Author:
Al Mulhim, Noura S K

Title:
Investigations of the classical and non-classical axis of the renin angiotensin system in dementia

Investigations of the classical and non-classical axis of the renin angiotensin system in dementia

Noura Saad Khalifa Al Mulhim

A dissertation submitted to the University of Bristol in accordance with the requirements for award of the degree of Doctor of Philosophy in the Faculty of Health Sciences.

School of Clinical Sciences

February 2020

Word count: 61,282

Abstract

Hyperactivity of the classical renin angiotensin system (cRAS) (ACE-1/Ang-II/AT_1R) within the brain exerts damaging effects and contributes to the pathogenesis of Alzheimer's disease (AD). Alternative 'downstream' regulatory RAS pathways: the non-classical RAS axis (ACE-2/Ang (1-7)/MasR) and the alternative regulatory RAS axis (rRAS) (APA/Ang-III/APN/Ang-IV/IRAP) have recently been discovered that counter-regulate the damaging effects of cRAS signalling, whilst also regulating synaptic function and boosting learning and memory. Despite a strong association of an imbalance in brain RAS pathways in relation to AD pathology and cognitive decline, the role of ACE-1 and the involvement of the other rRAS pathways in relation to AD pathogenesis remains unclear. This thesis describes a series of investigations of both cRAS and rRAS, and non-classical RAS components, in AD in post-mortem brain tissue aimed to test the general hypothesis that alterations of both the classical and regulatory axes of brain RAS can influence AD pathogenesis and are related to vascular dysfunction.

For this thesis I have studied mid-frontal cortex (Brodmann area 8/9) from post-mortem confirmed AD cases (n= 70) and age-matched controls (n= 48) that were matched closely for age-at-death and post-mortem delay (PMD). I developed specific ACE-1 N-domain and C-domain activity assays using immunocapture-based fluorogenic substrates. I measured the level of angiotensin peptides (Ang-I and Ang (1-7)) and characterised the expression, enzyme activity and distribution of rRAS receptors including MasR, Ang-IV, and IRAP by ELISA and immunohistochemistry. I used previously measured markers of disease pathology (parenchymal Aβ/Tau and insoluble Aβ40 and 42) and measured markers of cerebrovascular dysfunction including brain ischaemia (VEGF) and tissue oxygenation (MAG:PLP1 ratio) and examined the relationship between alterations of brain RAS components with these markers. I also explored the novel non-AT_1R and non-AT_2R receptor (Neurolysin) and its substrate (Neurotensin) using an ELISA.

Divergent ACE-1 C-domain (increased) and N-domain (reduced) enzyme activity was observed in AD that potentially favours Ang-II production and limits Aβ clearance and provides further insight into the complex role of ACE-1 in AD. These data potentially indicate that C-domain ACEIs may have greater therapeutic benefit for AD. Ang-I level was reduced and the ratio of Ang-II:Ang-I was increased in AD - as would be expected with overactivation of ACE-1. Changes were observed in mid-frontal cortex in the rRAS pathways indicative of dysregulation in AD: the Ang-II:Ang (1-7) ratio, a proxy marker of ACE-2 activity, was reduced in AD; IRAP activity was also reduced in AD, however, other components of the rRAS pathways including Ang (1-7), and MasR and Ang-IV and IRAP protein level remained unchanged in AD (although they were related to ischaemic damage). Interestingly, the non-AT_1R and non-AT_2R binding protein (neurolysin), previously not studied in AD, was reduced in relation to disease severity and ischaemia in AD.

In conclusion, these data support recent findings within the field that indicate that regulatory RAS pathways are dysfunctional in AD associated with disease pathology and vascular function. This thesis also offers insights into novel RAS components, such as neurolysin and neurotensin and their involvement in AD, that will require further investigation. The RAS remains a pivotal and complex system that underpins disease pathogenesis in AD and may offer new therapeutic targets in the future.

Publications

I confirm that some data presented in this thesis has been published in multi-author papers where my contributions are specified in this statement of contribution.

Kehoe PG, Wong S, **AL Mulhim N**, Palmer LE, Miners JS.

Angiotensin-converting enzyme 2 is reduced in Alzheimer's disease in association with increasing amyloid-β and tau pathology.

Alzheimers Res Ther. 2016 Nov 25;8(1):50. doi: 10.1186/s13195-016-0217-7

Contribution to paper: NAM carried out the angiotensin (1–7) measurements, performed statistical analysis and helped draft the manuscript.

AL Mulhim N, Kehoe PG, Miners JS.

Divergence in the activity of the N- and C- catalytic domains of ACE1 - implications for the role of the renin-angiotensin system in Alzheimer's disease.

Acta Neuropathol. Commun. 2019 Apr 24;7(1):57. doi: 10.1186/s40478-019-0718-2.

Contribution to paper: NAM was responsible for acquisition of ACE1 domain specific activity measurements; JSM and NAM analysed and interpreted the data.

Kehoe PG, **Al Mulhim N**, Zetterberg H, Blennow K, Miners JS.

Cerebrospinal Fluid Changes in the Renin-Angiotensin System in Alzheimer's Disease.

J Alzheimers Dis. 2019 Nov 12;72(2):525-535. doi: 10.3233/JAD-190721.

Figure 1.12 and Table 1.1 presented in this thesis contributed to Kehoe PG. 2018 J Alzheimers Dis. 2018;62(3):1443-1466.

PhD student: Noura S. Al Mulhim Signature:

First author: Patrick G. Kehoe Signature:

Last author: Scott J. Miners Signature:

Acknowledgements

I am extremely grateful and thankful to ALLAH for giving me the strength to complete this thesis. I would like to express my gratitude to the Imam Abdulrahman Bin Faisal University for funding my PhD scholarship. I would like to extend my sincere gratitude and thank my supervisors, Professor Patrick Kehoe and Dr Scott Miners for their continues support, invaluable comments, guidance, patience and encouragement from the start to the end of my PhD study. I would also like to thank all members of the Dementia Research Group and SWDBB for their help during my laboratory work. Special thank to Dr Hannah Tayler and Dr Kevin Kemp for their invaluable advices and suggestions during my annual evaluation.

I would like to give my special thanks to my partner, Mohammed and my superhero son, Rashed for their love, support, patience and have been a source of motivation and comfort to me. I wish to acknowledge the endless love and support of my mother, Badriyah for me and my son. Without her help and prayers I would not have been able to complete my study. I would also like to thank all of my sisters and brothers who have always loved and supported me. I also like to thank all my friends for their help and encouragement. Special thanks to my friend Dr Mayada for her kindness, advice, help and always being there for me in my ups and downs.

Finally, I dedicate this thesis to my mother and the soul of my beloved father, Saad who have raised me, loved and encouraged me to do my best. I will always make sure that you are proud of me.

Declaration

I declare that the work in this dissertation was carried out in accordance with the requirements of the University of Bristol *Regulations and Code Practice for Research Degree Programmes* and that it has not been submitted for any other academic award. Except where indicated by specific reference in the text, the work is the candidate's own work. Work done in collaboration with, or with the assistance of, others, is indicated as such. Any views expressed in the dissertation are those of the author.

Signed: Date: 18 February 2020

List of Contents

List of Figures

List of Tables

Abbreviations

ABC	Avidin-biotin complex
ABCA7	Encoding ATP-binding cassette transporter A7
Abz	o-aminobenzoic acid
ACE-1	Angiotensin converting enzyme 1
ACE-2	Angiotensin converting enzyme 2
ACE1	Encoding angiotensin-converting enzyme 1
ACEIs	Angiotensin converting enzyme inhibitors
AD	Alzheimer's disease
ADAM10	Encoding a disintegrin and metalloproteinase 10
ADAMTS1	Encoding a disintegrin and metalloprotease domain with TSP repeats protein-1
ADRDA	Alzheimer's Disease and Related Disorders Association
AGT	Angiotensinogen
AGTR1	AT_1R gene
AGTR2	AT_2R gene
AICD	APP intracellular domain
Ang (1-5)	Angiotensin (1-5)
Ang (1-7)	Angiotensin (1-7)
Ang (1-9)	Angiotensin (1-9)
Ang A	Angiotensin A
Ang-I	Angiotensin I
Ang-II	Angiotensin II
Ang-III	Angiotensin III
Ang-IV	Angiotensin IV
ANOVA	Analysis of variance
APA	Aminopeptidase A
APB	Aminopeptidase B
APES	3-amin-propyl-triethoxy-saline
Aph-1	Anterior pharynx defective 1
APN	Aminopeptidase N
APOE	Encoding apolipoprotein E

ApoE	Apolipoprotein E
APP	Amyloid precursor protein
APP	Encoding amyloid precursor protein
ARBs	Angiotensin-II receptor blockers
ASAP	Aspartyl aminopeptidase
AT_1aR	Angiotensin II type-1 a receptor
AT_1bR	Angiotensin II type-1 b receptor
AT_1R	Angiotensin II type-1 receptor
AT_2R	Angiotensin II type-2 receptor
AT_4R	Angiotensin IV receptor also called insulin regulated aminopeptidase (IRAP)
Aβ	Amyloid beta
Aβ40	Amyloid beta 40
Aβ42	Amyloid beta 42
BACE1	β-secretase
BBB	Blood-brain barrier
BDNF	Brain-derived neurotrophic factor
BIN1	Encoding bridging integrator 1
BP	Blood pressure
BSA	Bovine serum albumin
c-MET	A tyrosin type 1 receptor
C21	Compound 21
C83	C-terminal fragment 83
C99	C-terminal fragment 99
CA1	Region I of hippocampus proper
CAA	Cerebral amyloid angiopathy
cAMP/PKA	Edenosine 3',5'-cyclic monophosphate (cAMP)-dependent protein kinase (PKA)
Carb-P	Carboxypeptidase B
CASS4	Encoding cas scaffolding protein family member 4
CBF	Cerebral blood flow
CD2AP	Encoding CD2-associated protein
CD33	Encoding CD33 molecule (sialic acid–binding immunoglobulin (Ig)–like lectin)
CERAD	Consortium to Establish a Registry for Alzheimer's disease
CLU	Encoding clustrin

CNS	Central nervous system
COX-2	Cyclooxygenase 2
CR1	Encoding complement receptor one
cRAS	Classical axis of RAS or classical RAS
CSF	Cerebral spinal fluid
CV	Coefficient of variation
CVD	Cardiovascular diseases
CVLM	Caudal ventrolateral medulla
DAB	Diaminobenzidin
DAP	Dipepidyl aminopeptidases
dH2O	Distilled water
DIZE	Diminazene aceturate
DLB	Dementia with Lewy bodies
DM	Diabetic mellitus
DMEM	Dulbecco's modified Eagle medium
DMM	Dorsomedial medulla
DMSO	Dimethyl Sulfoxide
Dnp	2,4-dinitrophenyl
DOCA-salt rat	Deoxycorticosterone acetate -salt rat
ECE-1	Endothelin converting enzyme 1
ECE-2	Endothelin converting enzyme 2
ECHDC3	Encoding enoyl CoA hydratase domain containing 3
ECL	Enhanced chemiluminescence
EDTA	Ethylenediamine tetraacetic acid
ELISA	Enzyme linked immunosorbant assay
eNOS	Endothelial nitric oxide synthase (NOS)
EOAD	Early-onset Alzheimer's disease
EPHA1	Encoding ephrin receptor A1
ET-1	Endothelin-1
FAD	Familial Alzheimer's disease
FBS	Foetal bovine serum
FDA	Food and drug administration
FERMT2	Encoding fermitin family member

FRET	Fluorescence resonance energy transfer
FTD	Fronto-temporal dementia
gACE-1	Germinal angiotensin converting enzyme 1 (ACE-1)
GFAP	Glial fibrillary acidic protein
GFP	Green fluorescent protein
GLUT4	Glucose transporter type 4
GPCRs	G-protein coupled receptors
GSK3β	Glycogen synthase kinase 3β
GWAS	Genome Wide Association Studies
H_2O_2	Hydrogen peroxide
HEK	Human embryo kidney
HGF	Hepatic growth factor
HLA-DQB1	Encoding major histocompatibility complex class II, DQ beta 1
HTN	Hypertension
I/D	ACE intron 16 insertion/deletion polymorphism
ICV	Intracerebroventricular
IDE	Insulin-degrading enzyme
IHC	Immunohistochemistry
IL-1b	Interleukin 1b
IL-6	Interleukin 6
INPP5D	Encoding inositol polyphosphate-5-phosphatase, 145 kDa
IQCK	Encoding IQ motif containing K
IRAP	Insulin regulated aminopeptidase
ISF	Interstitial fluid
L-Leu-pNA	L-Leucine-p-nitroanilide
LOAD	Late-onset Alzheimer's disease
LRP1	Low-density lipoprotein receptor-related protein 1
LTD	Long-term depression
LTP	Long-term potentiation
MAG	Myelin-associated glycoprotein
MAPK	Mitogen-activated protein kinase
MasR	MAS receptor
MCI	Mild cognitive impairment

MMP-2	Matrix metalloproteinase 2
MMP-3	Matrix metalloproteinase 3
MMP-9	Matrix metalloproteinase 9
MMSE	Mini Mental State Examination
MoCA	Montreal Cognitive Assessment
MrgD	Mas-related G protein-coupled receptor D
Mrgprd	MrgD gene
MRI	Magnetic resonance imaging
MS4A4E	Encoding membrane-spanning 4-domain, subfamily A, member 4E
MS4A6A	Encoding membrane-spanning 4-domain, subfamily A, member 6A
MW	Molecular weight
NEP	Neprilysin
NF-κB	Nuclear factor- kappa B
NFTs	Neurofibrillary tangles
NIA-RI	National Institute on Aging and the Alzheimer's Association
NMDA	N-methyl-D-aspartate
NO	Nitric oxide
NOS	Nitric oxide synthase
NP	Neuritic plaques
NSE	Neuron-specific enolase
NTSR1	Neurotensin type-1 receptor
NTSR2	Neurotensin type-2 receptor
NTSR3	Neurotensin type-3 receptor
NYAP1	Encoding neuronal tyrosine phosphorylated phosphoinositide-3-kinase adaptor 1
p-tau	Phosphorylated tau
P3	A 3-kDa peptide
PBS	Phosphate buffered saline
PDD	Parkinson's disease dementia
Pen-2	Presenilin enhancer 2
PEP	Prolyl endopeptidase
PET	Positron emission tomography
PI3K/Akt	Phosphatidylinositol 3-kinase/Protein Kinase B
PiB	C Pittsburgh compound B

PICALM	Encoding phosphatidylinositolbinding clathrin assembly protein
PLP1	Proteolipid protein-1
PMD	Post-mortem delay
PMSF	Phenylmethylsulphonyl fluoride
PO	Proly oligopeptidase
proNGF	Precursor form of nerve growth factor
PSEN1	Presenilin-1
PSEN1	Encoding presenilin-1
PSEN2	Presenilin-2
PSEN2	Encoding presenilin-2
PTK2B	Encoding protein tyrosine kinase 2 beta
RAS	Renin angiotensin system
r.f.u	Relative fluorescence units
rhACE-2	Recombinant human angiotensin converting enzyme 2
ROS	Reactive oxygen species
ROUT	Robust regression and Outlier removal
rpm	Revolutions-per-minute
rRAS	Non-classical axis of RAS or regulatory RAS
RT-PCR	Reverse transcription-Polymerase chain reaction
RVLM	Rostral ventrolateral medulla
sACE-1	Somatic angiotensin converting enzyme 1 (ACE-1)
SAD	Sporadic Alzheimer's disease
sAPPα	Soluble N-terminal ectodomain of APP
SD	Standard deviation
SDR	Sprague-Dawley rats
SDS	Sodium dodecyl sulphate
SEM	Standard error of mean
SHR	Spontaneously hypertensive rat
SIVD	Subcortical ischaemic vascular dementia
SLC24A4	Encoding (sodium/potassium/calcium exchanger), member 4
SNPs	Single nucleotide polymorphisms
SORL1	Encoding sortilin-related receptor, L(DLR class) A repeats containing
SPECT	Single photon emission computed tomography

SPI1	Encoding transcription factor PU.1
Strep-HRP	HRP-conjugated streptavidin
SWDBB	South West Dementia Brain Bank
TAC	Tumor necrosis factor-α convertase
TBS	Tris-buffered saline
TBST	Tris-buffered saline containing Tween®-20
TDP-43	Transactive response DNA-binding protein 43kDa
TMB	Tetramethylbenzidine
TNF-a	Tumour necrosis factor alpha
TREM2	Triggering receptor expressed on myeloid cells-2
TREM2	Encoding triggering receptor expressed on myeloid cells-2
VaD	Vascular dementia
VCAM	Vascular cells adhesion molecules
VEGF	Vascular endothelial cell growth factor
VLDLR	Very low-density lipoprotein receptor
WML	White matter lesions

Chapter 1. Introduction

1.1 Dementia

Dementia is characterised clinically by a progressive decline in higher cognitive functions, such as thinking, memory, planning, problem-solving and associated behavioural impairment, that together significantly affects a patient's daily functioning activities (1). Dementia is a multi-aetiological syndrome that mainly affects the elderly and is caused by different neurodegenerative diseases including Alzheimer's disease (AD), vascular dementia (VaD), mixed dementia, dementia with Lewy bodies (DLB), Fronto-temporal dementia (FTD), Parkinson's disease dementia (PDD) and less common causes including Huntington's disease and Creutzfeldt-Jakob disease and multiple sclerosis (2). One of the early symptoms of dementia is impairment of short-term memory. As dementia progresses, a variety of symptoms including progressive cognitive impairment, disorientation, confusion, mood swings and transient behavioural issues, language impairment, difficulties in movement and progressive disabilities occur (3). The severity and duration of these symptoms vary amongst people with different types of dementia and at different stages of the disease.

1.1.1 Types of Dementia

AD is the most common type of dementia and accounts for 60-80% of all dementia cases (Figure 1.1) (4). AD was first described in 1906 when Alois Alzheimer observed the unusual clinical symptoms of his patient (Auguste Deter) that included loss of memory, hallucination, disorientation and delusions (5). Seventy years later, AD, which was now widely recognized as a common type of dementia also became recognised as a major cause of death (6). Early clinical symptoms of AD are forgetfulness and short-term memory loss, which together are known as mild cognitive impairment (MCI). Other symptoms such as apathy and depression appear later (7). In addition to these clinical symptoms, AD has the two distinct neuropathological hallmarks that differentiate it from other types of dementia; extracellular accumulation of amyloid beta (Aβ) plaques that triggers an intracellular accumulation of neurofibrillary tangles (NFTs) and intiates a series of pathological events attributed to neurotoxicity in the AD brain (3).

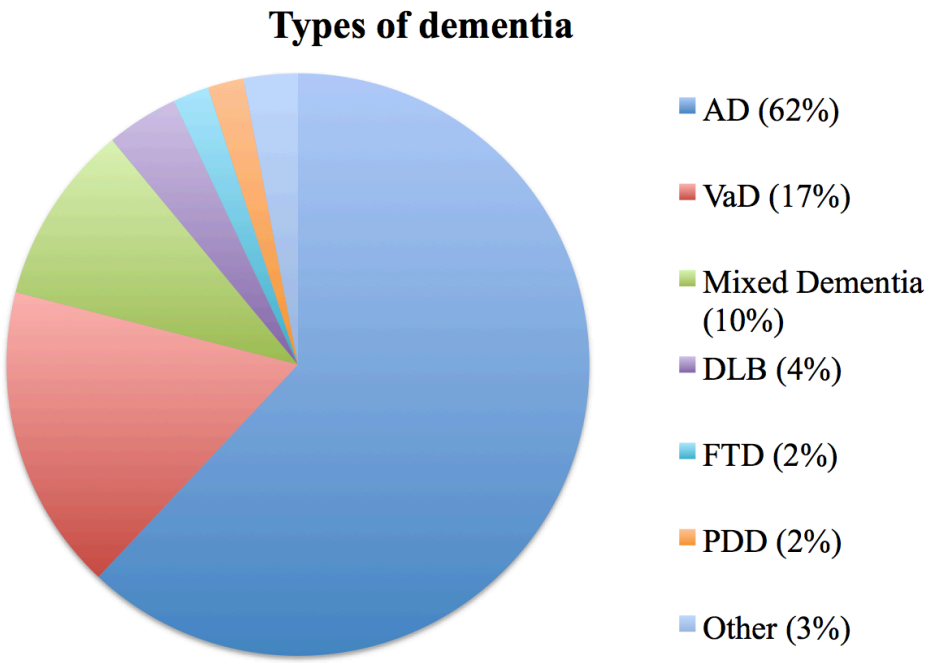

Figure 1.1 Types of dementia.

Pie chart showing the estimated percentages of different types of dementia.
AD - Alzheimer's disease; VaD - Vascular dementia; Mixed dementia (a condition when more than one type of dementia co-occur; DLB - Dementia with Lewy bodies; FTD - Fronto-temporal dementia; PDD - Parkinson's disease dementia; Others include numerous less common causes of dementia Huntington's disease and Creutzfeldt-Jakob disease, multiple sclerosis, infections, metabolic disease and tumours (sourced and adapted from Alzheimer's Society UK, 2015)(7).

The second most common type of dementia is VaD and accounts for 15-20% of all dementia cases (7). Early symptoms that first appear in patients with VaD include impaired judgement, poor planning and impaired ability to organise that are called executive cognitive functions, in contrast to deficits in memory and language functions observed in AD (8). The underlying mechanisms of VaD are associated with ischaemic tissue damage as a result of reduced cerebral blood flow (CBF) either by blocked or damaged blood vessel that result in infarcts or haemorrhage (9). VaD is divided into several sub-categories that include: multi-infarction dementia, strategic infarction dementia, haemorrhagic dementia, mixed dementia, subcortical ischaemic vascular dementia (SIVD) and other forms of VaD (10, 11). There is evidence that many forms of dementia also have vascular abnormalities and thus of all the dementias, VaD is possibly one of the biggest contributors to co-morbidity and mixed dementias (11-13).

DLB, as a singular cause of dementia, accounts for approximately 5% of all dementia cases (7). DLB is characterised neuropathologically by abnormal accumulation of alpha-synuclein in cortical neurons

associated with brain atrophy (14). In addition to the common clinical symptoms of AD, patients with DLB also have disturbances in sleep pattern, visual hallucinations, gait imbalance and other parkinsonian movement abnormalities (15). If the onset of movement disorders precedes dementia by twelve months, likely as a result of alpha-synuclein aggregation in the substantia nigra resulting in degeneration of the dopaminergic neurons, it is diagnosed as PDD, which accounts for approximately 2% of all cases of dementia. Both clinical diagnosis and neuropathological assessment are required to differentiate between DLB and PDD (16).

Dementia with more than one cause is known as mixed dementia and has been suggested to account for about 10% of all other dementia types (7). However as mentioned, many people with dementia also have vascular changes or dysfunction that are also associated with VaD and so mixed dementia is likely to be under recognised. The most common combination of mixed dementia is AD-VaD, this is followed by AD-DLB, and then AD-VaD-DLB. VaD-DLB is less commonly observed (12). Mixed dementia is increased with age and is more prevalent in older people (age 85 or older) (17, 18).

FTD is a heterogenous neurodegenerative group of dementias with different clinical and pathological characteristics compared to AD and accounts for about 2% of all dementia cases (7, 19). FTD is characterised pathologically by atrophy of both frontal and temporal lobes, neuronal loss and gliosis and spongiosis due to abnormal aggregation of protein inclusions that mainly comprise tau protein or the transactive response DNA-binding protein 43kDa (TDP-43) (20). FTD is divided into three subgroups that include FTD-tauopathies such as Pick's disease, corticobasal degeneration, argyrophilic grain disease and others such as FTD-ubiquitin and FTD-without tau or ubiquitin (19). FTD tends to affect people at a younger age where approximately 60% of people with FTD are aged between 40-60 years old (21). Early symptoms of patients with FTD include behavioural and personality changes and language impairment, while memory function is spared at the early stage of the disease (4).

There are other less common causes of dementia such as Huntington's disease and Creutzfeldt-Jakob disease, multiple sclerosis, infections, metabolic disease and tumours (16).

1.1.2 Prevalence of Dementia

Dementia is considered as a major cause of death and a global health burden with around 50 million people suffering from dementia worldwide (22). Every 3 seconds someone develops dementia and every year there are around 10 million new cases globally (23). This number has been predicted by some researchers to double every 20 years, reaching 75 million in 2030 and 131.5 million in 2050 (24). Currently, around 850,000 people in the UK are estimated to have dementia where the incidence of dementia has been predicted to rise to over 1 million by 2025 and over 2 million by 2051 (7). A recent modelling study estimated the number of people that will have dementia in the UK by 2040 is more than 1.2 million with an increase by 57% from 2016 (25). However, more recent research and findings are pointing to a slowing in incidence rates although there will still be high prevalence of AD with an increasingly ageing population and the current absence of any disease-modifying treatments (26, 27).

AD is the most common form of dementia accounting for between 60-80% of all dementia cases (4). The prevalence of AD increases with age and ranges from ~1% in 60-64 year olds compared to ~30% in the 90-94 year olds (2). The majority of AD cases, between 95-99%, are regarded as sporadic in origin (SAD) also known as late-onset AD (LOAD) (28), whereas 1-5% of AD cases are familial (FAD) (early-onset, EOAD) (3).

1.2 Alzheimer's disease

AD is a complex, progressive chronic neurodegenerative disorder. Characterised clinically by cognitive decline associated with behavioural impairment and neuropathologically by the presence of cortical extracellular senile Aβ plaques and intracellular NFTs. In addition, AD has a complex aetiology including a combination of genetic and lifestyle factors (29).

1.2.1 Neuropathology of AD

Multiple macroscopic changes are visible in the AD brain that include cortical atrophy predominantly affecting the frontal and medial temporal lobes, widening of the sulci and enlargement of the lateral and third ventricles. These changes can be detected clinically by a magnetic resonance imaging (MRI)

scan (30). Cortical micro-infarcts and white matter changes, associated with cerebrovascular disease, may also be present (29).

At a microscopic level, the two major and most commonly referred to pathological hallmarks of AD are extracellular Aβ plaques and intracellular NFTs (31). Aβ plaques are extracellular proteinaceous deposits primarily formed from abnormal accumulation of the Aβ peptide derived from the sequential enzymatic actions of β- and γ- secretase on the transmembrane amyloid precursor protein (APP). Plaques are characterised as either being diffuse (composed mainly of Aβ42 and thought to be the earliest form of amyloid deposits (32), or neuritic (senile) that contain a central core of fibrillar amyloid peptide (Aβ40 and Aβ42), which is surrounded by dystrophic neurites, reactive astrocytes and microglial cells (33). Both forms of amyloid plaques have been thought to play a significant role in the pathogenesis of AD, but more recently the presence of (more neurotoxic) soluble oligomeric forms has been attributed with the greatest levels of neurotoxicity in the brain in AD (34).

NFTs are composed of intracellular aggregated phosphorylated tau. Tau is a microtubule-associated protein that normally plays a physiological role in microtubule stabilisation (35). However, in AD there is an imbalance in the hyperphosphorylation state of tau (36). Hyperphosphorylated tau impairs axonal transport and synaptic function (37). The levels of hyperphosphorylated tau proteins are increased in the AD brain (35). The distribution of NFTs is important in the post-mortem diagnosis of AD (38). Studies indicate a synergistic role of Aβ and tau in AD (39-41). However, much uncertainty still exists about the relationship between the Aβ and tau proteins and their interaction in AD.

A third, less often referred to, but arguably as common as senile plaques and tangles, is cerebral amyloid angiopathy (CAA) that contributes to AD pathogenesis. CAA affects around 90% of elderly with AD and approximately 30% of normal elderly (42, 43). Accumulation of Aβ in and around cerebral blood vessels can alter blood-brain barrier (BBB) integrity and limit blood supply (44), or can increase risk of haemorrhage which is another risk factor for dementia (45). The exact mechanisms of Aβ accumulation in AD and CAA are still unknown.

1.2.2 Pathological hypotheses of Alzheimer's disease

1.2.2.1 The amyloid cascade hypothesis

The amyloid cascade hypothesis, perhaps the most widely accepted and predicted cause of AD pathogenesis, states that the accumulation of Aβ is central to the pathogenesis of AD and triggers a series of downstream events that ultimately result in nerve cell injury/death and cognitive impairment (Figure 1.2) (46). This pathogenic cascade starts when there is accumulation and increased levels of pathogenic Aβ42 (either oligomeric or fibrillar) or an increase in the ratio of Aβ42:40. Elevated Aβ causes a subsequent cascade resulting in tissue damage such as activation of microglia and astrocytes, altered ionic homeostasis and oxidative injury in neurons and activation of kinases, which lead to hyperphosphorylation of the tau protein, synaptic dysfunction, and ultimately neuronal death (47, 48). Several imaging and brain biomarker studies, and recent disease-modelling studies indicate that abnormal accumulation of Aβ in the brain begins up to 10-20 years before the onset of AD clinical symptoms (31, 49, 50).

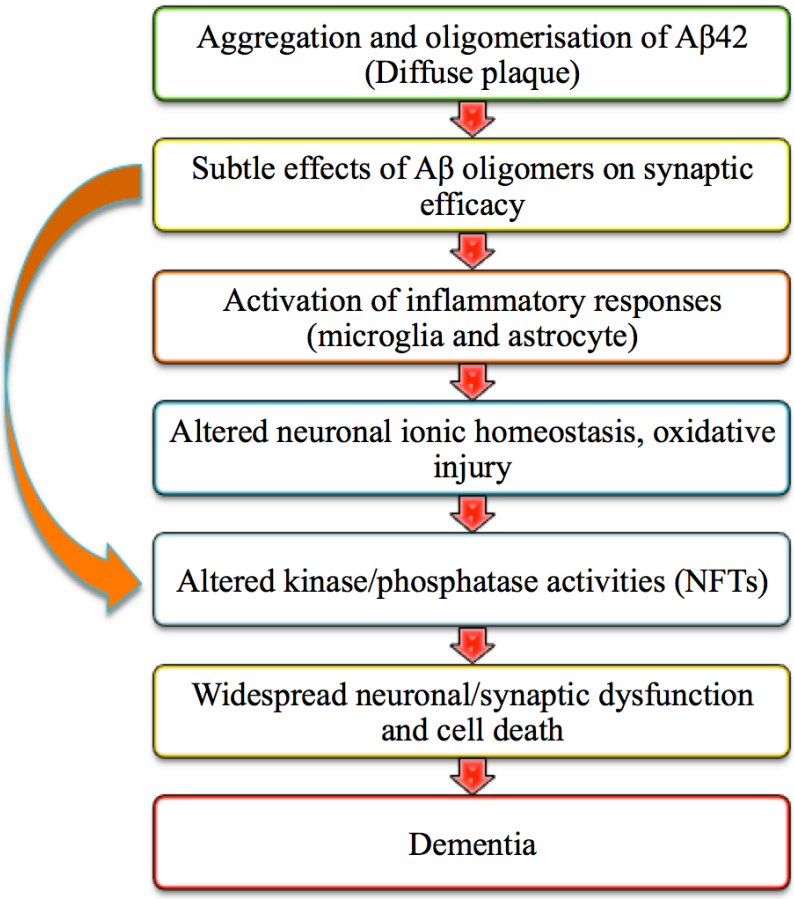

Figure 1.2 The amyloid (Aβ) cascade hypothesis of AD pathogenesis.

The figure illustrates the proposed sequence of major pathogenic effects of Aβ accumulation leading to AD. The pathogenic sequence is initiated by accumulation of Aβ42 that alters tau phosphorylation, activates inflammation, oxidative stress and other neurotoxic events and leads to synaptic remodelling and neuronal death. More recently, the direct neurotoxic effects of oligomeric Aβ, indicated by the curved orange arrow have been recognised. Aβ42 - Amyloid beta 42. NFTs - Neurofibrillary tangles (adapted from Selkoe and Hardy. 2016)(48).

1.2.2.1.1 Aβ Production

The Aβ peptide is a product of the proteolytic cleavage of APP, an integral trans-membrane glycoprotein consisting of a large extracellular N-terminus and a smaller cytoplasmic C-terminus (51). APP usually comprises 770 amino acids and is encoded for by *APP* located on chromosome 21 (52). APP can be cleaved by α-secretase that includes members of the ADAM (a disintegrin and metalloproteinase) family enzymes (ADAM 9, ADAM 10 and TAC (tumor necrosis factor-α

convertase, ADAM 17); β-secretase (BACE1) and γ-secretase (made up of presenilins (presenilin-1(PSEN1) and presenilin-1(PSEN2)), nicastrin, anterior pharynx defective 1 (Aph-1) and presenilin enhancer 2 (Pen-2) (53-55).

When APP is hydrolysed by α-secretase at residues 16–17 of the Aβ domain, a large non-pathogenic peptide known as soluble N-terminal ectodomain of APP (sAPPα) and a C-terminal fragment (C83) are generated. These non-pathogenic fragments are further cleaved by γ-secretase to produce the APP intracellular domain (AICD) and a 3-kDa peptide (P3) – collectively this pathway is called non-amyloidogenic processing. Toxic amyloidogenic processing of APP, generates heterogeneous polypeptides with 40 to 42 amino acids are produced in the brain when APP is first hydrolysed by β-secretase to produce a soluble fragment of APP (sAPPβ) and the C-terminal fragment (C99) followed by cleavage by γ-secretase (Figure 1.3) (56). Autosomal dominant mutations in *APP* that are located within the Aβ sequence increase the production and aggregation of Aβ, and account for around 10% of mutations in FAD (57). The remaining 90% of identified mutations in FAD are located in *PSEN1* and *PSEN 2* that are linked to increased production of Aβ42 or those that increase the ratio of Aβ42/Aβ40 in humans (48, 58).

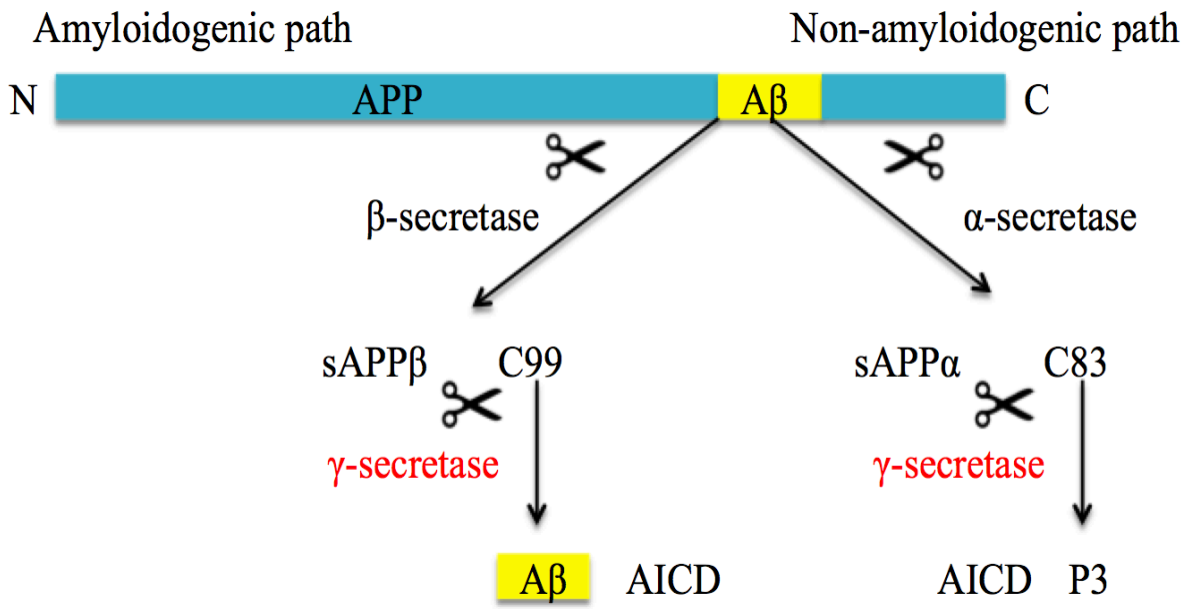

Figure 1.3 APP processing showing the amyloidogenic and non-amyloidogenic pathways.

APP is cleaved by β-secretase (BACE1) to produce sAPPβ followed by cleavage of the sAPPβ fragment by γ-secretase (presenilins, nicastrin, Aph-1, and Pen-2) to produce Aβ and AICD (amyloidogenic pathway). APP is cleaved by α-secretases (ADAM 19, ADAM 10, TACE) to produce sAPPα followed by cleavage of the soluble fragment by γ-secretase to release AICD and P3 (non-

amyloidogenic pathway). APP - amyloid precursor protein, Aβ - Amyloid beta, sAPPβ - soluble fragment of APP β, C99 - C-terminal fragment 99, AICD - APP intracellular domain, sAPPα - soluble fragment of APP α, C83 - C-terminal fragment 83, P3 – a 3-kDa peptide (adapted from Kehoe et al. 2009)(56).

1.2.2.1.2 Aβ aggregation

Soluble Aβ monomers aggregate in a dynamic, reversible process into small soluble multimers that can be converted by further oligomerisation to form micelles and protofibrils. In the final irreversible step of this process, protofibrils undergo conformational change to form insoluble fibrils that aggregate and form the Aβ plaque (Figure 1.4) (59, 60). The most common species of Aβ that are produced and aggregate during plaque formation are Aβ40 and Aβ42 (61). The ratio of Aβ40:Aβ42 in brain tissue is predicted to be approximately 9:1 in the healthy non-diseased individuals (62). In contrast to Aβ40, Aβ42 is highly insoluble, amyloidogenic and deposits in the parenchyma as senile plaques. Aβ42 also more-readily forms neurotoxic oligomeric aggregates that impair neuronal synaptic function, trigger the inflammatory responses through activation of microglia and astrocytes and alters neuronal activity leading to loss of neurons (63-65). Aβ43 is an early depositing Aβ species in both SAD and FAD and is potently amyloidogenic and toxic (66, 67), while Aβ40 is less prone to aggregation and may actually be an anti-amyloidogenic form of Aβ in addition to be the major amyloid species found in CAA (68).

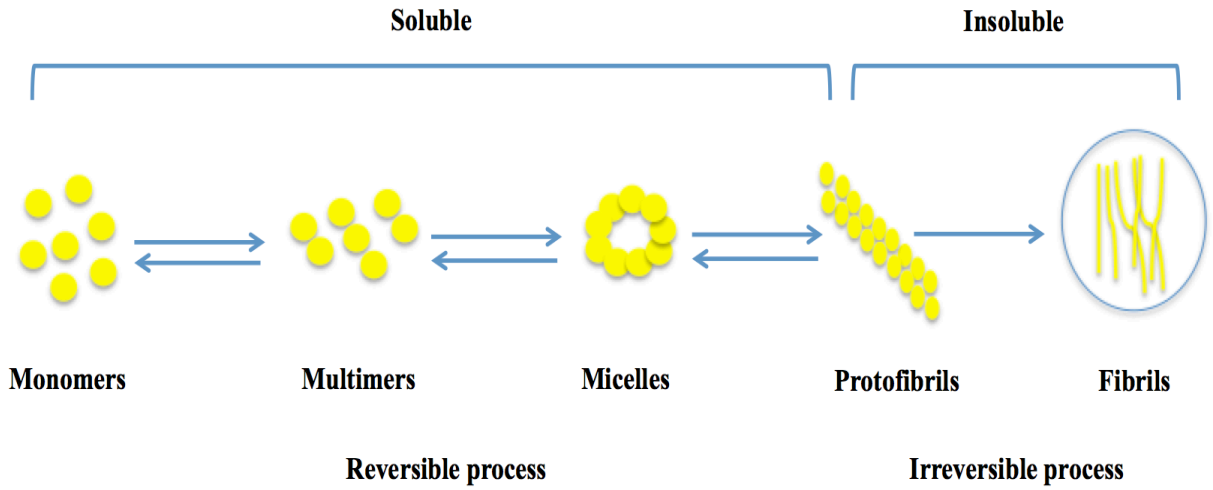

Figure 1.4 The Aβ Aggregation process.

Soluble Aβ monomers readily aggregate to form small soluble multimers followed by more aggregated forms such as micelles and protofibrils. Protofibrils undergo conformational changes to form insoluble fibrils that deposit in the extracellular space as plaques. The process then becomes irreversible (adapted from Walsh and Selkoe. 2007) (61).

1.2.2.1.3 Aβ clearance

Accumulation of Aβ in the brain may result from either increased neuronal production of Aβ or reduced clearance of Aβ as a result of defective transport across the BBB or decreased degradation by proteolytic Aβ degrading enzymes (69). Previous studies indicate that accumulation of Aβ in SAD and CAA is due to impaired clearance rather than overproduction of Aβ peptides that leads to Aβ peptide deposition (70). There are several clearance routes of Aβ from the brain: bulk flow of interstitial fluid (ISF) into the cerebral spinal fluid (CSF); transport across the BBB that is mediated by a series of clearance receptors such as low-density lipoprotein receptor-related protein 1 (LRP1), very low-density lipoprotein receptor (VLDLR) and P-glycoprotein (71); the uptake and phagocytosis of Aβ by microglial or astrocytic phagocytosis in the early stage of AD (72). Dysfunction of these clearance pathways has been shown to increase Aβ accumulation in the brain associated with cognitive impairment in AD (73, 74). The routes of Aβ clearance that are proposed to be impaired in AD are illustrated in (Figure 1.5).

Proteolytic degradation of Aβ involves multiple enzymes known to cleave at a single or multiple sites within Aβ such as neprilysin (NEP), insulin-degrading enzyme (IDE), endothelin converting enzymes (ECE-1 and ECE-2), angiotensin converting enzyme (ACE-1 and ACE-2), plasmin and matrix metalloproteinases (MMP-2, MMP-3 and MMP-9) (75). Alterations of the level and activity of these Aβ degrading enzymes have been linked to reduced Aβ metabolism (76-78). *In vitro* studies showed that the Aβ degrading enzymes cleave the full-length Aβ to produce small peptide fragments, which are less neurotoxic and thus more easily cleared (71). ACE-2 was recently reported to convert Aβ43 (earliest and potent amyloidogenic form of Aβ) to Aβ42, which in turn is converted to a shorter and less toxic form, Aβ40, by ACE-1 (79), which indicate that the combined effects of ACE-1 and ACE-2 in degradation of Aβ are protective in AD. All degrading enzymes are thought to be able to cleave monomeric Aβ but only few appear to degrade oligomeric and fibrillar forms of Aβ including NEP, plasmin and MMP-2 and MMP-9 (80). Knowing the important roles of these degrading enzymes on Aβ metabolism makes them an interesting therapeutic target for AD.

ACE-1 has been reported to degrade both Aβ40 and Aβ42 and convert the neurotoxic Aβ42 into less toxic form Aβ40 *in vitro* (81-83). Several earlier genetic studies showed a strong association between ACE-1 and AD and found that the *ACE* indel polymorphism (I/I) increased risk of LOAD (84-90). In

human studies, both ACE-1 level and activity are increased in AD (78, 91, 92). The potential role of ACE-1 in the pathogenesis of AD is discussed further in chapter 1 (sections 1.2.4 and 1.5.1.2).

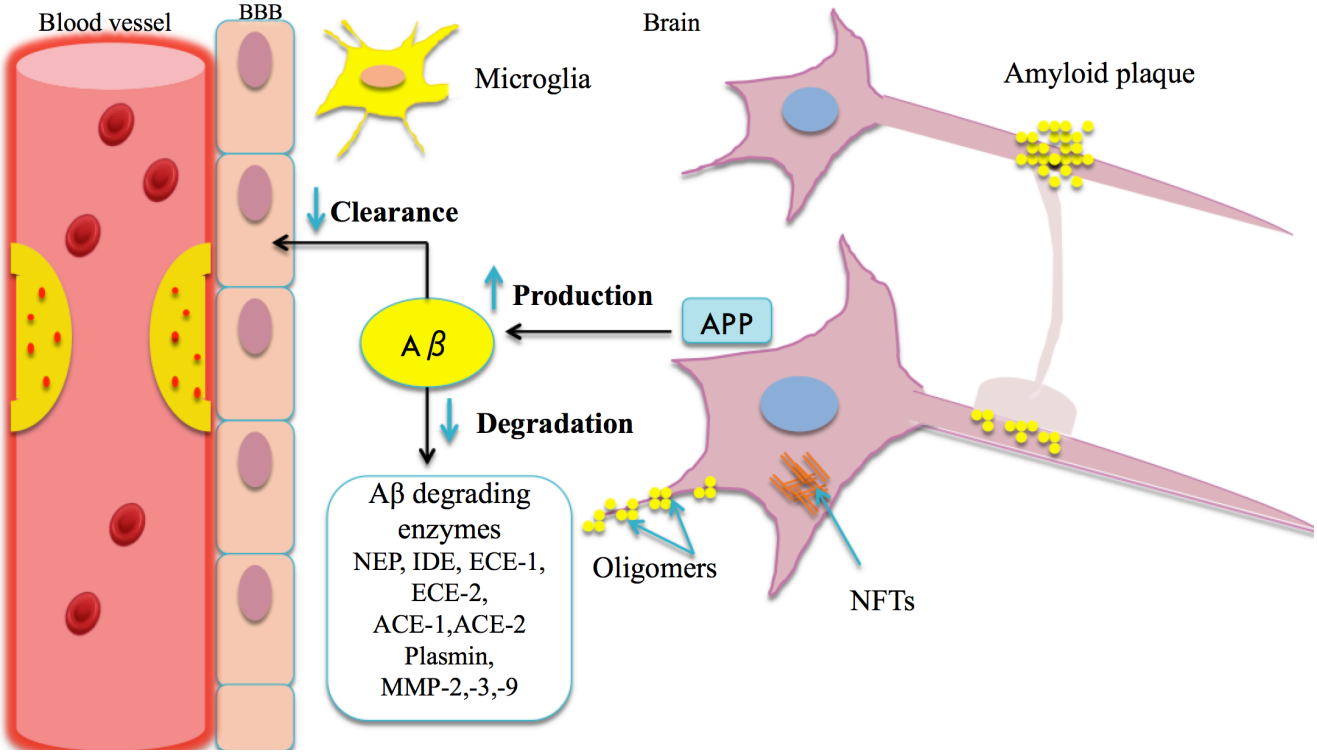

Figure 1.5 Metabolism of Aβ in AD brain.

The metabolic processing of Aβ is impaired in AD. Accumulation of Aβ in brain tissue may result from either increased production of Aβ (due to genetic mutation in *APP* or decreased Aβ clearance (from several routes including: impaired bulk flow of the interstitial fluid (ISF) into the cerebral spinal fluid (CSF), the uptake of Aβ by microglial or astrocytic phagocytosis in the early stage of AD; receptor-facilitated transport of Aβ across the BBB or via enzymatic degradation of Aβ (e.g. NEP, IDE, ECE-1, -2, ACE-1,-2, plasmin, MMP-2, -3, -9). BBB - blood brain barrier; NFTs - neurofibrillary tangles; APP - amyloid precursor protein; NEP - neprilysin; IDE - insulin degrading enzyme; ECE-1; ECE-2 - Endothelin converting enzymes 1 and 2; ACE-1, ACE-2 - angiotensin II converting enzymes 1 and 2. Downward pointing blue arrows = decrease, Upward pointing blue arrow = increase (adapted from Huang and Mucke. 2012) (69).

1.2.2.2 The Tau hypothesis

NFTs are composed of abnormally hyperphosphorylated tau proteins and defined as one of the pathological hallmarks of AD (93, 94). The tau hypothesis proposes that abnormal accumulation and distribution of hyperphosphorylated tau proteins is closely linked to the progression of AD and related to cognitive decline (95). Based on this abnormal distribution, AD has been described as having six

disease stages known as Braak tangle stages (96) (Figure 1.6). In the human adult brain, six isoforms of tau are expressed and these play an important role in the stability of microtubules (97). Under pathological conditions, tau proteins undergo many modifications including phosphorylation that can be triggered by the accumulation of Aβ, and the activation of kinases such as Glycogen synthase kinase 3β (GSK3β) that are involved in tau phosphorylation (98-100). The hyperphosphorylated tau proteins have increased propensity to aggregate and form NFTs and therefore affect the synaptic and axonal transport functions of neurons (37, 101). Several studies have shown that Aβ aggregation precedes and accelerates tau pathology in AD both *in vitro* and *in vivo* (39, 102-104). However, the pathophysiological conditions of tau proteins in relation to AD pathogenesis are not fully understood.

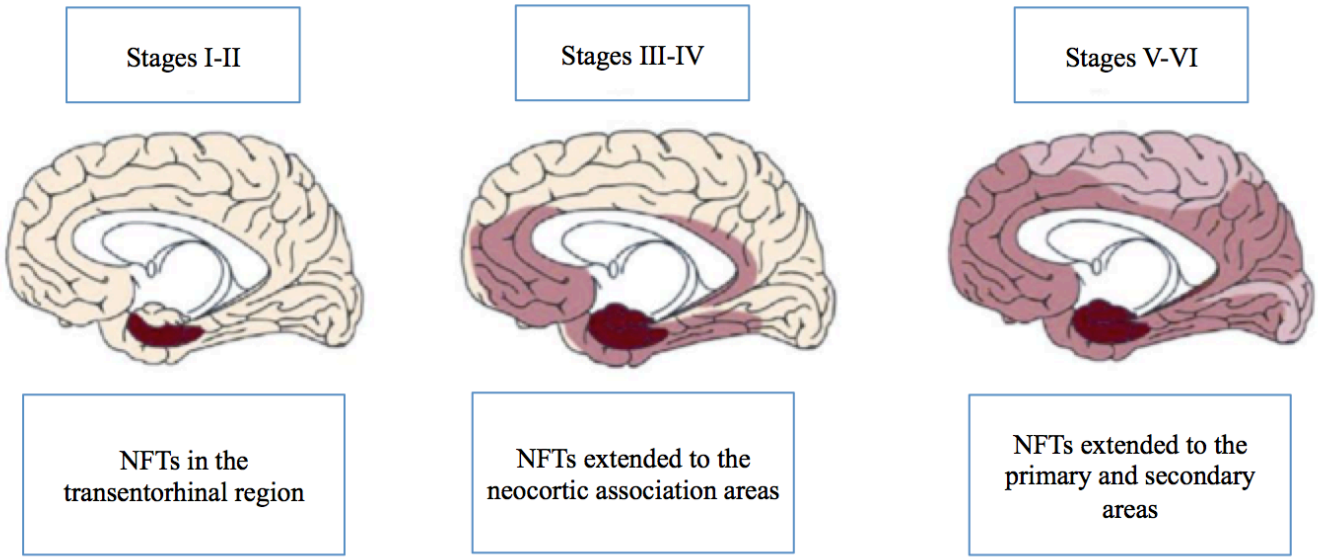

Figure 1.6 Stages of tau pathology in the development of AD.

The distribution and spread of NFTs in human brain tissue can be used to describe disease-stage severity into six stages. In the Braak tangle stage I-II, NFTs accumulate in the transentorhinal region. In stage III-IV they spread to the neocortic association areas and then extend to the primary and secondary areas in stage V-VI (adapted from Braak et al. 2011) (105). NFTs - neurofibrillary tangles.

1.2.2.3 The cholinergic hypothesis

The cholinergic hypothesis was the first established hypothesis of AD based on findings of dysfunction and loss of cholinergic neurons (106). Early studies identified cholinergic dysfunction as an early hallmark of AD (107). Acetylcholine, the major neurotransmitter of the cholinergic system, which has been implicated in several brain physiological functions such as learning, memory, attention, stress

response, sleep and processing of sensory information (108). Cholinergic dysfunction was associated with cognitive impairment in AD. Post-mortem brain tissue from AD patients showed reduced activity of choline acetyltransferase, reduced acetylcholine synthesis, choline uptake and acetylcholine release (35). Currently available drugs that have been approved by the food and drug administration (FDA) for AD treatment that were discovered and developed from research on the cholinergic hypothesis include tacrine, donepezil, rivastigmine and galantamine (109). Although there is currently no cure for AD, these cholinesterase inhibitors provide some but time-limited symptomatic relief of mild to moderate AD.

1.2.2.4 The vascular hypothesis

The vascular hypothesis, is currently gaining a new popularity but this hypothesis, which has been around for several decades proposes and states that reduced cerebral perfusion and vascular dysfunction play a significant role in AD pathogenesis (110), particularly in the early stages of disease (111-113). Most AD cases have evidence of vascular lesions including CAA and SVD (43, 45). Data from several studies highlighted the relationship between cerebrovascular diseases on the production and clearance process of Aβ peptide (114) and more recently Tau (115). Cerebral hypoxia or ischaemia caused by cerebrovascular diseases may also contribute to neurodegeneration in AD through several pathways, including acceleration of Aβ deposition, neuronal or synaptic dysfunction, and white matter changes (116, 117) (Figure 1.7). Results from multifactorial data-driven analysis suggest that brain vascular dysregulation including reduced CBF and BBB breakdown are early pathological changes in AD that contribute to cognitive decline and disease progression (118).

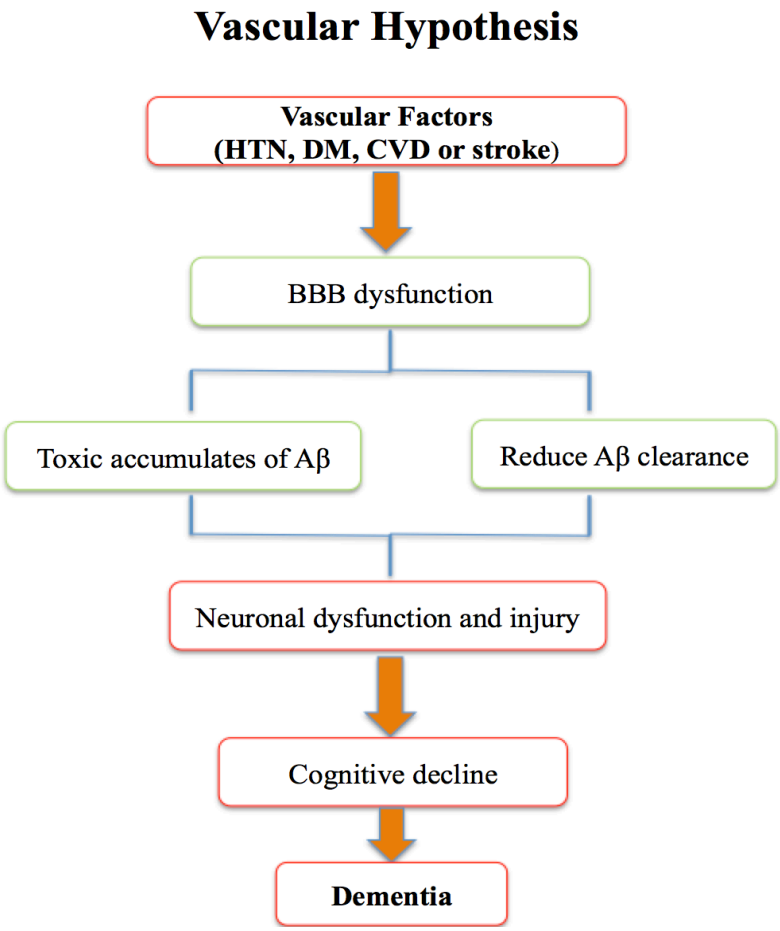

Figure 1.7 The vascular hypothesis for AD pathogenesis.

According to vascular hypothesis, the presence of one or more vascular risk factors including BBB dysfunction and a reduction in cerebral blood flow can lead to either increased accumulation of Aβ or reduced Aβ clearance that can exacerbate the toxic effects of Aβ (adapted from Zlokovic. 2011) (117). HTN - hypertension, DM - diabetic mellitus, CVD - cardiovascular diseases, BBB - blood brain barrier, Aβ - amyloid beta.

1.2.2.5 The inflammation hypothesis

Neuroinflammation is considered as a hallmark of AD. Dysfunctional microglia and astrocytes are believed to play a central role in the inflammatory process of AD (119, 120). The role of the inflammatory system in AD is further supported by more recent Genome Wide Association Studies (GWAS) studies that have identified that genetic variants in genes that regulate inflammation, such as triggering receptor expressed on myeloid cells-2 (TREM2), increase AD risk (121-123). In the early stages of AD, accumulation of Aβ is proposed to activate microglia and lead to the increased secretion of pro-inflammatory cytokines (72, 124). Activated microglia, TREM2 and the complement system

contribute to neurotoxicity and synapse loss associated with dysregulated proinflammatory cascades (125, 126). Targeting the inflammatory system is currently under investigation as a therapeutic approach for the treatment of AD (127-129).

1.2.3 Common Risk factors for AD

AD is a multifactorial neurodegenerative disease and advanced age remains the greatest non-modifiable risk factor for AD (130, 131). The risk of AD is increased with age with the largest incidence rates observed after the sixth decade of life (4, 132). As the ageing population is growing globally, the number of aged people aged 60 years or over has been predicted to double by 2050 and as a result the incidence of AD has been estimated to increase dramatically (131).

1.2.3.1 Genetic Risk factors

The known causative genetic mutations for FAD (or EOAD) are in genes that encode proteins involved in the processing of APP including *APP (*encoding amyloid precursor protein) on chromosome 21, *PSEN1* (encoding presenilin 1) on chromosome 14, *PSEN2* (encoding presenilin 2) on chromosome 1. There are 32 *APP,* 221 *PSEN1* and 19 *PSEN2* gene mutations associated with autosomal-dominant FAD (133). These genetic mutations lead to accelerated Aβ40 and Aβ42 production, or increased Aβ42:Aβ40, all of which are proposed as diagnostic biomarkers of FAD (134, 135).

In contrast, the most common form of AD, the SAD (or LOAD) is thought to be mainly caused by the interaction between several susceptibility genes and environmental risk factors (29). Among all of the known susceptibility genes that are associated with increased risk of AD, the *APOE* gene (encoding apolipoprotein E (ApoE)) is the strongest genetic risk factor and accounts for 50% of the genetic cause of AD (136-138). ApoE is a cholesterol transporter and plays a key role in regulating cholesterol metabolism in brain tissue (139). *APOE* is located in chromosome 19 and in humans there are three ApoE isoforms coded for by three alleles of *APOE*, ε2, ε3 and ε4 (140). The level of *APOE* expression has been associated with the different *APOE* genotypes, with ε4 associated with the lowest *APOE* expression (141). People carrying a single *APOE* ε4 allele have two to three fold increased risk of AD,

while having two *APOE* ε4 alleles increase the risk five-fold (142). Studies have found that patients with an *APOE* ε4 allele have more Aβ deposition, increased Aβ oligomer level, reduced level and activity of Aβ degrading enzymes and greater hippocampal volume loss (76, 143-145).

The major GWAS have identified several novel susceptibility genes for LOAD (Table 1.1). The ten genes that reached genome-wide significance in most GWAS studies are *APOE* ε4, *BIN1*, *CLU*, *ABCA7*, *CR1*, *PICALM*, *MS4A6A*, *CD33*, *MS4A4E* and *CD2AP*. A number of these susceptibility genes are clustered together and are involved in three main biological pathways related to AD that include APP processing and lipid metabolism (*APOE, CLU, ABCA7*) (29, 146-148), immune response (*CLU, CR1, ABCA7, CD33, MS4A6A, MS4A4E, CD2AP*) (29, 146, 148-150) and endocytosis (*BIN1, PICALM*) (149-152). Most recently, a large GWAS study has confirmed twenty previously identified risk loci (*APOE* ε2, ε3 and ε4, *BIN1*, *CLU*, *ABCA7*, *CR1*, *PICALM*, *MS4A6A*, *CD33*, *MS4A4E*, *CD2AP, INPP5D, HLA-DQB1, TREM2, NYAP1, EPHA1, PTK2B, ECHDC3, SPI1, SORL1, FERMT2, SLC24A4, CASS4)* and identified four novel genome-wide loci for LOAD (*IQCK*, *ACE1 ADAM10*, *ADAMTS1*) that have been implicated in immune system, lipid metabolism, tau bindings protein and APP processing (153).

Table 1.1 Summary of the sporadic AD susceptibility genes implicate in APP processing, lipid metabolism, immunity and tau processing.

Gene	Chromosome	Polymorphism	Protein
APOE ε2/3/4	19	APOE_e2/3/4	apolipoprotein E
BIN1	2	rs744373	bridging integrator 1
CLU	8	rs11136000	clustrin
ABCA7	19	rs3764650	ATP-binding cassette transporter A7
CR1	1	rs3813861	complement receptor one
PICALM	11	rs541458	phosphatidylinositol binding clathrin assembly protein
MS4A6A	11	rs610932	membrane-spanning 4-domain, subfamily A, member 6A
CD33	19	rs3865444	CD33 molecule (sialic acid–binding immunoglobulin (Ig)–like lectin)
MS4A4E	11	rs670139	membrane-spanning 4-domain, subfamily A, member 4E
CD2AP	6	rs9349407	CD2-associated protein

INPP5D	2	rs10933431	inositol polyphosphate-5-phosphatase, 145 kDa
HLA-DQB1	6	rs78738018	major histocompatibility complex class II, DQ beta 1
TREM2	6	rs75932628	triggering receptor expressed on myeloid cells-2
NYAP1	7	rs12539172	neuronal tyrosine phosphorylated phosphoinositide-3-kinase adaptor 1
EPHA1	7	rs11762262	ephrin receptor A1
PTK2B	8	rs73223431	protein tyrosine kinase 2 beta
ECDH3	10	rs7920721	enoyl CoA hydratase domain containing 3
SPI1	11	rs3740688	transcription factor PU.1
SORL1	11	rs11218343	sortilin-related receptor, L(DLR class) A repeats containing
FERMT2	14	rs17125924	fermitin family member
SLC24A4	14	rs12881735	(sodium/potassium/calcium exchanger), member 4
CASS4	20	rs6024870	cas scaffolding protein family member 4
IQCK	16	rs7185636	IQ motif containing K
ACE1	17	rs138190086	angiotensin-converting enzyme 1
ADAM10	15	rs593742	a disintegrin and metalloproteinase 10
ADAMTS1	21	rs2830500	a disintegrin and metalloprotease domain with TSP repeats protein-1

ACE, the gene that encodes ACE-1, is one of the most studied susceptibility genes for LOAD. First reported by Kehoe *et al.* (84) who found that an insertion (I)/ deletion (D) polymorphism (indel) within intron 16 of *ACE* on chromosome 17q23 was associated with increased AD risk. Since then, several studies replicated this finding and supported the strong relationship between the *ACE* indel polymorphism (I/I) and increased risk of LOAD (85, 86, 88, 89, 154, 155). As mentioned, ACE-1 is one of the Aβ degrading enzymes and genetic variation in *ACE* has been associated with Aβ level, particularly soluble Aβ species. Miners *et al.* (90) found that (II) genotype and other nearby proxy SNPs were associated with increased levels of soluble Aβ in AD. The rarer *ACE* polymorphism (rs138190086) on chromosome 17 was also more recently reported as a new genome-wide significance

loci implicated in Aβ processing (153). Together these genetic studies strongly suggest an association between *ACE* indel polymorphism and increased risk of AD that may also link to Aβ pathogenesis and thus have helped to generate renewed interest in the role of ACE in AD pathogenesis and implications with respect to the therapeutic intervention of AD.

Modifiable lifestyle factors such as midlife hypertension, midlife diabetes, stroke, obesity, high cholesterol level and smoking also increase the risk of AD (156-161). Among all the cardiovascular risk factors, hypertension seems to be the most common risk factor for AD (162). Recently, numerous studies have focused on describing the role of hypertension in causing or increasing the progression of AD (163-165). Based on the previously published literature, there is considerable evidence to support a strong association between hypertension and AD. However, to date, potential mechanisms that explain a pathophysiological link between hypertension and the development or progression of AD are less clear. Therefore, explaining how the primary regulatory system of blood pressure might alter the progression of AD will provide important insights into the mechanisms between these two diseases and potentially provide important data to inform therapeutic strategies.

Based on epidemiological studies, several preventable lifestyle risk factors have been found to increase the risk of cognitive impairment and AD such as head trauma, depression, sleep disturbances (166-171). Several observational and randomized controlled trials have also shown that achievable life adjustments, such as maintaining an active lifestyle including regular physical activity, a balanced diet, cognitive training and social engagement are all associated with a decreased risk of cognitive impairment and lower incidence of AD (172-178). It is important to consider these preventable risk factors to ensure a healthy lifestyle for the elderly and help reduce the risk of AD.

1.2.5 Diagnosis

The clinical diagnosis of AD is mainly based on clinical symptoms that are measured by a variety of cognitive assessment tests, some of which include the measurement of different cognitive domains (179). However, the sensitivity of some screening tools, such as the Mini Mental State Examination (MMSE) to detect MCI is limited (180). Other cognitive screening tools such as the Montreal Cognitive Assessment (MoCA) has been found to be able to detect early cases of MCI and are more

sensitive than MMSE to disturbance to executive function, which can be attributed to vascular issues (181).

In addition to the memory tests, there are numbers of neuroimaging procedures that are increasingly used, depending on availability, to detect the brain changes and accumulation of Aβ within the brain. This includes MRI to look at brain atrophy, or the use of F-florbetapir or C Pittsburgh compound B (PiB) positron emission tomography (PET) to assess amyloid burden, whilst single photon emission computed tomography (SPECT) is another modality that allows assessment of brain structural change (182-185). Together these neuroimaging tools could be used as an early detection method of AD in people at high risk. CSF biomarkers (Aβ, tau) are also considered to be of use to help facilitate earlier and more accurate diagnosis of AD and help differentiate it from other types of dementia (186). Both plasma level of Aβ and tau have also been proposed but have, as yet, to be shown to be reliable as diagnostic biomarkers (187). All of these diagnostic approaches are included in the Alzheimer's Disease and Related Disorders Association (ADRDA) guidelines, which take into account clinical symptoms, cognitive results, neurological assessment and biomarkers (188).

Overall, the accuracy of clinical diagnosis of AD has been shown to vary somewhat and can range, according to various groups from 80% to 100%. Yet, it is more realistic and acknowledged that post-mortem neuropathological examination is in fact the most accurate diagnostic test for AD among all these diagnostic approaches and is likely to be the only one that can confirm with the greatest accuracy the diagnosis of AD and other dementias (16). In post-mortem diagnosis, the brain tissue is examined at both macroscopic and microscopic levels and is assessed according to specific criteria of the Consortium to Establish a Registry for Alzheimer's disease (CERAD), which is based on semi-quantitative assessment of the density of neocortical neuritic plaques (NP) (189), in addition to the use of Braak staging for distribution of NFTs recommended by the National Institute on Aging and the Alzheimer's Association (NIA-RI) (190). This information is viewed alongside the clinical medical history to provide a more in depth diagnosis.

1.2.6 Treatment

None of the currently available pharmacological drugs slow or stop the progression of AD. Six drugs are clinically available for the symptomatic treatment of AD including cholinesterase inhibitors

(rivastigmine, galantamine, donepezil) (191-193) and the N-methyl-D-aspartate (NMDA) receptor antagonist (memantine). Memantine combined with donepezil and tacrine have also been approved by the FDA (194). All cholinesterase inhibitors are approved for the treatment of mild to moderate stages of AD and help facilitate synaptic transmission due to increasing the level of the neurotransmitter acetylcholine. However, cholinesterase inhibitors may not benefit mild cognitive impairment (195). Memantine was originally developed for use in more severe (moderate to late) stages of AD and works by preventing the excitotoxicity of glutamate and inhibiting tau hyperphosphorylation and aggregation (196). Although, 244 drugs for Alzheimer's have been tested in registered clinical trials, memantine is the only drug that successfully completed clinical trials and is approved by the FDA (197).

In more recent years there have been several clinical trials and efforts to investigate drugs that target Aβ, tau and inflammation (3, 198). However, most of these Aβ-focussed targeting approaches have been unsuccessful. With continually growing knowledge about the pathogenesis of AD and the potential role of modifiable risk factors, particularly in the early stages of disease, many researchers are now focusing on modulating vascular risk factors of AD and exploring new and what some might view as alternative new therapeutic approaches. Examples of which include ongoing efforts to re-position anti-hypertensive drugs that include angiotensin converting enzyme inhibitors (ACEIs) and angiotensin-II receptor blockers (ARBs) (56). Other non-pharmacological approaches have also been attempted and some have been found to relieve behavioural symptoms and improve cognitive function such as exercise and cognitive stimulation (199-201). Thus far, the available pharmacological and non-pharmacological approaches for AD, which may be beneficial are still unable to cure or prevent AD, but some may be able to slow or halt the progression of the disease. Thus, there is now a strong focus on the need for developing effective disease-modifying treatment for AD, whilst research will continue to find the earliest triggers for AD that will then lead to the potential identification of a cure.

1.3 Relationship between hypertension and AD

One possible therapeutic approach to prevent and slow progression of AD has been suggested to involve maintaining a healthy and normal blood pressure (202). Meta-analysis of secondary investigations in cardiovascular clinical trials and observational research of populations has showed evidence that high blood pressure was associated with subsequent cognitive decline (203, 204). The Framingham study was one of the first study to find a positive association between high blood pressure and cognitive decline (205). Several other longitudinal studies have replicated this positive observation of a relationship (206-211). Several epidemiological studies have reported a strong relationship

between mid-life hypertension and increase risk of AD in later life (206, 212-215). However, some longitudinal studies showed either no significant association or a negative association between hypertension and AD (216-218).

There is also some debate about whether mid-life hypertension increased risk of AD or late-life hypertension is more strongly associated with reduced risk of AD. Some studies indicated that late-life hypertension could be protective against cognitive decline and reduce the risk of AD (162, 219). This physiological compensatory mechanism of increase blood pressure in elderly may help maintain adequate CBF and normal cognition. Although the previous studies revealed divergent effects of high blood pressure with respect to increased risk of AD, which could be due to an age-dependent effect of hypertension on AD pathogenesis. Most recently, post hoc analysis of data from a randomized trial (NILVAD) indicated that mild-moderate AD patients with blood pressure variability had a greater deterioration in cognitive decline that was associated with progression of AD (220).

The effect of hypertension on brain cerebrovascular homeostasis has been investigated by several studies. Hypertension may increase the risk of AD by disturbing the integrity of the BBB, resulting in the accumulation of Aβ in brain tissue (116). Hypertension also causes white matter lesions (WML) and is associated with cognitive impairment (221, 222). Hypertension has also been shown to increase blood vessel fibrosis resulting in narrowing and stiffness of the blood vessel walls that leads to reduced cerebral blood flow and WML (223-227). An association between mid-life hypertension and increased rate of progression of vascular brain injury and worsening cognitive function has been reported (159). Beauchet *et al.* (228) has shown using meta-analysis that high blood pressure is associated with reduced cortical and hippocampal brain volumes. Several potential pathological mechanisms that might explain how hypertension and vascular dysfunction and damage might lead to cognitive decline are summarised in (Figure 1.8).

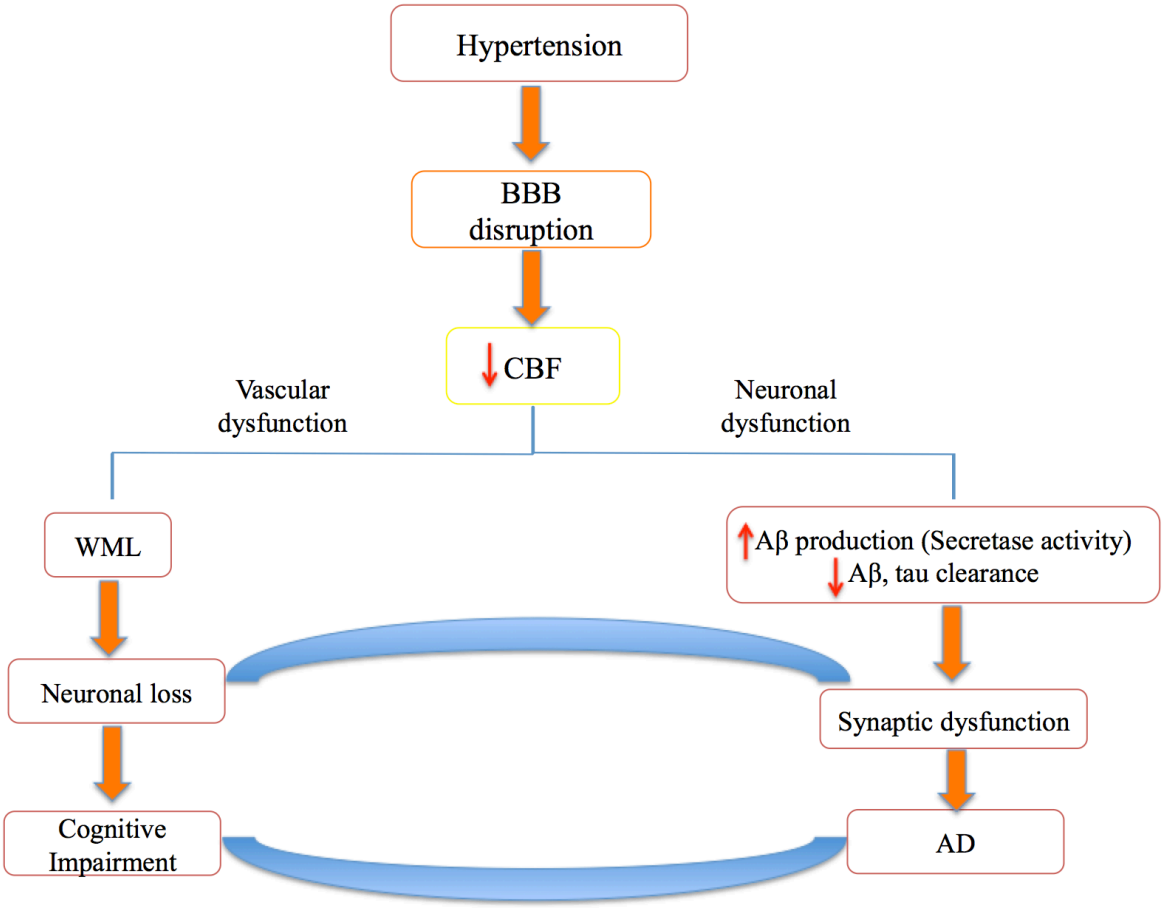

Figure 1.8 Proposed underlying mechanisms of the relationship between hypertension and AD.

Hypertension leads to both vascular dysfunction and brain structure abnormalities such as white matter lesions, and neuronal dysfunction, through direct and indirect effects of increased Aβ production and reduced Aβ and tau clearance. In turn, accumulation of AD pathological hallmarks may lead to synaptic dysfunction and neuronal loss that both result in cognitive impairment and AD. BBB - blood brain barrier, CBF - cerebral blood flow, WML - white matter lesion, Aβ - amyloid beta, AD - Alzheimer's disease. Down pointed red arrows = decrease, Up pointed red arrow = increase (adapted from Iadecola and Gottesman. 2019) (229).

Further evidence of the relationship between hypertension and AD pathogenesis is reported in several post-mortem studies, *in vivo* neuroimaging studies and experimental studies. In post-mortem brain tissue, accumulation of AD pathological hallmarks, including Aβ plaques and NFTs, was greater in hypertensive elderly patients (230-233). *In vivo* PET scan studies have found that Aβ accumulation is associated with higher blood pressure, both systolic and diastolic, in normal, mild cognitive impairment and AD patients (234-237). Induced hypertension in experimental animal models following administration of the vasoconstrictor, angiotensin II (Ang-II) has also been shown to increase microvascular accumulation of Aβ and neuronal deposition of phosphorylated tau (p-tau), suggesting a role of Ang-II on APP processing and Aβ production (238, 239). Moreover, the

relationship between hypertension and AD biomarkers was observed. In elderly patients, high pulse pressure was associated with increased levels of p-tau in CSF and decreased Aβ42 level (240, 241).

In several observational studies, treatment with anti-hypertensive drugs was associated with improvement of cognitive function. The first prospective randomised study (FOCUS study) found that anti-hypertensive drugs (felodipine, a calcium channel blocker and enalapril, an ACEI) in elderly patients with cognitive impairment resulted in significant improvement in overall cognitive function at 12 and 24 weeks (242). Moreover, the SCOPE study showed a trend in risk reduction of dementia in elderly patients that received angiotensin receptor antagonists (candesartan and cilexetil) (243). More details of the use of anti-hypertensive drugs in AD are described below (see sections 1.5.1.2 and 1.5.4).

1.4 The Renin Angiotensin System (RAS)

The RAS is a complex enzymatic and peptide system that acts either locally or centrally to maintain body fluid homeostasis, control blood pressure and regulate hormone secretion (244). The first understanding of the RAS was gathered from its function in the periphery. The RAS involves the synthesis and release of angiotensinogen (AGT) by hepatocytes into the circulation. AGT is the only known substrate of renin. The latter, an acid protease enzyme that is synthesised and released from the juxtaglomerular apparatus of the kidney into the circulation in response to a reduction in peripheral blood pressure, cleaves AGT 10 amino acids from the N-terminus to generate angiotensin I (Ang-I) (245). Centerally, AGT and renin are produced within neurons and astrocytes (246). Ang-I, in turn, is hydrolysed by ACE-1 (a member of the M2 metalloprotease family), at the C-terminus to form angiotensin II (Ang-II). Ang-II is the main effector of the classical RAS pathway but more recently has been identified to have central functions where it exerts neuro-damaging effects by interaction with the angiotensin II type-1 receptor (AT_1R) or protective effects by binding to angiotensin II type-2 receptor (AT_2R) (247). This ACE-I/Ang-II/AT_1R pathway is now more commonly known as the classical axis of RAS or classical RAS (cRAS). Hyperactivity of cRAS has traditionally been viewed to contribute to pathogenesis of cardiovascular and renal diseases associated with hypertension (248).

It has more recently emerged that cRAS is counter-regulated by activation of the non-classical axis of RAS or regulatory RAS (rRAS) pathways. These downstream pathways are involved in the metabolism of Ang-II. Angiotensin converting enzyme 2 (ACE-2) is the enzyme mainly involved in

the regulation of the rRAS (249, 250). ACE-2 is a zinc metallopeptidase comprising of 805 amino acids and shares 42% sequence identity with the catalytic regions of ACE-1 metalloprotease (250). The main role of ACE-2 is in the metabolism of Ang-II to generate angiotensin (1-7) (Ang (1-7)). ACE-2 is also capable of converting Ang-I to angiotensin (1-9) (Ang (1-9)) (251). Binding of Ang (1-7) to the MAS receptor (MasR), a G-protein-coupled receptor that has been found within the brain (252), causes vasodilation through stimulation of bradykinin and nitric oxide release (253). It has also been shown to have other protective actions such as diuresis, anti-inflammatory, anti-proliferative and anti-fibrotic effects (254). This pathway is often termed the ACE-2/Ang (1-7)/MasR axis. Dysregulation of this pathway is associated with organ-specific diseases, such as hypertension (cardiovascular disease), stroke (cerebrovascular diseases) and AD (neurodegenerative disease) (255).

Another regulatory pathway (Ang-III/APN/Ang-IV/IRAP) of cRAS involves the formation of angiotensin III (Ang-III) following cleavage of Ang-II by aminopeptidase A (APA). Ang-III binds to AT_1R, as well as AT_2R, and has similar actions to Ang-II such as vasoconstriction, stimulation of aldosterone secretion, cell growth, and inflammation through AT_1R signalling (256). Ang-III can be subsequently cleaved by aminopeptidase N (APN) to form angiotensin IV (Ang-IV) (244). Ang-IV exerts actions on the central nervous system (CNS) via binding to angiotensin IV receptor (AT_4R) (also called insulin regulated aminopeptidase (IRAP) and another AT_4R binding site identified as c-MET, a tyrosine kinase receptor), which includes improved learning and memory and protection from cerebral hypoxia (257). In addition to the classical and non-classical pathways there are a number of additional pathways and smaller angiotensin peptides (Figure 1.9). The current view of RAS is thus relatively complex with much to still learn about more recently identified angiotensins such Ang (1-9), angiotensin (1-5) (Ang (1-5)), angiotensin A (Ang A) and alamandine (253).

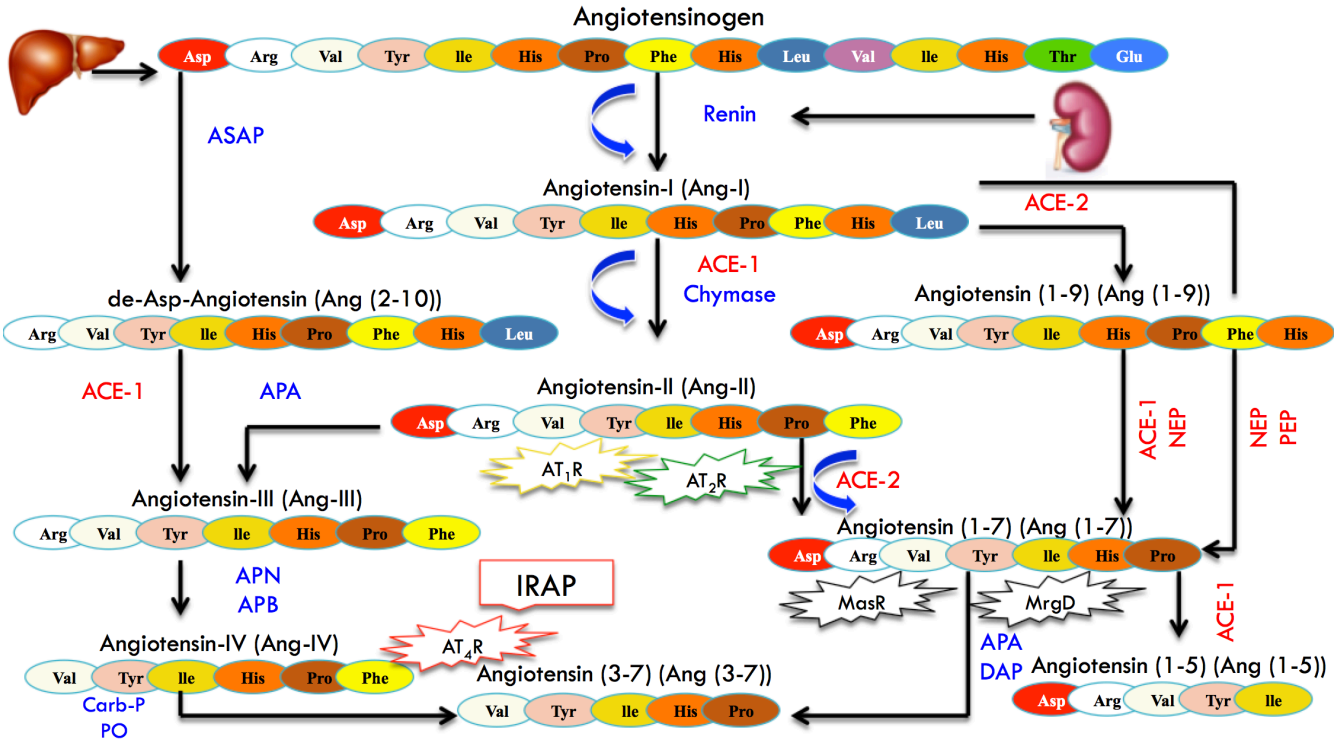

Figure 1.9 The renin angiotensin system.

A schematic of the enzymes, substrates and effector molecules related to RAS function. Angiotensin peptides in the brain are produced from angiotensinogen through several enzymatic pathways. Angiotensin-I (Ang-I) is formed by renin acting on angiotensinogen that is then converted into the main effector, angiotensin-II (Ang-II), by angiotensin II converting enzyme 1 (ACE-1) that acts on both AT_1R and AT_2R. This pathway was first identified and is known as the classical axis of RAS. Ang-II is converted into the active Ang (1-7) by angiotensin II converting enzyme 1 (ACE-2) that acts on both MasR and MrgD, this pathway is known as the non-classical regulatory axis of RAS. Ang-II can be converted to angiotensin III (Ang-III) by aminopeptidase A (APA) and is further converted into angiotensin IV (Ang-IV) by aminopeptidase N (APN). The resultant Ang-IV acts on AT_4R (also referred to as Insulin-regulated aminopeptidase (IRAP)). These pathways giving rise to Ang (1-7) and Ang-IV from the cleavage of Ang-II are known as the alternative regulatory pathways of RAS (rRAS). Both Ang (1-7) and Ang-IV can be further converted into small inactive peptide fragments. Other but less involved components of the RAS include APB - Aminopeptidase B, ASAP - Aspartyl aminopeptidase, Carb-P - Carboxypeptidase B, DAP - dipepidyl aminopeptidases, PEP - prolyl endopeptidase PO - Proly oligopeptidase, NEP - Neprilysin (adapted from Puertas et al. 2013) (258).

In addition to the well-known crucial role of the peripheral circulating RAS in the maintenance of fluid balance and regulation of blood pressure, several studies demonstrated the vital role of a local RAS in different tissues such as the brain, heart, kidney, peripheral blood vessels, adipose tissue, liver, endocrine tissue, reproductive tissues, immune cells, hematopoietic tissue and gastrointestinal tract (259-266). Dysregulation of the local RAS underlies various cardiovascular, renal, vascular and neurodegenerative disorders and can include inflammation, fibrosis and oxidative stress as well as other tissue-specific pathological conditions (267-269). It is now widely accepted that there is a fully

functioning local RAS within the brain (270). This comprises both the classical and regulatory pathways that are likely to function independently from, but also probably synchronously with, the peripheral RAS (253, 254). In the following sections I will discuss in more detail the role of the brain RAS and its importance and relevance to AD.

1.4.1 The role of brain RAS in regulating blood pressure

Most of the active components of brain RAS are involved in regulating blood pressure. Overactivity of cRAS in the brain is associated with hypertension. Several experimental studies have demonstrated the effect of Ang-II administration in increasing neuronal activity in brain areas responsible for cardiovascular regulation, osmoregulation and energy homeostasis (271). Through activation of AT_1R, Ang-II was found to inhibit barosensitive neurons and increase blood pressure (BP) (272). Furthermore, Ang-II induces vasoconstriction, endothelial dysfunction, inflammation, growth and remodelling of the vasculature through several mechanisms that include, modulating sympathetic tone, stimulation of aldosterone secretion and sodium reabsorption (248). Intracerebroventricular (ICV) administration of ACEIs enhanced baroreceptor reflex sensitivity due to reduced production of Ang-II (273). Furthermore, similar to Ang-II, Ang-III binds to AT_1R and contributes to increased blood pressure (274), whilst similarly both Ang-II and Ang-III were also found to bind to a recently discovered non-AT_1R and non-AT_2R site. Reduction of this binding protein, called neurolysin, was found in spontaneously hypertensive rats, suggesting the important role of this binding protein in the development of hypertension (275). On the other hand, rRAS in the brain, including ACE-2/Ang (1-7)/MasR, exerts an anti-hypertensive effect. The effects of Ang (1-7) on blood pressure are also mainly effected via modulating the baroreflex (276). Several animal studies demonstrated the effect of long-term administration of Ang (1-7) on reduced blood pressure and attenuated the development of hypertension (277-279). A MasR antagonist completely reversed the cerebroprotective effect of Ang (1-7) (280). Further support for the protective role of the rRAS in the brain was a recent study that showed that increased expression of ACE-2 reduced the development of neurogenic hypertension through reduced oxidative stress and inflammation (281).

1.4.2 Involvement of brain RAS in inflammation

The classical and non-classical axes of brain RAS are implicated in the inflammatory responses in brain tissue. ACE-1/Ang-II/AT_1R is known as a proinflammatory axis due to the effect of the powerful

proinflammatory mediator Ang-II and its activation of AT_1R (282). Ang-II mediates an inflammatory response through activation of several pathways that stimulate the production of prostaglandins and vascular endothelial cell growth factor (VEGF) (283), upregulates adhesion molecules and vascular cell adhesion molecules on vascular endothelial cells and smooth muscle cells, and activates monocytes (284, 285). In addition, Ang-II upregulates potent chemoattractants and activators of neutrophils (286), and mediates reactive oxygen species (ROS) production and nuclear factor- kappa B (NF-κB) activation (287). ARBs have been found to suppress the inflammatory responses mediated by Ang-II (288-291). On the other hand, the rRAS exerts anti-inflammatory effects mediated by the action of Ang (1-7) on MasR. Supporting evidence demonstrated that Ang (1-7) suppressed leukocyte migration, cytokine expression and release, and fibrogenic pathways. In the brain, ICV administration of Ang (1-7) in a stroke model in Sprague-Dawley rats (SDR) was associated with a reduction in oxidative stress, suppression of NF-κB activity and reduced levels of pro-inflammatory cytokines (292). Overexpression of ACE-2 in the paraventricular nucleus attenuated the increase in the expression of tumour necrosis factor alpha (TNF-a), interleukin (IL-1b) and (IL-6) that had been induced by Ang-II (293). Moreover, in the *APOE* knockout mouse, genetic ACE-2 deficiency enhanced vascular inflammation and atherosclerosis through increased gene expression of vascular cells adhesion molecules (VCAM), cytokines, chemokines and MMP (294). Activation of ACE-2/Ang (1-7)/MasR axis by ACE-2 activator, diminazene aceturate (DIZE) in the D-Galactose-Ovariectomized rat model of AD showed upregulation of ACE-2 and MasR expression along with downregulation of AT1R and inflammatory proteins such as glial fibrillary acidic protein (GFAP), NF-kB p65 and TNF-a, indicating the anti-inflammatory role of the non-classical axis of brain RAS in AD (295).

1.4.3 The role of brain RAS in cerebral hypoperfusion/ ischaemia

AD is associated with cerebrovascular dysfunction such as cerebral hypoperfusion, CAA and BBB dysfunction (117, 296-299). Several experimental studies have revealed that hypoxic or ischaemic conditions are associated with increased amyloidogenic APP processing, stimulating the production and the accumulation of Aβ that dysregulates calcium homeostasis in both neurons and astrocytes, leading to neuronal cell death and activated microglia (300-304). Hypoperfusion is evident in the early stages of AD and is related to cognitive decline (118, 305-307). Moreover, cerebral ischaemia leads to cognitive decline in AD and aggravates cognitive deficiency induced by accumulation of Aβ (308-310). The mechanism linking cerebral hypoperfusion/ischaemia and Aβ accumulation is related to interaction between Aβ degrading enzymes in both the brain endothelin system (ECE-1, ECE-2) and

RAS (ACE-1). Miners and colleagues (311) reviewed the evidence that indicates upregulation of ECE-1, ECE-2 and ACE-1 activities are increased in the cerebral cortex in AD in human post-mortem brain tissue are associated with increased production of the potent vasoconstrictors (endothelin-1(ET-1) and Ang-II), which both result in reduced CBF and aggravated Aβ-related pathology (Figure 1.10).

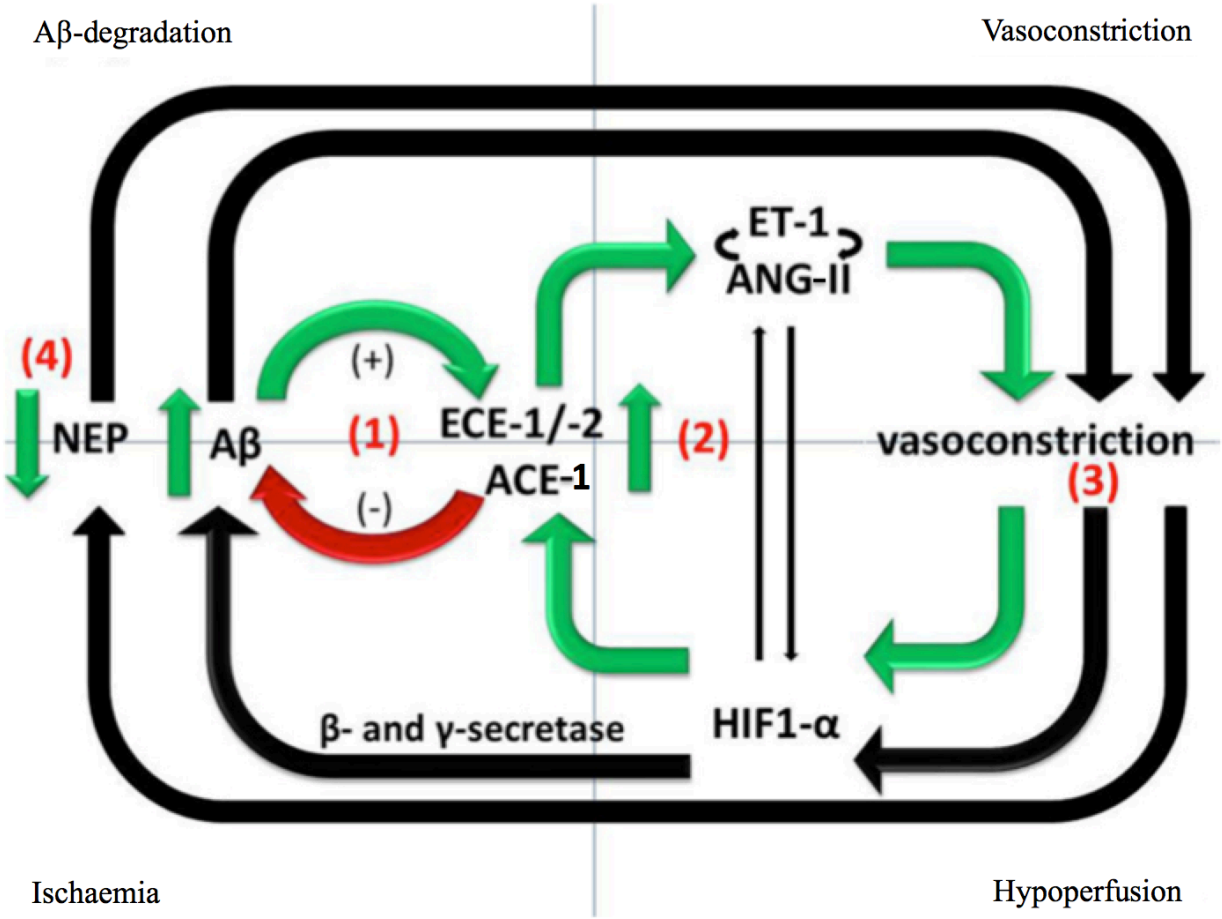

Figure 1.10 Possible mechanisms linking cerebral hypoperfusion/ischaemia and Aβ degrading enzymes in AD.

Upregulation of ECE-1, ECE-2 and ACE-1 activities are a physiological feedback response of Aβ accumulation in AD. These result in increased production of vasoconstrictors (ET-1 and Ang-II) that lead to reduced CBF, increase Aβ production and accumulation mediated by reduced NEP activity in ischaemia that all aggravate Aβ-related pathology (adapted from Miners et al. 2014) (311).

Recently, two novel methods to quantify ischaemic injury in post-mortem brain tissue have been developed. These involve the comparison of the levels of two myelin proteins, myelin-associated glycoprotein (MAG), which is highly susceptible to reduced tissue oxygenation, and proteolipid protein-1 (PLP1), which is relatively resistant to reduced tissue oxygenation and thus reduction in

MAG:PLP1 ratio would be indicative of ischaemic (reduced tissue oxygenation) injury (prior to death as the myelin proteins are resistant to PM-delay and have a slow turnover rate of several months). This was recently shown in the mid-frontal and medial parietal cortex (precuneus) in human post-mortem brain tissue in AD (312-315). A reduction in MAG:PLP1 is also related to increased levels of VEGF, a potent angiogenic and neuroprotective factor that is upregulated in response to tissue hypoxia and is thus considered another independent sensitive marker of ischaemia. VEGF level has been shown to be increased in mid-frontal cortex and parahippocampal cortex in human post-mortem brain tissue in AD and was positively correlated with insoluble Aβ42 level and Aβ42:Aβ40 ratio (314). In addition, the reduction in cortical MAG:PLP1 ratio was inversely correlated with VEGF level (314, 315). Together these studies demonstrate an involvement of ischaemia in early AD pathogenesis.

The ACE-1/Ang-II/AT_1R pathway (also known as a pressor axis of brain RAS) is involved in cerebrovascular damage after stroke. Experimental studies have shown the association between increased Ang-II level and vascular damage following stroke (316). AT_1R activation is linked to ischaemic damage through a change in cerebral nitric oxide synthase (NOS) in genetic hypertensive rats, while treatment with ARBs reduced the risk of cerebrovascular ischaemia and neuronal injury (317, 318). In addition, ARBs reduced infarct size and increased cerebral blood flow in an animal stroke model (319-324). Conversely, activation of the depressor or regulatory axis of brain RAS, i.e. the ACE-2/Ang (1-7)/MasR axis was found to induce baroreflex activity, reduce blood pressure and increase release of nitric oxide (NO) that protects cerebrovascular function during ischaemic injury (251). Several experimental studies demonstrated the cerebroprotective effects of centrally administered Ang (1-7) (325). ICV administration of Ang (1-7) in animal stroke models caused a reduction of the infarct size associated with increased neuron survival in the cortex and striatum (326, 327). Ang (1-7) stimulates NO release and upregulates endothelial NOS (eNOS) expression (328). Chen and colleagues (329), demonstrated that overexpression of neuronal ACE-2 in an animal model with central Ang-II overproduction protected the brain from the ischaemic injury by changing the Ang (1-7)/Ang-II ratio. Supporting this protective effect of ACE-2, it has been shown that overexpression of ACE-2 reduced ischaemic neuronal damage such as cell swelling and death (330). Overexpression of ACE-2/Ang (1-7)/MasR has been shown after acute cerebral ischaemia as a compensatory mechanism to protect the brain (331). All these previous studies support the important role of the brain RAS in ischaemia and highlight the need to either block the effect of the pressor axis or activate the depressor axis as a therapeutic approach for cerebrovascular disorders.

1.5 The brain RAS and AD

Over the last decade and a half, experimental and clinical studies have focused on the role of brain RAS on neuronal and cognitive function, particularly in neurodegenerative conditions such as AD. It was recently demonstrated that overactivation of brain cRAS was associated with AD pathogenesis. More recently, data from post-mortem brain tissue and *in vivo* models have indicated that alterations within the downstream alternative and regulatory RAS pathways contribute to cRAS overactivation and AD pathology. These changes are present in areas of the brain, such as the mid-frontal cortex, that are affected in AD and are distinct from those brain regions involved in blood pressure regulation.

1.5.1 The classical RAS of the brain in relation to cognitive function and AD pathology

The cRAS regulates blood pressure but functions independently within the brain and is implicated in higher brain functions including cognition and learning and memory. Overaction of cRAS has damaging effects such as vasoconstriction, fibrosis, hypertrophy and inflammation (Figure 1.11).

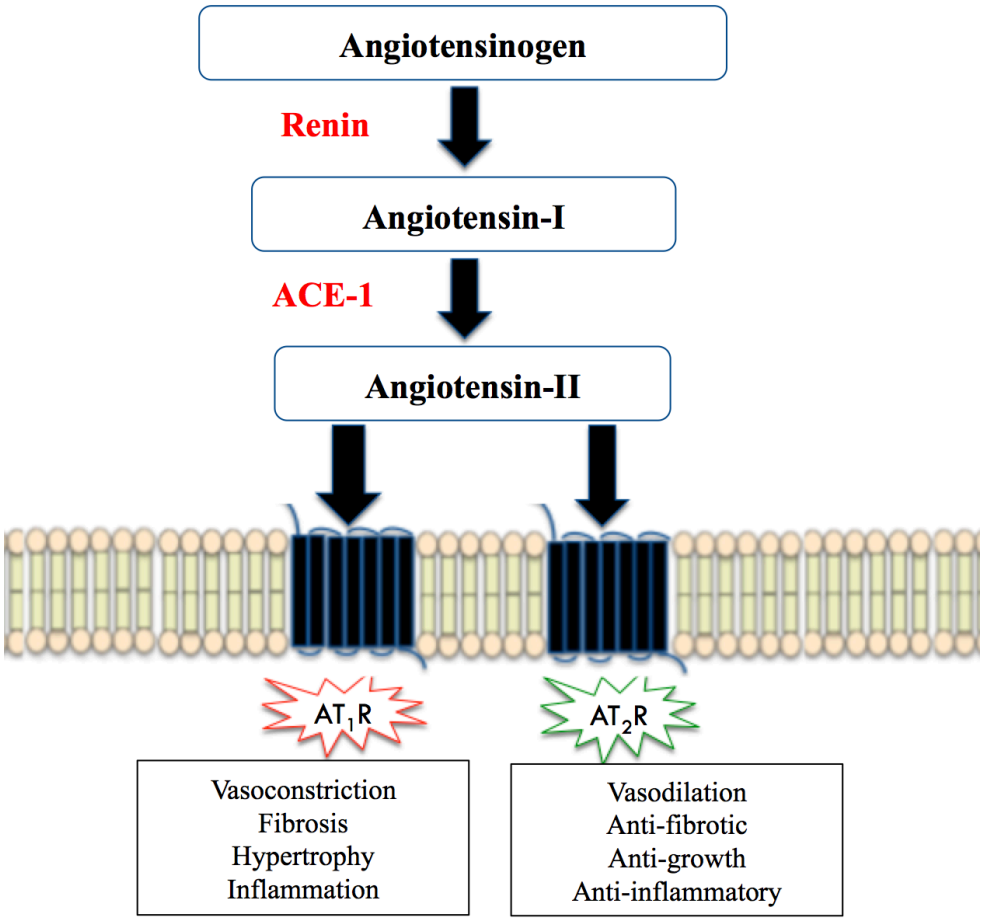

Figure 1.11 Effects of the classical axis of brain RAS.

Angiotensin II (Ang-II) is the main effector in the classical axis of brain RAS. Ang-II/AT_1R coupling results in damaging effects to neurons that include vasoconstriction, fibrosis, hypertrophy and inflammation. While, angiotensin II (Ang-II) /AT_2R interaction counter-regulate the Ang-II/AT_1R mediated effects. Ang-II has a higher affinity toward AT_1R and responsible for the major effects of the classical brain RAS c(RAS). ACE-1 – angiotensin II converting enzyme 1; AT_1R - angiotensin II type 1 receptor, AT_2R - angiotensin II type 2 receptor.

1.5.1.1 Angiotensinogen (AGT) and Angiotensin I (Ang-I)

Activation of the cRAS begins with the synthesis of renin, a protease and a rate-limiting enzyme responsible for cleaving the N-terminal portion of AGT to form Ang-I, this conversion can also be processed by other enzymes such as elastase, proteinease 3, cathepsin D and E. Although, the AGT and Ang-I are biologically inactive and their functions are still generally unknown in the brain especially in relation to AD, both act as important precursors for the major active metabolites in RAS,

including Ang-II, Ang (1-7) and Ang (1-9). The decapeptide Ang-I serves as a substrate for ACE-1, the main protease in cRAS to yield the biologically active metabolite Ang-II (257).

1.5.1.2 Angiotensin converting enzyme (ACE-1)

ACE-1 (dipeptidyl-dipeptidase) is a membrane-bound zinc metalloprotease (332). In humans, there are two isoforms of ACE-1: somatic ACE-1 (sACE-1) and germinal ACE-1 (gACE-1) (333). Somatic ACE-1 is a large protein (150-180 KDa) and has two homologous domains, commonly referred to as the N-domain and the C-domain. sACE1- is found in various types of endothelial, epithelial and neural cells. gACE-1 is a smaller protein (100-110 KDa) that has a single catalytic domain identical to the C-domain of sACE-1 and is expressed only in developing spermatids and in mature sperm cells (334, 335). In addition, sACE-1 can be found as a soluble enzyme distributed into many types of extracellular fluids including plasma, serum and cerebrospinal fluids (336). For convenience and given the high tissue specificity of gACE-1, sACE-1 will henceforth be referred to as ACE-1 for the remainder of this thesis and thus will refer to the form of ACE-1 with two catalytic domains.

ACE-1 is abundantly distributed within the human brain where it is expressed widely in dendrite cells, is predominantly expressed within neurons and in pyramidal neurons in the cortex (layer V), and within the cerebral vasculature (78, 91, 337, 338). In addition to the main role of ACE-1 as an enzyme responsible for production of Ang-II, a previous study indicated that ACE-1 was involved in the metabolism of neurotensin, a major endogenous substrate of the non-AT_1R and non-AT_2R binding protein (i.e. that was determined to be neurolysin) (339). Several studies also indicated a neuroprotective role of neurotensin in learning and memory function (340-342), which had yet to be investigated with respect to the pathophysiology of AD.

With respect to two different and independent catalytic domains of ACE-1, which as mentioned are called the N-domain and C-domain according to the N- to C- end orientation of ACE-1 when it is synthesised (Figure 1.12). Although both domains share greater than 60% overall sequence homology, several important biophysical and biochemical similarities and differences have been described. Both the N-domain and C-domain contain a zinc binding site (HExxH) that is a functional site and joined by a shorter linker sequence. The N-domain and most of the C-domain are normally extracellular but a portion of the C-domain is intracellular (C-terminus) (332). Important catalytic differences between the catalytic activities of the N-domain and C-domain of ACE-1 have been described. Oba *et al.* (82)

demonstrated that the N-domain of ACE-1 was primarily responsible for Aβ degradation by inhibiting the aggregation and cytotoxicity of Aβ in vitro, whereas the C-domain showed less inhibitory effects on Aβ accumulation. Another study demonstrated that Aβ42 to Aβ40 converting activity by ACE-1 was limited to N-domain activity and that Ang-II production was mainly attributed to the C-domain of ACE-1 (343). In addition, an *in vivo* study conducted by Fuchs *et al.* (344) showed that the C-domain of ACE-1 was predominantly involved in Ang-II production. However, not all studies are in agreement with these reported distinct roles for each domain, some studies have suggested that both domains participate in Aβ degradation (345, 346). Thus, the potential contributory role of the two domains of ACE-1 in Aβ pathology remains unresolved.

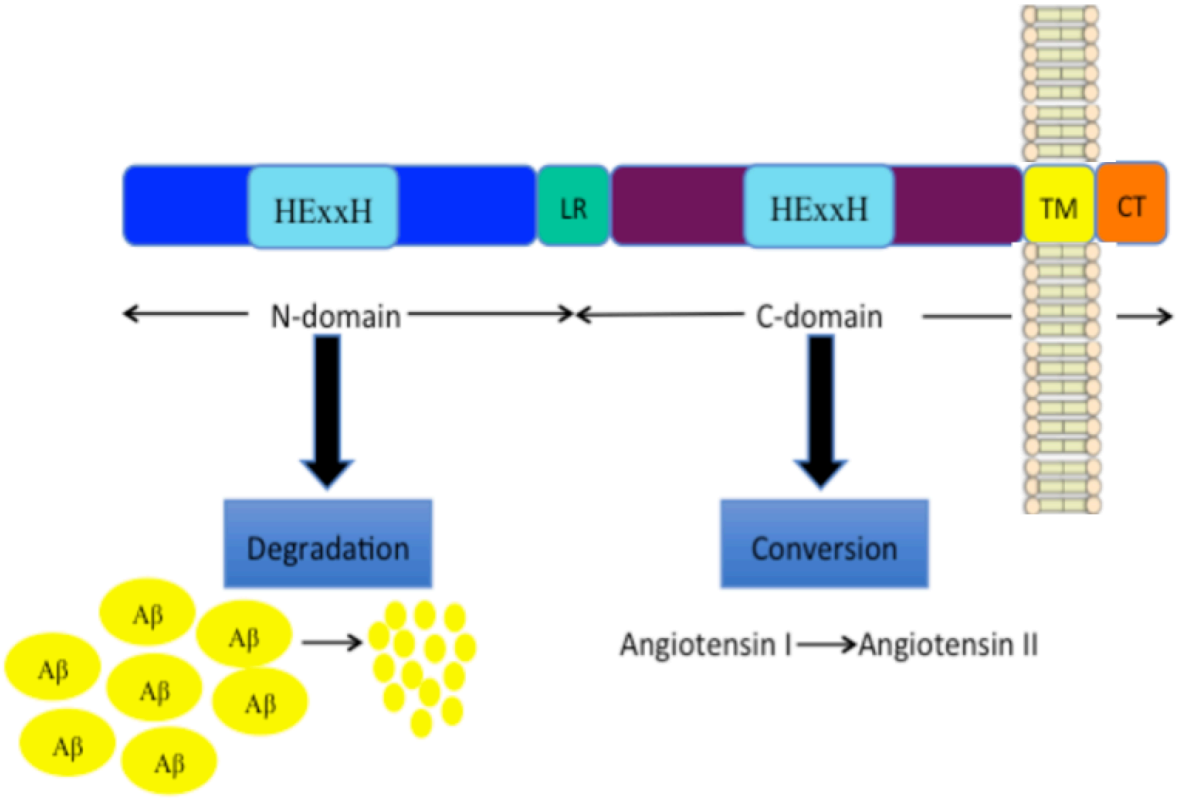

Figure 1.12 Human $_S$ACE-1 structure and domain specificity.

Schematic representation of human $_S$ACE-1 domain structure. The two homolgous domains (N-domain and C-domain) have a catalytic active zinc binding site (HExxH). The N-domain and most of C-domain are extracellular. Both domains are linked by a linker sequence (LR). Transmembrane (TM) domain joined the C-domain with an intracellular C-terminus (CT) adapted from Harrison and Acharya. 2014 (332). There is an important catalytic difference between the N- and C-domains of sACE-1 as illustrated in this figure, N-domain is thought to be primarily responsible for amyloid beta (Aβ) degradation by inhibiting its aggregation and cytotoxicity (82, 343), whereas the C-domain is mostly responsible for the angiotensin II converting activity (343, 344).

In vitro ACE-1 has similarly been reported to degrade Aβ (81, 82, 347). ACE-1 was found to cleave the neurotoxic Aβ species (Aβ42) to a less neurotoxic species (Aβ40) (83). The physiological role of ACE-1 in the metabolism of Aβ *in vivo* remains unclear. Eckman *et al.* (348) found no relationship between inactivation of brain ACE-1 in mice and Aβ pathology. A later study by Zou *et al.* (83) found that administration of captopril (ACEI) into mice resulted in elevated Aβ deposition. This controversy is possibly due to differences between the study designs including age of animals, dosage and duration of exposure (which ranged from a single dose to several months of exposure) to ACEIs that suggests the need for further investigation in more internally and externally validated animal studies to improve clinical translation. Although animal models can be improved to mimic the human clinical conditions, the unmodifiable features such as animal-human differences are considered as ongoing issues (349, 350).

There is also some supportive evidence from genetic association studies in AD patients. A number of studies reported strong evidence of a genetic association between *ACE1* and AD. The first genetic study to describe this association was by Kehoe and colleagues (84), which showed that an insertion (I)/ deletion (D) polymorphism within intron 16 of *ACE1* associates with increased AD risk. This association has replicated in several meta-analyses with data regularly showing that the presence of the (I) allele (II and ID genotypes) in individuals was associated with increased the risk for AD, whereas homozygosity of the (D) allele was at reduced risk of AD (85, 86, 88, 89). Additional single nucleotide polymorphisms (SNPs) have also been shown to be associated with AD risk (351). In a study that set out to investigate the relationship between *ACE1* variants and the levels of different species of Aβ, Miners *et al.* (90) found that the (II) genotype and other nearby SNPs were associated with increased levels of soluble Aβ in AD. More recently, case-control studies supporting the association between *ACE1* polymorphism and increased risk of AD continue to emerge (155), agreeing with previous meta-analyses (89). *ACE1* DD allele polymorphism was associated with higher serum ACE-1 level compared to other genotypes (ID and II) and therefore people with this polymorphism could degrade Aβ more effectively than those with II homozygotes (352). Collectively, these data outline another layer of complexity implicating ACE-1 in AD in modulating Aβ metabolism in the brain.

Experimental animal and clinical human studies also provide strong supportive evidence that the brain RAS is involved in maintaining normal brain function, specifically in learning and memory, and that overactivation, or hyperactivity of cRAS axis is involved in the pathogenesis of AD (78, 270, 353). Previous work in human brain tissue indicated that the cRAS was overactive in AD. The activity of

ACE-1 was significantly increased within the mid-frontal cortex in human post mortem brain tissue (78, 354) and the increased level and activity of ACE-1 was demonstrated in the hippocampus, frontal and temporal cortex of AD patients (78, 355, 356). It has also been found that ACE-1 activity correlated with Aβ senile plaque load (78) and correlated with levels of Aβ deposition in blood vessels (311, 357). These observations of upregulated ACE-1 have been suggested to be a response to Aβ accumulation. Some animal studies have shown that brain-penetrating ACEIs such as captopril and perindopril, or ARBs such as losartan, olmesartan and valsartan, protect against cognitive decline (358-362). Not all studies agree, Ferrington *et al.* (363) did not find any alteration in either intraneuronal Aβ or oligomeric Aβ levels in a triple transgenic mouse model of AD after administration of ACEI (captopril) and ARBs (eprosartan and valsartan) for two months. The discrepant findings to date could indicate variation and inconsistencies in animal models and length of exposure times to drugs and require further work.

Yet, these animal data are overall, relatively consistent with the data observed from large epidemiological studies where several have indicated that treatment with anti-hypertensive medications, including ACEIs and ARBs protect against cognitive decline (364, 365). Data from some studies suggest that ARBs were more effective than ACEIs in decreasing the incidence and the rate of progression of AD (366-369), although more recently Ding and colleagues (370) found no difference afforded between different blood pressure treatment class and AD. The discrepant findings from animal and human studies could be related to the utility and validaty of animal models of hypertention including representative of discrete form of hypertension, responses to therapy and studies quality (371). In addition, the inconsistent observations in both *in vivo* and *in vitro* studies, as well as in population studies, regarding the role of ACEIs on Aβ metabolism and cognitive decline, and potentially on AD risk and progression indicate that there may be a complex interaction between ACE-1 and Aβ and it may point to the variable affinities of different ACEIs for each ACE-1 domain, in addition to other properties such as their ability to cross the BBB. Several experimental studies have reported specificities of some commonly used ACEIs on ACE-1 catalytic domains (Table 1.2). Some ACEIs were reported to inhibit both ACE-1 domains equally, whilst other ACEIs appeared to be either C-domain specific and accordingly thus would reduce Ang-II production, or N-domain specific and potentially interfere with Aβ degradation. Thus, considering the ACE-1 domains specificity is important to study the contribution of ACEIs on AD pathology.

Table 1.2 Reported specificities of ACE-1 catalytic domains of some licensed and experimental ACEIs

ACEIs	N-domain specificity	C-domain specificity	N- and C-domain specificity	References
Captopril	++	NONE	+	(343, 344, 372, 373)
Lisinopril	NONE	++	+	(343, 344, 372, 373)
Lisinopril-tryptophan	NONE	+	NONE	(373-375)
Enalapril	++	NONE	+	(343, 372, 373)
Ramipril	NONE	NONE	+	(373)
Perindopril	NONE	NONE	+	(343)
* RXP407	++	NONE	NONE	(372, 373, 376)
*RXP380	NONE	++	NONE	(372, 373, 376)

Experimental compounds are highlighted by *. The degree of affinity is indicated by the number of + while NONE indicates no evidence of binding.

Clinical trials are currently underway to test the possible role of ACEIs or ARBs as possible treatments against cognitive decline. Examples of these are the RADAR trial of losartan (377) (EuDraCT No.2012-003641-15), and the SARTAN-AD study (Identifier NCT02085265) involving both telmisartan and perindopril in AD patients with hypertension. In addition, smaller sized studies will aim to compare the effects of different ARBs on: CSF levels of RAS components, the HEART study (378) (Identifier NCT02471833); executive function in hypertensive patients with mild cognitive impairment, the CALIBREX study (Identifier NCT01984164); cardiovascular outcomes in people with mild cognitive impairment, the CEDAR study (Identifier NCT02646982); cognitive performance in older adults at high risk of AD, the rrAD study (Identifier NCT02913664). The findings of these important clinical trials will provide us with the further critical detail of the potential involvement of RAS in the pathogenesis of AD.

1.5.1.3 Angiotensin II (Ang-II)

Ang-II is the central active peptide in the ACE-1/Ang-II/AT_1R (cRAS) axis and is produced predominantly by ACE-1-mediated cleavage of Ang-I. Ang-II can also be produced directly from AGT by cathepsin G, tonin, elastase and protease-3 although the abundance of these in the brain is not clear. As described, Ang-II exerts its functions through binding to the specific G-protein coupled receptors (GPCRs), AT_1R and AT_2R (379). Ang-II is widely distributed throughout the brain and is detected in neurons, present at axon terminals and plasma membranes of dendrites, and astroglia (380, 381). Positive immunoreactivity of Ang-II has been reported in areas of the brain responsible for memory function and has a reported effect on supressing both long-term potentiation (LTP) and long-term depression (LTD) (382, 383).

The current knowledge about cRAS in the brain is largely based upon studies that have investigated how Ang-II affects brain functions including learning and memory. The major physiological effects of Ang-II are mainly mediated through AT_1R and produce neuronal damage and interfere with memory acquisition and recall in several *in vivo* studies. Infusion of Ang-II, the main effector in the classical axis of RAS, has been found to interfere with memory acquisition and recall in animal models of learning and memory (384, 385). Chronic Ang-II activation decreases synaptic plasticity through activation of neuroinflammatory pathway (386). Prolonged administration of Ang-II for three months in adult male C57BL/6 mice showed an association with BBB leakage, microglial activation, myelin loss and short-term memory impairment (387). In addition, infusion of Ang-II into AD mice model (AβPP/PS) resulted in exacerbation of AD pathological changes such as reduced CBF, spatial learning and functional dis-connectivity (388). A study conducted by Zhu *et al.* (238) found that ICV infusion of Ang-II into aged rats altered various components of the APP processing pathway (i.e. increased Aβ production and altered Aβ42/Aβ40 ratio), while AT_1R deletion inhibited production of Aβ and plaque formation (389). In addition, ICV infusion of Ang-II increased the levels of phosphorylated tau (390). This collection of animal studies suggest that the underlying mechanisms between increased level of Ang-II and both cognitive dysfunction and AD could be related to Aβ and tau-related pathology including impaired BBB integrity (391) and enhanced neuroinflammatory and oxidative stress (392).

Further support for the involvement of Ang-II in cognition and AD comes from recent *human post-mortem* studies. Kehoe *et al.* (393) found an increase in Ang-II level in frontal cortex of AD patients that results from increased level and activity of ACE-1. In addition to preclinical trials and population studies that suggested the role of ARBs may reduce the risk and development of AD (367, 394, 395),

these studies suggest that the increased level of Ang-II, and the effects of AT_1R activation, may be central to the pathogenesis of AD.

1.5.1.4 Angiotensin-II receptors

AT_1R is composed of 359 amino acids and has an approximate molecular weight around 40-42 kDa. AT_1R is coupled by guanyl nucleotide binding proteins to phospholipase C, calcium and adenosine 3',5'-cyclic monophosphate (cAMP) second messenger systems and thus is a GPCR. In humans, the AT_1R gene (*AGTR1*) is located on chromosome 3q and there are two subtypes of AT_1R known as AT_1aR and AT_1bR in rodents (396). Within the human adult brain, AT_1R is expressed more densely than AT_2R and is located on neurons, astrocytes, oligodendrocytes and microglia of the cortex, hippocampus and basal ganglia (397).

ACE-1 upregulation significantly increased production of Ang-II and subsequent activation of AT_1R and activates several pathways that result in vasoconstriction, apoptosis (cell death) and neuroinflammation that collectively exacerbate cognitive impairment (397). In animal studies, activation of AT_1R was shown to accelerate cell death of cholinergic and non-cholinergic neurons in the cortex and hippocampus after ischaemic injury (398) and was involved in the release of pro-inflammatory cytokines and inflammation that also led to cell death (282). Several ARBs that block AT_1R activation, such as telmisartan, valsartan, losartan and candesartan, have been shown to improve memory impairment and normalize spatial learning and memory in animal studies (291, 399-403). In addition, as mentioned, numerous clinical and epidemiological studies have provided clinical evidence of the neuroprotective effects of ARBs in reducing the incidence and progression of AD (404-407).

The neurotoxic effects that have been attributed to Ang-II/AT_1R binding can be countered by Ang-II-mediated activation of AT_2R, which is also a 7-transmembrane GPCR composed of 363 amino acids and weighs approximately 42 kDa sharing 32-34% homology with the AT_1R. In humans, the AT_2R gene (*AGTR2*) is located on the X chromosome (396). Although, AT_1R and AT_2R belong to one receptor family and have comparable potency and binding efficiency for Ang-II, each type is expressed in different areas of the brain and each mediates opposing functions of Ang-II. While AT_1R are widely distributed in adult brain tissue, AT_2R are limited to certain areas, including the thalamus, hypothalamus, brainstem nuclei and learning-associated areas (407, 408).

In the brain, AT_2R activation cause vasodilation, facilitates cognitive function, promotes cell survival and has both antioxidant and anti-inflammatory effects (408). Activation of AT_2R has been shown to attenuate cognitive impairment in several animal studies of brain injury. In a model of cerebral ischaemia, activation of AT_2R induced neuronal synthesis of VEGF and enhanced survival of cortical neurons (409). Direct stimulation of AT_2R by administration of an AT_2R agonist (compound 21, (C21)) enhanced spatial memory and prevented cognitive decline in a model of AD (410). C21 has also also been shown to attenuate ischaemic damage in other animal models of ischaemia (411, 412). In addition, AT_2R deficient mice showed impaired spatial memory and dendritic spine abnormalities (385). AT_2R knock out animals showed cognitive impairment and reduced hippocampal neurons in females (413). Together these studies demonstrated that inhibition of Ang-II/AT_1R or activation of Ang-II/AT_2R axis could be promising targets for improvement of cognitive impairment in AD.

1.5.2 Non-classical regulatory axis of RAS in the brain in AD

We are becoming increasingly aware that downstream brain RAS pathways may have a major impact on AD pathogenesis. The non-classical axis or rRAS axis of brain RAS (ACE-2/Ang (1-7)/MasR) has regulatory and depressor functions. The protective effect of the non-classical axis may be related to its vasodilatory, anti-fibrotic, anti-growth and anti-inflammatory actions (Figure 1.13). Reduction in ACE-2/Ang (1-7)/MasR activities have been linked to several neurodegenerative diseases such as Multiple sclerosis, Parkinson's disease and AD (414-416). Reduced level and activity of ACE-2 have been reported in human post-mortem studies and are strongly related to disease pathology (417). The role of each component of ACE-2/Ang (1-7)/MasR axis in relation to AD pathogenesis will be discussed in the following sections.

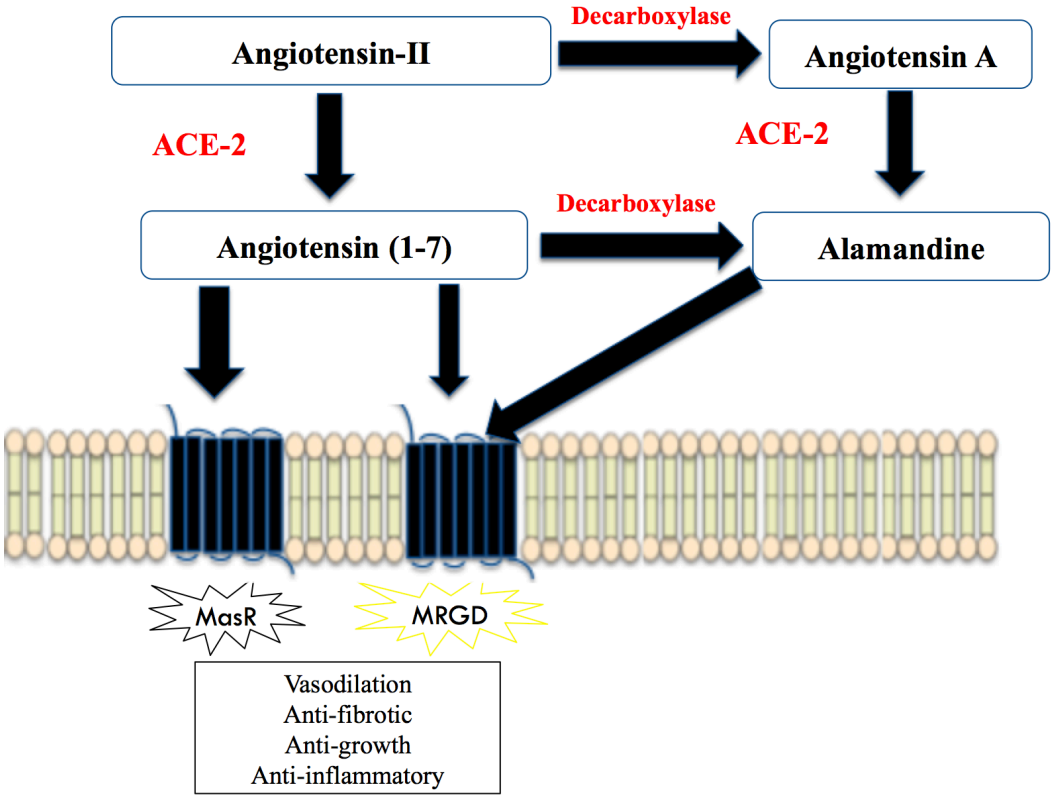

Figure 1.13 Effects of the non-classical axis of brain RAS.

Angiotensin (1-7) (Ang (1-7)) is the main effector of the non-classical axis of brain RAS. Ang (1-7) mainly acts on MasR and results in the neuroprotective effects include vasodilatory, anti-fibrotic, anti-growth and anti-inflammatory actions. Also, Ang (1-7) binds to another receptor known as MrgD and produces similar protective effects. Ang (1-7) can be further converted by decarboxylase into another active peptide known as alamandine that interacts with MrgD. Ang (1-7) has a higher affinity toward MasR and is responsible for the major effects of the non-classical axis of brain RAS (ACE-2/Ang (1-7) /MasR). ACE-2 - Angiotensin converting enzyme 2. MasR - Mas receptor. MrgD - Mas-related G protein-coupled receptor D.

1.5.2.1 Angiotensin converting enzyme 2 (ACE-2)

ACE-2 is a zinc metallopeptidase and the main enzyme involved in the non-classical rRAS axis (249, 250). ACE-2 comprises 805 amino acids and shares 42% sequence identity with ACE-1 metalloprotease, but unlike ACE-1 has only one catalytic domain (250). A major role of ACE-2 is in the metabolism of Ang-II forming Ang (1-7). Also, ACE-2 converts Ang-I to Ang (1-9) (251). Like ACE-1, ACE-2 is widely distributed in brain tissue, predominantly in neurons and perivascular areas involved in the regulation of cardiovascular function and learning and memory, such as the hippocampus and cerebral cortex (331, 417-419). In addition, a cell culture study reported that ACE-2

is also highly expressed in glial cells and astrocytes (420), although this remains to be confirmed in human brain tissue.

Several studies have described the interaction between ACE-2 and AD pathogenesis. Liu S et al., 2014 found that ACE-2 was involved in metabolism of Aβ where it was able to convert Aβ43 to Aβ42, which in turn could be cleaved by ACE-1 to less neurotoxic Aβ40 and Aβ41 species. In addition, they found that ACE-2 activity was reduced in the serum of AD patients, suggesting a potentially important role of ACE-2 in relation to Aβ neurotoxicity and development of AD. In ACE-2 knockout mice, the lack of ACE-2 resulted in cognitive impairment due to enhanced oxidative stress and reduced brain-derived neurotrophic factor (419). More recently, we found that ACE-2 activity was reduced in human post-mortem brain tissue of AD patients and this reduction was associated with increased AD pathological hallmarks (total Aβ load and p-tau levels) (417). In addition, the observed reduction in ACE-2 activity was inversely correlated with increased ACE-1 activity (417). Together our findings indicated the potentially vital role of ACE-2 as a regulator of the brain cRAS and how dysregulation of ACE-2 might be a precursor and important factor in the involvement of cRAS in AD pathogenesis. Furthermore, activation of ACE-2 by administration of DIZE, an ACE-2 activator in AD animal model, in a D-galactose-ovariectomized rat model of AD, resulted in improved learning and memory function in the Morris water maze and novel object recognition tests (295). More recently a very similar observation was made in a Tg2576 mouse model of Aβ-related cognitive impairment and pathology whereby DIZE both prevented the development of Aβ-related cognitive impairment in pre-symptomatic and restored cognition in mid-age cognitively impaired Tg2576 mice (421).

1.5.2.2 Angiotensin 1-7 (Ang (1-7))

The heptapeptide Ang (1-7) is a bioactive endogenous peptide of the brain RAS. Ang (1-7) has been found in different areas of the brain including the cerebellar cortex, hippocampus, hypothalamus, substantia nigra, medulla oblongata and amygdala in rat and human brain (422-425). There is more than one enzymatic pathway involved in the production of Ang (1-7) in the brain. The dominant pathway involved in the conversion of Ang-II into Ang (1-7) directly by the action of ACE-2 (426). Also, ACE-2 can produce Ang (1-7) indirectly from converting Ang-I into Ang (1-9) and then ACE-1 and/or NEP act on Ang (1-9) to form Ang (1-7) (427). Another pathway involved in Ang (1-7) production is via Ang-I cleavage by prolyl oligopeptidase, thimet oligopeptidase or NEP although how

prominent these are active in the brain, where their relative contributions to the formation of Ang (1-7) compared to that via ACE-2 is also still not fully known. It is widely accepted that Ang (1-7) exerts its physiological actions through binding to a GPCR namely, MasR (252). Coupling of Ang (1-7) with MasR generates several downstream signalling pathways such as stimulation of phospholipase A2, increased production of arachidonic acid, release of Ca+ independent activation of NOS, activation of phosphatidylinositol 3-kinase/Protein Kinase B (P13K/Akt), Mitogen-activated protein kinase (MAPK) and adenosine 3',5'-cyclic monophosphate (cAMP)-dependent protein kinase (PKA) (cAMP/PKA) (428).

Although the role of Ang (1-7) has been extensively explored in the cardiovascular and renal system, less is known of the neurobiological functions of Ang (1-7). Previous animal studies have focused on the role of brain Ang (1-7) as a vasodilator and other vascular related effects. Indeed, brain Ang (1-7) plays an important role in maintaining cerebral blood flow. Xie *et al.* (429) demonstrated that central administration of Ang (1-7) in rats with chronic cerebral hypoperfusion restored the cerebral blood flow and improved cognitive function. Also, this effect was associated with additional neuroprotective actions including increased NO generation, attenuated neuronal loss and suppressed astrocyte proliferation in the rat hippocampus. This was further supported by another animal study that showed intracerebrovascular infusion of Ang (1-7) in rats promoted brain angiogenesis and increased capillary density via a Mas/eNOS dependent pathway (430). Furthermore, other underlying cerebroprotective mechanisms of Ang (1-7) have been reported such as increased bradykinin production and higher eNOS expression in the brain (328, 431). Collectively, these studies outline a critical role of the active RAS metabolite, Ang (1-7), in maintaining homeostasis of brain functions.

In addition to the vascular actions of brain Ang (1-7), a few animal studies have investigated the role of this peptide in learning and memory. It has been shown that Ang (1-7), via its action on MasR, enhances LTP in the CA1 region of the hippocampus in mice (432). Similarly, Albrecht D. (433) showed that Ang (1-7) promoted stable LTP in mice amygdala mediated by cyclooxygenase (COX-2) and NO. Moreover, dysregulation of the Ang (1-7)/Mas axis caused memory deficits and affected object recognition memory in Mas knockout mice (353). One study examined the role of Ang (1-7) in relation to AD pathology, in an animal model of sporadic AD, Jiang *et al.* (416) found that Ang (1-7) levels were reduced in cerebral cortex and hippocampus and inversely correlated with hyperphosphorylated tau. In accordance, Uekawa *et al*. (434) showed that ICV infusion of Ang (1-7) alleviates cognitive impairment and improves cerebrovascular reactivity in the AD mouse model.

Despite the extensive investigation on the role of Ang (1-7) in previous animal studies, there is very little published data on the function of this peptide in humans in relation to AD. The plasma level of Ang (1-7) was found to be reduced in AD patients (n= 110) compared to age-matched controls (n= 128), suggesting that Ang (1-7) could be a potential biomarker for AD (435). In our previous study, we found that Ang-II to Ang (1-7) ratio was increased in AD, indicating a reduction in conversion of Ang-II to Ang (1-7) related to the observed reductions in ACE-2 activity (417).

1.5.2.3 Mas receptor (MasR)

The MasR was originally identified as a proto-oncogene due to its ability to transform NIH 3T3 cells and induce tumorigenicity in mice. MasR encodes a genetic sequence characteristic of the GPCR subfamily and has seven hydrophobic transmembrane domains (436). Recently, the MasR gene has been characterised as the most complex gene structure among the GPCR family group (437). In rats, the highest MasR expression was found in brain and testis (436). MasR was also found to be expressed in different peripheral tissues including heart, kidney, lung, liver, spleen, tongue, skeletal muscle and endothelial cells of blood vessels (254). In rat brain, high MasR level was detected within the hippocampus, cerebral cortex and in cardiovascular-related areas of the brain such as the hypothalamus and medulla (438, 439). The high expression of MasR in the hippocampus reinforces the hypothesis that binding of Ang (1-7) to MasR enhances LTP and modulates synaptic plasticity and further suggests that alterations to the non-classical axis of RAS may play a role in the cognitive decline in AD (432, 433).

MasR knockout mice showed memory deficit and defective novel and spatial object recognition memory performance (353). In contrast, MasR activation in the hippocampus and basal ganglia promoted cell survival, enhanced synapse formation and improved cognition in rodent and humans (425). Accordingly, activation of MasR by Ang (1-7) administration attenuated cognitive decline, reduced expression of AD pathological hallmarks (phosphorylated tau, Aβ oligomer and both Aβ40 and Aβ42 levels) in hippocampus of an AD rat model and co-administration of MasR antagonist reversed all of these protective effects (440), suggesting that dysregulation of (ACE-2/Ang (1-7)/MasR) axis might be highly relevant to cognitive decline in AD.

Several lines of evidence suggest an interaction between MasR and the neuroprotective AT_2R (441). In the mouse heart, Ang (1-7) was found to produce vascular effects by an interaction of the MasR with AT_1R and AT_2R, resulting in the release of prostaglandins and NO (442). More recently, a study conducted by Tetzner *et al.* (443) offered contradictory findings. They posed the possibility for interaction between the MasR and other receptors, including AT_2R, but excluded AT_2R as a receptor for Ang (1-7) and identified a second receptor for Ang (1-7) known as Mas-related GPCR, member D (MrgD). The coupling of Ang (1-7) with both MasR and MrgD activates intracellular signalling pathways involving increased cAMP and phosphokinase A activity. In addition to the complexity of the MasR, several studies reported variable selectivity of MasR upon stimulation by angiotensin peptides other than Ang (1-7), such as Ang-III and Ang-IV (444, 445). Considering these data, future examination and improved understanding of the direct interactions between Ang (1-7)/MasR and the intracellular signalling cascade in brain tissue is now of interest and which may also help to inform the role of the non-classical axis of RAS in AD pathogenesis.

1.5.2.4 Alamandine and MrgD receptor

Alamandine is one of the newly discovered active peptides in the brain RAS. It is an agonist of the MrgD receptor and is a heptapeptide that differs by one amino acid from Ang (1-7), where there is an alanine instead of aspartate (446, 447). Alamandine is produced from Ang (1-7) by decarboxylase or from Ang A, which is generated from the decarboxylation of Ang-II and then subsequent cleavage by ACE-2 (Figure 1-12) (448). Due to the sequence homology between Ang (1-7) and alamandine, both exert similar protective effects in circulatory and peripheral tissues. Several *in vivo* studies have demonstrated the cardioprotective effects of alamandine. Similar to Ang (1-7), alamandine has vasodilatory, anti-inflammatory and anti-hypertrophic actions (449-452). These protective effects result from binding of alamandine to the MrgD receptor that is encoded by *Mrgprd* gene in animals and humans (453). Within the brain, MrgD was detected in sensory neurons and has been implicated in the perception of neuropathic pain (454). MrgD had also been extensively studied in non-neuronal tissue especially cardiovascular tissue where it was found in arterial smooth muscles, endothelial cells of blood vessels, and cardiomyocytes (455). MrgD has been found to be expressed within the cardiovascular centre of the mouse brain (456). Despite the well know effects of alamandine/MrgD in the cardiovascular system, the role of this coupling system in relation to cognitive dysfunction and AD pathogenesis is less well studied.

1.5.3 Role of the APA/Ang-III/APN/Ang-IV/IRAP pathway in cognitive function and AD

In addition to the main brain RAS pathways described, another downstream regulatory pathway of RAS has been identified in the brain involving APA/Ang-III/APN/Ang-IV/IRAP (457). This is another rRAS pathway that regulates cerebral blood flow, maintains memory and learning acquisition, and enhances synaptic plasticity and has neuroprotective effects in the CNS (458) (Figure 1.14). The role of each component of the APA/Ang-III/APN/Ang-IV/IRAP regulatory axis in relation to AD pathogenesis will be discussed in the following sections.

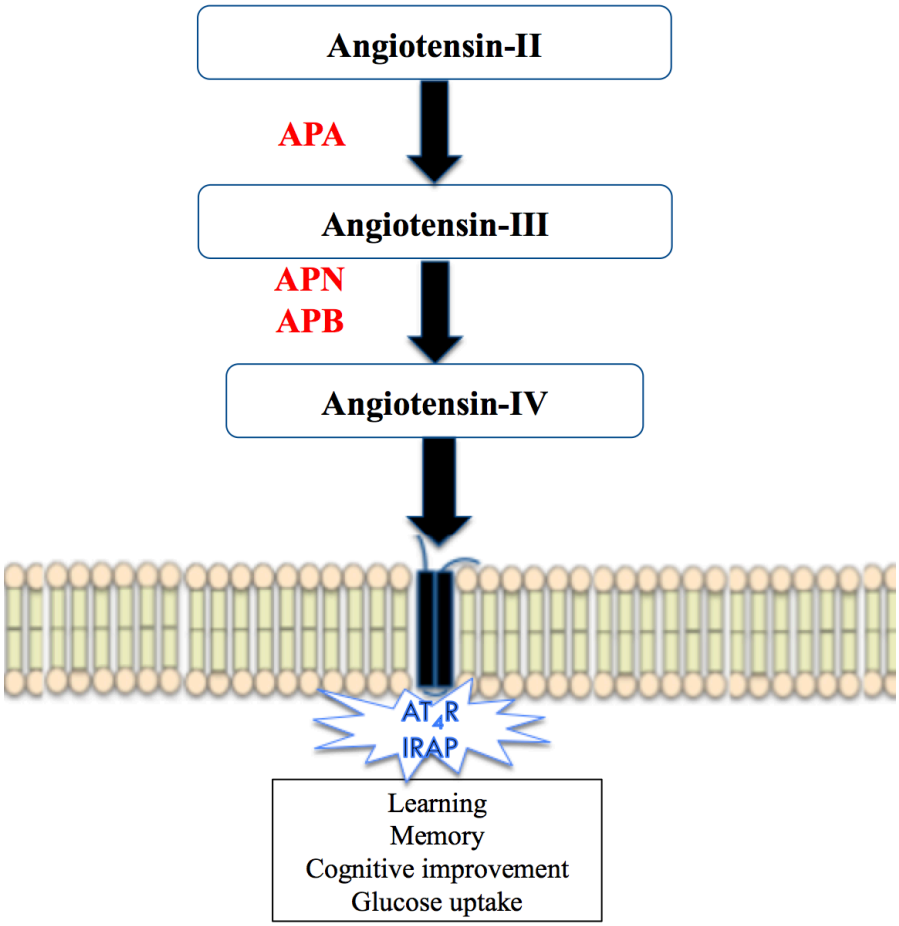

Figure 1.14 Effects of the regulatory pathway of brain RAS.

Ang-IV is the main effector of the regulatory pathway of brain RAS. Ang-IV acts on AT_4R binding sites, including IRAP, to activate neuroprotective signalling resulting in maintaining memory and learning, regulating cerebral blood flow, increasing glucose uptake, and enhancing synaptic plasticity that together lead to cognitive improvement. The APA/Ang-III/APN/Ang-IV/IRAP enzymatic pathway is known as the regulatory pathway of brain RAS. APN -Aminopeptidase A, APN - Aminopeptidase N, APB - Aminopeptidase B, AT_4R - Angiotensin 4 receptor, IRAP - Insulin-regulated aminopeptidase.

1.5.3.1 Angiotensin III (Ang-III)

Ang-III is a heptapeptide and a biologically active endogenous peptide in the brain RAS that is derived from and exerts similar pressor effects to Ang-II. Ang-III is generated from the cleavage of Ang-II by the action of APA but can also result from alternative enzymatic steps, such as APA-mediated conversion of angiotensinogen to des-Asp-Angiotensin followed by cleavage by ACE-1 to make Ang-III (256). Although, some studies found that Ang-III has less affinity than Ang-II toward AT_1R and AT_2R (459), several studies have shown that Ang-III does mediate effects on the regulation of blood pressure, fluid homeostasis and vasopressin release (460).

It is well established that Ang-III has significant cardiovascular actions (269). *In vivo* studies have found that Ang-III infusion increases BP, promotes vasoconstriction and stimulates aldosterone production (461). *In vitro*, it stimulates growth, production of proinflammatory mediators, and deposition of extracellular matrix proteins (462). Ang-III binds to AT_1R, as well as to AT_2R. However, most of the effects of Ang-III are mediated by AT_1R. The role of Ang-III within the brain, in relation to AD pathogenesis, is less studied. Recently, our group found increased Ang-III level in human post-mortem brain tissue of AD patients that correlated strongly with parenchymal Aβ and tau load (393). The increase in Ang-III level in AD might reflect hyperactivity of the classical axis of brain RAS (ACE-1/Ang-II/AT_1R) and reduced activity of the downstream regulatory pathway APA/Ang-IV/APN/IRAP, which might limit the metabolism of Ang-III in AD.

1.5.3.2 Aminopeptidases in the brain RAS

A group of enzymes, that are central to the proteolytic processing of many of the bioactive peptides in the brain RAS, are known as aminopeptidases. The two main aminopeptidases implicated in the synthesis, metabolism and actions of angiotensins are APA and APN, although APB might also be involved (463). All of these enzymes have previously been proposed to be involved in regulation of the brain RAS and are implicated in learning and memory (464).

APA is a type II membrane bound monozinc aminopeptidase that is responsible for the hydrolysis of Ang-II, the main effector peptides of the brain RAS, to generate Ang-III. APA is also known as glutamyl aminopeptidase as its main function involves cleavage of the N-terminal glutamyl residue

from Ang-II (465). APA is expressed in many peripheral tissues and within the brain, where it has been identified in several brain nuclei sensitive to angiotensins that are involved in regulation of blood pressure. APA has been shown to localise to neurons and microglia (393, 466). In the brain RAS, APA has been proposed to be involved in two main enzymatic pathways that include the conversion of Ang-II to Ang-III and also the hydrolysis of the protective peptide Ang (1-7) into less active small peptide Ang (2-7) (467).

Previous experimental animal studies have reported increased activity of APA in different hypertensive animal models such as the spontaneously hypertensive rat (SHR) and in a salt-dependent model of hypertension, the deoxycorticosterone acetate (DOCA)-salt rat (466, 468). One of the novel treatment strategies for hypertension is targeting APA activity to reduce production of Ang-III (467), suggesting an association between hyperactivity of brain RAS and hypertension. Moreover, a number of human studies have investigated the role of APA in relation to AD pathogenesis. APA was able to generate the neurotoxic form of Aβ (Aβ42) and contribute directly to AD pathogenesis (469). Other studies indicated a reduction in APA activity in plasma and serum of AD patients (258, 464). In human post-mortem tissue, APA level and activity was similarly found to be reduced but not significantly so in AD (393). These findings suggest that the dysregulation in the upstream pathway of the alternative RAS axis may be altered in AD and could contribute to AD pathogenesis.

APN is a type II transmembrane zinc-dependent aminopeptidase that is responsible for the hydrolysis of Ang-III to generate the neuroprotective Ang-IV peptide. APN is also known as alanyl aminopeptidase since alanine is most efficiently cleaved by APN (467). APN has been found in the wall of microvessels in the rat brain and in other brain areas such as the cortex, thalamus, hippocampus, substantia nigra, hypothalamus and in neurons of frontal cortex in human brain (393, 470). In the brain RAS, APN is predominantly responsible for the conversion of Ang-III to Ang-IV and also, hydrolyses the small peptide Ang (2-7) into a less active smaller peptide Ang (3-7) (258). To-date, several studies have shown a reduction of APN activity in association with AD pathogenesis. Puertas *et al.* (258) found that plasma APN activity was reduced in AD patients and associated with cognitive decline. In addition, reduced APN activity has been found in AD patients in both serum and in mid-frontal cortex of human post-mortem tissue (393, 464). Together these studies indicate that dysregulation of APN mediated production of Ang-IV is implicated in cognitive decline in AD.

APB is a type II transmembrane zinc-dependent aminopeptidase that hydrolyse basic amino acid (Arginine) from the N-terminal of several peptides. APB is also known as arginine aminopeptidase

(467). Similar to APN, APB is also involved in the conversion of Ang-III into Ang-IV. Two studies have shown a reduction of APB activity in early stage of AD. Puertas *et al.* (258) found that plasma APB activity was reduced in AD patients and associated with cognitive decline. In addition, reduced APB activity has been found in serum of AD patients in the early stage of the disease (464). Both studies indicate that dysregulation of APB occur in early stage of AD and associated with cognitive decline.

1.5.3.3 Angiotensin IV (Ang-IV)

Originally, Ang-IV was thought to be an inactive, small fragment of RAS, however, recent studies have shown the hexapeptide to be a bioactive peptide in the brain RAS that plays a role in several physiological functions within the brain including facilitation of cognitive processing. Ang-IV is produced from Ang-III by the action of APN and APB (471). Within the brain, the Ang-IV binding site has been found in neurons in different brain areas including the cortex, hippocampus and basal ganglia (246, 472, 473). Accumulating evidence demonstrates that Ang-IV regulates CBF, maintains memory and learning acquisition, enhances synaptic plasticity and has neuroprotective effects (458). These beneficial effects of Ang-IV are mediated by binding to AT_4R. There was a debate for many years about the identity of an Ang-IV specific binding site. Albiston *et al.* (474) discovered that IRAP was a specific binding site for Ang-IV. Later in 2008, Wright *et al.* (473) indicated that Ang-IV also binds and activates c-Met, a type 1 tyrosine kinase receptor. It seems that Ang-IV binds to these two binding sites independently and mediates different functional effects through inhibiting IRAP activity and stimulating the c-Met receptor pathway (475).

Several experimental studies have focused on the effects of Ang-IV and Ang-IV analogues on cognitive function, especially in learning and memory. Both Ang-IV and its analogue (Nle^1-Ang IV) facilitated LTP induction in hippocampal and dentate granule cells both *in vitro* and *in vivo* (476-478). ICV administration of Ang-IV or Ang-IV analogues have been shown to enhance both spatial working memory and object recognition memory. Administration of Ang-IV into the lateral ventricle of normal rat (male SDR) enhanced spatial working memory in the plus maze spontaneous alteration task (479). Similarly, two studies showed improvement in cognitive performance after treatment with Ang-IV alone or combined with an Ang-IV analogue (Nle^1-Ang IV or LVV-haemorphin-7) (480, 481). Braszko *et al.* (482) demonstrated that the enhancement of memory after ICV administration of Ang-II

in male WR was caused by the shorter peptide, Ang-IV. In addition, Golding and colleagues found improvement in object recognition after subcutaneous administration of Ang-IV in the same animal model (483). Consistent with all these studies, ICV infusion of Ang-IV rapidly improved novel object recognition in a mouse model (male C57BL/6J mice) that was dependent on AT_4R expression (484). In contrast, two studies found no effects of Ang-IV on the rate of acquisition of cognitive task or on object recognition performance after subcutaneous administration of Ang-IV (485, 486).

Ang-IV and a number of its analogues have been found to restore cognitive function and enhance spatial working memory in an animal model of Scopolamine-induced memory deficits (487-492). More recently, blocking the effects of AT_4R with divalinal was found to counter ARBs (losartan) effects to rescue spatial learning and memory in a mouse model of AD (493). In addition to the neuroprotective effects of Ang-IV, previous results from animal studies support the cerebroprotective role of Ang-IV/AT_4R in increasing CBF by stimulation of NO production (458, 494, 495). Overall, these findings suggest that Ang-IV/AT_4R pathway is potentially a promising target for improving cognitive decline in AD.

1.5.3.4 Insulin regulated aminopeptidase (IRAP)

The AT_4R binding site has been identified as IRAP, a type II transmembrane protein that belongs to the M1 zinc dependent aminopeptidase family that also contains APA, APN, and APB. IRAP is predominantly localised to glucose transporter type 4 (GLUT4) vesicles in insulin-responsive cells, which include the pyramidal cell of the hippocampus and cerebral cortex (474, 496, 497). This identification was based on observed similarities between human brain AT_4R and the known IRAP structure, both were found to have high sequence homology and a similar molecular weight of around 160 kDa. IRAP consists of a 110 amino acid N-terminal hydrophilic intracellular domain that includes two dileucine motifs. The hydrophobic transmembrane domain consists of 22 amino acids that continue with an 893 amino acid C- terminal extracellular domain associated with its catalytic site (459). IRAP also has been known as oxytocinase, cysteine aminopeptidase, and placental leucine aminopeptidase (479).

IRAP has the ability to cleave the N-terminal amino acids from a number of active neuropeptides such as, vasopressin, somatostatin, eNOS, met-enkephalin and many others (498, 499). Two groups of IRAP inhibitor have been identified that show memory enhancing properties, especially enhancing

spatial working memory in animal models: peptide inhibitors (Ang-IV and its analogues, LVV haemorphin7) and benzopyran-based inhibitors (HFI-419, HFI-435 and HFI-437) (500-502). Based on the physiological actions of IRAP, two potential mechanisms have been proposed to explain the role of Ang-IV/IRAP interaction as a memory enhancer in the brain (Figure 1.15). First, Ang-IV competitively inhibits the catalytic activity of IRAP toward several neuropeptides such as oxytocine, vasopressin, somatostatin, eNOS, met-enkephalin and as a result extends their half-life. Second, Ang-IV binds to IRAP and inhibits the intracellular GLUT4 vesicular trafficking resulting in sustained presence of both IRAP and GLUT4 on the cell surface, thus enhancing memory by increasing neuronal glucose uptake (496, 497, 503).

Contrary to previous animal studies showing the cognitive-enhancing effects of IRAP inhibitors, a recent animal study in IRAP knockout mice resulted in significant deficit both spatial and object recognition memory (504). In accordance, plasma activity of IRAP was found to be significantly reduced in AD patients and correlated with worsening MMSE scores (258). Together these studies support the hypothesis that IRAP has a vital role in cognitive function, while the implication of Ang-IV/IRAP pathway in AD pathogenesis is less studied.

1.5.3.5 Angiotensin type 4 receptor (AT_4R) subtype (c-Met)

Ang-IV interacts with another AT_4R binding site identified as c-MET, a tyrosine kinase receptor (473). The c-Met receptor consists of an α-chain (50 kDa) and a β-chain (140 kDa) linked by disulfide bonds. Hepatic growth factor (HGF) binds to c-Met resulting in tyrosine phosphorylation leading to the activation of a number of biological activities (505). This identification was based on several research findings that showed a partial similarity between Ang-IV and HGF in chemical structure and physiological function (458). Distribution of the c-MET receptor in the brain was similar with the extensive distribution pattern of AT_4R in areas responsible for cognitive and motor processing including the amygdala, hippocampus, cerebral cortex, substantia nigra, striatum, and thalamus (384, 472, 492, 506, 507). There is an overlap between many functions mediated by HGF/c-MET and Ang-IV/AT_4R; both coupling systems facilitated memory consolidation, enhanced hippocampal LTP, calcium signalling, CBF, synaptic transmission and have been implicated in AD (459, 508). Increased HGF level was found in the CSF in AD patients associated with the white matter damage (509).

Ang-IV activation of the c-Met receptor induces several signalling pathways (Figure 1.15), Ang-IV increases:

i) intracellular calcium and enhances eNOS production (495);

ii) calcium entry via different calcium channels and enhances synaptic transmission and LTP (478, 510);

iii) acetylcholine synthesis and release (511);

iv) dendritic growth in the hippocampus (512).

Together these studies suggest that Ang-IV activation of these intracellular signalling pathways facilitates CBF, enhances synaptogenesis and LTP and increases neuroprotection (475). Moreover, recent neural imaging indicates that an Ang-IV analogue (Nle^1-Ang-IV) stimulates the production of new dendritic spines and increases spine head size in hippocampal neurons and reverses learning deficits in a scopolamine dementia rat model (491). In summary, Ang-IV seems to mediate its neuroprotective functions by interacting with both IRAP and AT_4R subtype (c-MET).

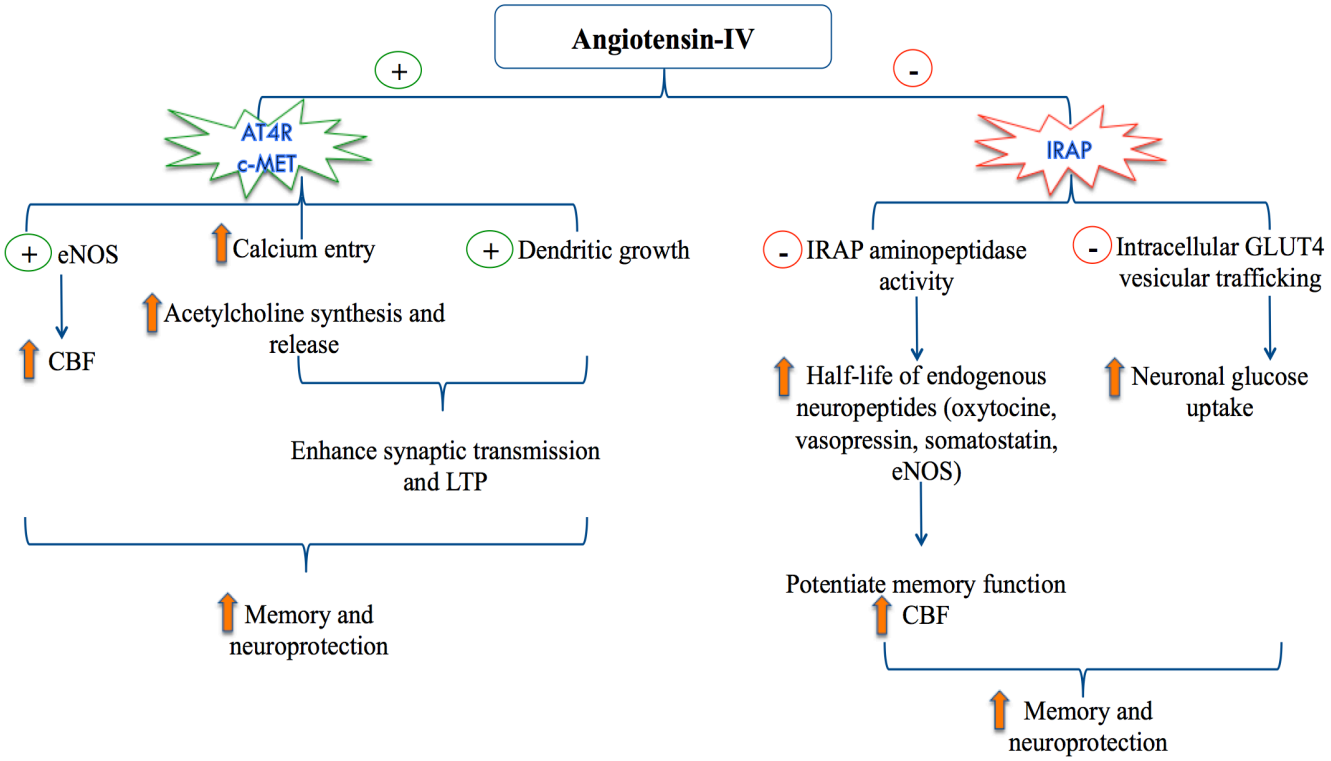

Figure 1.15 The possible mechanisms of the neuroprotective effects of Ang-IV.

Ang-IV mediates several neuroprotective effects through binding to two binding sites independently, IRAP and AT_4R/c-Met receptor. Ang-IV binds to IRAP and inhibits its aminopeptidase activity resulting in increased half-life of several endogenous neuropeptides such as oxytocine, vasopressin, somatostatin and eNOS, altogether known to potentiate memory and increase CBF. Also, Ang-IV inhibits intracellular GLUT4 vesicular trafficking and increases neuronal glucose uptake. Other effects of Ang-IV are mediated trough stimulation of the AT_4R/c-Met pathway that stimulates eNOS production and increased CBF, increased calcium entry and acetylcholine synthesis and release, and stimulates dendritic growth that altogether lead to enhanced synaptic transmission, LTP, increased memory functions and neuroprotection. IRAP - Insulin-regulated aminopeptidase, GLUT4 - Glucose transporter type 4, eNOS - endothelial nitric oxide synthase, CBF - cerebral blood flow, AT_4R - Angiotensin 4 receptor, c-MET - a tyrosin type 1 receptor, LTP - Long-term potentiation. Up pointed orange arrows = increase, red circle minus signs = inhibit, green circle plus signs = stimulate.

1.5.4 Potential therapeutic targets of brain RAS in AD

Improved understanding of the critical roles of brain RAS in neurodegenerative diseases has opened new ideas as to potential therapeutic approaches for AD. Although, the development of brain RAS targeting drugs that are able to cross the BBB remains challenging, several published data provide novel evidence that regulation of brain cRAS and rRAS may provide therapeutic benefit in AD.

Currently, the possible RAS pharmacological targets in AD aim to inhibit the overactive cRAS (ACE-1/Ang-II/AT_1R) but novel targets that activate the downstream rRAS (ACE-2/Ang (1-7)/MasR) and (APN/Ang-IV/IRAP) might prove to be more efficacious. There are currently eight potential targets/approaches (Figure 1.16):

i. Renin inhibitors:

Renin inhibitors are a class of cRAS targeting anti-hypertensive drugs that inhibit the enzymatic activity of renin and prevent formation of Ang-I, the first step toward Ang-II production in the RAS. Aliskiren, a highly specific and potent renin inhibitor has been shown to exert neuroprotection against Aβ toxicity in cortical neurons of rats (513) and reduce brain damage and working memory deficits in a mouse model of chronic cerebral ischaemia (514). However, there is limited evidence about the effects of renin inhibitors on cognitive functions and AD pathogenesis in human since the drug is relatively new compared to all other RAS medications.

ii. ACE-1 inhibitors (ACEIs)

ACEIs are the most commonly prescribed RAS targeting anti-hypertensive drugs that inhibit the enzymatic activity of ACE-1 and prevent the production of Ang-II from Ang-I. A number of currently used ACEIs have variable effects on cognitive functions and are associated with decreased risk of developing AD (364, 365). However, findings from *in vitro* and *in vivo* studies regarding the effects of ACEIs on Aβ level are inconsistent and sometimes conflicting. Most of the *in vitro* studies have shown that ACEIs increase both Aβ40 and Aβ42 level and inhibit degradation of Aβ42 (79, 81, 343, 347). In contrast, several animal studies have shown the beneficial effect of ACEIs, such as perindopril, captopril and enalapril, which are associated with decreased Aβ42 level, reduced Aβ plaque and ROS accumulation and improved CBF in brain of AD models (361, 515-517). Other studies have showed either no effect of ACEIs on Aβ level (518) or increased Aβ level after administration of ramipril in mice model of AD (ACE 10/10 mice) (519). Despite the inconsistency of ACEIs effects on Aβ level, a large body of evidence from observational and clinical studies support a beneficial effect of ACEIs on reducing cognitive decline and slowing the progression of AD in patients using ACEIs compared to non-RAS targeting anti-hypertensive drugs (364, 365, 367, 520, 521).

iii. AT_1R blockers (ARBs)

Ang-II acts on AT_1R to exert its neurotoxic effects, thus inhibiting Ang-II by blocking AT_1R is one of the therapeutic targets of AD. Data from experimental studies have demonstrated the beneficial effects of several ARBs such as losartan, valsartan, olmesartan, telmisartan and candesartan on both cognitive functions and Aβ pathology in human APP mice (238, 358, 359, 522-526). Moreover, supportive data from observational and clinical studies has indicated the neuroprotective effects of ARBs on cognition and Aβ pathology (366, 367, 377, 527). Some recent clinical studies suggest that ARBs are more effective than ACEIs in delaying the onset or reducing the rate of cognitive decline in AD (366-369).

iv. AT_2R agonists

Ang-II also acts on AT_2R and mediates beneficial signalling mechanisms opposing those of AT_1R, and thus activation of AT_2R by AT_2R agonists could potentially modulate the cognitive deficit in AD. Direct activation of AT_2R by administration of AT_2R agonist (C21) has been shown to enhance spatial learning in wild-type mice that were given intracerebral injection of Aβ40 (410). AT_2R has a higher affinity toward Ang-III, thus stimulation of this receptor through targeting Ang-III analogues that are able to penetrate the BBB could be a new therapeutic approach for AD (528).

Together all of these targets aim to inhibit or reduce the deleterious effects of the classical RAS axis (ACE-1/Ang-II/AT_1R). In contrast, other agents that target the downstream regulatory RAS axis include:

v. ACE-2 activators

Direct activation of ACE-2 results in reduced effects of Ang-II through conversion of Ang-II into the neuroprotective peptide Ang (1-7). Experimental studies have shown that DIZE, a trypanocidal drug that can activate ACE-2 (529) has neuroprotective effects against ischaemic stroke in rats and improved learning and memory in an AD rat model (295, 326, 441). Mascolo and colleagues (530) suggests that direct administration of recombinant human ACE-2 (rhACE-2) previously investigated in relation to cardiovascular diseases (531), could provide therapeutic benefit in AD. However, this targeting strategy still remains less studied in relation to cognitive function and AD pathogenesis.

vi. MasR agonists

Ang (1-7) acts on MasR and mediates the cerebroprotective and neuroprotective effects. Reduced level of Ang (1-7) was found in both AD patients and a mouse model of sporadic AD (416, 435). Direct activation of MasR through ICV administration of Ang (1-7) has been shown to improve cognitive performance in an animal model with induced cognitive deficit (429, 434). Another non-peptide MasR agonist, AVE 0991, in combination with renin inhibitors, showed a beneficial cardiovascular effect of lowering blood pressure in hypertensive rats (532). Its potential protective role in relation to cognitive function and AD pathogenesis warrants further study.

Together these pharmacological approaches might potentiate the protective effects of the non-classical axis (ACE-2/Ang (1-7) /MasR).

vii. IRAP inhibitors

IRAP inhibitors include both the peptide (Ang-IV and Ang-IV analogues) and the non-peptide mimetic (HFI-419) that have been shown to promote memory especially enhancing spatial working memory in animal models with induced cognitive impairment (500-502). Several attempts were made to develop new Ang-IV analogues for the treatment of AD (458), however, the short half-life and inability to cross the BBB limited the use of these compounds in clinical studies. Developments of Ang-IV analogues that result in more stable smaller molecules that are able to cross the BBB (e.g. dihexa) have been shown to facilitate spatial memory in scopolamine-induced deficits in Morris water maze (492).

All of these pharmacological manipulated targets aim to potentiate the neuroprotective effects of the brain RAS regulatory axis (APN/Ang-IV/IRAP).

viii. APA inhibitors

APA inhibitors inhibit the conversion of Ang-II to Ang-III, which is reported to be increased in AD patients and was associated with AD pathology (393). Oral administration of APA inhibitors reduced blood pressure (533). Two new drugs targeting APA (EC33 and QGC001) that reduce the blood pressure have been shown to cross the BBB (534, 535). In addition, APA was able to generate the neurotoxic form of Aβ (Aβ42) and contribute directly to AD pathogenesis (469). Thus, targeting APA

activity through APA inhibitors can modulate the toxic effects of Ang-III on blood pressure and APA on Aβ metabolism.

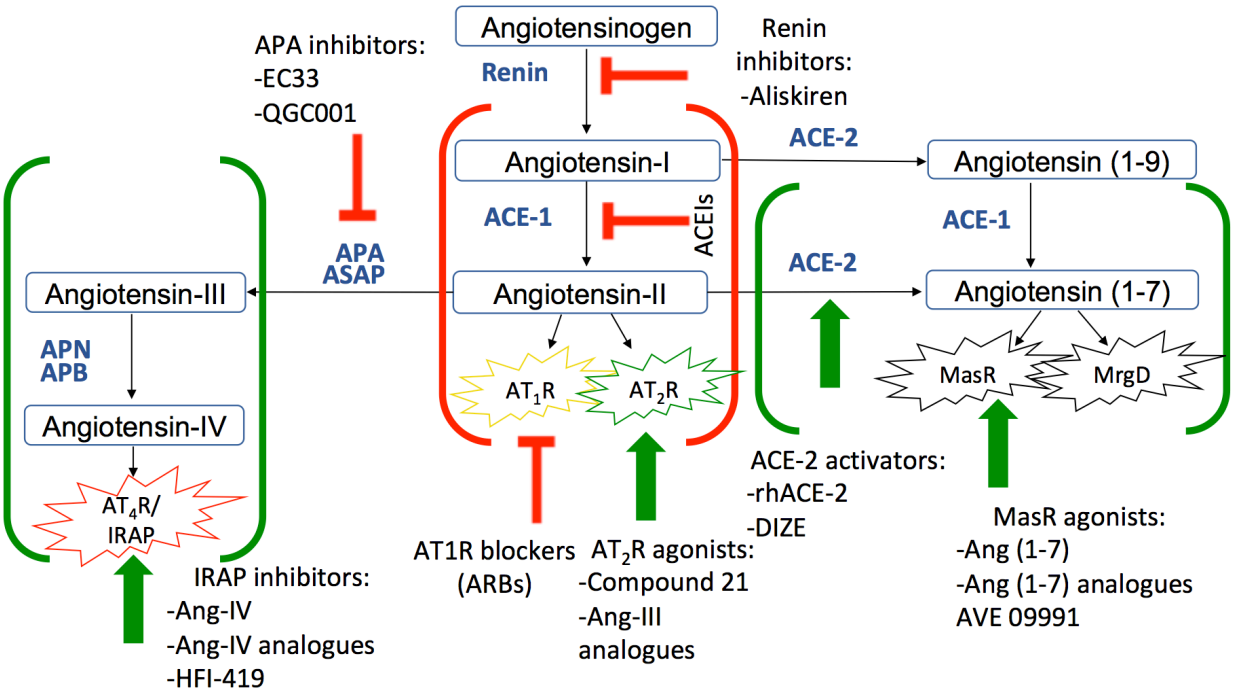

Figure 1.16 The possible therapeutic targets of brain RAS in AD.

Eight basic approaches can be considered as new therapeutic targets for AD that aim to inhibit the overactive classical axis (ACE-1/Ang-II/AT_1R) and/or activate the downregulatory non-classical axes (ACE-2/Ang (1-7)/MasR) and (APN/Ang-IV/IRAP). Inhibition of the overactive classical axis (ACE-1/Ang-II/AT_1R) can be achieved by the use of renin inhibitors (Aliskiren), Angiotensin converting enzyme-1 inhibitors (ACEIs), AT_1R blockers (ARBs) or activators of the the protective AT_2R by AT_2R agonists (compound 21 and Ang-III analogues). Activation of the non-classical axis (ACE-2/Ang (1-7)/MasR) can result from either the use of ACE-2 activators (rhACE-2 and DIZE) or MasR agonists (Ang (1-7), Ang (1-7) analogues AVE 09991). IRAP inhibitors (Ang-IV, Ang-IV analogues and HFI-419) are promising targets to activate the regulatory pathway (APN/Ang-IV/IRAP). One of the new therapeutic targets within RAS aims to inhibit APA activity by using APA inhibitors (EC33, QGC001). rhACE-2 - recombinant human angiotensin converting enzyme 2, DIZE - diminazene aceturate. Flat red arrows = inhibition or blocking, Up pointed green arrows = activation (adapted from Mascolo et al., 2017) (530).

1.6 Hypothesis and aims

Recent studies indicate that an imbalance in brain RAS, due in part to defective rRAS signalling and overactive cRAS activity, is associated with disease pathology in human studies. Collective data from genetic, *in vitro* and *in vivo*, as well as clinical and observational studies support a strong association of a dysfunctional brain RAS in the mediation of disease pathology and cognitive decline in human and animal studies although there is much to still be understood of the brain RAS in AD.

In this study, I explored the general hypothesis that alterations of both the classical (overactive) and non-classical axes of brain RAS (underactive) can influence AD pathogenesis and are related to vascular dysfunction.

The main aims were to characterise the expression and distribution of cRAS and rRAS pathways, and novel RAS mediators, in AD in relation to disease pathology and markers of vascular dysfunction in human post-mortem brain tissue.

The specific aims of the studies in this thesis were:

(i) To determine the relevant contributions of ACE-1 C-domain and N-domain activities to the overall increased activity of ACE-1 in AD.
(ii) To systematically characterise the expression and distribution of major non-classical RAS axis pathways (ACE-2/Ang (1-7)/MasR) in AD in relation to AD pathology,
(iii) To characterise the expression and distribution of the alternative regulatory axis of brain RAS (APN/Ang-IV/IRAP) in AD in relation to AD pathological markers.
(iv) To examine the relationship between alterations of brain RAS markers (Ang (1-7)/MasR), (Ang-IV/IRAP) with markers of cerebrovascular dysfunction including brain ischaemia (VEGF) and tissue oxygenation (MAG:PLP1 ratio).
(v) To investigate the level and examine the distribution of the non-AT_1R and non-AT_2R binding protein (neurolysin) in AD in relation to both AD pathological hallmarks and vascular markers, and to measure the level of its substrate (neurotensin) in relation to AD pathology.

Chapter 2. Materials and Methods

2.1 Materials

All the details of laboratory equipments, consumable suppliers, constituents of regulary used solutions, summary of primary and secondary antibodies, standard proteins and assay kits used in this study are listed and presented in chapter 9 (Appendix II).

2.2 Brain tissue acquisition and processing

Human post-mortem brain tissue used in this study was obtained from the Human Tissue Authority-licensed South West Dementia Brain Bank (SWDBB), University of Bristol, Southmead Hospital, UK with local Research Ethics Committee approval (reference 08/H0106/28 + 5).

Brain tissue dissection was performed following a standard procedure that has previously been described (78). In summary, for the majority of cases, brain tissue was obtained and processed within 72 hours of death. The left cerebral hemisphere had been sliced and stored at -80°C for further biochemical assessment. The right cerebral hemisphere was fixed in 10% buffered formalin for a minimum of three weeks before being sliced coronally into slices of approximately 1 cm thickness and embedded into wax blocks. All tissue blocks were used for creating tissue sections using a sledge microtome of 7 μm thickness for both pathological assessment and other relevant histological investigations.

2.2.1 Cohort selection

Brain tissue used in this study was taken from the mid-frontal cortex (Brodmann area 8/9). AD cases (n= 70) were selected with a definite AD diagnosis according to the criteria of the CERAD (189). The controls (n= 48) used were selected with no history of dementia and other neuropathological disorders. This cohort was selected on the basis that it had also been previously used to study other RAS components in relation to AD pathology and from which some data was already available (78). Where such data is used in this thesis in various analyses the contributions of any relevant persons for these data is made clear.

Brain tissue homogenates were made from AD cases (n= 70) that ranged from 47-98 years of age-at-death (Mean= 77.9, SD= 10.5), which included 44 females and 26 males, and had a post mortem delay time ranging from 4 to 99 hours (Mean= 46.7, SD= 25.7). The control group (n= 48) ranged from 43-95 years of age-at-death (Mean= 78.9, SD= 10.5), included 19 Females and 29 males, and had a PMD time that ranged from 3-216 hours (Mean= 47.5, SD= 38). Although some cases had a long PMD time and different cause of death that could have an influence on tissue processing, there were no significant differences in age-at-death or PMD time between controls and AD cases (p= 0.657; p= 0.525) respectively. The demographic features of the AD and control cohorts are summarised in Table 2.1. The details of the study cohorts are described in chapter 9 (Appendix I: Table 9.1 and Table 9.2).

Table 2.1 Characteristics of the control and AD cases include: age-at-death, gender and PMD time.

	Control (n= 48)	AD (n= 70)
Age-at-death (Years)		
Range	43-95	47-98
Mean ± SD	78.9 ±10.5	77.9 ± 10.5
Gender		
Females (%)	19 (39.58 %)	44 (62.86 %)
Males (%)	29 (60.42 %)	26 (37.14 %)
PMD (hours)		
Range	3-216	4-99
Mean ± SD	47. 5 ± 38	46.7 ± 25.7

The fixed tissue used in this study was from a cohort selected from SWDBB, University of Bristol, with local Research Ethics Committee approval. The cohort comprised a total of 7 AD cases, 7 vascular dementia (VaD) cases and 10 age-matched controls. There were no significant differences in age-at-death or PMD time between controls and AD cases (p= 0.349; p= 0.987) respectively. The demographic features of the fixed tissue cohort are summarised in Table 2.2. The details of the fixed-tssue study cohorts are described in chapter 9 (Appendix I: Table 9.3, Table 9.4 and Table 9.5).

Table 2.2 Characteristics of fixed tissue cohort. Control, AD and VaD cases include: Age-at-death, Gender and PMD time.

	Control (n= 10)	AD (n= 7)	VaD (n= 7)
Age-at-death (Years)			
Range	71-89	57-85	76-90
Mean ± SD	79.1 ± 6.22	74.86 ± 10.12	83.42 ± 4.96
Gender			
Females (%)	2 (20 %)	6 (85.71 %)	4 (57.14 %)
Males (%)	8 (80 %)	1 (14.28 %)	3 (42.86 %)
PMD (hours)			
Range	15-80	9-85	22-70
Mean ± SD	43.8 ± 21.28	44 ± 28	39.86 ± 20.33

2.2.2 Brain tissue homogenisation

Homogenates of mid-frontal cortex (Brodmann area 8/9) made from approximately 200 mg pieces of tissue that were prepared in a Precellys 24 homogenizer with 5-10 silica beads (2.3 mm) (Stretton Scientific) in either 1% SDS buffer, or 0.5% Triton X-100. The tissue was kept on ice throughout the process and homogenised using program comprising 2 rounds of 6000 revolutions-per-minute (rpm) for 15 seconds each. The resultant homogenates were then centrifuged at 13,000 x g for 15 minutes at 4°C using a refrigerated centrifuge (Eppendorf). The supernatants were sub-aliquoted into 100 µl volumes and stored at -80°C for later use.

2.3 Total protein measurement

Total protein concentrations of the tissue homogenates were made to allow for adjustments within various assays and to help with standardised loading of samples. Total protein was measured using the Total Protein Assay Kit (Sigma-Aldrich). The protein assay solution was prepared by mixing one volume of protein dye reagent with four volumes of distilled water (dH_2O). 5 µl of tissue homogenates

were diluted 1:10 in 0.85% NaCl and added in triplicate to wells on a 96 well plate. Then 5 µl of 0.85% NaCl as blank and protein standard comprising 0.3mg/ml albumin were added in triplicate to wells followed by 250 µl of the protein dye reagent. The absorbance of the samples was then read at 595 nm and the protein concentration was determined using the following formula. The sample values determined from the formula were then multiplied by the dilution factor (i.e. 10).

$$\text{Protein concentration (mg/ml)} = \frac{\text{Absorbance of sample} \times \text{Concentration of standard (0.3mg/ml)}}{\text{Absorbance of standard}}$$

2.4 Western blotting

Western blotting was used to identify the presence of specific proteins in tissue homogenates and cell lysates, as well as help determine the specificity of antibodies. In this technique, specific proteins are separated by gel electrophoresis according to molecular weight. The samples are then transferred to a nitrocellulose membrane by a blotting approach that relies on capillary action and then the nitrocellulose membranes processed to eventually yield a visible band of measurable weight for each protein. This was made possible by allowing the membrane to be incubated with specific antibodies to allow the detection and visualisation of the target protein band.

2.4.1 Gel electrophoresis

Samples of tissue homogenates or cell lysates were diluted (1:2) in SDS sample buffer (reducing buffer) that was prepared prior to use by adding 25 µl of β-mercaptoethanol (Sigma-Aldrich, UK) to 475 µl SDS reducing buffer under a fume hood. Samples were boiled at 95°C for 5 minutes and then allowed to cool at room temperature and spun briefly in a bench top centrifuge. A total volume of 25 µl per sample and 5 µl of a molecular weight ladder (Precision Plus Protein™ WesternC™; Bio-Rad Laboratories) was added into respective wells in a 4-20% Tris-HCl pre-cast gels (Mini-PROTEAN® TGX™; Bio-Rad Laboratories). The electrophoresis module (Mini-PROTEAN® 3; Bio-Rad Laboratories) was used to separate the proteins using 1x running buffer. After loading the samples into wells, the module was ran at 150 V for 1 hour.

2.4.2 Blotting

The electrophoretic transfer cell (Mini Trans-Blot®; Bio-Rad Laboratories) was used to transfer proteins from the gel to a nitrocellulose membrane. The gel and the membrane were placed between two filter papers and two filter pads to form a gel sandwich within the gel holder cassette. The cassette was placed in the transfer cell tank and filled up with 1x blotting buffer and a small magnetic stirrer with an ice pack were used to cool the transfer process. The gel was blotted at 150 V for 1 hour.

2.4.3 Protein detection

The membrane was washed briefly in 0.05% TBST and incubated with 10% milk/TBST blocking buffer for 1 hour. The membrane was washed in 0.05% TBST (3x 15 minutes) at room temperature on a shaker. The membrane was then incubated with primary antibody diluted in 5% milk/TBST antibody buffer overnight at 4°C (in the fridge) on a shaker. The membrane was washed in 0.05% TBST (3x 15 minutes) at room temperature on a shaker. Next, the membrane was incubated with peroxidase-labelled secondary antibody for 1 hour at room temperature on the shaker. After 3 x 15 minutes washing steps with 0.05% TBST, a chemiluminescent HRP substrate (ECL) (Millipore) was added to the membrane in a 1:1 ratio (5 ml of reagent 1 and 5 ml of reagent 2) for 5 minutes. Excess substrate was removed and the membrane was carefully placed on the centre of the imaging platform which was then smoothed out with a roller to remove any bubbles and ensure a uniform imaging. The resultant images were captured using ChemiDoc XRS+ and Image Lab software, version 0.5 (Bio-Rad).

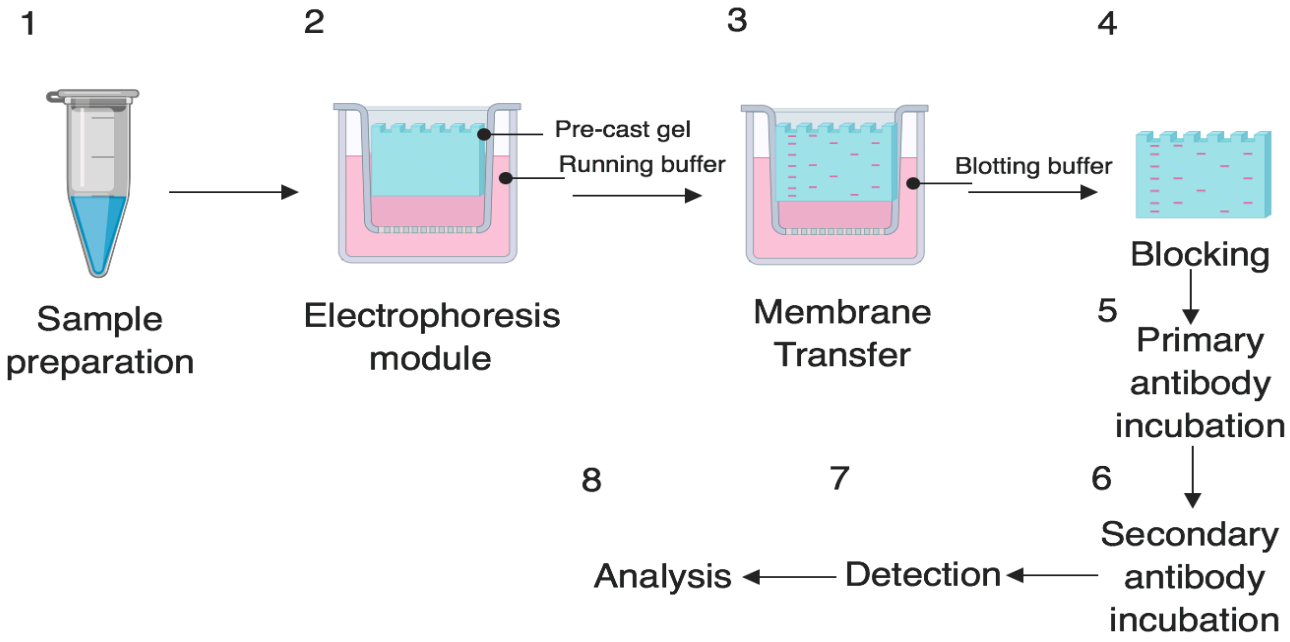

Figure 2.1 Summary of Western blotting technique.

2.5 Immunohistochemistry

Immunohistochemistry (IHC) is a specific method used to detect and examine the cellular distribution of proteins of interest in formalin-fixed brain tissue or frozen tissue. In this thesis the descriptions of IHC relate only to formalin fixed tissue.

2.5.1 Slide preparation

Microscope slides (1.0-1.2mm square) (Cell Path) were soaked overnight in 10% decon detergent, then washed in 60°C running water for 1 hour. The slides were then rinsed with distilled water and dried in an oven at 60°C overnight. After drying overnight, the slides were immersed for 15 seconds in different solutions: 2% APES, ethanol and distilled water. The slides were then dried at 40°C for 24 hours and stored in boxes until used.

2.5.2 Tissue preparation

A total of 5 sections (7 μm in thickness) were cut using a sledge microtome (LEICA Biosystems) from paraffin-embedded wax blocks of fixed brain tissue of mid-frontal cortex (Brodmann area 8/9). The sections were collected on APES-coated slides and dried at 40°C overnight and stored in boxes at room temperature until used. The slides were incubated at 60°C for 24 hours prior to IHC.

2.5.3 Immunolabelling

After overnight incubation at 60°C, the slides were dewaxed 2 $_X$ 5 minutes in clearene and dehydrated 2_X 5 minutes in 100% ethanol. Endogenous peroxidase activity was blocked by immersing the slides in 3% hydrogen peroxide in methanol for 90 minutes. After washing in running tap water for 10 minutes, a pre-treatment step was undertaken (sections were immersed in either EDTA or citrate buffer and boiled for 10 minutes in a microwave). The sections were then washed in running tap water for 5 minutes before equilibration in PBS. Non-specific binding was blocked by incubation with normal blocking serum (Vectastain®) for 20 minutes. The sections were incubated with a primary antibody against MasR, IRAP and neurolysin respectively and incubated overnight (see primary antibody list, Table 2.4). A control slide was incubated with PBS only and was included in each experiment. On the second day of immunolabelling, sections were rinsed in two changes of PBS for 3 minutes each and incubated with Vectastain biotinylated universal secondary antibody for 20 minutes. After another wash in two changes PBS for 3 minutes each, sections were incubated with VectaElite Avidin-biotin complex (ABC) for 20 minutes, rinsed again and incubated with diaminobenzidine (DAB) for 10 minutes. The sections were again washed in running water for 10 minutes after incubation with DAB and immersed in copper sulphate solution for 4 minutes followed by further washing in running water for 5 minutes. The sections were then counterstained with haematoxylin Gill II for 3 seconds, dehydrated, cleared and mounted.

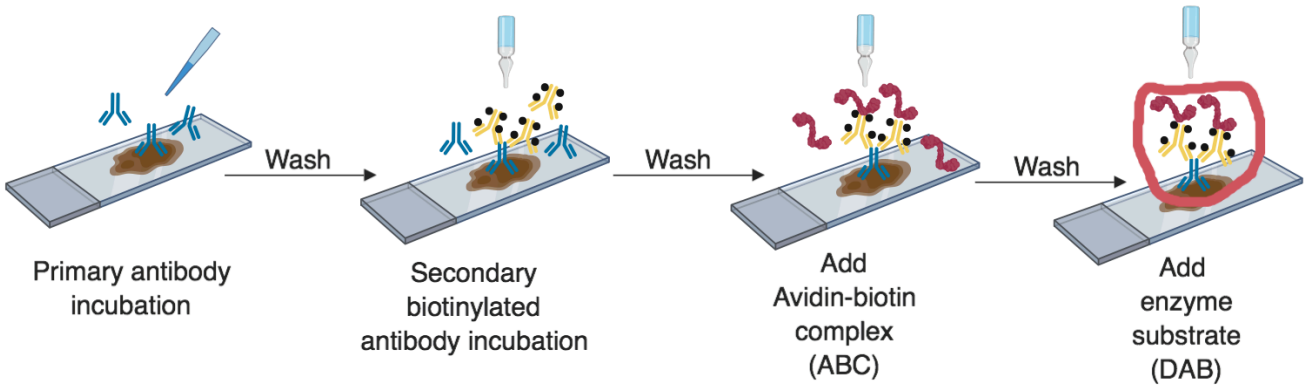

Figure 2.2 Immunolabelling sections based on ABC method with VECTASTAIN® Elite ABC kit.

2.6 ACE-1 domain specific activity assay

An ACE-1 activity assay was previously developed by Dr. Scott Miners using a fluorescence resonance energy transfer (FRET) substrate Abz-FRK(Dnp)p-OH for somatic ACE-1 (78). This FRET assay is a sensitive method for quantitative measurement of ACE-1 enzyme activity, using a FRET substrate containing o-aminobenzoic acid (Abz) as a fluorescence group (donor) and 2,4-dinitrophenyl (Dnp) as the quencher acceptor. ACE-1 enzyme activity is related to the fluorescence generated due to the breakdown of the peptide bond between the donor and acceptor pair. This assay measured total ACE-1 activity but did not discriminate between domains. In this study, we aimed to measure ACE-1 N-domain and C-domain activity using selective FRET substrate for N-domain (Abz-SDK(Dnp)-p) and for C-domain (Abz-LFK(Dnp)-OH trifluoroacetate salt) (536).

2.6.1 ACE-1 N-domain fluorogenic activity assay

ACE-1 N-domain activity was measured in 1% SDS homogenates using an N-domain-specific fluorogenic peptide substrate (Abz-SDK(Dnp)-p (Enzo Life Sciences). The assay was performed in black FlouroNUNC 96-well plates. Captopril (10 µl), an ACE-1 inhibitor, at concentration of 10 µM was added to all wells to be inhibited and 10 µl of dH_2O was added to all paired uninhibited wells. 50 µl of brain tissue homogenate (27.5 µl in 82.5 µl PBS) and a serial dilution of recombinant human

ACE (1000-15.625 ng/ml) (R&D systems) were prepared in a total volume of 50 µl and added in duplicate and incubated for 10 minutes at 37°C in either captopril or dH_2O. The N-domain-specific fluorogenic peptide substrate (Abz-SDK(Dnp)-p was diluted (5:200) in N/C domain assay buffer and 50 µl of the diluted substrate was added to each well and incubated in the dark at 37°C. Fluorescence was measured with excitation at 320 nm and emission at 405 nm in a fluorescent plate reader a FLUOstar OPTIMA (BMG Labtech) at 10, 15, 30 minutes and 1 hour.

2.6.2 ACE-1 C-domain fluorogenic activity assay

ACE-1 C-domain activity was measured in 1% SDS homogenates using a C-domain-selective fluorogenic peptide substrate Abz-LFK(Dnp)-OH Trifluroacetate) (Sigma-Aldrich). The assay was performed in black FlouroNUNC 96-well plates. Captopril (10 µl) (ACE-1 inhibitor) at a concentration of 10 µM was added to all wells to be inhibited and 10 µl of dH_2O was added to all paired uninhibited wells. Brain tissue homogenate (27.5 µl in 82.5 µl PBS) and a serial dilution of recombinant human ACE (1000-15.625 ng/ml) (R&D systems) respectively were prepared in a total volume of 50 µl and added in duplicate and incubated with captopril and dH_2O for 10 minutes at 37°C. The C-domain-specific fluorogenic peptide substrate Abz-LFK(Dnp)-OH Trifluroacetate) was diluted (5:200) in the N/C domain assay buffer and 50 µl of the diluted substrate was added to each well and incubated in the dark at 37°C. Fluorescence was measured with excitation at 320 nm and emission at 405 nm in a fluorescent plate reader a FLUOstar OPTIMA (BMG Labtech, UK) at 10, 15, 30 minutes and 1 hour.

2.6.3 ACE-1 N-domain immunocapture-based FRET assay

ACE-1 N-domain activity was measured using an immunocapture-based FRET assay. Mouse monoclonal anti-human ACE (R&D systems) diluted in PBS (0.5 mg/ml) was coated on a Nunc MaxiSorp 96-well plate overnight at room temperature. The plate was washed five times with wash buffer (0.05% Tween 20 in PBS) and blocked by addition of PBS:1% bovine serum albumin (BSA) for 2 hours at room temperature. After another wash step, serial dilutions of recombinant human ACE (1000-15.625 ng/ml) (R&D systems) and 100µl of 1% SDS brain tissue homogenates diluted (1:17) in PBS were incubated at 26°C with continuous shaking (300 rpm) for 2 hours. After the plate was washed a further five times, 40µl assay buffer was added to each well and 10µl of Captopril (10uM) or 10µl of distilled water was added to inhibited and uninhibited wells respectively and incubated for 10

minutes at 37°C. Fluorogenic substrate Abz-SDK(DnP)-P (Enzo Life Sciences) (0.68 mM) diluted in N/C domain assay buffer was added and incubated at 37°C in the dark. Fluorescence was measured with excitation at 320 nm and emission at 405 nm in a FLUOstar OPTIMA plate reader (BMG labtech). Each sample was measured in duplicate and the activity was calculated after subtracting the fluorescence in the captopril samples. A serial dilution of ACE-1 was used to minimise variation between plates.

2.6.4 ACE-1 C-domain immunocapture-based FRET assay

ACE-1 C-domain activity was also measured by immunocapture-based FRET assay. Mouse monoclonal anti-human ACE (R&D systems) diluted in PBS (0.5 mg/ml) was coated on Nunc MaxiSorp 96-well plate overnight at room temperature. The plate was washed five times with wash buffer (0.05% Tween 20 in PBS) and blocked by addition of PBS:1% BSA for 2 hours at room temperature. After another wash step, serial dilutions of recombinant human ACE (500-7.8125 ng/ml) (R&D systems) and 100µl of 1% SDS brain tissue homogenates diluted (1:5) in PBS were incubated at 26°C with continuous shaking (300 rpm) for 2 hours. After the plate was washed a further five times, 40 µl assay buffer was added to each well and 10 µl of Captopril (10 µM) or 10 µl of distilled water was added to the inhibited and uninhibited wells respectively and incubated for 10 minutes at 37°C. Fluorogenic substrate (Abz-LFK(Dnp)-OH trifluoroacetate salt) (Sigma-Aldrich) (0.14 mM) diluted in N/C domain assay buffer was then added to each well and incubated at 37°C in the dark. Fluoroscence was measured with excitation at 320 nm and emission at 405 nm in a FLUOstar OPTIMA plate reader (BMG labtech) after 24 hours incubation at 37°C.

2.7 Direct ELISA

Ang-I and Ang (1-7) levels were measured by direct Enzyme linked immunosorbant assay (ELISA) in human brain tissue. Both assays were developed in-house by Dr. Scott Miners and Noura AL Mulhim. A direct ELISA is a type of ELISA used for detection of specific enzyme labelled antigen-antibody complex in biological samples such as brain tissue homogenates to allow accurate quantification of a protein of interest (Figure 2.3).

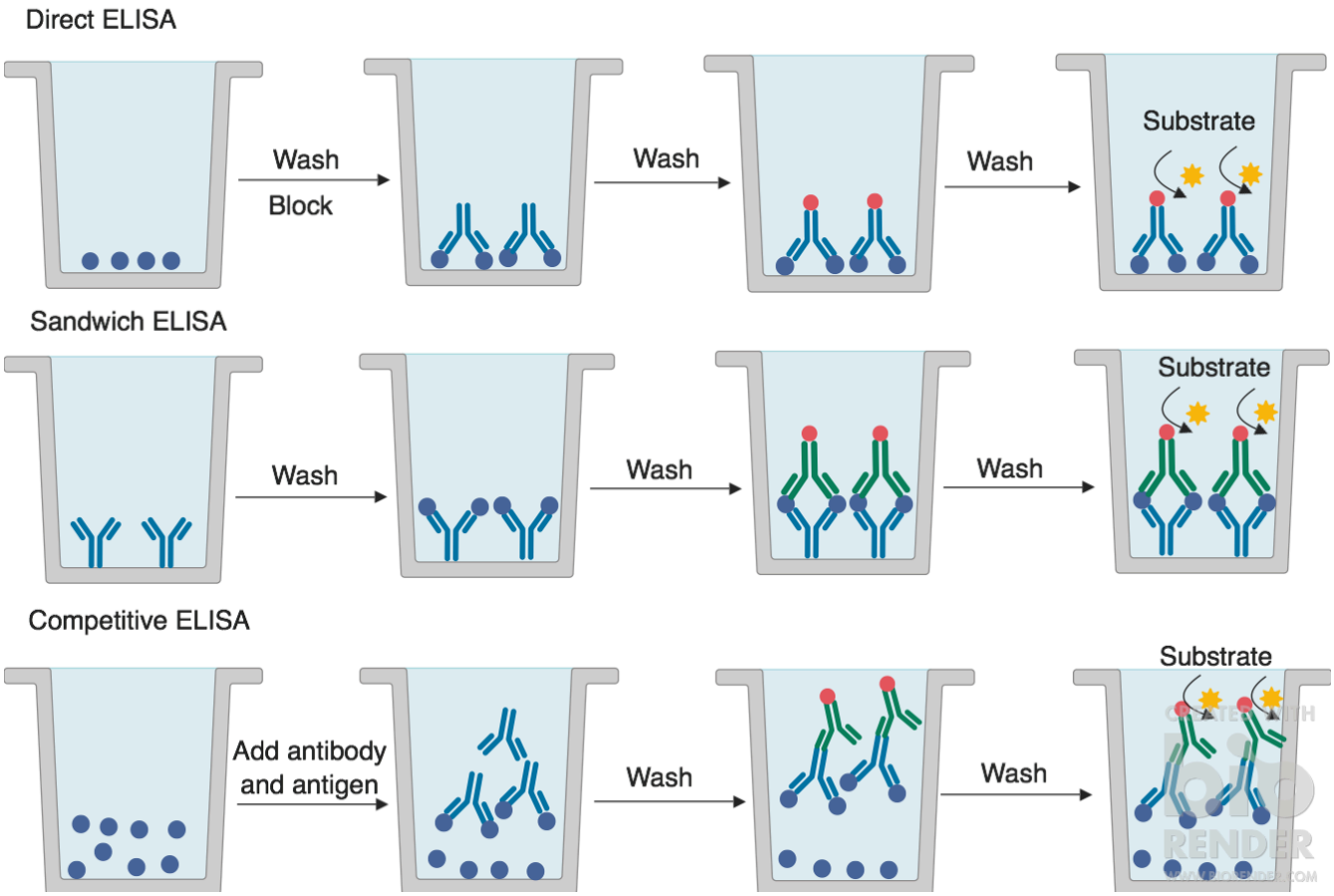

Figure 2.3 Summary of general steps for a direct ELISA, sandwich ELISA and competitive ELISA.

2.7.1 Angiotensin I direct ELISA

Ang-I levels were measured in human brain tissue homogenates prepared in 1% SDS lysis buffer. The measurements were performed using an in-house direct ELISA. A two-fold serial dilution of recombinant human Ang-I (625-9.76 pg/ml) and human brain tissue homogenates (diluted 1 in 25 in PBS) were added into a clear, high-binding capacity 96-well plate (Nunc® MaxisorpTM; Fisher Scientific) and incubated for 2 hours at 26°C with shaking. The wells were washed five times with wash buffer (0.05% Tween 20 in PBS) and then blocked with 1% BSA in PBS for 1 hour at 26°C with shaking. The wells were washed five times with wash buffer and incubated with biotinylated anti-human Ang-I (1:100 in PBS) (Cloud-Clone Corp) for 2 hours at 26°C with shaking. After another five washsteps, 100 µl of Strep-HRP (1:200) in PBS were added to each well and incubated for 20 minutes at room temperature in dark. The wells were washed five times and 100 µl of tetramethylbenzidine (TMB) substrate (R&D Systems) was added to each well and left in the dark for 20 minutes and the

reaction was stopped by adding 50 µl of 2N sulphuric acid (stop solution). The absorbance was read at 450 nm using a FLUOstar OPTIMA plate reader (BMG labtech). Each sample was measured in duplicate. Concentrations were interpolated from standard curve interpolation generated from serial dilutions of recombinant human Ang-I.

2.7.2 Angiotensin (1-7) direct ELISA

Ang (1-7) levels were measured in human brain tissue homogenates in 1% SDS lysis buffer. Five-fold serial dilutions of recombinant human Ang (1-7) (5000-0.32 pg/ml) and human brain tissue homogenates (diluted 1 in 40 in PBS) were used with the biotin-linked polyclonal detection antibody to Ang (1-7) (200 µg/ml) diluted 1:100 in PBS. First, 100 µl of recombinant human Ang (1-7) and diluted homogenates (1:67) were incubated for 2 hours at 26°C with shaking. After five washing steps, the wells were blocked for 1 hour in 1% BSA-PBS (300 µl). Following five washes, 100 µl of biotin-linked polyclonal antibody to Ang (1-7) was added to each well and incubated for 2 hours at 26°C with shaking. The wells were washed and incubated with strep-HRP (1:200) in PBS at room temperature for 20 minutes in dark. Then, following a further wash step, TMB substrate was added and incubated in the dark for 20 minutes. Finally, the reaction was terminated by adding 50 µl of stop solution to each well and the absorbance was read at 450 nm using a FLUOstar OPTIMA plate reader (BMG labtech). Each sample was measured in duplicate. Concentrations were determined by interpolation of standard curve generated from serial dilution of recombinant Ang (1-7). Carry-overs samples in each plate were used to adjust for any plate-to plate variation.

2.8 Sandwich ELISA

A sandwich ELISA is another form of quantitative and highly sensitive technique used for the detection and quantification of a specific antigen in a biological sample using two specific antibodies. A microplate is first coated with a 'capture' antibody specific for a protein (antigen) of interest. Any remaining binding sites are blocked using a suitable blocking buffer e.g. BSA. In commercial kits, plates are normally supplied pre-coated and blocked. Standards and samples are then added into the wells and any antigen presented binds to the capture antibody. After removing any unbound substances and washing, a specific 'detection' antibody (raised against a different epitope on the same target protein) is then added into the wells. An enzyme-linked secondary antibody is then used to bind the detection antibody which is followed by the addition of a substrate to allow detection of the secondary antibody. The amount of colour change detected is in proportion of the amount of bound target antigen in the samples (Figure 2.3).

2.8.1 MasR sandwich ELISA

MasR protein levels were measured using a commercially available quantitative sandwich ELISA (MyBiosource). The assay was performed following the manufacturer's protocol. 50 µl of undiluted brain tissue homogenates, 50 µl of serial diluted standards (1000-31.2 pg/ml) and 50 µl of sample diluent as a blank were added to the respective wells. 100 µl of HRP-conjugated reagent was added to each well then incubated for 1 hour at 37°C. After 4 washes step using proprietary wash buffer, 50 µl of chromogen A and chromogen solution B was added to each well and incubated for 15 minutes at 37°C. The reaction was stopped by adding 50 µl of stop solution. Absorbance was measured at 450 nm using a FLUOstar OPTIMA plate reader (BMG labtech). Each sample was measured in duplicate. Concentrations of MasR were interpolated from standard curve generated from serial diluted standards. Carry-overs samples in each plate were used to measure and adjust for plate-to plate variation.

2.8.2 Angiotensin IV sandwich ELISA

Commercial sandwich ELISA kits were used for measuring Ang-IV level in brain tissue homogenates according to the manufacturer's protocol (MyBioSource). All reagents were allowed to reach a room temperature (18 -25°C). 50 µl of each of the following was added to wells: sample diluent as blank,

serial dilution of standards (1000-31.2 pg/ml) and undiluted 1% SDS brain tissue homogenates. HRP-conjugated reagent (100 µl) was added to each well then incubated for 1 hour at 37°C. Following 4 washing steps, 50 µl of chromogen A and chromogen B solution (1:1) was added to each well and incubated for 15 minutes at 37°C in the dark. A 50 µl of stop solution was added to each well to stop the reaction. Absorbance was measured at 450 nm using a FLUOstar OPTIMA plate reader (BMG labtech). Each sample was measured in duplicate. Concentrations were determined by interpolation of standard curve generated by dilution of recombinant Ang-IV. Carry-overs samples in each plate were used to measure and adjust for plate-to plate variation.

2.8.3 IRAP sandwich ELISA

IRAP levels were measured using a commercial sandwich ELISA kit able to quantified IRAP in human tissue homogenates and other biological fluids (Cloud-Clone Corp.). This kit is supplied with a microplate pre-coated with an antibody specific to IRAP. The assay was performed following the manufacturer's protocol. All reagents were allowed to reach room temperature before use. Serial diluted standards (10-0.156 ng/ml), standard diluent as a blank and brain tissue homogenates diluted (1:10) in PBS (all 100 µl) were incubated for 1 hour at 37°C. After aspiration, 100 µl of detection reagent A was added to each well and incubated for 1 hour at 37°C. Following three washes, 100 µl of detection reagent B was added to each well and incubated for 30 minutes at 37°C. After five washes, 90 µl of Tetramethylbenzidine (TMB) substrate solution was added to each well and incubated for 20 minutes at 37°C in the dark. Absorbance was measured at 450 nm using a FLUOstar OPTIMA plate reader (BMG labtech) after adding 50 µl of stop solution to each well. Each sample was measured in duplicate. Concentrations were interpolated from standard curve interpolation generated from serial diluted standards. Carry-overs samples in each plate were used to measure and adjust for plate-to plate variation.

2.8.4 Neurotensin sandwich ELISA

The level of neurotensin was measured in 1% SDS brain tissue homogenates using a commercially available quantitative sandwich ELISA kit (CUSABIO). Following the manufacturer's protocol, all reagents were allowed to reach a room temperature before use. Human neurotensin standard (1000-15.6 pg/ml), standard diluent as a blank and tissue homogenates diluted (1:10) in sample diluent (all

100 µl) were incubated for 2 hours at 37°C. After aspiration, 100 µl of biotin-labelled detection antibody was added to each well and incubated for 1 hour at 37°C. Following three wash steps, HRP-avidin (100 µl) was added to each well and incubated for 1 hour at 37°C. Washes were repeated five times before adding 90 µl of TMB substrate to each well and incubated for 30 minutes at room temperature in the dark. 50 µl of stop solution was added to each well to stop the reaction. Absorbance was measured at 450 nm using a FLUOstar OPTIMA plate reader (BMG labtech). Each sample was measured in duplicate. Concentrations were determined by interpolation of standard curve generated from serially diluted standards. Carry-overs samples in each plate were used to measure plate-to plate variation.

2.8.5 Human Vascular Endothelial Growth Factor (VEGF) sandwich ELISA

A commercially available DuoSet ELISA kit (R&D systems) was used to measure VEGF level in 1% SDS brain tissue homogenates. The assay was performed following the manufacture's protocol. A 96-well microplate was coated with mouse anti-human VEGF capture antibody diluted 1:120 to the working concentration (1.00 µg/ml) and incubated overnight at room temperature. After 4 washes, the plate was blocked with 300 µl/well of blocking buffer (1% BSA in PBS) and incubated for 1 hour at 26°C with agitation. Following 4 washing cycles with washing buffer, a 100 µl of two-fold serial dilutions of human VEGF standard (2000-31.3 pg/ml), brain tissue homogenates diluted in 1% BSA in PBS (1:10) and PBS:BSA blanks were added to respective wells and incubated for 2 hours at 26°C with agitation. After 4 further washes, 100 µl of biotinylated human VEGF detection antibody (100 ng/ml) diluted (1:60) was added to each well and incubated for 2 hours at 26°C with agitation. 100 µl of Strep-HRP diluted (1:40) was added to each well and incubated in the dark at room temperature for 20 minutes. After the last wash step, 100 µl of Substrate A and B in a 1:1 ratio was added to each well and incubated in dark for 20 minutes. Absorbance was measured at 450 nm using a FLUOstar OPTIMA plate reader (BMG labtech) after adding 50 µl of stop solution to each well. Each sample was measured in duplicate. Concentrations were interpolated from standard curves generated from serial diluted standards. Carry-overs samples in each plate were used to measure plate-to plate variation.

2.8.6 Human Proteolipid Protein 1 (PLP1) sandwich ELISA

PLP1 level was measured in 1% SDS brain tissue homogenates using a commercially available sandwich ELISA kit (Cloud-clone Corp.). The assay was performed according to the manufacturer's protocol. All reagents were brought at room temperature before use. Recombinant PLP (10-0.156 ng/ml), diluted samples (1:50) in PBS and a PBS blank (all 100 µl) were added to microplate pre-coated with an antibody specific to PLP1 and incubated for 1 hour at 37°C. Following five wash steps, a 100 µl of detection reagent A was added to each well and incubated for 1 hour at 37°C. After another five wash steps, a 100 µl of detection reagent B was added to each well and incubated for 30 minutes at 37°C. After further wash steps, 90 µl of TMB substrate was added to each well and incubated for 10 minutes at 37°C in the dark. The reaction was stop by adding 50 µl of stop solution and the absorbance was measured at 450 nm using a FLUOstar OPTIMA plate reader (BMG labtech). Each sample was measured in duplicate. Concentrations were determined by interpolation of standard curve generated from serially diluted standards. Carry-over samples on each plate were used to measure and adjust for plate-to plate variation.

2.8.7 Neurolysin competitive ELISA

Neurolysin concentration was measured in 1% SDS human post-mortem brain tissue homogenates using a competitive ELISA kit (MyBioscource) (see Figure 2.3 for general description of a competitive ELISA). The assay was performed following the manufacturer's protocol. Recombinant neurolysin (10-0 ng/ml), diluted samples (1:10) in PBS, and a PBS blank, were incubated with NLN-HRP conjugate in a pre-coated plate for 1 hour at 37 °C. Following 5 wash steps, 50 µl of chromogen A and chromogen solution B (1:1) was added to each well and incubated for 15 minutes at 37°C. A 50 µl of stop solution was added to each well to stop the reaction. Absorbance was measured at 450 nm using a FLUOstar OPTIMA plate reader (BMG labtech). Each sample was measured in duplicate. Concentrations were interpolated from standard curve generated from serial diluted standards. Carry-overs samples in each plate were used to measure plate-to plate variation.

2.10 IRAP activity assay

IRAP enzyme activity was determined in brain tissue homogenates prepared in 0.5% Triton X-100 buffer using a substrate, L-Leucine-p-nitroanilide (L-Leu-pNA) (Sigma-Aldrich) as previously described (464). 50 µl of brain tissue homogenates diluted (1:20) in Tris assay buffer (0.05 M Tris, 0.14 M NaCl, pH 7.4) were incubated with 200 µl of L-Leu-pNA (1mM) diluted (1:16) in assay buffer at 37°C in 96-well plates. Absorbance was measured at 405 nm after 1 hour, 90 minutes and overnight.

2.11 Cell culture

Cell culture is the technique of growing live cells within a controlled and sterile environment. Cells can be derived directly from source tissue (primary cells) or originated from continuous immortalised cell lines. In this section, general methods used to grow and maintain healthy cell cultures and preparing cell lysate are discussed in detail. All work was conducted in a class II laminar flow hood (Holten) to maintain a sterilised air flow. The hood was switched on for 15 minutes before use and UV light was used to sterilise the surface for 15 minutes before and after use. Prior to work, pipette tips, tubes, reagents and the hood surface were sprayed with 70% ethanol solution.

2.11.1 Cell line

SH-SY5Y neuroblastoma cells (European Collection of Authenticated Cell Cultures (ECACC) were used in this experiment. The culture medium to maintain SH-SY5Y cells was Dulbecco's modified Eagle's medium (DMEM) consisting of amino acids, salts (calcium chloride, potassium chloride, magnesium sulphate, sodium chloride, and monosodium phosphate), glucose, vitamins (folic acid, nicotinamide, riboflavin, B12), iron and phenol red) (Sigma-Aldrich) and supplemented with 15% foetal bovine serum (Sigma-Aldrich) and 2 mM L- Glutamine (Sigma-Aldrich).

2.11.2 Growing cells and maintaining healthy cell cultures

Culture medium, PBS and other solutions were warmed in water bath to 37°C for 30 minutes prior to use. T75cm^3 flasks (Greiner Bio-One: T75; surface area of 75 cm^2) were used to grow cells after adding 10 ml of growth medium. Vial of cells were carefully removed from storage and warmed in a

water bath to 37°C for 1 minute. 1 ml of cells was transferred into the flask and gently agitated from side to side, then placed in incubator under conditions set to a temperature 37°C and 5% CO_2 overnight. The treating freezing medium, which contains Dimethyl Sulfoxide (DMSO), was replaced the next day with fresh 10 ml DMEM. Every two days the growth medium was replaced until cells reached 90% confluent then cells were either used for experimentation or passaged.

2.11.3 Cell Passaging

Cells were passaged when approximately 90% confluent. Old growth medium was aspirated and the flask was washed with 10 ml pre-warmed PBS. After removal of PBS, 3 ml Trypsin with EDTA (Sigma-Aldrich) was added to detach cells from the flask surface following 5 minutes. incubation at 37°C. 7 ml of fresh pre-warmed complete growth medium (to neutralise trypsin) was added to the flask. The cell suspension was transferred into 15 ml centrifuge tube and centrifuged for 3 minutes at 1000 x g. The cell medium was aspirated with a glass pipette and the pelleted cells were mixed with 1.0 ml of fresh complete growth medium. 200 µl of cell suspension was added into new labelled flasks prepared with 10 ml of fresh growth medium. Flasks then placed into the incubator and media changed every tow days.

2.11.4 Preparation of cell lysates

Following the experiment (details described later in chapter 9). Medium from each flask was transferred into 10 ml centrifuged tube and stored at -80°C. Cells were washed with 10 ml sterile PBS and following aspiration of PBS, 3 ml of accutase (Sigma-Aldrich) was added and the flask was incubated for 5 minutes to detach the cells. 7 ml of PBS was then added into each flask and the solution was transferred to a 10 ml tube and spun for 3 minutes at 1000 x g. The supernatant was carefully aspirated and the cell pellet was collected and lysed using 70 µl of cell lysis buffer (CelLytic M reagent (Sigma-Aldrich). Cell lysates were left at incubator (26°C) with shaking for 1 hour (as per manufacturer's instruction) before the tube was stored at -80 °C. Total protein concentrations of the cell lysates were measured using the Total Protein Assay Kit (Sigma-Aldrich) (previously described in detail in section (2.3)).

2.12 Statistical analysis

Statistical tests were performed using either SPSS (version 21) or GraphPad Prism version 7. Normal distribution of all data sets was tested with the Shapiro-Wilk normality test and presented in chapter 9 (Appendix III). If the data sets were normally distributed, an unpaired samples t-test was used to compare one variable between control and AD groups. For correlation between two variables, a Pearson's correlation coefficient was used. One-way ANOVA with Dunnett's post-hoc was used to compare differences between three groups.

When the data sets were not normally distributed, non-parametric tests were used to identify differences between two groups (control vs. AD) using the Mann-Whitney U test. For correlations using non-parametric data, the Spearman's correlation coefficient was used. A non-parametric equivalent of an analysis of variance (ANOVA), the Kruskal-Wallis test with Dunn's post-hoc test was used to determine if there is an overall significant difference between three groups. Log transformation or square-root transformation was performed to attempt to reach normal distribution. Parametric tests were performed on the transformed data and presented in chapter 9 (Appendix VI). For all data sets, the Robust regression and Outlier removal (ROUT) method was used to detect outliers in all datasets and in case of outliers, the data was re-analysed after outliers were removed and presented in chapter 9 (Appendix VII). For all tests applied, a P-value < 0.05 was considered statistically significant.

Chapter 3. The classical axis of RAS in Alzheimer's disease - investigating the divergent role of ACE-1 in AD

3.1 Abstract

The cRAS (ACE-1/Ang-II/AT_1R) within the brain is overactive in AD and ACE-1, the central enzyme involved in the production of Ang-II, is increased in AD (78, 393). Despite a central role in the production of Ang-II, the role of ACE-1 remains unclear since it has also been shown to cleave Aβ42 in to less harmful shorter Aβ fragments that are less toxic and more easily cleared (83). ACE-1 consists of two homologous N- and C-domains, which show different substrate specificities. The N-domain is mainly involved in Aβ degradation whereas the C-domain is largely responsible for Ang-II production. This apparent divergent role of ACE-1 in the pathogenesis of AD may be explained by the domain-specific actions of ACE-1 in AD.

Human post-mortem brain tissue was obtained from the SWDBB, University of Bristol, with local Research Ethics Committee approval. We studied mid-frontal cortex (Brodmann area 8/9) from AD cases (n= 70) and age-matched controls (n= 48) that were matched closely for age-at-death and PMD. ACE-1 N-domain and C-domain activities were measured using specific fluorogenic substrates and immunocapture-based enzyme activity assays. Ang-I level was measured using a direct ELISA method for all cases. Previous measurement of ACE-1 activity (total), Ang-II, parenchymal Aβ and tau load, and ELISA-measurements of insoluble Aβ40 and Aβ42 concentrations were previously measured and available for further analysis.

ACE-1 C-domain activity was significantly elevated in AD and ACE-1 N-domain activity was significantly reduced in AD compared to age-matched controls. Ang-I level was reduced and the ratio of Ang-II:Ang-I was increased in AD - as would be expected with overactivation of ACE-1. Together, these novel data indicate a disease-related alteration of domain-specific activity of ACE-1 in AD that potentially favours Ang-II production and limits Aβ42 clearance. These data provide further mechanistic insight into the role of ACE-1 in AD and suggest that selective inhibitors of ACE-1 C-domain could prove to be a more effective treatment strategy for AD compared to non-domain specific ACEIs currently being investigated.

3.2 Introduction

The RAS is implicated in the pathogenesis of AD (56, 537). Overactivation of cRAS within the brain, in regions associated with disease pathology and cognition, is associated with the pathogenesis of AD. ACE-1 is the rate-limiting enzyme in the production of Ang-II, which, via activation of AT_1R, is thought to be primarily responsible for most AD-related pathology. Previous human post-mortem studies have shown that elevated ACE-1 activity and increased Ang-II level in AD are associated with increased Aβ and Tau levels (reviewed in (538)). Infusion of Ang-II in aged SDR elevated the formation of Aβ (238) and mediated phosphorylation of tau (390) indicating the direct involvement of cRAS in disease pathology in addition to vaso-modulatory influences.

Previous evidence ranging from genetic, cell-culture based, animal, epidemiological, and human post-mortem studies have supported an association between ACE-1 activity and disease progression in AD (78, 84, 347, 354, 367, 539, 540). Moreover, epidemiological population-based studies and clinical-based studies have provided evidence that ACEIs or ARBs delay the progression of cognitive decline and reduce the incidence of AD (367, 369, 406, 541). In addition, several animal studies show that brain-penetrating ACEIs such as captopril and perindopril or AT_1R blockers, such as losartan, olmesartan and valsartan protect against cognitive decline and AD-related disease pathology (359-362). Some of these animal studies have, however, highlighted potential differences between the effectiveness ACEIs and ARBs (358, 522) whilst others e.g. Ferrington *et al.* (363) did not find any alteration in either intraneuronal Aβ or oligomeric Aβ levels in a triple transgenic mouse model of AD after administration of ACEI (Captopril) and ARBs (eprosartan and valsartan). The discrepant findings to date may simply relate to variation in the drug treatment periods and modes of administration and differences in the animal models used and it is noteworthy that on balance the vast majority of studies agree to the potential protective effect of these drugs against AD. Clarification may yet emerge from ongoing exploratory clinical trials in humans testing various rRAS inhibitor drugs in AD and AD-related clinical populations (reviewed in (538)). In summary, most of the data support a role of ACE-1 in cRAS overactivation in support of the detrimental effects of Ang-II overproduction in the pathogenesis of AD.

The *ACE1* was first reported to be a genetic risk factor for AD by Kehoe *et al.* (84). The study reported that an insertion (I)/ deletion (D) polymorphism of an Alu repeat sequence within intron 16 of *ACE1* was associated with AD risk. Furthermore, this association has been demonstrated by several subsequent genetic studies that indicate that inheritance of the (I) allele increased the risk for AD,

whereas homozygosity of the (D) allele was protective (85, 86, 88, 89). This genetic relationship has continued to be published over a period of almost two decades (155). Furthermore, there is a gene dose-dependent partial association between *ACE1* genotypes and ACE-1 activity, such that possession of an I/I genotype is associated with the lowest peripheral plasma ACE-1 activity, homozygotes for DD with the highest levels and heterozygotes having intermediate levels (352). This was initially puzzling with respect to how an *ACE1 II* genotype i.e. lower ACE-1 activity, was associated with increased AD risk. However, our previous studies in brain tissue indicate that brain ACE-1 activity does not simply match serum changes. In this study, Miners and colleagues (90) found that (II) genotype and other nearby SNPs on *ACE1* were associated with increased levels of soluble Aβ in AD. This data indicates that ACE-1 may be involved in Aβ clearance, which is supported, by *in vitro* studies and data from animal models of AD. Hu and colleagues (81) reported that ACE-1 was able to degrade Aβ in vitro. Several other *in vitro* and *in vivo* studies also supported these findings (82, 347). Zou and colleagues (83) found that ACE-1 was able to convert the long neurotoxic species of Aβ (Aβ42) to a short and less neurotoxic species (Aβ40) and that administration of captopril (ACEI) into mice resulted in elevated Aβ deposition. These findings placed a different perspective on the how risk variants in *ACE1,* which ordinarily might be associated with lower levels of ACE-1, are associated with AD. These findings also posed a suggestion that the inheritance of *ACE1* I alleles may be associated with an individual's reduced capacity to degrade Aβ throughout life which may contribute to or exacerbate the development of AD.

As previously described, ACE-1 within the brain comprises N- and C- catalytic domains that have different substrate specificities (332). The N-domain favours cleavage of Aβ at Asp5His6, as well as having endopeptidase activity that promotes the conversion of Aβ42 to Aβ40, whilst the C-domain is reported to preferentially convert Ang-I to Ang-II. However, not all studies supported the reported dual properties of the N- and C- domains and some have suggested that both domains participate to similar extents in Aβ degradation (345, 346). Until now, this has remained an unresolved controversy concerning the involvement of ACE-1 in AD, where it may also have a bearing on the sometimes conflicting findings as to the involvement of different ACEIs in conferring protection (360, 361, 364, 542, 543) or increased risk (368, 544) in the incidence and progression of AD.

3.3 Study aims and hypothesis

In this chapter, I have explored the hypothesis that there is domain-specific variation in ACE-1 activity in AD such that N-domain activity (favouring Aβ-degradation) is decreased and C-domain activity (favouring Ang-II production) is increased in AD compared to age-matched controls and that changes in ACE-1 domain activity will be related to markers of disease pathology in AD.

The aims of the study were:

(i) To measure ACE-1 N-domain and C-domain activities in post-mortem brain tissue homogenates from mid-frontal cortex of human AD and control brains and explore the relationship between ACE-1 domain specific activities and AD pathological hallmarks (Aβ and tau).

(ii) To measure Ang-I level and through access to existing data on Ang-II, examine whether the Ang-II:Ang-I ratio is a proxy indicator of ACE-1 activity and to determine whether changes in Ang-I level, or the Ang-II:Ang-I ratio, were associated with AD pathological hallmarks (Aβ and tau).

3.4 Methods

3.4.1 Study cohort

Human post-mortem brain tissue homogenates from mid-frontal cortex (Brodmann area 8/9) were used for measurements of ACE-1 N-domain activity, C-domain activity and Ang-I level. The study cohort included controls (n= 48) and AD cases (n= 70). Demographic features of study cohort are described in chapter 2 (Table 2.1) for full details (Appendix I: Table 9.1 and Table 9.2).

3.4.2 ACE-1 N-domain fluorogenic activity assay

Measurements of ACE-1 N-domain activity in brain homogenates from mid-frontal cortex were described in the general methods (section 2.6.1). In this experiment, brain homogenates were prepared

in 0.5% Trition X-100 buffer, as described in the methods (section 2.2.2). The N-domain specific fluorogenic substrate (Abz-SDK(Dnp)-p (Enzo Life Sciences) was optimised before use in this experiment (see results section (3.5.1)). Samples were measured in triplicate and four carry-overs samples were repeated in each plate.

3.4.3 ACE-1 C-domain fluorogenic activity assay

The ACE-1 C-domain activity was measured in brain homogenates prepared as previously described in the general methods (section 2.2.2). Brain homogenates used in this experiment were homogenised in 0.5% Trition X-100 buffer. Different dilutions of C-domain specific fluorogenic substrate (Abz-LFK(Dnp)-OH Trifluroacetate) (Sigma-Aldrich) were tested prior to use in this assay (see results section (3.5.2)). ACE-1 C-domain activity was measured using the method described in the methods (section 2.6.2). Samples were measured in triplicate and four carry-overs samples were repeated across all plates.

3.4.4 ACE-1 N-domain immunocapture-based FRET assay

An immunocapture-based FRET assay, in which ACE-1 was isolated prior to addition on the FRET substrate (to improve specificity), was developed to measure ACE-1 N-domain activity using the N-domain specific fluorogenic substrate (Abz-SDK(Dnp)-p (Enzo Life Sciences). The details of the assay were described in the general methods (section 2.6.3). The N-domain activity was measured in brain tissue homogenates from mid-frontal cortex homogenised in 1% SDS lysis buffer. The homogenisation process was described in the methods (section 2.2.2). The assay conditions, such as optimising the concentration of N-domain specific fluorogenic substrate (Abz-SDK(Dnp)-p (Enzo Life Sciences) and the effect of time on reaction were tested prior to use in this assay (Appendix II: Figure 9.5). Samples were measured in triplicate and four carry-overs samples were repeated across all plates.

3.4.5 ACE-1 C-domain immunocapture-based FRET assay

An ACE-1 C-domain immunocapture enzyme activity assay, in which specificity was improved by capturing ACE-1 prior to the addition of the FRET substrate, was developed measure C-domain activity. The general method using an immunocapture-based FRET assay is described in detail in method (section 2.6.4). Brain homogenates used in this experiment were from mid-frontal cortex and homogenised in 1% SDS lysis buffer described previously in the methods (section 2.2.2). The assay conditions e.g. substrate concentration and incubation times were optimised (Appendix II: Figure 9.6) prior to use. ACE-1 C-domain activity was measured in triplicate and four carry-overs samples were repeated across all plates.

3.4.6 Angiotensin I direct ELISA

The concentration of Ang-I was measured in each sample in brain homogenates from mid-frontal cortex prepared in 1% SDS as previously described in the general methods (section 2.2.2). Ang-I level was measured using a direct ELISA method. A general description of the method has been described in method (section 2.7.1). Ang-I measurement was adjusted for total protein level to account for any variation in total protein between samples. The method used for total protein measurement is described in the methods (section 2.3). Samples were measured in duplicate and four carry-overs samples were repeated across all plates.

3.4.7 Statistical analysis

The distributions of all datasets were initially analysed by the Shapiro-Wilk normality test. A p value, $p < 0.05$ indicated that the data sets were not normally distributed. The ACE-1 N-domain activity assay, ACE-1 C-domain activity assay and Ang-I direct ELISA data did not follow a normal distribution (even after log transformation for ACE-1 C-domain activity assay) (Appendix III: Table 9.21) and therefore comparisons of the data (ACE-1 N-domain activity, ACE-1 C-domain activity and Ang-I level) between controls and AD cases were tested with a non-parametric test, Mann-Whitney test. Comparison of the data between Braak tangle stage groups (Braak stage 0-II, Braak stage III-IV, Braak stage V-VI) was performed with a non-parametric Kruskal-Wallis test and Dunn's post-hoc test

was used to determine if there was an overall significant difference between the three groups. Correlations of ACE-1 N-domain activity and ACE-1 C-domain activity data with total Aβ load, tau load, insoluble Aβ40, insoluble Aβ42, confounding factors (age-at-death, PMD) were assessed by the Spearman's correlation coefficient. Association of ACE-1 N-domain activity and ACE-1 C-domain activity with gender and *APOE* genotype were explored using a Mann-Whitney test. The relationship between Ang-I level, total Aβ load, tau load, confounding factors (age-at-death, PMD) and ACE-1 activity were assessed using the Spearman's correlation coefficient. Associations of Ang-I level with gender and *APOE* genotype were explored using a Mann-Whitney test. Also, comparison of Ang-II:Ang-I ratio between controls and AD cases was analysed using a non-parametric Mann-Whitney test. Log transformed data for ACE-1 N-domain activity and Ang-I level is presented in chapter 9 (Appendix VI: Section 9.6.1). For all tests applied, a p-value < 0.05 was considered statistically significant.

For all datasets, the ROUT method was applied to detect outliers. In datasets where outliers were removed, the data was re-analysed and the data is presented in chapter 9 (Appendix VII: Section 9.7.1)

3.5 Results

3.5.1 Optimisation of ACE-1 N-domain activity

Preliminary experiments were performed to optimise the ACE-1 N-domain enzyme activity assay using the domain-selective substrate (Abz-SDK(Dnp)-p in human brain tissue homogenates (Appendix II: Figure 9.1). The concentration of the FRET substrate, inhibitor and the effect of time on substrate cleavage were characterised (Appendix II: Figure 9.2). The variation between measurements was determined by calculating the coefficient of variation (CV%) (Appendix IV: Table 9.22). Optimal conditions identified from these preliminary experiments were substrate concentration at (10 μM) inhibitor at (10 μM) and time at (2 hours) at 37°C (that are used in subsequent experiments). Activity was expressed as relative fluorescence units (r.f.u).

3.5.1.1 Comparisons of ACE-1 N-domain FRET activity between control and AD

ACE-1 N-domain activity in the mid-frontal cortex was compared between AD cases and age-matched controls. The median for ACE-1 N-domain activity in the AD group (13728 (r.f.u)) was numerically lower than in controls (15229 (r.f.u)) after 2 hours. However, a Mann-Whitney test showed that this difference was not statistically significantly different between the groups (p= 0.981) (Figure 3.1).

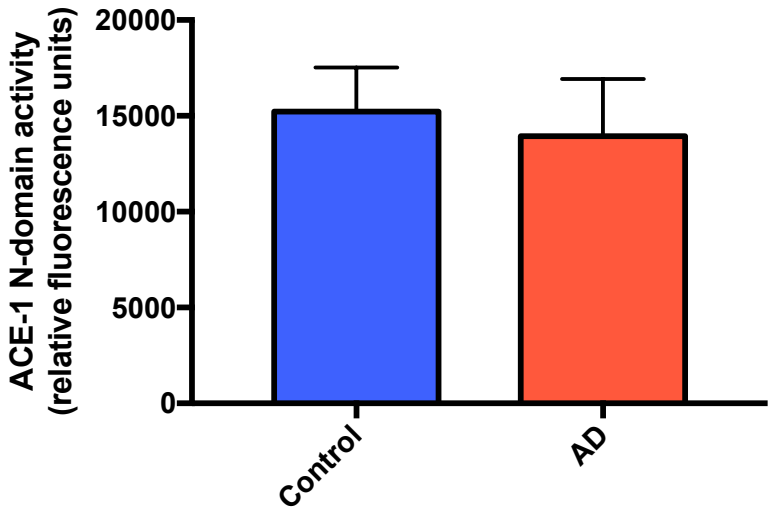

Figure 3.1 ACE-I N-domain activity in AD cases compared to controls.

Bar chart showing ACE-1 N-domain activity in AD (n= 70) compared to age-matched controls (n= 48) in the mid-frontal cortex measured using an ACE-1 N-domain fluorogenic activity assay. Mann-Whiney test showed no significant difference between groups (p= 0.981). Bars show the median and 95% confidence intervals.

3.5.1.2 ACE-1 N-domain FRET activity in relation to disease severity

ACE-1 N-domain activity was not found to change in relation to Braak tangle stage pathology (0-II, III-IV and V-VI) (p = 0.783) (Figure 3.2). The median values according to Braak stages were: 0-II = 15267 (r.f.u), III-IV = 15233 (r.f.u) and V-VI = 13707 (r.f.u). Although there appeared to be a numerical reduction in Braak stage V-VI compared to the other groupings, this was not found to be statistically significant.

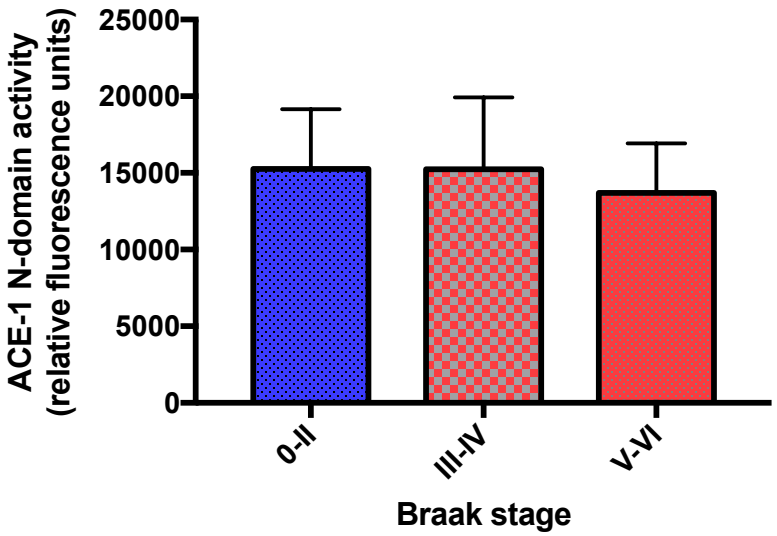

Figure 3.2 ACE-1 N-domain activity in relation to Braak tangle stage.

Bar chart showing relationship between ACE-1 N-domain activity and Braak tangle stage. No significant differences (p= 0.783) were found by Kruskal-Wallis test for ACE-1 N-domain activity between Braak tangle stages 0-II (n= 36), III-IV (n= 20), V-VI (n= 61). The bars indicate the median values and 95% confidence intervals.

3.5.2 Optimisation of ACE-1 C-domain activity

Preliminary experiments were first performed to optimise the use of the C-domain substrate (Abz (LFK(DnP)-OH Trifluroacetate) in human brain tissue homogenates. First, the optimal concentration of the FRET substrate was determined and the effect of incubation time on the reaction was characterised (Appendix II: Figure 9.3). Range of captopril concentrations was also tested (Appendix II: Figure 9.4). The variation between duplicate measurements was determined by calculating the intra-assay CV% (Appendix IV: Table 9.23). The resultant optimal conditions included using a substrate concentration at (10 μM), a concentration of inhibitor at (10 μM) and an assay time at (2 hours) at 37°C (these conditions were used for all subsequent assays). Activity was expressed as r.f.u.

3.5.2.1 ACE-1 C-domain FRET activity in control and AD

In mid-frontal cortex, ACE-1 C-domain activity measured by FRET activity assay was compared between AD cases (n=70) and controls (n=48). The median for ACE-1 C-domain activity was numerically higher in AD cases (7088 r.f.u) compared to controls (5938 r.f.u). However, a Mann-Whitney test showed that there was no statistical significant difference in enzyme activity between groups (p= 0.132) (Figure 3.3).

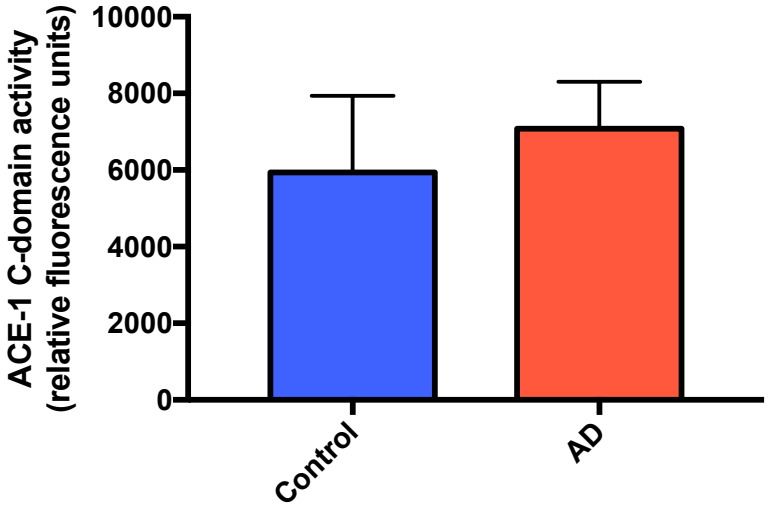

Figure 3.3 ACE-1 C-domain activity in control and AD cases.

Bar chart showing ACE-1 C-domain enzyme activity in AD (n= 70) compared to age-matched controls (n= 48) in the mid-frontal cortex measured using an ACE-1 C-domain fluorogenic activity assay. Mann-Whitney test showed no significant difference between groups (p= 0.132). Bars show the median and 95% confidence intervals.

3.5.2.2 ACE-1 C-domain FRET activity in relation to disease severity

ACE-1 C-domain activity was also examined in relation to Braak tangle stage (Braak stage 0-II, Braak stage III-IV, Braak stage V-VI) that equate to moderate/early and severe/end stage AD). A Kruskal-Wallis test revealed no statistically significant difference of the median between all groups (p= 0.466) (Figure 3.4).

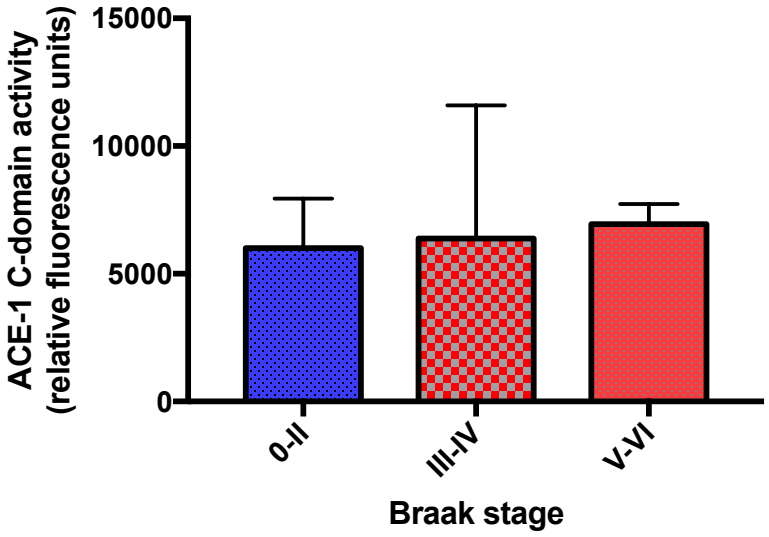

Figure 3.4 ACE-1 C-domain activity in relation to Braak tangle stage.

ACE-1 C-domain activity did not vary significantly between Braak tangle stage groups (Braak stages 0-II (n= 36), III-IV (n= 20), V-VI (n= 61)) according to Kruskal-Wallis test (p= 0.466). The bars indicate the median and 95% confidence intervals.

3.5.3 Optimisation of ACE-1 N-domain immunocapture-based activity

An assay to measure ACE-1 N-domain activity using an immunocapture-based FRET activity approach was developed. These assays benefit from using an 'immunocapture step' to pull-down and capture ACE-1 from biological samples prior to the addition of the FRET substrate and therefore reduce the risk of non-specific proteolytic cleavage of the substrate. Previous studies found that immunocapture-based fluorometric assays for the measurement of Aβ degrading enzymes (IDE and NEP) allowed sensitive and specific measurement of enzyme activity (77, 78). As before the optimal reaction conditions for the assay were first identified and a substrate concentration (0.68 mM) inhibitor (10 μM) and time (24 h) were used in subsequent experiments (Appendix II: Figure 9.5). Activity was expressed as r.f.u. Variation between measurements was determined by calculating the intra-assay CV% (Example in Appendix VI: Table 9.24).

3.5.3.1 ACE-1 N-domain immunocapture-based activity in controls and AD

The ACE-1 N-domain activity in mid-frontal cortex measured by immunocapture-based FRET activity assay showed that ACE-1 N-domain activity was significantly reduced in AD cases (n= 70) compared

to aged-mated controls (n= 48) by 49%. The Mann-Whitney test revealed that the median for ACE-1 N-domain activity in AD cases (6708 (r.f.u)) was significantly lower in AD (p= 0.024) compared to activity in controls (13248 (r.f.u)) (Figure 3.5).

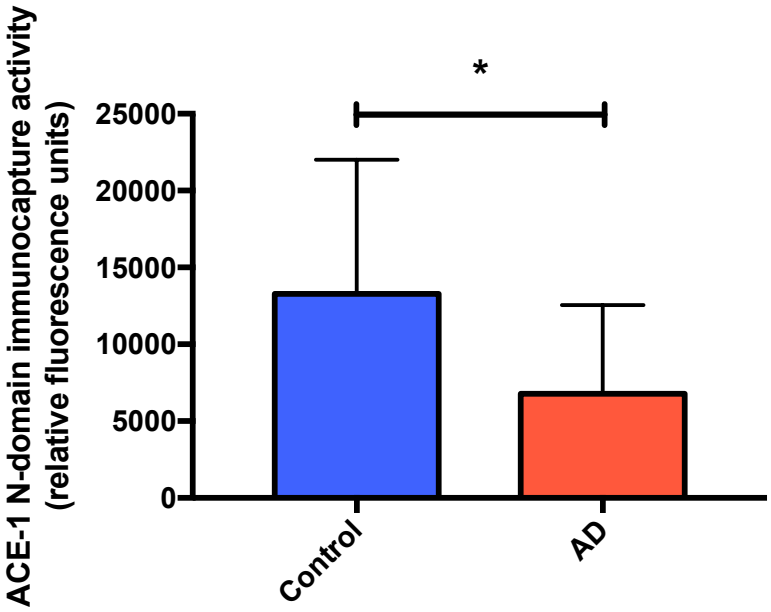

Figure 3.5 Reduction in ACE-1 immunocapture N-domain activity in Alzheimer's disease.

Bar chart showing ACE-1 N-domain enzyme activity measured by immunocapture-based FRET activity assay in AD (n= 70) compared to age-matched controls (n= 48) in the mid-frontal cortex. A Mann-Whiney test showed a significant difference between groups (p= 0.024). Bars show the median and 95% confidence intervals.

3.5.3.2 ACE-1 N-domain immunocapture-based activity in relation to disease severity

The relationship between ACE-1 N-domain activity and Braak tangle stages (0-II, III-IV, V-VI) was explored. ACE-1 N-domain activity was numerically lower in cases with end-stage AD i.e. Braak stage V-VI group compared to controls and early-mid stage AD (III-IV), however, Kruskal-Wallis test did not detect a statistical difference between the medians across all Braak stages, Kruskal-Wallis test (p= 0.126). The medians for the various Braak stages was: 0-II= 13282 (r.f.u), III-IV= 11655.1 (r.f.u), V-VI= 6336 (r.f.u) (Figure 3.6).

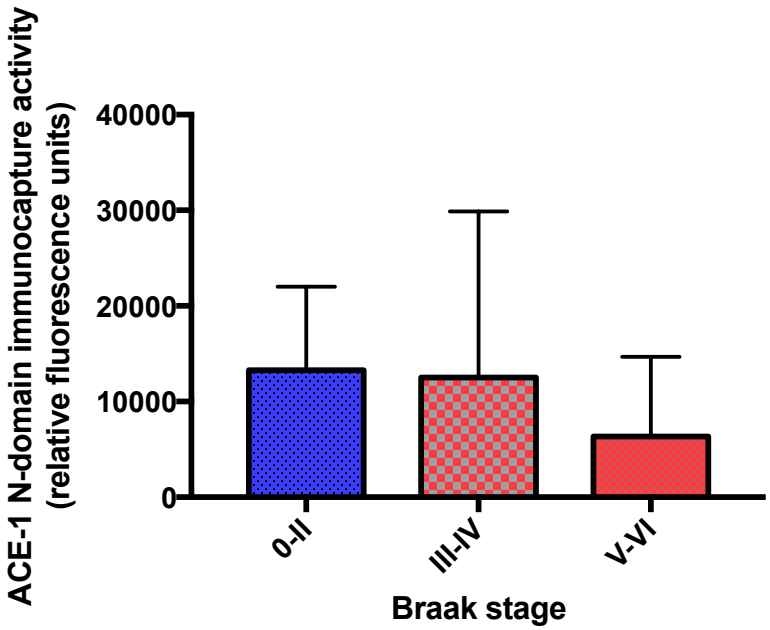

Figure 3.6 ACE-1 N-domain immunocapture-based activity in relation to disease severity.

No significant difference was found for ACE-1 N-domain activity measured by immunocapture-based activity assay between Braak tangle stage groups (0-II (n= 36), III-IV (n= 20), V-VI (n= 61)), Kruskal-Wallis test (p= 0.126). The bars indicate the median and 95% confidence intervals.

3.5.4 Optimisation of ACE-1 C-domain immunocapture-based activity

We next developed, optimised and measured C-domain activity using a more specific immunocapture-based FRET activity assay. Optimal conditions for the immunocapture C-domain activity assay were observed with substrate concentration (0.14 mM) inhibitor (10 μM) and time (24 hours) (Appendix II: Figure 9.6). Activity was expressed as r.f.u. All samples were measured in duplicate and ran alongside one sample in the presence of the inhibitor. The variation between measurements of samples was determined by calculating the intra-assay CV% (Example in Appendix IV: Table 9.25).

3.5.4.1 Comparison of ACE-1 C-domain immunocapture-based activity between controls and AD patients

In mid-frontal cortex, ACE-1 C-domain activity measured by immunocapture-based FRET activity assay was found to be significantly higher in AD cases (n= 70) compared to age-matched controls (n= 48). The median for ACE-1 C-domain activity was increased by ~30% in AD = 30656 (r.f.u) compared to controls = 23515 (r.f.u). A Mann-Whitney test detected a significant difference between the medians (p = 0.011) (Figure 3.7).

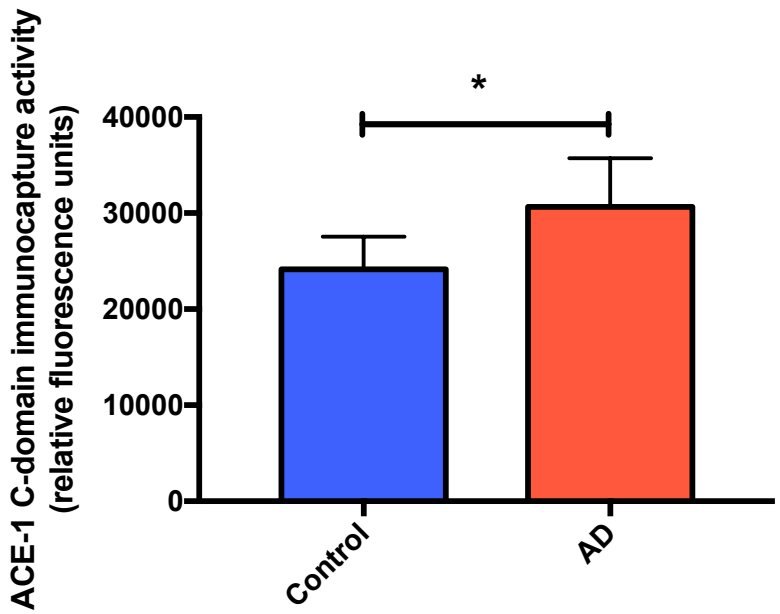

Figure 3.7 Immunocapture-based ACE-1 C-domain activity in control and AD cases.

Bar chart showing ACE-1 C-domain activity in mid-frontal cortex, measured by immunocapture-based FRET activity assay, in AD (n= 70) and age-matched controls (n= 48). Mann-Whitney test revealed that ACE-1 C-domain activity was significantly higher in the AD group compared to age-matched controls group (p= 0.011). The bars indicate the median and 95% confidence intervals.

3.5.4.2 ACE-1 C-domain immunocapture-based activity in relation to disease severity

ACE-1 C-domain activity measured by an immunocapture-based FRET activity assay was assessed in relation to Brake tangle stage (0-II (n= 36), III-IV (n= 20), V-VI (n= 61)). Kruskal-Wallis test found no significant difference of the medians between all Braak stage groups (p= 0.104) (Figure 3.8). The medians according to Braak stage were 0-II= 25597.5 (r.f.u), III-IV = 22979 (r.f.u), and V-VI = 30000 (r.f.u).

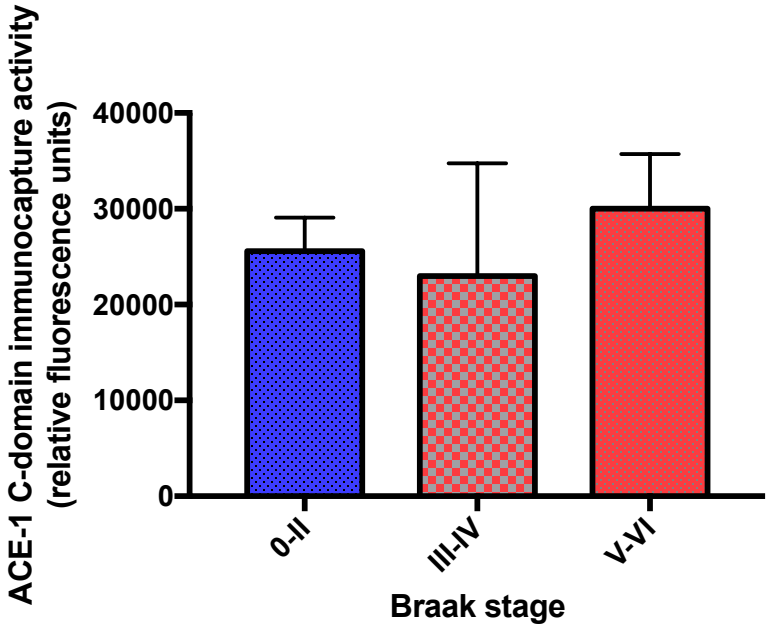

Figure 3.8 ACE-1 C-domain immunocapture-based activity in relation to Braak tangle stage.

No significant difference was found for ACE-1 C-domain activity between (Braak tangle stages 0-II (n= 36), III-IV (n= 20), V-VI (n= 61)) using a Kruskal-Wallis test (p= 0.104). The bars indicate the median and 95% confidence intervals.

3.5.4.3 Relationships between ACE-1 N- and C-domain immunocapture-based activity and AD pathological hallmarks

Given the significant differences between the ACE-1 N- and C-domains in AD cases and controls it was next important to examine the relationship between domain-specific activity and variables associated with AD pathology. The relationship between immunocapture-based ACE-1 N- and C-domain activity and previously measured guanidine Aβ (measured by ELISA) and tau load (determined by IHC-field fraction), and levels of insoluble Aβ42 and insoluble Aβ40 that were

previously measured by ELISA, were assessed. Insoluble Aβ levels measured by sandwich ELISA were available for controls (n= 28) and AD cases (n= 61)) (545) and Tau load was previously measured for all cases as part of routine pathological assessment of AD cases within the SWDBB by field fraction analysis and was available (for controls (n= 29) and AD cases (n= 89)). Both insoluble Aβ42 and insoluble Aβ40 were also previously measured by sandwich ELISA, for a subset of the cases studied (insoluble Aβ42 measures were available for controls (n= 20) and AD cases (n= 33)), as well as insoluble Aβ40 data for controls (n= 20) and AD cases (n= 34) (314).

Spearman's correlation coefficient test showed no significant correlations between ACE-1 N-domain activity and any of the AD pathological hallmarks (Figure 3.9 A-D).

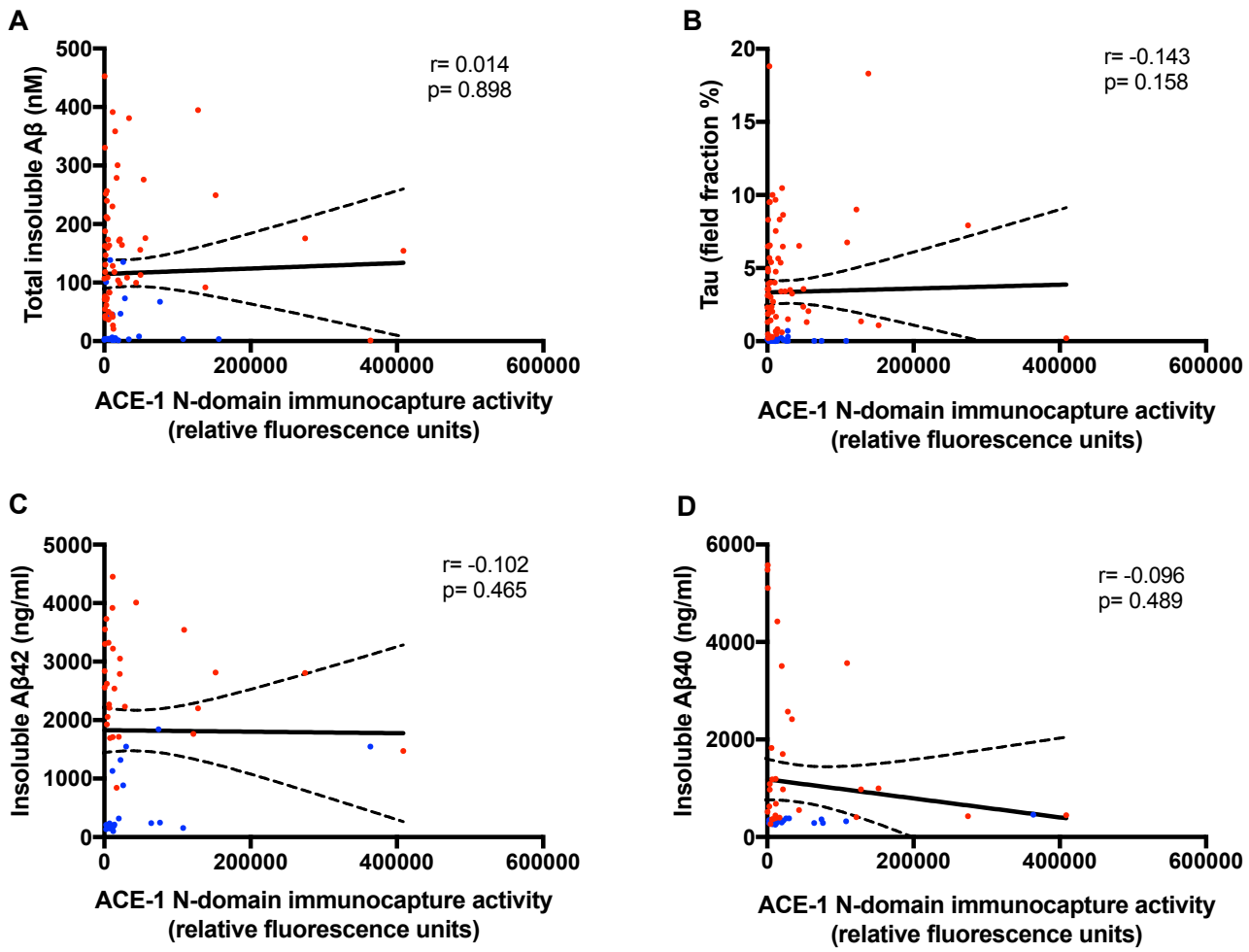

Figure 3.9 Relationships between ACE-1 N-domain activity and AD pathological hallmarks (total insoluble Aβ load, tau load, insoluble Aβ42 and insoluble Aβ40).

A. Scatterplots showing no correlation between ACE-1 N-domain activity and total insoluble Aβ load (measured by enzyme-linked immunosorbent assay), Spearman's correlation coefficient test (r= 0.014, p = 0.898). B. No significant correlation found between ACE-1 N-domain activity and tau load (measured by field fraction analysis), Spearman's correlation coefficient test (r= -0.143, p= 0.158). C-D. Scatterplots showing no correlation between ACE-1 N-domain activity and both insoluble Aβ42 and insoluble Aβ40 (measured by enzyme-linked immunosorbent assay), for insoluble Aβ42 Spearman's correlation coefficient test (r= -0.102, p= 0.465) and for insoluble Aβ40 Spearman's correlation coefficient test (r= -0.096, p= 0.489). The solid inner line indicates the best-fit linear regression and the outer lines the 95% confidence intervals. Blue dots = controls, red dots = AD cases.

ACE-1 C-domain activity was positively correlated with total insoluble Aβ load and Spearman's correlation coefficient test detected a significant relationship (r= 0.251, p= 0.017) indicate that increased ACE-1 C-domain activity in AD is associated with increased level of insoluble Aβ (Figure 3.10 A). In contrast, there was no significant correlation between ACE-1 C-domain activity and tau load (r= 0.181, p= 0.073) (Figure 3.10 B). Spearman's correlation coefficient test revealed a significant

positive correlation between ACE-1 C-domain activity and insoluble Aβ42 levels (r= 0.318, p= 0.020) (Figure 3.10 C) but no significant correlation was found for insoluble Aβ40 levels (r= 0.233, p= 0.089) (Figure 3.10 D).

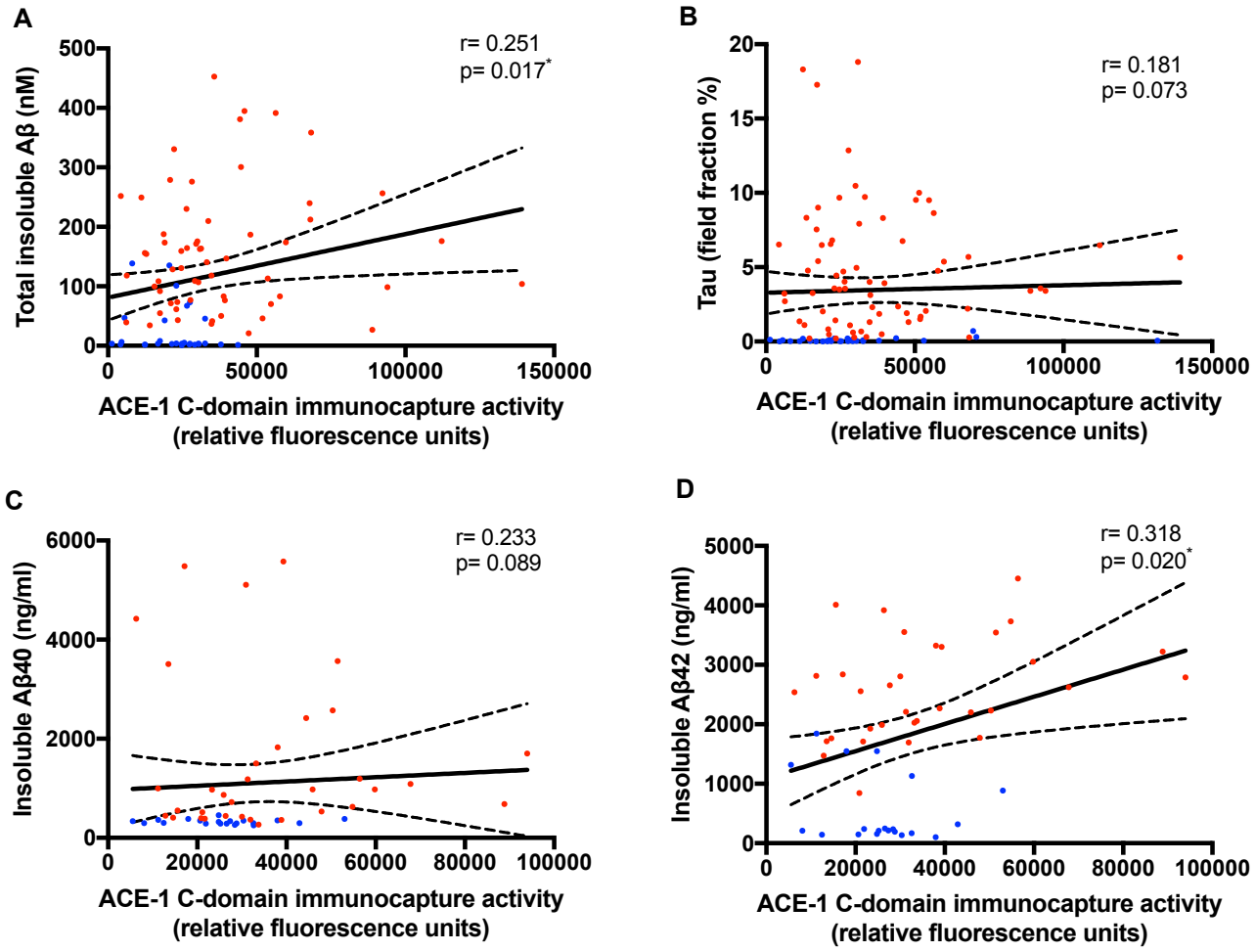

Figure 3.10 Correlations between ACE-1 immunocapture C-domain activity and AD pathological hallmarks (total insoluble Aβ load, tau load, insoluble Aβ42 and insoluble Aβ40).

A. Scatterplot showing a positive relationship between ACE-1 C-domain activity and total insoluble Aβ load (measured by enzyme-linked immunosorbent assay), Spearman's correlation coefficient test (r= 0.251, p= 0.017). B. Scatterplot showing no correlation between ACE-1 C-domain activity and tau load (measured by field fraction analysis), Spearman's correlation coefficient test (r= 0.181, p= 0.073). C. Scatterplot showing no correlation between ACE-1 C-domain activity and insoluble Aβ40 (measured by enzyme-linked immunosorbent assay), Spearman's correlation coefficient test (r= 0.233, p= 0.089). D. Scatterplot showing positive correlation between ACE-1 C-domain activity and insoluble Aβ42 (measured by enzyme-linked immunosorbent assay), Spearman's correlation coefficient test (r= 0.318, p = 0.020). The solid inner line indicates the best-fit linear regression and the outer lines the 95% confidence intervals. Blue dots = controls, red dots = AD cases.

3.5.4.4 Relationships between ACE-1 N- and C-domain immunocapture-based activity and possible confounding factors

Age and *APOE* genotype (*APOE* ε4 allele) are the major risk factors of AD and females have a higher risk for AD than males (131). PMD has been shown to affect the protein measurement (546). All these possible confounders could affect protein measurements and/or enzyme activity. The relationship between ACE-1 N- and C-domain activity, measured by immunocapture-based activity assay, and potential confounding factors including age-at-death, PMD and gender were explored. Spearman's test showed no correlations between ACE-1 N-domain activity with age-at-death or PMD. Also, there was no significant difference of ACE-1 N-domain activity between females and males (Appendix V: Table 9.37). There was no difference in ACE-1 N-domain activity depending on the presence or absence of *APOE* ε4 allele (Appendix V: Table 9.38). Spearman's test also showed no correlation between ACE-1 C-domain activity with age-at-death or PMD, or between females and males (Appendix V: Table 9.37). Also, there was no significant difference of ACE-1 C-domain activity depending on the presence or absence of *APOE* ε4 allele (Appendix V: Table 9.38).

3.5.5 Measurement of Angiotensin I level in AD

Given that Ang-I is a pre-cursor to Ang-II, mediated by the action of ACE-1 activity, it was helpful to explore the levels of Ang-I relative to Ang-II that could also serve to provide information regarding ACE-1 activity. Ang-I level in the mid-frontal cortex was measured using a direct ELISA on post-mortem brain homogenates from the cohort described. The variation of this assay was determined by calculating the intra-assay CV% (Example in Appendix IV: Table 9.26). Both unadjusted Ang-I measurements and protein-adjusted measurements were used for comparisons between control and AD. Relationships between Ang-I level and disease severity (Braak tangle stage), AD pathological hallmarks (Aβ load, Tau load) and possible confounding factors (age-at-death, PMD, gender and *APOE* genotype) were examined.

3.5.5.1 Comparisons of Ang-I level between controls and AD cases

Ang-I level was significantly reduced in the AD group compared to age-matched controls (p= 0.006) (Figure 3.11). The median for Ang-I level was lower in the AD group (median= 1546 (pg/ml)) compared to the control group (median= 1736 (pg/ml)). When Ang-I level was adjusted for total protein concentration, a significant reduction of Ang-I level was also observed in the AD group compared to age-matched controls (p= 0.013). The Mann-Whitney test allowed comparison of the median Ang-I level of the AD group (median= 4601 (pg/mg total protein)) in comparison to the control group (median= 4762 (pg/mg total protein)) (data shown in Appendix IX: Figure 9.47).

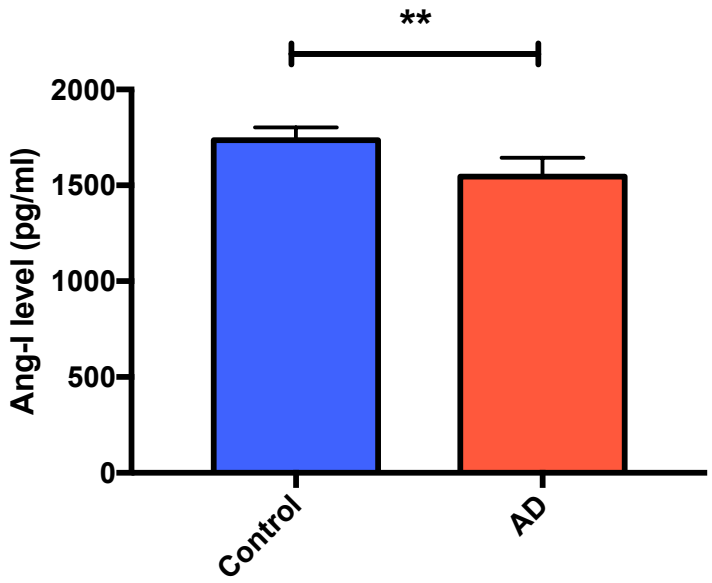

Figure 3.11 Angiotensin-I level (Ang-I) was reduced in mid-frontal cortex in Alzheimer's disease (AD).

Ang-I level was reduced in AD (n= 70) compared with age-matched control (n= 48) in mid-frontal cortex measured using an in-house Ang-I direct ELISA. Mann-Whitney test revealed that Ang-I level was significantly lower in AD (p= 0.006) compared to controls. The bars indicate the median and 95% confidence intervals.

3.5.5.2 Ang-I level in relation to disease severity

Ang-I level was assessed in relation to Braak tangle stage (0-II, III-IV, V-VI). Kruskal-Wallis test revealed a significant difference in the median between all groups (p= 0.008). Post-hoc analysis (Dunn's Test) revealed a significant reduction of Ang-I level in Braak stage (V-VI) compared to Braak stage (0-II) (p= 0.004) (Figure 3.12 A).

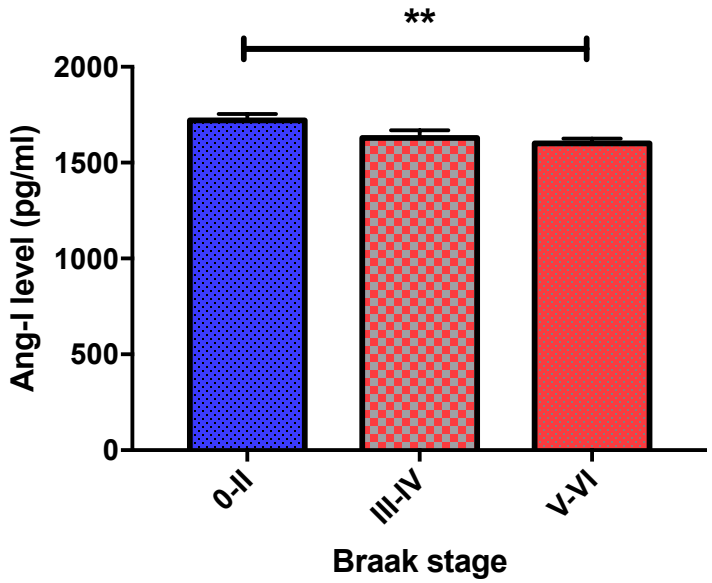

Figure 3.12 Ang-I level in relation to Braak tangle stage.

Ang-I level differed with disease severity measured by Braak tangle stage groups (0-II (n= 36), III-IV (n= 20), V-VI (n= 61)) when analysed with a Kruskal-Wallis test (p= 0.008). Ang-I level was significantly lower in cases with Braak stage (V-VI) compared with cases in Braak stage (0-II) (post-hoc Dunn's multiple comparisons test, p= 0.004). The bars indicate the median and 95% confidence intervals.

3.5.5.3 Correlation between Ang-I level and AD pathological hallmarks

Ang-I level unadjusted to protein concentration was inversely correlated with both insoluble Aβ and tau load, Spearman's correlation coefficient test found a strong inverse significant correlation between Ang-I level and insoluble Aβ (r= -0.389, p= 0.0001) (Figure 3.13 A) and between tau load (r= -0.347, p= 0.0004) (Figure 3.13 B). Correlations between protein adjusted data and AD pathological hallmarks presented in chapter 9 (Appendix IX: Figure 9.48).

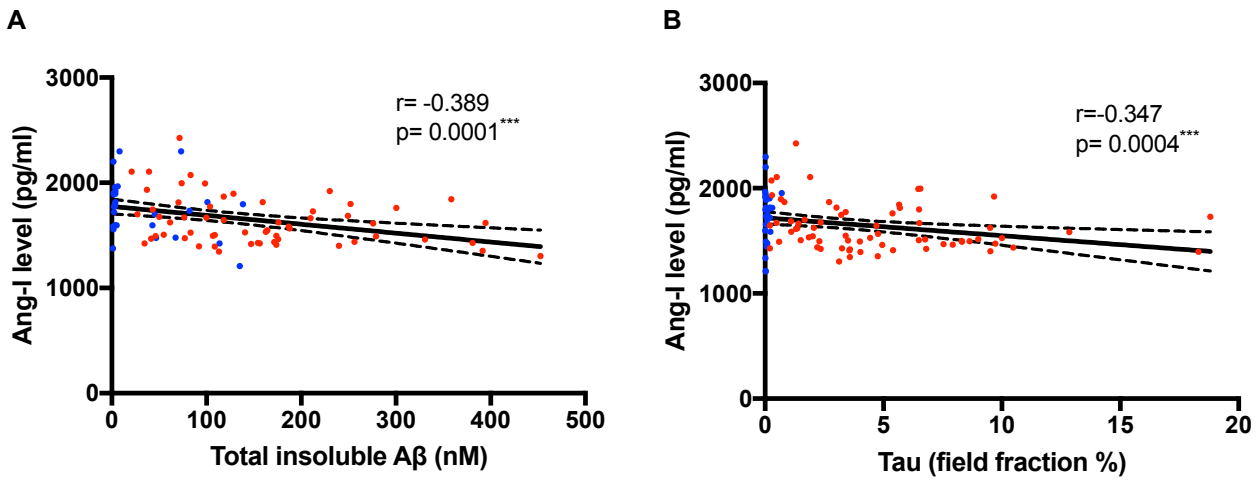

Figure 3.13 Inverse correlation between Angiotensin-I level and AD pathological hallmarks (Aβ load and tau load).

A. Scatterplot showing an inverse relationship between Ang-I level and total insoluble Aβ load (measured by enzyme-linked immunosorbent assay), Spearman's correlation coefficient test (r = -0.389, p= 0.0001). B. Scatterplot showing that Ang-I level was inversely correlated with tau load (measured by field fraction analysis), Spearman's correlation coefficient test (r= -0.347, p= 0.0004). The solid inner line indicates the best-fit linear regression and the outer lines the 95% confidence intervals. Blue dots = controls, red dots = AD cases.

3.5.5.4 Relationship between Ang-I level and ACE-1 activity

Ang-I is a major substrate for ACE-1. The relationship between Ang-I level and ACE-1 activity was assessed. Previous measurements of ACE-1 activity by FRET activity assay were available for controls (n= 43) and AD cases (n= 66) (78). Spearman's correlation coefficient test detected a weak but nonetheless significant inverse correlation between Ang-I level unadjusted to total protein concentration and ACE-1 activity (r= -0.189, p= 0.048) (Figure 3.14). Correlations between protein adjusted data and ACE-1 activity presented in chapter 9 (Appendix IX: Figure 9.49).

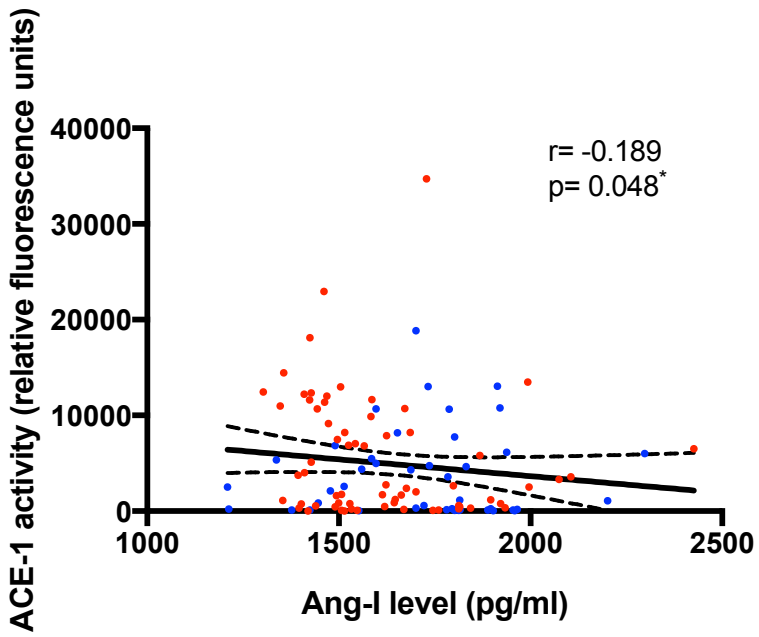

Figure 3.14 Relationship between Ang-I level and ACE-1 activity.

Scatterplot showing an inverse correlation between Ang-I level unadjusted to protein concentration and ACE-1 activity measured by FRET activity assay in mid-frontal cortex. Spearman's correlation coefficient test (r= -0.189, p= 0.048). The solid inner line indicates the best-fit linear regression and the outer lines the 95% confidence intervals. Blue dots= controls, red dots= AD cases.

3.5.5.5 Investigating the Ang-II:Ang-I ratio in AD

The Ang-II:Ang-I ratio is potentially a useful proxy marker of ACE-1 activity. The previous measurements of Ang-II level measured by sandwich ELISA were available for controls (n= 43) and AD cases (n= 70) and were showed to be significantly increased in AD (393). The median for Ang-II:Ang-I ratio was significantly increased in AD (median = 0.0131) compared to controls (median = 0.0086) indicating an increase in Ang-II relative to reduced Ang-I, which would be predicted in the presence of higher ACE-1 activity. Mann-Whitney test detected a significant p value (p= 0.0003) (Figure 3.15).

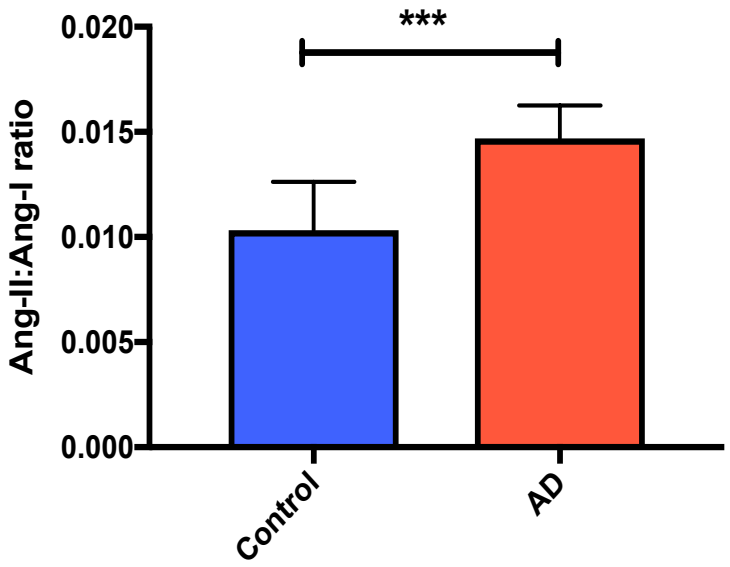

Figure 3.15 The ratio of Ang-II to Ang-I is increased in AD compared with age-matched controls.

Increased Ang-II:Ang-I ratio in AD (n= 70) compared to controls (n= 43) in mid-frontal cortex. Differences between groups were compared using Mann-Whitney test (p= 0.0003). The bars indicate the median and 95% confidence intervals.

3.5.5.6 Relationship between Ang-II:Ang-I ratio and ACE-1 activity

The Ang-II:Ang-I ratio is a potential proxy marker of ACE-1 activity. The relationship between Ang-II:Ang-I ratio and ACE-1 activity was assessed. ACE-1 activity was measured previously by FRET activity assay in controls (n= 43) and AD cases (n= 66) (78). Spearman's correlation coefficient test detected a significant positive correlation between the Ang-II:Ang-I ratio and ACE-1 activity (r= -0.229, p= 0.016) (Figure 3.16).

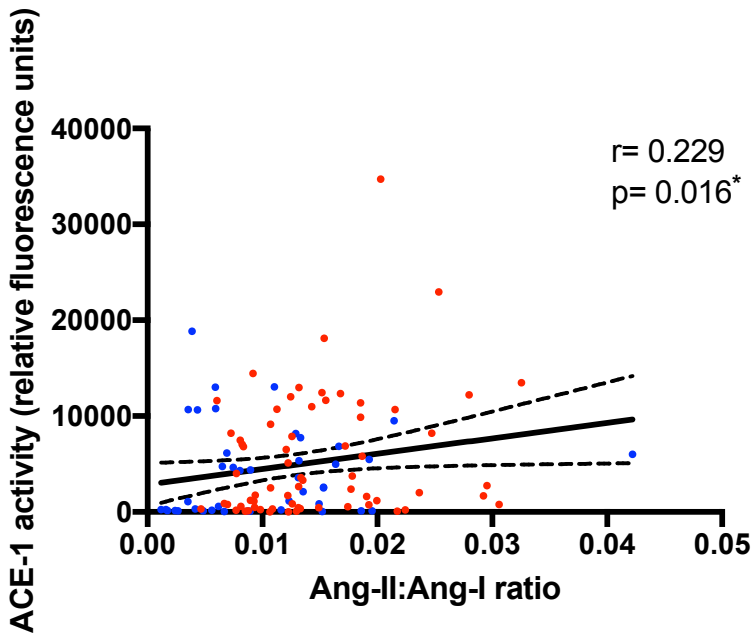

Figure 3.16 Relationship between Ang-II:Ang-I ratio and ACE-1 activity.

Scatterplot showing a positive correlation between the Ang-II:Ang-I ratio and ACE-1 activity measured by FRET activity assay in mid-frontal cortex. Spearman's correlation coefficient test (r= 0.229, p= 0.016). The solid inner line indicates the best-fit linear regression and the outer lines the 95% confidence intervals. Blue dots= controls, red dots= AD cases.

3.5.5.7 Relationship between Ang-I and APOE genotype

Ang-I level was analysed in relation to *APOE* ε4 allele for both unadjusted and protein–adjusted data. Mann-Whitney test revealed that Ang-I level unadjusted to total protein was reduced in cases with one or two *APOE* ε4 allele. The median for Ang-I level in cases with absence of *APOE* ε4 allele, median =1734 (pg/ml) was higher compared to cases with presence of one or two *APOE* ε4 allele, median = 1533 (pg/ml), (p= 0.02). There was no difference in protein-adjusted Ang-I level depending on the presence or absence of *APOE* ε4 allele (Appendix V: Table 9.38).

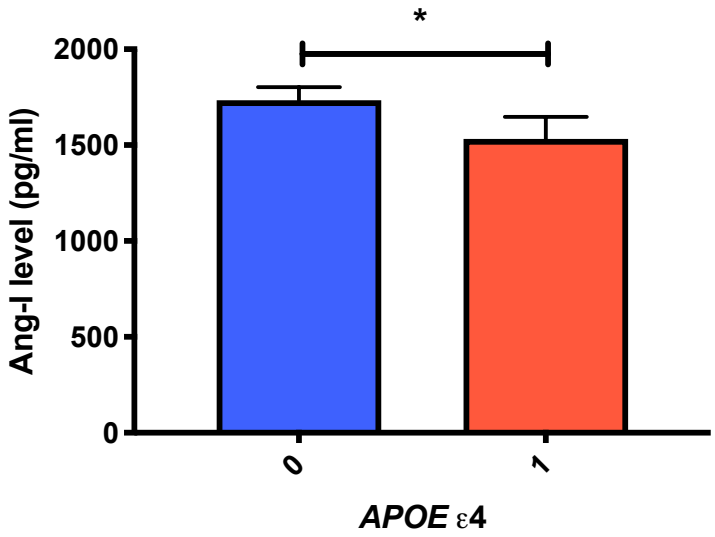

Figure 3.17 Ang-I level in relation to *APOE* genotype.

Ang-I level was significantly lower in cases with one or two *APOE* ε4 allele (1) compared with cases with absence of *APOE* ε4 allele (0). Differences between groups were compared using Mann-Whitney test (p= 0.02). The bars indicate the median and 95% confidence intervals.

3.5.5.8 Relationships between Ang-I level and confounding factors

The potential relationships between Ang-I level and protein-adjusted Ang-I level data with confounding factors of age-at-death, gender and PMD were investigated. There was no correlation between both unadjusted and protein-adjusted levels of Ang-I with age-at-death or PMD. Similarly, there was no significant difference in Ang-I level between males and females for either comparison of Ang-I levels (Appendix V: Table 9.37).

3.6 Discussion

This chapter involved an in-depth study of ACE-1 in relation to AD and explored the association between ACE-1 activity and pathological hallmarks of AD. The first question we sought to determine was whether changes in ACE-1 N-domain and C-domain activities were apparent in AD compared to controls and then we assessed the relationship between these domain-specific activities and AD pathological hallmarks. Secondly, we determined whether Ang-I level, as the precursor to Ang-II and a main substrate of ACE-1, and the Ang-II:Ang-I ratio (a potential proxy marker of ACE1 activity),

were altered in AD in relation to pathological hallmarks of AD. The latter provided an alternative means to explore ACE-1 activity and allow the determination of whether these measurements were potentially useful proxy markers of ACE-1 activity. The data highlighted divergent changes in ACE-1 domain activity that suggest that in AD there are disease-specific alterations in ACE-1 domain activity that potentially favour increased Ang-II production and interfere with Aβ degradation. The data also indicate that Ang-I level was reduced and the Ang-II:Ang-I ratio was increased in AD and may be a useful proxy marker of ACE-1 activity.

ACE-1 is the central and rate-limiting enzyme in the classical RAS pathway. It is responsible for the generation of Ang-II and total ACE-1 activity is elevated in AD in relation to parenchymal Aβ level (78). ACE-1 also cleaves and degrades Aβ42, facilitating its removal from the brain. This apparent divergent role of ACE-1 in AD underpins the complex relationship between ACE-1 and cRAS activation in AD. Here, we show that ACE-1 C-domain activity, largely responsible for converting Ang-I to Ang-II (547), is elevated in AD. Overactivation of C-domain activity would support an idea that elevated Ang-II mediated AT_1R signalling contributes to AD progression in accordance with the angiotensin hypothesis of AD (393). We also found that ACE-1 C-domain activity positively correlated with insoluble total Aβ and insoluble Aβ42 level but not with Aβ40 level or tau load. Ang-II mediated AT_1R activation, which has been shown to cause increased Aβ expression in adult SDR by stimulating amyloidogenic processing of APP metabolism (238) may be responsible for the positive correlations with Aβ. No significant association was found between ACE-1 C-domain activity in mid-frontal cortex and Braak tangle stage, age-at-death, PMD, gender or APOE genotype.

ACE-1 has been shown to degrade Aβ peptides in various pre-clinical investigations. Cleavage products of Aβ are less toxic and more easily cleared. Several *in vitro* studies found that ACE-1 was involved in the degradation of Aβ peptides (81-83, 345, 346) and in some animal studies, ACE-1 inhibitor administration is associated with elevated Aβ-related pathology (519, 548). The N-domain has been reported to favour Aβ degradation (82, 343, 549). We report novel evidence in post-mortem brain tissue of reduced N-domain activity that was associated with AD. We hypothesised that reduced N-domain activity could contribute to elevated Aβ in AD, however surprisingly and contrary to expectations, we did not find any significant correlations with N-domain ACE-1 activity and guanidine extracted Aβ load, Aβ42 or Aβ40 levels or tau load. A recent study proposed that N-domain activity enhanced the risk of AD by generating a toxic endogenous Aβ isoform (isoAβ(6-x) that is extremely susceptible to oligomerisation (550). Perhaps reduced N-domain activity is a protective compensatory response to elevated Aβ pathology but a more comprehensive assessment of Aβ species in relation to

ACE-1 activity is required. ACE-1 N-domain activity did not vary with age-at-death, PMD, gender or *APOE* genotype.

We report for the first time that there is imbalance in the activity of the two catalytic domains of ACE-1 in AD. Together, these data provide a potential explanation into seemingly paradoxical roles in ACE-1 in AD. This could be explained by common differences between N-domain and C-domain in substrate specificiteis, physiological properties (glycolysation level) and structural characteristics (551). Both glycolysation and peptide binding target the C-terminal in N-domain that is thought to affect glycolsation and its vital role in folding, localisation and enzyme activity as well (552). Reduced N-domain potentially impedes Aβ metabolism whereas increased ACE-1 C-domain activity could contribute to overproduction of Ang-II, for which we recently reported is elevated in AD. This possible relationship and the domain-specific changes may also provide an explanation for some of the inconsistences observed in previous studies linking ACE-1 and AD risk or progression. A number of animal and epidemiological studies have shown beneficial effects of ACEIs on cognition and reduce the risk of AD (361, 364, 365, 367, 542), whereas other studies have shown that ACEIs were associated with increased risk of AD or have no effect on AD risk (218, 363, 368, 370). The domain-selectivity of ACEIs, which remains unknown for most types of ACEI, may therefore have dramatic effects on disease progression in AD depending of its domain-specificity.

We also found that domain-specific immunocapture-based activity assays were more sensitive at detecting changes in AD compared to the equivalent FRET-based assays. We found that although ACE-1 N- and C-domain activity, when measured by FRET activity assay, showed trends towards lower N-domain activity in AD and higher C-domain activity in AD, these trends were not statistically significant in AD cases compared to controls. In contrast, ACE-1 N-domain activity, when measured by the more sensitive immunocapture-based FRET activity assay, was significantly lower in AD cases by ≈ 50% compared to controls. Similarly, the immunocapture-based C-domain activity assay revealed a significant increase in C-domain activity in AD cases by more than 25%. The reason for these differences is likely to be due to the improved specificity of the immunocapture assays and the longer incubation time, which is likely to have improved the sensitivity of the assay. These data highlight the possible need to further investigate and perform a more comprehensive analysis to try and better understand the potential causes and effects of ACE-1 domain specific changes in AD.

Finally, we measured Ang-I level and calculated the ratio of Ang-II:Ang:I in mid-frontal cortex to provide an additional way to help inform and support the ACE-1 activity findings. I found that Ang-1

level was reduced and the Ang-II:Ang:I ratio was increased in AD. This is the first study to show that Ang-I levels are reduced in AD, and that the reduction in Ang-I was related to disease severity according to Braak tangle stage such that it was more pronounced in more severe AD. Interestingly, a reduction in Ang-I level (that would occur through overactivity of ACE-1 that has been previously shown (78, 354)) was inversely correlated with increased levels of two AD pathological hallmarks (guanidine Aβ and tau load). That the ratio of Ang-II:Ang-I was significantly increased in AD cases compared to controls, is also consistent with increased activity of ACE-1. This analysis was possible through the availability of Ang-II data that were previously measured in the mid-frontal cortex and were found to be increased in AD (393). Both the reduction in Ang-I levels and the observed inverse correlation between Ang-I level and ACE-1 activity thus support the previous findings of increased ACE-1 level and activity in AD (78, 354). It also suggests that the Ang-II:Ang-I ratio can be used as a proxy marker for ACE-1. Moreover, the reduction of Ang-I level was associated with the presence of one or two *APOE* ε4 alleles and implies an association between RAS and *APOE* as suggested by another earlier study (417).

In conclusion, the data presented in this chapter provides further support and novel insights into the role of the brain cRAS in AD. For the first time, we provide evidence of divergent catalytic activity of ACE-1 catalytic domains in AD, which may begin to explain some of the conflicting findings in previous studies that have used various and perhaps different domain-binding ACEIs across diverse models of AD (343, 345, 346, 547). The potential impact of ACEI on disease pathogenesis, depending on domain-binding, may also provide a means to better explore the specificities of clinically used ACEIs for the ACE-1 catalytic domains in future studies (343, 344, 373-376). We report that, in addition, Ang-I is reduced and the ratio of Ang-II:Ang-I is increased in AD, which is consistent with increased ACE-1 activity and which also provides support for the utility of the Ang-II:Ang-I ratio as an alternative measure to estimate ACE-1 activity. These findings pose some questions as to the potential value of better discrimination of existing ACEIs as selective C-domain ACEIs that would preferentially target Ang-II production (whilst leaving Aβ-degradation unimpaired) and which could then be used exclusively to manage hypertension either in people at risk or in the early stages of AD, or in a wider population approach, to lower risk of AD.

Chapter 4. Non-classical axis of RAS in Alzheimer's disease

4.1 Abstract

The cRAS (ACE-1/Ang-II/AT_1R) exerts damaging effects and hyperactivity of this axis locally within the brain contributes to the pathogenesis of AD. Alternative 'downstream' RAS pathways have recently been discovered that counter-regulate the damaging effects of cRAS signalling, whilst also regulating synaptic function and boosting learning and memory. Yet, the expression of these rRAS pathways remains poorly characterised within the brain and their possible association with AD pathogenesis remains unclear. We previously showed that ACE-2 activity was reduced in AD in association with disease pathology (Aβ/Tau) and overactivity of ACE-1 (417). In this chapter, I have further characterised the ACE-2/Ang (1-7)/MasR pathway in AD. I have characterised the distribution and expression of angiotensin (1-7), MasR and the lesser known MrgD receptor involved in the alternative rRAS signalling pathway in relation to disease pathology in a well-characterised cohort of post-mortem brains.

Human post-mortem brain tissue was obtained from the SWDBB, University of Bristol, with local Research Ethics Committee approval. We studied mid-frontal cortex (Brodmann area 8/9) from AD cases (n= 70) and age-matched controls (n= 48) that were matched closely for age-at-death and PMD. The level of Ang (1-7) was measured in the mid-frontal cortex by an in-house direct ELISA. The expression and distribution of MasR was determined by ELISA and IHC. The expression of MrgD was determined by western blotting. Pre-existing data on Braak tangle stage, total insoluble Aβ, insoluble Aβ40 and Aβ42 and tau load was also available for analysis. We also calculated the ratio of Ang-II:Ang (1-7) to determine if it was a useful potential proxy marker for ACE-2 activity.

In this chapter we show that MasR was expressed primarily in neurons and that the level of Ang (1-7) and MasR were unaltered in AD and were not associated with AD pathological hallmarks. MrgD was also found to be expressed in human post-mortem brain tissue with no obvious difference between controls and AD cases. We also report that the Ang-II:Ang (1-7) ratio was significantly increased in AD compared to controls, consistent with recent findings of reduced ACE-2 activity (and thus reduced conversion of Ang-II to Ang (1-7)) in AD.

Together, these studies provide novel evidence that components of the alternative rRAS pathways i.e. Ang (1-7) and MasR are unchanged in AD, despite our findings of increased Ang-II:Ang (1-7) ratio, indicative of reduced ACE-2 activity in AD (which supports previous findings).

4.2 Introduction

The non-classical rRAS is composed of and relies heavily on the function and activity of ACE-2, the rate-limiting enzyme in the conversion of Ang-II to Ang (1-7), the primary agonist of MasR (ACE-1/Ang (1-7)/MasR). This rRAS pathway counter-regulates the disease-associated actions that are generally attributed to the cRAS axis (254). Ang (1-7) activation of MasR activates signalling pathways associated with several protective actions such as vasodilation, anti-inflammatory, anti-proliferative and anti-fibrotic effects (455). Ang (1-7) activation of the MasR is associated with LTP and boosts memory and cognition in mouse models of AD (432-434).

There is evidence that the rRAS (ACE-2/Ang (1-7)/MasR) pathway is dysregulated in AD. Our previous study showed a reduction in ACE-2 activity in AD human post-mortem brain tissue in the mid-frontal cortex, which was inversely associated with Aβ and tau pathology (417). The reduction of ACE-2 activity was also inversely correlated with ACE-1 activity, and the ratio of ACE-1 to ACE-2 (proxy markers of the activity of cRAS and rRAS respectively) was increased, suggesting an imbalance in brain RAS (favouring excess cRAS activity) in AD. Notably, serum ACE-2 activity was found to be reduced in AD patients compared to controls (79). Cognitive impairment and disease pathology, associated with increased oxidative stress and decreased brain-derived neurotrophic factor (BDNF) in the hippocampus, due to cRAS activation, has also been reported in ACE-2 knock-out mice (419), whilst activation of the ACE-2/Ang (1-7)/MasR axis has previously been shown to boost learning and memory in an AD rat model (295). Interestingly, ACE-2 has been shown to convert the neurotoxic form of Aβ (Aβ43) into (Aβ42), which in turn is cleaved by ACE-1 to less toxic Aβ species (Aβ40 and Aβ41) (79).

The beneficial effects of Ang (1-7) against disease-pathology and cognitive dysfunction has been reported to be mediated via activation of a GPCR, namely MasR (252). Activation of MasR by the binding of Ang (1-7) stimulates several downstream signalling pathways that counter-regulate cRAS disease-associated signalling including: stimulation of phospholipase A2, increased arachidonic acid,

release of Ca+ independent activation of NOS, activation of PI3K/Akt, MAPK and cAMP/PKA (428). ICV administration of Ang (1-7) into rats has been shown to restore cerebral blood flow and improve cognitive function through increased NO generation (429), promotion of brain angiogenesis and increased capillary density via a Mas/eNOS dependent pathway (328, 430, 431). In accordance, cerebroprotective mechanisms of ICV infusion of Ang (1-7) are due to reduced levels of oxidative stress and pro-inflammatory cytokines in the ischaemic area (292). Collectively, these studies outline a critical role of the active RAS metabolite (Ang (1-7)) in maintaining the physiological homeostasis of cerebrovascular function.

It has been shown that Ang (1-7) is implicated in learning and memory via its action on MasR. MasR was originally identified as a proto-oncogene and it encodes a genetic sequence characteristic of the GPCR subfamily and has seven hydrophobic transmembrane domains (436). High expression of MasR has been detected in rat brain within the hippocampus, cerebral cortex and also in cardiovascular function related areas in the brain such as hypothalamus and medulla (438, 439). Ang (1-7) also enhances LTP in the CA1 region of the hippocampus and amygdala in mice (432, 433). Moreover, dysregulation of Ang (1-7)/MasR axis has been found to cause memory deficit and affect the object recognition memory in MasR knockout mice (353). MasR activation in hippocampus and basal ganglia promoted cell survival, enhanced synapse formation and improved cognition in rodent and humans (425). In accordance, activation of MasR by Ang (1-7) administration attenuated cognitive decline and reduced expression of AD pathological hallmarks (phosphorylated tau, Aβ oligomer and both Aβ40 and Aβ42 levels) in the hippocampus of an AD rat model. Co-administration of a MasR antagonist reversed the protective effects (440). These findings suggested that dysregulation of (ACE-2/Ang (1-7)/MasR) axis might contribute to cognitive decline and disease pathology seen in AD. Activity of the main enzyme in the protective axis, ACE-2 was reduced in human post-mortem brain tissue of AD patients and this reduction was associated with increased AD pathological hallmarks (total Aβ load and p-tau levels) (417). Activation of ACE-2 by administration of DIZE, an ACE-2 activator in AD animal model, resulted in both prevented development of cognitive deficit and improved learning and memory function (295, 421). Jiang *et al.* (416) found that Ang (1-7) levels were reduced in AD and inversely correlated with hyperphosphorylated tau. Recently, Uekawa *et al.* (434) showed that ICV infusion of Ang (1-7) alleviated cognitive impairment and improved cerebrovascular reactivity (i.e. CBF) in an AD mouse model. In addition, a recent study has shown the beneficial effects of an Ang (1-7) analogue on cognitive function (553).

Together, these data indicate an important role of the ACE-2/Ang (1-7)/MasR pathway in AD, but the characterisation of this pathway in human brain tissue remains poorly described. In humans, plasma levels of Ang (1-7) were significantly reduced in AD patients compared to controls. The study by Jiang *et al.* (435) suggested that Ang (1-7) may be considered as a potential biomarker in AD diagnosis. However, cerebral Ang (1-7) levels in AD patients have not been investigated. Finally, MrgD is a member of the GPCR family group and has been reported to be expressed in neurons (554). Tetzner and colleagues (443) recently identified MrgD as a second receptor for Ang (1-7) although much is still unknown about this receptor. The coupling of Ang (1-7) with both MasR and MrgD has been shown to activate intracellular signalling pathways that induce increased cAMP and phosphokinase A activity. However, the role of both of these receptors in relation to AD-associated pathology and cognitive dysfunction is less studied.

In this chapter, we have characterised the rRAS pathway (downstream of ACE-2) and have measured the expression of Ang (1-7) and the expression and distribution of both the MasR and MrgD receptors in human-post mortem brain tissue in the mid-frontal cortex in AD in relation to markers of disease pathology.

4.3 Study aims and hypothesis

The aims of the study described in this chapter were:

(i) To determine if the level of Ang (1-7) and/or the ratio of Ang-II/Ang (1-7) in mid-frontal cortex is altered in AD in relation to disease pathology

(ii) To characterise the expression and distribution of MasR and MrgD receptors in the mid-frontal cortex in AD in relation to markers of disease pathology

We wished to test the hypothesis that the downstream components of the rRAS pathway beyond ACE-2 i.e. Ang (1-7), MasR and MrgD expression was altered in mid-frontal cortex of AD brains compared to controls and was related to Aβ and Tau levels.

4.4 Methods

4.4.1 Study cohort

Human post-mortem brain tissue homogenates from mid-frontal cortex (Brodmann area 8/9) were used for measurements of Ang (1-7) level and MasR level. The study cohort included a total of controls (n= 48) and AD cases (n= 70). Demographic features of study cohort are described in the methods section (see Table 2.1) for full details (Appendix I: Table 9.1 and Table 9.2). Previous measurements of total insoluble Aβ by sandwich ELISA were available for controls (n= 28) and AD cases (n= 61) (545). Tau load was previously measured for all cases as part of routine assessment of AD cases within the SWDBB by field fraction analysis and was available for controls (n= 29) and AD cases (n= 89). Both insoluble Aβ40 and insoluble Aβ42 were previously measured by sandwich ELISA and were available for controls (n= 20) and AD cases (n= 33) for insoluble Aβ42, and for controls (n= 20) and AD cases (n= 34) for insoluble Aβ40 (314). The previous measurements of Ang-II level measured by sandwich ELISA were available for controls (n= 43) and AD cases (n= 70). All these previous measurements of AD pathological hallmarks and RAS marker were used for analysis in this chapter.

4.4.2 Angiotensin (1-7) direct ELISA

The level of Ang (1-7) was measured in brain homogenates from mid-frontal cortex using an in-house direct ELISA as described in detail in the general methods (section 2.7.2). Brain homogenates were prepared in 1% SDS lysis buffer as described in the methods (section 2.2.2). Recombinant Ang (1-7) (serially diluted to produce a 1000-15.62 pg/ml standard curve) and tissue samples diluted 1:40 in PBS were incubated in a clear high-binding capacity NUNC maxisorp plate (Fisher Scientific) for 2 hours at room temperature with shaking. After washing in PBS/0.05% Tween-20 five times, wells were blocked for 1 hour using PBS:1% BSA (Sigma Aldrich). Following a further wash step, a biotinylated detection antibody against Ang (1-7) (100 µl) (Cloud-Clone) (diluted 1:100 in PBS) was incubated for 2 hours at 26°C with shaking. After five washes, the wells were incubated with strep:HRP (R&D System) (1:200) in PBS with 0.01% Tween-20 at room temperature for 20 minutes in dark. Following a further wash step, TMB substrate (R&D systems) was added and incubated in the dark for 20 minutes. 50 µl of Sulfuric acid (stop solution) (Sigma-Aldrich) was added to each well and the absorbance at 450nM was read using a FLUOstar OPTIMA plate reader (BMG labtech). The assay

showed minimal cross reactivity with a number of closely related angiotensin peptides, namely Ang-I, Ang-II, Ang-III and Ang-IV (Figure 4.1).

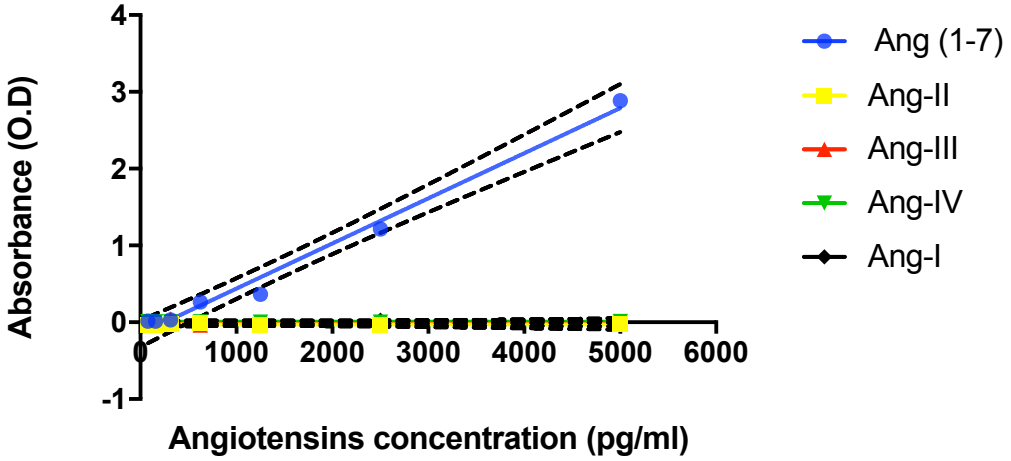

Figure 4.1 Cross reactivity test of the Ang (1-7) direct ELISA using biotin-linked polyclonal antibody to Ang (1-7) (Cloud-Clone Corp) with serial dilutions of closely-related recombinant human angiotensins (Ang (1-7), Ang-II, Ang-III, Ang-IV and Ang-I).

The solid inner line indicates the best-fit linear regression and the outer lines the 95% confidence intervals.

Ang (1-7) measurements were adjusted for total protein level determined using a method described in chapter 2 (section 2.3). Ang (1-7) level was measured in duplicate and four carry-over samples were used and repeated in each plate assayed. The variation between Ang (1-7) measurements was determined by calculating the intra-assay CV% (Appendix IV: Table 9.27).

4.4.3 Angiotensin (1-7) sandwich ELISA

The level of Ang (1-7) in brain homogenates from the mid-frontal cortex was also measured in a subset of control (n= 19) and AD cases (n= 19) using a quantitative commercially available sandwich ELISA (Human Angiotensin 1-7 (ANG1-7) ELISA kit) (MyBioSource), according to the manufacturer's instructions. A detailed method is described in the chapter 2 (section 2.8.1). Brain homogenate samples were added in duplicate and averaged and the variation of this assay was determined by calculating the intra-assay CV% (Example in Appendix IV: Table 9.28).

4.4.4 Expression of MasR in human brain tissue

4.4.4.1 Western blot for MasR expression

The standard protocol for western blotting is described in detail in chapter 2 (section 2.4). Details of the primary and secondary antibodies used are listed in chapter 9 (Appendix II: Table 9.13) and (Table 9.14) respectively. In summary for detection of MasR in brain homogenate samples, the membrane was blocked in 10% milk/TBST buffer for 1 hour. After it had been washed with 0.05% TBST (3x 15 minutes) at room temperature on a shaker, the membrane was then incubated with anti-MAS1 antibody diluted 1:800 in 5% milk/TBST antibody buffer overnight at 4°C (in the fridge) on a rotating platform. Following a wash step with 0.05% TBST (3x 15 minutes) at room temperature on the rotating platform, the membrane was incubated with the secondary antibody (peroxidase conjugated anti-rabbit) diluted 1: 5000 in 5% milk/TTBS for 1 hour. After 3x 15 minutes wash steps with 0.05% TBST, a chemiluminescent HRP substrate (ECL) (Millipore) was added to the membrane in a 1:1 ratio (5 ml of reagent 1 and 5 ml of reagent 2) for 5 minutes. Images were acquired using Image Lab (ChemiDoc XRS+, Bio-RAD) and Image Lab software, version 5.0 (Bio-RAD).

4.4.4.2 Immunohistochemistry for MasR

The specificity of the anti-MAS1 antibody (ab66030) was further tested by immunohistochemistry to examine the distribution of the MasR in formalin-fixed brain tissue. The standard protocol used for immunohistochemical staining is described in detail in chapter 2 (section 2.5). Immunohistochemical staining of MasR was initially optimised by comparing standardised antigen retrieval pre-treatment steps with either EDTA or citrate buffer and optimising the dilution of the primary antibody (1:100, 1:500, 1:1000). The best assay conditions for MasR staining were achieved when slides were pre-treated with EDTA and boiled in the microwave for 10 minutes. After washing with running tap water for 5 minutes, slides were incubated with blocking serum for 20 minutes then incubated with the primary antibody (anti-MAS1 antibody (ab66030)) diluted 1:100 in PBS (10 µg/ml) at 4°C overnight. After rinsing the sections in two changes of PBS for 3 minutes each, sections were incubated with Vectastain biotinylated universal secondary antibody for 20 minutes followed by another wash with PBS and then the VectaElite ABC complex for 20 minutes and rinsed again. Sections were then incubated with DAB for 10 minutes then washed in running water for 10 minutes and immersed in copper sulphate solution for 4 minutes followed by washing in running water for 5 minutes. The

sections were then counterstained with haematoxylin Gill II for 3 seconds, dehydrated, cleared and mounted.

4.4.5 MasR sandwich ELISA

The level of MasR in brain homogenates from the mid-frontal cortex was measured using a quantitative commercially available sandwich ELISA (Human Mas Proto-Oncogen (MAS1) ELISA kit) (MyBioSource), according to the manufacturer's instructions. A detailed method is described in chapter 2 (section 2.8.2). Brain homogenate samples were added in duplicate and averaged and measurements of four carry-overs samples were repeated across all plates. MasR measurements were adjusted to total protein level for each brain homogenate sample. The variation of this assay was determined by calculating the intra-assay CV% (Example in Appendix IV: Table 9.29). Both unadjusted MasR measurements and protein-adjusted measurements were used for comparisons between control and AD. Relationships between MasR level and disease severity (Braak tangle stage), AD pathological hallmarks (total insoluble Aβ, insoluble Aβ40, insoluble Aβ42 and tau load) were also examined.

4.4.6 Expression of MrgD in brain tissue

4.4.5.1 Western blotting for MrgD

A standard protocol for western blotting was used and is described in detail in chapter 2 (section 2.4). Details of the primary and secondary antibodies used are described in chapter 9 (Appendix II: Table 9.13) and (Table 9.14) respectively. In summary, for detection of MrgD in brain homogenate samples, the membrane was blocked in 10% milk/TBST buffer for 1 hour. Following a wash step with 0.05% TBST (3x 15 minutes) at room temperature on a shaker, the membrane was then incubated with MRGPRD antibody (NBP1-91964) diluted 1:500 in 5% milk/TBST antibody buffer overnight at 4°C (in the fridge) on a rotating platform. After it had been washed with 0.05% TBST (3x 15 minutes) at room temperature on a shaker, the membrane was incubated with a secondary antibody (peroxidase conjugated anti-rabbit) diluted 1:5000 in 5% milk/TBST for 1 h. After 3x 15 minutes wash steps with 0.05% TBST, a chemiluminescent HRP substrate (ECL) (Millipore) was added to the membrane in a

1:1 ratio (5 ml of reagent 1 and 5 ml of reagent 2) for 5 minutes. The images were then acquired using Image Lab (ChemiDoc XRS+, Bio-RAD) and Image Lab software, version 5.0 (Bio-RAD).

4.4.6 Statistical analysis

All datasets were initially analysed by the Shapiro-Wilk normality test to determine whether they were normally distributed. A significant p value $p< 0.05$ was used to indicate if the data were not normally distributed. Ang (1-7) direct ELISA were normally distributed whilst MasR sandwich ELISA data were not normally distributed.

Comparison of Ang (1-7) level between controls and AD cases was tested using an Unpaired samples t-test. Protein–adjusted data was not normally distributed and therefore a non-parametric test, Mann-Whitney test was used. Correlations of Ang (1-7) data with total insoluble Aβ and tau load were assessed by the Pearson's correlation coefficient for unadjusted data and Spearman's correlation coefficient for protein-adjusted data. Comparison of Ang-II:Ang (1-7) ratio between controls and AD cases was analysed using a parametric test, unpaired samples t-test.

Both MasR and protein-adjusted MasR data were not normally distributed. A non–parametric Mann-Whitney test was therefore performed to compare AD cases and controls for both datasets. Comparison of MasR and protein-adjusted MasR data between Braak tangle stage groups (Braak stage 0-II, Braak stage III-IV, Braak stage V-VI) was assessed using a non-parametric Kruskal-Wallis test. MasR and MasR protein-adjusted level correlations with total insoluble Aβ, tau load, insoluble Aβ40 and insoluble Aβ42 were assessed by the Spearman's correlation coefficient.

Log transformation for unadjusted and protein-adjusted MasR data was performed to attempt to reach normal distribution (Appendix VI: Section 9.6.2). Unpaired sample t-tests were used for log transformed unadjusted and protein-adjusted data to compare between AD cases and controls. A one-Way ANOVA test was performed to compare log transformed MasR data between Braak tangle stage groups. Correlations between log-transformed MasR data and total insoluble Aβ, tau load, insoluble Aβ40 and insoluble Aβ42 were assessed by Pearson's correlation coefficient. For all tests applied, a P-value < 0.05 was considered statistically significant.

For all datasets, the ROUT method was used to detect outliers, in datasets where outliers were removed, the data was re-analysed and is presented in chapter 9 (Appendix VII: Section 9.7.2).

4.5 Results

4.5.1 Comparison of Angiotensin (1-7) level in controls and AD

In the mid-frontal cortex, Ang (1-7) level measured by direct ELISA, was not significantly different in AD cases compared to age-matched controls. The mean and standard error of mean (SEM) for controls was (31668 ± 1014) and for AD cases (32572 ± 892.4) (Figure 4.2 A). The Ang (1-7) measurements were then adjusted to total protein level where Mann-Whitney test similarly revealed no significant difference between AD cases (median = 121204 pg/mg) and controls (median = 111555 pg/mg) (Figure 4.2 B).

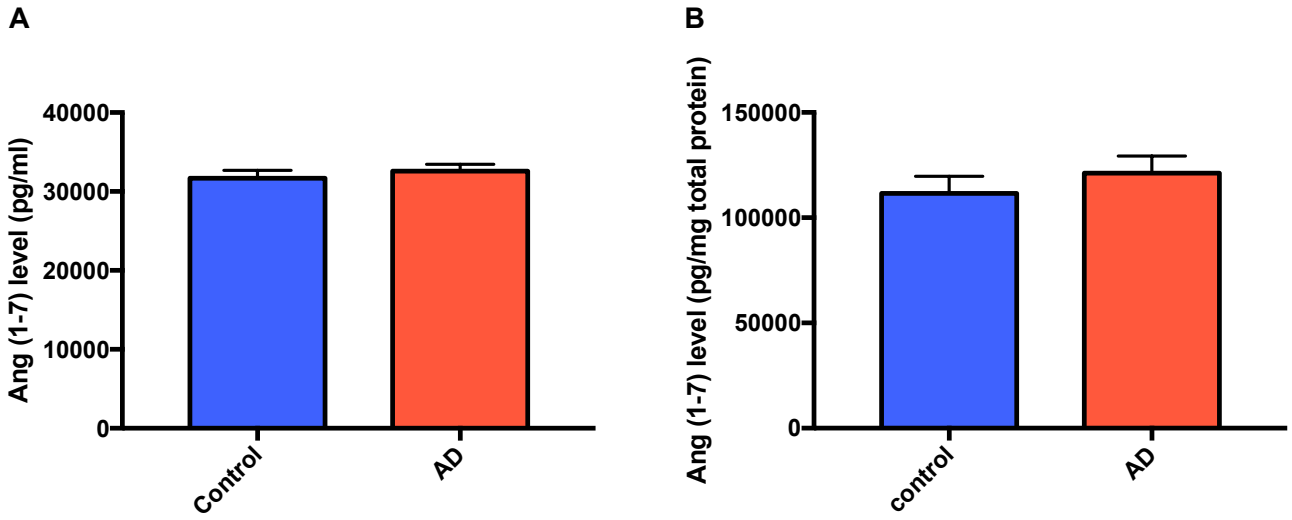

Figure 4.2 Comparison of Angiotensin (1-7) level between controls and AD cases.

A. Bar chart showing unchanged Ang (1-7) level in AD (n= 70) compared with age-matched control (n= 48) in mid-frontal cortex measured using an in-house Ang (1-7) direct ELISA. Unpaired samples t-test revealed no significant difference between AD and controls (p= 0.514). The bars indicate the mean ± SEM. B. Bar chart showing protein-adjusted Ang (1-7) level did not differ between AD group compared to age-matched group, Mann-Whitney test (p= 0.222). The bars indicate the median and 95% confidence intervals.

Similar to the results of Ang (1-7) direct ELISA, Ang (1-7) measured by sandwich ELISA was not significantly different in AD cases (n= 19) compared to age-matched controls (n= 19). The median total Ang (1-7) level was: controls = 22.92 (pg/ml) and AD = 25.06 (pg/ml). Mann-Whitney test showed no statistical significance between groups (p= 0.220) (Figure 4.3 A). The median for Ang (1-7) protein-adjusted data in AD cases (125.5 (pg/mg total protein)) did not differ from controls (131.9 (pg/mg total protein)). Mann-Whitney test similarly revealed no statistical significance between groups (p= 0.402) (Figure 4.3 B). Ang (1-7) level measured by direct ELISA was not correlated with data measured by sandwich ELISA in the subsets of AD cases (n= 19) and age-matched controls (n= 19) (Pearson's correlation coefficient r= 0.194, p= 0.243).

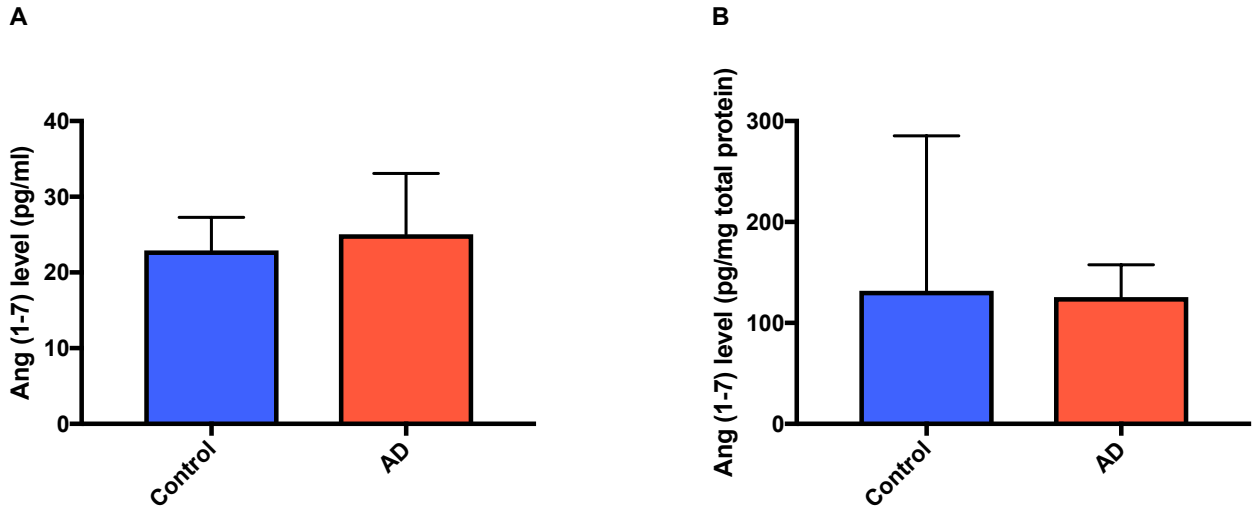

Figure 4.3 Comparison of Angiotensin (1-7) level between controls and AD cases using a commercial sandwich ELISA.

A. Bar chart showing unchanged Ang (1-7) level in AD (n= 19) compared with age-matched control (n= 19) in mid-frontal cortex measured using an Ang (1-7) sandwich ELISA. Mann-Whitney test revealed no significant difference between AD and controls (p= 0.220). The bars indicate the median and 95% confidence intervals. B. Bar chart showing protein-adjusted Ang (1-7) level did not differ between AD group compared to age-matched group, Mann-Whitney test (p= 0.402). The bars indicate the median and 95% confidence intervals.

4.5.1.1 Relationship between Ang (1-7) and Aβ and Tau load

The relationship between Ang (1-7) level (measured by direct ELISA) and levels of insoluble Aβ load and Tau load in mid-frontal cortex were assessed. Both total Ang (1-7) and protein-adjusted measurements showed no correlation with either insoluble Aβ load (Pearson's correlation coefficient r= 0.096, p= 0.381; Spearman's correlation coefficient r= 0.114, p= 0.306) respectively (Figure 4.4 A

and B). No significant correlations were found between both unadjusted Ang (1-7) and protein-adjusted measurements with tau load (Pearson's correlation coefficient r= 0.095, p= 0.358; Spearman's correlation coefficient r= 0.165, p= 0.113) respectively (Figure 4.4 C and D).

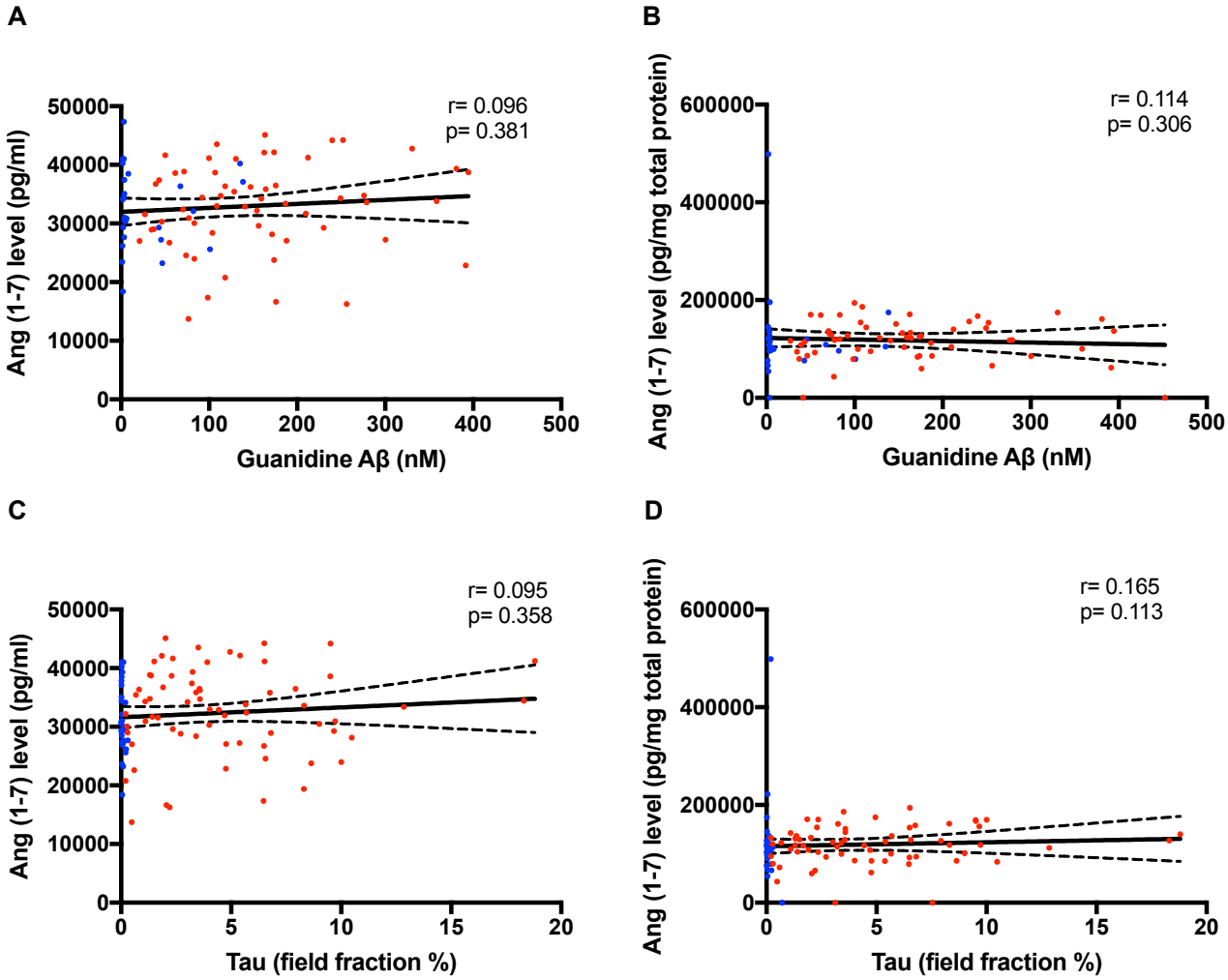

Figure 4.4 Relationships between Ang (1-7) level and Aβ and tau load.

A. Scatterplot showing no correlation between Ang (1-7) level and guanidine Aβ load (measured by enzyme-linked immunosorbent assay), Pearson's correlation coefficient (r= 0.096, p= 0.381). B. Scatterplot showing no significant correlation between Ang (1-7) protein-adjusted level and guanidine Aβ load, Spearman's correlation coefficient (r= 0.114, p= 0.306). C. Scatterplot showing no correlation between Ang (1-7) level and tau load (measured by field fraction analysis), Pearson's correlation coefficient (r= 0.095, p= 0.358). D. Scatterplot showing no significant correlation between Ang (1-7) protein-adjusted level and tau load, Spearman's correlation coefficient (r= 0.165, p= 0.113). The solid inner line indicates the best-fit linear regression and the outer lines the 95% confidence intervals. Blue dots= controls, red dots= AD cases.

4.5.1.2 The Ang-II:Ang (1-7) ratio is increased in AD

We next calculated the Ang-II:Ang (1-7) ratio, which is potentially a proxy indicator of ACE-2 activity. The previous measurements of Ang-II level were available for controls (n= 42) and AD cases (n= 68). The mean ± SEM for Ang-II:Ang (1-7) ratio was significantly increased in AD compared to controls, unpaired samples t-test (p= 0.004) (Figure 4.5). An increased ratio of Ang-II:Ang (1-7) in AD is in-keeping with reduced ACE-2 activity.

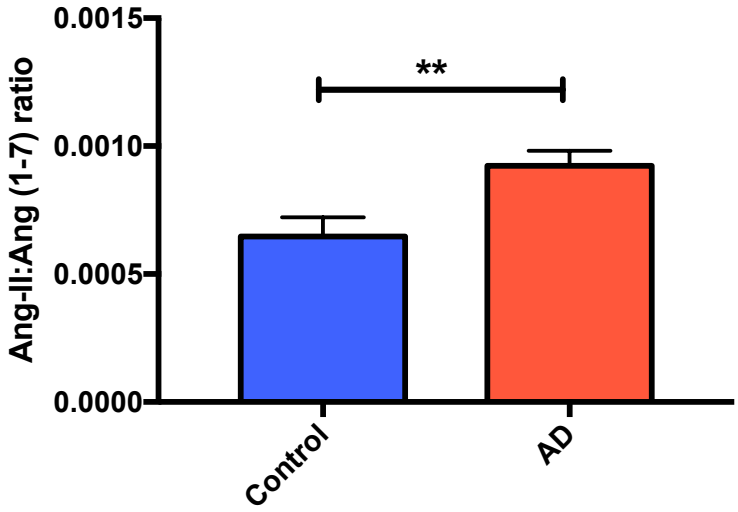

Figure 4.5 The ratio of Ang-II:Ang (1-7) in AD compared with age-matched controls.

Bar chart showing increased Ang-II:Ang (1-7) ratio in AD (n= 68) compared to controls (n= 42) in the mid-frontal cortex. Differences between groups were compared using Unpaired samples t-test at **P= 0.004. The bars indicate the mean ± SEM.

4.5.2 Expression of MasR in human brain tissue

To detect and examine the distribution of MasR in the mid-frontal cortex, the specificity of MasR antibody was first tested by western blot and then by immunohistochemical staining. Four AD cases and controls were used for this experiment. Details of the chosen samples are described in chapter 9 (Appendix I: Table 9.6).

4.5.2.1 Validation of MasR antibody specificity

A representative image of the MasR western blot is shown (Figure 4.6). The antibody detected a band at approximately 37 kDa, which is the expected molecular weight (MW) for the MasR protein (440). An additional lower band was detected at 20 kDa – the identity of this band is unknown but could possibly be a protein degradation product. There was no obvious difference in the levels of expression of MasR in AD and controls (see Figure 4.6) although this was a small sample set (n= 4). Densitometry was performed but no significant difference in band volume (p= 0.221) was observed between AD and controls.

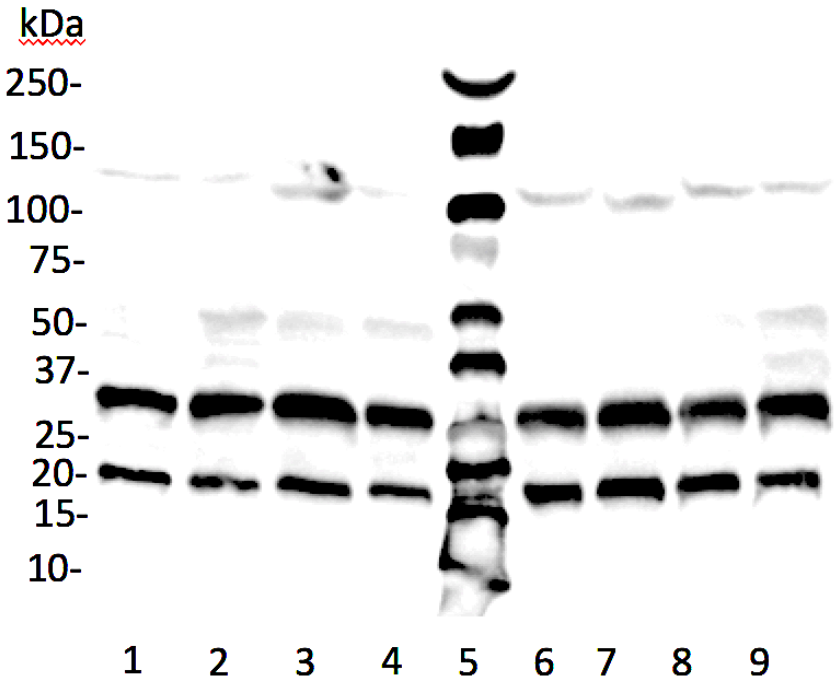

Figure 4.6 MasR expression in human post-mortem brain tissue homogenates detected by Western blot.

MasR expression in human brain tissue was studied by Western blotting: left side represents expression of MasR in human brain tissue from non-diseased controls (lines 1-4). Right side shows MasR expression in AD cases (lines 6-9). Lane 5 includes MW markers. The membrane was blotted with polyclonal rabbit antibody to MAS1 (ab66030). The reported size of MasR is predicted to be approximately 37 kDa. The smaller bands at MW 20 kDa are possibly protein degradation products.

4.5.2.2 Immunolabelling of MasR in human brain tissue

MasR labelling was mainly localised to neurons in control, AD and VaD cases. In a control case, positive MasR staining was predominantly observed in parenchymal neurons (Figure 4.7 A and B). In a vascular case, positive labelling was also seen around some blood vessels (Figure 4.7 C-F).

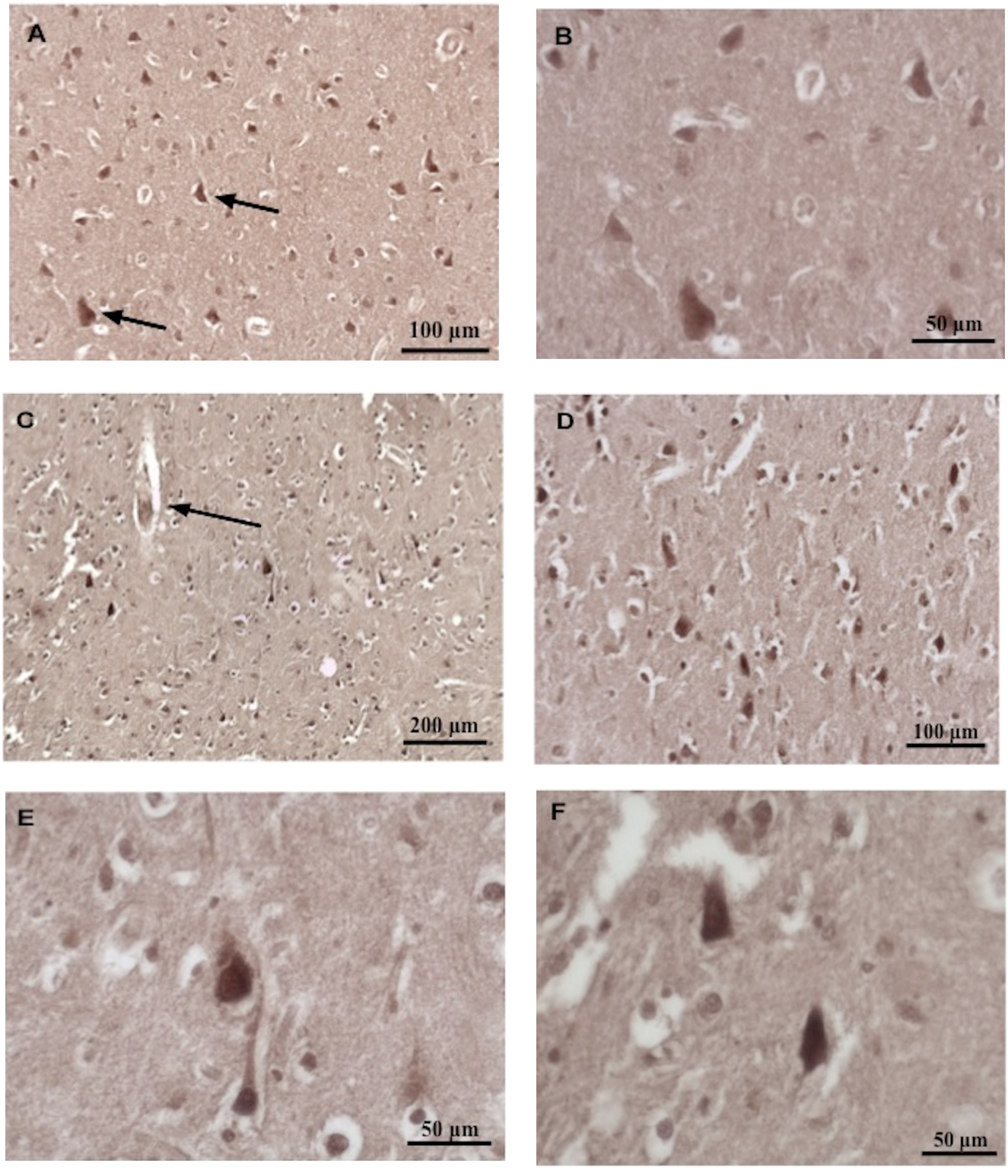

Figure 4.7 Immunolabelling of MasR in the mid-frontal cortex.

A-B. MasR labelling in brain sections from a non-diseased control case was mainly detected in parenchymal neurons (indicated by arrows). C-F. immunohistochemical staining of MasR in brain sections from a vascular case indicates that MasR was mostly present in neurons but with some additional staining of blood vessels evident (indicated by arrows). Images were taken by Professor Seth Love. (Image taken at 10x magnification for C, at 20x magnification for A and D, at 40x magnification for B, E and F).

4.5.3 Measurement of MasR level in AD

4.5.3.1 Comparison between control group and AD group

The level of MasR and MasR adjusted for total protein did not significantly differ between AD cases (n= 70) and controls (n= 48) (Figure 4.8 A and B). These data were not normally distributed. The median total MasR level was: controls= 51.39 (pg/ml) and AD= 57.56 (pg/ml). Mann-Whitney test showed no statistical significance between groups (p= 0.359). The median for MasR protein-adjusted data in AD cases (347 (pg/mg total protein)) did not differ from controls (327.9 (pg/mg total protein)). Mann-Whitney test showed no statistical significance between groups (p= 0.343).

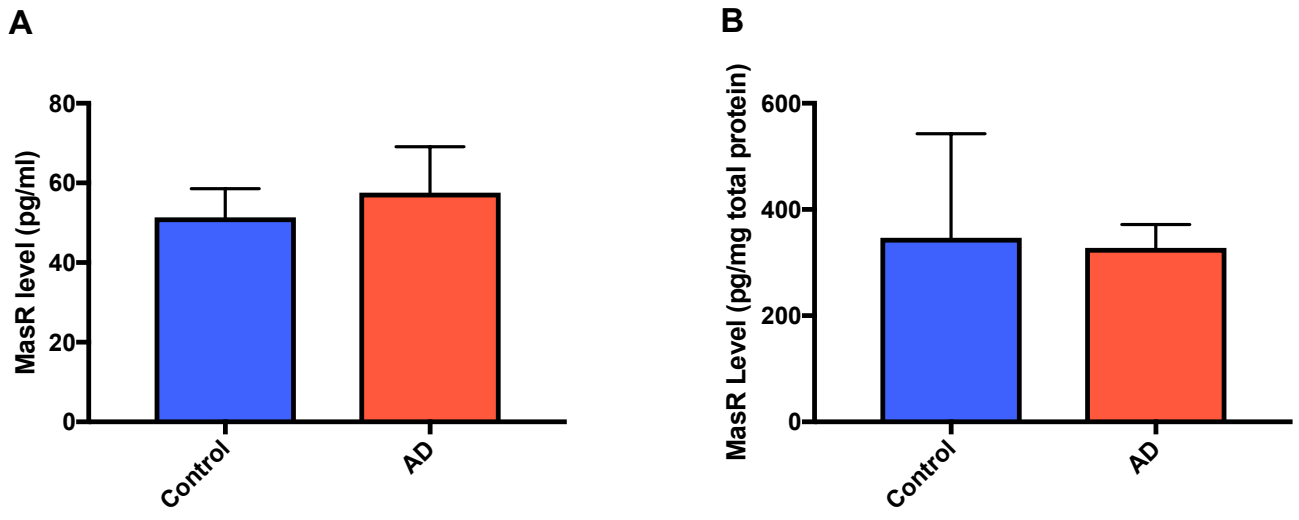

Figure 4.8 MasR level in mid-frontal cortex in Alzheimer's disease (AD).

A. Bar chart showing MasR concentration was unchanged in AD (n= 70) compared with age-matched control (n= 48) in mid-frontal cortex measured using a MasR sandwich ELISA, Mann-Whitney test (p= 0.359). The bars indicate the median and 95% confidence intervals. B. Bar chart showing protein-adjusted MasR level did not differ in the AD group compared to age-matched group, Mann-Whitney test (p= 0.343). The bars indicate the median and 95% confidence intervals.

4.5.3.2 Relationship between MasR and Braak tangle stage pathology

Both MasR level and MasR protein-adjusted level were assessed in relation to Braak tangle stage (Braak stage 0-II (n= 36), Braak stage III-IV (n= 20), Braak stage V-VI (n= 61)). Kruskal-Wallis test indicated that there was no significant difference in MasR medians between all Braak stage groups (p= 0.309) (Figure 4.9 A). The median of Braak stage 0-II = 55.305 (pg/ml), Braak stage III-IV= 47.265 (pg/ml) Braak stage V-VI= 60.61 (pg/ml). Similarly, no significant difference was observed between the MasR protein-adjusted medians in relation to Braak tangle stage (p= 0.794). The corresponding medians in this case were for Braak stage 0-II= 325.177 (pg/mg total protein), Braak stage III-IV= 281.641 (pg/mg total protein) Braak stage V-VI= 338.564 (pg/mg total protein) (Figure 4.9 B).

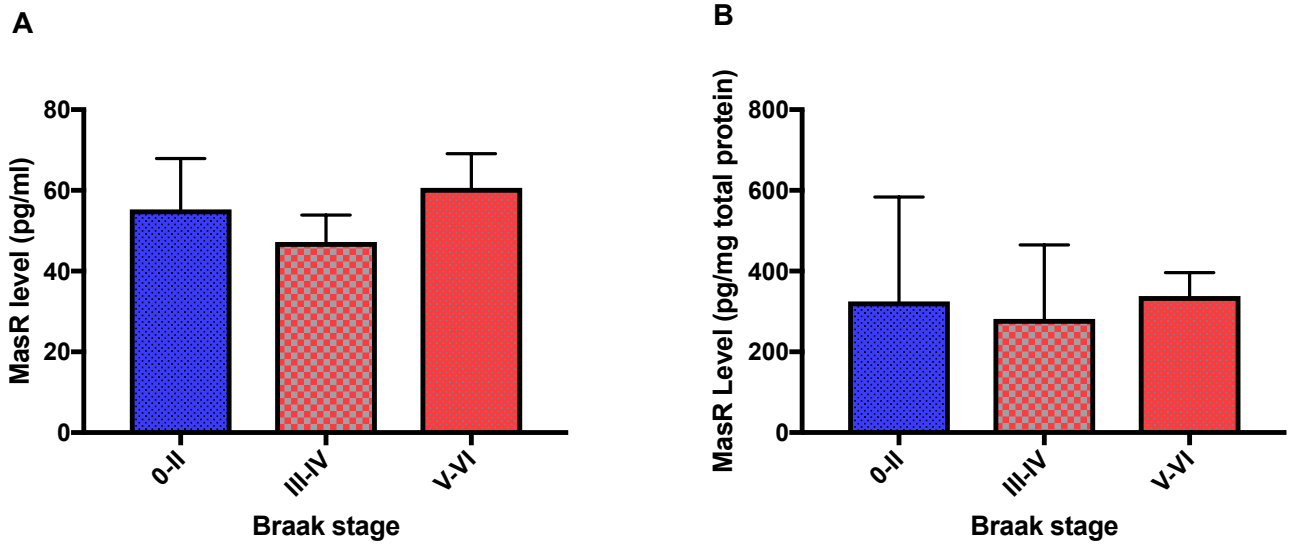

Figure 4.9 MasR level in relation to Braak tangle stage.

A. Bar chart showing no significant difference in MasR level measured by sandwich ELISA assay in relation to Braak tangle stage groups (Braak stage 0-II (n= 36), Braak stage III-IV (n= 20), Braak stage V-VI (n= 61)), Kruskal-Wallis test (p= 0.309. The bars indicate the median and 95% confidence intervals. B. Bar chart showing no difference between MasR protein-adjusted level and Braak tangle stage groups: (Braak stage 0-II (n= 36), Braak stage III-IV (n= 20), Braak stage V-VI (n= 61)), Kruskal-Wallis test (p= 0.794). The bars indicate the median and 95% confidence intervals.

4.5.3.3 Relationship between MasR and AD pathology hallmarks

The association between total MasR and protein-adjusted MasR measurements with AD pathology hallmarks was examined in the mid-frontal cortex. No significant correlation was found between MasR

level and total insoluble Aβ when Spearman's correlation coefficient test was applied (r= 0.008, p= 0.939). Protein-adjusted MasR level was also not correlated with total insoluble Aβ (r= 0.019, p= 0.855) using Spearman's correlation coefficient (Figure 4.10 A and B).

Similarly, no correlation was seen between total MasR level and tau load when Spearman's correlation coefficient test applied (r= 0.105, p= 0.296). Spearman's correlation coefficient test also showed a non-significant correlation between protein-adjusted MasR measurements and tau load (r= 0.079, p= 0.433) (Figure 4.10 C and D).

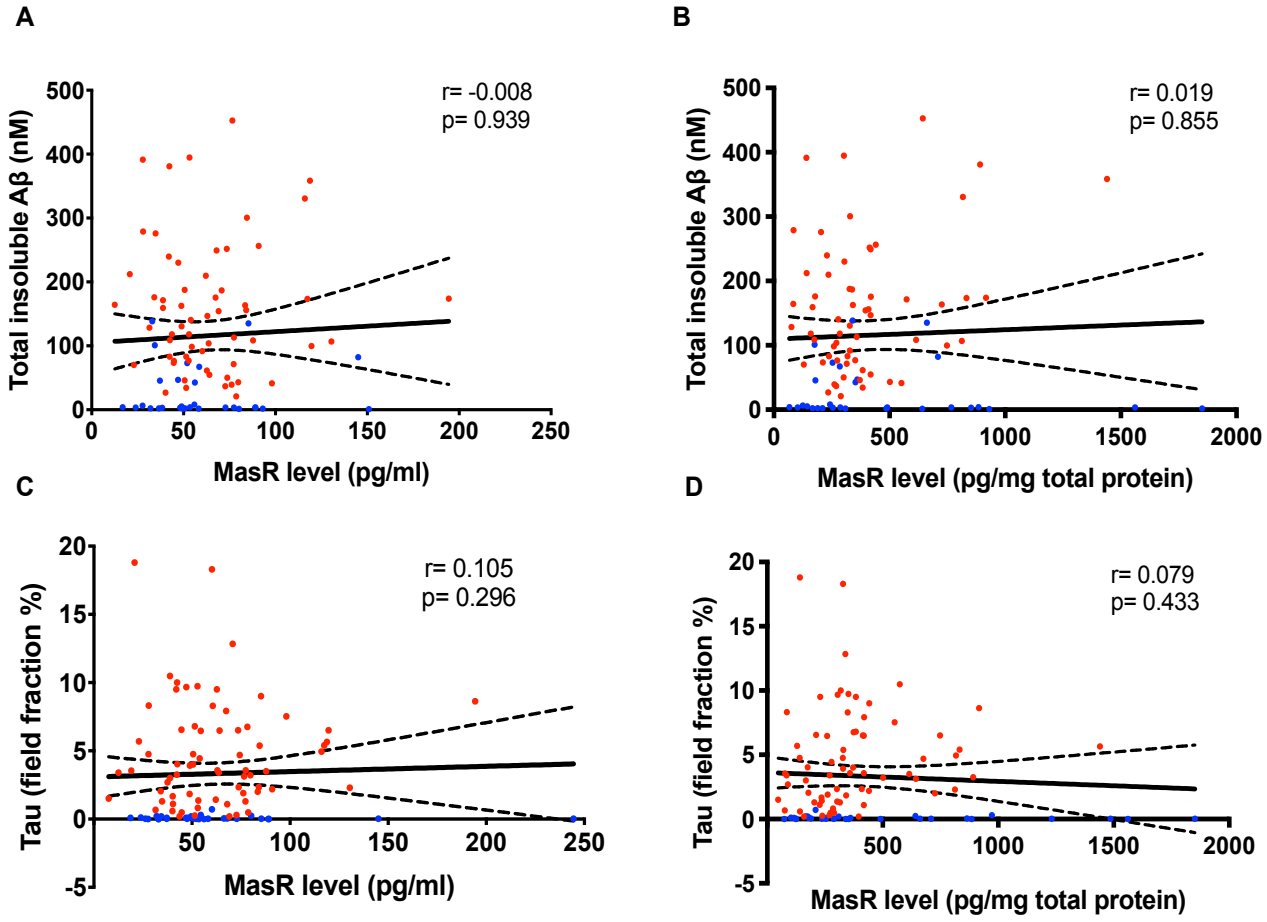

Figure 4.10 Relationship between MasR level and total insoluble Aβ and tau load.

A. Scatterplot showing no correlation between total MasR level and total insoluble Aβ (measured by enzyme-linked immunosorbent assay), Spearman's correlation coefficient (r= -0.008, p= 0.939). B. Scatterplot showing no significant correlation between protein-adjusted MasR level and total insoluble Aβ, Spearman's correlation coefficient (r= 0.019, p= 0.855). C-D. Scatterplot showing no significant correlation between both total MasR level and MasR protein-adjusted level and tau load (measured by field fraction analysis), Spearman's correlation coefficient (r= 0.105, p= 0.296), Spearman's

correlation coefficient (r= 0.079, p= 0.433). The solid inner line indicates the best-fit linear regression and the outer lines the 95% confidence intervals. Blue dots = controls, red dots = AD cases.

MasR was not associated with different isoforms of Aβ, Spearman's correlation coefficient test showed no significant correlations between total MasR level and both insoluble Aβ40 (r= -0.011, p= 0.936) and Aβ42 (r= -0.024, p= 0.861) (Figure 4.11 A and C). MasR protein-adjusted level was not correlated with either insoluble Aβ40 (r= -0.164, p= 0.229) or Aβ42 (r= -0.163, p= 0.238) in mid-frontal cortex using Spearman's correlation coefficient (Figure 4.11 B and D).

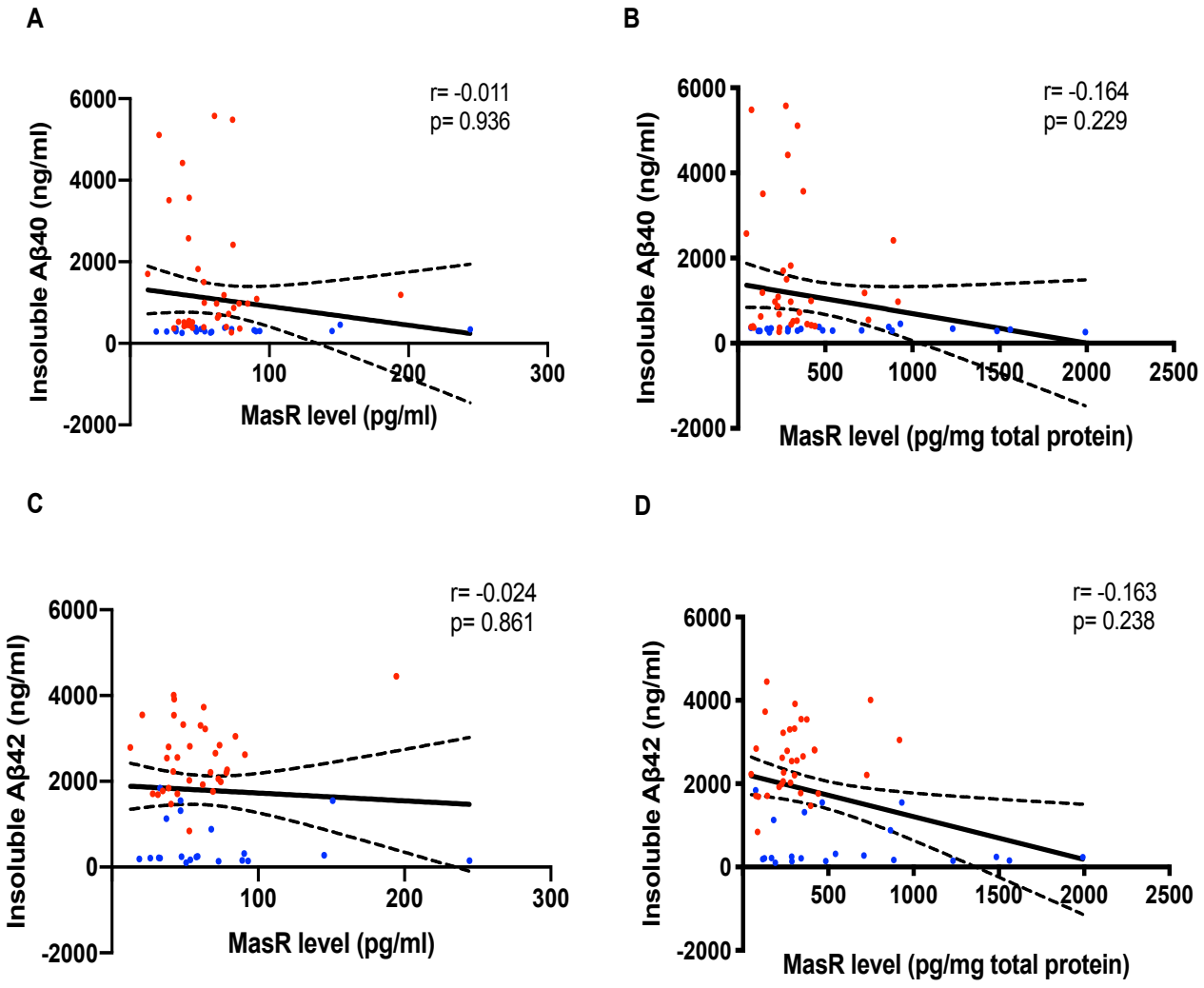

Figure 4.11 Relationship between MasR level and insoluble Aβ40 and insoluble Aβ42.

A and C. Scatterplots showing no correlation between total MasR level and both insoluble Aβ40 and insoluble Aβ42 (measured by enzyme-linked immunosorbent assay), Spearman's correlation coefficient (r= -0.011, p= 0.936), (r= -0.024, p= 0.861). B and D. Scatterplot showing no significant correlation between MasR protein-adjusted level and both insoluble Aβ40 and insoluble Aβ42,

Spearman's correlation coefficient (r= -0.164, p= 0.229) and (r= -0.163, p= 0.238) respectively. The solid inner line indicates the best-fit linear regression and the outer lines the 95% confidence intervals. Blue dots = controls, red dots = AD cases.

4.5.4 Expression of MrgD in human brain tissue

To detect the expression of MrgD in human post-mortem brain tissue, the specificity of MrgD antibody, (NB1-91964) was tested by western blot. Four AD cases and four non-diseased controls were chosen randomly for this experiment. Details of the chosen samples are described in chapter 9 (Appendix I: Table 9.7).

4.5.4.1 Validation of MrgD antibody specificity using western blot

A representative image is shown of the western blot with the MrgD antibody (Figure 4.12). A prominent single band at approximately 37 kDa is observed, consistent with expected MW of MrgD (555). The identity of some very faint lower bands detected at a MW 25 kDa is unknown but is potentially representative of a degradation product of MrgD or non-specific binding. Very faint higher MW bands at ~ 150 kDa are also observed; the identity of these bands is also unknown. There was no significant difference in band volume in AD and controls (p= 0.574).

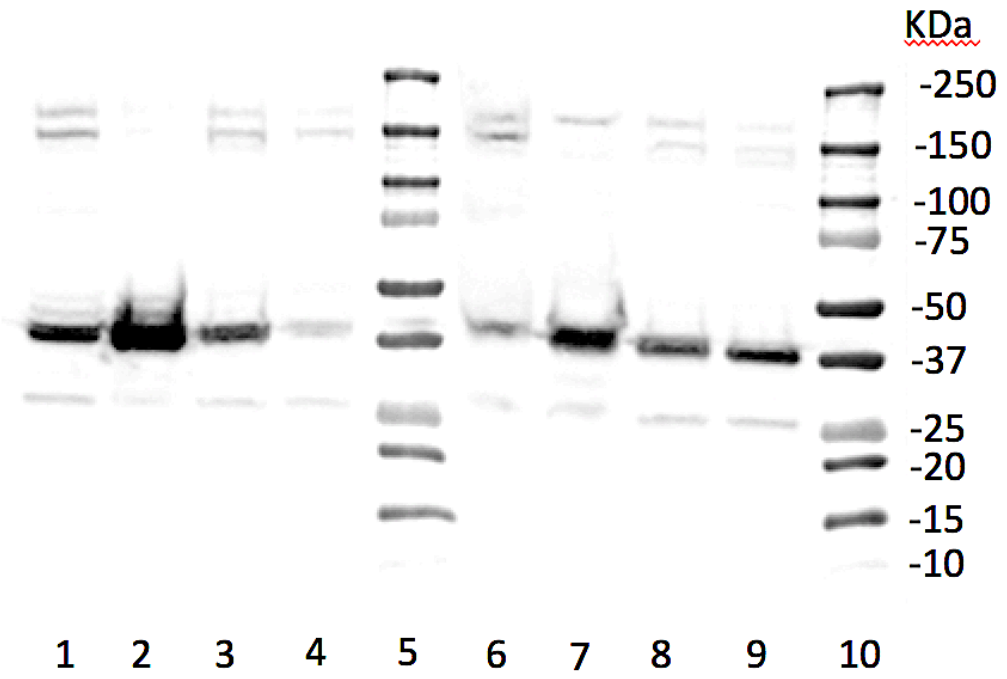

Figure 4.12 Detection of MrgD in mid-frontal cortex in human post-mortem brain tissue homogenates using Western blot.

MrgD expression in human brain tissue was studied by Western blotting: left side represents expression of MrgD in human brain tissue of controls (lines 1-4). Right side shows MrgD expression in AD cases (lines 6-9). Lanes (5 and 10) include MW markers. The membrane was blotted with polyclonal rabbit antibody to MRGD (NBP1-91964). The reported molecular weight of MrgD was around 37 kDa. The smaller bands at MW 25 kDa are likely to be protein degradation products.

4.6 Discussion

In this study, the downstream rRAS (ACE-2/Ang (1-7)/MasR) pathway that has recently been shown to be dysregulated in AD was further investigated. The brain rRAS pathway has been shown to counter-regulate the cRAS in various disease-associated scenarios. ACE-2 activity has been reported to be reduced in AD in relation to increased amyloid and tau load (417). Here we measured the levels of Ang (1-7) and explored the distribution of MasR in AD in relation to disease pathology. We found that the ratio of Ang:II:Ang (1-7) is increased in AD in keeping with our previous study showing that ACE-2 activity, the rate limiting enzyme in the ACE-2/Ang (1-7)/MasR pathway, is reduced in AD. Surprisingly, however, the level of Ang (1-7) was unaltered in AD as was MasR expression, which was predominantly expressed by pyramidal neurons within the neocortex. As opposed to ACE-2 activity, neither Ang (1-7) or MasR expression was related to amyloid or tau pathology. These data suggest that changes in rRAS downstream of ACE-2 remain unaltered in AD.

Our findings in human post-mortem brain tissue contrast with previous studies in animal models of AD that found reduced Ang (1-7) level in SAMP8 mice (an animal model of overproduction of APP) and P301S mice - an animal model of pure tauopathy. Ang (1-7) level was inversely correlated with tau hyperphosphorylation (416). This inconsistency may simply be due to the differences in species (animal vs. human). These animal models in previous studies have more aggressive Aβ pathology and tauopathy, which is associated with more extensive oxidative stress and brain damage, compared to brain changes in the human brain of an AD patient (556). Some of the differences may also relate to regional differences. The hippocampus was studied in mice, whereas here we studied the mid-frontal cortex. An important next step would be to validate my initial findings in other regions such as the entorhinal cortex and hippocampus. Some of the discrepancies could also simply be a reflection of different methods used to measure Ang (1-7): we measured Ang (1-7) using in-house direct ELISA while the previous study used commercially ELISA kits (S-1330; Bachem Inc.). Although we have also measured Ang (1-7) in a subset of cases, control (n= 19) and AD cases (n= 19) using a commercially available ELISA (Human angiotensin (1-7) ELISA kit) (MyBiosource) and found no difference in AD. It will be important to validate our data using another approach such as western blotting or another sandwich ELISA.

It is also important to consider that there are alternative pathways that might give rise to the generation of Ang (1-7) in brain tissue e.g. from conversion of Ang (1-9) into Ang (1-7) by the action of ACE-1. Since the activity of ACE-1 has been found to be increased in AD (78), the production of Ang (1-7) from this pathway may compensate for the reduced production of Ang (1-7) from the ACE-2 mediated action on Ang-II. This would also suggest the potentially important role of Ang (1-9) as a reservoir to potentially help offset dysregulation of the rRAS in AD and thus requires further study. Despite the unchanged Ang (1-7) level in AD, the ratio of Ang-II to Ang (1-7) was increased in AD. This is consistent with observed reports of reduced ACE-2 activity and in turn reduced ACE-2 mediated production of Ang (1-7) (417). Although these data support recent studies that ACE-2 is dysregulated in AD, that levels of Ang (1-7) and MasR (downstream of ACE-2) are unaltered in AD may suggest the involvement of additional mechanisms that have yet to be identified and explored in AD. Furthermore, additional validation studies would be helpful in confirming or refuting these unexpected findings across different regions in human post-mortem brain tissue.

Immunohistochemical staining sought to determine the expression of MasR in human brain tissue. Immunolabelling of MasR showed positive staining in parenchymal neurons in the human mid-frontal cortex. This result is in keeping with the IHC findings of Becker *et al.* (438) who previously detected

MasR in neurons within the rat brain and previous studies that also detected MasR in neurons (253, 326, 557, 558). The immunostaining showed no obvious difference in the expression of MasR between AD, VaD and age-matched controls, however, the nature of this very small pilot study prevented any meaningful statistical analysis. MasR staining of some blood vessels was observed in vascular cases, which supports a previous study showing positive MasR immunolabelling in small and large cerebral vessels (327) and others report positive staining of MasR in microglia (327), a finding that we did not replicate on initial inspection.

Whilst there has been an observed reduction of ACE-2 activity in the mid-frontal cortex of AD cases (417), there are no previous studies that have measured MasR level in AD patients. Previous studies in animal models of stroke have been inconsistent: Lu *et al.* (331) found increased expression of MasR and cerebral Ang (1-7) level in an ischaemic rat model with overactivation of ACE-2 activity. Similarly, MasR was observed in an area surrounding ischaemia in rodents (559). These results are in contrast to earlier findings that indicated a decline in MasR with advanced age (397) and down-regulation of (Ang (1-7)/MasR) axis in an ischaemic model (560). These apparent discrepancies could be attributed to the rat ischaemic model used in these studies and the type of ischaemia induced (e.g. acute vs. chronic). The combined and unknown potential confounding effects of cerebrovascular damage on MasR expression in AD cases is similarly not known in this study and has the potential to mask any pure AD-related changes.

This study was limited by the characterisation of expression of rRAS markers in one brain area (mid-frontal cortex) while investigating other brain regions (temporal and hippocampus) will be interesting. Another limitation of this study was the measurement of Ang (1-7) was through one limited methodological approaches (direct and sandwich ELISA). However, this peptide has a short half-life and arguably needs to be detected by more sensitive methods. While we did not find any significant difference of PMD in our cohort, degradation of Ang (1-7) in brain tissue might be affected by PMD. It is also conceivable that a larger cohort sample size might have allowed detection of any alterations in Ang (1-7) or MasR, however the similarities in the existing levels, both unadjusted and adjusted suggests this might be unlikely. Further research should be undertaken to characterise the expression of these rRAS markers Ang (1-7) and MasR (and the other less known MrgD receptor) in different brain regions and by more than one method such as IHC for MrgD and RT-PCR for both receptors. Some additional work to investigate other RAS metabolites such as Ang (1-9) might also be timely, as it provides another means to the production of Ang (1-7) and possibly has a bearing on the scale and overall consequences of dysregulation of this rRAS pathway in AD. More investigation on the

expression of MrgD and its agonist (Alamandine) in human post-mortem brain tissue will be informative about the role of this peptide in AD pathogenesis

In conclusion, this chapter provides some evidence in support of previous findings of reduced ACE-2, the rate-limiting enzyme in the non-classical axis of brain rRAS in AD. However, the levels of downstream mediators within this pathway, including Ang (1-7) and MasR, are unchanged in AD and not related to disease pathology. It is unclear if changes in other alternative downstream rRAS pathways are associated with AD pathology.

Chapter 5. Alternative regulatory pathway of brain RAS (APA/Ang-III/APN/Ang-IV/IRAP) in Alzheimer's disease

5.1 Abstract

Hyperactivity of the brain cRAS is associated with AD pathogenesis. In addition to a common ACE-2 mediated rRAS pathway, there are also additional alternative downstream pathways in RAS that have been identified in the brain, including the APA/Ang-III/APN/Ang-IV/IRAP axis, which is immediately downstream of Ang-II and is believed to regulate cerebral blood flow and has been implicated in memory and learning acquisition and synaptic plasticity. It has previously been shown that the upstream pathway of the alternative brain RAS axis (APA/Ang-III/APN) is dysregulated in AD in association with disease pathology. However, the involvement of the further downstream elements of this alternative regulatory RAS pathway (i.e. Ang-IV/IRAP) in relation to AD pathogenesis remains unclear. In this chapter, we investigated the expression and distribution of Ang-IV and the Ang-IV binding receptor, IRAP, in AD in a well-characterised cohort of post-mortem brains.

Human post-mortem brain tissue was obtained from the SWDBB, University of Bristol, with local Research Ethics Committee approval. We studied mid-frontal cortex (Brodmann area 8/9) from AD cases (n= 70) and age-matched controls (n= 48) that were matched closely for age-at-death and PMD. The level of Ang-IV was measured by sandwich ELISA. The expression and distribution of IRAP was determined by sandwich ELISA and IHC. The enzyme activity of IRAP was also measured using an in-house developed catalytic activity assay. Pre-existing data on Braak tangle stage and pathological hallmarks (total insoluble Aβ, insoluble Aβ40 and Aβ42 and tau load) was also available for analysis.

The levels of both Ang-IV and IRAP remained unchanged in AD whereas IRAP enzyme activity was significantly reduced in AD (p= 0.003). IRAP activity, which is arguably the most biological meaningful measure for this part of the pathway, was inversely correlated with total insoluble Aβ and tau load.

In conclusion, my studies extend previous work on downstream alternative regulatory pathways of brain RAS in AD and show that they extend further through to the Ang-IV/IRAP (AT_4R) elements of this pathway in a way that is associated with AD pathology.

5.2 Introduction

The brain RAS has a vital role in the pathophysiology of hypertension but is also involved in cognitive function and has been implicated in several neurodegenerative disorders of the CNS (255). As previously mentioned, the overall balance of this peptidergic system is reliant on the function of two main opposing axes: the cRAS (ACE-1/Ang-II/AT_1R) and the rRAS (ACE-2/Ang (1-7)/MasR) (56, 253). However, an additional regulatory pathway also exists that is downstream of where both cRAS and rRAS interact, which is the production or degradation of Ang-II. This pathway has been identified in the brain comprising the APA/Ang-III/ APN/Ang-IV/IRAP axis (457) (Figure 1.14). In short it is an additional or alternative mechanism to ACE-2 mediated regulation of Ang-II levels and through a series of sequential enzymatic steps can generate additional downstream Ang-II metabolites. There is already some evidence that dysregulation of the upper part of this axis (APA/Ang-III/ APN) is associated with AD pathology. Elevated Ang-III in AD was found in relation to increased APA activity and reduced APN activity and was strongly related to both Aβ and tau load (to a greater extent than had previously been found for Ang-II) (393).

The APA/Ang-III/APN/Ang-IV/IRAP, rRAS pathway controls cerebral blood flow, modulates memory and learning acquisition. It also enhances synaptic plasticity and has neuroprotective effects in the CNS (458). These protective effects have largely been attributed to the active peptide, Ang-IV (270), which is produced from Ang-III by the action of APN. Ang-III is itself generated from Ang-II by APA and/or DAP cleavage (427). Thus, both APA and DAP perform a similar function to ACE-2 in serving to lower Ang-II levels but produce different metabolites that in turn serve as different substrates for different receptors. Originally, Ang-IV was considered be an inactive small fragment of RAS, however, recent studies have shown that this hexapeptide regulates several physiological functions within the brain (528). What has given rise to some confusion and debate in the field is the discussion in relation to the identity of the Ang-IV specific binding site and effector receptor of Ang-IV. Some groups have described this as the AT_4R receptor whilst others have suggested it to be the insulin- regulated aminopeptidase (IRAP) (474, 496, 561). Some of the studies designed to define and characterise the AT_4R binding site in the human brain showed that it was highly distributed in the cerebral cortex, hippocampus and claustrum (472) but also the similarities with those seen for IRAP led to the proposal that IRAP was AT_4R (474). Yet, there still remains some controversy and debate because more recently, Ang-IV was also found to bind and activate c-Met - a type 1 tyrosine kinase receptor (499), the function of which in the brain still remains largely unknown.

Several previous studies have focused on the effect of Ang-IV on cognitive function, especially in learning and memory. Brazko *et al.* (482) demonstrated that enhanced memory following ICV administration of Ang-II was caused by the shorter (Ang-IV) peptide. ICV administration of Ang-IV into the lateral ventricle in non-diseased rats was also found to enhance spatial working memory in the plus maze spontaneous alteration task (479). In addition, ICV infusion of Ang-IV rapidly improved novel object recognition in a C57BL/6J mouse model that was dependent on AT_4R expression (484). More recently, activation of Ang-IV/AT_4R was found to restore Aβ-related cognitive deficit and cerebrovascular deficits in transgenic C57BL/6 mice overexpressing the human APP, carrying the Swedish and Indiana mutations (APP mice, J20 line) (493). A cerebroprotective role of Ang-IV/AT_4R was shown to be associated with increased CBF through stimulation of NO production (458, 494, 495). Overall, these findings suggested that an Ang-IV/AT_4R pathway was a potential target for improving cognitive decline and cerebrovascular deficits in AD.

As mentioned, several studies identified IRAP as a specific binding site for Ang-IV and likely candidate for the AT_4R (474, 496, 561). IRAP is a type II transmembrane protein and belongs to the M1 aminopeptidase family that includes two other homologous aminopeptidases including APA and APN (458). Localisation of both IRAP mRNA and IRAP protein were found in areas similar to the distribution of Ang-IV (AT_4R) binding site in mouse brain (474). The highest distribution of IRAP was found in brain areas associated with cognitive functions such as prefrontal cortex, entorhinal cortex, hippocampus and amygdala (496). Notably IRAP was also found to co-localise with GLUT4, in the same vesicles in the pyramidal neurons of the hippocampus and was found to facilitate glucose intake in active neurons (497).

Ang-IV has been reported to improve cognition by acting on two different receptors, IRAP and the c-Met receptor. First, Ang-IV acts as an IRAP inhibitor by binding to and inactivating IRAP. Ang-IV-mediated inhibition of IRAP catalytic activity, in turn prevents the degradation and prolongs the half-life of neuropeptides that have also been implicated in learning and memory such as oxytocin, vasopressin, met-enkephalin and Ang-III that are normally cleaved by IRAP (498, 500). Second, Ang-IV acts on the c-Met receptor and activates several signaling pathways that positively modulate synaptic plasticity and facilitate memory acquisition. These include:

i) Ang-IV increases intracellular calcium and enhances NO synthase (495);

ii) Ang-IV increases calcium entry via different calcium channels and enhances synaptic transmission and LTP (478, 510);

iii) Ang-IV increases acetylcholine synthesis and release (511);

iv) Ang-IV stimulates dendritic growth in the hippocampus (512).

Several animal studies have shown the beneficial effects of IRAP inhibitors (Ang-IV and LVV haemorphin-7) on cognitive function, especially spatial working memory (479, 500). In addition, other small molecule IRAP inhibitors (benzopyran compounds) have been developed to enhance learning and memory by increasing hippocampal dendritic spine density via a GLUT4 mediated mechanism in animal models (498, 502, 562-565). In a recent animal study, regional-specific IRAP knockout in the postnatal forebrain in mice resulted in a decline in spatial and object recognition memory (504).

In related research, plasma activity of IRAP was studied and found to be significantly reduced in AD patients compared to controls and there was some evidence that the IRAP activity correlated with the MMSE result (258). These studies support the hypothesis that IRAP has a vital role in cognitive function but seem to contradict earlier findings. More recently, we showed that dysregulation of the upper part of this IRAP regulatory pathway was associated with Aβ and tau pathology (393). However, there is little data on the role of the Ang-IV/IRAP pathway in AD pathogenesis, whilst understanding of the behaviour of each of the components of the APA/Ang-III/APN/Ang-IV/IRAP pathway in AD remains poorly characterised, particularly in human post-mortem tissue in AD.

5.3 Study aims and hypothesis

The aims of the study described in this chapter were:

(i) To measure the level of Ang-IV and calculate the ratio of Ang-III:Ang-IV in mid-frontal cortex in AD in relation to disease pathology
(ii) To characterise the expression and distribution of IRAP in AD in relation to markers of disease pathology
(iii) To measure the catalytic activity of IRAP in AD and examine the relationship between IRAP activity and AD pathological hallmarks

We wished to test the hypothesis that the lower downstream components of the alternative regulatory axis of brain RAS (Ang-IV/IRAP) are altered in mid-frontal cortex in AD and are associated with pathological markers of AD.

5.4 Methods

5.4.1 Study cohort

Human post-mortem brain tissue homogenates from mid-frontal cortex (Brodmann area 8/9) were used in this study and included a total of controls (n= 48) and AD cases (n= 70) for measurements of Ang-IV level, IRAP level and IRAP activity. Demographic features of study cohort are described in the methods section (Table 2.1) or for full details (Appendix I: Table 9.1 and Table 9.2).

Previous measurements of total insoluble Aβ by sandwich ELISA were available for controls (n= 28) and AD cases (n= 61) (545). Tau load was previously measured for all cases as part of routine assessment of AD cases within the SWDBB by field fraction analysis and was available for controls (n= 29) and AD cases (n= 89). Both insoluble Aβ40 and insoluble Aβ42 were previously measured by sandwich ELISA and were available for controls (n= 20) and AD cases (n= 33) for insoluble Aβ42, for controls (n= 20) and AD cases (n= 34) for insoluble Aβ40 (314). Ang-III level was previously measured by direct ELISA in mid-frontal cortex and available for controls (n= 31) and AD (n= 62) (393). All these previous measurements of AD pathological hallmarks and Ang-III level were included for analysis in this chapter.

5.4.2 Ang-IV sandwich ELISA

The level of Ang-IV in brain homogenates (1% SDS) from the mid-frontal cortex was measured using a quantitative commercially available sandwich ELISA (Human Angiotensin 4 (ANG4) ELISA kit) (MyBioSource) according to the manufacturer's protocol (described in detail in chapter 2 section 2.8.3). Ang-IV was measured in duplicate for each case. Carry-over samples were repeated across all plates to facilitate adjustment for plate-to-plate variation. Ang-IV measurements were adjusted to total protein level for each brain homogenate sample where indicated. The variation of this assay was determined by calculating the intra-assay CV% (Example in Appendix IV: Table 9.30).

5.4.3 Expression of IRAP in human brain tissue

5.4.3.1 Western blot detection of IRAP in human post-mortem samples

The standard protocol for western blotting used in this study is as described in detail in chapter 2 (section 2.4). Details of the primary and secondary antibodies used are described in chapter 9 (Appendix II: Table 9.13) and (Table 9.14) respectively. In summary, for detection of IRAP in brain homogenate samples, the membrane was blocked in 10% milk/TBST buffer for 1 hour. After it had been washed with 0.05% TBST (3x 15 minutes) at room temperature on a shaker, the membrane was incubated with anti-LNPEP (an alias for IRAP) antibody (aa 1-50, IHC-plus) diluted 1:2000 in 5% milk/TBST antibody buffer overnight at 4°C (in the fridge) on a shaker. Following a wash step with 0.05% TBST (3x 15 minutes) at room temperature on a shaker, the membrane was incubated with secondary antibody (peroxidase conjugated anti-rabbit) diluted 1:5000 in 5% milk/TBST for 1 hour. After 3x 15 minutes wash steps with 0.05% TBST, A chemiluminescent HRP substrate (ECL) (Millipore) was added to the membrane in a 1:1 ratio (5 ml of reagent 1 and 5 ml of reagent 2) for 5 minutes. The images then were acquired using (ChemiDoc XRS+, Bio-RAD) and Image Lab software, version 5.0 (Bio-RAD).

5.4.3.2 Immunohistochemistry of IRAP in formalin-fixed paraffin-embedded tissue sections

The anti-LNPEP antibody ((aa 1-50) IHC-plus (LS-B12918)) was further tested by immunohistochemistry to detect and examine the distribution of IRAP in formalin-fixed brain tissue. A standard immunohistochemical staining protocol was used as described in detail in the chapter 2 (section 2.5). The immunohistochemical staining procedure was initially optimised by comparing antigen retrieval pre-treatment steps with either EDTA or citrate buffer and testing a range of dilutions of the primary antibody (1:100, 1:200, 1:500). The best assay conditions for IRAP staining were achieved when slides were pre-treated with citrate buffer and boiled in microwave for 10 minutes. After washing with running water for 5 min, slides were incubated with blocking serum for 20 minutes then incubated with the primary antibody (Anti-LNPEP antibody (aa 1-50) IHC-plus (LS-B12918)) diluted 1:200 in PBS (5 μg/ml) overnight. After rinsing the sections in two changes of PBS for 3 minutes each, the sections were incubated with Vectastain biotinylated universal secondary antibody for 20 minutes followed by another wash with PBS and then VectaElite ABC complex for 20 minutes,

rinsed again and incubated with DAB for 10 minutes, then washed in running water for 10 minutes and immersed in copper sulphate solution for 4 minutes, followed by washing in running water for 5 minutes. The sections were then counterstained with haematoxylin Gill II for 3 seconds, dehydrated, cleared and mounted.

5.4.4 IRAP sandwich ELISA

The level of IRAP in brain homogenates from the mid-frontal cortex was measured using a quantitative commercially available sandwich ELISA (Human Leucyl/Cystinyl aminopeptidase (LNPEP) ELISA Kit) (Cloud-Clone Corp.), according to the method described previously in chapter 2 (section 2.8.4). Unlike the anti-LNPEP (aa 1-50) IHC-plus (LS-B12918) used in IHC, the immunogen characteristic of anti-LNPEP in this kit was unspecified. Optimisation stepts to select appropriate homogenate dilutions are described in chapter 9 (Appendix II: Section 9.2.3.1). Brain homogenate samples were assayed in duplicate and four carry-over samples were repeated across all plates. The variation of this assay was determined by calculating the intra-assay CV% (Example in Appendix IV: Table 9.31).

5.4.5 IRAP activity assay

IRAP activity was measured in brain homogenates from mid-frontal cortex prepared as previously described (chapter 2, section 2.2.2). Brain homogenates used in this experiment were homogenised in 0.5% Triton X-100 buffer. This homogenisation method is also described in chapter 2 (section 2.10). All samples were measured in duplicate, whilst four carry-over samples were repeated in each plate. The variation between measurements was determined by calculating the intra-assay coefficient of variation (CV%) (Appendix IV: Table 9.32).

Preliminary experiments were performed to optimise the use of IRAP substrate L-Leucine-p-nitroanilide (L-Leu-pNA) (Sigma-Aldrich) in human brain tissue homogenates. The optimal concentration of the colorimetric substrate was first determined by testing 10-fold serial dilutions of the substrate ranging from (25- 25×10^{-6} mg/ml) on brain homogenates diluted 1:40 in assay buffer (0.05 M Tris, 0.14 M NaCl, pH 7.4) (Appendix II: Figure 9.8 A). Next, the optimal substrate dilution was tested by adding serial dilutions of the substrate ranging from (125-1.95 mg/ml) on brain homogenates diluted 1:40 in assay buffer (0.05 M Tris, 0.14 M NaCl, pH 7.4) (Appendix II: Figure 9.8

B). The optimal substrate concentration was chosen and tested on two different homogenate dilutions (1:10 and 1:20). Also, the effect of incubation length (1 hour, 2 hours and overnight) was determined. (Appendix II: Figure 9.9). Optimal conditions were achieved when the substrate L-Leu-pNA stock (1mM) was diluted (1:16), the homogenate was diluted (1:20) and the reaction proceeded overnight at 4°C. These conditions were used in all subsequent experiments. Enzyme activity was expressed as relative absorbance units (OD).

5.4.6 Statistical analysis

The Shapiro-Wilk normality test was applied to test the normal distribution of all datasets. A significant p value, $p < 0.05$ was used to indicate if the individual data sets were not normally distributed. Ang-IV and protein-adjusted Ang-IV data were not normally distributed. Both log transformed and square-root transformed data did not pass the normality test and therefore a non–parametric Mann-Whitney test, was used for both Ang-IV and protein-adjusted Ang-IV data when comparing between AD cases and controls. Comparison of the total Ang-IV level and Ang-IV protein-adjusted data between Braak tangle stage groups (Braak stage 0-II, Braak stage III-IV, Braak stage V-VI) was performed with the non-parametric Kruskal-Wallis test. Correlations between total Ang-IV level and protein-adjusted Ang-IV with total insoluble Aβ, tau load, insoluble Aβ40 and insoluble Aβ42 were assessed using Spearman's correlation coefficient analysis. The Ang-III-Ang-IV ratio data were not normally distributed and comparison of the Ang-III-Ang-IV ratio in controls and AD was tested using a non-parametric test, Mann-Whitney test.

IRAP level and protein-adjusted IRAP data were similarly not normally distributed. A non–parametric test, Mann-Whitney test, was performed to compare both IRAP and protein-adjusted IRAP between AD cases and controls. Comparison of the IRAP level and protein-adjusted IRAP data between Braak tangle stage groups (Braak stage 0-II, Braak stage III-IV, Braak stage V-VI) was performed using a non-parametric Kruskal-Wallis test. Correlations between IRAP level and protein-adjusted data with total insoluble Aβ, tau load, insoluble Aβ40 and insoluble Aβ42 were assessed using the Spearman's correlation coefficient. Log transformation for unadjusted and protein-adjusted data was performed to attempt to reach normal distribution. In this case, the transformed data was normally distributed and unpaired samples t-test was used for log transformed unadjusted and protein-adjusted data to compare between AD cases and controls. The transformed data is presented separately in chapter 9 (Appendix VI: Section 9.6.3.1).

IRAP activity data was not normally distributed. A non–parametric test, Mann-Whitney test was performed to compare between AD cases and controls. Comparison of the IRAP activity data between Braak tangle stage groups (Braak stage 0-II, Braak stage III-IV, Braak stage V-VI) was performed using a non-parametric Kruskal-Wallis test. Correlations between IRAP activity with total insoluble Aβ, tau load, insoluble Aβ40 and insoluble Aβ42 were assessed using the Spearman's correlation coefficient. Square-rooted transformation for IRAP activity data was shown to normalise the data. Unpaired samples t-test was used for transformed IRAP activity data to compare between AD cases and controls. A One-Way ANOVA test was performed to compare transformed IRAP activity data between Braak tangle stage groups. Correlations between transformed IRAP activity data and total insoluble Aβ, tau load, insoluble Aβ40 and insoluble Aβ42 were assessed by the Pearson's correlation coefficient. Analysis of the transformed data is presented in chapter 9 (Appendix VI: Section 9.6.3.2). For all tests, a P-value < 0.05 was considered statistically significant.

5.5 Results

5.5.1 Comparison of Ang-IV level in controls and AD

Ang-IV and protein-adjusted Ang-IV levels were unchanged between AD cases (n= 70) and controls (n= 48) (Figure 5.1 A and B). The median for Ang-IV level was lower in controls (21.71 pg/ml) than AD (26.55 pg/ml) but the Mann-Whitney test showed no statistical significance between groups (p= 0.501). The median for Ang-IV protein-adjusted data did not differ between AD cases (130.5 pg/mg total protein) compared to controls (150.6 pg/mg total protein). A Mann-Whitney test showed no statistical significance between groups (p= 0.744).

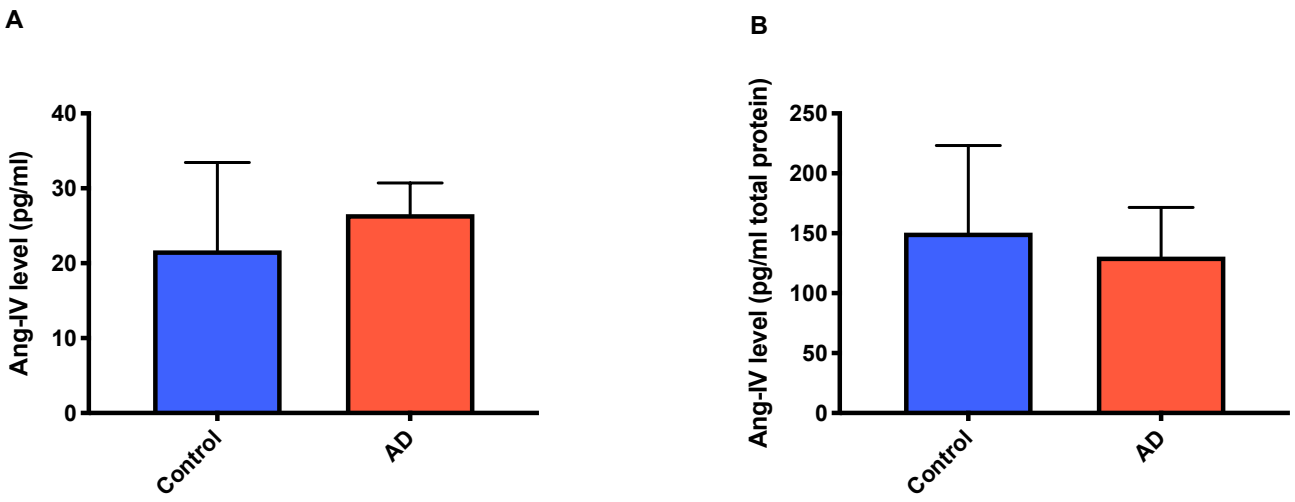

Figure 5.1 Angiotensin-IV level in mid-frontal cortex in Alzheimer's disease (AD).

A. Bar chart showing Ang-IV level is unchanged in AD (n= 70) compared with age-matched control (n= 48) in mid-frontal cortex measured using an Ang-IV sandwich ELISA, Mann-Whitney test (p= 0.501). The bars indicate the median and 95% confidence intervals. B. Bar chart showing protein-adjusted Ang-IV level did not differ in the AD group (n= 70) compared to age-matched group (n= 48), Mann-Whitney test (p= 0.744). The bars indicate the median and 95% confidence intervals.

5.5.1.2 Ang-IV level in relation to disease severity

The total Ang-IV level and Ang-IV protein-adjusted level were assessed in relation to Braak tangle stage (Braak stage 0-II (n= 36), Braak stage III-IV (n= 20), Braak stage V-VI (n= 61)). Kruskal-Wallis test indicated no significant difference of the total Ang-IV medians between Braak stage groups (p= 0.499) (Figure 5.2 A). The median of Braak stage 0-II= 29.176(pg/ml), Braak stage III-IV= 20.064 (pg/ml) Braak stage V-VI= 26.933(pg/ml). The medians of Ang-IV protein-adjusted level were unchanged between Braak stages. The median of Braak stage 0-II= 163.235 (pg/mg total protein), Braak stage III-IV= 130.487 (pg/mg total protein) Braak stage V-VI= 135.459 (pg/mg total protein) (Figure 5.2 B).

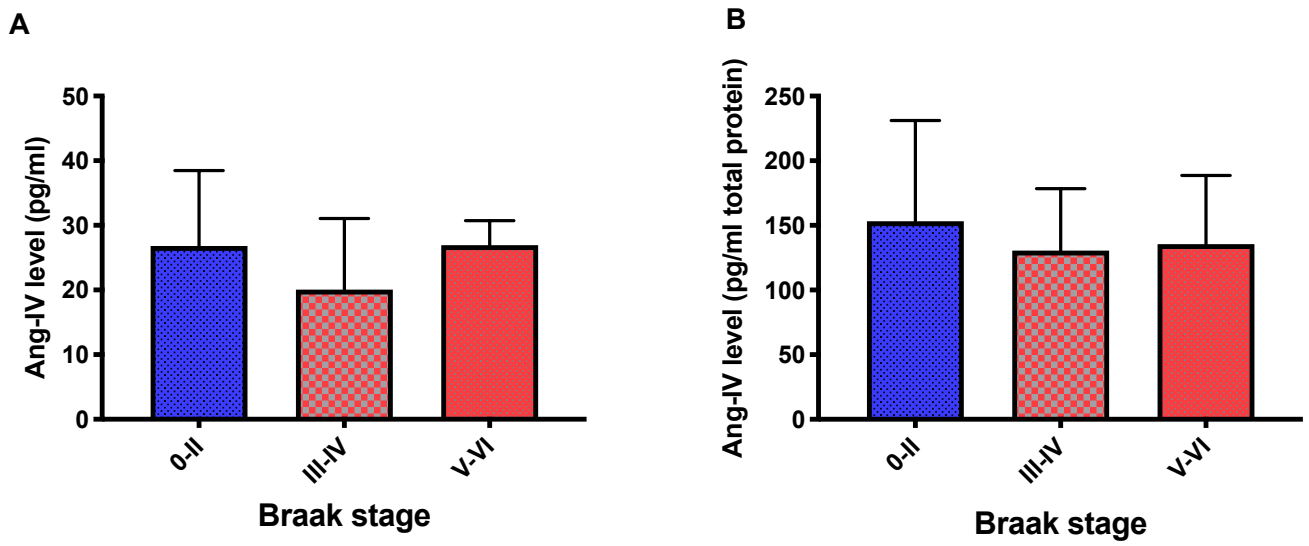

Figure 5.2 Angiotensin-IV level in relation to Braak tangle stage.

A. Bar chart showing no significant difference for total Ang-IV level measured by sandwich ELISA between Braak tangle stage groups (Braak stage 0-II (n= 36), Braak stage III-IV (n= 20), Braak stage V-VI (n= 61)), Kruskal-Wallis test (p= 0.499). The bars indicate the median and 95% confidence intervals. B. Bar chart showing Ang-IV protein-adjusted level was unchanged between Braak tangle stages groups (Braak stage 0-II (n= 36), Braak stage III-IV (n= 20), Braak stage V-VI (n= 61)), Kruskal-Wallis test (p= 0.577). The bars indicate the median and 95% confidence intervals.

5.5.1.3 Relationship between Ang-IV level and AD pathology hallmarks

No significant correlation was found between total Ang-IV level and total insoluble Aβ (Spearman's correlation coefficient r= 0.034, p= 0.746) and between Ang-IV protein-adjusted level and total insoluble Aβ (Spearman's correlation coefficient r= 0.065, p= 0.536) (Figure 5.3 A and B). Similarly, no correlation was seen between both total Ang-IV level and tau load (Spearman's correlation coefficient r= 0.087, p= 0.388) and between Ang-IV protein-adjusted level and tau load (Spearman's correlation coefficient r= 0.085, p= 0.399) (Figure 5.3 C and D).

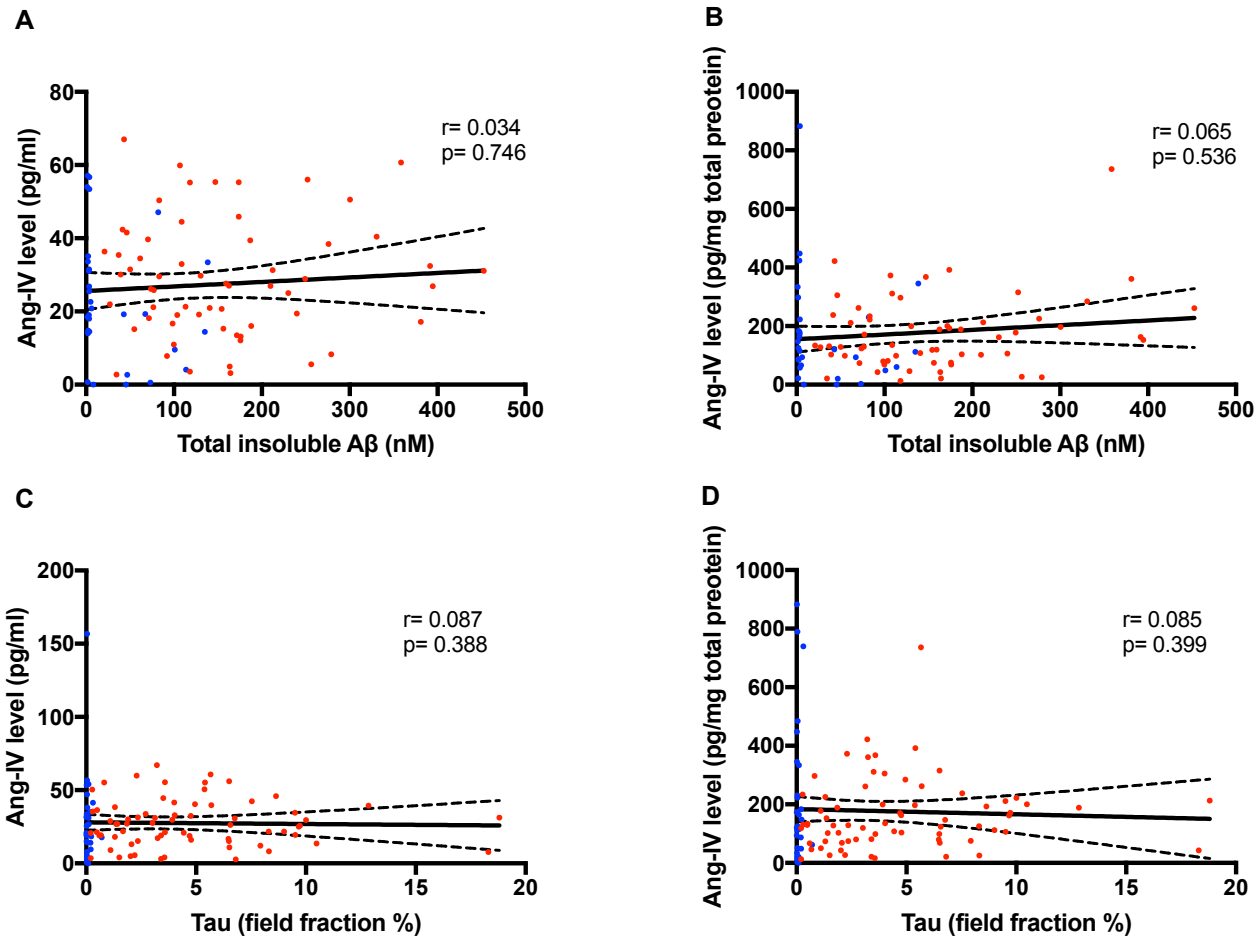

Figure 5.3 Relationships between Angiotensin-IV level and total insoluble Aβ and tau load.

A and B. Scatterplots showing no correlation between total Ang-IV level and Ang-IV protein-adjusted level and total insoluble Aβ (measured by enzyme-linked immunosorbent assay), Spearman's correlation coefficient (r= 0.034, p= 0.746) and (r= 0.065, p= 0.536). C and D. Scatterplots showing no significant correlation between total Ang-IV and Ang-IV protein-adjusted level and tau load (measured by field fraction analysis), Spearman's correlation coefficient (r= 0.087, p= 0.388) and (r= 0.085, p= 0.399). The solid inner line indicates the best-fit linear regression and the outer lines the 95% confidence intervals. Blue dots= controls, red dots= AD cases.

No significant correlations were observed between total Ang-IV level and both insoluble Aβ40 (Spearman's correlation coefficient r= -0.110, p= 0.419) and Aβ42 (Spearman's correlation coefficient r= -0.189, p= 0.167) (Figure 5.4 A and C). Ang-IV protein-adjusted level was not correlated with either insoluble Aβ40 (Spearman's correlation coefficient r= -0.197, p= 0.146) and Aβ42 (Spearman's correlation coefficient r= -0.203, p= 0.136) (Figure 5.4 B and D).

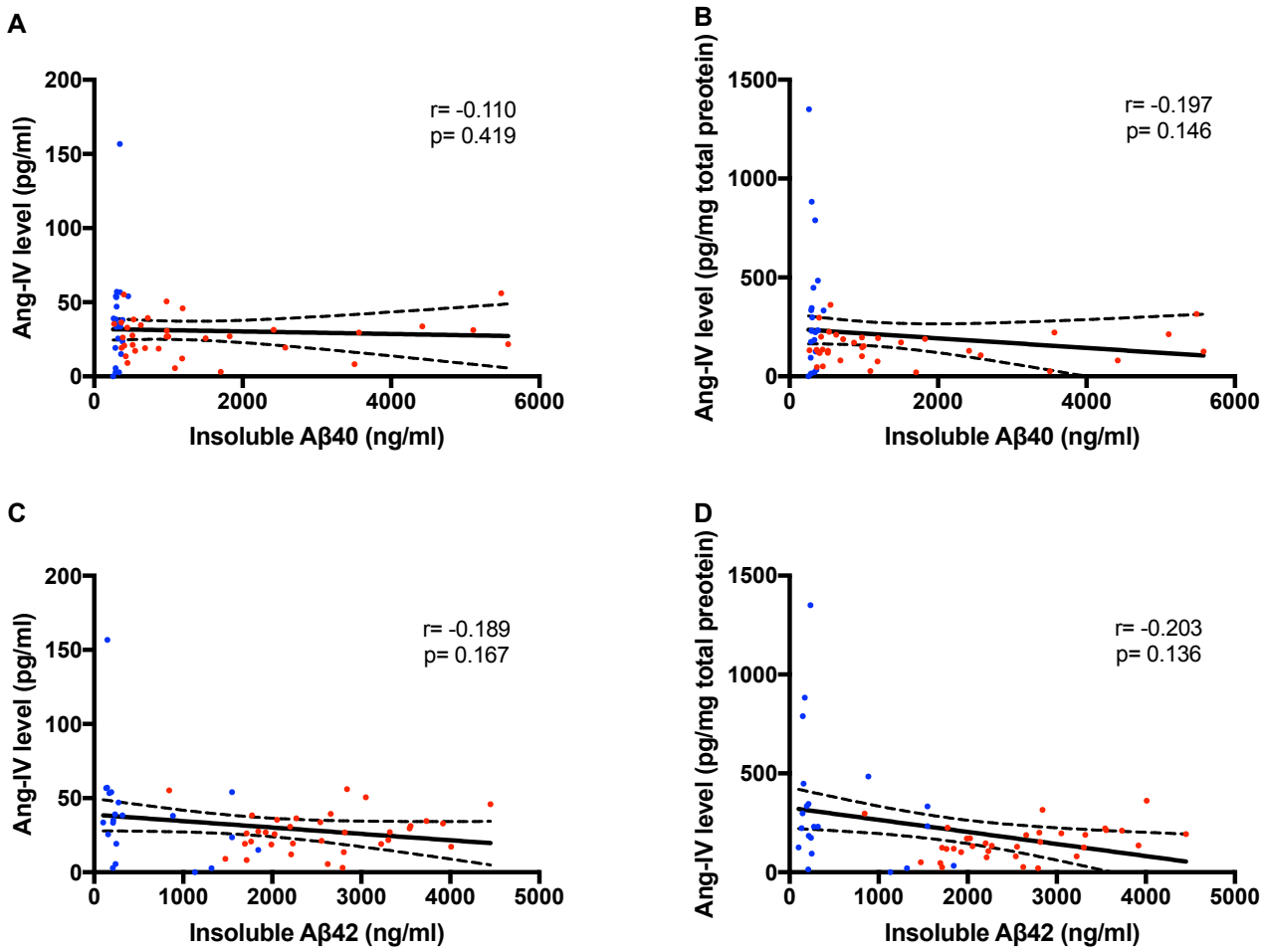

Figure 5.4 Relationship between Angiotensin-IV level and insoluble Aβ40 and insoluble Aβ42.

A and C. Scatterplots showing no correlation between total Ang-IV level and both insoluble Aβ40 (measured by enzyme-linked immunosorbent assay), Spearman's correlation coefficient (r= -0.110, p= 0.419), and insoluble Aβ42, Spearman's correlation coefficient (r= -0.189, p = 0.167). B and D. Scatterplots showing no significant correlation between Ang-IV protein-adjusted level and both insoluble Aβ40, Spearman's correlation coefficient (r= -0.197, p= 0.146) and insoluble Aβ42, Spearman's correlation coefficient (r= -0.203, p= 0.136). The solid inner line indicates the best-fit linear regression and the outer lines the 95% confidence intervals. Blue dots= controls, red dots= AD cases.

5.5.1.7 The Ang-III:Ang-IV ratio is unchanged in AD

The Ang-III:Ang-IV ratio can be viewed as a possible proxy marker for APN enzyme activity (responsible for the production of Ang-IV from Ang-III) in the Ang-III/APN/Ang-IV/IRAP pathway. Ang-III level was previously measured by direct ELISA in mid-frontal cortex of controls (n= 31) and AD (n= 62) and was shown to be significantly increased in AD (393). The median for Ang-III:Ang-IV

ratio was numerically slightly higher in AD cases (= 549.4) compared to the median of controls (= 370.5), suggestive of reduced APN enzyme activity, however, a Mann-Whitney test showed no statistical significance between the groups (p= 0.072) (Figure 5.5).

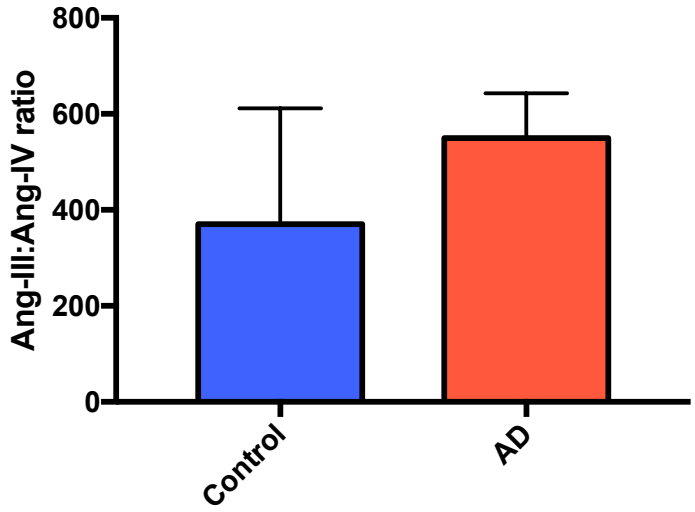

Figure 5.5 The ratio of Angiotensin-III:Angiotensin-IV in mid-frontal cortex in Alzheimer's disease (AD).

Bar chart showing the Ang-III:Ang-IV ratio in AD (n= 62) compared to age-matched controls (n= 31) in the mid-frontal cortex. Mann-Whitney test showed no significant difference between groups (p= 0.072). Bars show the median and 95% confidence intervals.

5.5.2 Expression of IRAP in human brain tissue

The specificity of the IRAP antibody (anti-LNPEP antibody (aa 1-50) IHC-plus (LS-B12918)), used for immunohistochemical staining to examine the distribution of IRAP in mid-frontal cortex, was first tested by western blot. This polyclonal antibody is raised against specific region between residue 1 to 50 of human LNPEP using the portion of GeneID: 4012. Randomly chosen samples from four AD and four control homogenates were used for this experiment. Details of the chosen samples are described in chapter 9 (Appendix I: Table 9.6). The western blot shown below in (Figure 5.6) shows distinct bands at the expected MW150 kDa. There was no obvious difference in the expression of IRAP in AD and controls. Volumetric analysis, using Image Lab software, version 5.0 (Bio-RAD) revealed that the band volume when averaged across groups, did not differ between AD and controls (p= 0.492).

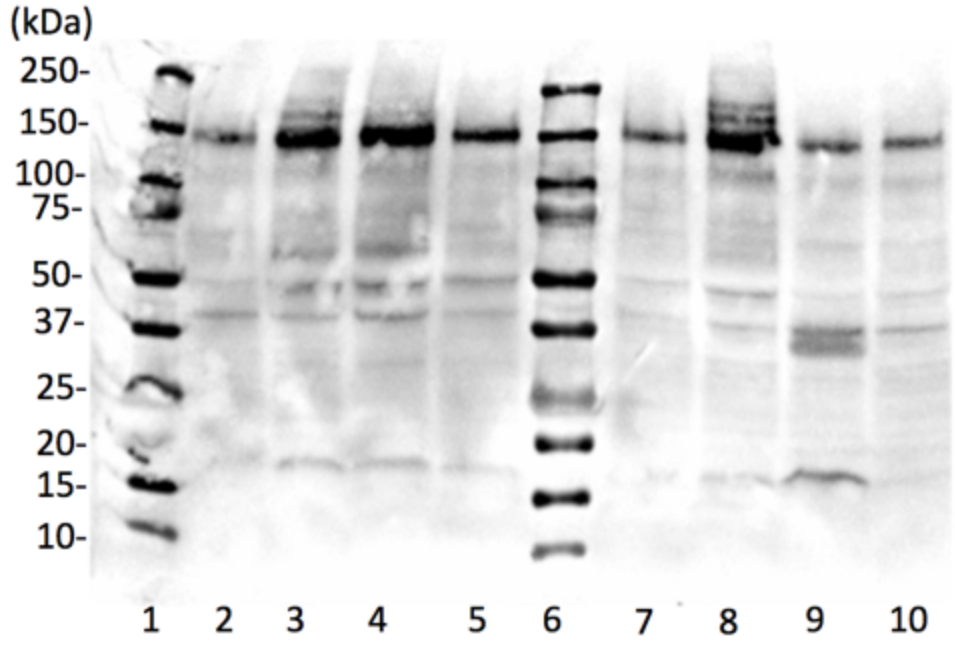

Figure 5.6 Insulin-regulated aminopeptidase (IRAP) expression determined by western blot in human post-mortem brain tissue homogenates.

IRAP expression in human brain tissue in controls (lanes 2-5) and AD cases (lanes 7-10). Lanes (1 and 6) include MW markers. The membrane was blotted with polyclonal rabbit antibody to IRAP (Anti-LNPEP antibody (aa 1-50) IHC-plus (LS-B12918)). The reported size of IRAP is predicted to be ~ 150 kDa.

5.5.2.2 Immunolabelling of IRAP in human brain tissue

IRAP labelling was predominantly neuronal in all studied sections of control, AD and VaD cases. Positive IRAP staining was mainly observed in pyramidal neurons with strong staining of dendrites (See Figure 5.7 B from an indicative AD case). There was no obvious observed difference in the level of IRAP staining between controls and VaD/AD cases, although we did not perform quantitative analysis because the number of sections studied was small and intended for a qualitative examination of the distribution and nature of IRAP staining only.

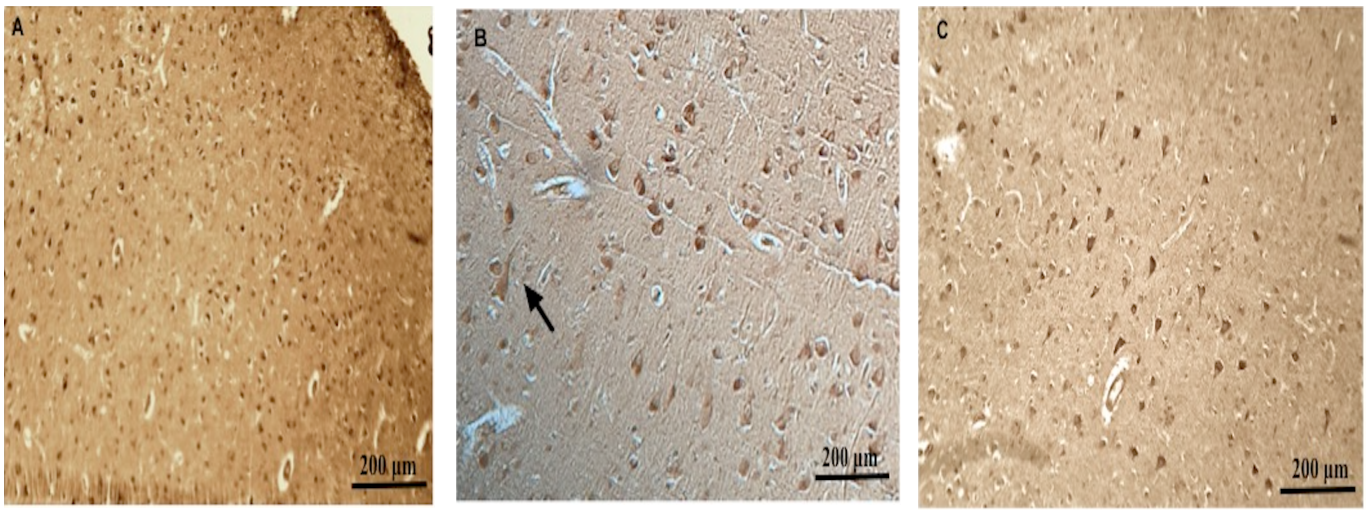

Figure 5.7 Immunolabelling of IRAP in the mid-frontal cortex.

IRAP labelling in brain sections from a control case (A), AD case (B) and vascular case (C) showed IRAP was mainly expressed in parenchymal neurons. In B. IRAP was present mainly in pyramidal neurons and dentrites (indicated by the arrow) (Images taken at 10x magnification).

5.5.3 Measurement of IRAP level by ELISA in controls and AD

IRAP level was not significantly different between AD cases (n= 70) and controls (n= 48) (Figure 5.8 A). The median for IRAP level was - controls= 12.26 (ng/ml) and AD= 11.46 (ng/ml). The data was not normally distributed so a Mann-Whitney test was performed but showed no statistical significance between groups (p= 0.997). The IRAP protein-adjusted level was similarly unchanged in AD cases compared to controls. Again, these data were not normally distributed. The median for IRAP protein-

adjusted level was - controls= 20.09 (ng/ml) and AD= 23.33 (ng/ml). Mann-Whitney test showed no statistical significance between groups (p= 0.405) (Figure 5.8 B).

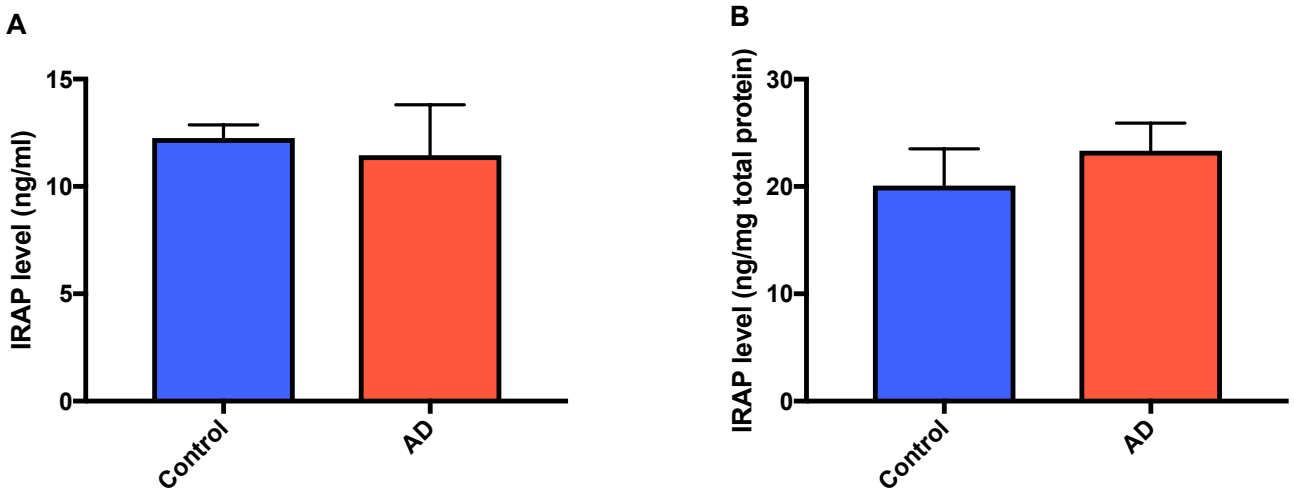

Figure 5.8 Measurement of IRAP level between controls and AD cases.

A. Bar chart showing IRAP level was unchanged in AD (n= 70) compared with age-matched control (n= 48) in mid-frontal cortex measured using an IRAP sandwich ELISA, Mann-Whitney test (p= 0.997). The bars indicate the median and 95% confidence intervals. B. Bar chart showing protein-adjusted IRAP level did not differ in AD group compared to age-matched group, Mann-Whitney test (p= 0.405). The bars indicate the median and 95% confidence intervals.

5.5.3.2 IRAP level in relation to disease severity

Both IRAP level unadjusted to protein concentration and protein-adjusted level were assessed in relation to Braak tangle stage (0-II (n= 36), III-IV (n= 20), V-VI (n= 61)). As for IRAP level, both datasets were not normally distributed. A Kruskal-Wallis test found no significant difference of the unadjusted IRAP medians between Braak stage groups (p= 0.885) (Figure 5.9 A). The median IRAP level in Braak stage 0-II= 11.757 (ng/ml), Braak stage III-IV= 12.524 (ng/ml) and Braak stage V-VI= 11.537 (ng/ml). The medians of IRAP protein-adjusted level were similarly unchanged between all Braak stages (p= 0.675). The median for Braak stage 0-II= 18.377 (ng/mg total protein), Braak stage III-IV= 21.002 (ng/mg total protein) and Braak stage V-VI= 23.667 (ng/mg total protein) (Figure 5.9 B).

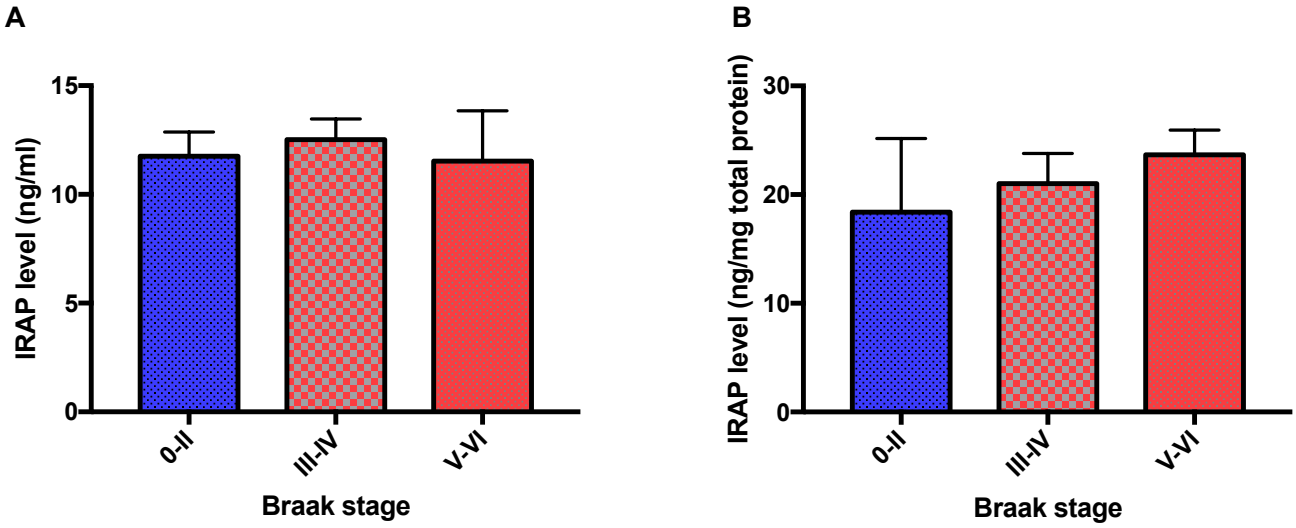

Figure 5.9 IRAP level in relation to Braak tangle stage.

A. Bar chart showing no significant difference for unadjusted IRAP level measured by sandwich ELISA assay and between Braak tangle staged groups (Braak stage 0-II (n= 36), Braak stage III-IV (n= 20), Braak stage V-VI (n= 61)), Kruskal-Wallis test (p= 0.885). The bars indicate the median and 95% confidence intervals. B. Bar chart showing IRAP protein-adjusted level was unchanged between Braak tangle staged groups (Braak stage 0-II (n= 36), Braak stage III-IV (n= 20), Braak stage V-VI (n= 61)), Kruskal-Wallis test (p= 0.675). The bars indicate the median and 95% confidence intervals.

5.5.3.3 Relationship between IRAP level and Aβ and Tau level

No significant correlation was found between unadjusted IRAP level and total insoluble Aβ (Spearman's correlation coefficient r= -0.087, p= 0.412) (Figure 5.10 A). IRAP protein-adjusted level similarly did not correlate with total insoluble Aβ in mid-frontal cortex, (Spearman's correlation coefficient r= -0.081, p= 0.445) (Figure 5.10 B). Similarly there was no correlation between unadjusted IRAP level (Spearman's correlation coefficient r= 0.023, p= 0.831) (Figure 5.10 C) or IRAP protein-adjusted level (Spearman's correlation coefficient r= 0.127, p= 0.207) (Figure 5.10 D) and tau load.

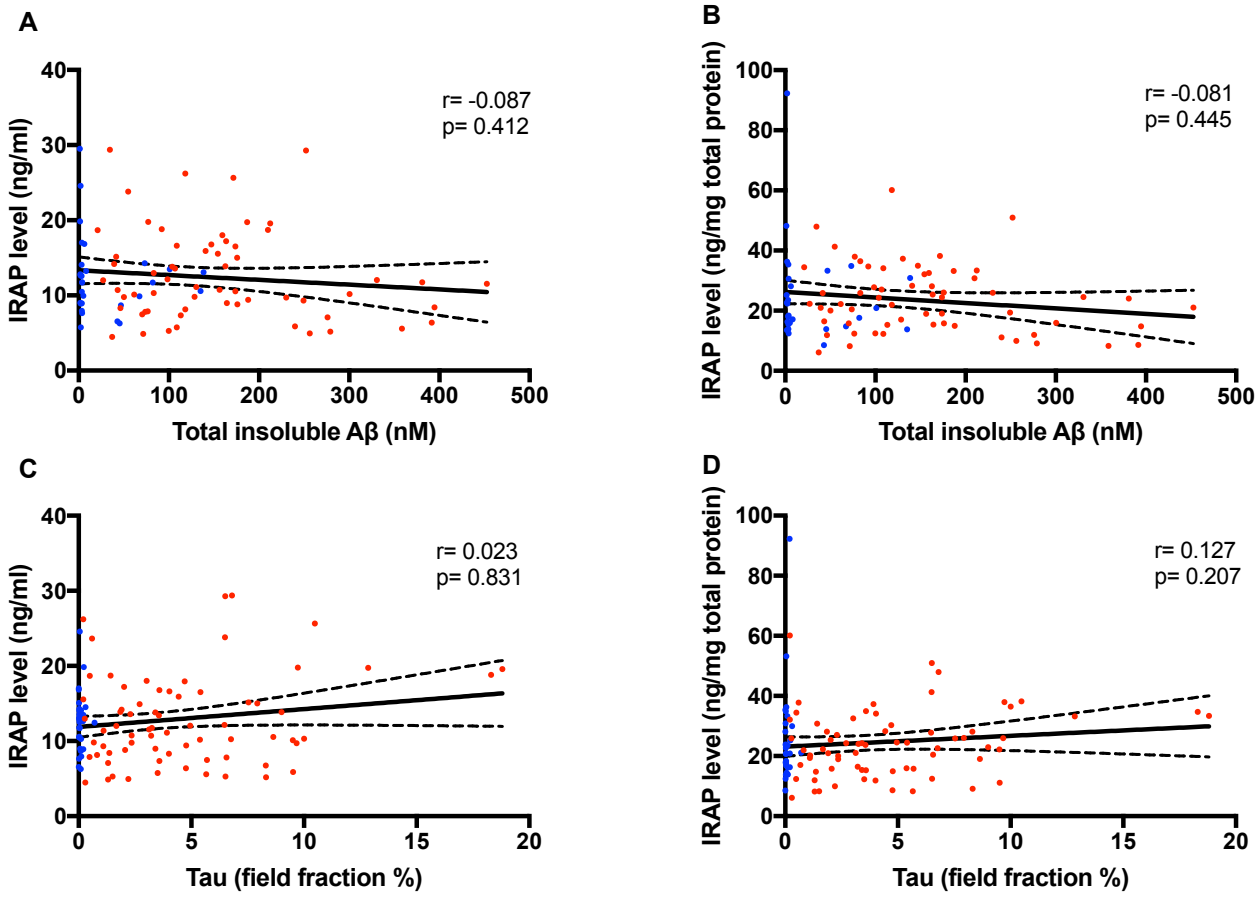

Figure 5.10 Relationships between IRAP level and total insoluble Aβ and tau load.

A and C. Scatterplots showing no correlation between unadjusted IRAP level and both total insoluble Aβ (measured by enzyme-linked immunosorbent assay), Spearman's correlation coefficient (r= -0.087, p= 0.412) and tau load (measured by field fraction analysis), Spearman's correlation coefficient (r= 0.023, p= 0.831). B and D. No significant correlation was found between IRAP protein-adjusted level and both total insoluble Aβ, Spearman's correlation coefficient (r= -0.081, p= 0.445) and tau load Spearman's correlation coefficient (r= 0.127, p= 0.207). The solid inner line indicates the best-fit linear regression and the outer lines the 95% confidence intervals. Blue dots = controls, red dots = AD cases.

Next we examined IRAP levels and Aβ40 and Aβ42. First, there were no significant correlations observed between unadjusted IRAP level and both insoluble Aβ40 (r= -0.055, p= 0.685) and Aβ42 (Spearman's correlation coefficient r= 0.069, p= 0.616) (Figure 5.11 A and C). Similarly, IRAP protein-adjusted level also did not correlate with either insoluble Aβ40 (r=0.186, p= 0.169) or Aβ42 (r= 0.206, p= 0.131) in mid-frontal cortex using Spearman's correlation coefficient test (Figure 5.11 B and D).

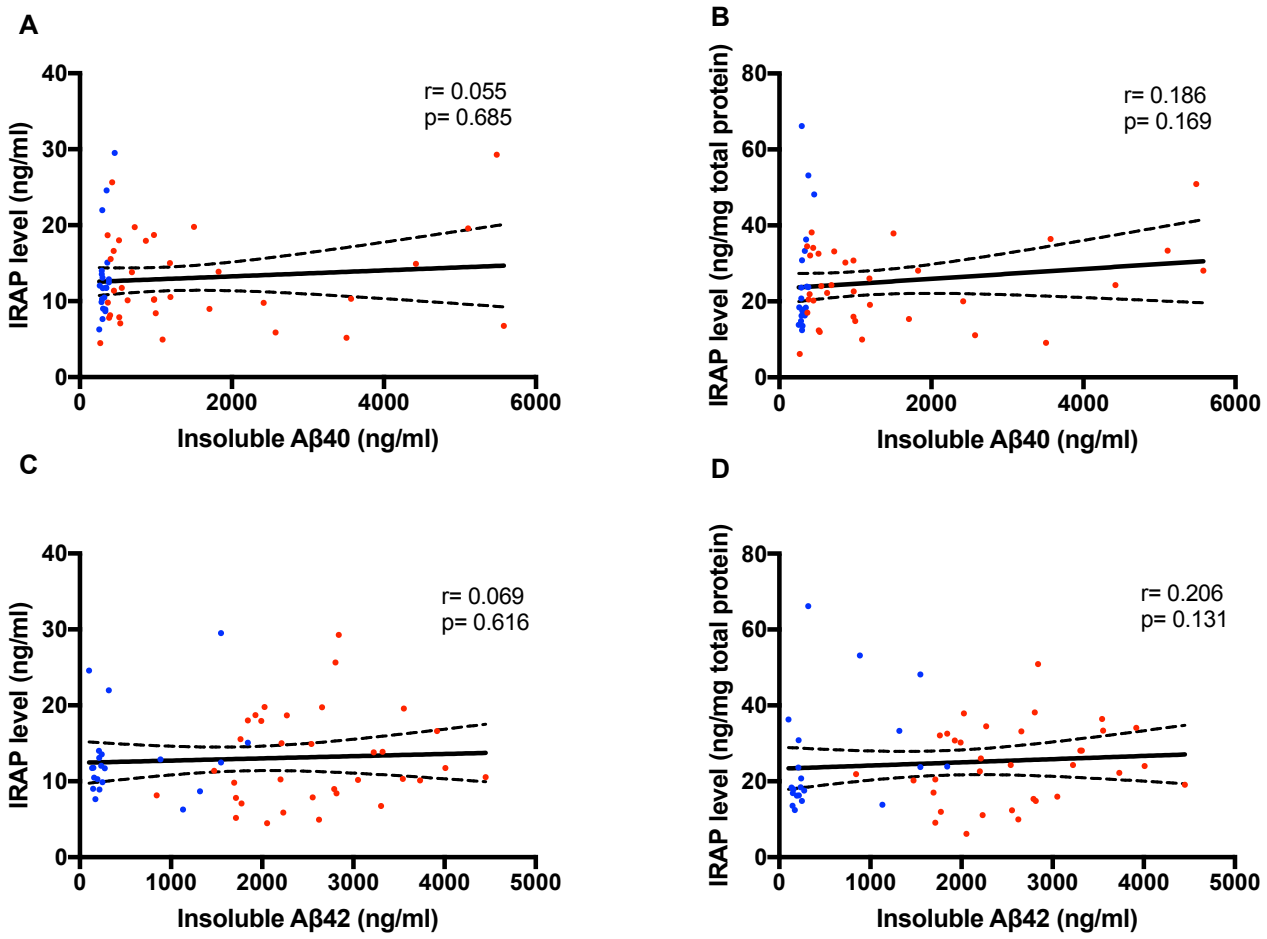

Figure 5.11 Relationship between IRAP level and insoluble Aβ40 and insoluble Aβ42.

A and C. Scatterplots showing no correlation between IRAP level and both insoluble Aβ40 (measured by enzyme-linked immunosorbent assay), Spearman's correlation coefficient (r= 0.055, p= 0.685), and insoluble Aβ42 (r= 0.069, p= 0.616). B and D. No significant correlation was found between IRAP protein-adjusted level and both insoluble Aβ40, Spearman's correlation coefficient (r= 0.186, p= 0.169) and insoluble Aβ42, Spearman's correlation coefficient (r= 0.206, p= 0.131). The solid inner line indicates the best-fit linear regression and the outer lines the 95% confidence intervals. Blue dots = controls, red dots = AD cases.

5.5.4 Comparison of IRAP activity in controls and AD

In mid-frontal cortex, IRAP enzyme activity was measured in AD (n= 70) and age-matched controls (n= 48). IRAP activity was found to be significantly reduced in AD cases compared to controls by 28.5%. A Mann-Whitney test revealed that the median OD for IRAP activity in AD cases (= 0.5623 (relative absorbance units (Abs))) was significantly lower than in controls (= 0.7863 (Abs)) (p= 0.003) (Figure 5.12 A).

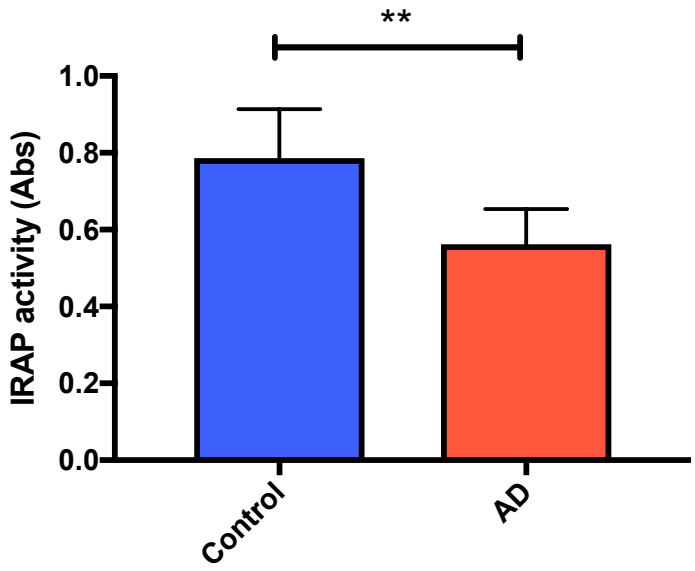

Figure 5.12 Reduction in IRAP enzyme activity in Alzheimer's disease.

Bar chart showing reduced IRAP enzyme activity in AD (n= 70) compared to age-matched controls (n= 48) in mid-frontal cortex measured using an in-house IRAP activity assay. Mann-Whitney test showed a significant difference between groups (p= 0.003). Bars show the median and 95% confidence intervals.

5.5.4.1 IRAP enzyme activity in relation to disease severity

IRAP enzyme activity was also assessed in relation to Braak tangle stage (0-II (n= 36), III-IV (n= 20), V-VI (n= 61)). Kruskal-Wallis test revealed a significant difference of the median between all groups (p= 0.008). Furthermore, a significant reduction of IRAP activity was observed in end-stage severe AD cases (Braak stages (V-VI)) compared to controls Braak stages (0-II) (p= 0.034) and earlier (less severe) AD cases (Braak stages (III-IV)) (p= 0.024) using Dunn's multiple comparisons test (Figure 5.13).

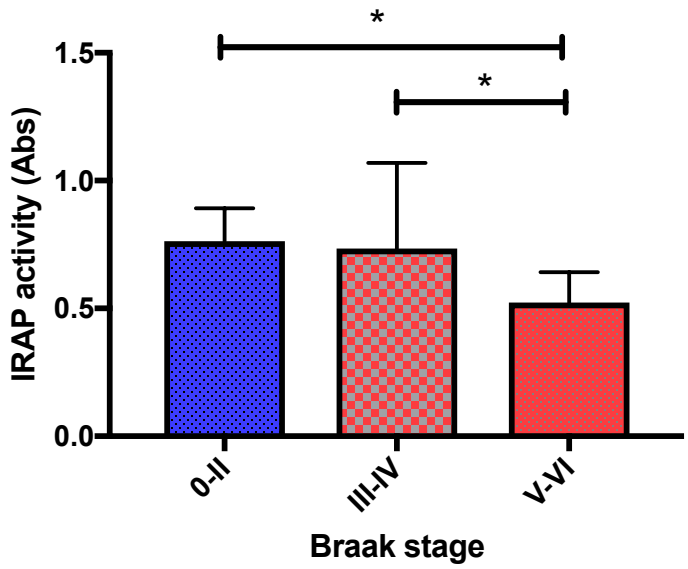

Figure 5.13 IRAP activity in relation to Braak tangle stage.

Bar chart showing a significant difference in IRAP activity between all groups (Braak stage 0-II (n= 36), Braak stage III-IV (n= 20), Braak stage V-VI (n= 61)) when analysed with Kruskal-Wallis test (p= 0.008). IRAP activity was found to be significantly lower in cases with higher Braak stage (V-VI) compared with cases in Braak stage (0-II) (post-hoc Dunn's multiple comparisons test, p= 0.034) and Braak stage (III-IV) (post-hoc Dunn's multiple comparisons test, p= 0.024) and. The bars indicate the median and 95% confidence intervals.

5.5.4.2 Relationship between IRAP enzyme activity and Aβ and Tau

Spearman's correlation coefficient test revealed a significant inverse correlation between IRAP enzyme activity with both total insoluble Aβ (r= -0.311, p= 0.003) (Figure 5.14 A) and tau load in mid-frontal cortex (r= -0.297, p= 0.003) (Figure 5.14 B). Spearman's correlation coefficient similarly revealed a significant inverse correlation between IRAP activity and insoluble Aβ40 (r= -0.312, p= 0.019) (Figure 5.14 C) but no significant correlation between IRAP activity and insoluble Aβ42 (r= -0.164, p= 0.229) (Figure 5.14 D).

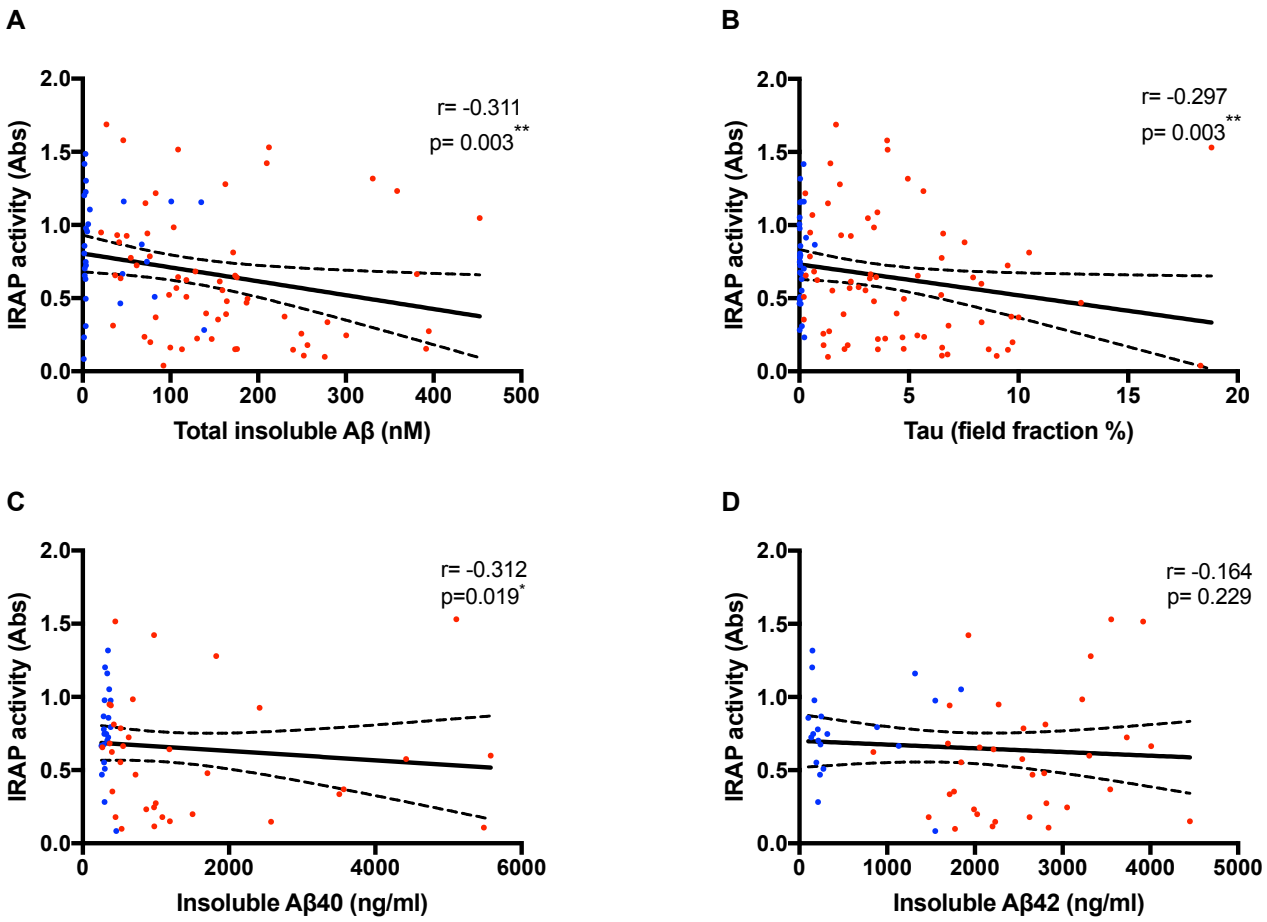

Figure 5.14 Relationships between IRAP enzyme activity and total insoluble Aβ, tau load, insoluble Aβ40 and insoluble Aβ42.

A. Scatterplot showing a significant inverse correlation between IRAP activity and total insoluble Aβ (measured by enzyme-linked immunosorbent assay), Spearman's correlation coefficient (r= -0.311, p= 0.003). B. Scatterplot showing a significant inverse correlation between IRAP activity and tau load (measured by field fraction analysis), Spearman's correlation coefficient (r= -0.297, p= 0.003). C. Scatterplot showing a significant inverse correlation between IRAP activity and insoluble Aβ40 (measured by enzyme-linked immunosorbent assay), Spearman's correlation coefficient (r= -0.312, p= 0.019). D. Scatterplot showing no correlation between IRAP activity and insoluble Aβ42 (measured by enzyme-linked immunosorbent assay), Spearman's correlation coefficient (r= -0.164, p= 0.229). The solid inner line indicates the best-fit linear regression and the outer lines the 95% confidence intervals. Blue dots= controls, red dots= AD cases.

5.5.4.3 Relationships between IRAP enzyme activity and confounding factors

Given the association between IRAP activity and variables associated with AD, we also explored and tested for relationships with confounding factors including age-at-death, gender, PMD and *APOE* genotype. On investigation no correlation between IRAP enzyme activity (either untransformed or square-root transformed) with age-at-death, PMD or gender (Appendix V: Table 9.37) was found. There was no difference in IRAP activity depending on the presence or absence of *APOE* ε4 allele (Appendix V: Table 9.38).

5.6 Discussion

This chapter explored changes in the main components of the downstream alternative pathway of brain rRAS (APA/Ang-III/APN/Ang-IV/IRAP) in relation to AD pathogenesis. In this chapter, we found that Ang-IV and IRAP protein expression within the mid-frontal cortex, the latter being predominantly expressed in pyramidal neurons, were unchanged in AD. In contrast, IRAP enzyme activity, arguably the most biologically relevant indicator, was reduced in AD in association with disease severity and Aβ and tau load. These data suggest that dysregulated IRAP activity in AD could contribute to disease pathogenesis.

Dysregulation of the upstream pathway of the alternative RAS axis (APA/Ang-III/APN/Ang-IV/IRAP) has previously been reported and is associated with AD pathogenesis. A previous study showed that increased Ang-III was strongly related to Aβ load and tau load, much more so than Ang-II. Furthermore, increased Ang-III level in AD was associated with increased APA activity (responsible for conversion of Ang-II to Ang-III) and reduced APN activity (responsible for conversion of Ang-III to Ang-IV). These data viewed together indicate that dysregulation within this major regulatory rRAS pathway was strongly associated with disease pathology in AD (393). I wanted to extend these findings with further investigations to characterise the expression of the components further downstream of Ang-III i.e. Ang-IV and IRAP, which both remained poorly characterised in human brain tissue in AD at the time of undertaking this work.

Despite observed changes in Ang-III and APA and APN (393) we did not find a change in Ang-IV expression in AD. This is the first study, to our knowledge, to characterise Ang-IV expression in

human post-mortem brain tissue from AD patients and compared with aged-matched controls. As such, and to provide greater confidence in my findings, it will be necessary to repeat these studies in different, preferably larger, indpendent studies.

Immunohistochemical staining was performed to qualitatively assess the expression and distribution of IRAP in the brain tissue of AD patients and controls. Immunolabelling revealed positive staining of pyramidal neurons and dendrites in the mid-frontal cortex. This is consistent with previous studies that reported IRAP expression was mainly restricted to neurons in the cortex, hippocampus and basal ganglia (425, 472). A few studies in rodent brain, however, reported positive IRAP staining within astrocytes (504, 566). Although I did not specifically perform co-labeling to identify astrocytes, based on morphology, we did not observe obvious positive staining of IRAP in non-neuronal cells. IRAP immunostaining did not appear to be different between control, AD and VaD cases. This was in agreement with the ELISA measurements of IRAP in a larger dataset that also found no change in the IRAP level in AD.

In contrast, IRAP enzyme activity was reduced in AD associated with disease severity and inversely correlated with Aβ load, tau load and insoluble Aβ40 level. These novel and interesting observations could indicate that IRAP – the terminal effector receptor of the rRAS pathway may contribute to disease pathology in AD. These findings are in keeping with a previous study that reported a reduction of IRAP activity in the plasma of AD patients (258). In contrast, a study of Gard *et al.* (464) reported no difference in serum IRAP activity in patients with early stage AD. These apparent differences in IRAP activity in AD might reflect differences in the tissue studied (e.g. brain versus serum versus plasma) or stage of disease, or possibly differences in the methodological approach (fluorogeneic or colorometric) used to measure IRAP activity. Together, these studies indicate possible disruption of IRAP activity within the CNS and periphery in AD that need to be evaluated and confirmed in larger independent studies.

A reduction of IRAP activity in our study is incongruent with previous studies in animal models that have found protective effects of IRAP inhibitors against cognitive decline (474, 479, 484, 493). These studies suggest that loss of IRAP activity is likely to be protective in AD possibly suggestive that loss of IRAP is a compensatory response as AD progresses. Yet, not all studies support these earlier findings. In a recent animal study, IRAP knockout in the postnatal forebrain in mice resulted in a decline in spatial and object recognition memory (504). In accordance, plasma activity of IRAP has also been found to be significantly reduced in AD patients and correlated with the MMSE result (258).

In AD, reduction in IRAP activity (and reduced formation of Ang-IV) may minimise the effect of the intrinsic negative feedback mechanism of IRAP on Ang-III and thus result in maintenance of higher Ang-III levels that contribute to AD pathogenesis.

The colocalisation of IRAP and GLUT4 in glucose storage vesicles in the hippocampus could explain the cognitive enhancing role of IRAP by increasing neuronal glucose entry through inhibition of intracellular trafficking of GLUT4 and maintaining the presence of GLUT4 on the plasma membrane (497). Reduction in IRAP activity in AD could feasibly minimise the inhibition on the intracellular trafficking of GLUT4 and result in decrease GLUT4 translocation at the plasma membrane which in turn could decrease neuronal glucose entry and impair cognition. Neuronal glucose entry is a requirement for cognitive enhancement by hippocampal Ang-IV (567). An *in vivo* study found that intrahippocampal administration of Aβ42 in rats impaired spatial working memory through reduced plasma membrane translocation of GLUT4 (568). Together these findings strongly support a key role of IRAP/GLUT4 on cognitive function that requires further study.

Possible weaknesses of the current study include the potential unknown effect of a PMD on the level of endogenous Ang-IV and IRAP. Ang-IV, for example, has a short half-life in serum/plasma (528), yet, as for other peptides, such as Ang-II and endothelin-1, we were able to measure it in brain tissue (393, 569). Although we found no evidence that Ang-IV and IRAP levels were related to PMD it would be important to confirm the stability of the peptide and receptor in brain tissue by performing post-mortem simulated studies (354). Another possible limitation of our study was that measurement of these RAS markers was restricted to one brain tissue region (mid-frontal cortex). It would be of interest to explore the distribution of Ang-IV/IRAP in the temporal cortex and hippocampus of AD patients, especially since studies in rodents indicate that IRAP, and Ang-IV, are highly enriched within the hippocampus. As well as AD, it would be interesting to know if this rRAS pathway, and especially IRAP activity, was dysregulated in other types of dementia.

Future studies should focus on confirming that Ang-IV level remains unchanged in AD by other methodologies and in different brain regions in independent cohorts. In addition, it would be informative to measure the level of other less-abundant angiotensin metabolites such as Angiotensin 3-7 in AD, which has also been shown to have high affinity for IRAP and has been implicated in learning and memory (570, 571). It would also be interesting to determine whether dysregulation in IRAP is restricted to enzyme activity in AD by measuring IRAP mRNA level that might be expected to be similarly unchanged as was found for IRAP levels. The measurement of IRAP activity by using

other substrates (e.g. fluorometric substrate) to provide supportive trends of change would also be worthwhile. The apparent divergence between unchanged IRAP level and reduced IRAP activity in our study might also be related to post-translational modification of IRAP that warrants future study. *S*-acylation, a type of post-translational modification of protein, has been shown to regulate IRAP and to a lesser degree affect intracellular trafficking of GLUT4 in rat brain (572). Further studies could also explore alternative rRAS pathways and receptors e.g. HGF/c-MET receptor in human post-mortem tissue in AD, since Ang-IV facilitates memory by activation of c-MET receptor via several signalling pathways (495, 510, 512).

In conclusion, my findings provide novel evidence of reduced catalytic activity of IRAP in AD associated with pathological hallmarks of disease pathogenesis that warrant further study.

Chapter 6. Alternative regulatory RAS pathways in relation to markers of brain ischaemia in Alzheimer's disease

6.1 Abstract

Overactivity of the brain cRAS is associated with neurogenic hypertension and neurodegenerative disorders including AD and is associated with an imbalance in the brain RAS as a result of cRAS overactivity and underactivity of rRAS pathways. Brain rRAS pathways are composed of two main axes: the non-classical axis (ACE-2/Ang (1-7)/MasR) and the alternative (APN/Ang-IV/IRAP) pathway. These pathways counter-regulate cRAS signalling and dysregulation of the rRAS has been implicated in neurodegenerative and cerebrovascular disorders. Despite the obvious importance of rRAS in potentially reducing disease pathology, and the direct involvement and potential contribution of rRAS pathways in learning and memory, there is very little information about the dysregulation of these two protective arms of brain RAS in relation to disease pathology (Aβ and Tau) and similarly in relation to markers of hypoperfusion and ischaemia in AD. Previous chapters discussed the exploration of the relationship between rRAS pathways and classical neuropathological hallmarks of AD. In this chapter, I investigate the relationship between the major angiotensins and related receptors in brain rRAS pathways in AD in relation with markers of cerebral hypoperfusion and ischaemia: VEGF that is increased in relation to ischaemia, and MAG:PLP1 ratio that is reduced in poorly perfused tissue and is reduced in AD.

Human post-mortem brain tissue was obtained from the SWDBB, University of Bristol, with local Research Ethics Committee approval. We studied mid-frontal cortex (Brodmann area 8/9) from AD cases (n= 35) and age-matched controls (n= 17) that were matched closely for age-at-death and PMD. The level of VEGF was determined by sandwich ELISA. Pre-existing data on MAG level was available and PLP1 level was measured by sandwich ELISA allowing the MAG:PLP1 ratio to be calculated for all cases. Existing brain RAS markers (Ang (1-7), MasR, Ang-IV and IRAP level and activity) were available for analysis.

We found that MasR reduction in AD correlated with two independent markers of reduced oxygenation of brain tissue i.e. MasR was negatively associated with VEGF and positively associated with the ratio of MAG:PLP1. In contrast, no correlations were found between Ang (1-7) level and both

VEGF and MAG:PLP1 ratio. Both Ang-IV and IRAP level negatively correlated with VEGF but no correlation was observed with the MAG:PLP1 ratio. No correlations were found between IRAP activity and both VEGF and MAG:PLP1 ratio. Together, these findings indicate that rRAS dysregulation in AD is associated with markers of vascular dysfunction.

6.2 Introduction

The brain rRAS pathways (ACE-2/Ang (1-7)/MasR and APN/Ang-IV/IRAP) are the major counter-regulatory pathways of the cRAS axis and mediate both depressor and neuroprotective actions in the brain (455). The cRAS and rRAS pathways are inter-dependent and loss of rRAS activity is often associated with cRAS overactivation. Loss of rRAS signalling has been implicated in oxidative stress (573), cerebral ischaemia (330, 430, 574), and inflammation (575-577) associated with CNS injury, including cognitive impairment and dementia (419, 429, 433). The brain rRAS pathway (APN/Ang-IV/IRAP) has also notably been shown to regulate CBF, maintain memory, learning acquisition and enhance synaptic plasticity and has neuroprotective effects in the CNS (reviewed by (458)).

Brain ischaemia, as a result of reduced cerebral blood flow (i.e. cerebral hypoperfusion), is the defining pathological process that underlies vascular dementia. There is now also overwhelming evidence that cerebral hypoperfusion and ischaemia also contributes to disease pathogenesis in AD and is evident even in the early stages of AD. The extent of cerebral hypoperfusion is now recognized as a sensitive predictor of cognitive decline (118, 305-307). Moreover, cerebral ischaemia associated with cerebral hypoperfusion and cognitive decline aggravates Aβ-related pathology (308-310). Overactivation of the classical RAS axis (ACE-1/Ang-II/AT1R), resulting in overproduction of the potent vasoconstrictor peptide Ang-II, is thought to contribute toward cerebral hypoperfusion and ischaemic injury in AD (559, 578), while activity within rRAS (ACE-2/Ang (1-7)/MasR), which is protective (579), is reduced in AD.

We have previously shown that activity within the (ACE-2/Ang (1-7)/MasR) pathway, specifically a 50% loss of ACE-2 activity, is strongly associated with the Aβ and Tau parenchymal load in post-mortem brain tissue in AD (417). However, despite the role of RAS in the regulation of cerebral blood flow and the likely involvement of cRAS in mid-life hypertension (a modifiable risk factor for AD), the association between dysregulation of the two alternative rRAS pathways with markers of perfusion

and ischaemia in AD remains relatively unexplored. In this chapter, I have examined the relationship between alterations of (Ang (1-7)/MasR) and (Ang-IV/IRAP) with markers of brain ischaemia (VEGF) and reduced brain tissue oxygenation i.e. cerebral hypoperfusion (MAG:PLP1 ratio).

Our group has previously developed two novel independent markers of cerebral perfusion in post-mortem human brain tissue. The ratio of two myelin proteins, MAG and PLP1 has been shown to a useful marker of tissue oxygenation and is reduced under conditions of cerebral hypoperfusion. MAG is expressed distally at the adaxonal loop of the myelin sheath i.e. furthest away from the oligodendrocyte cell body and is the first part of the cell to degenerate under conditions of hypoperfusion. In contrast, PLP1 is widely distributed throughout the myelin sheath and is more resistant to ischaemia and hypoperfusion, illustrated in (Figure 6.1). The utility of MAG:PLP1 as a post-mortem marker of tissue perfusion prior to death has been developed and validated across multiple independent cohorts (45). A reduction in the MAG:PLP1 ratio has been shown not only in VaD but also in mid-frontal and medial parietal cortex (precuneus) in human post-mortem brain tissue in AD (312-315). VEGF is a protein that is induced under hypoxic conditions and is an ischaemic-sensitive marker. The level of brain VEGF has previously been shown to be elevated in the mid-frontal cortex in AD and was inversely related to a reduction in MAG:PLP1 (314). The increase in VEGF in AD has also been shown to be positively correlated with insoluble Aβ42 level and the Aβ42:Aβ40 ratio. Collectively these studies demonstrate the now accepted direct relationship between ischaemia and AD pathogenesis.

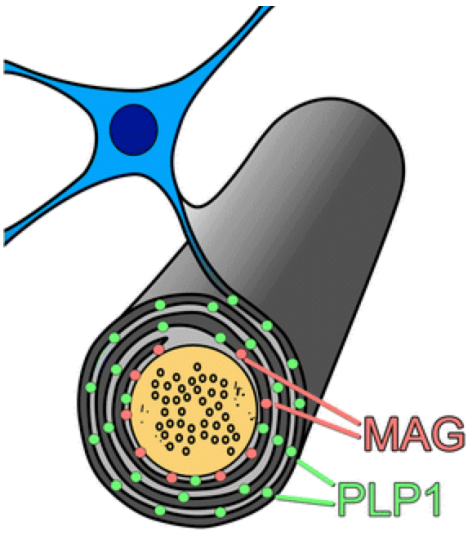

Figure 6.1 Schematic illustration of the distribution of both MAG (Pink dots) and PLP1 (Green dots) in the myelin sheath (Taken from Love S and Miners JS, 2016) (45).

Expression of myelin proteins, MAG and PLP1, is an energy dependent process. Reduced cerebral perfusion of the oligodendrocyte (blue) results is more significant loss of MAG (expressed distally from the oligodendrocyte) compared to PLP, which is expressed throughout the myelin sheath and is more resistant to reduced perfusion.

6.3 Study aims and hypothesis

The aims of the work described in this chapter were:

(i) To examine the relationship between Ang (1-7) and MasR expression with the markers of ischaemia (VEGF) and cerebral hypoperfusion (MAG:PLP1 ratio)

(ii) To examine the relationship between Ang-IV and IRAP level and activity with markers of ischaemia (VEGF) and cerebral hypoperfusion (MAG:PLP1 ratio)

(iii) To pilot the effect of ischaemia on expression of MasR in neuronal SH-SY5Y cells cultured under hypoxic conditions i.e. 2% oxygen for 24 hours to model chronic low-level perfusion in AD. Presented in chapter 9 (Appendix X).

The aims were designed to test the hypothesis that the dysregulation and loss of activity within the rRAS pathways (Ang (1-7), MasR, Ang-IV and IRAP level and activity) are associated with cerebral hypoperfusion and ischaemia in AD.

6.4 Methods

6.4.1 Study cohort

Human post-mortem brain tissue homogenates were prepared from mid-frontal cortex (Brodmann area 8/9) in aged-matched controls (n= 17) and AD cases (n= 35). The demographic features of this study cohort are described in detail (Appendix I: Table 9.8 and Table 9.9). Previous measurements of MAG (312) and RAS markers (Ang (1-7), MasR, Ang-IV and IRAP) were available for analysis.

6.4.2 Human vascular endothelial growth factor (VEGF) sandwich ELISA

The level of VEGF was measured in 1% SDS brain homogenates from the mid-frontal cortex using the quantitative commercially available DuoSet ELISA kit (R&D systems) according to the manufacturer's protocol described previously in the general methods (section 2.8.5). Measurements were made in duplicate and four carry-over samples were repeated on each plate to adjust for plate-to-plate variation. The variation of this assay was determined by calculating the intra-assay CV% (Example in Appendix IV: Table 9.33).

6.4.3 Human proteolipid protein 1 (PLP1) sandwich ELISA

PLP1 level was measured in 1% SDS brain tissue homogenates using a commercially available sandwich ELISA kit (Cloud-clone Corp.). The assay was performed according to the manufacturer's protocol described previously in the methods (section 2.8.6). Each sample was measured in duplicate and the mean was presented. Concentrations were determined by interpolation from the standard curve. Carry-over samples were repeated across all plates to adjust for any plate-to plate variation. The variation of this assay was determined by calculating the intra-assay CV% (Example in Appendix IV: Table 9.34).

6.4.4 Statistical analysis

The distributions of all datasets in this chapter were analysed by the Shapiro-Wilk normality test. A significant p value, $p< 0.05$ indicated that the data sets were not normally distributed. The data from Ang (1-7) direct ELISA was normally distributed while data from MasR, Ang-IV and IRAP sandwich ELISA did not follow a normal distribution.

Correlations of both total Ang (1-7) and Ang (1-7) protein-adjusted data with VEGF level and MAG:PLP1 ratio were assessed by the Pearson's correlation coefficient test. MasR unadjusted and protein-adjusted data were not normally distributed and therefore correlations between total MasR level and MasR protein-adjusted data with VEGF level and MAG:PLP1 ratio were assessed using Spearman's correlation coefficient. Log transformation for unadjusted and protein-adjusted MasR data was performed to attempt to reach normal distribution (Appendix VI: Section 9.6.4). Correlations between log-transformed MasR data and VEGF level and MAG:PLP1 ratio were assessed by the Pearson's correlation coefficient test.

Ang-IV protein concentration and protein-adjusted Ang-IV data were both not normally distributed. Log transformation and square-root transformation did not 'normalise' the distribution of the datasets and therefore both total Ang-IV level and Ang-IV protein-adjusted level correlations with VEGF level and MAG:PLP1 ratio were assessed by the Spearman's correlation coefficient. Both IRAP level and protein-adjusted data were not normally distributed. IRAP unadjusted to protein concentration and protein-adjusted data correlations with VEGF level and MAG:PLP1 ratio were assessed by the Spearman's correlation coefficient. Log transformation of unadjusted and protein-adjusted data was performed to attempt to reach normal distribution (Appendix VI: Section 9.6.4). Correlations between log-transformed IRAP data and VEGF level and MAG:PLP1 ratio were assessed by the Pearson's correlation coefficient test. Correlations between IRAP activity data and VEGF and MAG:PLP1 ratio were assessed by the Pearson's correlation coefficient test. For all tests applied, a P-value < 0.05 was considered statistically significant.

For all data sets, the ROUT method was used to detect outliers, where outliers existed and were removed the data was re-analysed and presented in chapter 9 (Appendix VII: Section 9.7.3)

6.5 Results

6.5.1 Relationship between Ang (1-7) and MasR expression and markers of ischaemia in AD

Ang (1-7) and protein-adjusted Ang (1-7) level showed no evidence of a correlation with VEGF level (Pearson's correlation coefficient, r= -0.269, p= 0.061; r= -0.223, p= 0.124) respectively (Figure 6.2 A and B).

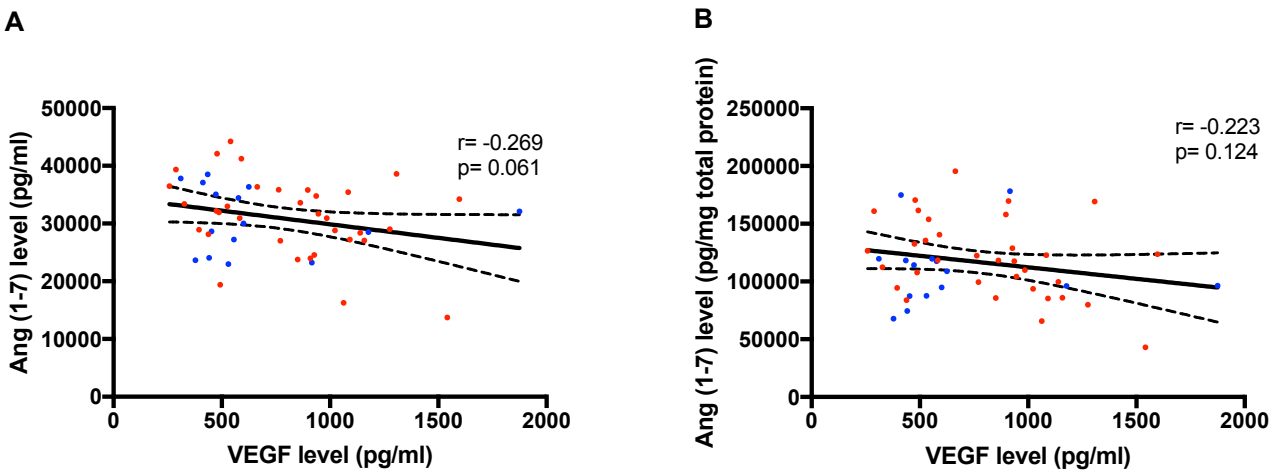

Figure 6.2 Relationship between Ang (1-7) level and VEGF level.

A. Scatterplot showing no correlation between Ang (1-7) level and VEGF level (measured by sandwich enzyme-linked immunosorbent assay), Pearson's correlation coefficient test (r= -0.269, p= 0.061). B. Scatterplot showing no significant correlation between Ang (1-7) protein-adjusted level and VEGF level, Pearson's correlation coefficient test (r= -0.223, p= 0.124). The solid inner line indicates the best-fit linear regression and the outer lines the 95% confidence intervals. Blue dots = controls, red dots = AD cases.

The relationship between total MasR level and MasR protein-adjusted data with VEGF level in mid-frontal cortex was similarly assessed. Again, no evidence of correlation was seen between total MasR levels and VEGF level when Spearman's Pearson's correlation coefficient test was applied (r= -0.046, p= 0.750) (Figure 6.3 A). However, MasR protein-adjusted level was inversely correlated with VEGF level in mid-frontal cortex, (r= -0.424, p= 0.002) using Spearman's Pearson's correlation coefficient test (Figure 6.3 B). Simillary, MasR protein-adjusted level was inversely correlated with VEGF level after removal of outliers (Appendix VII, Figure 9.35).

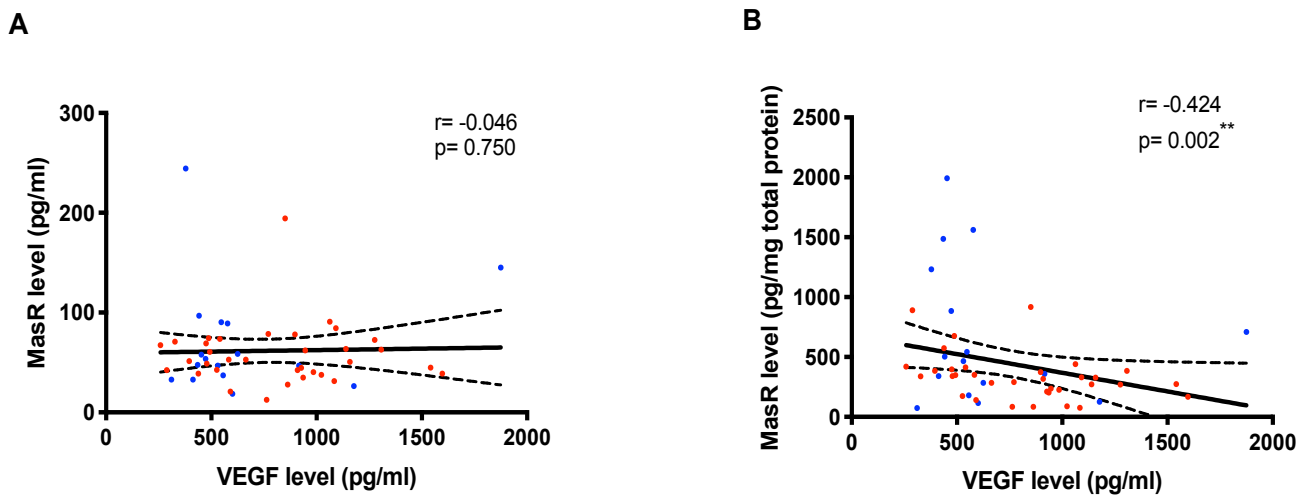

Figure 6.3 Relationship between MasR level and VEGF level.

A. Scatterplot showing no correlation between total unadjusted MasR level and VEGF level (measured by sandwich enzyme-linked immunosorbent assay), Spearman's correlation coefficient (r= -0.046, p= 0.750). B. Scatterplot showing a moderate inverse correlation between MasR protein-adjusted level and VEGF level, Spearman's correlation coefficient (r= -0.424, p= 0.002). The solid inner line indicates the best-fit linear regression and the outer lines the 95% confidence intervals. Blue dots = controls, red dots = AD cases.

6.5.2 Relationship between Ang (1-7) and MasR and markers of brain tissue oxygenation in AD

The relationship between unadjusted Ang (1-7) and protein adjusted Ang (1-7) level with the MAG:PLP1 ratio was also assessed in the mid-frontal cortex. There was no evidence of correlation with the MAG:PLP1 ratio (Pearson's correlation coefficient, r= -0.039, p= 0.786; r= -0.244, p= 0.091) respectively (Figure 6.4 A and B).

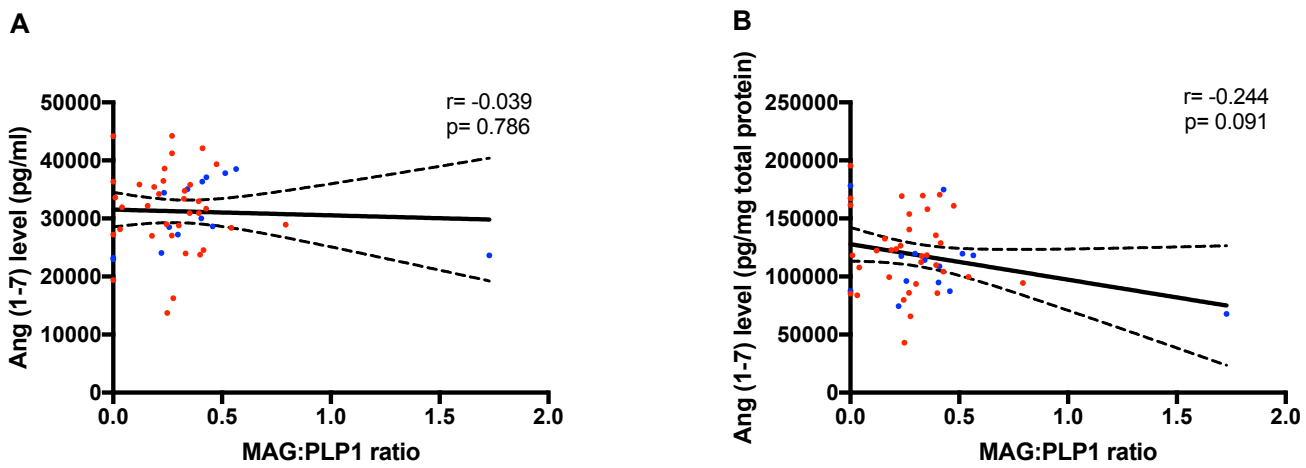

Figure 6.4 Relationship between Ang (1-7) level and the MAG:PLP1 ratio.

A. Scatterplot showing no correlation between Ang (1-7) level and MAG:PLP1 ratio, Pearson's correlation coefficient test (r= -0.039, p= 0.786). B. Scatterplot showing no significant correlation between Ang (1-7) protein-adjusted level and MAG:PLP1 ratio, Pearson's correlation coefficient test (r= -0.244, p= 0.091). The solid inner line indicates the best-fit linear regression and the outer lines the 95% confidence intervals. Blue dots= controls, red dots= AD cases.

Similarly, the association between both total unadjusted MasR level and protein-adjusted MasR measurement and the MAG:PLP1 ratio was examined. No significant correlation was found between total MasR level and MAG:PLP1 ratio (Spearman's correlation coefficient, r= -0.056, p= 0.696) (Figure 6.5 A). MasR protein-adjusted level was also not correlated with MAG:PLP1 ratio in mid-frontal cortex, (Spearman's correlation coefficient, r= 0.066, p= 0.644) (Figure 6.5 B).

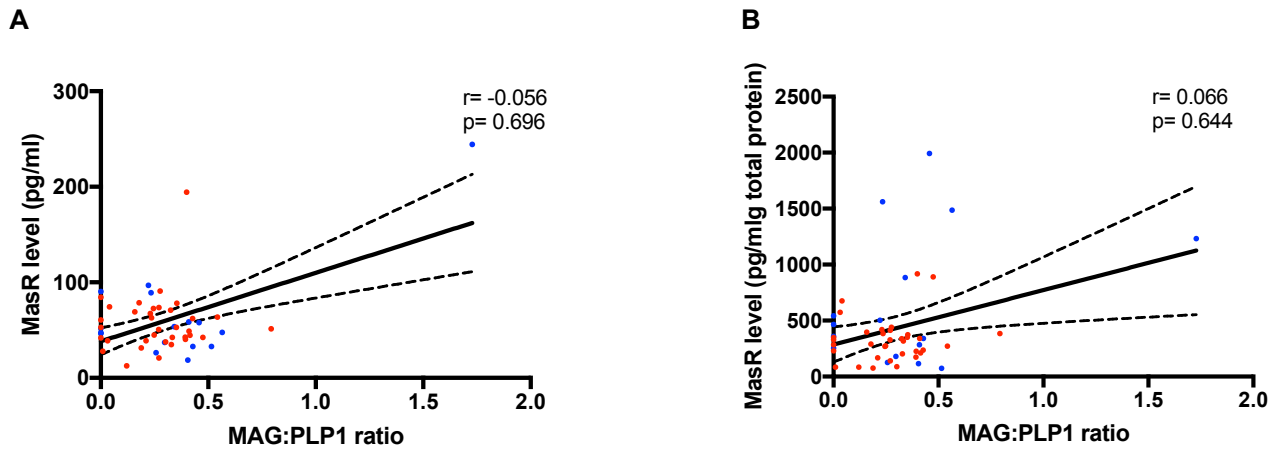

Figure 6.5 Relationship between MasR level and brain MAG:PLP1 ratio.

A. Scatterplot showing no correlation between total MasR level and MAG:PLP1, Spearman's correlation coefficient test (r= -0.056, p= 0.696). B. Scatterplot showing no significant correlation between MasR protein-adjusted level and MAG:PLP1 ratio, Spearman's correlation coefficient test (r= 0.066, p= 0.644). The solid inner line indicates the best-fit linear regression and the outer lines the 95% confidence intervals. Blue dots = controls, red dots = AD cases.

6.5.3 Relationship between Ang-IV and IRAP with marker of brain ischaemia in AD

Total unadjusted Ang-IV level did not significantly correlate with VEGF level (Spearman's correlation coefficient, r= -0.013, p= 0.931) (Figure 6.6 A). In contrast, Ang-IV protein-adjusted level was inversely correlated with VEGF level (Spearman's correlation coefficient, r= -0.337, p= 0.019) (Figure 6.6 B) in mid-frontal cortex.

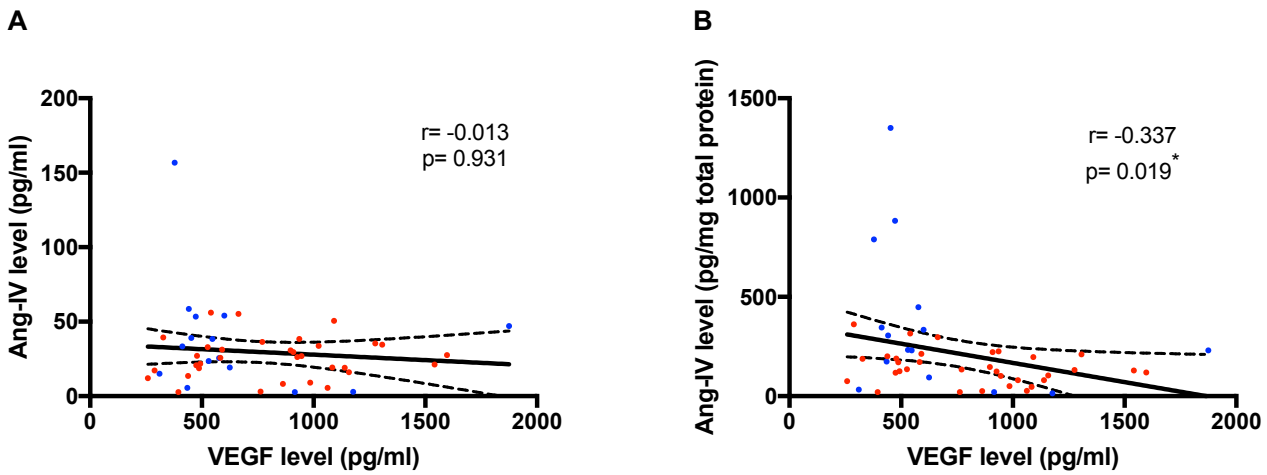

Figure 6.6 Relationship between Ang-IV level and VEGF level.

A. Scatterplot showing no correlation between total Ang-IV level and VEGF level (measured by sandwich enzyme-linked immunosorbent assay), Spearman's correlation coefficient test (r= -0.013, p= 0.931). B. Scatterplot showing a significant inverse correlation between Ang-IV protein-adjusted level and VEGF level, Spearman's correlation coefficient test (r= - 0.337, p= 0.019). The solid inner line indicates the best-fit linear regression and the outer lines the 95% confidence intervals. Blue dots = controls, red dots = AD cases.

The relationship between total unadjusted IRAP level and protein-adjusted IRAP with VEGF level in mid-frontal cortex were similarly assessed. In the case of total unadjusted IRAP level an inverse correlation was seen with VEGF level (Spearman's correlation coefficient, r= -0.398, p= 0.004) (Figure 6.7 A). When protein-adjusted IRAP levels were similarly compared to VEGF level, a similar significant inverse correlation was observed (Spearman's correlation coefficient, r= -0.398, p= 0.015) (Figure 6.7 B).

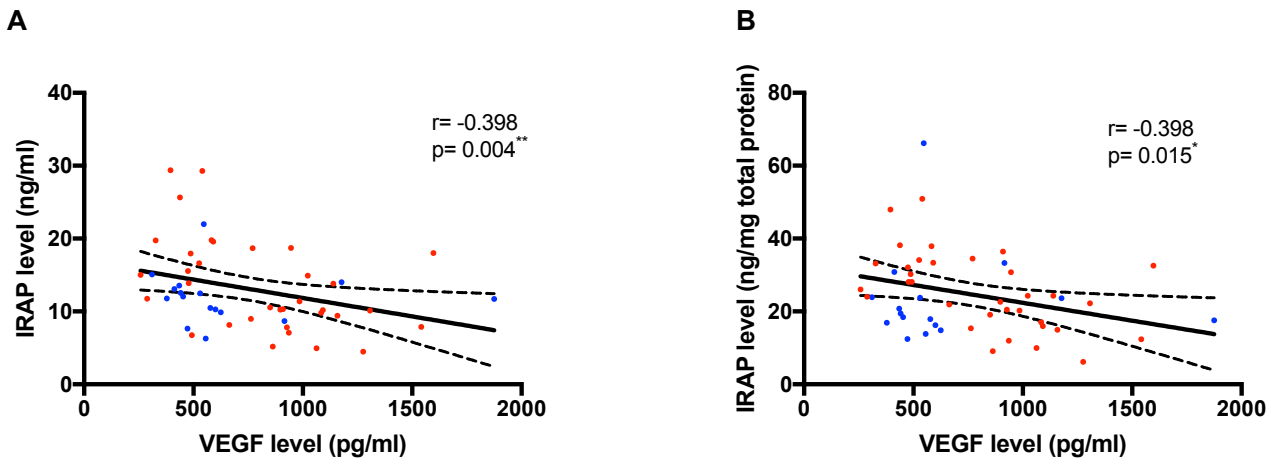

Figure 6.7 Relationship between IRAP level and VEGF level.

A. Scatterplot showing a moderately strong inverse correlation between total IRAP level and VEGF level (measured by sandwich enzyme-linked immunosorbent assay), Spearman's correlation coefficient test (r= -0.398, p= 0.004). B. Scatterplot showing a significant inverse correlation between IRAP protein-adjusted level and VEGF level, Spearman's correlation coefficient test (r= -0.398, p= 0.015). The solid inner line indicates the best-fit linear regression and the outer lines the 95% confidence intervals. Blue dots= controls, red dots= AD cases.

The relationship between IRAP activity and VEGF level was assessed. No significant correlation was found between IRAP activity and VEGF level in mid-frontal cortex (Pearson's correlation coefficient, r= -0.131, p= 0.363) (Figure 6.8).

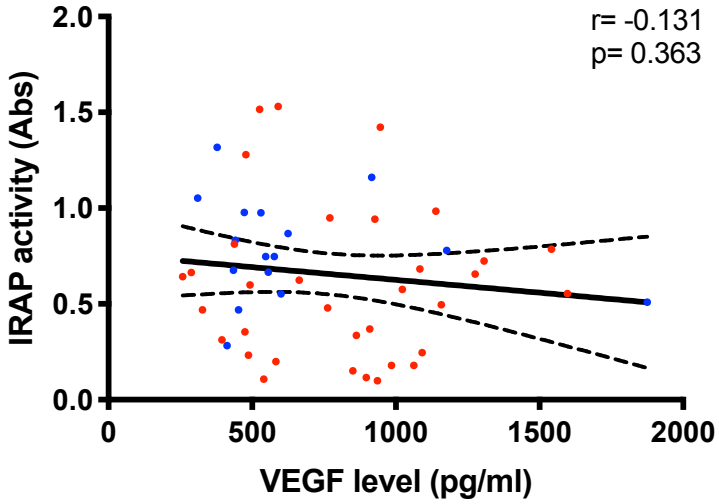

Figure 6.8 Relationship between IRAP activity and VEGF level.

A. Scatterplot showing no correlation between IRAP activity and VEGF level (measured by sandwich enzyme-linked immunosorbent assay), Pearson's correlation coefficient test (r= -0.131, p= 0.363). The solid inner line indicates the best-fit linear regression and the outer lines the 95% confidence intervals. Blue dots= controls, red dots= AD cases.

6.5.4 Relationship between Ang-IV and IRAP with markers of brain tissue oxygenation

Following the investigations with VEGF, similar investigations were undertaken with MAG:PLP1 ratio. No significant correlation was found between total unadjusted Ang-IV level and MAG:PLP1 ratio (Spearman's correlation coefficient, r= 0.017, p= 0.907) and between protein-adjusted Ang-IV level and MAG:PLP1 ratio (Spearman's correlation coefficient, r= 0.151, p= 0.301) (Figure 6.9 A and B).

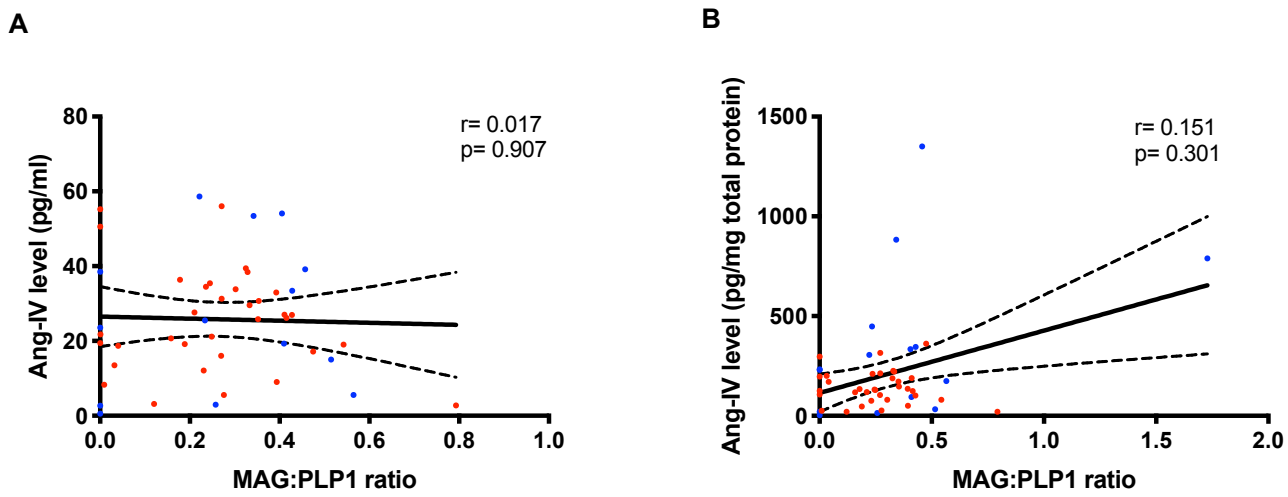

Figure 6.9 Relationship between Ang-IV level and the MAG:PLP1 ratio.

A. Scatterplot showing no correlation between total Ang-IV level and MAG:PLP1 ratio, Spearman's correlation coefficient test (r= 0.017, p= 0.907). B. Scatterplot showing no significant correlation between Ang-IV protein-adjusted level and MAG:PLP1 ratio, Spearman's correlation coefficient test (r= 0.151, p= 0.301). The solid inner line indicates the best-fit linear regression and the outer lines the 95% confidence intervals. Blue dots= controls, red dots= AD cases.

Investigation of total unadjusted IRAP level showed no evidence of a correlation with the MAG:PLP1 ratio in mid-frontal cortex (Spearman's correlation coefficient, r= 0.154, p= 0.279) (Figure 6.10 A). Similarly IRAP protein-adjusted level did not correlate with MAG:PLP1 ratio (Spearman's correlation coefficient, r= -0.029, p= 0.839) (Figure 6.10 B).

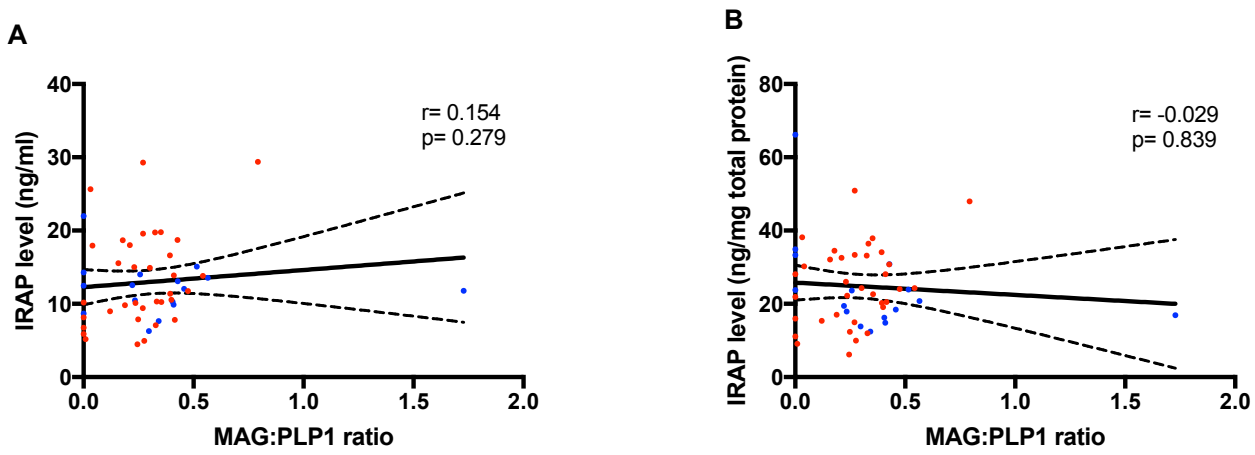

Figure 6.10 Relationship between IRAP level and brain tissue oxygenation marker (MAG:PLP1 ratio).

A. Scatterplot showing no correlation between total IRAP level and MAG:PLP1, Spearman's correlation coefficient test (r= 0.154, p= 0.279). B. Scatterplot showing no significant correlation between IRAP protein-adjusted level and MAG:PLP1 ratio, Spearman's correlation coefficient test (r= -0.029, p= 0.839). The solid inner line indicates the best-fit linear regression and the outer lines the 95% confidence intervals. Blue dots = controls, red dots = AD cases.

Similarly, no significant correlation was found between IRAP activity and MAG:PLP1 ratio in mid-frontal cortex assessed using Pearson's correlation coefficient, r= 0.229, p= 0.015) (Figure 6.11).

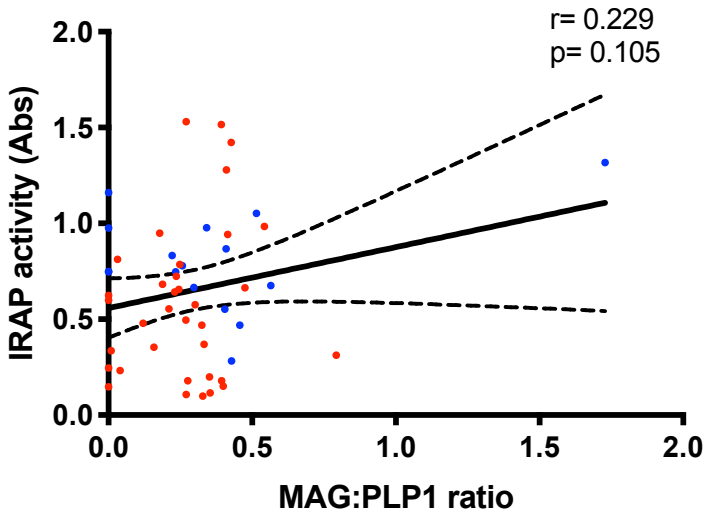

Figure 6.11 Relationship between IRAP activity and brain tissue oxygenation marker (MAG:PLP1 ratio).

A. Scatterplot showing no correlation between total IRAP activity and MAG:PLP1, Pearson's correlation coefficient test (r= 0.229, p= 0.105). The solid inner line indicates the best-fit linear regression and the outer lines the 95% confidence intervals. Blue dots = controls, red dots = AD cases.

6.6 Discussion

In this chapter, I explored the relationship between brain rRAS pathways and markers of cerebral ischaemia and hypoperfusion. We report for the first time that MasR expression, when adjusted to total protein level, was inversely correlated with VEGF, a marker of brain ischaemia. However, there was no correlation with a marker of brain tissue oxygenation, namely MAG:PLP1. In contrast, Ang (1-7) was not found to be associated with markers of ischaemia and or hypoperfusion. In relation to the components of another rRAS pathway, Ang-IV and IRAP levels, both were inversely correlated with VEGF but not with MAG:PLP1. While, IRAP activity was not found to be associated with both VEGF and MAG:PLP1 ratio. These data suggest that dysregulation of brain rRAS pathways is associated, to some extent with vascular dysfunction in AD, reinforcing the hypothesis that there is an interaction between RAS, cerebrovascular disease and neurodegenerative disease.

As mentioned, reduction of ACE-2 activity, the rate-limiting enzyme in the brain rRAS axis (ACE-2/Ang (1-7)/MasR) has been associated with AD pathogenesis (417) and contributes to the pathogenesis of cerebral ischaemia (441, 580). Here I have investigated the relationship between

expression of the downstream elements of the pathway i.e. Ang (1-7) and MasR), in relation to markers of brain ischaemia and cerebral hypoperfusion in AD. Whilst I did not find a relationship between Ang (1-7) and MasR expression with Aβ or tau in a larger cohort presented previously in chapter 4, I did find an interesting relationship showing that reduced MasR expression in mid-frontal cortex was inversely associated with cerebral ischaemia. This was indicated by a negative correlation with VEGF levels that increase under conditions of cerebral ischaemia in AD. We did not, however, observe a similar relationship with an independent marker of cerebral hypoperfusion (MAG:PLP1 ratio).

Cerebral ischaemia has been shown to reduce Ang (1-7) and MasR expression whilst inducing Ang-II/AT_1R signalling in a rat model of stroke (560). Directly supporting this, Ang (1-7) administration and subsequent induction of the ACE-2/Ang (1-7)/MasR pathway protected against cerebral ischaemia in animal models of stroke (326, 329, 330). Indeed, administration of a MasR agonist (Ang (1-7)) in an animal model of stroke showed a reduction in infarct volume and improved CBF (327, 430, 573). In a rat model of focal cerebral ischaemia, Ang (1-7) contributed to the neuroprotection that was observed from the administration of the ACE-inhibitor captopril in ischaemic stroke (581).

These findings highlight the vital protective role that rRAS signalling provides in ischaemia. In contrast, Lu *et al.* (331) showed that components of the ACE-2/Ang (1-7)/MasR pathway are upregulated after acute ischaemic stroke in rat, which could represent a compensatory physiological response to acute ischaemia. Contrary to expectations, we did not find a significant correlation between Ang (1-7) level with either VEGF levels or MAG:PLP1. My results are likely to be related to unchanged level of Ang (1-7) in the AD group compared to significant reductions of Ang (1-7) observed in both human plasma and brain tissue in an animal model of sporadic AD (senescence-accelerated mouse prone 8 (SAMP8) mice) (416, 435). The different findings may also be due to differences in the method used to measure Ang (1-7) (direct ELISA used in my study vs. sandwich ELISA kit used in previous studies), the species of study sample (human vs. animal) or (plasma vs. brain tissue), or the potential effect of PMD on Ang (1-7) degradation, however, I did not find any significant difference of PMD in our cohort (chapter 2: Section 2.2.1).

Dysregulation of the downstream components of the alternative RAS axis (APA/Ang-III/APN/Ang-IV/IRAP) have previously been studied in AD in relation to disease pathology: Ang-III was increased in AD and strongly associated with both Aβ and Tau pathology (393). The lower downstream pathway elements of brain rRAS pathway (Ang-IV/IRAP) have also been reported to regulate cerebral blood

flow and have been implicated in cerebral ischaemia (495). Other research has shown that boosting this pathway was also associated with improved cognition and mediated the cerebrovascular and cognitive effects of treatment with the ARB (Losartan) (362, 493, 582). In this study, we wanted to investigate whether these downstream components of rRAS pathway (i.e. Ang-IV and IRAP) were related to markers of ischaemia and hypoperfusion in AD, which has not received much attention.

Ang-IV and IRAP protein levels were found to be unchanged in the AD cohort (presented in chapter 5) and these markers did not correlate with Aβ or tau. However and interestingly, both Ang-IV and IRAP were negatively correlated with VEGF level, but no associations were found with MAG:PLP1 - a marker of cerebral hypoperfusion for both Ang-IV and IRAP level and activity. In contrast, IRAP activity was not found to be associated with markers of ischaemia. Activation of the Ang-IV/AT4R axis has previously been shown to be cerebroprotective against ischaemia in animal models of stroke (494, 583-585). In contrast, there is also counter evidence of cerebrovascular protection seen in IRAP knockout mice where reduced cerebral infarcts volume was observed (586). This rather contradictory result may be due to difference in the study subject (rat vs. mice). There are still many unknown roles of this brain rRAS pathway in relation to cerebral ischaemia and further studies in this area will be very valuable.

One of the limitations in this study, which could have affected the evaluation of the relationship between brain rRAS markers and ischaemic and hypoperfusion markers was the small sample size of previously available VEGF and MAG:PLP1 ratio measurements. Caution must also be applied to the interpretation of the results as some of the significant correlations might be caused by the potential impact of outliers (Appendix VII: Section 9.7.3). Another limitation of our study was that the effect of ischaemia in cell culture was focused on expression of MasR only and due to some limitations at the end of my study I was unable to complete this pilot investigation. Further characterisation of the effect of ischaemia on expression of IRAP in neuronal SH-SY5Y cells would provide more insight about the relationship between brain rRAS (APN/Ang-IV/IRAP) and cerebral ischaemia. Little is known regarding the role of rRAS pathway in vascular dementia that will be important to explore in future studies. Exploring the relationship between brain rRAS and other neuronal markers such as neuron-specific enolase (NSE) and markers of glial injury would be interesting to investigate, to confirm the relationship between brain rRAS pathways and damage associated with cerebral ischaemia.

In conclusion, this study provides preliminary evidence in human post-mortem tissue that dysregulation in rRAS axis, specifically MasR and IRAP, are related to markers of vascular

dysfunction in AD. Together, these findings suggest that dysregulation of downstream rRAS pathways are more closely associated with vascular dysfunction than established Aβ and Tau-related pathology. Larger independent studies are required to validate our preliminary observations in humans and studies in animal models should be focussed on addressing causality and the direction of the observed relationship.

Chapter 7. Non-AT_1R and non-AT_2R binding proteins in Alzheimer's disease

7.1 Abstract

The RAS has traditionally been viewed to elicit its biological effects via activation of more widely known GPCRs (AT_1R, AT_2R, MasR) and IRAP. However, another element of the RAS complexity has been shown through the reported existence of a non-AT_1R and non-AT_2R binding protein, which has been reported to occur in the human and rat brain. This binding site was subsequently identified as the zinc metalloendopeptidase - neurolysin. Furthermore, dysregulation of neurolysin has been implicated in the pathophysiology of cardiovascular and cerebrovascular disorders including stroke. However, its contribution to neurodegenerative diseases including AD remains unknown. Another consideration of a possible role of neurolysin in AD is the neuropeptide neurotensin, which is metabolised by ACE-1 but is also a major endogenous substrate of neurolysin. Changes in neurotensin level have been associated with dysregulation of blood pressure, the pathophysiology of stroke and some neurodegenerative diseases (Parkinson's disease and AD). In this study, I have undertaken the first investigation of the expression and distribution of neurolysin and neurotensin in AD in a well-characterised cohort of post-mortem brains.

Human post-mortem brain tissue was obtained from the SWDBB, University of Bristol, with local Research Ethics Committee approval. We studied mid-frontal cortex (Brodmann area 8/9) from AD cases (n= 70) and the age-matched controls (n= 48) that were matched closely for age-at-death and PMD. The expression and distribution of neurolysin was assessed using a competitive ELISA and IHC. The level of neurotensin was measured by sandwich ELISA. Pre-existing data on Braak tangle stage, pathological hallmarks (total insoluble Aβ, insoluble Aβ40 and Aβ42 and tau load), brain RAS markers (Ang-II, Ang-III and Ang-II:Ang (1-7) ratio), and markers of brain tissue oxygenation and ischemia (MAG:PLP1 ratio and VEGF) were available for analysis.

I found that the level of neurolysin was significantly reduced in AD, compared to controls, and the reduction was in association with increased levels of brain RAS markers (Ang-II, Ang-II:Ang (1-7) ratio, and Ang-III). Similarly, neurolysin levels were also inversely associated with the level of VEGF

(a marker of brain ischaemia). In contrast the level of expression of neurotensin remained unchanged in AD and was not associated with any other RAS markers or markers of ischaemia.
Together, these studies have produced a novel finding that the level of neurolysin was dysregulated in post-mortem AD brain tissue in association with RAS markers and with a marker of ischaemia, suggesting some association with vascular dysfunction in AD. These studies highlight additional components of RAS that are potentially involved in the pathogenesis of AD and in doing so broaden the level of RAS dysfunction that appears evident in AD.

7.2 Introduction

The main components of RAS have been well-characterised in renal, cardiac and neurological diseases (255, 267, 269). However, as discussed, the role and function of major angiotensin receptors, due in part to a lack of specific antibodies for some of the main receptors, remains unclear, especially within the brain. An additional level of complexity was identified in the RAS when a novel non-AT_1R and non-AT_2R binding protein was discovered in rat brain. The same group also identified that there was a similar binding site in human brain tissue (587). This binding protein was reported to have different properties from the more established angiotensin receptors (AT_1R, AT_2R, MasR and AT_4R) that had already been identified (588). For example, this new molecule was found to have a higher molecular mass than most of the established GPCRs. Additionally, the new protein did not appear to undergo post-translational N-glycosylation, nor did it seem to be coupled to a G-protein. Most importantly perhaps was the finding that it acts independently of the main cRAS receptors, as it was not stimulated or inhibited by selective AT_1R and AT_2R agonists and antagonists respectively (275, 588). This non-AT_1R and non-AT_2R receptor was later identified as a zinc metalloendopeptidase and was found to correspond to the previously characterised neurolysin, which is a monomeric protein containing 704 amino acids with an approximate MW of 78 kDa (589, 590). Known endogenous substrates for neurolysin include neurotensin, Ang-I and Ang-II, bradykinin, substance P, hemopressin and somatostatin (591, 592). Neurolysin has since become considered an important component of brain RAS function and has been reported to be involved in the pathophysiology of cardiovascular and cerebrovascular diseases (275, 590, 593). The expression of neurolysin in human post-mortem tissue in AD remained uncharacterised at the time this work was first undertaken.

Neurolysin has been reported to be widely distributed in rodent and mammalian tissues and is expressed centrally within the brain and peripheral tissues including the testis (587, 588, 594). At a subcellular level, neurolysin has been localised to the plasma membrane but is also present in the cytosol and mitochondria (595, 596). Within the brain, neurolysin has been reported to be expressed in both neurons and glia (595-597).

Neurolysin has also been reported to have numerous roles in RAS. It has been reported to generate (Ang (1-7)) from Ang-I and degrades Ang-II and Ang-III into more inactive peptides Ang (1-4) and Ang (5-8). Neurolysin has also been reported to act as a novel clearance Ang-II/Ang-III receptor that works to internalise Ang-II and Ang-III and thus counter-regulate the function of AT_1R (275, 593, 598, 599). Together these studies indicate a significant potentially protective role of neurolysin in the regulation of the brain cRAS, which could acts as a neuroprotective enzyme by generating Ang (1-7) and inactivating Ang-II. The proposed neuroprotective roles that neurolysin might provide are summarized in Figure 7.1.

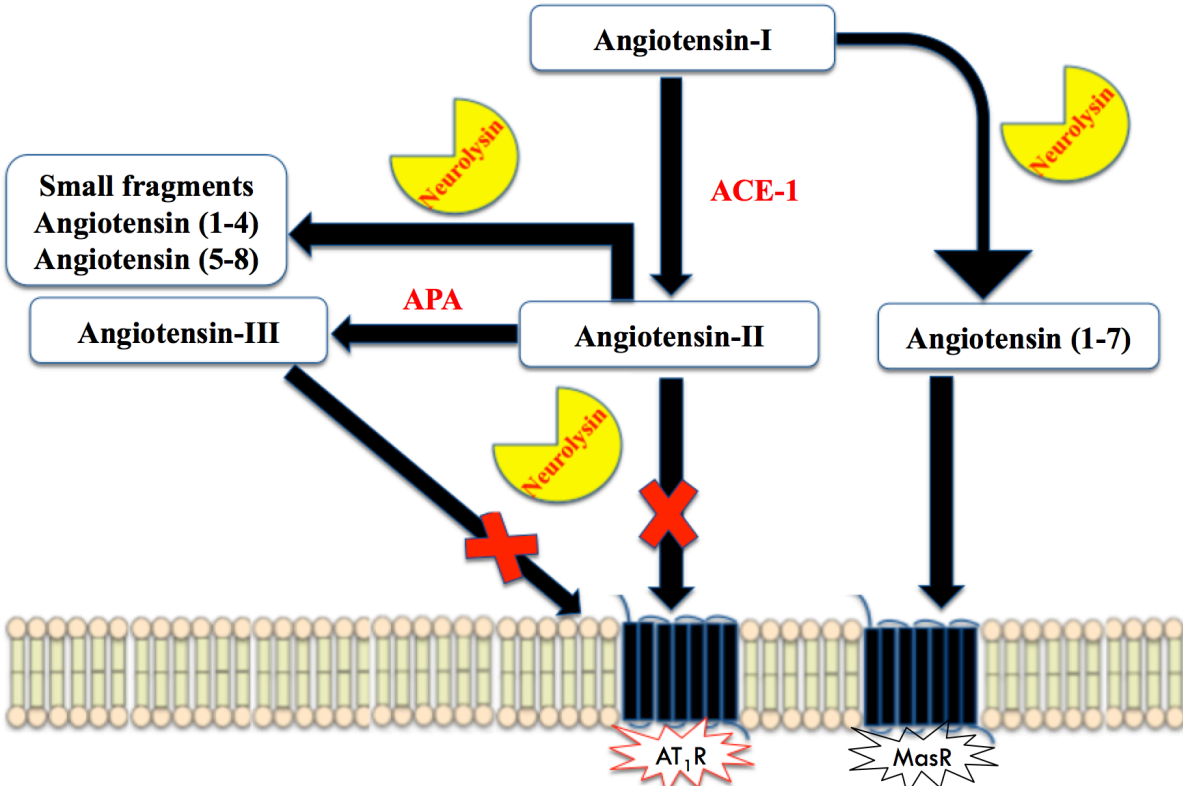

Figure 7.1 Schematic of suggested neuroprotective roles of neurolysin in the brain RAS.

Neurolysin can convert Ang-I into the neuroprotective Ang (1-7), which via stimulation of the MasR counter-regulates the disease-associated effects of cRAS signalling. Neurolysin has also been shown to degrade Ang-II and Ang-III into small inactive peptides (Ang (1-4) and Ang (5-8)), which are less

neurotoxic and more easily cleared. Neurolysin also binds to and facilitates the clearance of Ang-II and Ang-III and limits the access of Ang-II and Ang-III to AT_1R.

Previous studies have highlighted the involvement of neurolysin in the pathophysiology of cerebrovascular diseases associated with overactive RAS such as stroke (593, 600). In a mouse model of stroke, neurolysin activity was upregulated in the frontoparietal cortex 7 days post-stroke (593). A similar increase in neurolysin expression in mouse brain was previously associated with neuronal cell death (601) and these studies suggest that neurolysin plays a role in the pathophysiology of stroke. In SHR, an animal model of hypertension, neurolysin was significantly reduced in the brainstem's cardiovascular regulatory centres (rostral ventrolateral medulla (RVLM), caudal ventrolateral medulla (CVLM), as well as dorsomedial medulla (DMM)), compared to normotensive Wistar–Kyoto rats. This finding suggested a possible role of neurolysin in the regulation of blood pressure through its regulation of the main angiotensins (Ang-II and Ang-III) (275). Neurolysin has also been shown to be involved in metabolism of Aβ. In a recent *in vitro* study, human mitochondrial neurolysin degraded Aβ peptide (Aβ40), cleaving the hydrophobic fragment of the peptide (Aβ35-40) (602). Despite these potentially neuroprotective functions of neurolysin, together these studies indicate a complex and poorly understood role in the pathophysiological of stroke. Little is known regarding its function in AD.

The 13 amino acid neuropeptide neurotensin, is also worthy of consideration as an endogenous active substrate of neurolysin within the brain and which has been shown to play a vital role in brain functions including learning and memory (603, 604). A previous study revealed that ACE-1 was involved in the metabolism of neurotensin (339), and thus would be consistent of memory related deficits resulting from increased levels of ACE-1 activity that have also been reported in the AD brain (354). Immunohistochemical studies have also identified high levels of expression of neurotensin in several brain regions including the prefrontal areas, amygdala and hypothalamus (605-607). This tridecapeptide is also densely distributed in the entorhinal cortex in the hippocampus (608) indicative perhaps of a central role in learning and memory.

Neurotensin has been reported to bind to three different receptors, in addition to neurolysin including: neurotensin type-1 receptor (NTSR1), neurotensin type-2 receptor (NTSR2) and neurotensin type-3 receptor (NTSR3). Both NTSR1 and NTSR2 are GPCRs while NTSR3 is a trans-membrane single domain like sortilin/gp95 family receptor (595, 609). NTSR1 is widely distributed in neurons while

NTSR2 has been found in glia (610, 611). This overall pattern of distribution is thought to suggest a predominant role of NTSR1 on cognitive function compared to NTSR2.

Some studies have suggested a neuroprotective role of neurotensin in AD. Reduction in neurotensin level and its receptors have been found in several brain regions of AD patients such as the suprachiasmatic nucleus, amygdala, entorhinal area, dentate gyrus and temporal gyrus (606, 612-615). Neurotensin was also found to increase the neuronal excitability and improve spatial learning and memory (340), as well as block neurotoxicity of the sortilin-induced precursor form of nerve growth factor (proNGF) (616). In addition, the density of amyloid plaques in the occipital cortex was negatively associated with neurotensin sensitive neurons in the suprachiasmatic nucleus in AD patients (615). Findings from experimental animal studies are controversial. Neurotensin administration was found to increase spatial learning and memory, improve cognitive function and play an inhibitory role in memory related to fear (340-342). Whilst another study found that an NTSR1 agonist did not improve cognitive function in Long Evan rats, an animal model of neuropsychiatric disorders (341). Further studies are needed to clarify the role of neurotensin on cognitive function and the possible implication of this neuropeptide in the pathophysiology of AD remains unexplored.

7.3 Study aims and hypothesis

The aims of the investigations described in this chapter were:

(i) To characterise the expression and distribution of neurolysin in post-mortem AD brain tissue and examine the relationship with markers of brain RAS, vascular dysfunction and disease pathology in AD
(ii) To measure neurotensin level in mid-frontal cortex in AD and explore the relationship with markers of disease pathology

I wished to test the hypothesis that the expression of both neurolysin and neurotensin were altered in mid-frontal cortex in AD and were associated with markers of AD pathogenesis and brain RAS markers.

7.4 Methods

7.4.1 Study cohort

Human post-mortem brain tissue homogenates from mid-frontal cortex (Brodmann area 8/9) were used in this study and neurolysin and neurotensin levels were measured in age-matched controls (n= 48) and AD cases (n= 70). Demographic features of the study cohort are described in the methods section (Table 2.1) for full details (Appendix I: Table 9.1 and Table 9.2). Previous measurements of insoluble Aβ, measured by sandwich ELISA, were available for controls (n= 28) and AD cases (n= 61) (545). Tau load was previously measured by field fraction analysis and was available for controls (n= 29) and AD cases (n= 89) (analysis performed by routine histological assessment of tau load in cases from the SWDBB). Both insoluble Aβ40 and insoluble Aβ42 were previously measured by sandwich ELISA and were available for controls (n= 20) and AD cases (n= 33) for insoluble Aβ42, and for controls (n= 20) and AD cases (n= 34) for insoluble Aβ40 (314). Previous measurement of Ang-II level, measured by sandwich ELISA, were available for controls (n= 43) and AD cases (n= 70) (393). Ang-III level was also previously measured by direct ELISA in mid-frontal cortex and available for controls (n= 31) and AD (n= 62) (393). The Ang-II:Ang (1-7) ratio was also calculated and available for controls (n= 42) and AD (n= 68) (417). Previous measurements of VEGF level and MAG:PLP1 ratio were measured by sandwich ELISA and were available for controls (n= 17) and AD cases (n= 35) (314).

7.4.2 Expression of neurolysin in human brain tissue

7.4.2.1 Western blotting for neurolysin

A standard protocol for western blotting used is described in detail in chapter 2 (section 2.4). Details of the primary and secondary antibodies used are described in chapter 9 (Appendix II: Table 9.13) and (Table 9.14) respectively. In summary, for detection of neurolysin in brain homogenate samples, the membrane was blocked in 10% milk/TBST buffer for 1 hour. After it had been washed with 0.05% TBST (3x 15 minutes) at room temperature on a shaker, the membrane was then incubated with a mouse anti-human neurolysin antibody (1D6) (NBP2-01693) diluted 1:500 in 5% milk/TBST antibody buffer overnight at 4°C (in the fridge) on a shaker. Following a wash step with 0.05% TBST (3x 15 minutes) at room temperature on shaker, the membrane was incubated with a secondary antibody

(peroxidase conjugated anti-mouse) diluted 1:5000 in 5% milk/TBST for 1 hour. After 3x 15 minutes wash steps with 0.05% TBS with tween-20 (TBST), a chemiluminescent HRP substrate (ECL) (Millipore) was added to the membrane in a 1:1 ratio (5 ml of reagent 1 and 5 ml of reagent 2) for 5 minutes. The images then were acquired using (ChemiDoc XRS+, Bio-RAD) and Image Lab software, version 5.0 (Bio-RAD).

7.4.2.2 Immunohistochemistry

The neurolysin antibody (1D6) (NBP2-01693) was used by IHC to detect and examine the distribution of neurolysin in formalin-fixed brain tissue. The standard protocol used for immunohistochemical staining is described in detail in the method (section 2.5). The immunohistochemical protocol was initially optimised by comparing the antigen retrieval pre-treatment step using either EDTA or citrate buffer and optimising the dilution of the primary antibody (1:150, 1:300, 1:500). The optimal assay conditions for neurolysin staining were achieved with microwave- EDTA pre-treatment and an antibody dilution at 1:150 in PBS. After washing with running tap water for 5 minutes, slides were incubated with blocking serum for 20 minutes then incubated with the primary antibody diluted 1:150 in PBS (5 μg/ml) overnight. After rinsing the sections in two changes of PBS for 3 minutes each, sections were incubated with Vectastain biotinylated universal secondary antibody for 20 minutes followed by another wash with PBS and then the VectaElite ABC complex for 20 minutes. The sections were rinsed again and incubated with DAB for 10 minutes then washed in running water for 10 minutes and immersed in copper sulphate solution for 4 minutes followed by washing in running water for 5 minutes. The sections were then counterstained with haematoxylin Gill II for 3 seconds, dehydrated, cleared and mounted.

7.4.3 Neurolysin competitive ELISA

The level of neurolysin in brain homogenates from the mid-frontal cortex, prepared in 1% SDS, was measured using a quantitative commercially available competitive ELISA (Human Neurolysin, (NLN) ELISA kit) (MyBioSource)) according to the manufacturers protocol, which is described in detail in chapter 2 (section 2.9). Different homogenate dilutions (1:2, 1:4, 1:10 and 1:20) were initially tested to identify the dilution of homogenate that fell within the linear part of the standard curve (Appendix II:

Table 9.19) and a dilution of 1 in 10 was chosen for further studies. Neurolysin level was initially determined in two controls and two AD cases to confirm that the chosen dilution was within the range of standard curve (Appendix II: Figure 9.10 and Table 9.19). Neurolysin was then measured in the entire cohort in duplicate and averaged for all cases. Measurements from four carry-over samples were repeated across all plates to help measure and minimise plate-to-plate variation. Neurolysin measurements were adjusted to total protein level for each brain homogenates sample. The variation of this assay was determined by calculating the intra-assay CV% (Example in Appendix IV: Table 9.35). Both unadjusted neurolysin measurements and protein-adjusted measurements were used for comparisons between control and AD.

7.4.4 Neurotensin sandwich ELISA

The level of neurotensin in brain homogenates from the mid-frontal cortex, prepared in 1% SDS, was measured using a commercially available sandwich ELISA (Human Neurotensin (NT) ELISA kit) (CUSABIO) according to the manufacturer's protocol described in detail in the general methods (section 2.8.5). Different homogenate dilutions (1:2, 1:4, 1:10 and 1:20) were initially tested and a 1:10 dilution fell within the linear range of the standard curve and was chosen for further experiments (Appendix II: Table 9.20). Neurotensin level were calculated in two controls and two AD cases to confirm whether the selected dilution was appropriate and fell within the range of the standard curve (Appendix II: Figure 9.11 and Table 9.20). Neurotensin level was then measured across the entire cohort in duplicate and averaged and measurements from four carry-overs samples were repeated across all plates. Neurotensin measurements were adjusted to total protein level for each brain homogenates sample. The variation of this assay was determined by calculating the intra-assay CV% (Example in Appendix IV: Table 9.36). Both unadjusted neurolysin measurements and protein-adjusted measurements were used for comparisons between control and AD.

7.4.5 Statistical analysis

The Shapiro-Wilk normality test was applied to test the normal distribution of all datasets in this chapter. A significant p value, $p < 0.05$ indicated that the data sets were not normally distributed. Neurolysin concentration and protein-adjusted levels were not normally distributed. Both log transformation and square root transformation of the data did not pass the normality test and therefore

a non–parametric, Mann-Whitney test, was used to assess whether total and protein-adjusted levels varied between AD cases and controls, male and females and in the presence or absence of the *APOE* ε4 allele. Comparison of both neurolysin and protein-adjusted data between Braak tangle stage groups (Braak stage 0-II, Braak stage III-IV, Braak stage V-VI) was made using a non-parametric Kruskal-Wallis test. Correlations between both neurolysin unadjusted data and protein-adjusted data with total insoluble Aβ, tau load, insoluble Aβ40, insoluble Aβ42, Ang-II, Ang-III, Ang-II:Ang (1-7) ratio, MAG:PLP1 ratio, VEGF, age and PMD were assessed by the Spearman's correlation coefficient.

Neurotensin data was normally distributed. Comparison of neurotensin level between controls and AD cases were tested with a parametric, Unpaired samples t-test. Comparison of the neurotensin unadjusted data between Braak tangle stage groups (Braak stage 0-II, Braak stage III-IV, Braak stage V-VI) was made by use of a parametric One-Way ANOVA test. Protein–adjusted data was not normally distributed and the comparison was tested with a non-parametric test, Mann-Whitney test. Both log transformation and square root transformation of the data did not pass the normality test and therefore non–parametric tests were applied for protein-adjusted data. A non-parametric Kruskal-Wallis test was performed to compare neurotensin protein-adjusted between Braak tangle stage groups. Correlations of neurotensin unadjusted data with total insoluble Aβ, tau load, insoluble Aβ40 and insoluble Aβ42 were assessed by the Pearson's correlation coefficient and Spearman's correlation coefficient was used for protein-adjusted data. For all datasets, the ROUT method was used to detect outliers and the data was re-analysed following the removal of potential outliers and is presented in chapter 9 (Appendix VII: Section 9.7.4).

7.5 Results

7.5.1 Expression of neurolysin in human brain tissue

The specificity of the neurolysin antibody used for immunohistochemical staining to detect and examine the distribution of neurolysin in mid-frontal cortex was first tested by western blot. Four AD and four controls homogenates were used for this experiment and chosen randomly. Details of the chosen samples are described in chapter 9 (Appendix I: Table 9.7).

7.5.1.1 Validation of neurolysin antibody

A representative image of the western blot is shown below in (Figure 7.2). It shows a predominant band at the anticipated estimated MW of 75-79 kDa using the neurolysin antibody ((1D6, Catalogue number NBP2-01693)). There was no obvious difference in the expression of neurolysin in AD and controls, although this is a small sample set (n= 4). Densitometry was performed but no significant difference in band volume was observed between AD and controls (p= 0.351). The identity of the very faint lower band detected at approximately 37 kDa is unknown but could potentially be a protein degradation product.

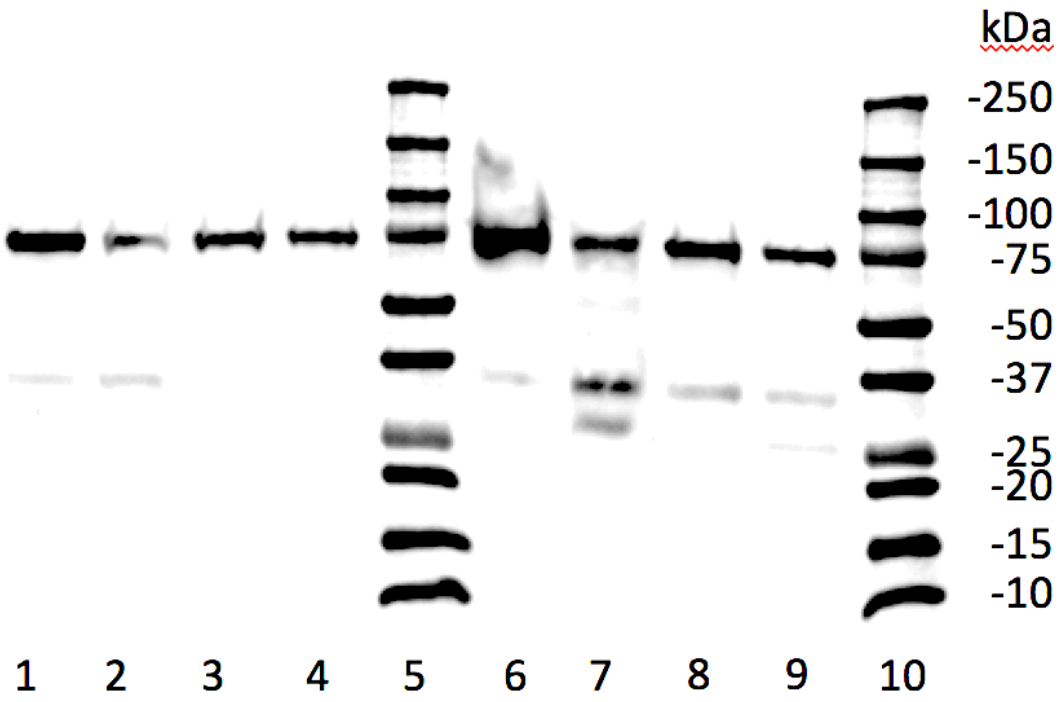

Figure 7.2 Western blot of neurolysin expression in human post-mortem brain tissue.

Neurolysin expression in human brain tissue was studied by Western blotting: left side represents expression of neurolysin in human brain tissue from AD cases (lines 1-4). Right side shows neurolysin expression in controls (lines 6-9). Lanes (5 and 10) include MW markers. The membrane was blotted with monoclonal mouse antibody to neurolysin (Neurolysin Antibody (1D6) (NBP2-01693)). The reported size of neurolysin was between 75-79 kDa. The smaller bands at MW 37 kDa are unknown but are potentially protein degradation products.

7.5.1.2 Immunolabelling of neurolysin in human brain tissue

Neurolysin predominantly labelled neurons in a control, AD and VaD case in the mid-frontal cortex. No obvious difference in the level of neurolysin immuno-positive staining was observed between controls, AD and VaD cases; although the staining was not quantified since the staining was intended to be principally qualitative (Figure 7.3 A-C).

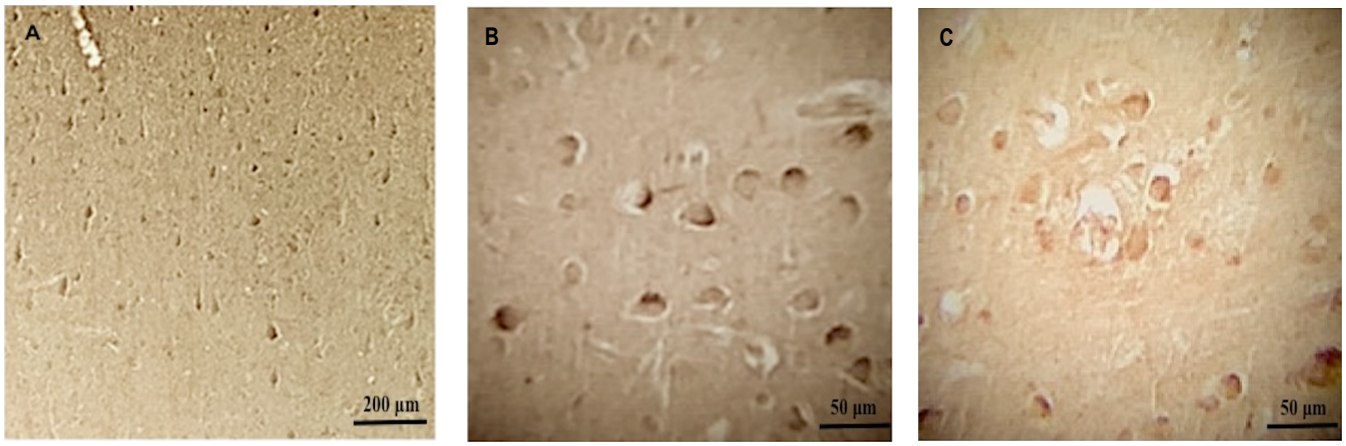

Figure 7.3 Immunolabelling of neurolysin in mid-frontal cortex.

Neurolysin labelling in the mid-frontal cortex of control (A), AD case (B) and VaD case (C) showed neurolysin was mainly present in neurons. (Image taken at 10x magnification for A and at 40x magnification for B and C).

7.5.2 Measurement of neurolysin level in AD

7.5.2.1 Reduction of neurolysin level in AD

Neurolysin protein level, measured by ELISA, was significantly reduced in the AD group compared to age-matched controls (p= 0.004) (Figure 7.4 A). The median for total neurolysin level was lower in the AD group (median= 7.368 (ng/ml)) compared to control group (median= 8.164 (ng/ml)). When neurolysin level was adjusted to total protein concentration to account for any variations in sample concentration, a significant reduction of neurolysin level was still evident in the AD group compared to age-matched controls (p= 0.008). A Mann-Whitney test compared the median of AD group (median= 20.4 (ng/mg total protein)) to control group (median= 23.66 (ng/mg total protein)) (Figure 7.4 B).

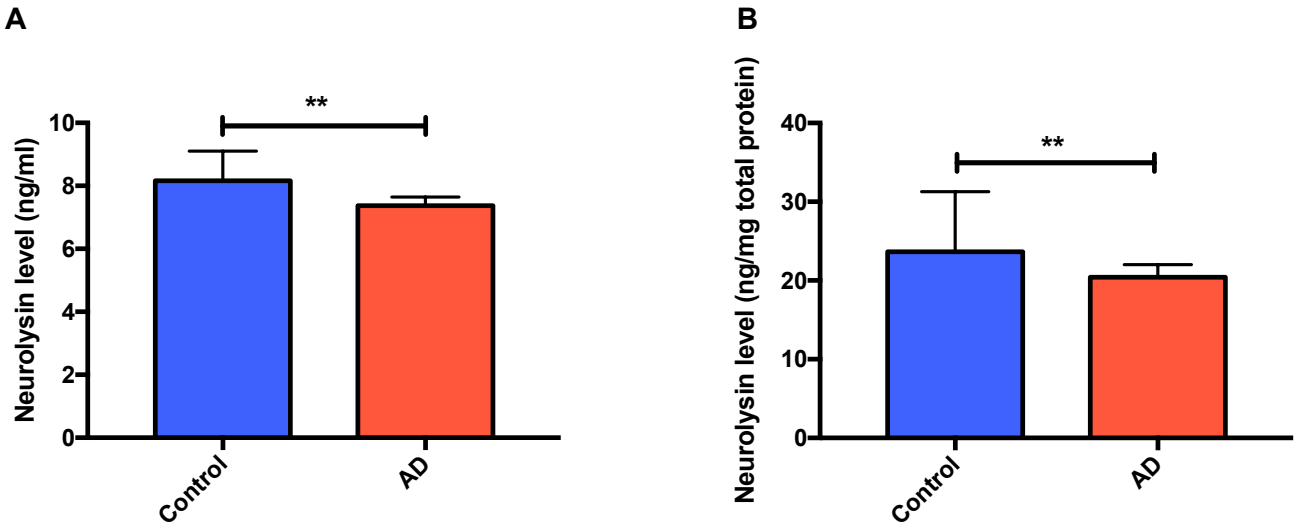

Figure 7.4 Neurolysin level, measured by ELISA, in Alzheimer's disease compared to age-matched controls.

A. Bar chart showing total neurolysin level was significantly reduced in AD (n= 70) compared with age-matched control (n= 48) in mid-frontal cortex measured using a neurolysin competitive ELISA. Mann-Whitney test revealed that total neurolysin level was lower in AD (p= 0.004) compared to controls. B. Neurolysin protein-adjusted measurement was significantly reduced in AD cases (n= 70) compared to age-matched controls (n= 48). Difference between groups was compared using Mann-Whitney test at P= 0.008. The bars indicate the median and 95% confidence intervals.

7.5.2.2 Neurolysin level in relation to disease severity

Neurolysin level and protein-adjusted neurolysin level was assessed in relation to Braak tangle stages (0-II, III-IV, V-VI). A Kruskal-Wallis test revealed a significant difference of the median between all groups for neurolysin level (p= 0.005): the median level of Braak stage 0-II= 8.273 (ng/ml), Braak stage III-IV= 7.145 (ng/ml), and Braak stage V-VI= 7.447 (ng/ml). A significant reduction of neurolysin level was observed in Braak stage (III-IV) compared to Braak stage (0-II) (p= 0.035) and between cases in Braak stage (V-VI) and Braak stage (0-II) (p= 0.004) using Dunn's multiple comparisons test (Figure 7.5 A). For neurolysin protein-adjusted data, no significant variation of the median between all groups was observed (p= 0.059). The median of Braak stage 0-II= 24.183 (ng/ml), Braak stage III-IV= 19.795 (ng/ml), Braak stage V-VI= 21.438 (ng/ml). (Figure 7.5 B).

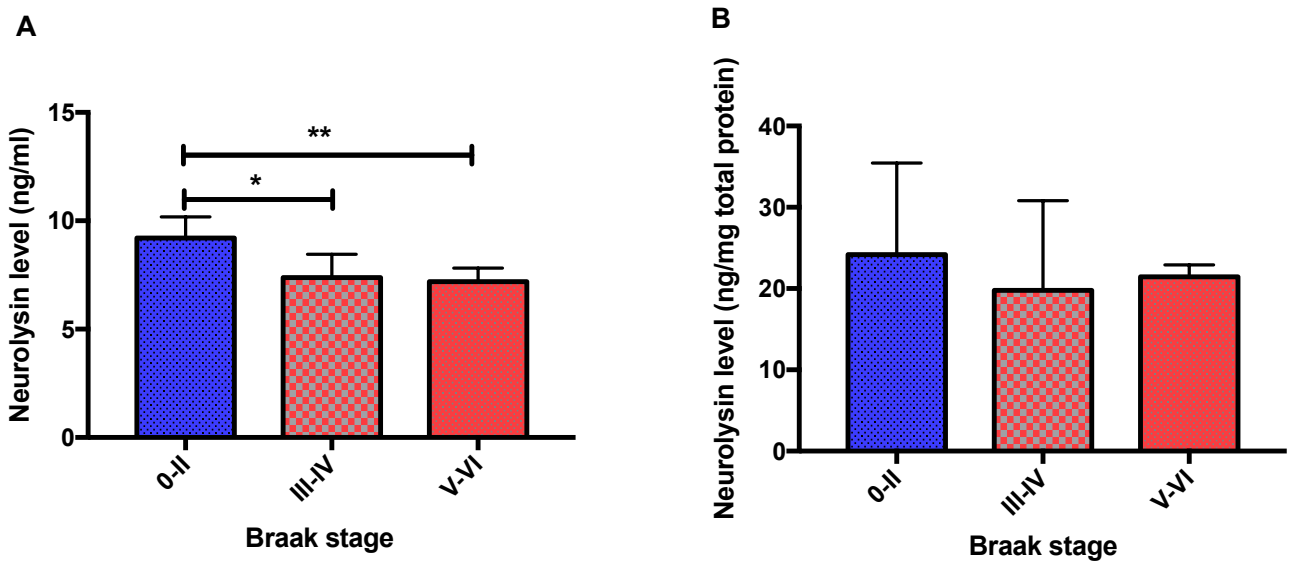

Figure 7.5 Neurolysin level in relation to Braak tangle stage pathology.

A. Bar chart showing significant variation in neurolysin level between Braak groups (Braak stage 0-II (n= 36), Braak stage III-IV (n= 20), Braak stage V-VI (n= 61)) when analysed with Kruskal-Wallis test (p= 0.005). Neurolysin level was significantly lower in Braak stage (III-IV) compared with cases in Braak stage (0-II) (p= 0.035) and between cases in Braak stage (V-VI) and Braak stage (0-II) (p= 0.004) (post-hoc Dunn's multiple comparisons test). The bars indicate the median and 95% confidence intervals. B. No significant difference was found for neurolysin protein-adjusted measurement between Braak tangle stage groups (Braak stage 0-II (n= 36), Braak stage III-IV (n= 20), Braak stage V-VI (n= 61)), Kruskal-Wallis test (p= 0.059). The bars indicate the median and 95% confidence intervals.

7.5.2.3 Neurolysin level in relation to AD pathological hallmarks

Correlations between neurolysin level and insoluble total Aβ, tau load, and insoluble Aβ40 and Aβ42 level were also examined. Unadjusted neurolysin data was not correlated with either total insoluble Aβ or tau load using (Spearman's correlation coefficient r= -0.108, p= 0.311) and (Spearman's correlation coefficient r= -0.077, p= 0.446) respectively (Figure 7.6 A and C). Spearman's correlation coefficient test showed no significant correlations between protein-adjusted neurolysin data and either total insoluble Aβ and tau load (r= -0.077, p= 0.474) and (r= -0.029, p= 0.774) respectively (Figure 7.6 B and D).

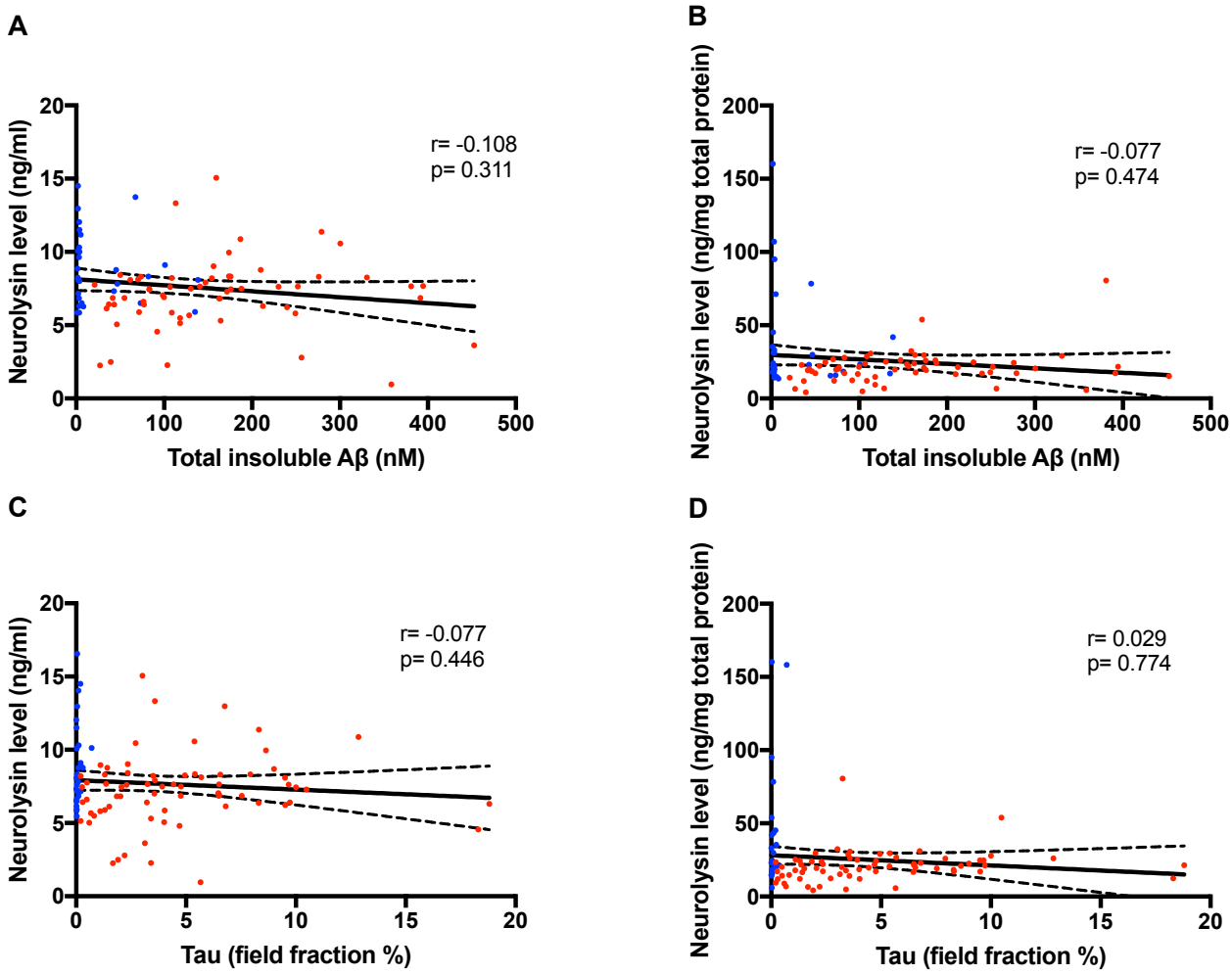

Figure 7.6 Relationship between neurolysin level and total insoluble Aβ and tau load.

A and C. Scatterplots showing no correlation between neurolysin level and both total insoluble Aβ (measured by enzyme-linked immunosorbent assay), Spearman's correlation coefficient (r= -0.108, p= 0.311) and tau load (measured by field fraction analysis), Spearman's correlation coefficient (r= 0.077, p= 0.446). B and D. Scatterplots showing no significant correlation between neurolysin protein-adjusted level and both total insoluble Aβ, Spearman's correlation coefficient (r= -0.077, p= 0.474) and tau load, Spearman's correlation coefficient (r= 0.029, p= 0.774). The solid inner line indicates the best-fit linear regression and the outer lines the 95% confidence intervals. Blue dots = controls, red dots = AD cases.

Neurolysin level did not correlate with either insoluble Aβ40 and insoluble Aβ42 (Spearman's correlation coefficient r= -0.095, p= 0.484) and (Spearman's correlation coefficient r= -0.207, p= 0.130) respectively (Figure 7.7 A and C). Similarly, neurolysin protein-adjusted data did not correlate with either insoluble Aβ40 and insoluble Aβ42 (Spearman's correlation coefficient r= -0.081, p= 0.555) and (Spearman's correlation coefficient r= -0.014, p= 0.917) respectively (Figure 7.7 B and D).

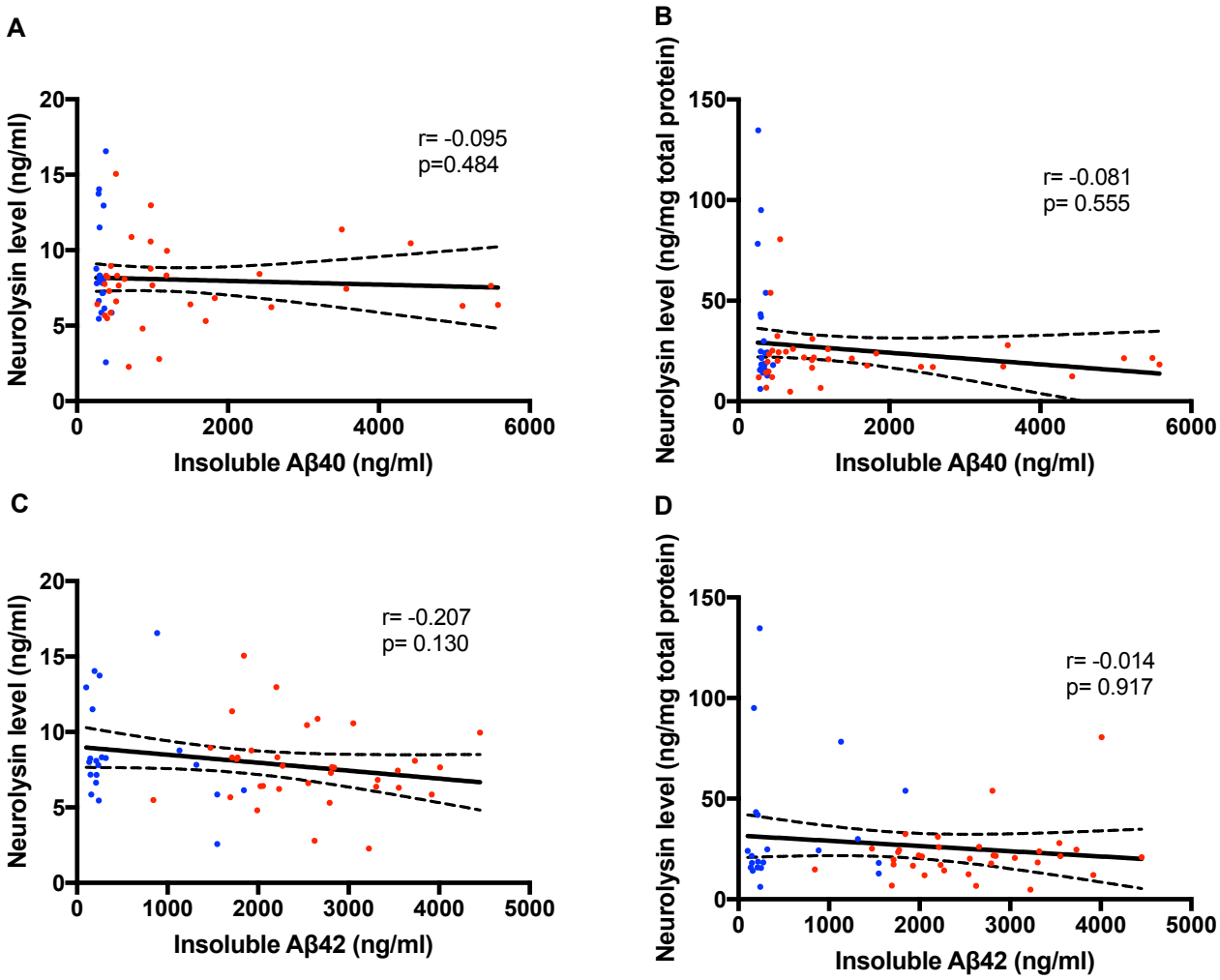

Figure 7.7 Relationships between neurolysin level and insoluble Aβ40 and insoluble Aβ42.

A and C. Scatterplots showing no correlation between neurolysin level and both insoluble Aβ40 (measured by enzyme-linked immunosorbent assay), Spearman's correlation coefficient (r=-0.095, p= 0.484), and insoluble Aβ42 (r= -0.207, p= 0.130). B and D. No significant correlation found between neurolysin protein-adjusted level and both insoluble Aβ40, Spearman's correlation coefficient (r= -0.081, p= 0.555) and insoluble Aβ42, Spearman's correlation coefficient (r= -0.014, p= 0.917). The solid inner line indicates the best-fit linear regression and the outer lines the 95% confidence intervals. Blue dots= controls, red dots= AD cases.

7.5.2.4 Relationship between neurolysin level and age-at-death, gender and PMD

In additional analyses, total and protein-adjusted neurolysin level did not correlate with either age-at-death or PMD. Neurolysin level did not vary between male and female, however, neurolysin protein-adjusted level was significantly reduced in females (p= 0.009) (Appendix V: Table 9.37).

7.5.2.5 Relationship between neurolysin level and APOE genotype

APOE genotype (*APOE* ε4 allele) is one of the major risk factors of AD. The relationship between neurolysin and *APOE* genotype was explored. Neurolysin level was significantly reduced in AD cases or individuals with one or two *APOE* ε4 alleles. The median for unadjusted neurolysin level in *APOE* ε4 negative cases= 8.037 (ng/ml) compared to *APOE* ε4 positive cases= 7.449 (ng/ml), (p= 0.045) (Figure 7.8 A). There was no difference in protein-adjusted neurolysin level in relation to the presence or absence of *APOE* ε4 allele (p= 0.219) (Figure 7.8 B).

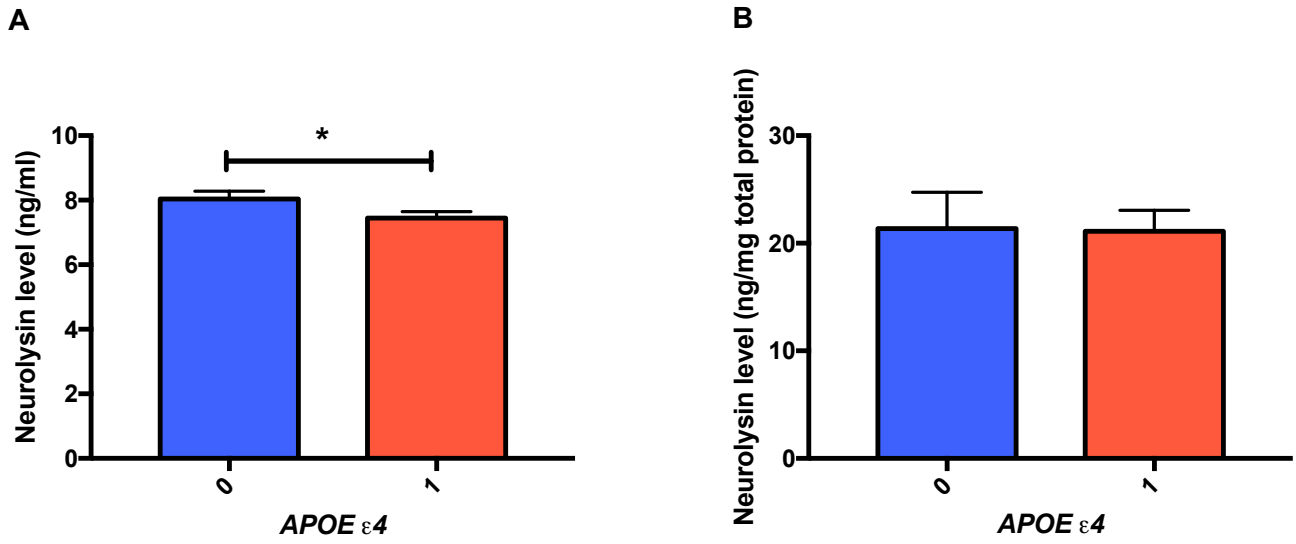

Figure 7.8 Relationship between neurolysin level and *APOE* genotype

A. Bar chart showing reduced neurolysin level in the presence of one or two *APOE* ε4 alleles (1) compared to cases with the absence of an *APOE* ε4 allele (0). Differences between groups were compared using Mann-Whitney test (p= 0.045). The bars indicate the median and 95% confidence intervals. B. Bar chart showing no significant difference in neurolysin protein-adjusted measurement in association with the presence or absence of *APOE* ε4 allele (p= 0.219). The bars indicate the median and 95% confidence intervals.

7.5.2.6 Neurolysin level in relation to brain RAS markers

The relationship between Ang-II level and neurolysin level was also assessed. Total unadjusted neurolysin level and protein-adjusted neurolysin level both correlated inversely with Ang-II level (Spearman's correlation coefficient r= -0.238, p=0.012) and (r= -0.258, p= 0.006) (Figure 7.9 A and B).

Similar investigations with Ang-III showed that unadjusted neurolysin was also correlated inversely with Ang-III level (Spearman's correlation coefficient r= -0.224, p= 0.030) but no significant correlation was found between protein-adjusted neurolysin data and Ang-III level (Spearman's correlation coefficient r= -0.005, p= 0.595) (Figure 7.9 C and D).

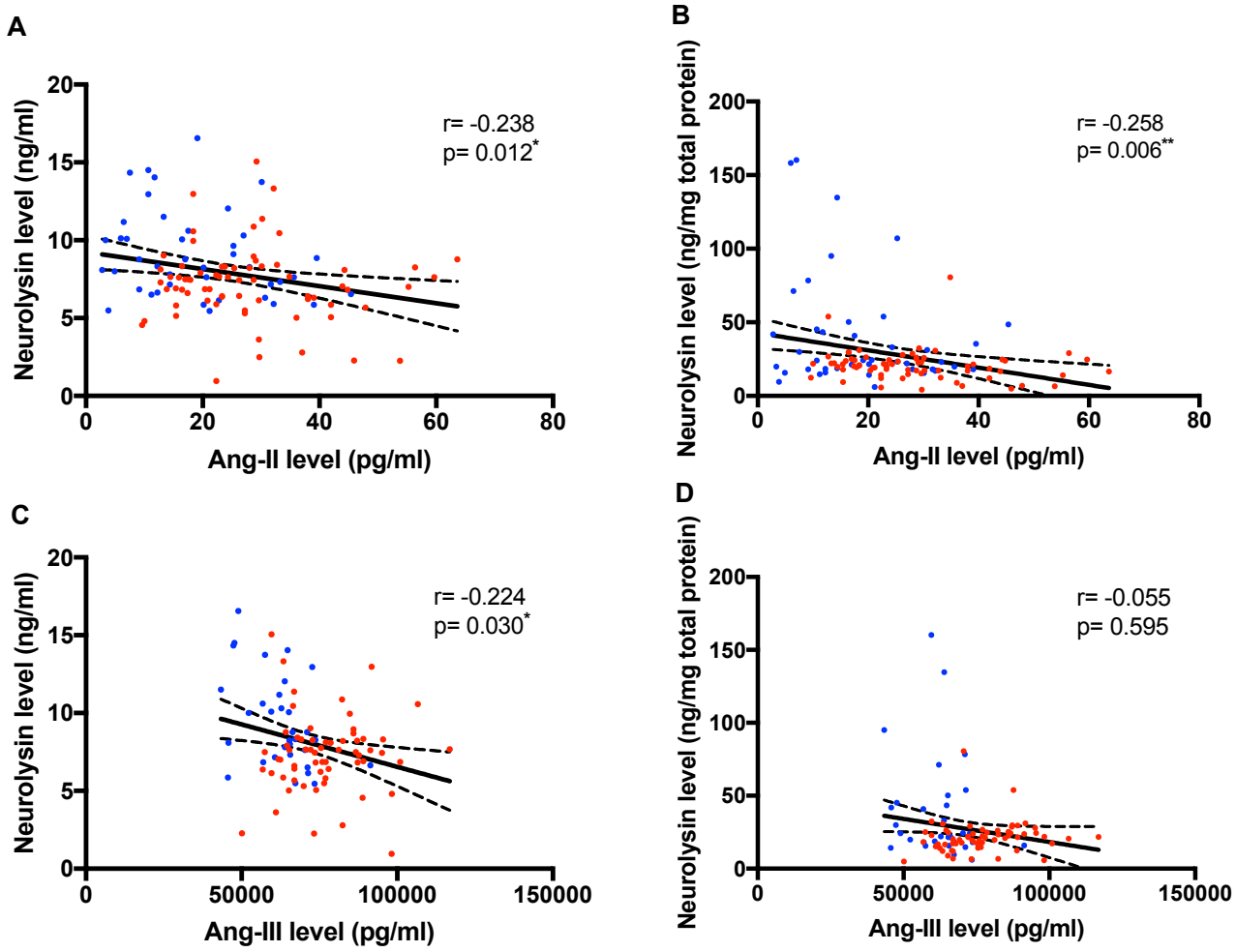

Figure 7.9 Relationship between neurolysin level and Angiotensin-II and Angiotensin-III.

A. Scatterplot showing a significant inverse correlation between neurolysin level and Ang-II level (measured by enzyme-linked immunosorbent assay), Spearman's correlation coefficient (r= -0.238, p= 0.012). B. Scatterplot showing a significant inverse correlation between neurolysin protein-adjusted level and Ang-II level, Spearman's correlation coefficient (r= -0.258, p= 0.006). C. Scatterplot showing a significant inverse correlation between neurolysin level and Ang-III level (measured by enzyme-linked immunosorbent assay), Spearman's correlation coefficient (r= -0.224, p= 0.030). D. Scatterplot showing no correlation between neurolysin protein-adjusted level and Ang-III level, Spearman's correlation coefficient (r= -0.055, p= 0.595). The solid inner line indicates the best-fit linear regression and the outer lines the 95% confidence intervals. Blue dots = controls, red dots = AD cases.

Both unadjusted neurolysin and protein-adjusted neurolysin level were also significantly inverse correlated with the Ang-II:Ang (1-7) ratio (Spearman's correlation coefficient r= -0.192, p= 0.043) and (Spearman's correlation coefficient t r= -0.276, p= 0.003) respectively (Figure 7.10 A and B).

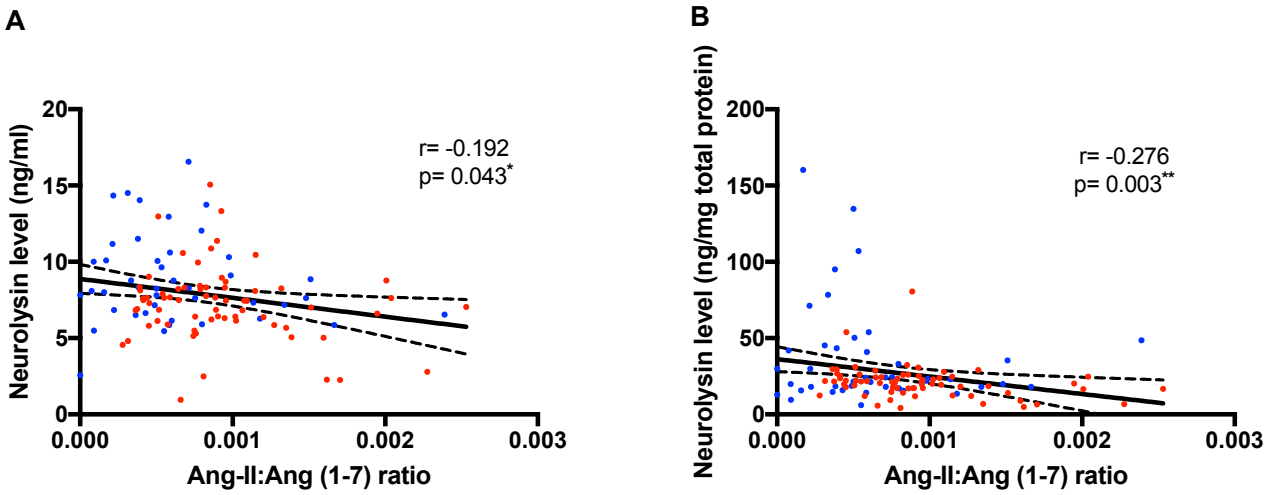

Figure 7.10 Relationship between neurolysin level and the ratio of Ang-II:Ang (1-7).

A. Scatterplot showing a significant inverse correlation between neurolysin level and the Ang-II:Ang (1-7) ratio, Spearman's correlation coefficient (r= -0.129, p= 0.043). B. Scatterplot showing a significant inverse correlation between neurolysin protein-adjusted level and Ang-II:Ang (1-7) ratio, Spearman's correlation coefficient (r= -0.276, p= 0.003). The solid inner line indicates the best-fit linear regression and the outer lines the 95% confidence intervals. Blue dots = controls, red dots = AD cases.

7.5.2.7 Neurolysin level in relation to markers of ischaemia and brain tissue oxygenation

Neurolysin level was dysregulated in relation to cerebral ischaemia (593). VEGF level is increased and the MAG:PLP1 ratio reduced in AD (314). I explored the relationship between neurolysin and markers of ischaemia and tissue oxygenation in AD. A significant inverse correlation was observed between protein-adjusted neurolysin level and VEGF level (Spearman's correlation coefficient r= -0.345, p= 0.015) (Figure 7.10 B). No significant correlation was found between unadjusted neurolysin and VEGF level (Spearman's correlation coefficient r= 0.129, p= 0.369) (Figure 7.11 A). In contrast, both unadjusted neurolysin and protein-adjusted neurolysin data were not associated with MAG:PLP1 ratio (Spearman's correlation coefficient r= 0.045, p= 0.753; Spearman's correlation coefficient r= 0.145, p= 0.315) respectively.

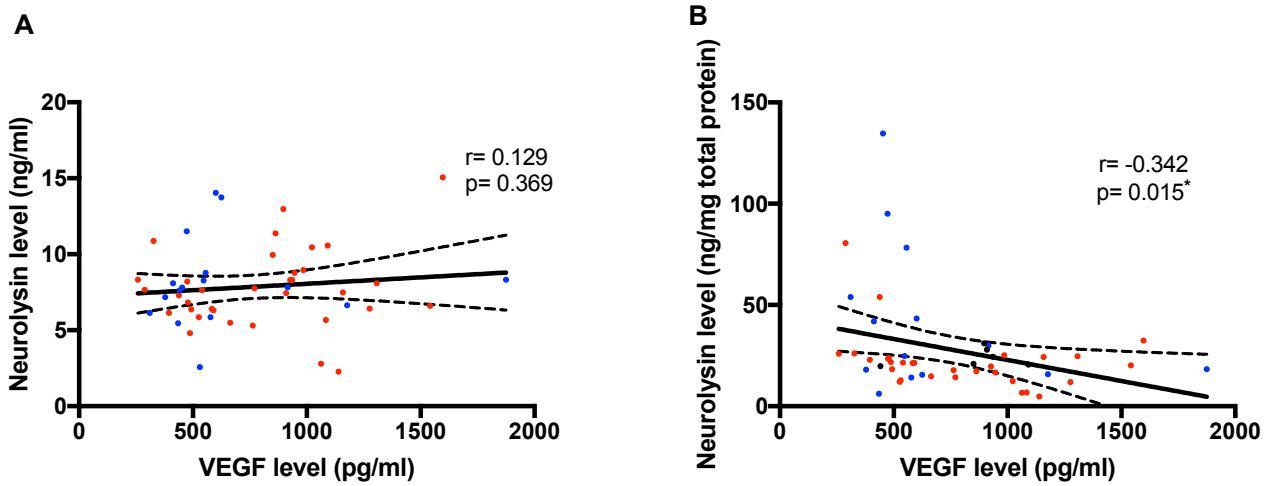

Figure 7.11 Relationship between neurolysin level and ischemic marker (VEGF)

A. Scatterplot showing no significant correlation between neurolysin level and VEGF level (measured by enzyme-linked immunosorbent assay), Spearman's correlation coefficient (r= 0.129, p=0.369). B. Scatterplot showing a significant inverse correlation between neurolysin protein-adjusted level and VEGF level, Spearman's correlation coefficient (r= -0.342, p= 0.015). The solid inner line indicates the best-fit linear regression and the outer lines the 95% confidence intervals. Blue dots= controls, red dots= AD cases.

7.5.3 Neurotensin level in AD

7.5.3.1 Comparison of neurotensin level in controls and AD

Neurotensin level and protein-adjusted neurotensin levels were not statistically different between AD cases (n= 70) and controls (n= 48) (Figure 7.12 A and B). The mean ± SEM for unadjusted neurotensin level was: controls= 746.9 ± 19.2pg/ml and AD= 751 ± 16.47pg/ml. Unpaired samples t-test showed no statistical significance between groups (p= 0.875). The median for neurotensin protein-adjusted data in AD cases was slightly numerically lower in AD (= 2096 (pg/mg total protein)) than in controls (= 2245 (pg/mg total protein)), however, a Mann-Whitney test showed no statistical significant difference between the groups (p= 0.259).

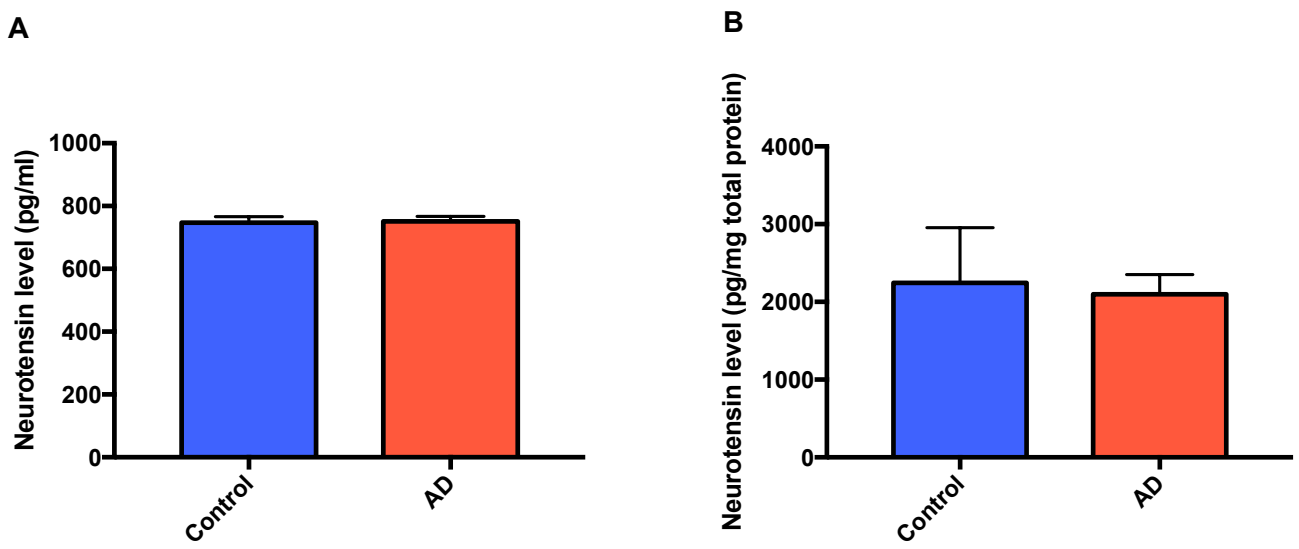

Figure 7.12 Measurement of neurotensin level in Alzheimer's disease compared to age-matched controls.

Neurotensin level was measured by sandwich ELISA in AD (n= 70) and age-matched controls (n= 48) in mid-frontal cortex measured using a neurotensin sandwich ELISA. A. Bar chart showing neurotensin level was unchanged in AD, unpaired samples t-test (p= 0.875). The bars indicate the mean ± SEM. B. Bar chart showing protein-adjusted neurotensin level did not differ in AD, Mann-Whitney test (p= 0.259). The bars indicate the median and 95% confidence intervals.

7.5.3.2 Neurotensin level in relation to disease severity

The neurotensin level in mid-frontal cortex was assessed in relation to Braak tangle stages (0-II (n= 36), III-IV (n= 20), V-VI (n= 61)). One-Way ANOVA test indicated no significant difference was present when the mean neurotensin levels were compared between Braak stage groups (p= 0.528) (Figure 7.13 A). The mean of Braak stage 0-II= 749.245 (pg/ml), Braak stage III-IV= 719.254 (pg/ml) Braak stage V-VI= 759.076 (pg/ml). For neurotensin protein-adjusted level, Kruskal-Wallis test indicated no significant difference of the medians between Braak stage groups (p= 0.683) (Figure 7.13 B). The median of Braak stage 0-II= 2157.280 (pg/mg total protein), Braak stage III-IV= 2093.885 (pg/mg total protein) Braak stage V-VI= 2197.430 (pg/mg total protein).

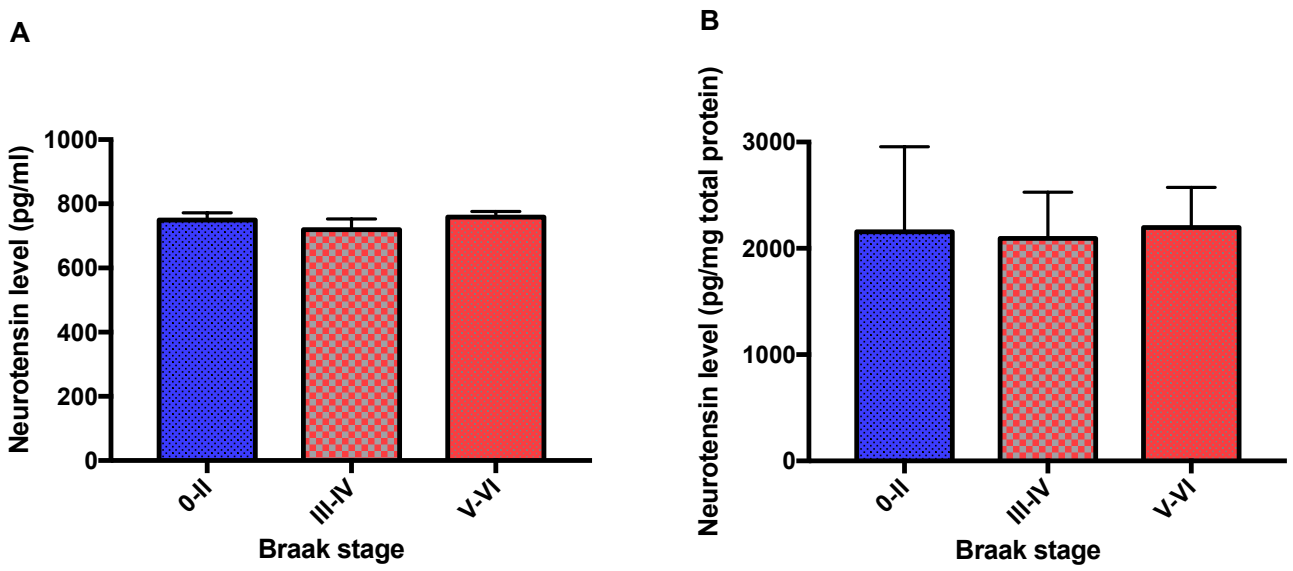

Figure 7.13 Neurotensin level in relation to Braak tangle stage.

A. Bar chart showing no significant difference in neurotensin level measured by sandwich ELISA between Braak tangle stage groups (Braak stage 0-II (n= 36), Braak stage III-IV (n= 20), Braak stage V-VI (n= 61)), One-Way ANOVA test (p = 0.528). The bars indicate the mean ± SEM. B. Bar chart showing no significant difference in neurotensin protein-adjusted measurement between Braak tangle stage groups (Braak stage 0-II (n= 36), Braak stage III-IV (n= 20), Braak stage V-VI (n= 61)), Kruskal-Wallis test (p= 0.683). The bars indicate the median and 95% confidence intervals.

7.5.3.3 Neurotensin level in relation to traditional pathological hallmarks

No significant correlation was found between neurotensin level and total insoluble Aβ (Pearson's correlation coefficient r= 0.023, p= 0.831) (Figure 7.14 A) or tau load in mid-frontal cortex (Pearson's correlation coefficient r= 0.067, p= 0.510) (Figure 7.14 C). Spearman's correlation coefficient test showed no significant correlation between neurotensin protein-adjusted level and both total insoluble Aβ (Spearman's correlation coefficient r= 0.003, p= 0.977) and tau load (Spearman's correlation coefficient r= 0.154, p= 0.125) (Figure 7.14 B and D).

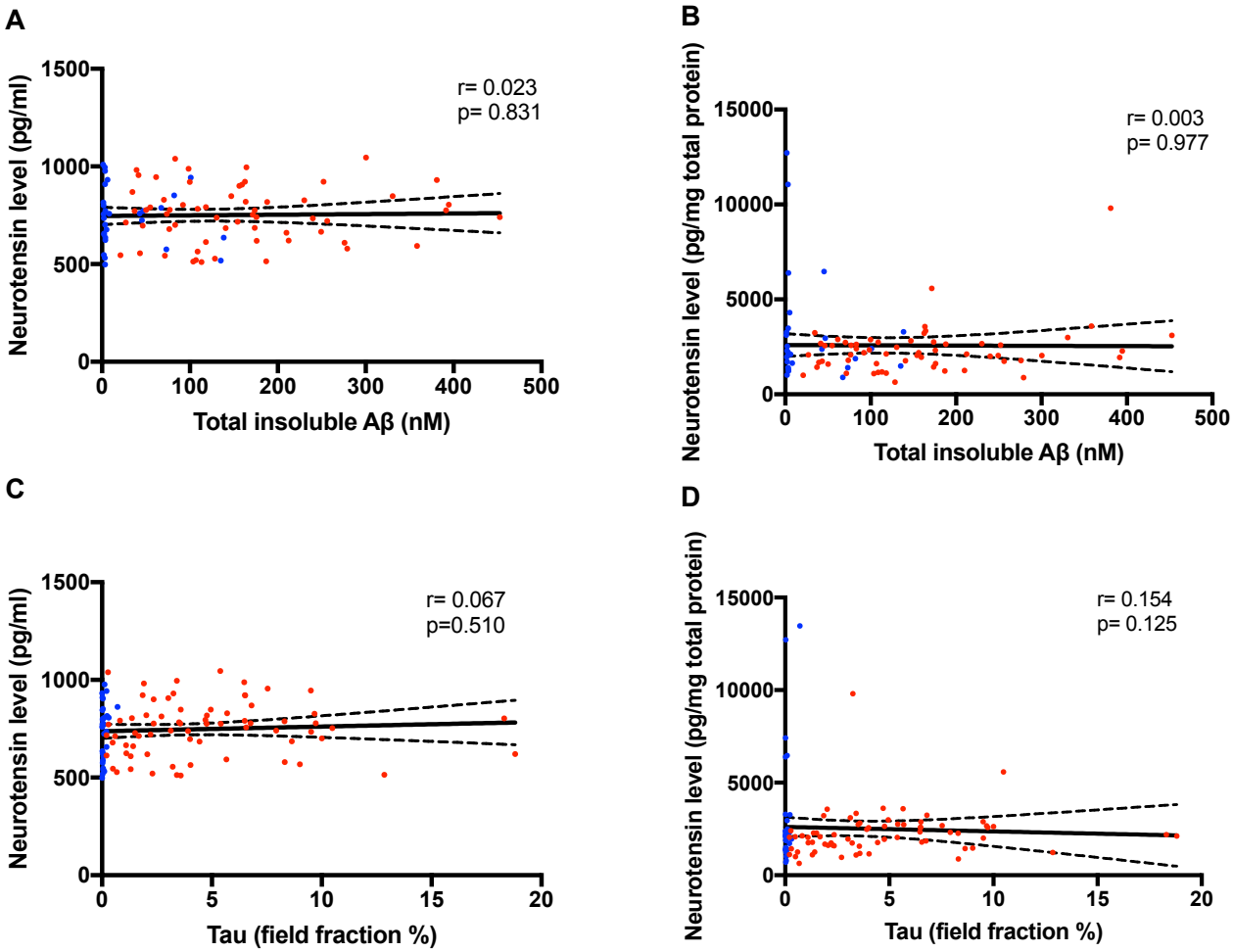

Figure 7.14 Relationship between neurotensin level and total insoluble Aβ and tau load.

A and C. Scatterplots showing no correlation between neurotensin level and total insoluble Aβ (measured by enzyme-linked immunosorbent assay), Pearson's correlation coefficient (r= 0.023, p= 0.831) and tau load (measured by field fraction analysis), Pearson's correlation coefficient (r= 0.067, p= 0.510). B and D. Scatterplots showing no significant correlation between neurotensin protein-adjusted level and total insoluble Aβ, Spearman's correlation coefficient (r= 0.003, p= 0.977) and tau load Spearman's correlation coefficient (r= 0.154, p= 0.125). The solid inner line indicates the best-fit linear regression and the outer lines the 95% confidence intervals. Blue dots = controls, red dots = AD cases.

Neurotensin level did not correlate with insoluble Aβ40 (Pearson's correlation coefficient= 0.056, p= 0.682) or Aβ42 (r= 0.036, p= 0.791) (Figure 7.15 A and C). Protein-adjusted neurotensin level was not correlated with either insoluble Aβ40 (r= -0.030, p= 0.825) or Aβ42 (r= 0.074, p= 0.589) using Spearman's correlation coefficient (Figure 7.15 B and D).

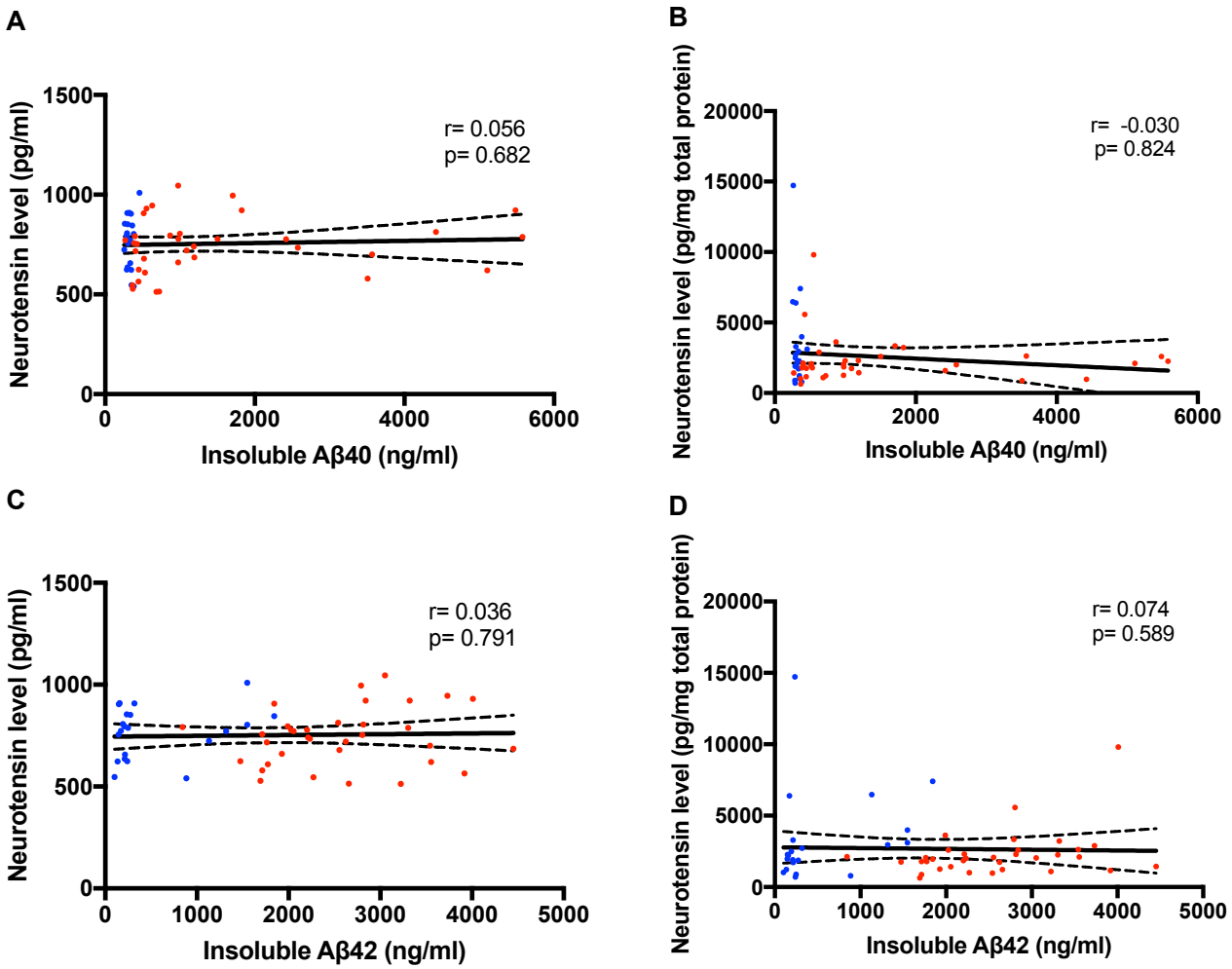

Figure 7.15 Relationship between neurotensin level and insoluble Aβ40 and insoluble Aβ42.

A and C. Scatterplots showing no correlation between neurotensin level and insoluble Aβ40 (measured by enzyme-linked immunosorbent assay), Pearson's correlation coefficient (r= 0.056, p= 0.62), and insoluble Aβ42 (r= 0.036, p= 0.791). B and D. Scatterplots showing no significant correlation between neurotensin protein-adjusted level and insoluble Aβ40, Spearman's correlation coefficient (r= -0.030, p= 0.824) or insoluble Aβ42, Spearman's correlation coefficient (r=0.074, p= 0.589). The solid inner line indicates the best-fit linear regression and the outer lines the 95% confidence intervals. Blue dots = controls, red dots = AD cases.

7.6 Discussion

This chapter explored the expression and distribution of the non-AT_1R and non-AT_2R RAS binding site (neurolysin) and its substrate (neurotensin) in relation to AD pathogenesis. I report for the first time that neurolysin expression in the mid-frontal cortex was reduced in AD in association with disease severity, brain RAS markers, *APOE* ε4 and a marker of ischaemic damage (VEGF). In contrast, neurotensin level in the mid-frontal cortex was unchanged in AD and was not associated with disease pathology. These data suggest that dysregulation of neurolysin may play an important role in modulating brain RAS and vascular dysfunction in AD and has been largely overlooked to-date.

The role of neurolysin as a metalloendopeptidase that is involved in the degradation of numerous bioactive peptides makes it interesting in relation to AD. That it has been identified as a novel non-AT_1R/AT_2R binding site in brain RAS and cleaves both Ang-II and Ang-III (275, 590, 593, 598) is also interesting in relation to the angiotensin hypothesis of AD (538). Dysregulation of neurolysin has been previously associated with the pathophysiology of stroke and hypertension, both of which are risk factors for AD, yet few studies have explored its potential role in AD pathogenesis (275, 593, 617).

This is the first study, to the best of my knowledge, of neurolysin expression in human post-mortem brain tissue in AD. My novel findings indicated that neurolysin level was significantly reduced in the mid-frontal cortex in post-mortem brain tissue in AD in association with markers of disease severity. This reduction was inversely correlated with Ang-II, Ang-III levels and the Ang-II:Ang (1-7) ratio in AD. These observations are in keeping with previous studies that reported a neuroprotective role of neurolysin in the degradation of both Ang-II and Ang-III into inactive metabolites (275, 593) but also consistent as a possible contributory factor for the excess levels of Ang-II and Ang-III that have been reported in AD (393, 417). Thus, these findings suggest that reduction of neurolysin could be an important contributor to the overactivation of the cRAS in AD.

Despite observed lower levels of neurolysin in AD and a relationship with some of the key markers of cRAS, I did not find any significant correlations between neurolysin level and total insoluble Aβ, tau load, insoluble Aβ40 and insoluble Aβ42. These findings are unexpected given recent data indicating a role of neurolysin in degradation of Aβ (602). Neurolysin level did not significantly change with age and PMD but was significantly reduced in female and in AD cases or individuals with one or two *APOE* ε4 alleles. Neurolysin level was inversely correlated with VEGF level, a marker of brain ischaemia that is elevated in AD (314). Yet, these findings of reduced neurolysin in association with

VEGF in AD, might appear at odds with a previous study that found neurolysin was up-regulated in stroke (593, 601). These differences might be explained by the duration or scale of the cerebral ischaemia that is evident in both diseases, where up-regulation of neurolysin expression observed after stroke corresponded to acute ischaemia, possibly as a compensatory mechanism, whilst in AD there is a lower and more chronic level of ischaemia. Yet, together these data indicate a consistent role of neurolysin in different degenerative disorders of the brain and point to a possibly important role in vascular dysfunction in AD that requires further characterisation in future studies.

Immunohistochemical staining was also performed to explore the expression and distribution of neurolysin. This revealed positive neuronal staining in the mid-frontal cortex. This supports previous findings that also reported similar neurolysin expression patterns in neurons within the brain (595-597). Immunohistochemical studies in rodent brains have also reported positive neurolysin staining within glia (596), however, I did not observe obvious positive staining of neurolysin in non-neuronal cells. Neurolysin immunostaining was similar between controls, AD and VaD brain tissue sections examined, although quantification of neuronal labelling was not possible and the study was performed in a small sample set in contrast to the ELISA measurements of neurolysin in a larger cohort.

Neurotensin is a neuroendocrine peptide that metabolised by neurolysin. Previous studies with a small sample size have reported reduced neurotensin protein and mRNA levels, as well as reduced levels of two of its receptors (NTSR1 and NTSR2) in post-mortem brain tissue of AD patients (614, 618). Contrary to expectation, we did not find a significant difference in neurotensin level, measured by ELISA, between AD cases and age-matched controls in the mid-frontal cortex. The discrepant findings may be explained by regional differences and/or different methodological approaches, as previous studies have examined neurotensin expression in the amygdala by IHC (606) or neurotensin level has been measured by real time-RT-PCR in the temporal cortex (614). In these studies, a modest reduction in neurotensin mRNA was observed compared to more obvious loss of expression of NTSR1 and NTSR2 in AD. Reduced NTSR was also reported in post-mortem hippocampal tissue, using autoradiography the authors detected a 57% reduction in entorhinal region (612). However, the small sample size of this study (8 AD cases compared to 9 controls) warrants caution in interpreting these results. To the best of our knowledge this is the first study to have measured neurotensin level by quantitative ELISA in the mid-frontal cortex of AD patients in a large cohort. The discrepant findings for neurotensin level in AD prompts a need for further investigations in independent cohorts, using a

combination of different methodological approaches, to confirm or refute the involvement of neurotensin in AD pathogenesis.

This study has several limitations: we only measured neurotensin expression in AD by one methodological approach (ELISA) and this was restricted to one brain area (mid-frontal cortex) in AD. Other studies indicate that neurotensin is highly distributed in the hippocampus so this should be an area of interest in future studies. It will also be of interest to explore the distribution of neurotensin in different brain areas and by other methods such as reverse transcription-polymerase chain reaction (RT-PCR) and immunohistochemical studies. It would be interesting to determine if neurotensin expression varied in other types of dementia especially vascular dementia. In addition, further characterisation of the NTSR in human post-mortem brain tissue would also provide further information about this pathway in AD.

In conclusion, my findings provide novel evidence of reduced neurolysin level and its association with brain RAS markers and vascular dysfunction in AD. Further studies are now required to characterise and study this system more broadly in AD.

Chapter 8. General discussion and Conclusions

The now increasingly recognised association between overactivity within the cRAS and AD has framed a rapid growth in research to better understand the mechanisms behind this interaction and the scope for translational and intervention opportunities not only for AD but also increasingly in a number of related, overlapping neurodegenerative conditions.

Studies in animal models have indicated that ICV infusion of Ang-II accelerated both Aβ and Tau deposition, which was associated with cognitive decline. Notably, cRAS-blockers that are available for the treatment of hypertension, a risk factor for AD, rescued these deficits to varying degrees or reduced the extent of pathology and rate of progression observed. The translational potential and importance of these pre-clinical findings are consistent with the reported findings of several clinical and epidemiological studies that indicate that ACEIs and ARBs reduce the incidence and delay the progression of AD. The real test will come from the results of various clinical trials that are underway in AD patients or related populations of mild cognitive impairment to determine if cRAS-targeting medication may be of therapeutic benefit in AD patients (538).

Despite our increased understanding of RAS in AD there are still many gaps in our knowledge. Herein I have presented data that explores the divergent role of ACE-1 activity in AD. I have explored the apparent contradictory role of ACE-1 to generate Ang-II (disease-promoting) but also potentially cleave and degrade Aβ42 (disease-protective) in AD. I have also investigated further the expression and behaviour of two major rRAS pathways in AD (ACE-2/Ang (1-7)/MasR) and the alternative (APA/Ang-III/APN/Ang-IV/IRAP) in relation to AD. These more recently identified pathways are thought to counter-regulate the potentially harmful effects of cRAS and are also notably directly implicated in learning and memory. Lastly, I have undertaken exploratory studies on a number of new and less well characterised RAS pathways. These include the non-AT_1R and non-AT_2R binding receptor and associated enzyme (Neurolysin) within RAS in relation to AD. I have also undertaken some exploratory studies to try and further our understanding of the specificity of commercial antibodies for the AT_1R and AT_2R receptors (presented in Appendix XI). In summary, this thesis presents data that continues to indicate and support previously findings that both cRAS and rRAS pathways are dysfunctional in AD and provides further insights into the complex relationship between the RAS and AD pathogenesis. With these new findings the following research questions can be posed and explored further.

8.1 Could divergent ACE-1 C-domain and N-domain activities provide a new therapeutic target for AD?

The role of ACE-1 has been extensively investigated in AD. Several reports have demonstrated an association between increased ACE-1 and AD pathogenesis (78, 90, 155, 311, 354, 357). The role of ACE-1 in AD is certainly complex. On the one hand, ACE-1 is responsible for the generation of Ang-II and is associated with several aspects of disease pathogenesis. ACE-1 activity is elevated in AD in human post-mortem studies in relation to parenchymal Aβ load (78, 311, 354, 357). ACEIs improve cognitive function and disease pathology in animal models of AD (360, 361, 515, 619) and slow the progression and reduce the incidence of AD in human epidemiological studies (364, 365, 367-370, 520, 542). In contrast, ACE-1 has also been shown to cleave and degrade Aβ42 in vitro (81-83, 347, 549, 550) – ACE-1 mediated degradation of Aβ generates cleavage products that are potentially less neurotoxic and therefore potentially more easily cleared. There is also an established literature in which *in vitro* and *in vivo* studies have shown that the use of ACEIs increases both Aβ40 and Aβ42 level and inhibits the degradation of Aβ42 (79, 81, 343, 347, 518, 519). Previous genetic evidence has linked lower serum/CSF ACE-1 level with increased AD risk indicated by an association with *ACE* genotype and accumulation of Aβ in the brain (86, 620, 621). We propose that the inconsistencies in some previous findings reflect the variable affinities of different ACEIs for each ACE-1 domain (which are responsible for Ang-II generation and Aβ cleavage respectively).

Herein, I have shown for the first time a disease-related change in ACE-1 catalytic domain activity in AD. Previous studies have highlighted the domain-specificity of ACE-1: the C-domain is largely responsible for converting Ang-I to Ang-II (547) whereas the N-domain is involved in Aβ degradation (82, 343, 549). I have now found that in AD, ACE-1 C-domain activity, largely responsible for Ang-II production (343, 344, 547) was increased and was positively correlated with insoluble total Aβ and insoluble Aβ42 level, whilst N-domain activity, potentially contributing to Aβ cleavage and clearance, was reduced in AD. These novel data provide further insight and a possible explanation for the apparent divergent role of ACE-1 in AD where the combined effect of the domain-specific alterations would favour Ang-II mediated disease progression but also result in impeded Aβ clearance (via reduced N-domain activity) (550). This imbalance in the activity of the two ACE-1 catalytic domains might therefore resolve the conflicting findings in previous studies regarding the role of ACE-1 domains in AD e.g. both ACE-1 catalytic domains involved in Aβ cleavage (345, 346).

My findings may also provide for the first time, a possible mechanistic explanation for the apparent discrepant findings in previous pharmaco-epidemiological studies comparing different ACEIs and AD risk and progression i.e. where some have been found to reduce risk of AD (364, 365), where following adjustment for prescribing bias that they have no protective effect, or that ACEIs might even be more harmful (368, 544). My findings point to potentially far-reaching implications in clinical populations since different ACEIs have been reported to have higher affinities and domain selectivity e.g. clinically prescribed lisinopril, or experimental drugs like RXP380 and proline-rich oligopeptides (PRO8)) have C-domain specificity (343, 344, 372, 373, 376, 622). Any selective C-domain inhibitors will likely inhibit Ang-II production while preserving Aβ metabolism i.e. since N-domain activity should not be unaltered. These findings warrant further experimental investigations to characterise the domain-specificity of the ACEIs currently prescribed for the treatment of hypertension with respect to their inhibitory effects on the activity of the two ACE-1 domains. I suggest that selective C-domain ACEIs may have greater therapeutic benefit for AD.

8.2 Are the rRAS pathways altered in AD in relation to vascular dysfunction?

The cRAS pathway and its associated elevated activity is well-established in AD. However, attention has more recently begun to be focussed on the brain rRAS pathways. The rRAS pathways are responsible for the metabolism of Ang-II. These metabolites, that were originally thought to be inactive, have now been shown to have important biological functions. The two main axes of rRAS: the non-classical axis (ACE-2/Ang (1-7)/MasR) and the alternative (APA/Ang-III/APN/Ang-IV/IRAP) pathway counter-regulate cRAS signalling. Importantly, dysregulation of the rRAS has been implicated in several neurodegenerative and cerebrovascular disorders (330, 419, 429, 430, 433, 458, 574). Interestingly, these pathways are highly expressed within the hippocampus and basal forebrain and have been shown to be directly involved in learning and memory. The role of these pathways in AD is now becoming an area of increased interest and investigation. In recent studies, we found that the activity of ACE-2 (an enzyme involved in the generation of Ang (1-7) from Ang-II) was reduced in AD, concomitantly with increased ACE-1, and was strongly related to disease pathology. Notably, restoration of ACE-2 activity, or Ang (1-7) infusion, has been shown to be protective against cognitive decline and disease pathology in mouse models of AD (295, 434, 440). Yet, the expression and behaviour of these rRAS pathways remains poorly characterised in the human brain and its possible association with AD pathology and vascular dysfunction remains unclear. The intention of the work

described in chapters 4, 5 and 7 was to further investigate the major components of the rRAS pathways (Ang (1-7), MasR, Ang-IV, IRAP level and activity) in relation to AD pathogenesis and vascular dysfunction in post-mortem human brain tissue.

In these studies, I found that the ratio of Ang-II:Ang (1-7) was increased in AD in keeping with our previous study showing reduced ACE-2 activity in AD (417). Despite the observed reduction of ACE-2 activity in AD, I present new data showing that the levels of Ang (1-7) were unaltered in AD as was MasR expression in the same cases. MasR was predominantly expressed by pyramidal neurons within the neocortex, although neither Ang (1-7) nor MasR expression was related to amyloid or tau pathology. The implications of these findings are somewhat difficult to interpret as to-date there are only a few studies that have investigated the Ang (1-7)/MasR pathways in AD. These were two studies with different study samples, one using animal brain tissue and the other reporting on human plasma and both used different methods to those I employed here. In the first study, Ang (1-7) levels were reduced in an animal model of sporadic AD in two different brain regions (hippocampus and cerebral cortex) and inversely correlated with tau hyperphosporylation. Despite the reduction of Ang (1-7) and similar to our finding, this study reported no significant reduction of MasR expression in AD (416). The same group conducted another study in human plasma and reported that plasma Ang (1-7) levels were reduced in AD patients and positively correlated with cognitive decline. However, in this study no reduction of ACE-2 activity was observed (435). These findings, along with my own findings are somewhat puzzling as one might expect to see changes in levels of Ang (1-7) with respect to reduced ACE-2 activity. Similarly, one might expect to see any changes in Ang (1-7) reflected by some changes in MasR given their relationship with respect to signalling.

Some of the apparent inconsistence across studies may simply reflect differences in study subjects (animal vs. human), the methods used to measure Ang (1-7)(different ELISA, in-house direct vs. commercially ELISA kit), different methods to measure MasR (western blot vs. ELISA) and ACE-2, and regional difference (hippocampus vs. mid-frontal cortex). Aspects of PMD or sample processing of blood plasma and timelines for the preparation of animal tissue might also contribute however this is largely speculative. Another possible explanation is that ACE-1 is involved in the formation of Ang (1-9) forming alternate processing pathways involved in rRAS signalling. These angiotensin peptides and alternative processing pathways remain almost completely uncharacterised in human brain tissue at present. It will be important to confirm in future studies whether Ang (1-7) and MasR are related to AD, as well achieve a better understanding of both ACE-1 and ACE-2 in the dynamics of this

relationship. My studies here suggest that although ACE-2 activity is reduced in AD that some of the downstream pathways remain unaltered although, as mentioned, alternative uncharacterised rRAS pathways may be involved.

In this thesis I also investigated the main components of the downstream alternative pathway of brain RAS (APA/Ang-III/APN/Ang-IV/IRAP) in relation to AD pathogenesis and vascular dysfunction. Previous findings indicated that the upstream components of this rRAS pathway (e.g. Ang-III) are dysregulated and associated with AD pathogenesis (393). Based on this previous evidence and other experimental animal studies that showed beneficial effects of Ang-IV treatment on Aβ related cognitive decline (479, 482, 484, 493), I expected to see a reduction of the downstream rRAS pathway in AD. Contrary to expectations, I found that Ang-IV and IRAP protein expression within the mid-frontal cortex, the latter being predominantly expressed in pyramidal neurons, were unchanged in AD. IRAP enzyme activity, arguably the more biologically relevant measure, was reduced in AD in association with disease severity and Aβ and tau load. These findings are in keeping with a previous study that reported a reduction of IRAP activity in the plasma of AD patients (258). Yet, these findings seem incongruent with previous studies in animal models that have reported the protective effects of IRAP inhibitors (i.e. that would lower IRAP activity) against cognitive decline (474, 479, 484, 493). Considering the complex structure and function of IRAP and its complex role in AD and in relation to other RAS markers (459), these novel preliminary findings require further investigation in the context of AD. It is possible that the observed reduction in IRAP activity in AD in this study corresponds to a compensatory response to disease pathology. Yet, Ang-IV and IRAP protein levels were unchanged in AD. The reason for the discrepancy between protein and enzyme activity is unclear; future studies should perhaps try to characterise the expression and distribution of the RNA transcript to clarify this surprising observation or the extent to which the activity of the enzyme might be influenced by post-translational modifications that are also modulated by the disease process. Thus, levels of IRAP protein might continue to be maintained, or even slightly elevated to try and compensate for the lack of activity that the disease might be directly influencing.

I also explored the relationship between brain rRAS pathways and markers of cerebral ischaemia (VEGF) and hypoperfusion (MAG:PLP1). In this smaller cohort, I found for the first time that MasR expression adjusted to total protein level was inversely correlated with VEGF, a marker of brain ischaemia. Similarly, I found that Ang-IV and IRAP protein levels, which were unchanged in AD, were both inversely correlated with VEGF. In contrast, the expression of MasR, Ang-IV and IRAP did

not correlate with MAG:PLP1 ratio, a novel marker of brain tissue oxygenation in post-mortem brain tissue, which reflects changes in brain perfusion several months prior to death (312-315). These data suggest that the downstream brain rRAS pathways are associated with cerebral ischaemia in AD, reinforcing the interaction between rRAS and cerebrovascular dysfunction in AD. Larger independent studies are now required to further investigate and validate these preliminary observations and should be focussed on addressing causality and the direction of the observed relationships. In summary, my data supports previous studies suggesting that downstream rRAS pathways are potentially dysfunctional in AD in relation to vascular changes, rather than classical markers of disease pathology, namely Aβ and Tau.

8.3 Is non-AT_1R and non-AT_2R binding protein expression in AD related to markers of disease pathology and vascular dysfunction in AD?

The cRAS elicits its biological effects through activation of the GPCRs (AT_1R and AT_2R) (255, 267, 269). A novel non-AT_1R and non-AT_2R binding protein was discovered in human and rat brain and was identified as a zinc metalloendopeptidase known as neurolysin (587, 588). Dysregulation of neurolysin has been reported to be associated with the pathophysiology of stroke and hypertension with little evidence of its role in AD pathogenesis (275, 593, 617). My novel findings indicate that neurolysin level is significantly reduced in the mid-frontal cortex in post-mortem brain tissue in AD in association with disease severity (Braak tangle stage). This reduction in neurolysin was inversely correlated with Ang-II, Ang-III levels and the Ang-II:Ang (1-7) ratio in AD. These interesting observations are in agreement with previous studies that have reported a neuroprotective role of neurolysin in the degradation of both Ang-II and Ang-III into inactive metabolites (275, 593). The possible role of neurolysin in Ang-II and Ang-III metabolism, which works by internalising and facilitating the degradations of these angiotensins, thus limiting their access to AT_1R, is interesting. Thus the observed reduction of neurolysin in AD is another level of evidence in support of the angiotensin hypothesis of AD.

I also investigated whether the reduction of neurolysin was related to markers of ischaemia e.g. VEGF and hypoperfusion e.g. MAG:PLP1 in AD. Interestingly, the reduced level of neurolysin was inversely correlated with VEGF level, a marker of brain ischaemia (that is elevated in AD brain), but not with MAG:PLP1 in these tissue samples (314). These findings contrast with those in a previous study

reporting that neurolysin was up-regulated in early phase (after 7 days) post-acute stroke in mouse brain (593, 601). The duration of cerebral ischaemia (acute vs. chronic) and study subject (animal vs. human) could explain the inconsistences with previous studies.

In summary, my novel findings suggest that a reduction of neurolysin could contribute to the overactivation of cRAS reported in AD (because the levels of Ang-II and Ang-III signaling are less well controlled), and similarly are associated with vascular dysfunction, both of which now require further characterisation in future studies.

8.4 Study Limitations

In this study, I have attempted to map the distribution and expression of human RAS in AD. These studies have been performed in relatively large cohorts that were previously characterised in terms of disease pathology (Aβ and Tau) and disease severity. I have identified a number of novel findings in relation to RAS changes in AD: domain specific alterations in ACE-1, reduction in IRAP enzyme activity and lower neurolysin activity in AD in relation to increased Ang-II and Ang-III. In contrast, I did not detect any change in angiotensin level (Ang-IV and Ang (1-7)) and failed to detect any change in the expression of MasR and IRAP protein level in AD. Preservation of brain proteins is an important factor that could affect the stability of the endogenous protein level (546, 623). Both Ang (1-7) and Ang-IV for example ordinarily have a short half-life in serum/plasma that could be affected by long PMD in post-mortem brain tissue (528). Other peptides, such as Ang-II and another vasoconstrictor ET-1, are measurable and stable in post-mortem brain tissue (393, 569). Although I found no evidence that the measured proteins were altered by PMD and my tissue sample groups were matched in relation to PMD, it will be important to confirm the stability of selected angiotensin peptides in brain tissue by performing, as for other study, an experimental simulation of PMD on samples for up to 72 hours, at room temperature or 4°C. (354). Post-mortem stability may also account for the observation that MasR protein levels were unaltered in AD although this would need to be confirmed in larger independent studies using more than one experimental approach.

Another limitation of these studies in general is that characterisation of the RAS markers were restricted to one brain area (mid-frontal cortex). Investigating other brain regions that are affected in AD, such as the temporal cortex and hippocampus, will be interesting especially since studies in rodents have indicated that expression of rRAS, for instance, are highly enriched within the

hippocampus (246). Again, a general limitation throughout is the reliance on RAS marker measurements that were limited to one methodological approach such as ELISA only. It will be important to explore the expression and distribution of these proteins by other methods such as RT-PCR, RNAscope and immunohistochemical studies and to validate our original findings in larger independent cohorts. Another limitation in this study, which could have affected the evaluation of the relationship between brain RAS markers and AD pathological hallmarks, and that of ischaemic and hypoperfusion markers, was the small sample size used, which was determined partly by the numbers of tissue samples with previously collected data on VEGF and MAG:PLP1.

8.5 Future work

My novel findings of divergent catalytic activity of ACE-1 C-domain and N-domain in AD warrant further experimental investigation to explain the underlying mechanisms of this imbalance in AD.
Some related research questions on this could include the following:

i. What are the disease-related changes and mechanisms that alter domain-specific ACE-1 activity in AD?
ii. Are domain-specific changes related to post-translational modifications?
iii. Does disease-modified ACE-1 have a higher specificity for Ang-I than in controls?
iv. Is ACE-1 mediated Aβ cleavage impaired in AD in vivo?
v. Do certain ACEIs alter levels of ACE-mediated degradation of Aβ and thus pose as potential risk factors for AD?
vi. Are more selective C-domain targeting ACEIs a new therapeutic option for AD?

Other findings of note relate to reduced neurolysin levels that warrant further study. Questions arising include:

i. What is the combined effect of reduced neurolysin and ACE-2 on Ang-II and Ang-III levels, compared with ACE-1 activity?
ii. Are there any licensed pharmacological compounds that might activate neurolysin, which might have a net detrimental effect in AD?

Other general questions worth exploring include further study on other RAS metabolites, currently not studied, which could influence the activity of rRAS pathways. These include Ang (1-9) and

Angiotensin (3-7). Ang (1-9) is a pre-cursor in the production of Ang (1-7) and might be implicated in the rRAS pathway in AD. Angiotensin 3-7 also has a high affinity for IRAP and has been implicated in learning and memory.

Similarly, further investigations would be beneficial into the expression of less well known RAS receptors, such as MrgD and its agonist (Alamandine), AT_4R/ HGF/c-MET subtype receptor in human post-mortem brain tissue. These are necessary and will provide new data to broaden our understanding of the role of these rRAS components in AD pathogenesis. Further expanded investigations of IRAP activity would also be worthwhile as well as exploring the impact of AD-associated IRAP changes on glucose metabolism considering the normal intimate relationship between IRAP and GLUT4 trafficking (497).

I also undertook some initial pilot studies of the possible use of SH-SY5Y cells as a tool to allow more experimental investigations of the RAS, particularly allowing investigation of the effects of ischaemia and potentially other exposures (e.g. Aβ) on numerous RAS components that could also allow subsequent testing or screening of potential pharmacological interventions. Similarly, the scope to explore the effects of ischaemia will allow the important study of the role of RAS in VaD, which could then be further validated in human tissue and subsequent *in vivo* studies.

8.6 Final conclusions

In this thesis, I have uncovered novel domain-specific changes in ACE-1 in AD that could account for the discrepant findings within the AD field in relation to more widely studied ACEIs and has the potential to pave the way to discovering ACEIs that might exacerbate AD pathology and also the identification of domain-specific ACE-1 inhibitors for AD treatment i.e. inhibit Ang-II production whilst allowing unhindered Aβ degradation. I have also been the first to explore and report a reduction in the non-AT_1R and non-AT_2R binding protein (neurolysin) in relation to Aβ, tau and ischaemia in AD that has a regulating role in both the cRAS and rRAS pathways but which now requires further study in AD. I also report changes of some components within the rRAS pathways (e.g. Ang-II:Ang (1-7) ratio and IRAP activity) that have recently been shown to be dysregulated in relation to AD pathogenesis (Figure 8.1) and some RAS changes (IRAP and Ang-IV level) that are associated with ischaemic markers. More detailed studies may indicate whether the newly identified brain RAS

components in the rRAS pathways contribute to AD and are associated with vascular dysfunction that could offer new therapeutic targets in AD.

I propose a summary of the role of changes to RAS in AD that I have identified in this thesis and present in the following schematic (Figure 8.1). With these newly found changes in mind I also provide a further summary update of reported changes in RAS to-date that incorporate my new findings and that clearly show the extent to which RAS changes continue to be found in relation to AD (Figure 8.2).

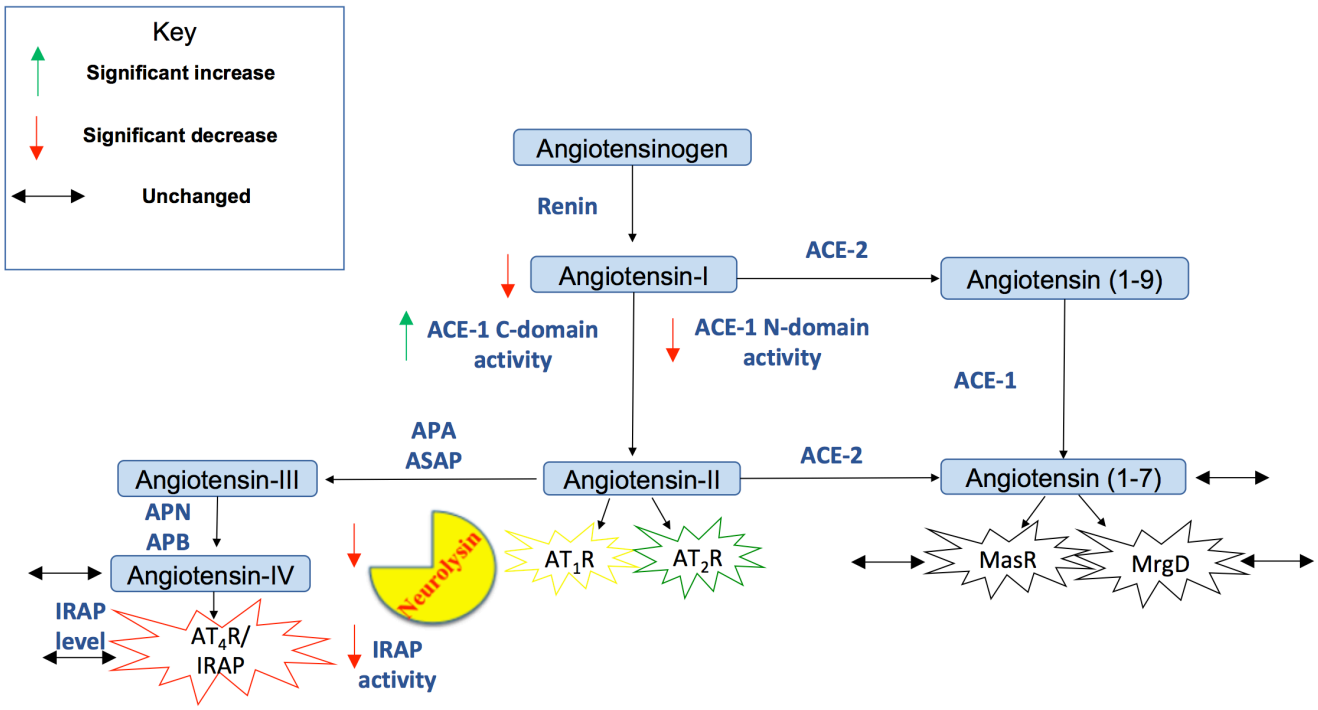

Figure 8.1 Levels and activities of RAS components in the AD brain compared to controls identified in this thesis.

Up pointed green arrow indicates a significant increase of the RAS component in AD compared to age-matched controls in the mid-frontal cortex. Down pointed red arrows indicates a significant decrease in either protein level or activity. Horizontal black arrows indicate unchanged of the protein level in AD compared to controls.
ACE-1 - Angiotensin converting enzyme 1, ACE-2 - Angiotensin converting enzyme 2, APA - Aminopeptidase A, APN - Aminopeptidase N, APB - Aminopeptidase B, ASAP - Aspartyl aminopeptidase, IRAP - Insulin-regulated aminopeptidase.

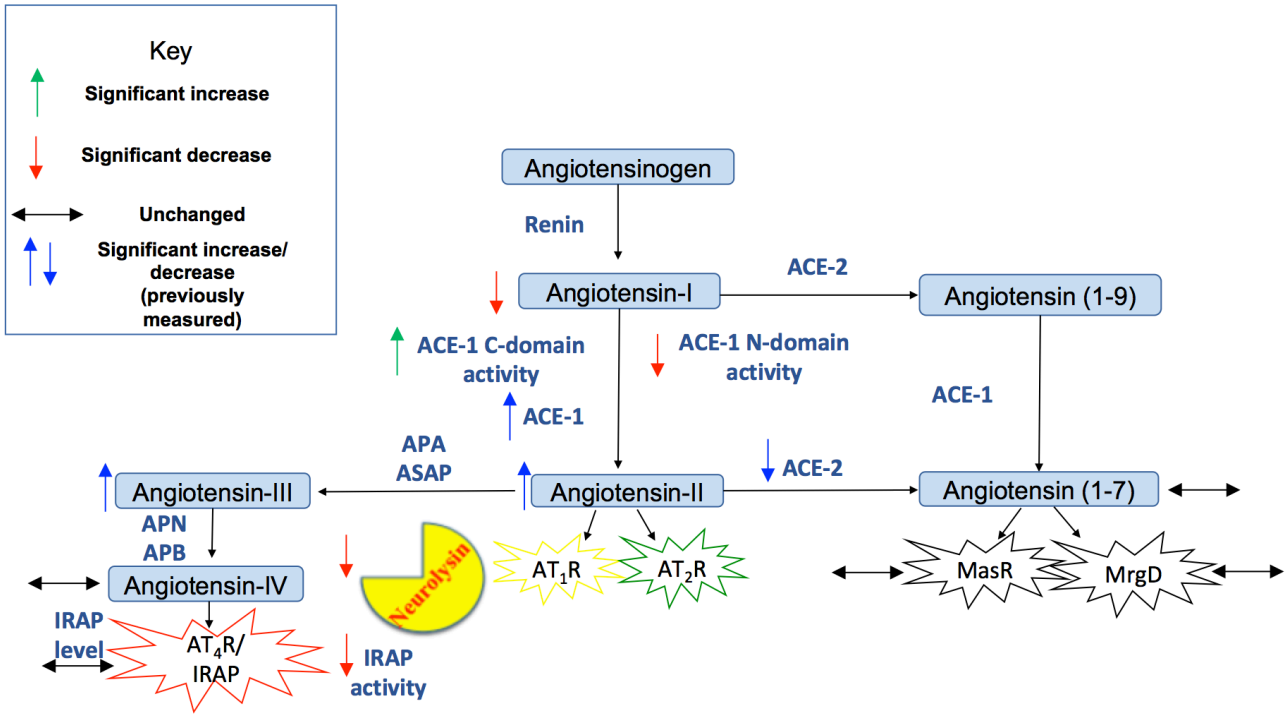

Figure 8.2 Summary update of reported changes in RAS components in the AD brain compared to controls.

Up pointed green arrow indicates significant increase of the RAS component in AD compared to age-matched controls in the mid-frontal cortex. Down pointed red arrows indicated significant decrease in either protein level or activity. Horizontal black arrows indicate unchanged of the protein level in AD compared to controls identified in this thesis. Up pointed and down pointed blue arrows indicated significant increase or decrease of other brain RAS components in AD identified previously (Miners et al., 2008; Kehoe et al., 2016; Kehoe et al., 2017).
ACE-1 - Angiotensin converting enzyme 1, ACE-2 - Angiotensin converting enzyme 2, APA - Aminopeptidase A, APN - Aminopeptidase N, APB - Aminopeptidase B, ASAP - Aspartyl aminopeptidase, IRAP - Insulin-regulated aminopeptidase.

Chapter 9. Appendices

9.1 Appendix I: Study cohorts

9.1.1 Control cohort

Table 9.1 Demographic and neuropathological characteristics for the control cohort cases used in this study

Brain Bank No.	Age-at-death (Years)	Gender	PMD (hours)	Braak stage	ACE genotype	APOE genotype
1	62	M	4	0	ID	3.4
16	95	F	46	II	ID	2.3
36	78	F	24	II	ID	
48	83	M	80	III	ID	3.3
50	71	M	25	I	DD	3.3
57	82	F	35	III	II	
66	64	M	12	II	ID	3.4
69	64	M	16	0	DD	3.3
72	72	M	42	I	ID	3.3
73	80	M	106	II	DD	3.3
74	90	M	45	II	DD	2.3
75	83	M	86	II	ID	
79	81	F	103	II	DD	3.3
81	64	M	23	II	DD	3.3
84	77	M	55	I	ID	3.3
95	73	M	36	II	ID	3.3
98	88	F	62	II	II	3.3
103	76	F	106	II	ID	3.3
106	88	F	72	0	DD	3.3
110	93	F	18	II	ID	3.3
112	80	F	92	0	DD	3.3
120	88	F	28	II	DD	3.3
122	82	M	30	II	II	3.3
127	84	M	48	III	II	3.3
128	90	M	48	II	DD	3.3
130	75	M	48	II	ID	3.3
141	89	F	15	I	ID	3.3
147	73	M	33	II	ID	2.3
150	69	M	66	II	DD	3.3
206	73	F	59	III	DD	3.3
254	90	M	40	II	DD	3.3
259	89	M	91	II	DD	3.4
269	83	F	24	II	ID	3.3
295	82	M	3	II	DD	3.3

328	43	F	12	.	DD	
333	84	F	17	I	ID	2.3
336	82	F	37	II	ID	4.4
338	53	M	7	III	ID	3.3
355	78	M	48	I	II	3.3
390	82	M	56	II	II	3.3
402	76	M	23	II	ID	3.3
412	82	F	96	III	ID	3.4
461	77	M	10	III	DD	2.3
467	75	M	6	III	.	
597	93	F	53	III	ID	2.4
678	84	F	216	II	DD	3.4
714	73	M	35	III	DD	3.3
733	93	M	38	III	DD	2.3
Mean SD	78.9 10.5		47.5 38			

9.1.2 AD cohort

Table 9.2 Demographic and neuropathological characteristics for the AD cohort cases used in this study

Brain Bank No.	Age-at-death (Years)	Gender	PMD (hours)	Braak stage	ACE genotype	APOE genotype
190	89	F	71	V	ID	3.3
196	78	F	77	VI	DD	4.4
205	78	F	9	V	ID	3.4
212	81	F	80	III	ID	3.4
213	81	F	42	VI	ID	3.4
219	77	F	43	IV	ID	3.4
223	71	F	67	V	ID	4.4
224	96	F	53	IV	ID	2.3
228	87	F	72	V	ID	3.4
241	87	F	67	V	II	2.4
242	79	F	70	III	ID	3.3
243	88	F	79	VI	DD	3.3
263	91	F	70	V	DD	2.4
278	78	F	35	VI	ID	3.3
284	82	F	24	VI	DD	3.4
287	85	M	58	IV	DD	3.4
289	91	M	43	III	ID	3.3
290	89	F	82	V	DD	3.3
302	70	F	25	VI	ID	3.4
326	69	M	48	V	DD	4.4
330	74	M	50	V	DD	3.4
341	95	M	48	III	ID	3.3
370	74	F	12	VI	ID	3.4

378	89	F	4	VI	ID	3.4
400	79	M	28	VI	ID	3.4
405	85	M	66	VI	DD	3.4
424	90	F	21	IV	ID	4.4
426	57	F	24	V	ID	3.4
435	54	F	24	VI	II	3.3
451	84	F	20	V	ID	3.4
470	79	F	72	V	DD	
488	74	F	53	V	II	4.4
495	80	M	49	V	DD	3.4
498	83	F	5	V	II	3.3
499	74	F	35	V	ID	3.3
508	80	M	5	V	II	3.4
512	77	F	26	VI	DD	3.4
538	63	M	43	VI	ID	3.3
541	60	F	68	VI	II	3.3
558	64	M	9	VI	ID	3.4
561	74	M	24	V	ID	3.4
562	85	F	49	V	II	3.4
567	68	F	87	VI	II	3.4
568	78	F	21	VI	ID	4.4
572	79	M	84	V	ID	3.4
573	89	F	39	V	DD	4.4
577	77	F	14	VI	ID	3.4
579	84	M	64	V	ID	3.4
580	65	M	90	VI	II	3.3
584	85	F	85	VI	II	3.4
586	80	F	71	VI	II	3.3
592	65	F	22	VI	II	3.3
601	68	M	61	VI	II	3.3
665	88	F	75	V	ID	3.4
670	83	F	85	VI	ID	4.4
681	47	F	54	VI	ID	
683	83	M	48	V	DD	3.3
685	74	M	48	V	ID	2.3
687	60	F	5	VI		
691	83	M	99	IV	DD	3.4
697	87	M	36	VI	DD	4.4
713	62	M	25	VI	II	3.4
715	78	M	50	VI	II	3.4
717	85	M	50	VI	DD	3.3
718	98	M	21	V	II	3.4
725	69	M	12	V	ID	3.4
726	61	M	38	V	DD	3.4
731	88	F	88	V	ID	3.3
737	67	F	24	VI	ID	4.4
745	84	F	21	VI		3.3
Mean	77.9		46.7			

SD	10.5		25.7			

9.1.3 Fixed-tissue control cases

Table 9.3 Demographic and neuropathological characteristics of fixed control brain samples used in immunohistochemistry study

Brain Bank No.	Age-at-death (Years)	Gender	PMD (hours)	Braak stage
48	83	M	80	III
50	71	M	25	I
72	72	M	42	I
84	77	M	55	I
106	88	F	72	0
122	82	M	30	II
130	75	M	48	II
141	89	F	15	I
355	78	M	48	I
402	76	M	23	II
Mean SD	79.1 6.22		43.8 21.28	

9.1.4 Fixed-tissue AD cases

Table 9.4 Demographic and neuropathological characteristics of fixed AD brain samples used in immunohistochemistry study

Brain Bank No.	Age-at-death (Years)	Gender	PMD (hours)	Braak stage
205	78	F	9	V
213	81	F	42	VI
223	71	F	67	V
426	57	F	24	V
451	84	F	20	V
584	85	F	85	VI
601	68	M	61	VI
Mean SD	74.86 10.12		44 28	

9.1.5 Fixed-tissue VaD cases

Table 9.5 Demographic and neuropathological characteristics of fixed VaD brain samples used in immunohistochemistry study

Brain Bank No.	Age-at-death (Years)	Gender	PMD (hours)	Braak stage
27	81	M	66	0
32	84	F	20	II
78	80	F	70	II
170	90	F	31	I
324	84	M	30	II
347	76	M	40	III
604	89	F	22	I
Mean SD	83.42 4.96		39.86 20.33	

9.1.6 AD cases and controls used for MasR and IRAP western blotting

Table 9.6 Demographic characteristics and total protein level of samples used in MasR and IRAP western blotting

Brain Bank No.	Age-at-death (Years)	Gender	PMD (hours)	Total protein level (mg/ml)
48	83	M	80	5.03
50	71	M	25	4.19
72	72	M	42	3.24
79	81	F	103	4.66
223	71	F	67	8.4
212	81	F	80	5.65
196	78	F	77	3.09
190	89	F	71	4.64

9.1.7 AD cases and controls used for MrgD and neurolysin western blotting

Table 9.7 Demographic characteristics and total protein level of samples used in MrgD and neurolysin western blotting

Brain Bank No.	Age-at-death (Years)	Gender	PMD (hours)	Total protein level (mg/ml)
336	82	F	37	2.61
106	88	F	72	6.82
333	84	F	17	3.47
120	88	F	28	5.38
219	77	F	43	3.72
426	57	F	24	3.83
243	88	F	79	2.72
242	79	F	70	5.39

9.1.8 Control cohort used in chapter 6

Table 9.8 Demographic and neuropathological characteristics of frozen control cohort cases used in this study (relationship between RAS components and marker of ischaemia and brain tissue oxygenation)

Brain Bank No.	Age-at-death (Years)	Gender	PMD (hours)	Braak stage	ACE genotype	APOE genotype
16	95	F	46	II	ID	2.3
50	71	M	25	I	DD	3.3
72	72	M	42	I	ID	3.3
74	90	M	45	II	DD	2.3
84	77	M	55	I	ID	3.3
98	88	F	62	II	II	3.3
141	89	F	15	I	ID	3.3
147	73	M	33	II	ID	2.3
150	69	M	66	II	DD	3.3
206	73	F	59	III	DD	3.3
269	83	F	24	II	ID	3.3
295	82	M	3	II	DD	3.3
336	82	F	37	II	ID	4.4
355	78	M	48	I	II	3.3
402	76	M	23	II	ID	3.3
714	73	M	35	III	DD	3.3
733	93	M	38	III	DD	2.3
Mean SD	80.23 8.28		37.42 17.91			

9.1.9 AD cohort used in chapter 6

Table 9.9 Demographic and neuropathological characteristics of frozen AD cohort cases used in this study (relationship between RAS components and marker of ischaemia and brain tissue oxygenation)

Brain Bank No.	Age-at-death (Years)	Gender	PMD (hours)	Braak stage	ACE genotype	APOE genotype
190	89	F	71	V	ID	3.3
205	78	F	9	V	ID	3.4
213	81	F	42	VI	ID	3.4
219	77	F	43	IV	ID	3.4
223	71	F	67	V	ID	4.4
224	96	F	53	IV	ID	2.3
228	87	F	72	V	ID	3.4
241	87	F	67	V	II	2.4
242	79	F	70	III	ID	3.3
278	78	F	35	VI	ID	3.3
289	91	M	43	III	ID	3.3
341	95	M	48	III	ID	3.3
370	74	F	12	VI	ID	3.4
400	79	M	28	VI	ID	3.4
405	85	M	66	VI	DD	3.4
451	84	F	20	V	ID	3.4
488	74	F	53	V	II	4.4
498	83	F	5	V	II	3.3
508	80	M	5	V	II	3.4
512	77	F	26	VI	DD	3.4
541	60	F	68	VI	II	3.3
577	77	F	14	VI	ID	3.4
579	84	M	64	V	ID	3.4
592	65	F	22	VI	II	3.3
601	68	M	61	VI	II	3.3
683	83	M	48	V	DD	3.3
685	74	M	48	V	ID	2.3
687	60	F	5	VI		
697	87	M	36	VI	DD	4.4
713	62	M	25	VI	II	3.4
715	78	M	50	VI	II	3.4
725	69	M	12	V	ID	3.4
726	61	M	38	V	DD	3.4
737	67	F	24	VI	ID	4.4
745	84	F	21	VI		3.3
Mean SD	77.83 9.59		40.43 21.11			

9.2 Appendix II: Materials and methods

9.2.1 Materials

9.2.1.1 Commercial supplies of equipment

Table 9.10 Details of laboratory equipment used in this study

Commercial suppliers of equipment	
Equipment	**Suppliers**
Balance	European Instruments
ChemiDoc XRS+	Bio-Rad Laboratories
Bench top centrifuge	MSE Scientific Instruments
Class II laminar flow hood	Holten
CO_2 incubator (maintained at 37°C and 5% CO_2)	Thermo Electron Corp.
Confocal microscope	Nikon
FLUOstar OPTIMA microplate reader	BMG Labtech
Fume hood	Surgipath Europe
Gilson Pipettes	Gilson
Magnetic stirrer and stir bars	VWR Jencons
Mini Trans-Blot®, electrophoretic transfer cell	Bio-Rad Laboratories
Mini-PROTEAN® 3, electrophoresis module	Bio-Rad Laboratories
Oven (37°C)	LTE Scientific
Oven (60°C)	Philip Harris
pH meter	Hanna Instruments
Plate Incubator/Shaker	Thermo Scientific
Plate shaker	Janke & Kunkel Gmbh
Precellys 24 automated homogeniser	Stretton Scientific
Refrigerated centrifuge	Eppendorf
Sledge Microtome	LEICA Biosystems
Water still	Bibby Scientific Ltd.

9.2.1.2 Commercial consumables

Table 9.11 Details of consumable suppliers used in this study

Commercial suppliers of consumables	
Consumables	**Suppliers**
3-amin-propyl-triethoxy-saline (APES)	Sigma-Aldrich
Accutase	Sigma-Aldrich
Acetonitrile	Fisher Scientific
Aprotinin	Sigma-Aldrich
B-mercaptoethanol	Sigma-Aldrich
Blotting paper	Fisher Scientific
Bovine serum albumin (BSA)	Fisher Scientific
Bromophenol blue	Sigma-Aldrich
Captopril	Biomol
Cell Lytic™ M reagent	Sigma-Aldrich
Clearene	Surgipath
Clear 96 well plates	R&D Systems
Colorometric substrate L-Leucine-p-nitroanilide (L-Leu-pNA)	Sigma-Aldrich
Cover slips	Surgipath
Decon detergent	Decon Laboratories Inc
Diaminobenzidine (DAB) substrate Kit	Vector Laboratories
Dimethyl Sulfoxide (DMSO)	Sigma-Aldrich
Dulbecco's modified Eagle medium (DMEM)	Sigma-Aldrich
ECL (Enhanced chemiluminescence) western blotting detection reagents	Millipore
Eppendorf tubes (0.5 ml, 1.5 ml, 2 ml)	Greiner Bio-One
Ethylenediamine tetraacetic acid (EDTA)	Sigma-Aldrich
Flasks, cell culture with filter cap (75 cm^2)	Greiner Bio-One
Fluorogenic substrate (Abz-LFK(DnP)-OH Trifluroacetate)	Sigma-Aldrich
Fluorogenic substrate (Abz-SDK(DnP)-P	Enzo Life Sciences
Foetal bovine serum (FBS)	Sigma-Aldrich
Glycerol	Sigma-Aldrich
Glycine	Fisher Scientific
Haemotoxylin (Gill II)	Surgipath
Horse serum (blocking serum)	Vector Laboratories
HRP-conjugated streptavidin (Strep-HRP)	R&D Systems
Hydrogen peroxide (H_2O_2)	Fisher Scientific
L-Glutamine	Sigma-Aldrich
Marvel™ skimmed milk powder	Premier Foods
Methanol	Fisher Scientific
Microplates: 96-well, black, Nunc® Maxisorp™	Fisher Scientific
Microscope slides (3" x 1.5")	Cell Path

Mini-PROTEAN® TGX ™ 4-20% pre-cast gels	Bio-Rad Laboratories
Nitrocellulose transfer membrane (0.45 µm)	Fisher Scientific
Pasteur Pipettes, plastic (3 ml)	Greiner Bio-One
PAP pen	Vector Laboratories
Phenylmethylsulphonyl fluoride (PMSF)	Sigma-Aldrich
Phosphate buffered saline (PBS)	Fisher Scientific
Pipettes, glass, single wrap (1ml, 5ml, 10 ml, 25ml, 50 ml)	Greiner Bio-One
Pipette tips (10µl, 200µl, 1000µl)	Greiner Bio-One
Plate sealers	R&D Systems
Precision Plus Protein™ WesternC™ standards	Bio-Rad Laboratories
Protease inhibitor cocktail	Sigma-Aldrich
Sodium Chloride (NaCl)	Fisher Scientific
Sodium dihydrogen orthophosphate 1-hydrate	Fisher Scientific
Sodium dodecyl sulphate (SDS)	Sigma-Aldrich
Sodium hydrogen orthophosphate 12-hydrate	Fisher Scientific
Substrate Reagent (A/B)	R&D Systems
Sulfuric Acid (stop Solution)	Sigma-Aldrich
Tris-HCl	Sigma-Aldrich
Triton X-100	Fisher Scientific
Trypsin-EDTA	Sigma-Aldrich
Tween®-20 (polysorbate-20)	Sigma-Aldrich
VECTASTAIN® ABC kit	Vector Laboratories
Zinc Chloride	Sigma-Aldrich
Zirconia/Silica (ceramic) beads (2.3 mm diameter)	Stratech Scientific

9.2.1.3 Constituents of commonly used solutions

Table 9.12 Constituents of regularly used solutions

Solutions	Constituents	Method
1% Bovine serum albumen (BSA)	1% BSA in PBS	ELISA
10x Blotting buffer	0.25 M Tris base, 1.92 M Glycine, 1L distilled water (dH_2O)	Western blot
1x Blotting buffer	200 ml Methanol, 100 ml 10x Blotting buffer, 700 ml dH2O	Western blot
10x Running buffer	0.25 M Tris base, 1.92 M Glycine 1% (w/v) SDS, dH_2O	Western blot
1x Running buffer	50ml 10x running buffer, 450 ml dH_2O	Western blot
1% SDS Lysis buffer	10 mM Tris base (pH 6.0) ,0.1	Brain tissue

	mM NaCl 1 µM PMSF 1 µg/ml Aprotinin	homogenisation
0.5% Triton X-100	20mM Tris (pH 7.4), 10% sucrose (w/v), 10 mM PMSF 1 µg/ml Aprotinin	Brain tissue homogenisation
Antibody buffer	5% Marvel in TBST	Western blot
Avidin-biotin complex (ABC)	Vectastain Universal Elite kit – 2 drops Reagent A, 2 drops Reagent B in 5 ml PBS.	IHC
Blocking serum	Vectastain Universal Elite kit – 1 drop horse serum in 5ml PBS	IHC
DAB	2 drops H_2O_2, 4 drops DAB solution, 2 drops buffer in 5 ml dH_2O	IHC
Citrate buffer	9 mM tri-sodium citrate, pH 6.0	IHC
Copper sulphate	0.16M Copper (II) sulphate 5-hydrate, 0.12M sodium chloride	IHC
EDTA	1 mM EDTA pH 8	IHC
N/C domain assay buffer	0.1 M Tris-HCL pH 7.0 , 0.05 M NaCl, 10 µM $ZnCl_2$	ACE-1 N/C domain activity assay
Phosphate buffered saline (PBS)	90 g sodium chloride, 126.8 g sodium dihydrogen orthophosphate 1-hydrate, 2.9 g sodium hydrogen orthophosphate 12-hydrate, 10 l dH_2O, pH 7.1	Various
SDS reducing buffer	0.5 M Tris-HCL (pH 6.8), 0.25% Glycerol, 10% (w/v) SDS 0.5% (w/v) Bromophenol blue	Western blot
Secondary biotinylated universal antibody	Vectastain Universal Elite kit – 2 drops horse serum and 2 drops secondary antibody in 5 ml PBS	IHC
Stop solution	2 N (1 M) Sulphuric acid	ELISA
Tris-buffered saline containing Tween®-20 (TBST)	10% 10x TBS, 0.05% Tween-20	Western blot
Tris-buffered saline 10x (TBS)	0.2 M Tris base, 5 M NaCl	Western blot
Tris assay buffer	0.05 M Tris, 0.14 M NaCl, pH 7.4	IRAP activity assay
Wash buffer	0.05% Tween 20 in PBS	Various

9.2.1.4 Primary antibodies

Summary of the primary antibodies used in this study are outlined in Table 9.13

Table 9.13 Summary of primary antibodies

Primary antibody	Clonality	Species raised in	Suppliers (Code)	Applications in this study
AGTR1 polyclonal antibody	Polyclonal	Rabbit	ThermoFischer Scientific (PA5-20812)	Western blotting
Anti-AGTR1 antibody	Polyclonal	Rabbit	Sigma-Aldrich (SAB3500209)	Western blotting
Anti-human ACE/CD143	Monoclonal	Mouse	R&D Systems (MAB9291)	Immunocapture activity assay
Anti-LNPEP antibody (aa 1-50) IHC-plus	Polyclonal	Rabbit	LifeSpan BioSciences (LS-B12918)	Western blotting Immunoperoxidase
Anti-MAS1 antibody	Polyclonal	Rabbit	Abcam (ab66030)	Western blotting Immunoperoxidase
AT1 receptor (extracellular) polyclonal antibody	Polyclonal	Rabbit	Enzo Life Sciences (BML-SA608)	Western blotting
AT1a non-selective receptor polyclonal antibody	Polyclonal	Rabbit	Kindly provided by Dr. Atticus Hainsworth, St George's, University of London	Western blotting
AT1a selective receptor polyclonal	Polyclonal	Rabbit	Kindly provided by Dr. Atticus Hainsworth, St	Western blotting

antibody			George's, University of London	
Biotin-Linked polyclonal antibody to Angiotensin I (AngI)	Polyclonal	Rabbit	Cloud-Clone Corp. (LAA811Hu71)	ELISA
Biotin-Linked polyclonal antibody to Angiotensin 1-7 (Ang1-7)	Polyclonal	Rabbit	Cloud-Clone Corp. (LAS085Hu71)	ELISA
MRGPRD antibody	Polyclonal	Rabbit	Novus Biologicals (NBP1-91964)	Western blotting
Neurolysin antibody (OTI1D6)	Monoclonal	Mouse	Novus Biologicals (NBP2-01693)	Western blotting Immunoperoxidase
Recombinant Anti-Angiotensin II Type 2 receptor antibody	Monoclonal	Rabbit	Abcam (ab92445)	Western blotting

9.2.1.5 Secondary antibodies

Table 9.14 Summary of secondary antibodies

Secondary antibody	Suppliers	Code
Anti-Rabbit IgG	Vector Laboratories	WB-1000
Anti-Mouse IgG	Vector Laboratories	WB-2000
Vectastain biotinylated universal secondary antibody	Vector Laboratories	PK-6200

9.2.1.6 Standard proteins

Table 9.15 Summary of standard proteins

Protein	Suppliers	Code
Angiotensin I (Ang-I)	Enzo Life Sciences	ALX-151-037-M005
Angiotensin 1-7 (Ang (1-7))	Enzo Life Sciences	ALX-151-041-M005
Amyloid beta 40 (Aβ 40)	rPeptide Anaspec Inc	A-1001-1 AS-24236
Amyloid beta 42 (Aβ 42)	rPeptide	A-1002-1
Recombinant human ACE-1 /CD143 somatic form	R&D Systems	929-ZN-010

9.2.1.7 Assay kits

Table 9.16 Commercial suppliers of assay kits used in this study

Assay Kits	Suppliers (Code)
DAB substrate Kit	Vector Laboratories (SK-4100)
Human Angiotensin II Receptor 2 (AGTR2) ELISA kit	Cloud-Clone Corp. (SEA973Hu)
Human Angiotensin 1-7 (ANG1-7) ELISA Kit	MyBioSource (MBS084052)
Human Angiotensin 4 (ANG4) ELISA Kit	MyBioSource (MBS028441)
Human Leucyl/Cystinyl aminopeptidase (LNPEP) ELISA Kit	Cloud-Clone Corp. (SEH723Hu)
Human Mas Proto-Oncogene (MAS1) ELISA Kit	MyBioSource (MBS9327239)
Human Mitochondrial Neurolysin (NLN) ELISA Kit	MyBioSource (MBS7207245)
Human Neurotensin (NT) ELISA Kit	CUSABIO (CSB-E09144h)
Human proteolipid protein 1 (PLP1) ELISA Kit	Cloud-Clone Corp. (SEA417Hu)
Human VEGF DuoSet ELISA kits	R&D systems

	(DY293B-05)
Total protein Kit	Sigma-Aldrich (TP0100)
Vectastain Elite ABC Kit	Vector Laboratories (PK-6200)

9.2.2 Optimisation steps of experiments from Chapter 3:

9.2.2.1 Optimisation steps of ACE-1 N-domain FRET activity assay

The optimal concentration of the N-domain selective substrate (Abz-SDK(Dnp)-p in human brain tissue homogenates was determined by testing different dilution ranges (10-0.625 µM). Optimal conditions identified from these preliminary experiments were substrate concentration at (10 µM) (Figure 9.1).

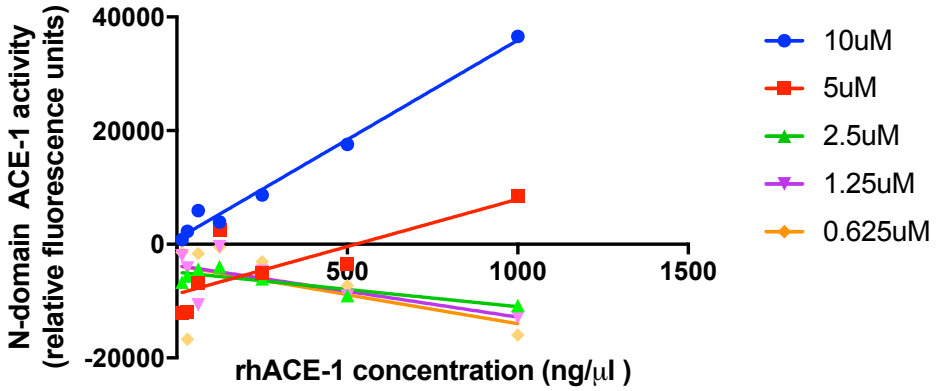

Figure 9.1. Test of Different dilutions of N-domain specific fluorogenic substrate Abz-SDK(Dnp)-P (Enzo Life Sciences).
Standard curves of recombinant human ACE-1 activity as measured using a range of concentrations of FRET substrate (Abz-SDK(Dnp)-P).

The effect of incubation time on the reaction was characterised (Figure 9.2 A). A range of captopril concentrations was also tested to determine the dose-related changes to the inhibition of substrate cleavage (Figure 9.2 B).

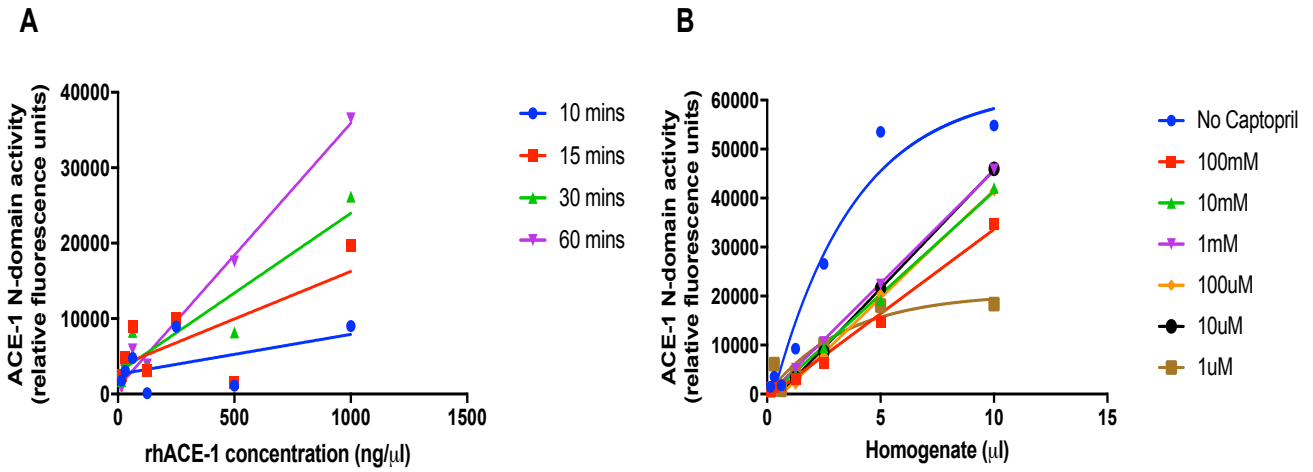

Figure 9.2. Standard curves of recombinant human ACE-1 activity as measured using a rang of FRET (Abz-SDK(Dnp)-P) substrate Measurements are based on substrate cleavage after incubation for 1 hour at 37°C. A. Effect of time on reaction. **B.** Captopril inhibition of fluorogenic peptide (**Abz-SDK(Dnp)-P**) substrate cleavage.

9.2.2.2 Optimisation of ACE-1 C-domain FRET activity assay

As for the N-domain assay, the concentration of C-domain selective substrate (Abz (LFK(DnP)-OH Trifluroacetate) in human brain tissue homogenates was characterised. The resultant optimal conditions that were found included using a substrate concentration at (10 μM) (Figure 9.3).

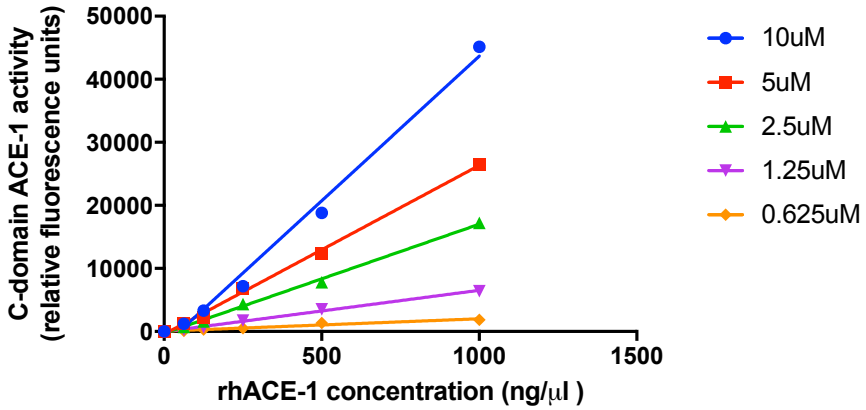

Figure 9.3. Test of Different dilutions of C-domain specific fluorogenic substrate (Abz-LFK(Dnp)-OH Trifluroacetate) (Sigma-Aldrich).
Standard curves of recombinant human ACE-1 activity as measured using a rang of FRET (Abz(LFK(DnP)-OH Trifluroacetate) substrate Measurements are based on substrate cleavage after incubation for 1 hour at 37°C.

The optimal concentration of inhibitor and the effect of time on substrate cleavage were characterised (Figure 9.4 A and B).

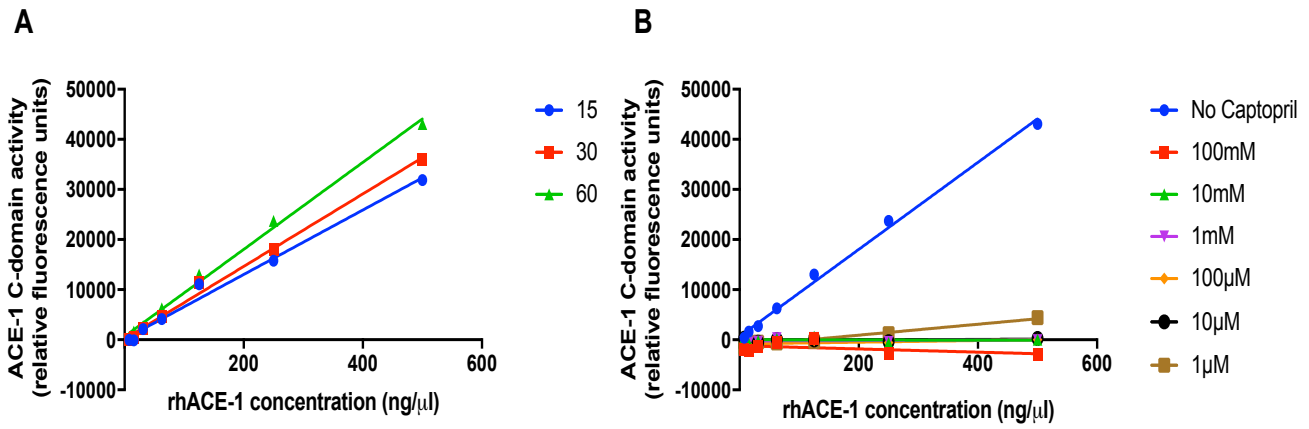

Figure 9.4. Standard curves of recombinant human ACE-1 activity as measured using a rang of FRET (Abz(LFK(DnP)-OH Trifluroacetate) substrate Measurements are based on substrate cleavage after incubation for 1 hour at 37°C. A. Effect of time on reaction. **B.** Captopril inhibition of fluorogenic peptide (Abz(LFK(DnP)-OH Trifluroacetate) substrate cleavage.

9.2.2.3 Optimisation of ACE-1 N-domain immunocapture-based activity assay

The effect of time on reaction and the inhibitor concentration were determined in optimising the immunocapture-based FRET activity assay. The reaction was measured after 1 hour, 20 and 24 hours (Figure 9.5 A). The effect of inhibitor at 10 µM was determined (Figure 9.5 B).

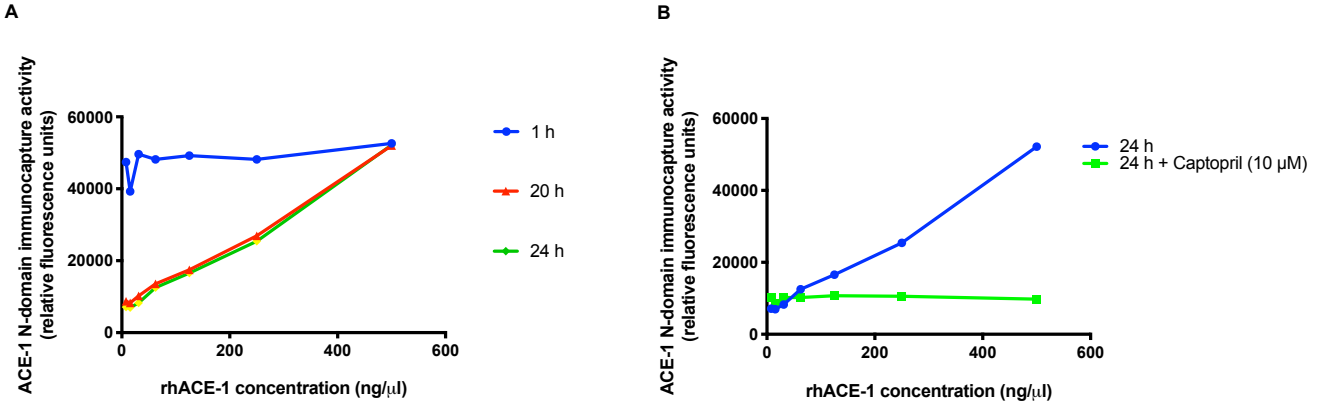

Figure 9.5. Standard curves of recombinant human ACE-1 activity as measured using of FRET substrate (Abz-SDK(Dnp)-P) at concentration (0.68 mM)**. Measurements are based on substrate cleavage after incubation for 1 hour, 20 and 24 hours at 37°C. A**. Effect of time on reaction. **B**. Captopril inhibition of (Abz-SDK(Dnp)-P) fluorogenic peptide substrate cleavage.

9.2.2.4 Optimisation of ACE-1 C-domain immunocapture-based activity assay

The effect of 2 and 24 hours incubation on the reaction of C-domain selective substrate (Abz(LFK(DnP)-OH Trifluroacetate) cleavage was measured. The inhibitor effect on the reaction at concentration (10 µM) was determined (Figure 9.6 A and B).

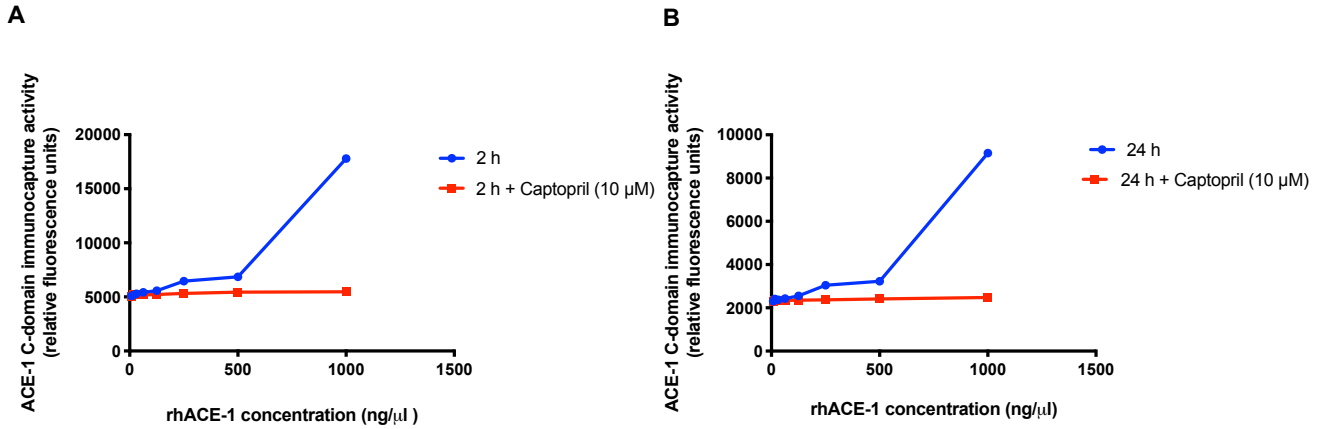

Figure 9.6. Standard curves of recombinant human ACE-1 activity as measured using of FRET substrate (Abz(LFK(DnP)-OH Trifluroacetate) at concentration (0.14 mM**). Measurements are based on substrate cleavage after incubation for 2 hours and 24 hours at 37°C. A**. Effect of 2 hours incubation on reaction and Captopril inhibition of (Abz-SDK(Dnp)-P) fluorogenic peptide substrate cleavage. **B**. Effect of 24 hours incubation on reaction and Captopril inhibition of (Abz-SDK(Dnp)-P) fluorogenic peptide substrate cleavage.

9.2.3 Optimisation steps of experiments from Chapter 5:

9.2.3.1 Optimisation steps of IRAP sandwich ELISA

Preliminary experiments were first performed to optimise the homogenate concentration to use for the IRAP sandwich ELISA. First, I tested different dilutions of homogenate (2-fold serial dilution of 1:10) (Table 9.17). Then I compared two dilutions 1:10 and 1:20 by measuring two samples of control and two AD cases. There was no difference in the concentration of IRAP level measured in homogenate diluted 1:10 and 1:20 (Table 9.18).

Table 9.17 Results from first optimisation step of IRAP sandwich ELISA

IRAP sandwich ELISA				
Homogenate dilution 2-fold serial dilution of 1:10	**Reading 1**	**Reading 2**	**Average Absorbance (O.D)**	**Concentration (ng/ml)**
1	0.488	0.414	0.451	1.299
2	0.465	0.397	0.431	1.102
3	0.419	0.342	0.3805	0.603
4	0.405	0.339	0.372	0.519
5	0.426	0.374	0.4	0.796
6	0.486	0.386	0.436	1.15
7	0.438	0.376	0.407	0.865
8	0.389	0.318	0.3535	0.337

Table 9.18 Results from second optimisation step of IRAP sandwich ELISA

IRAP sandwich ELISA				
Homogenate dilution	**Reading 1**	**Reading 2**	**Average Absorbance (O.D)**	**Concentration (ng/ml)**
Control case (1:10)	0.808	0.789	0.7985	5.350
Control case (1:20)	0.673	0.678	0.6755	5.971
AD case (1:10)	0.792	0.823	0.8075	5.515
AD case (1:20)	0.641	0.705	0.673	5.871

An Example of Standard curve of recombinant human IRAP measured using the sandwich ELISA (Figure 9.7).

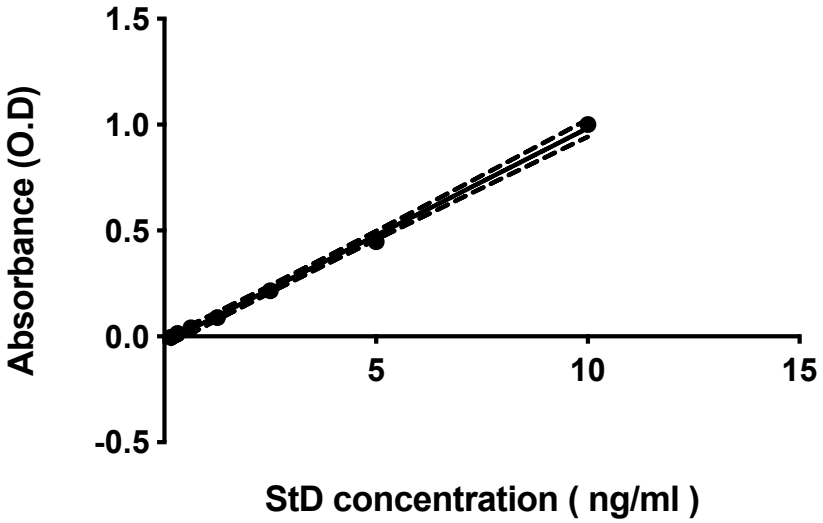

Figure 9.7. Standard (StD) curve of recombinant human IRAP as measured using (Human Leucyl/Cystinyl aminopeptidase (LNPEP) ELISA Kit) (Cloud-Clone Corp.)

9.2.3.2 Optimisation steps of IRAP activity assay

Preliminary experiments were performed to optimise the use of IRAP substrate L-Leucine-p-nitroanilide (L-Leu-pNA) (Sigma-Aldrich) in human brain tissue homogenates. The optimal concentration of the colorimetric substrate was first determined by testing 10-fold serial dilutions and 2-fold serial dilutions of the substrate on brain homogenates diluted 1:40 in assay buffer (Figure 9.8 A and B).

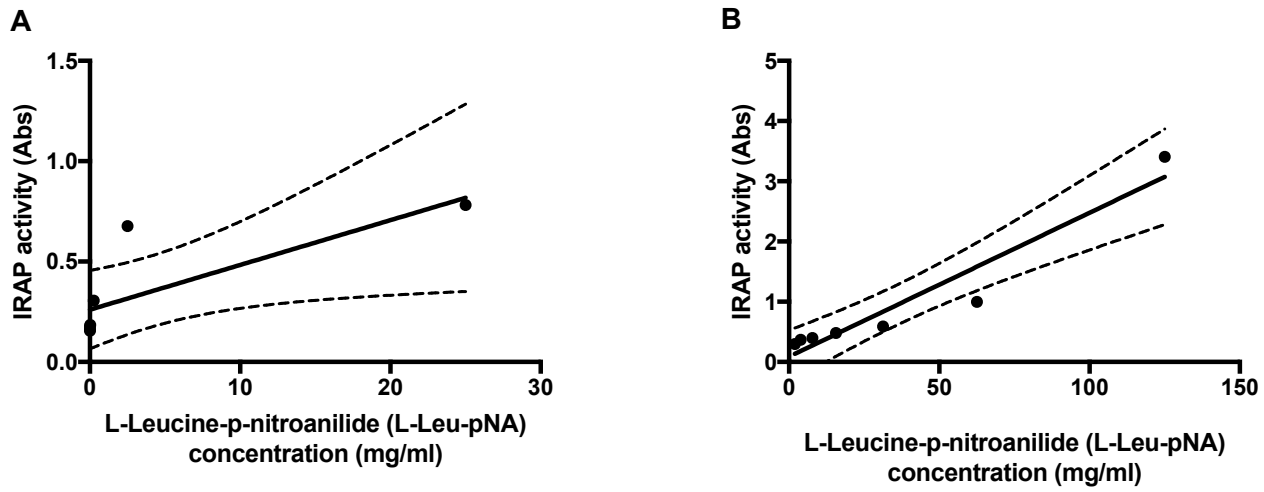

Figure 9.8. Test of different dilutions of colorimetric IRAP substrate L-Leucine-p-nitroanilide (L-Leu-pNA) (Sigma-Aldrich).
A. Standard curves of IRAP activity as measured using 10-fold serial dilutions of the substrate ranging from (25-0.000025 mg/ml). Measurements are based on substrate cleavage after incubation for 1 hour at 37°C. B. Standard curves of IRAP activity as measured using 2-fold serial dilutions of the substrate ranging from (125-1.95 mg/ml). Measurements are based on substrate cleavage after incubation for 1 hour at 37°C.

The effect of incubation length on the reaction (1 hour, 2 hours and overnight) was determined on two different homogenate dilutions (1:10 and 1:20) (Figure 9.9 A and B).

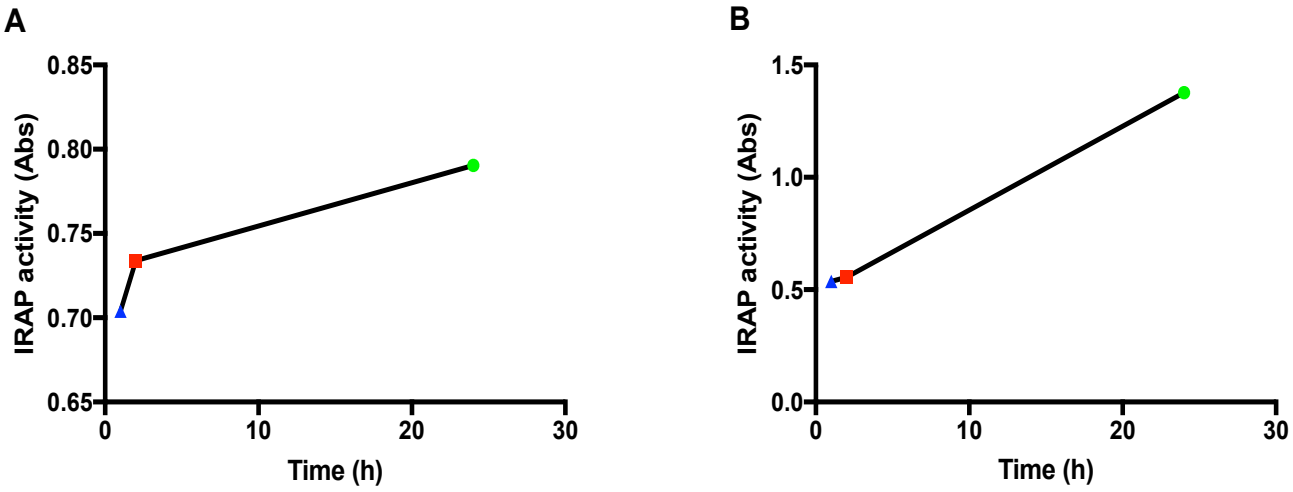

Figure 9.9. Testing the effect of time on colorimetric IRAP substrate L-Leucine-p-nitroanilide (L-Leu-pNA) (Sigma-Aldrich) cleavage.
A. The effect of time on reaction measured on homogenate diluted (1:10). B. The effect of time on reaction measured on homogenate diluted (1:20). Measurements are based on substrate cleavage after incubation for 1 hour (blue), 2 hours (red) and 24 h (green) at 4°C.

9.2.4 Optimisation steps of experiments from Chapter 7:

9.2.4.1 Optimisation steps of neurolysin competitive ELISA

The optimal concentration of brain homogenate was determined before using the neurolysin competitive ELISA. First, I tested different dilutions of homogenate (1:2, 1:4, 1:10 and 1:20) (Table 9.19). Homogenate diluted 1:10 was chosen for further studies.

Table 9.19 Results from optimisation steps of neurolysin competitive ELISA

Neurolysin competitive ELISA				
Homogenate dilution	**Reading 1**	**Reading 2**	**Average Absorbance – Blank (O.D)**	**Concentration (ng/ml)**
1:2	3.024	3.334	3.179	0.404
1:4	2.801	2.77	2.7855	0.613
1:10	2.828	2.76	2.794	0.608
1:20	2.851	2.915	2.883	0.558

An Example of Standard curve of recombinant human neurolysin measured using competitive ELISA (Figure 9.10).

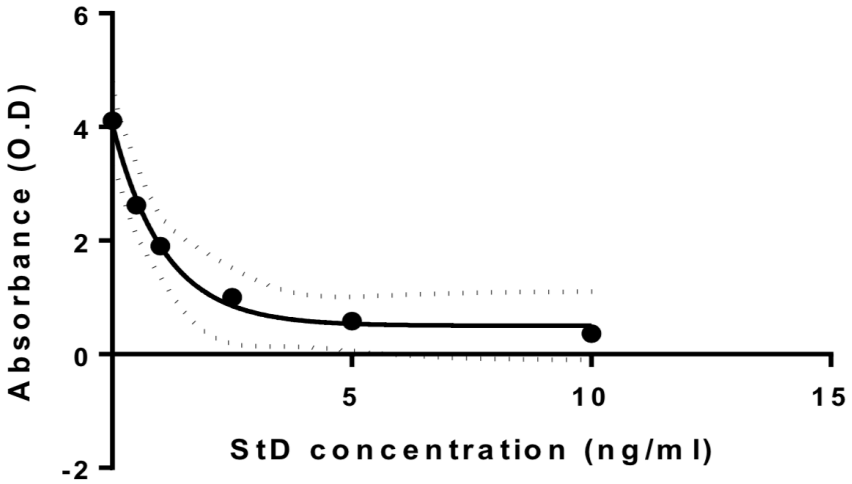

Figure 9.10. Standard (StD) curve of recombinant human neurolysin as measured using (NLN, competitive ELISA kit, MyBioSource).

9.2.4.2 Optimisation steps of neurotensin sandwich ELISA

Different homogenate dilutions (1:2, 1:4, 1:10 and 1:20) were initially tested and a 1:10 dilution fell within the linear range of the standard curve and was chosen for further experiments (Table 9.20).

Table 9.20 Results from optimisation steps of neurotensin sandwich ELISA

Neurotensin sandwich ELISA				
Homogenate dilution	**Reading 1**	**Reading 2**	**Average Absorbance - Blank (O.D)**	**Concentration (pg/ml)**
1:2	0.865	0.804	0.621	433.439
1:4	0.527	0.503	0.301	247.747
1:10	0.517	0.431	0.26	220.862
1:20	3.871	3.103	3.273	1390.358

An Example of Standard curve of recombinant human neurotensin measured using sandwich ELISA (Figure 9.11).

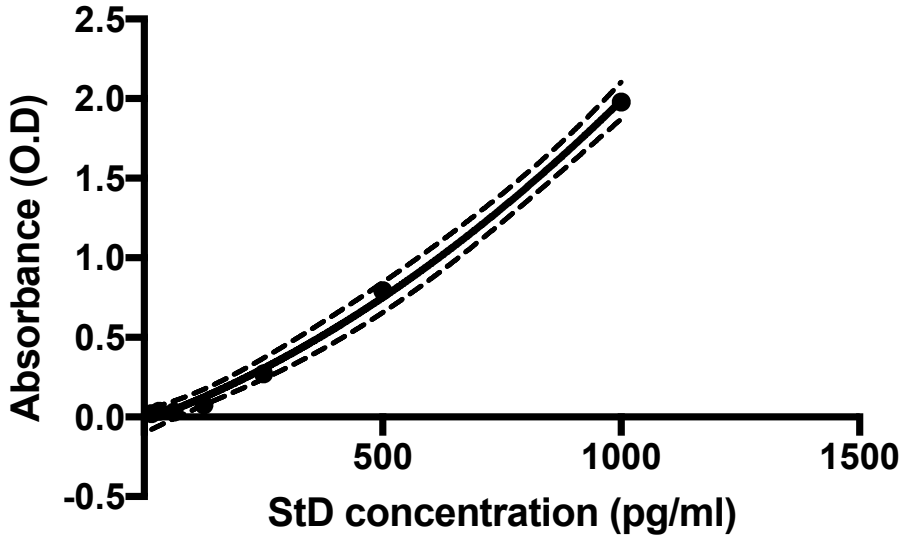

Figure 9.11. Standard (StD) curve of recombinant human neurotensin as measured using (Human Neurotensin (NT) ELISA kit, CUSABIO).

9.3 Appendix III: Shapiro-Wilk normality test

All datasets were analysed by Shapiro-Wilk test to determine the distribution of the data. P-value <0.05 were considered not normally distributed.

Table 9.21 Shapiro-Wilk normality tests

Data Sets	Shapiro-Wilk normality test	
	p-value	Normally distributed?
Chapter 3		
ACE-1 N-domain FRET activity	<0.0001	No
ACE-1 C-domain FRET activity	<0.0001	No
ACE-1 N-domain immunocapture-based activity	<0.0001	No
ACE-1 C-domain immunocapture-based activity	<0.0001	No
Total Ang-I level	0.001	No
Ang-I protein-adjusted level	<0.0001	No
Chapter 4		
Total Ang (1-7) level	0.405	Yes
Ang (1-7) protein-adjusted level	<0.0001	No
Total MasR level	<0.0001	No
MasR protein-adjusted level	<0.0001	No
Chapter 5		
Total Ang-IV level	<0.0001	No
Ang-IV protein-adjusted level	<0.0001	No
Total IRAP level	<0.0001	No
IRAP protein-adjusted level	<0.0001	No
IRAP activity	0.008	No
Chapter 6 (Ang (1-7), MasR, Ang-IV, IRAP) Small cohort (control, n= 17) and (AD, n= 35)		
Total Ang (1-7) level	0.733	Yes

Ang (1-7) protein-adjusted level	0.211	Yes
Total MasR level	<0.0001	No
MasR protein-adjusted level	<0.0001	No
Total Ang-IV level	<0.0001	No
Ang-IV protein-adjusted level	<0.0001	No
Total IRAP level	0.003	No
IRAP protein-adjusted level	0.003	No
IRAP activity	0.050	Yes
Chapter 7		
Total neurolysin level	0.0002	No
Neurolysin protein-adjusted level	<0.0001	No
Total neurotensin level	0.054	Yes
Neurotensin protein-adjusted level	<0.0001	No

9.4 Appendix IV: Intra-assay coefficient of variation (CV%) of measured proteins

9.4.1 Results and data analyses from chapter 3:

9.4.1.1 ACE-1 N-domain FRET activity data

Table 9.22 Intra-assay CV% of ACE-1 N-domain FRET activity assay from a 96 well plate. CV% was calculated using the following formula: CV%= (Standard deviation (SD)/Mean) *100

ACE-1 N-domain FRET activity					
Sample	**Reading 1**	**Reading 2**	**Mean**	**SD**	**CV%**
6	24682	24935	24808.5	178.89	0.72
16	22359	23013	22686	462.447	2.04
36	25371	25459	25415	62.22	0.24
48	5233	5290	5261.5	40.30	0.77
66	15513	15642	15577.5	91.22	0.58
74	18609	18473	18541	96.16	0.51
147	20578	20854	20716	195.16	0.94
190	21693	21957	21825	186.68	0.85
205	11922	12969	12445.5	740.34	5.95
213	20005	19909	19957	67.88	0.34
242	17964	17929	17946.5	24.75	0.14
269	15643	15609	15626	24.04	0.15
284	25089	24879	24984	148.49	0.59
321	17492	17216	17354	195.16	1.12
424	16496	17630	17063	801.86	4.69
426	10520	10661	10590.5	99.70	0.94
435	11012	10865	10938.5	103.94	0.95
451	15492	15097	15294.5	279.30	1.83
470	17403	17683	17543	197.99	1.13
721	16303	16391	16347	62.22	0.38
Mean					1.24

9.4.1.2 ACE-1 C-domain FRET activity data

Table 9.23 Intra-assay CV% of ACE-1 C-domain FRET activity assay from a 96 well plate. CV% was calculated using the following formula: CV%= (Standard deviation (SD)/Mean) *100

ACE-1 C-domain FRET activity					
Sample	**Reading 1**	**Reading 2**	**Mean**	**SD**	**CV%**
6	20400	22150	21275	1237.44	5.82
16	29147	28840	28993.5	217.08	0.75
36	22213	21336	21774.5	620.13	2.85

48	16189	16548	16368.5	253.85	1.55
66	11991	12530	12260.5	381.13	3.11
74	14211	16454	15332.5	1586.04	10.34
147	16699	19112	17905.5	1706.25	9.53
190	22477	24588	23532.5	1492.70	6.34
205	17419	22320	19869.5	3465.53	17.44
213	21000	23867	22433.5	2027.27	9.03
242	21214	23148	22181	1367.54	6.17
269	15501	16774	16137.5	900.15	5.58
284	29662	30589	30125.5	655.49	2.17
321	18368	22072	20220	2619.12	12.95
424	24008	23962	23985	32.53	0.13
426	15625	15721	15673	67.88	0.43
435	15919	10196	13057.5	4046.77	30.99
451	23565	25796	24680.5	1577.55	6.39
470	20673	23029	21851	1665.94	7.62
721	10914	11610	11262	492.15	4.37
Mean					7.18

9.4.1.3 ACE-1 N-domain immunocapture-based activity data

Table 9.24 Example of intra-assay CV% of ACE-1 N-domain immunocapture-based activity assay from a 96 well plate. CV% was calculated using the following formula: CV%= (Standard deviation (SD)/Mean) *100

ACE-1 N-domain immunocapture-based activity					
Sample	**Reading 1**	**Reading 2**	**Mean**	**SD**	**CV%**
66	14283	13947	14115	453.69	3.21
69	14073	14965	14519	889.28	6.12
461	14428	16109	15268.5	1991.88	13.04
467	16439	19232	17835.5	1828.50	10.25
597	15747	19212	17479.5	3729.61	21.33
678	24757	19158	21957.5	4893.26	22.28
219	14669	14269	14469	563.19	3.89
223	14646	15593	15119.5	635.64	4.20
601	14067	14952	14509.5	571.85	3.94
665	15828	16184	16006	1175.17	7.342
725	16329	18426	17377.5	877.881	5.051
670	17662	17191	17426.5	1854.36	10.64
681	20072	21026	20549	2099.05	10.21
683	24760	23073	23916.5	2148.93	8.98
592	19664	23206	21435	4392.19	20.49
687	14370	14137	14253.5	437.34	3.07
685	14216	15094	14655	514.82	3.51
691	14784	15427	15105.5	1628.46	10.78

697	13084	17020	15052	1638.86	10.89
713	15654	15558	15606	306.57	1.96
715	16200	16041	16120.5	1036.38	6.43
717	17651	18113	17882	939.88	5.26
718	15932	17126	16529	844.28	5.10
Mean					8.39

9.4.1.4 ACE-1 C-domain immunocapture-based activity data

Table 9.25 Example of intra-assay CV% of ACE-1 C-domain immunocapture-based activity assay from a 96 well plate. CV% was calculated using the following formula: CV%= (Standard deviation (SD)/Mean) *100

ACE-1 C-domain immunocapture-based activity					
Sample	**Reading 1**	**Reading 2**	**Mean**	**SD**	**CV%**
72	11568	12293	11930.5	512.65	4.29
73	12275	12123	12199	107.48	0.88
74	11843	12527	12185	483.66	3.97
75	11974	12821	12397.5	598.92	4.83
79	12900	13107	13003.5	146.37	1.12
81	12450	13097	12773.5	457.49	3.58
84	12769	13389	13079	438.41	3.35
95	12367	13396	12881.5	727.61	5.65
98	10563	10991	10777	302.64	2.81
103	12045	10898	11471.5	811.05	7.07
106	12498	12112	12305	272.94	2.22
110	12388	12244	12316	101.82	0.83
223	12914	12491	12702.5	299.11	2.35
224	12837	12714	12775.5	86.97	0.68
228	13598	13977	13787.5	267.99	1.94
241	12948	13620	13284	475.17	3.58
242	9964	9576	9770	274.36	2.81
243	10389	9691	10040	493.56	4.92
263	10510	10067	10288.5	313.25	3.04
278	11327	10819	11073	359.21	3.24
284	12098	12154	12126	39.59	0.33
287	12609	13276	12942.5	471.64	3.64
289	13184	12915	13049.5	190.21	1.46
290	13411	14039	13725	444.06	3.23
Mean					2.99

9.4.1.5 Ang-I level data

Table 9.26 Example of intra-assay CV% of absorbance values for Ang-I direct ELISA from a 96 well plate. CV% was calculated using the following formula: CV%= (Standard deviation (SD)/Mean) *100

Ang-I direct ELISA					
Sample	**Reading 1**	**Reading 2**	**Mean**	**SD**	**CV%**
1	0.292	0.298	0.295	0.004	1.44
16	0.326	0.321	0.3235	0.003	1.09
36	0.31	0.31	0.31	0	0
48	0.334	0.342	0.338	0.005	1.67
50	0.346	0.342	0.344	0.002	0.82
57	0.314	0.302	0.308	0.008	2.75
66	0.339	0.339	0.339	0	0
69	0.305	0.301	0.303	0.003	0.93
72	0.295	0.335	0.315	0.028	8.98
73	0.369	0.395	0.382	0.018	4.81
74	0.345	0.338	0.3415	0.005	1.45
75	0.311	0.308	0.3095	0.002	0.68
79	0.319	0.33	0.3245	0.008	2.39
81	0.349	0.345	0.347	0.002	0.81
95	0.275	0.315	0.295	0.028	9.59
98	0.317	0.303	0.31	0.009	3.19
106	0.31	0.339	0.3245	0.020	6.31
110	0.311	0.315	0.313	0.003	0.90
112	0.335	0.361	0.348	0.018	5.28
120	0.328	0.346	0.337	0.013	3.78
122	0.325	0.328	0.3265	0.002	0.65
127	0.297	0.348	0.3225	0.036	11.18
219	0.327	0.335	0.331	0.005	1.71
220	0.34	0.343	0.3415	0.002	0.62
223	0.33	0.338	0.334	0.006	1.69
224	0.347	0.329	0.338	0.013	3.77
228	0.349	0.356	0.3525	0.005	1.40
241	0.31	0.299	0.3045	0.008	2.55
242	0.34	0.347	0.3435	0.005	1.44
254	0.348	0.345	0.3465	0.002	0.61
256	0.323	0.325	0.324	0.001	0.43
257	0.296	0.292	0.294	0.003	0.96
259	0.307	0.336	0.3215	0.021	6.38
263	0.31	0.31	0.31	0	0
269	0.318	0.311	0.3145	0.005	1.57
277	0.277	0.288	0.2825	0.008	2.75
278	0.305	0.336	0.3205	0.022	6.84
284	0.315	0.346	0.3305	0.022	6.63
Mean					2.84

9.4.2 Results and data analyses from chapter 4:

9.4.2.1 Ang (1-7) direct ELISA data

Table 9.27 Intra-assay CV% of Ang (1-7) direct ELISA from a 96 well plate. CV% was calculated using the following formula: CV%= (Standard deviation (SD)/Mean) *100

Ang (1-7) direct ELISA					
Sample	**Reading 1**	**Reading 2**	**Mean**	**SD**	**CV%**
1	0.248	0.252	0.25	0.003	1.131
36	0.233	0.387	0.31	0.109	35.127
50	0.237	0.243	0.24	0.004	1.768
57	0.358	0.225	0.291	0.094	32.263
69	0.217	0.233	0.225	0.011	5.028
72	0.257	0.262	0.259	0.003	1.362
73	0.594	0.212	0.403	0.270	67.026
75	0.254	0.258	0.256	0.003	1.105
79	0.229	0.228	0.229	0.001	0.309
81	0.254	0.279	0.267	0.018	6.633
84	0.237	0.246	0.242	0.006	2.635
95	0.278	0.25	0.264	0.019	7.499
98	0.233	0.213	0.223	0.014	6.342
103	0.222	0.236	0.229	0.009	4.323
106	0.217	0.22	0.218	0.002	0.971
110	0.248	0.253	0.250	0.004	1.411
112	0.279	0.261	0.27	0.012	4.714
196	0.24	0.259	0.249	0.013	5.385
205	0.208	0.246	0.227	0.027	11.837
212	0.154	0.171	0.163	0.012	7.397
223	0.255	0.232	0.243	0.016	6.679
224	0.263	0.251	0.257	0.008	3.302
228	0.182	0.194	0.188	0.008	4.513
241	0.284	0.278	0.281	0.004	1.509
243	0.267	0.259	0.263	0.006	2.151
256	0.266	0.28	0.273	0.009	3.626
257	0.276	0.25	0.263	0.018	6.990
263	0.272	0.287	0.279	0.011	3.795
277	0.243	0.251	0.247	0.006	2.290
278	0.224	0.252	0.238	0.019	8.318
287	0.221	0.299	0.26	0.055	21.213
289	0.218	0.222	0.22	0.003	1.286
Mean					8.436

9.4.2.2 Ang (1-7) sandwich ELISA data

Table 9.28 Intra-assay CV% of Ang (1-7) sandwich ELISA from a 96 well plate. CV% was calculated using the following formula: CV%= (Standard deviation (SD)/Mean) *100

Ang (1-7) sandwich ELISA					
Sample	**Reading 1**	**Reading 2**	**Mean**	**SD**	**CV%**
66	0.391	0.369	0.38	0.015	4.094
69	0.361	0.389	0.375	0.019	5.279
72	0.317	0.306	0.311	0.008	2.497
73	0.273	0.273	0.273	0	0
74	0.411	0.388	0.399	0.016	4.071
75	0.375	0.361	0.368	0.009	2.691
79	0.348	0.333	0.340	0.011	3.115
81	0.389	0.401	0.395	0.008	2.148
84	0.319	0.334	0.326	0.011	3.248
95	0.397	0.419	0.408	0.015	3.813
98	0.301	0.309	0.305	0.005	1.855
103	0.399	0.428	0.413	0.020	4.959
106	0.425	0.458	0.441	0.023	5.285
110	0.369	0.392	0.380	0.016	4.274
120	0.386	0.394	0.39	0.006	1.450
122	0.415	0.472	0.443	0.040	9.088
127	0.433	0.448	0.440	0.011	2.408
128	0.583	0.602	0.592	0.013	2.267
130	0.388	0.449	0.418	0.043	10.307
190	0.382	0.426	0.404	0.031	7.701
196	0.443	0.434	0.438	0.006	1.451
205	0.41	0.476	0.443	0.047	10.535
212	0.325	0.344	0.334	0.013	4.016
213	0.347	0.361	0.354	0.009	2.796
219	0.415	0.393	0.404	0.015	3.850
223	0.398	0.388	0.393	0.007	1.799
224	0.39	0.358	0.374	0.022	6.050
228	0.349	0.39	0.369	0.029	7.846
241	0.462	0.45	0.456	0.008	1.861
243	0.38	0.446	0.413	0.047	11.300
263	0.358	0.374	0.366	0.011	3.091
278	0.361	0.566	0.463	0.145	31.274
284	0.518	0.829	0.673	0.219	32.651
287	0.455	0.677	0.566	0.157	27.734
290	0.48	0.436	0.458	0.031	6.793
341	0.345	0.396	0.370	0.036	9.733
370	0.405	0.434	0.419	0.020	4.888
378	0.367	0.377	0.372	0.007	1.901
Mean					6.582

9.4.2.3 MasR sandwich ELISA data

Table 9.29 Intra-assay CV% of MasR sandwich ELISA from a 96 well plate. CV% was calculated using the following formula: CV%= (Standard deviation (SD)/Mean) *100

MasR sandwich ELISA					
Sample	**Reading 1**	**Reading 2**	**Mean**	**SD**	**CV%**
66	0.279	0.277	0.278	0.001	0.509
69	0.259	0.232	0.245	0.019	7.778
72	0.198	0.197	0.197	0.001	0.358
74	0.288	0.288	0.288	0	0
75	0.22	0.226	0.223	0.004	1.902
79	0.203	0.219	0.211	0.011	5.362
84	0.185	0.219	0.202	0.024	11.902
95	0.289	0.263	0.276	0.018	6.661
98	0.235	0.256	0.245	0.015	6.048
103	0.274	0.307	0.290	0.023	8.032
106	0.318	0.333	0.325	0.011	3.258
110	0.209	0.255	0.232	0.032	14.020
112	0.202	0.24	0.221	0.027	12.158
120	0.254	0.308	0.281	0.038	13.588
122	0.375	0.302	0.338	0.051	15.249
127	0.274	0.274	0.274	0	0
128	0.393	0.389	0.391	0.002	0.723
130	0.312	0.331	0.321	0.013	4.179
220	0.304	0.295	0.299	0.006	2.125
223	0.241	0.252	0.246	0.008	3.155
224	0.234	0.227	0.230	0.005	2.147
228	0.321	0.209	0.265	0.079	29.885
241	0.338	0.283	0.310	0.039	12.525
242	0.305	0.371	0.338	0.046	13.807
256	0.397	0.348	0.372	0.035	9.301
257	0.268	0.319	0.293	0.036	12.287
263	0.269	0.238	0.253	0.022	8.647
277	0.252	0.281	0.266	0.020	7.694
278	0.273	0.356	0.314	0.059	18.661
284	0.438	0.478	0.458	0.028	6.176
287	0.272	0.293	0.282	0.014	5.256
288	0.226	0.231	0.228	0.003	1.547
289	0.34	0.367	0.353	0.019	5.401
290	0.358	0.336	0.347	0.015	4.483
291	0.251	0.283	0.267	0.023	8.475
302	0.299	0.414	0.356	0.081	22.809
319	0.321	0.339	0.33	0.013	3.856
1	0.285	0.284	0.284	0.001	0.248
213	0.219	0.282	0.250	0.044	17.783
216	0.257	0.297	0.277	0.028	10.211
Mean					7.955

9.4.3 Results and data analyses from chapter 5:

9.4.3.1 Ang-IV sandwich ELISA data

Table 9.30 Intra-assay CV% of Ang-IV sandwich ELISA from a 96 well plate. CV% was calculated using the following formula: CV%= (Standard deviation (SD)/Mean) *100

Ang-IV sandwich ELISA					
Sample	**Reading 1**	**Reading 2**	**Mean**	**SD**	**CV%**
1	0.255	0.279	0.267	0.017	6.356
16	0.403	0.341	0.372	0.044	11.785
36	0.438	0.385	0.411	0.037	9.107
50	0.202	0.245	0.223	0.030	13.604
328	0.184	0.184	0.184	0	0
333	0.268	0.262	0.265	0.004	1.601
336	0.21	0.213	0.211	0.002	1.002
338	0.263	0.27	0.266	0.005	1.857
355	0.325	0.421	0.373	0.068	18.199
390	0.289	0.278	0.283	0.008	2.744
412	0.24	0.246	0.243	0.004	1.746
461	0.247	0.325	0.286	0.055	19.285
597	0.213	0.223	0.218	0.007	3.244
678	0.448	0.435	0.441	0.009	2.082
326	0.214	0.217	0.215	0.002	0.984
330	0.291	0.273	0.282	0.012	4.513
573	0.378	0.385	0.381	0.005	1.297
577	0.209	0.215	0.212	0.004	2.001
579	0.282	0.263	0.272	0.013	4.930
580	0.262	0.275	0.268	0.009	3.424
584	0.403	0.491	0.447	0.062	13.921
586	0.222	0.222	0.222	0	0
592	0.221	0.288	0.254	0.047	18.615
601	0.251	0.271	0.261	0.014	5.418
665	0.267	0.271	0.269	0.003	1.051
670	0.237	0.233	0.235	0.003	1.203
681	0.302	0.294	0.298	0.006	1.898
683	0.305	0.282	0.293	0.016	5.541
685	0.233	0.248	0.240	0.011	4.410
687	0.28	0.289	0.284	0.006	2.237
691	0.291	0.298	0.294	0.005	1.680
697	0.31	0.323	0.316	0.009	2.904
Mean					5.062

9.4.3.2 IRAP sandwich ELISA data

Table 9.31 Intra-assay CV% of IRAP sandwich ELISA from a 96 well plate. CV% was calculated using the following formula: CV%= (Standard deviation (SD)/Mean) *100

IRAP sandwich ELISA					
Sample	**Reading 1**	**Reading 2**	**Mean**	**SD**	**CV%**
1	0.583	0.488	0.535	0.067	12.544
16	0.711	0.681	0.696	0.021	3.047
36	0.582	0.602	0.592	0.014	2.389
48	0.716	0.609	0.662	0.075	11.420
50	0.727	0.711	0.719	0.011	1.573
57	0.566	0.55	0.558	0.011	2.027
66	0.71	0.661	0.685	0.034	5.054
69	0.628	0.736	0.682	0.076	11.197
150	0.742	0.749	0.745	0.005	0.663
206	0.699	0.716	0.707	0.012	1.699
254	0.677	0.685	0.681	0.005	0.831
259	0.553	0.567	0.56	0.009	1.767
269	0.681	0.644	0.662	0.026	3.949
295	0.748	0.703	0.725	0.031	4.385
328	0.682	0.718	0.7	0.025	3.636
333	0.657	0.612	0.6345	0.032	5.015
336	0.683	0.493	0.588	0.134	22.848
338	0.554	0.477	0.515	0.054	10.562
72	0.738	0.648	0.693	0.063	9.183
84	0.746	0.671	0.708	0.053	7.485
190	0.911	0.725	0.818	0.131	16.078
196	0.621	0.606	0.613	0.011	1.728
205	0.753	0.813	0.783	0.042	5.418
212	0.964	0.948	0.956	0.011	1.183
213	0.531	0.472	0.501	0.041	8.318
219	0.612	0.538	0.575	0.052	9.100
302	0.658	0.618	0.638	0.028	4.433
405	0.509	0.483	0.496	0.018	3.706
424	0.534	0.576	0.555	0.029	5.351
426	0.621	0.561	0.591	0.042	7.178
435	0.71	0.637	0.673	0.052	7.664
451	0.605	0.586	0.595	0.013	2.256
470	0.687	0.722	0.704	0.025	3.513
478	0.692	0.614	0.653	0.055	8.446
488	1.049	1.141	1.095	0.065	5.941
495	0.531	0.478	0.504	0.037	7.428
498	0.666	0.661	0.663	0.003	0.533
499	0.627	0.603	0.615	0.016	2.759
223	0.711	0.65	0.680	0.043	6.338
224	0.599	0.593	0.596	0.004	0.711
Mean					5.734

9.4.3.3 IRAP activity data

Table 9.32 Intra-assay CV% of IRAP activity assay from a 96 well plate. CV% was calculated using the following formula: CV%= (Standard deviation (SD)/Mean) *100

IRAP activity assay					
Sample	**Reading 1**	**Reading 2**	**Mean**	**SD**	**CV%**
50	1.087	1.174	1.130	0.061	5.441
57	0.833	0.896	0.864	0.044	5.153
69	0.816	0.878	0.847	0.043	5.175
72	0.873	0.937	0.905	0.045	5.001
73	1.111	1.205	1.158	0.066	5.739
74	1.079	1.58	1.329	0.354	26.646
75	2.14	1.003	1.571	0.804	51.160
79	0.665	0.656	0.660	0.006	0.963
81	0.827	0.87	0.848	0.030	3.583
84	0.81	0.831	0.820	0.015	1.809
190	0.9	0.913	0.906	0.009	1.014
196	0.709	0.742	0.725	0.023	3.216
212	1.368	1.474	1.421	0.075	5.275
219	0.935	1.017	0.976	0.058	5.941
223	0.919	0.937	0.928	0.013	1.371
224	0.993	1.076	1.034	0.058	5.673
228	0.93	1.66	1.295	0.516	39.860
241	1.735	1.813	1.774	0.055	3.109
243	1.742	2.119	1.930	0.266	13.809
263	1.902	2.177	2.039	0.194	9.534
Mean					9.974

9.4.4 Results and data analyses from chapter 6:

9.4.4.1 VEGF level data

Table 9.33 Example of intra-assay CV% of absorbance values for VEGF sandwich ELISA from a 96 well plate. CV% was calculated using the following formula: CV%= (Standard deviation (SD)/Mean) *100

VEGF sandwich ELISA					
Sample	**Reading 1**	**Reading 2**	**Mean**	**SD**	**CV%**
72	1.421	1.434	1.427	0.009	0.643
73	1.126	1.061	1.093	0.046	4.203
74	1.19	1.218	1.204	0.019	1.644
75	1.347	1.281	1.314	0.046	3.551
79	1.161	1.089	1.125	0.051	4.525
81	1.904	1.713	1.808	0.135	7.468
84	1.077	1.048	1.062	0.020	1.929
95	1.115	1.103	1.109	0.008	0.765
98	1.158	1.157	1.157	0.001	0.061
103	1.13	1.139	1.134	0.006	0.561
106	0.902	0.921	0.911	0.013	1.474
110	1.173	1.172	1.172	0.001	0.060
112	1.011	1.026	1.018	0.011	1.041
120	0.745	0.758	0.751	0.009	1.223
122	1.442	1.311	1.376	0.092	6.729
127	0.76	0.755	0.757	0.003	0.467
128	1.151	1.121	1.136	0.021	1.867
130	1.073	0.992	1.032	0.057	5.547
141	1.236	1.178	1.207	0.041	3.397
147	1.395	1.316	1.355	0.056	4.121
223	2	1.98	1.99	0.014	0.711
224	1.147	1.095	1.121	0.037	3.280
241	1.878	1.726	1.802	0.108	5.964
242	1.596	1.501	1.548	0.067	4.338
243	1.159	1.088	1.123	0.050	4.468
263	1.482	1.416	1.449	0.046	3.221
278	0.911	0.88	0.895	0.022	2.448
284	1.013	0.985	0.999	0.019	1.982
287	1.697	1.632	1.664	0.046	2.761
290	1.711	1.482	1.596	0.162	10.142
291	0.79	0.782	0.786	0.005	0.719
665	1.107	0.963	1.035	0.102	9.838
326	1.049	0.902	0.975	0.104	10.655
330	1.442	1.024	1.233	0.295	23.972
341	1.316	0.996	1.156	0.226	19.574
370	1.057	0.866	0.961	0.135	14.046
378	1.045	0.857	0.951	0.133	13.978

400	1.418	1.041	1.229	0.266	21.681
Mean					5.448

9.4.4.2 PLP1 level data

Table 9.34 Example of intra-assay CV% of absorbance values for PLP1 sandwich ELISA from a 96 well plate. CV% was calculated using the following formula: CV%= (Standard deviation (SD)/Mean) *100

PLP1 sandwich ELISA					
Sample	**Reading 1**	**Reading 2**	**Mean**	**SD**	**CV%**
16	1.241	1.474	1.357	0.165	12.137
50	1.403	1.354	1.378	0.035	2.513
84	1.315	1.402	1.358	0.061	4.528
141	1.419	1.383	1.401	0.025	1.816
147	1.434	1.59	1.512	0.110	7.295
150	1.328	1.345	1.336	0.012	0.899
295	1.371	1.376	1.373	0.003	0.257
336	1.285	1.349	1.317	0.045	3.436
355	1.472	1.517	1.494	0.032	2.129
714	1.327	1.399	1.363	0.051	3.735
733	1.193	1.342	1.267	0.105	8.312
190	1.239	1.19	1.214	0.034	2.853
289	1.232	1.335	1.283	0.073	5.674
541	1.293	1.401	1.347	0.076	5.669
577	1.013	1.052	1.032	0.027	2.671
579	1.282	1.196	1.239	0.061	4.908
592	1.231	1.317	1.274	0.061	4.773
601	1.153	1.257	1.205	0.073	6.102
685	1.323	1.361	1.342	0.027	2.002
687	1.105	1.136	1.120	0.022	1.956
697	1.36	1.636	1.498	0.195	13.028
713	1.268	1.323	1.295	0.039	3.001
715	1.287	1.131	1.209	0.110	9.124
725	1.274	1.321	1.297	0.033	2.561
726	1.269	1.33	1.299	0.043	3.319
737	1.381	1.41	1.395	0.020	1.469
745	1.472	1.396	1.434	0.053	3.747
Mean					4.441

9.4.5 Results and data analyses from chapter 7:

9.4.5.1 Neurolysin level data

Table 9.35 Example of intra-assay CV% of absorbance values for neurolysin competitive ELISA from a 96 well plate. CV% was calculated using the following formula: CV%= (Standard deviation (SD)/Mean) *100

Neurolysin competitive ELISA					
Sample	**Reading 1**	**Reading 2**	**Mean**	**SD**	**CV%**
1	2.176	2.135	2.155	0.029	1.345
36	1.431	1.811	1.621	0.269	16.576
48	1.904	1.942	1.923	0.027	1.397
57	1.979	1.859	1.919	0.085	4.422
66	1.379	1.844	1.611	0.329	20.404
69	2.098	2.157	2.128	0.042	1.961
72	1.78	1.498	1.639	0.199	12.166
73	1.943	1.889	1.916	0.038	1.993
74	1.774	1.843	1.808	0.048	2.698
75	1.85	1.902	1.876	0.037	1.959
79	1.857	1.942	1.899	0.060	3.164
81	1.667	1.875	1.771	0.147	8.305
95	1.919	1.747	1.833	0.122	6.635
128	1.634	1.796	1.715	0.114	6.679
130	1.634	1.796	1.715	0.114	6.679
141	1.686	1.631	1.658	0.039	2.345
147	2.086	2.519	2.302	0.306	13.297
150	2	2.329	2.164	0.232	10.748
206	2.166	2.522	2.344	0.252	10.739
259	2.378	2.303	2.340	0.053	2.266
190	1.978	1.181	1.579	0.563	35.679
196	2.082	2.173	2.127	0.064	3.024
205	1.794	2.16	1.977	0.259	13.090
212	2.179	2.078	2.128	0.071	3.355
219	3.071	2.318	2.694	0.532	19.761
224	2.618	2.025	2.321	0.419	18.062
228	2.313	1.819	2.066	0.349	16.907
243	2.677	2.291	2.484	0.273	10.988
263	3.071	2.376	2.723	0.491	18.044
278	3.091	2.351	2.721	0.523	19.230
284	3.3	2.505	2.902	0.562	19.368
289	2.188	2.043	2.115	0.102	4.847
290	3.113	2.274	2.693	0.593	22.026
541	2.092	2.079	2.085	0.009	0.441
685	2.064	1.954	2.009	0.078	3.872
687	2.38	2.45	2.415	0.049	2.049
713	1.974	1.737	1.855	0.167	9.032

725	1.989	1.425	1.707	0.399	23.363
726	2.183	2.106	2.144	0.054	2.538
745	1.825	1.932	1.8785	0.076	4.027
Mean					9.476

9.4.5.2 Neurotensin level data

Table 9.36 Example of intra-assay CV% of absorbance values for neurotensin sandwich ELISA from a 96 well plate. CV% was calculated using the following formula: CV%= (Standard deviation (SD)/Mean) *100

Neurotensin sandwich ELISA					
Sample	**Reading 1**	**Reading 2**	**Mean**	**SD**	**CV%**
1	0.39	0.335	0.362	0.039	10.728
16	0.292	0.307	0.299	0.011	3.541
36	0.418	0.397	0.407	0.014	3.644
48	0.425	0.424	0.424	0.001	0.166
50	0.563	0.544	0.553	0.013	2.427
57	0.499	0.504	0.501	0.003	0.705
66	0.502	0.508	0.505	0.004	0.840
69	0.392	0.38	0.386	0.008	2.1982
72	0.541	0.583	0.562	0.029	5.284
73	0.551	0.564	0.557	0.009	1.649
74	0.515	0.556	0.535	0.029	5.413
75	0.566	0.569	0.567	0.002	0.374
79	0.715	0.678	0.696	0.026	3.756
81	0.307	0.317	0.312	0.007	2.266
84	0.619	0.58	0.599	0.027	4.600
95	0.48	0.435	0.457	0.031	6.955
98	0.513	0.479	0.496	0.024	4.847
103	0.593	0.532	0.562	0.043	7.668
106	0.351	0.342	0.346	0.006	1.837
110	0.463	0.42	0.441	0.030	6.887
190	0.519	0.429	0.474	0.063	13.426
196	0.526	0.474	0.5	0.037	7.354
205	0.38	0.352	0.366	0.019	5.409
212	0.467	0.504	0.485	0.026	5.389
213	0.411	0.346	0.378	0.046	12.143
219	0.584	0.517	0.550	0.047	8.606
223	0.576	0.559	0.567	0.012	2.118
224	0.334	0.34	0.337	0.004	1.259
228	0.535	0.509	0.522	0.018	3.522
241	0.441	0.449	0.445	0.005	1.271
242	0.516	0.553	0.534	0.026	4.895
243	0.485	0.463	0.474	0.015	3.282

263	0.469	0.505	0.487	0.025	5.227
278	0.333	0.315	0.324	0.013	3.928
284	0.395	0.384	0.389	0.007	1.997
287	0.67	0.795	0.732	0.088	12.066
289	0.362	0.34	0.351	0.015	4.432
290	0.778	0.741	0.759	0.026	3.445
302	0.342	0.377	0.3595	0.024	6.884
326	0.407	0.405	0.406	0.001	0.348
Mean					4.569

9.5 Appendix V: Relationships between measured proteins and confounding factors

9.5.1 Results and data analyses of altered measured RAS proteins

Table 9.37 Correlations between measured proteins and confounding factors

Chapter 3			
ACE-1 N-domain immunocapture-based activity (relative fluorescence units)			
	r	**p-value**	**Significant**
Age-at-death	0.117	0.209	No
PMD	- 0.059	0.525	No
Gender	-	0.326	No
ACE-1 C-domain immunocapture-based activity (relative fluorescence units)			
Age-at-death	0.040	0.666	No
PMD	- 0.107	0.249	No
Gender	-	0.701	No
Ang-I level (pg/ml)			
Age-at-death	0.008	0.925	No
PMD	0.094	0.305	No
Gender	-	0.410	No
Ang-I protein-adjusted level (pg/mg total protein)			
Age-at-death	-0.118	0.199	No
PMD	-0.132	0.150	No
Gender	-	0.071	No
Chapter 5			
IRAP activity (Abs)			
Age-at-death	0.155	0.093	No

PMD	0.036	0.695	No
Gender	-	0.712	No
Chapter 7			
Neurolysin level (ng/ml)			
Age-at-death	0.008	0.934	No
PMD	0.016	0.866	No
Gender	-	0.393	No
Neurolysin protein-adjusted level (ng/mg total protein)			
Age-at-death	-0.091	0.326	No
PMD	-0.083	0.371	No
Gender	-	0.009	Yes

9.5.2 Relationship between ACE-1 N-domain activity, ACE-1 C-domain activity, Ang-I level, IRAP activity and *APOE* genotype

Table 9.38 Relationship between ACE-1 N-domain activity, ACE-1 C-domain activity, Ang-I level, IRAP activity and *APOE* genotype

Presence or absence of *APOE* ε4 allelle	**ACE-1 N-domain activity**			
	p-value		**Significant**	
	0.189		No	
	ACE-1 C-domain activity			
	0.428		No	
	Ang-I level (pg/ml)		**Ang-I level (pg/mg total protein)**	
	p-value	**Significant**	**p-value**	**Significant**
	0.020	*	0.830	No
	IRAP activity (Abs)		**Sqrt transformed IRAP activity (Abs)**	
	0.068	No	0.079	No

9.6 Appendix VI: Transformed data

9.6.1 Log transformed data from chapter 3:

9.6.1.1 Log transformed data for ACE-1 N-domain immunocapture activity

Log transformation of ACE-1 N-domain activity was performed to attempt to reach normal distribution. The mean and standard error of mean (SEM) for controls was (4.108 ± 0.134) and for AD cases (3.920 ± 0.134). Unpaired samples t-test showed no significant difference between groups (p= 0.165) (Figure 9.12).

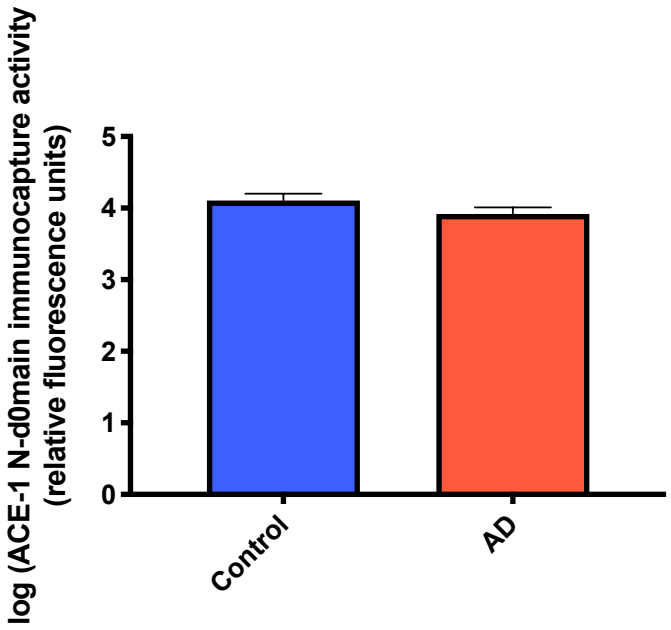

Figure 9.12. Measurement of log transformed ACE-1 N-domain activity compared between controls and AD cases.
Bar chart showing changes of log transformed ACE-1 N-domain enzyme activity measured by immunocapture-based FRET activity assay in AD (n= 70) compared to age-matched controls (n= 48) in the mid-frontal cortex. Unpaired samples t-test showed no significant difference between groups (p= 0.165). Bars show the mean ± SEM.

9.6.1.2 Log transformed data for Ang-I level

Ang-I level data was not normally distributed and log transformation was performed to attempt to reach normal distribution. Similar pattern of reduction of Ang-I level in AD group was observed. Unpaired samples t-test showed a significant difference between groups (p= 0.043). The mean and SEM for controls was (3.227 ± 0.01) and for AD cases (3.205 ± 0.0.01) (Figure 9.13).

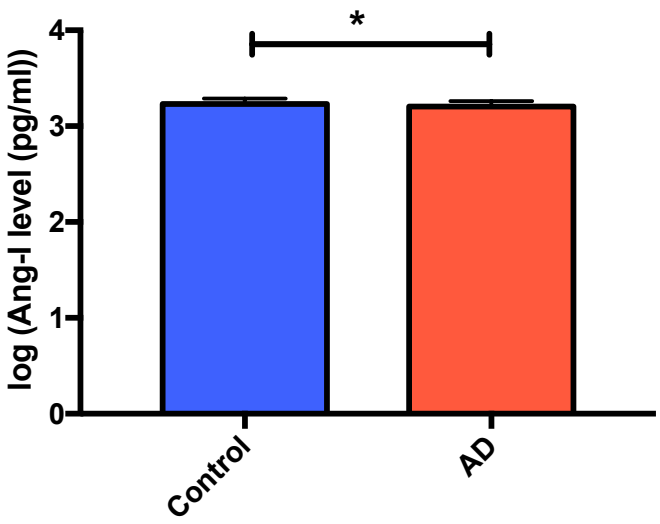

Figure 9.13. Measurement of log transformed Ang-I level compared between controls and AD cases.
Log transformed Ang-I level unadjusted to protein concentration was reduced in AD (n= 70) compared with age-matched control (n= 48) in mid-frontal cortex. Unpaired samples t-test revealed that Ang-I level was lower in AD (p= 0.043) compared to controls. The bars indicate the mean ± SEM.

9.6.2 Log transformed data from chapter 4:

9.6.2.1 Log transformed data for MasR level

Log transformation was performed to normalise the data. The mean and SEM for controls was (1.726 ± 0.034) and for AD cases (1.741 ± 0.028) (Figure 10.14 A). MasR protein-adjusted level after log transformation was unchanged between AD cases (2.486 ± 0.053) and controls (2.567 ± 0.034) (Figure 9.14 B).

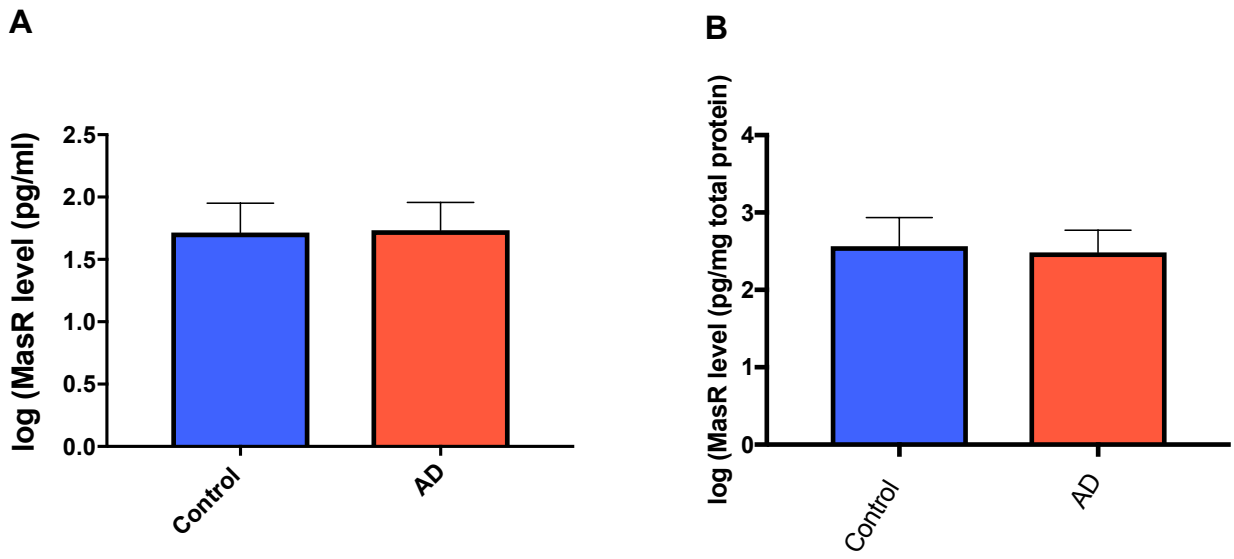

Figure 9.14. Measurement of log transformed MasR level compared between controls and AD cases.
A. Log transformed MasR level did not differ in AD cases compared to controls, Unpaired samples t-test revealed no significant difference between AD and controls (p= 0.982). The bars indicate the mean ± SEM. B. Log transformed MasR protein-adjusted level was unchanged in AD cases compared to controls, Unpaired samples t-test (p= 0.182). The bars indicate the mean ± SEM.

9.6.2.2 Relationship between MasR and disease severity

One-Way ANOVA test did not detect significant difference between the total MasR level and MasR protein-adjusted means of all Braak stages after log transformation (Figure 9.15).

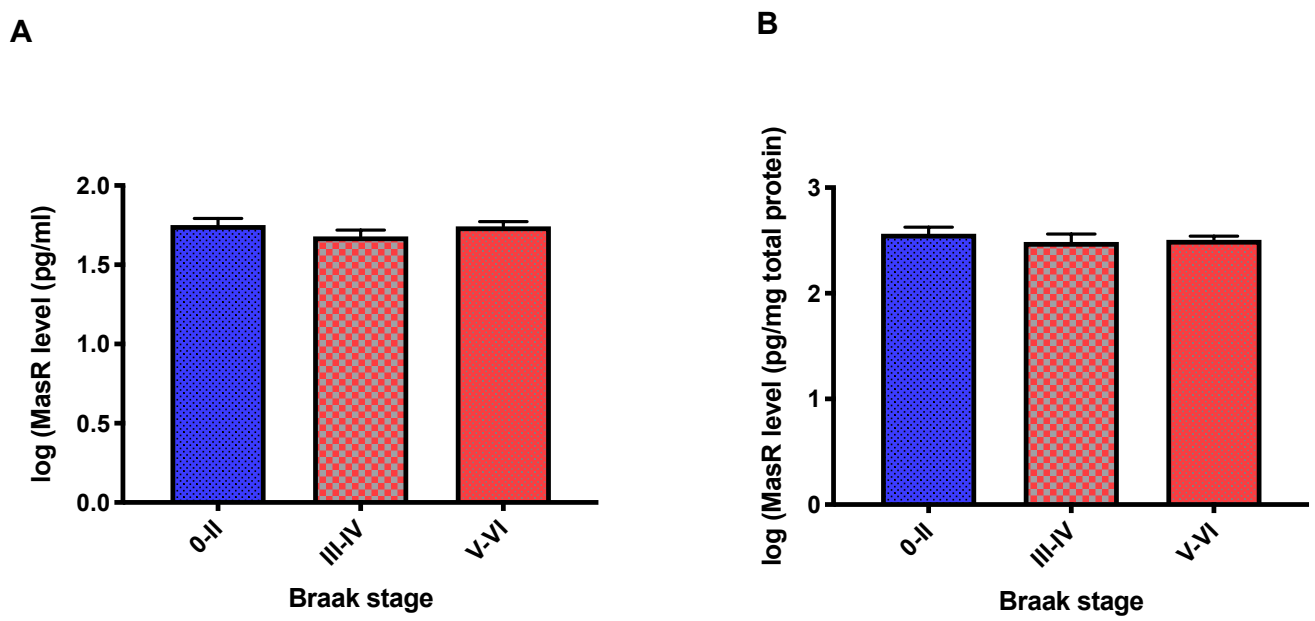

Figure 9.15. Log transformed MasR level in relation to Braak tangle stage.
A. No significant variations were found for log transformed total MasR level measured by sandwich ELISA assay between Braak tangle stage groups (Braak stage 0-II (n= 36), Braak stage III-IV (n= 20), Braak stage V-VI (n= 61)), One-Way ANOVA test (p= 0.510). The bars indicate the mean ± SEM. B. log transformed MasR protein-adjusted level was unchanged between Braak tangle stages groups (Braak stage 0-II (n= 36), Braak stage III-IV (n= 20), Braak stage V-VI (n= 61)), One-Way ANOVA test (p= 0.619). The bars indicate the mean ± SEM.

9.6.2.3 Relationship between MasR and AD pathology hallmarks

Log transformed data for both total MasR level and MasR protein-adjusted level was not correlated with total insoluble Aβ, tau load (Figure 9.16).

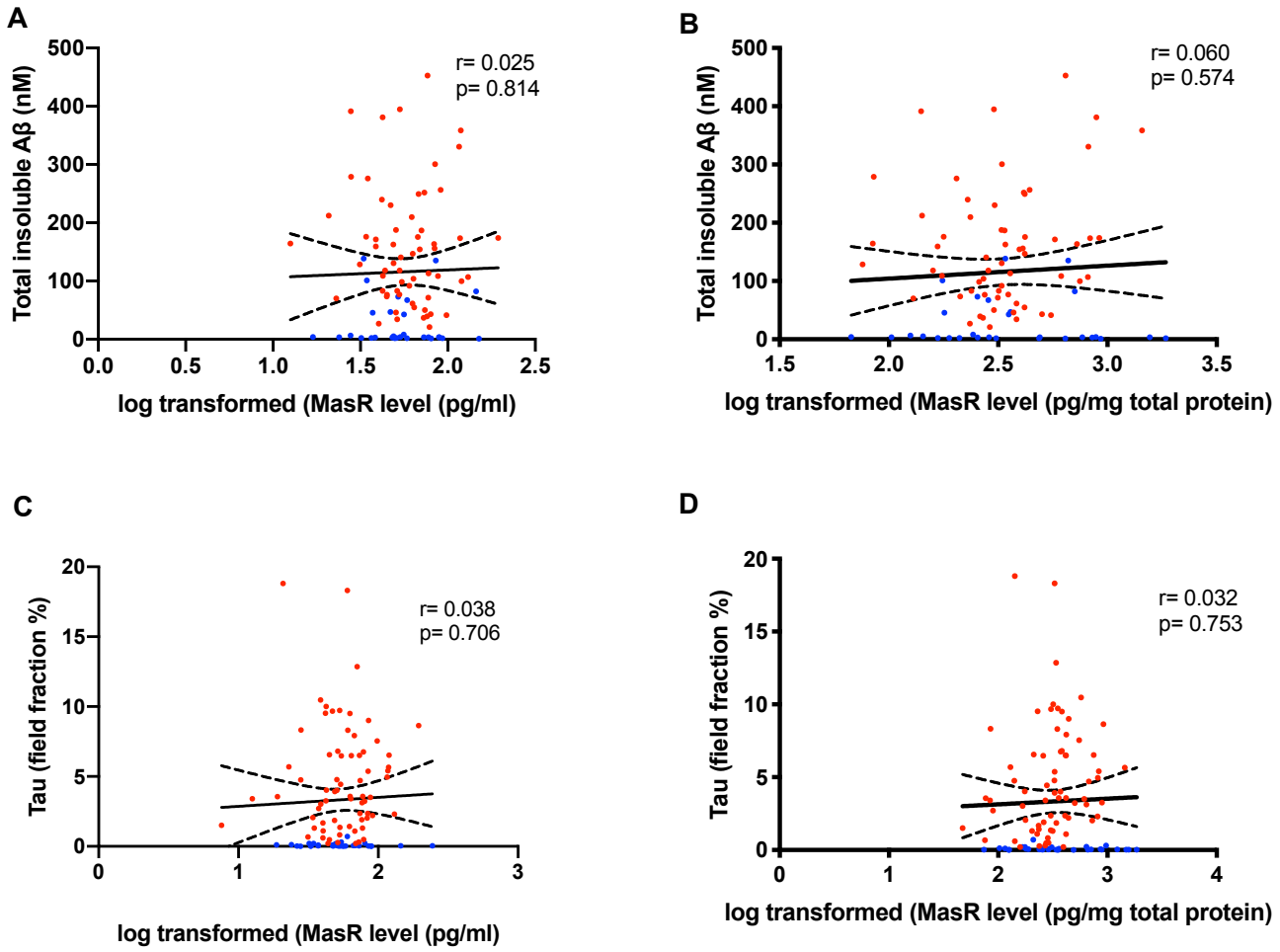

Figure 9.16. Relationships between log transformed MasR level and AD pathological hallmarks (total insoluble Aβ and tau load).
A. Scatterplots showing no correlation between log transformed total MasR level and total insoluble Aβ (measured by enzyme-linked immunosorbent assay), Pearson's correlation coefficient test (r= 0.025, p= 0.814). B. No significant correlation found between log transformed MasR protein-adjusted level and total insoluble Aβ, Pearson's correlation coefficient test (r= 0.060, p= 0.574). C-D. No significant correlation found between both log transformed total MasR level and MasR protein-adjusted level and tau load (measured by field fraction analysis), Pearson's correlation coefficient test (r= 0.038, p= 0.706), Pearson's r test (r= 0.032, p= 0.753). The solid inner line indicates the best-fit linear regression and the outer lines the 95% confidence intervals. Blue dots= controls, red dots= AD cases.

Similarly, no correlations were observed between Log transformed data for both total MasR level and MasR protein-adjusted level and insoluble Aβ40 and insoluble Aβ42 (Figure 9.17).

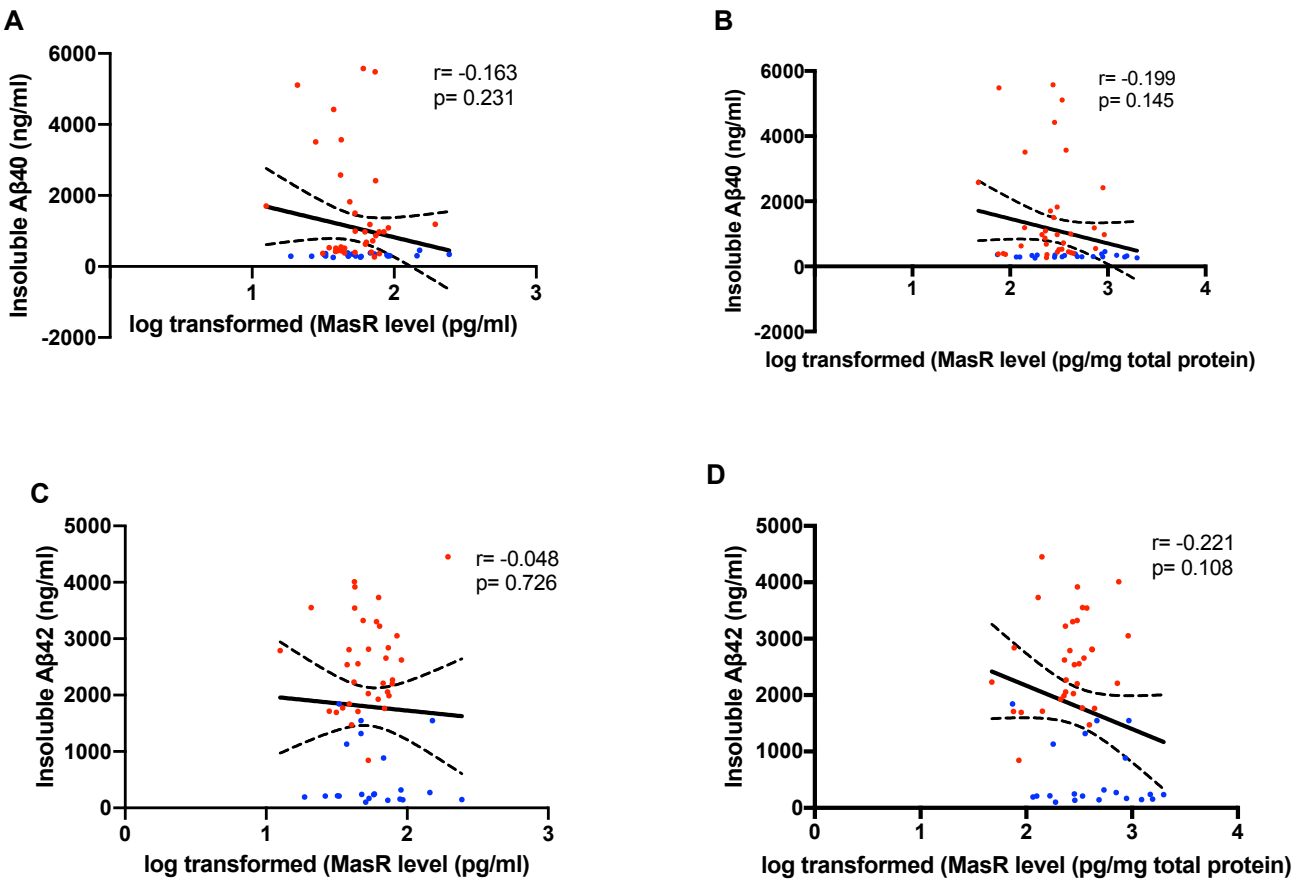

Figure 9.17. Relationships between log transformed MasR level and AD pathological hallmarks (insoluble Aβ40 and insoluble Aβ42).
A and C. Scatterplots showing no correlation between log transformed total MasR level and both insoluble Aβ40 and insoluble Aβ42 (measured by enzyme-linked immunosorbent assay), Pearson's correlation coefficient test (r= -0.163, p= 0.231), (r= -0.048, p= 0.726). B and D. No significant correlation found between log transformed MasR protein-adjusted level and both insoluble Aβ40 and insoluble Aβ42, Pearson's correlation coefficient test (r= -0.199, p= 0.145), (r= -0.221, p= 0.108). The solid inner line indicates the best-fit linear regression and the outer lines the 95% confidence intervals. Blue dots= controls, red dots= AD cases.

9.6.3 Log transformed data from chapter 5:

9.6.3.1 Log transformed data for IRAP level

Log transformation was performed to normalise the data. The mean and SEM for controls was (1.064 ± 0.021) and for AD cases (1.059 ± 0.024) (Figure 10.18 A). IRAP protein-adjusted level after log transformation was unchanged between AD cases (1.332 ± 0.026) and controls (1.332 ± 0.029) (Figure 9.18 B).

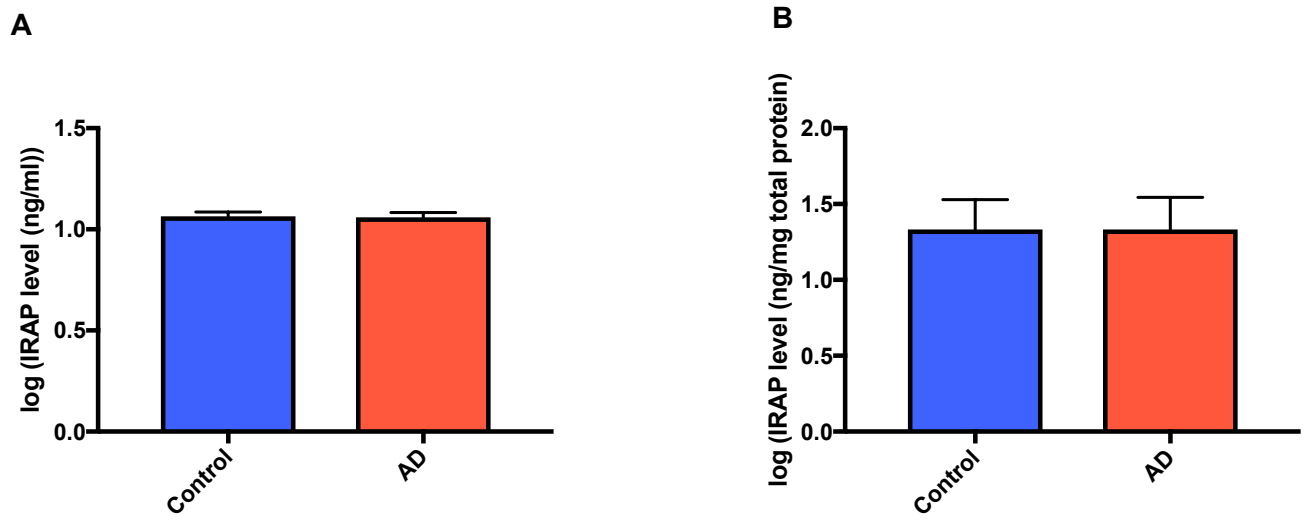

Figure 9.18. Measurement of log transformed IRAP level compared between controls and AD cases.
A. log transformed IRAP level unadjusted to protein concentration was unchanged in AD (n= 70) compared with age-matched control (n= 48) in mid-frontal cortex, Unpaired samples t-test (p= 0.892). The bars indicate mean ± SEM. B. log transformed protein-adjusted IRAP level did not differ in AD group compared to age-matched group, Unpaired samples t-test (p= 0.996). The bars indicate the mean ± SEM.

9.6.3.2 Comparison of IRAP activity in controls and AD

The data was not normally distributed so square-root transformation for IRAP activity data was performed to attempt to reach normal distribution. Following square-root transformation, the data was normally distributed. The mean for square-root IRAP activity was significantly lower in AD cases, mean ± SEM (= 0.736 ± 0.033 (Abs)) than in controls (= 0.875 ± 0.028 (Abs)) (p= 0.003) (Figure 9.19).

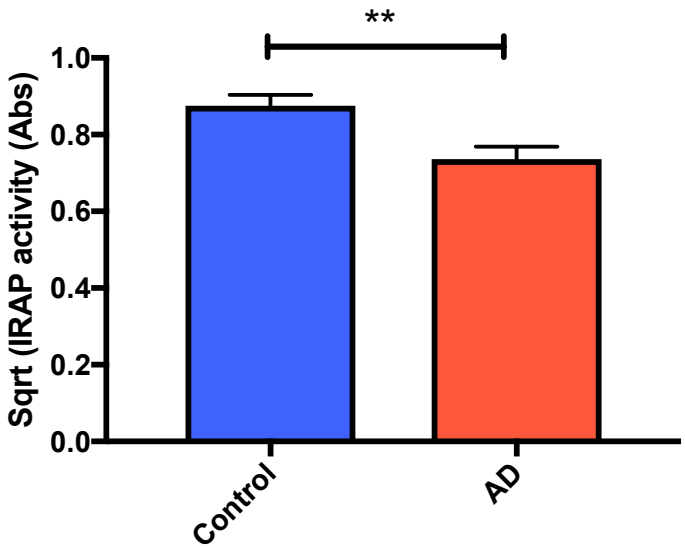

Figure 9.19. Measurement of square-rooted IRAP activity compared between controls and AD cases.
Square-rooted IRAP activity in AD (n= 70) compared to age-matched controls (n= 48) in mid-frontal cortex. Unpaired samples t-test showed a significant difference between groups (p= 0.003). Bars represent the mean ± SEM.

9.6.3.3 IRAP activity in relation to disease severity

Square-rooted IRAP activity was significantly reduced in cases with higher Braak tangle stage (V-VI) compared to Braak stage (0-II) (p= 0.043) and Braak stage (III-IV) (p= 0.023) using Dunn's multiple comparisons test. One-Way ANOVA test detected a significant difference of the mean between all groups (p= 0.008) (Figure 9.20).

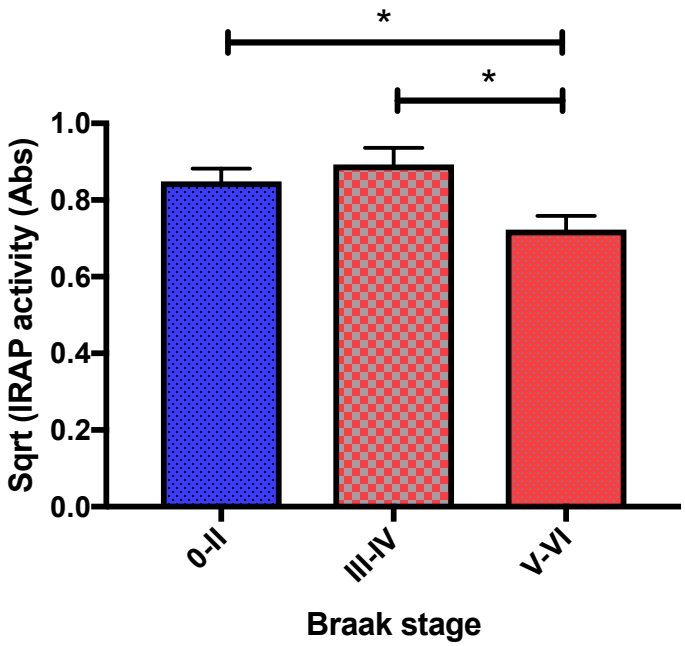

Figure 9.20. Square-rooted IRAP activity in relation to disease severity.
Square-rooted IRAP activity was significantly different between all groups (Braak stage 0-II (n= 36), Braak stage III-IV (n= 20), Braak stage V-VI (n= 61)) when analysed with One-Way ANOVA test (p= 0.008). IRAP activity was found to be significantly lower in cases with higher Braak stage (V-VI) compared with cases in Braak stage (0-II) (post-hoc Dunn's multiple comparisons test, p= 0.043) and Braak stage (III-IV) (post-hoc Dunn's multiple comparisons test, p= 0.023) and. The bars indicate the mean ± SEM.

9.6.3.4 Relationship between IRAP activity and AD pathology hallmarks

Square-rooted IRAP activity was inversely correlated with both total insoluble Aβ and tau load (Figure 9.21).

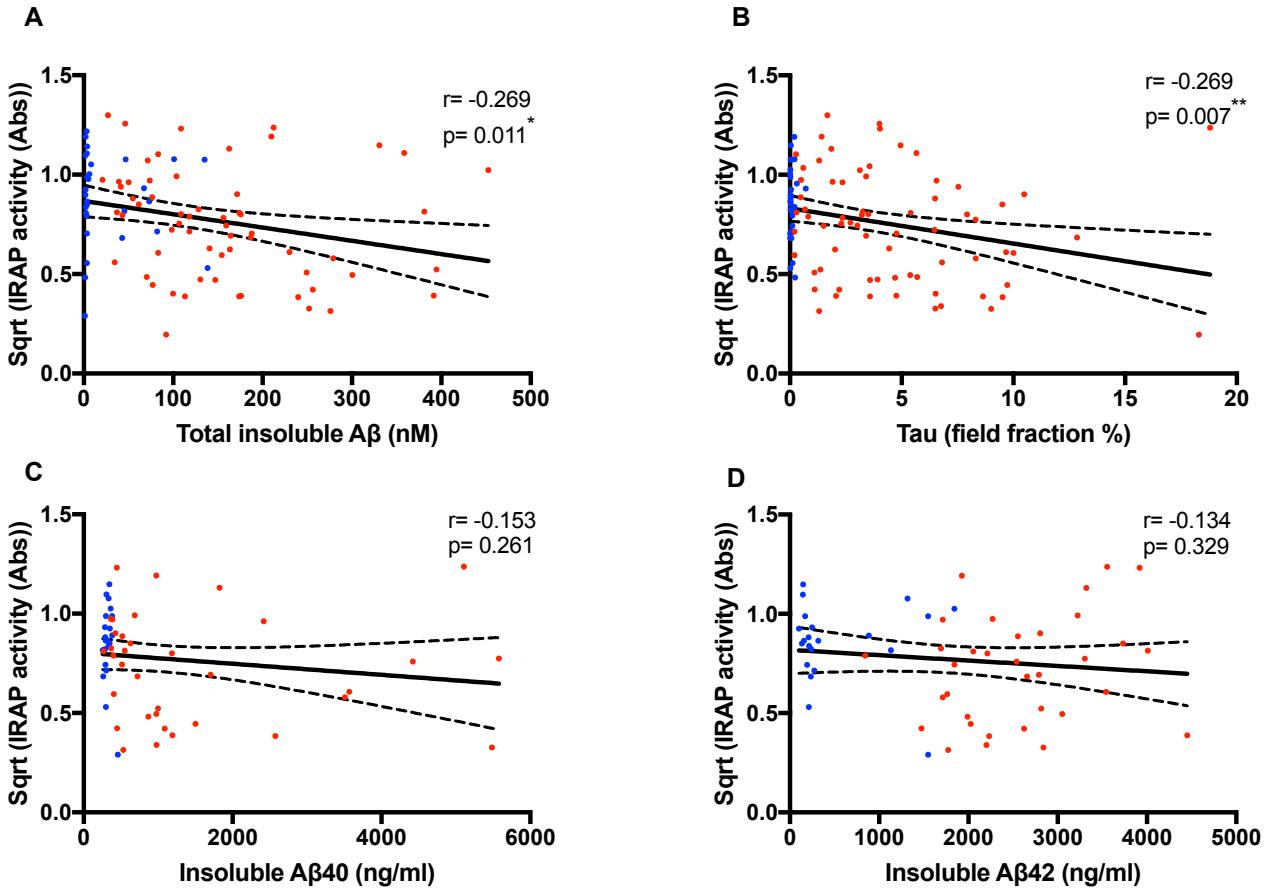

Figure 9.21. Relationships between square-rooted IRAP activity and AD pathological hallmarks (total insoluble Aβ, tau load, insoluble Aβ40 and insoluble Aβ42).
A. Scatterplots showing significant inverse correlation between sqrt IRAP activity and total insoluble Aβ (measured by enzyme-linked immunosorbent assay), Spearman's correlation coefficient test (r= -0.269, p= 0.011). B. Scatterplots showing significant inverse correlations between sqrt IRAP activity and tau load (measured by field fraction analysis), Spearman's correlation coefficient test (r= -0.269, p= 0.007). C. Scatterplots showing no correlation between sqrt IRAP activity and insoluble Aβ40 (measured by enzyme-linked immunosorbent assay), Spearman's correlation coefficient test (r= -0.153, p= 0.261). D. Scatterplots showing no correlation between sqrt IRAP activity and insoluble Aβ42 (measured by enzyme-linked immunosorbent assay), Spearman's correlation coefficient test (r= -0.134, p= 0.329). The solid inner line indicates the best-fit linear regression and the outer lines the 95% confidence intervals. Blue dots= controls, red dots= AD cases.

9.6.4 Log transformed data from chapter 6:

9.6.4.1 Relationship between MasR and marker of ischaemia in AD

MasR unadjusted and protein-adjusted data were not normally distributed. Log transformation for unadjusted and protein-adjusted data was performed to attempt to reach normal distribution. Correlations between log transformed total MasR level, MasR protein-adjusted data and VEGF level were assessed using Pearson's correlation coefficient. No significant correlations were observed between total MasR level and VEGF level (Pearson's correlation coefficient test, r= 0.031, p= 0.828), MasR protein-adjusted level and VEGF level (Pearson's correlation coefficient test, r= -0.267, p= 0.061) (Figure 9.22).

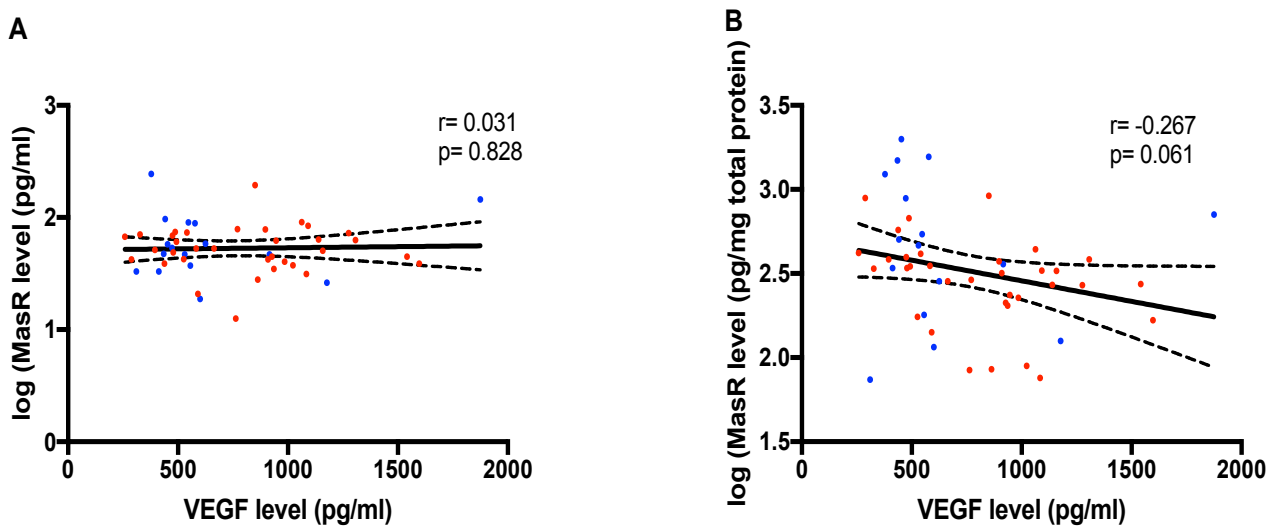

Figure 9.22. Relationships between MasR level and ischemic marker (VEGF level).
A-B. No significant correlations found between both log transformed total MasR level and log transformed MasR protein-adjusted level and VEGF level, Pearson's correlation coefficient test (r= 0.031, p= 0.828), Pearson's correlation coefficient test (r= -0.267, p= 0.061). The solid inner line indicates the best-fit linear regression and the outer lines the 95% confidence intervals. Blue dots= controls, red dots= AD cases.

9.6.4.2 Relationship between MasR and marker of brain tissue oxygenation in AD

Log transformation for MasR unadjusted and protein-adjusted data was performed to attempt to reach normal distribution. Correlations between log transformed total MasR level, MasR protein-adjusted data and MAG:PLP1 ratio were assessed using Pearson's correlation coefficient. A significant positive correlation was found between log transformed total MasR level and MAG:PLP1 ratio (Pearson's correlation coefficient test, r= 0.309, p= 0.027) (Figure 10.23 A). While, no correlation was found between log transformed MasR protein-adjusted level and MAG:PLP1 ratio (Pearson's correlation coefficient test, r= 0.254, p= 0.072) (Figure 9.23 B).

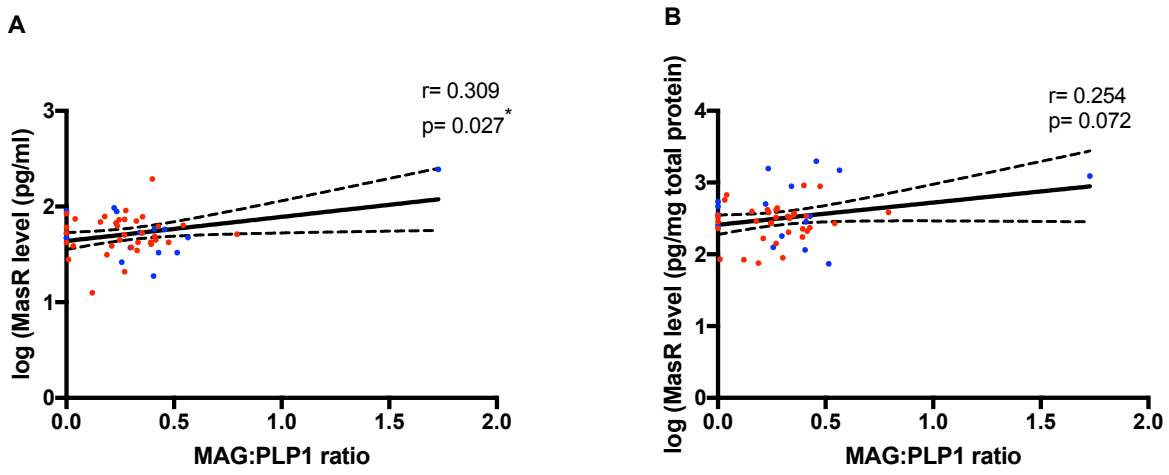

Figure 9.23. Relationships between MasR level and brain tissue oxygenation marker (MAG:PLP1 ratio).
A. Significant positive correlation between log transformed total MasR level and MAG:PLP1 ratio, Pearson's correlation coefficient test (r= 0.309, p= 0.027). B. No significant correlations found between log transformed MasR protein-adjusted level and MAG:PLP1 ratio, Pearson's correlation coefficient test (r= 0.254, p= 0.072). The solid inner line indicates the best-fit linear regression and the outer lines the 95% confidence intervals. Blue dots= controls, red dots= AD cases.

9.6.4.3 Relationship between IRAP and marker of brain ischaemia in AD

Both IRAP unadjusted to protein concentration and protein-adjusted data were not normally distributed. Log transformation for unadjusted and protein-adjusted data was performed to attempt to reach normal distribution. Correlations between log-transformed IRAP data and VEGF level and were assessed by the Pearson's correlation coefficient. Both log transformed IRAP unadjusted level and protein-adjusted level showed significant inverse correlations with VEGF level, (Pearson's correlation coefficient test, r= -0.329, p= 0.019) and (Pearson's correlation coefficient test, r= -0.349, p= 0.013) respectively (Figure 9.24 A and B).

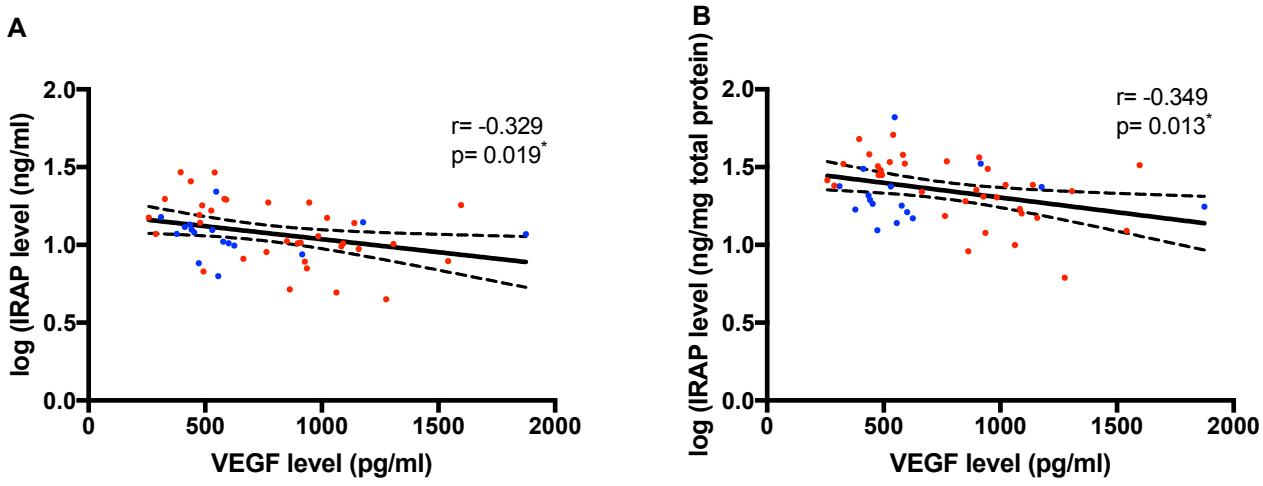

Figure 9.24. Relationships between IRAP level and ischemic marker (VEGF level).
A. Scatterplots showing significant inverse correlation between log transformed total IRAP level and VEGF level, Pearson's correlation coefficient test (r= -0.329, p= 0.019). B. Scatterplots showing significant inverse correlations between log transformed IRAP protein-adjusted level and VEGF level, Pearson's correlation coefficient test (r= -0.349, p= 0.013). The solid inner line indicates the best-fit linear regression and the outer lines the 95% confidence intervals. Blue dots= controls, red dots= AD cases.

9.6.4.4 Relationship between IRAP and marker of brain tissue oxygenation in AD

Correlations between log-transformed IRAP data and MAG:PLP1 ratio were assessed by the Pearson's correlation coefficient. Both log transformed IRAP unadjusted level and protein-adjusted level showed no significant correlations with MAG:PLP1 ratio, (Pearson's correlation coefficient test, r= 0.146, p=

0.307) and (Pearson's correlation coefficient test, r= -0.035, p= 0.808) respectively (Figure 9.25 A and B).

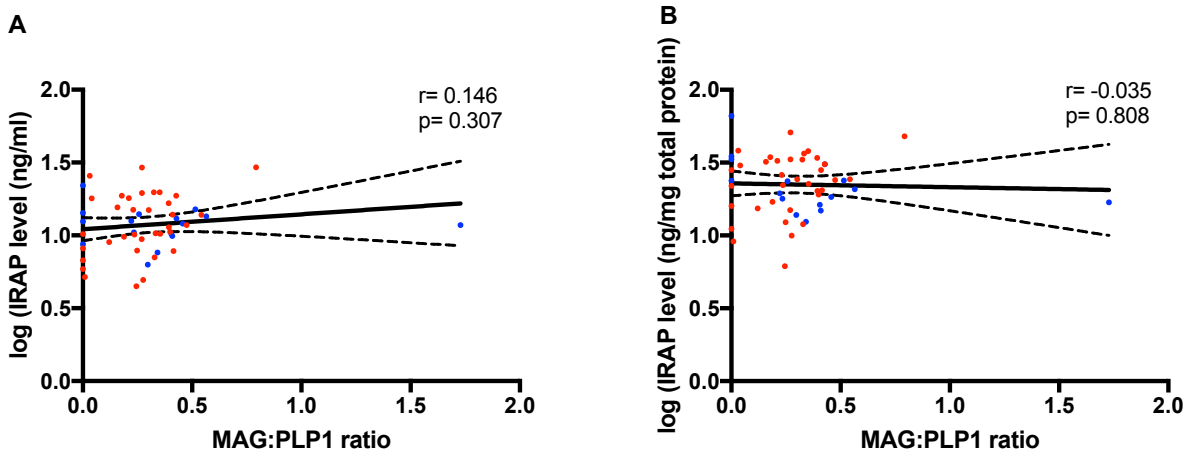

Figure 9.25. Relationships between IRAP level and brain tissue oxygenation marker (MAG:PLP1 ratio).
A-B. No significant correlations between both log transformed total IRAP level and log transformed IRAP protein-adjusted level with MAG:PLP1 ratio, Pearson's correlation coefficient test (r= 0.146, p= 0.307) and (r= -0.035, p= 0.808). The solid inner line indicates the best-fit linear regression and the outer lines the 95% confidence intervals. Blue dots= controls, red dots= AD cases.

9.7 Appendix VII: Data analysis after outliers removal

9.7.1 Data analysis after outliers removal from chapter 3:

9.7.1.1 ACE-1 N-domain immunocapture activity after removal of outliers

ACE-1 N-domain activity data was re-analysed after removal of outliers detected by ROUT method. Eighteen outliers was removed and ACE-1 N-domain activity was significantly reduced in AD group compared to age-matched controls (p= 0.037) (Figure 9.26).

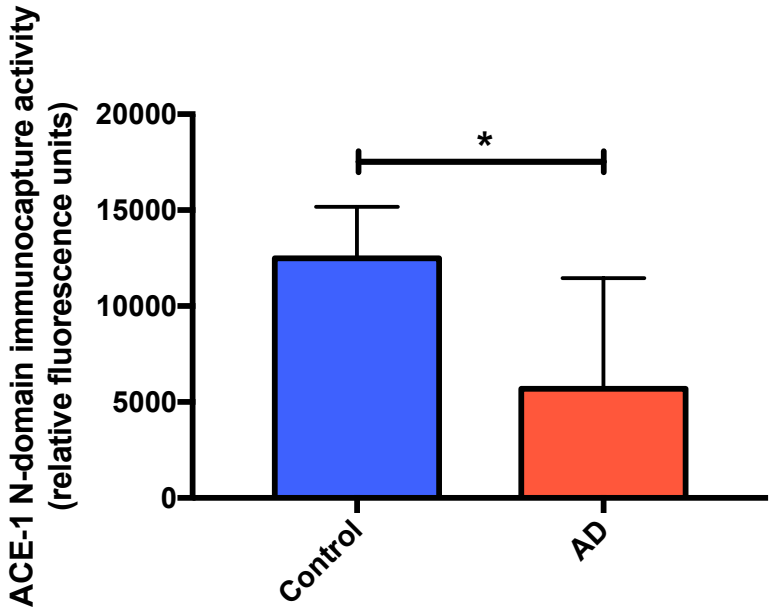

Figure 9.26. Reduction in ACE-1 N-domain activity in Alzheimer's disease.
Bar chart showing changes of ACE-1 N-domain enzyme activity measured by immunocapture-based FRET activity assay in AD (n= 59) compared to age-matched controls (n= 41) in the mid-frontal cortex. Mann-Whiney test showed a significant difference between groups (p= 0.037). Bars show the median and 95% confidence intervals.

9.7.1.2 ACE-1 C-domain immunocapture activity after removal of outliers

ACE-1 C-domain activity data was re-analysed after removal of outliers detected by ROUT method. Six outliers was removed and ACE-1 C-domain activity was significantly increased in AD group compared to age-matched controls (p= 0.001) (Figure 9.27).

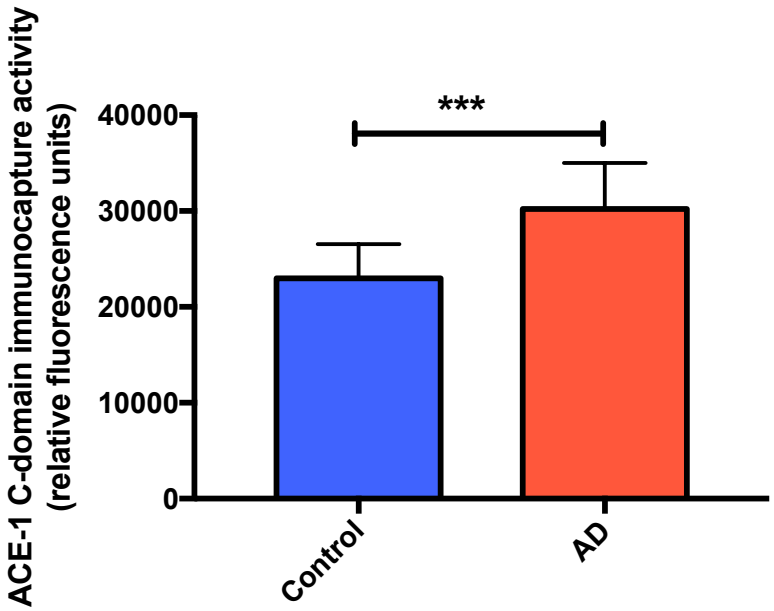

Figure 9.27. Change of ACE-1 C-domain activity in control and AD cases.
Bart chart showing changes of ACE-1 C-domain activity in mid-frontal cortex, measured by immunocapture-based FRET activity assay in AD (n= 68) and age-matched controls (n= 44). Mann-Whitney test revealed that ACE-1C-domain activity was higher in AD compared to age-matched controls (p= 0.001). The bars indicate the median and 95% confidence intervals.

9.7.1.3 Relationships between ACE-1 C-domain immunocapture-based activity and AD pathological hallmarks

ACE-1 C-domain activity data was re-analysed after removal of outliers detected by ROUT method. Ten outliers were removed in correlation between ACE-I C-domain activity and total insoluble Aβ load, (Figure 9.28).

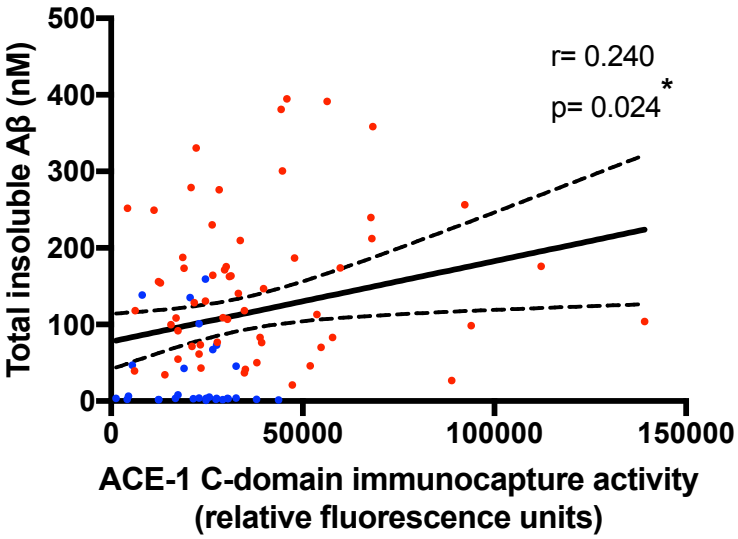

Figure 9.28. Correlations between ACE-1 C-domain activity and AD pathological hallmark (total insoluble Aβ load).
Scatterplots showing positive relationship between ACE-1 C-domain activity and insoluble total Aβ load (measured by enzyme-linked immunosorbent assay), Spearman's correlation coefficient test (r= 0.240, p= 0.024). The solid inner line indicates the best-fit linear regression and the outer lines the 95% confidence intervals. Blue dots= controls, red dots= AD cases.

9.7.1.4 Ang-I level after removal of outliers

Ang-I level data was re-analysed after removal of outliers detected by ROUT method. One outlier was removed and Ang-I level was significantly reduced in AD group compared to age-matched controls (p= 0.010) (Figure 9.29).

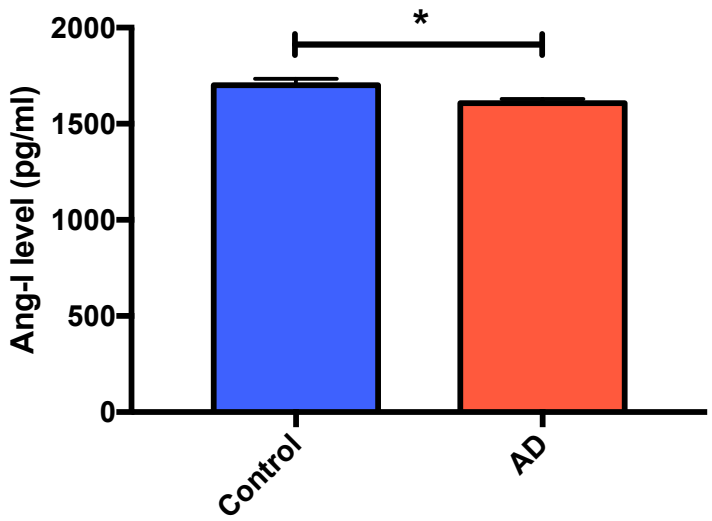

Figure 9.29. Measurement of Ang-I level compared between controls and AD cases.
Ang-I level unadjusted to protein concentration was reduced in AD (n= 69) compared with age-matched control (n= 48) in mid-frontal cortex. Mann-Whitney test revealed that Ang-I level was lower in AD (p= 0.010) compared to controls. The bars indicate the median and 95% confidence intervals.

9.7.1.5 Ang-I level in relation to disease severity

Ang-I level data was re-analysed after removal of outliers detected by ROUT method. One outlier was removed and Ang-I level was assessed in relation to Braak tangle stage (Braak stage 0-II, Braak stage III-IV, Braak stage V-VI). Kruskal-Wallis test revealed a significant difference of the median between all groups (p= 0.003) (Figure 9.30).

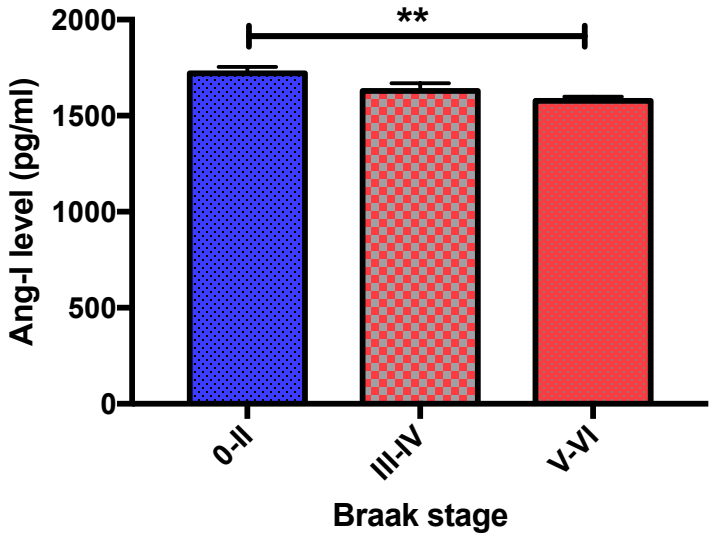

Figure 9.30. Ang-I level in relation to Braak tangle stage.
Significant variations were found between all groups (Braak stage 0-II (n= 36), Braak stage III-IV (n= 20), Braak stage V-VI (n= 60)) when analysed with Kruskal-Wallis test (p= 0.003). Ang-I level was

found to be significantly lower in cases with higher Braak stage (V-VI) compared with cases in Braak stage (0-II) (post-hoc Dunn's multiple comparisons test, p= 0.001). The bars indicate the median and 95% confidence intervals.

9.7.1.6 Ang-II:Ang-I ratio in AD

Ang-II:Ang-I ratio data was re-analysed after removal of outliers detected by ROUT method. One outlier was removed and Ang-II:Ang-I ratio level was significantly increased in AD group compared to age-matched controls (p< 0.0001) (Figure 9.31).

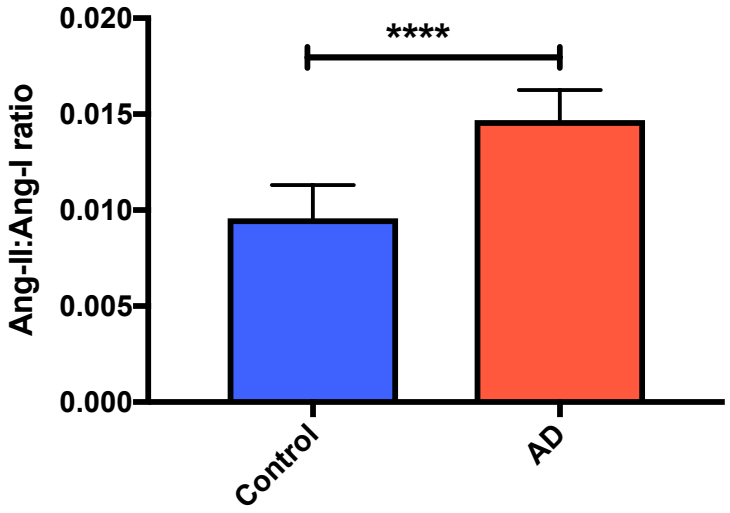

Figure 9.31. The ratio of Ang-II to Ang-I in AD compared with age-matched controls.
Reduced Ang-II:Ang-I ratio in AD (n= 70) compared to controls (n= 42) indicates an increase in ACE-1 activity in AD in mid-frontal cortex. Differences between groups were compared using Mann-Whitney test at P< 0.0001. The bars indicate the median and 95% confidence intervals.

9.7.1.7 Relationship between Ang-I level and ACE-1 activity

Ang-I level data was re-analysed after removal of outliers detected by ROUT method. Four outliers were removed in correlation between Ang-I level and ACE-I activity, (Figure 9.32).

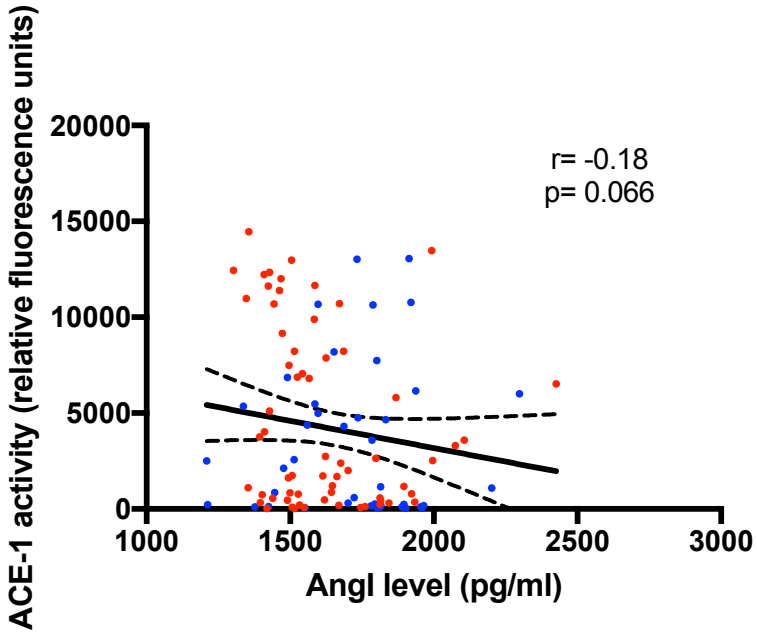

Figure 9.32. Correlation between Ang-I level and ACE-1 activity.

Scatterplots showing no correlation between Ang-I level unadjusted to protein concentration and ACE-1 activity measured by FRET activity assay in mid-frontal cortex. Spearman's correlation coefficient test (r= -0.18, p= 0.066). The solid inner line indicates the best-fit linear regression and the outer lines the 95% confidence intervals. Blue dots= controls, red dots= AD cases.

9.7.1.8 Relationship between Ang-II:Ang-I ratio and ACE-1 activity

Ang-II:Ang-I ratio data was re-analysed after removal of outliers detected by ROUT method. Four outliers were removed in correlation between Ang-II:Ang-I ratio and ACE-1 activity, (Figure 10.33).

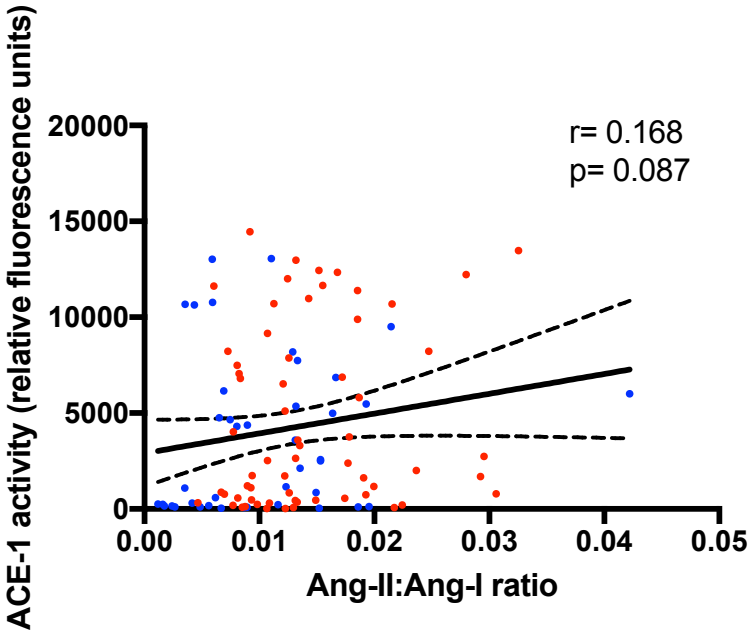

Figure 9.33. Correlation between Ang-II:Ang-I ratio and ACE-1 activity.

Scatterplots showing inverse correlation between Ang-II:Ang-I ratio and ACE-1 activity measured by FRET activity assay in mid-frontal cortex. Spearman's correlation coefficient test (r= 0.168, p= 0.087). The solid inner line indicates the best-fit linear regression and the outer lines the 95% confidence intervals. Blue dots= controls, red dots= AD cases.

9.7.2 Data analysis after outliers removal from chapter 4:

9.7.2.1 The Ang-II:Ang (1-7) ratio is increased in AD

Ang-II:Ang (1-7) ratio was re-analysed after removal of outliers detected by ROUT method. Tow outliers were removed and the mean ± SEM for Ang-II:Ang (1-7) ratio was significantly increased in AD compared to controls, Unpaired samples t-test detected a significant p value (p= 0.0008) (Figure 9.34).

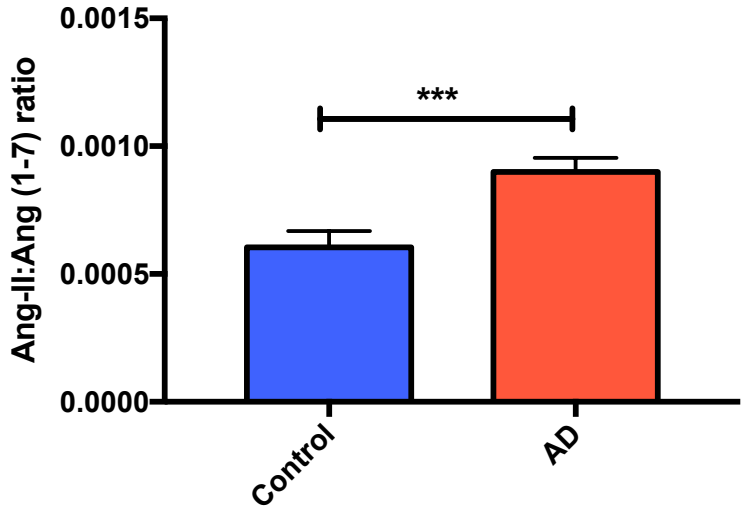

Figure 9.34. The ratio of Ang-II to Ang (1-7) in AD compared with age-matched controls. Increased Ang-II:Ang (1-7) ratio in AD (n= 67) compared to controls (n= 41) indicates a reduction in ACE-2 activity in AD in mid-frontal cortex. Differences between groups were compared using Unpaired samples t-test at ***P= 0.0008. The bars indicate the mean ± SEM.

9.7.3 Data analysis after removal of outliers from chapter 6

9.7.3.1 Relationship between MasR and marker of ischemia in AD

MasR protein-adjusted data was inversely correlated with VEGF after removed four outliers (Spearman's correlation coefficient r= -0.346, p= 0.018) (Figure 9.35).

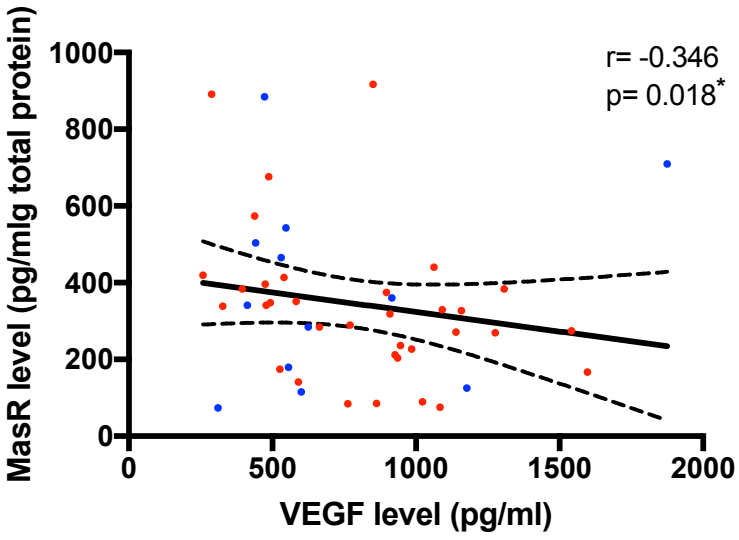

Figure 9.35. Relationships between MasR level and ischemic marker (VEGF level).

Significant inverse correlation found between MasR protein-adjusted level and VEGF level, Spearman's correlation coefficient test (r= - 0.346, p= 0.018). The solid inner line indicates the best-fit linear regression and the outer lines the 95% confidence intervals. Blue dots= controls, red dots= AD cases.

9.7.3.2 Relationship between MasR and markers of brain tissue oxygenation in AD

The association between both total unadjusted MasR level and protein-adjusted MasR measurement and the MAG:PLP1 ratio was examined after removed four outliers. No significant correlation was found between total MasR level and MAG:PLP1 ratio (Spearman's correlation coefficient, r= -0.115, p= 0.437) (Figure 9.36 A). MasR protein-adjusted level was also not correlated with MAG:PLP1 ratio in mid-frontal cortex, (Spearman's correlation coefficient, r= -0.087, p= 0.559) (Figure 9.36 B).

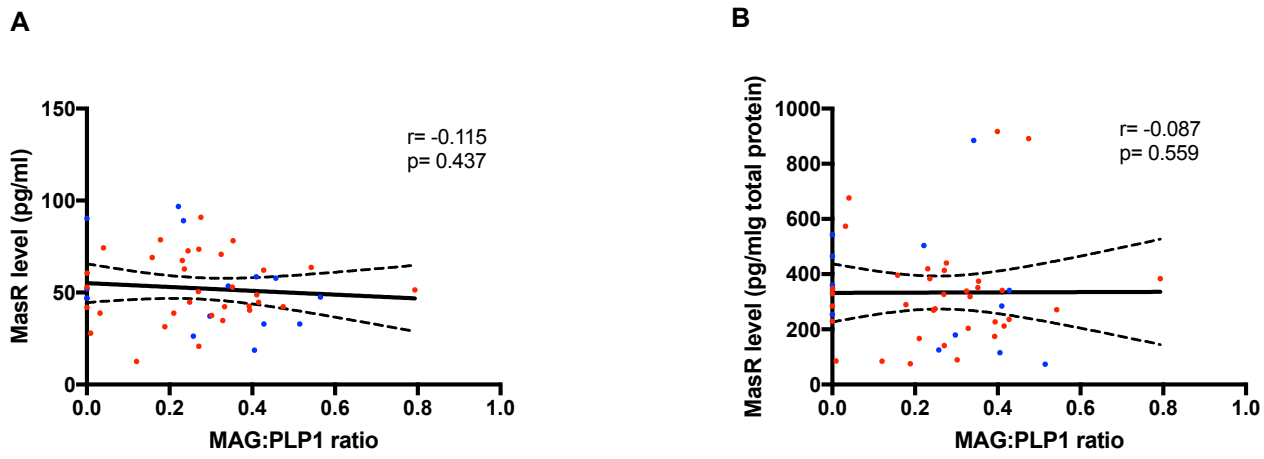

Figure 9.36. Relationship between MasR level and brain MAG:PLP1 ratio.
A. Scatterplot showing no correlation between total MasR level and MAG:PLP1, Spearman's correlation coefficient test (r= -0.115, p= 0.437). B. Scatterplot showing no significant correlation between MasR protein-adjusted level and MAG:PLP1 ratio, Spearman's correlation coefficient test (r= -0.087, p= 0.559). The solid inner line indicates the best-fit linear regression and the outer lines the 95% confidence intervals. Blue dots = controls, red dots = AD cases.

9.7.3.3 Relationship between Ang-IV and marker of brain ischaemia in AD

Ang-IV protein-adjusted data was not correlated with VEGF after removed three outliers (Spearman's correlation coefficient, r= -0.259, p= 0.084) (Figure 9.37).

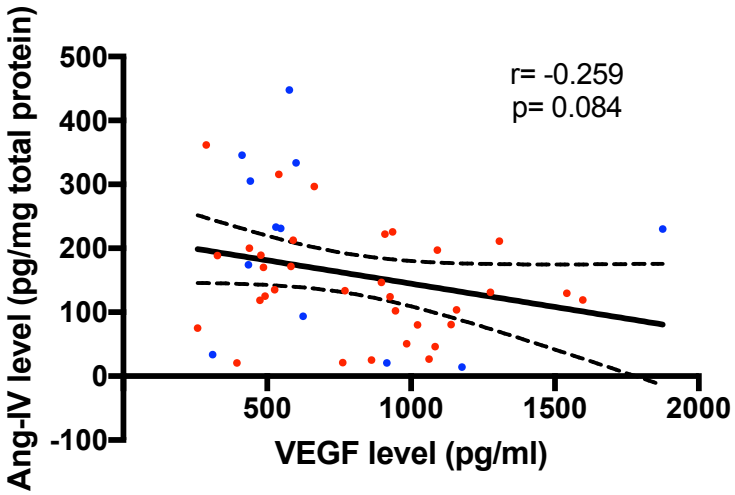

Figure 9.37. Relationship between Ang-IV level and ischemic marker (VEGF level).
Scatterplots showing no correlation between Ang-IV protein-adjusted level and VEGF level (measured by sandwich enzyme-linked immunosorbent assay), Spearman's correlation coefficient test (r= -0.259, p= 0.084). The solid inner line indicates the best-fit linear regression and the outer lines the 95% confidence intervals. Blue dots= controls, red dots= AD cases.

9.7.3.4 Relationship between Ang-IV and markers of brain tissue oxygenation in AD

Total unadjusted Ang-IV and Ang-IV protein-adjusted data were not correlated with MAG:PLP1 ratio after removed four outliers (Spearman's correlation coefficient, r= 0.017, p= 0.907) and (Spearman's correlation coefficient, r= 0.003, p= 0.982) respectively (Figure 9.38 A and B).

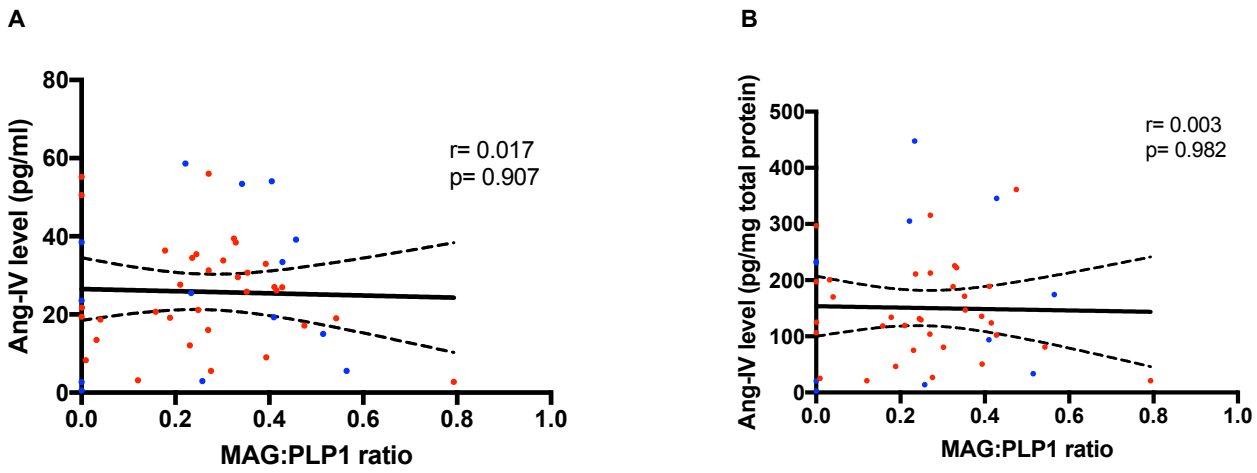

Figure 9.38. Relationship between Ang-IV level and brain MAG:PLP1 ratio.
A. Scatterplot showing no correlation between total Ang-IV level and MAG:PLP1, Spearman's correlation coefficient test (r= 0.017, p= 0.907). B. Scatterplot showing no significant correlation between Ang-IV protein-adjusted level and MAG:PLP1 ratio, Spearman's correlation coefficient test (r= 0.003, p= 0.982). The solid inner line indicates the best-fit linear regression and the outer lines the 95% confidence intervals. Blue dots = controls, red dots = AD cases.

9.7.3.5 Relationship between IRAP and marker of brain ischaemia in AD

IRAP protein-adjusted data was inversely correlated with VEGF after removed one outlier (Spearman's correlation coefficient, r= -0.336, p= 0.018) (Figure 9.39).

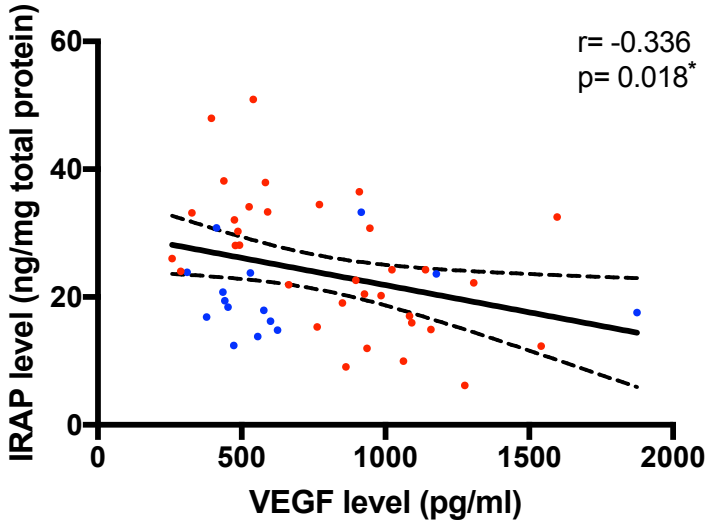

Figure 9.39. Relationship between IRAP level and ischemic marker (VEGF level).
Scatterplots showing significant inverse correlations between IRAP protein-adjusted level and VEGF level, Spearman's test (r= -0.398, p= 0.015). The solid inner line indicates the best-fit linear regression and the outer lines the 95% confidence intervals. Blue dots= controls, red dots= AD cases

9.7.3.6 Relationship between IRAP and markers of brain tissue oxygenation in AD

IRAP protein-adjusted data was not correlated with MAG:PLP1 ratio after removed one outlier (Spearman's correlation coefficient, r= 0.023, p= 0.873) (Figure 9.40).

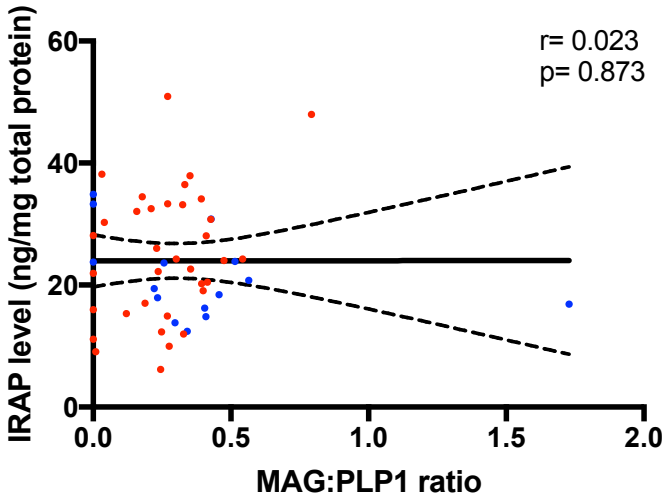

Figure 9.40. Relationship between IRAP level and brain MAG:PLP1 ratio.
Scatterplot showing no significant correlation between IRAP protein-adjusted level and MAG:PLP1 ratio, Spearman's correlation coefficient test (r= 0.023, p= 0.873). The solid inner line indicates the best-fit linear regression and the outer lines the 95% confidence intervals. Blue dots = controls, red dots = AD cases.

9.7.4 Data analysis after outliers removal from chapter 7

9.7.4.1 Neurolysin level after removal of outliers

Neurolysin data was re-analysed after removal of outliers detected by ROUT method. In neurolysin unadjusted data, one outliers was removed and Neurolysin level was significantly reduced in AD group compared to age-matched controls (p= 0.007) (Figure 9.41 A). The median for neurolysin level was lower in AD group (median= 7.368 (ng/ml)) compared to control group (median= 8.086 (ng/ml)). When neurolysin level was adjusted to total protein concentration, ten outliers was removed and neurolysin level was unchanged in AD group compared to age-matched controls (p= 0.119). Mann-Whitney test compared the median of AD group (median= 20.17 (ng/mg total protein)) to control group (median= 21.37 (ng/mg total protein)) (Figure 9.41 B).

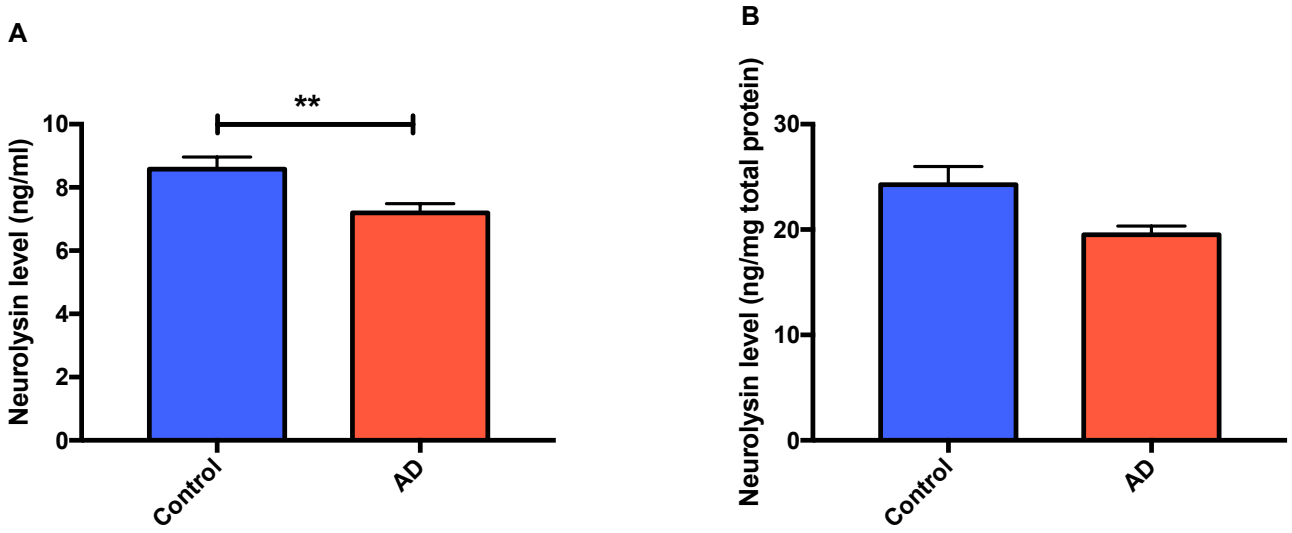

Figure 9.41. Measurement of neurolysin level compared between controls and AD cases.
A. Neurolysin level unadjusted to protein concentration was reduced in AD (n= 70) compared with age-matched control (n= 47) in mid-frontal cortex. Mann-Whitney test revealed that neurolysin level was lower in AD (p= 0.007) compared to controls. B. Neurolysin protein-adjusted measurement was unchanged in AD cases (n= 68) compared to age-matched controls (n= 40). Differences between groups were compared using Mann-Whitney test at P= 0.119. The bars indicate the median and 95% confidence intervals.

9.7.4.2 Neurolysin level in relation to disease severity

In neurolysin unadjusted data, one outliers was removed and Kruskal-Wallis test revealed a significant difference of the median between all Braak tangle stage groups (p= 0.003). A significant reduction of neurolysin level was observed in Braak stage (III-IV) compared to Braak stage (0-II) (p= 0.049) and between cases in Braak stage (V-VI) and Braak stage (0-II) (p= 0.004) using Dunn's multiple comparisons test (Figure 9.42 A). For neurolysin protein-adjusted data, ten outliers removed and no significant variation of the median between all groups was observed (p= 0.334) (Figure 9.42 B).

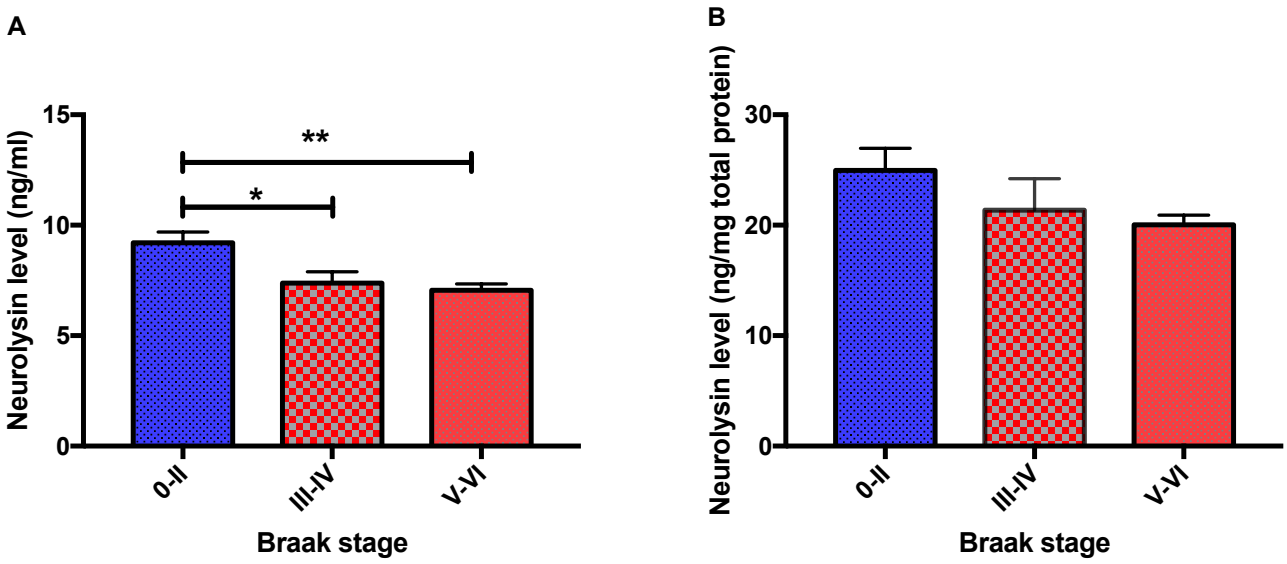

Figure 9.42. Neurolysin level in relation to Braak tangle stage.
A. Significant variations were found between all groups (Braak stage 0-II (n= 36), Braak stage III-IV (n= 20), Braak stage V-VI (n= 60)) when analysed with Kruskal-Wallis test (p= 0.003). Neurolysin level was found to be significantly lower in cases in Braak stage (III-IV) compared with cases in Braak stage (0-II) (p=0.049) and between cases in Braak stage (V-VI) and Braak stage (0-II) (p= 0.004) (post-hoc Dunn's multiple comparisons test). The bars indicate the median and 95% confidence intervals. B. No significant difference was found for neurolysin protein-adjusted measurement between Braak tangle stage groups (Braak stage 0-II (n= 30), Braak stage III-IV (n= 19), Braak stage V-VI (n= 59)), Kruskal-Wallis test (p= 0.334). The bars indicate the median and 95% confidence intervals.

9.7.4.3 Relationship between neurolysin level and APOE genotype

There was no difference in both neurolysin unadjusted data and protein-adjusted neurolysin level in relation to the presence or absence of *APOE* ε4 allelle after removal of outliers in unadjusted data (n= 1) (p= 0.062) and in protein-adjusted data (n= 8) (p= 0.992) (Figure 9.43).

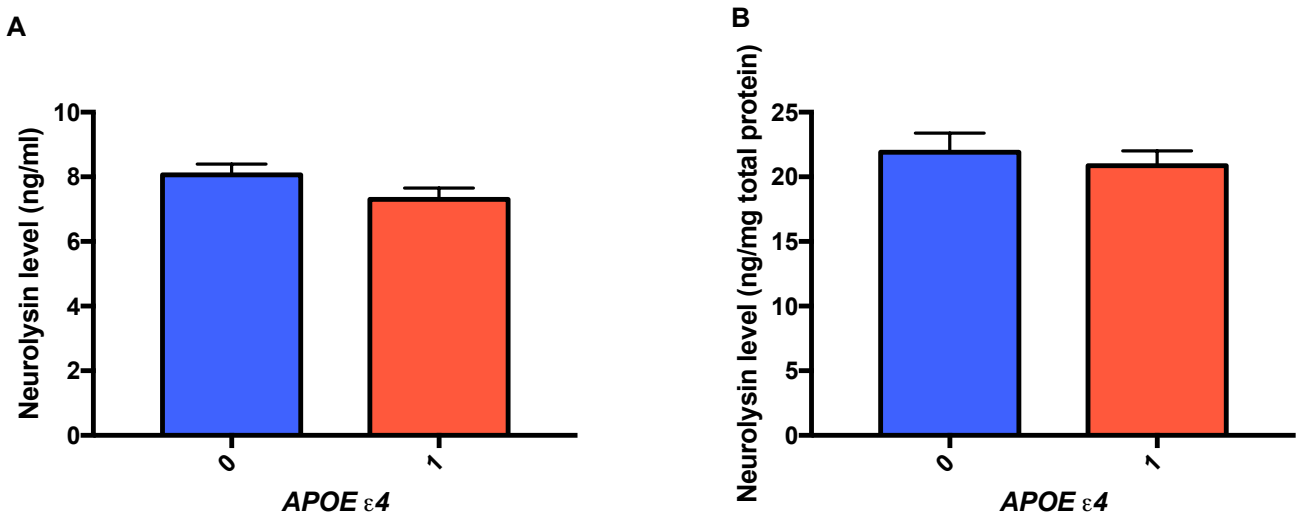

Figure 9.43. Relationship between neurolysin level and *APOE* genotype
A. Unchanged neurolysin level in presence of one or two *APOE* ε4 allelle compared to cases with absence of *APOE* ε4 allelle. Differences between groups were compared using Mann-Whitney test at p= 0.062. The bars indicate the median and 95% confidence intervals. B. No significant difference in neurolysin protein-adjusted measurement depending on the presence or absence of *APOE* ε4 allelle (p= 0.992). The bars indicate the median and 95% confidence intervals.

9.7.4.4 Neurolysin level in relation to brain RAS markers

The relationship between Ang-II level and neurolysin level was assessed after removal of outliers. Total neurolysin correlated inversely with Ang-II level after removed one outlier (Spearman's correlation coefficient, r= -0.234, p= 0.013) and no correlation was observed between neurolysin protein-adjusted level and Ang-II level after removed ten outliers (Spearman's correlation coefficient, r= -0.167, p= 0.093) (Figure 9.44 A and B). Unadjusted neurolysin correlated inversely with Ang-III level (Spearman's correlation coefficient, r= -0.224, p= 0.030), no outliers detected. No significant correlation was found between neurolysin protein-adjusted data and Ang-III level after removed eight outliers (Spearman's correlation coefficient, r= -0.013, p= 0.902) (Figure 9.44 C).

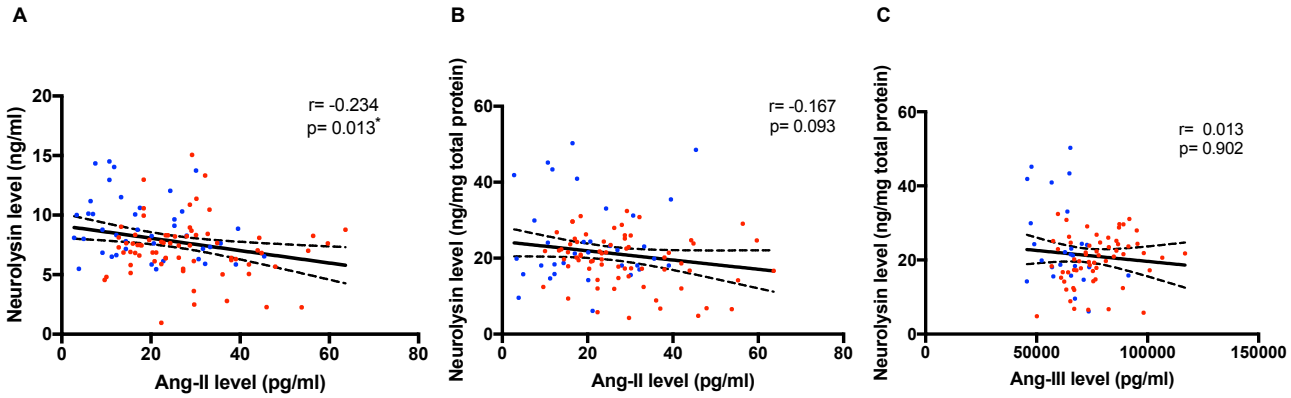

Figure 9.44. Relationships between neurolysin level and brain RAS markers (Ang-II and Ang-III).

A. Scatterplots showing significant inverse correlation between neurolysin level and Ang-II level (measured by enzyme-linked immunosorbent assay), Spearman's correlation coefficient test (r= -0.234, p= 0.013). B. No correlation found between neurolysin protein-adjusted level and Ang-II level, Spearman's correlation coefficient test (r= -0.167, p= 0.093). C. Scatterplots showing no correlation between neurolysin protein-adjusted level and Ang-III level, Spearman's correlation coefficient test (r= -0.013, p= 0.902). The solid inner line indicates the best-fit linear regression and the outer lines the 95% confidence intervals. Blue dots= controls, red dots= AD cases.

Neurolysin unadjusted data was inversely correlated with Ang-II:Ang (1-7) ratio after removed one outlier (Spearman's c correlation coefficient, r= -0.194, p= 0.042) and protein-adjusted levels was not correlated with the Ang-II:Ang (1-7) ratio after removed ten outliers (Spearman's correlation coefficient, r= -0.182, p= 0.068) (Figure 9.45 A and B).

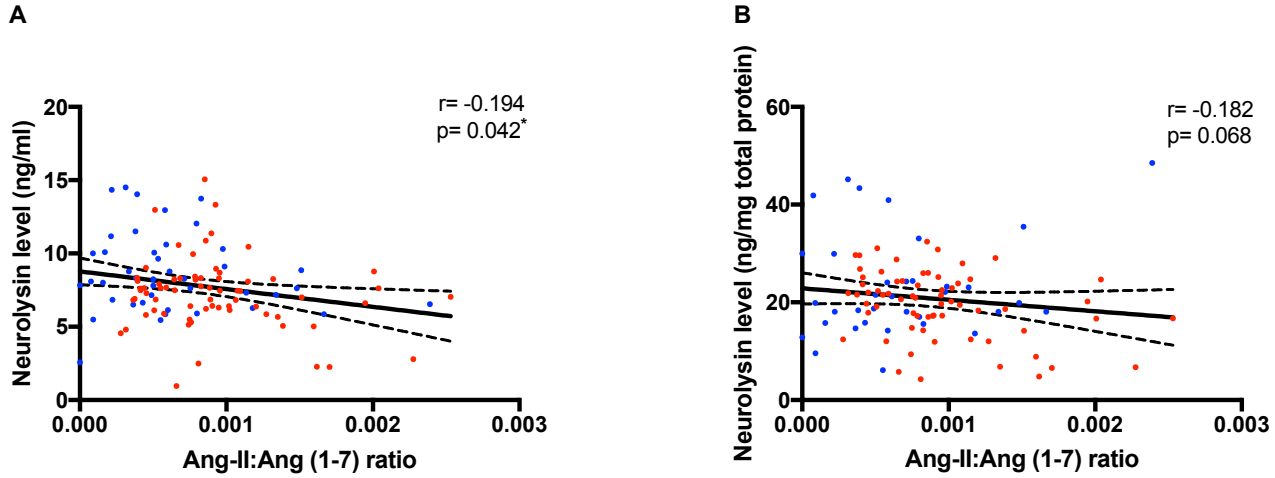

Figure 9.45. Relationship between neurolysin level and brain RAS markers (Ang-II:Ang (1-7) ratio).

A. Scatterplots showing significant inverse correlation between neurolysin level and Ang-II:Ang (1-7) ratio, Spearman's correlation coefficient test (r= -0.194, p= 0.042). B. No correlation found between neurolysin protein-adjusted level and Ang-II:Ang (1-7) ratio, Spearman's correlation coefficient test

(r= -0.182, p= 0.068). The solid inner line indicates the best-fit linear regression and the outer lines the 95% confidence intervals. Blue dots= controls, red dots= AD cases.

9.7.4.5 Neurolysin level in relation to markers of brain tissue oxygenation and ischaemia

No significant correlation was found between neurolysin protein-adjusted level and VEGF level after removed six outliers (Spearman's correlation coefficient, r= 0.129, p= 0.369) (Figure 9.46).

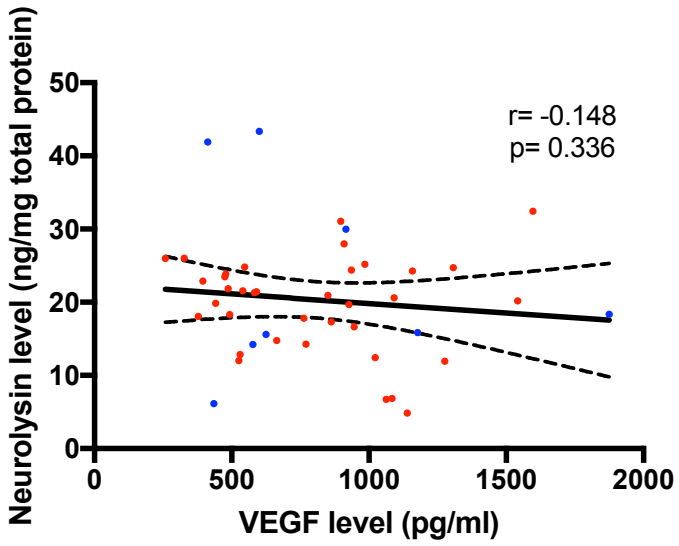

Figure 9.46. Relationship between neurolysin level and ischemic marker (VEGF)
Scatterplots showing no significant correlation between neurolysin protein-adjusted level and VEGF level (measured by enzyme-linked immunosorbent assay), Spearman's correlation coefficient test (r= -0.148, p= 0.336). The solid inner line indicates the best-fit linear regression and the outer lines the 95% confidence intervals. Blue dots= controls, red dots= AD cases.

9.8 Appendix VIII: Summary statistics of all measured proteins

Table 9.39 Summary statistics for all measured proteins in this thesis

Chapter 3					
Data set	**Cohort**	**Median**	**Mean**	**SEM**	**p-value**
ACE-1 N-domain FRET activity (r.f.u)	Control AD	15229 13728	-	-	0.981
ACE-1 C-domain FRET activity (r.f.u)	Control AD	5938 7088	-	-	0.132
ACE-1 N-domain immunocapture-based activity (r.f.u)	Control AD	13248 6708	-	-	0.024
ACE-1 C-domain immunocapture-based activity (r.f.u)	Control AD	23515 30656	-	-	0.011
Ang-I level (pg/ml)	Control AD	1736 1546	-	-	0.006
Ang-I protein-adjusted level (pg/mg total protein)	Control AD	4762 4601	-	-	0.013
Chapter 4					
Ang (1-7) level (pg/ml)	Control AD	-	31668 32572	1014 892.4	0.514
Ang (1-7) protein-adjusted level (pg/mg total protein)	Control AD	111555 121204	-	-	0.222
MasR level (pg/ml)	Control AD	51.39 57.56	-	-	0.359

MasR protein-adjusted level (pg/mg total protein)	Control AD	327.9 347	-	-	0.343
Chapter 5					
Ang-IV level (pg/ml)	Control AD	21.71 26.55	-	-	0.501
Ang-IV protein-adjusted level (pg/mg total protein)	Control AD	150.6 130.5	-	-	0.744
IRAP level (ng/ml)	Control AD	12.26 11.46	-	-	0.997
IRAP protein-adjusted level (ng/mg total protein)	Control AD	20.09 23.33	-	-	0.405
IRAP activity (Abs)	Control AD	0.7863 0.5623	-	-	0.003
Chapter 6					
Ang (1-7) level (pg/ml)	Control AD	-	30656 31502	1465 1206	0.686
Ang (1-7) protein-adjusted level (pg/mg total protein)	Control AD	-	110424 121279	8121 5824	0.301
MasR level (pg/ml)	Control AD	51.96 51.41	-	-	0.843
MasR protein-adjusted level (pg/mg total protein)	Control AD	465.2 318.6	-	-	0.082
Log MasR protein-	Control	-	2.641	0.102	0.047

adjusted level (pg/mg total protein)	AD	-	2.447	0.044	
Ang-IV level (pg/ml)	Control AD	29.49 26.00	-	-	0.533
Ang-IV protein-adjusted level (pg/mg total protein)	Control AD	232.1 130.5	-	-	0.059
IRAP level (ng/ml)	Control AD	12.05 11.38	-	-	0.907
IRAP protein-adjusted level (ng/mg total protein)	Control AD	19.45 24.27	-	-	0.405
Chapter 7					
Neurolysin level (ng/ml)	Control AD	8.164 7.368	-	-	0.004
Neurolysin protein-adjusted level (ng/mg total protein)	Control AD	23.66 20.4	-	-	0.008
Neurotensin level (pg/ml)	Control AD	-	746.9 751	19.2 16.47	0.875
Neurotensin protein-adjusted level (pg/mg total protein)	Control AD	2245 2096	-	-	0.259

9.9 Appendix IX: Ang-I protein adjusted data

9.9.1 Protein-adjusted data for Ang-I level

I analysed Ang-I level after adjustment to total protein. Similar to Ang-I unadjusted data, the median for Ang-I protein adjusted level was lower in AD group (median= 4601 (pg/mg total protein)) compared to the control group (median= 4762 (pg/mg total protein)). The Mann-Whitney test showed a significant difference between AD and controls (p= 0.012) (Figure 9.47 A). Kruskal-Wallis test showed no significant difference in the median between all groups (p= 0.366) when was assessed in relation to Braak tangle stages (0-II, III-IV, V-VI) (Figure 9.47 B).

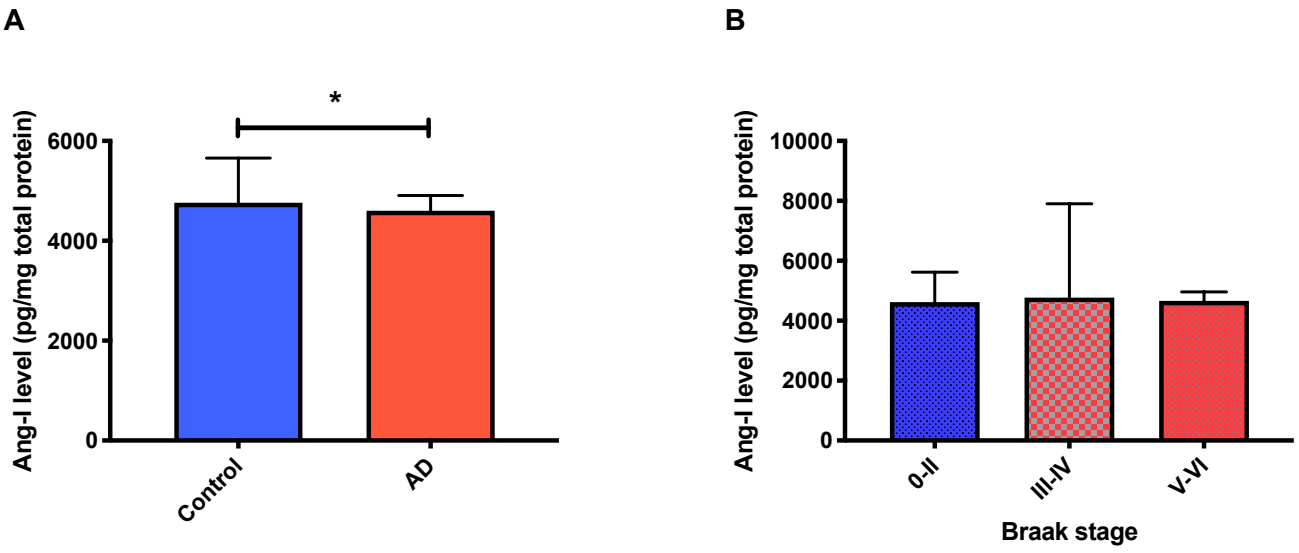

Figure 9.47. Measurement of Ang-I protein-adjusted level compared between controls and AD cases and in relation to Braak tangle stage.
A. Ang-I protein-adjusted level was reduced in AD (n= 70) compared with age-matched control (n= 48) in mid-frontal cortex. Mann-Whitney test revealed that Ang-I level was lower in AD (p= 0.012) compared to controls. The bars indicate the median and 95% confidence intervals. B. No variations were found between all groups (Braak stage 0-II (n= 36), Braak stage III-IV (n= 20), Braak stage V-VI (n= 61)) when analysed with Kruskal-Wallis test (p= 0.366). The bars indicate the median and 95% confidence intervals.

9.9.2 Correlation between Ang-I protein-adjusted level and AD pathological hallmarks

Ang-I protein-adjusted level was not correlated with both insoluble Aβ and tau load, Spearman's correlation coefficient test found no significant correlation between Ang-I protein-adjusted level and insoluble Aβ (Spearman's correlation coefficient, r= -0.2, p= 0.107) (Figure 9.48 A) and between tau load (Spearman's correlation coefficient, r= -0.016, p= 0.296) (Figure 9.48 B).

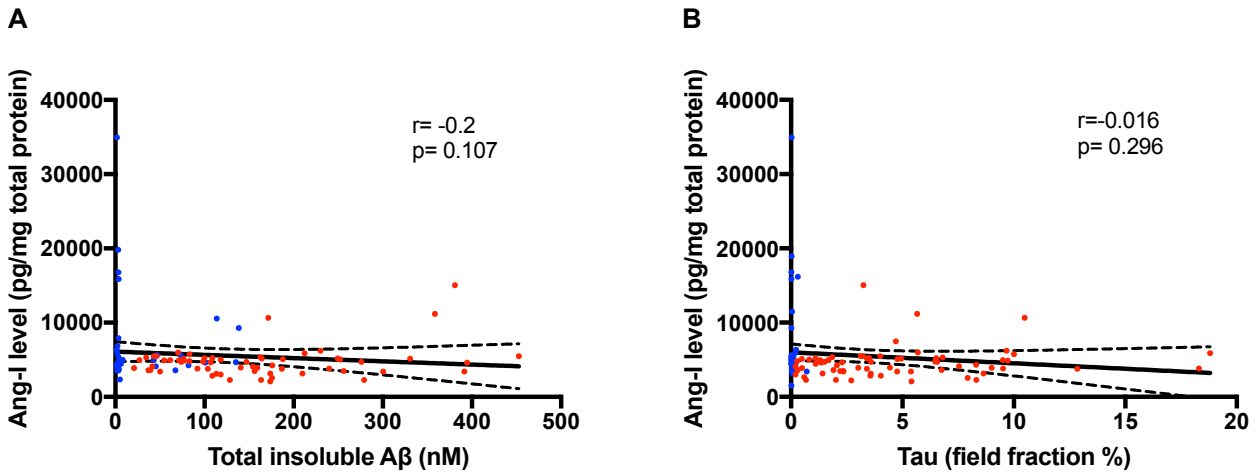

Figure 9.48. Correlation between Ang-I protein-adjusted level and AD pathological hallmarks (Aβ load and tau load). A. Scatterplots showing no relationship between Ang-I level and insoluble Aβ load (measured by enzyme-linked immunosorbent assay), Spearman's correlation coefficient test (r= -0.2, p= 0.107). B. Scatterplots showing no correlation between Ang-I protein-adjusted level and tau load (measured by field fraction analysis), Spearman's correlation coefficient test (r= -0.016, p= 0.296). The solid inner line indicates the best-fit linear regression and the outer lines the 95% confidence intervals. Blue dots= controls, red dots= AD cases.

9.9.3 Relationship between Ang-I protein-adjusted level and ACE-1 activity

Previous measurements of ACE-1 activity by FRET activity assay were available for controls (n= 43) and AD cases (n= 66). Spearman's correlation coefficient test shoed no significant correlation between Ang-I protein-adjusted level and ACE-1 activity (Spearman's correlation coefficient, r= -0.049, p= 0.616) (Figure 9.49).

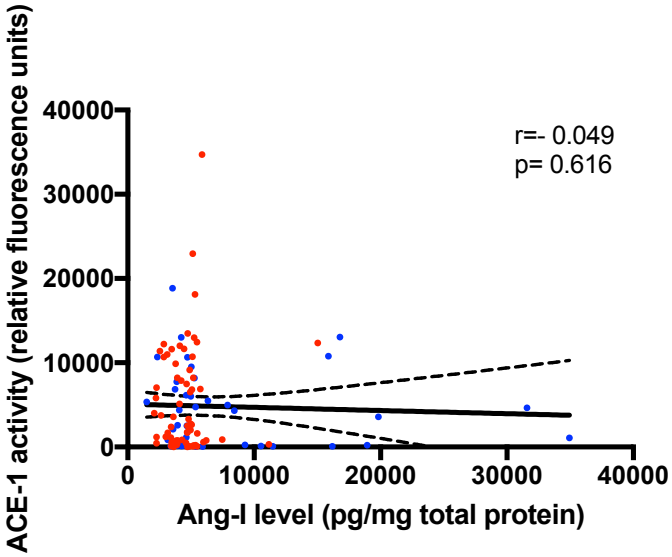

Figure 9.49. Correlation between Ang-I protein-adjusted level and ACE-1 activity.
Scatterplots showing no correlation between Ang-I protein-adjusted level and ACE-1 activity measured by FRET activity assay in mid-frontal cortex. Spearman's correlation coefficient test (r= -0.049, p= 0.616). The solid inner line indicates the best-fit linear regression and the outer lines the 95% confidence intervals. Blue dots= controls, red dots= AD cases.

9.10 Appendix X: Piloting the effect of hypoxia on MasR expression in SH-SY5Y neuroblastoma cells

We also modelled the effect of ischemia on MasR expression in neuronal SH-SY5Y cells cultured under hypoxic conditions (2% oxygen) for 24-hours.

9.10.1 Cell culture

SH-SY5Y neuroblastoma cells were cultured and maintained using standard conditions under aseptic conditions in T75 flasks as described previously in the method (section 2.11.2). Cells were seeded and cultured in T75 flasks until ~90% confluent. Prior to treatment of the cells with Aβ40 or Aβ42, the culture medium was replaced with serum-free medium and left to equilibrate for 4 hours, which was then replaced with SF medium containing either Aβ40 or Aβ42 (both at 1um), or serum-free (SF) medium alone (rPeptide). Aβ peptides stocks were dissolved in 35% acetonitrile at concentration of 1mM and stored at -20 until being diluted in SF medium immediately prior to addition to the cells. Duplicate flasks were prepared and then incubated overnight under standard culture conditions (5% CO_2 at 37 °C) (Normoxia) or 2% O_2 (Hypoxia) (using a Ruskin hypoxic chamber). At the end of the treatment, cell lysates were prepared in cell lysis buffer (CelLytic M reagent (Sigma-Aldrich) for western blotting as described in the method (section 2.11.4). Total protein concentrations of the cell

lysates were measured using the Total Protein Assay Kit (Sigma-Aldrich) as described in detail in method (section 2.3). Expression of MasR was tested by western blot, the standard protocol used is described in detail in method (section 2.4 and 4.4.3.1).

9.10.2 Expression of MasR in SH-SY5Y neuroblastoma cells

To test the feasibility of this pilot study I initially determined whether MasR was expressed in SH-SY5Y neuroblastoma cells. Western blot was used to probe SH-SY5Y cell lysates for the expression of MasR. A polyclonal rabbit antibody to MAS1 (Abcam, ab66030) was used to for the detection of MasR. A representative image showed three bands for MasR (Figure 9.50). One band between (35-37 kDa) was at the expected MW for MasR protein (440) and a second unidentified lower band at 20 kDa that possibly represents a protein degradation product. The third faint higher bands at 40 kDa could be a heterodimer of MasR and AT_2R that has been reported in previous studies (624, 625). Thus, MasR expression was detectable and levels were reduced in cell lysates that were diluted suggesting specificity of the antibody used.

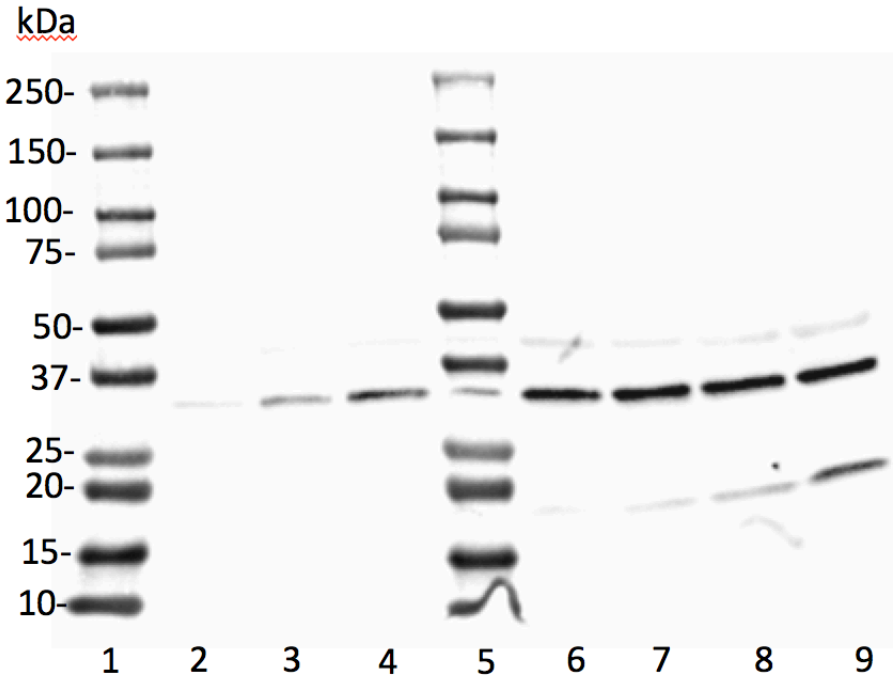

Figure 9.50 MasR western blot in SH-SY5Y neuroblastoma cell lysate.

MasR expression in SH-SY5Y neuroblastoma cell lysate was studied by Western blotting: Line 9 shows MasR expression in diluted sample (1:2) and (Line 8 to 2) show two fold serial dilution of cell lysates, bands intensity reduced with more diluted sample. Lines 1 and 5 include MW markers. The membrane was blotted with polyclonal rabbit antibody to MAS1 (Abcam, ab66030). The reported size of MasR was between (35-37 kDa). The smaller bands at MW 20 kDa are likely to be protein degradation products. The faint bands at MW 40 kDa, at a higher than the expected MW of MasR, could be a MasR/AT_2R heterodimer.

9.11 Appendix XI: Pilot investigations into the specificity of antibodies against the Angiotensin-type 1 and type-2 receptors

9.11.1 Abstract

The AT_1R and AT_2R are key components of the classical and regulatory axis of brain RAS. Activation of AT_1R promotes neurotoxic effects including vasoconstriction, inflammation, fibrosis, and hypertrophy. On the other hand, activation of AT_2R causes neuronal protective effects that counteract AT_1R activation. In AD, there is hyperactivity of the cRAS resulting in overproduction of Ang-II that via activation of AT_1R has been proposed to contribute to the pathogenesis of AD. Despite the suggested importance of these two receptors in AD, their expression remains poorly characterised in rodent models of AD and human brain tissue. It is therefore crucial to determine the expression of the AT_1R and AT_2R to better understand their role in AD. However, surprisingly, most commercially available AT_1R and AT_2R receptor antibodies have more recently been shown to be less specific than originally thought and do not to accurately discriminate between the two receptors. Therefore, accurate and specific characterisation of the two receptors in human brain tissue in AD is hampered and there is an urgent need for more specific antibodies within this area of research. In this chapter, I have begun to explore the specificity of several commercially available AT_1R and AT_2R antibodies to see if they hold potential for better characterisation of these receptors in AD.

Three commonly used and widely reported AT_1R antibodies (Alomone AAR-011; Santa Cruz sc-1173; Abcam 18801) have been found to be non-specific in the detection of AT_1R as they all showed cross-reactivity with AT_2R (626). These antibodies were also tested in another study in conjunction with three additional AT_1R antibodies (AT1 (306), rabbit polyclonal antibody, Santa Cruz sc-579; AT1, affinity purified rabbit polyclonal antibody, Millipore AB15552; (1E10-1A9) mouse monoclonal antibody, Abcam ab9391). Again, all of these antibodies showed cross-reactivity with AT_2R i.e. were nonspecific for AT_1R (627) despite the claims of the commercial providers.

Similarly, three commercially available AT_2R antibodies have been tested for specificity - two polyclonal antibodies (AT2 (H-143), rabbit Santa Cruz sc-9040; AT2, affinity purified rabbit Alomone AAR-012) and one monoclonal antibody (AT2, rabbit Epitomics Inc, 2818-1). Similar to the AT_1R antibodies all three AT_2R antibodies were unable to specifically detect AT_2R (628).

In this study, I have sought to extend these studies and examine the specificity of additional AT_1R and AT_2R antibodies.

These included three commercially available AT_1R antibodies:

a) Anti-AGTR1 polyclonal antibody (ThermoFisher, PA5-20812),

b) Anti-AGTR1 (Sigma-Aldrich, SAB3500209),

c) AT1 receptor polyclonal antibody (Enzo, BML-SA608))

and two AT_1aR antibodies (which are kindly gifted from Dr Atticus Hainsworth)

d) AT_1a non-selective receptor polyclonal antibody

e) AT_1a selective receptor polyclonal antibody

I also investigated one AT_2R antibody

f) Anti-Angiotensin II Type 2 Receptor antibody (Abcam, ab92445))

Specificity of these antibodies was determined in human embryo kidney (HEK) cells that were transfected to overexpress AT_1aR, AT_1bR and AT_2R (gifted from the Jeremy Henley Lab, University of Bristol). I also tested the specificity of a commercially available AT_2R sandwich ELISA kit (Human Angiotensin II Receptor 2 (AGTR2) ELISA, Cloud-Clone Corp.).

In this study, I demonstrate that none of the additional AT_1R antibodies tested were specific for AT_1R or AT_1aR as they showed cross-reactivity for AT_2R. In contrast, the anti-AT_2R antibody (Anti-Angiotensin II Type 2 Receptor antibody (Abcam, ab92445)) appeared to exhibit preferential binding to AT_2R in AT_2R-overexpressing HEK cell lysate suggesting potential specificity.

In conclusion, my studies indicate that the non-specific nature of all commercially available AT_1R antibodies is likely to result in unreliable characterisation of these receptors in previous and future studies. In contrast the Abcam, ab92445 antibody, holds some promise, at least for related research around the counteracting effects of AT_2R in cRAS function.

9.11.2 Introduction

The two major receptors in the brain RAS (AT_1R and AT_2R) have a crucial and contrasting role in the physiology and pathophysiology of AD. Ang-II mediates its effect mainly by binding to AT_1R, overactivity of AT_1R exacerbates tissue inflammation and oxidative stress (290), associated with hypertension and metabolic dysfunction (629, 630) and promotes cell death, neuronal injury and cognitive impairment (397). In contrast, activation of AT_2R exerts protective effects that counteract the signalling of AT_1R by inducing vasodilation, reducing inflammation and neuronal injury and inhibiting cellular growth, cell differentiation and apoptosis (631-634). Despite the great importance of these receptors, the exact role and balance of these receptors within the brain in AD remains unclear. This problem is mainly due to a lack of available antibodies that can successfully discriminate between AT_1R and AT_2R with genuine specificity.

AT_1R is a seven trans-membrane domain G-protein coupled receptor consisting of 359 amino acids with a molecular weight of approximately 41 kDa. There are two subtypes of AT_1R in rodents (AT_1aR and AT_1bR) that have a sequence homology of around 95% (499). This high degree of homology between these subtypes may result in difficulty of differentiation between them. Ang-II, the central effector of the cRAS, has a very high affinity for AT_1aR, which appears to be the main receptor for eliciting the effects of the cRAS (635).

In brain tissue, AT_1R is highly expressed in specific nuclei within the hypothalamus and brainstem areas, and is also expressed in neurons, astrocytes and microglia of the cortex, hippocampus and basal ganglia (246, 457). Dysregulation of AT_1R expression has been implicated in several pathophysiological conditions such as stroke (559, 560, 578), anxiety (636), Alzheimer's disease (366, 637, 638) and epilepsy (639, 640). Despite these extremely important functions of AT_1R, the accurate determination and localisation of this receptor in human post-mortem brain tissue and the potential dysregulation of its expression in relation to AD remains unclear. This issue is partly due to the lack of AT_1R antibodies that are specific and can successfully allow the discrimination of AT_1R from AT_2R. To date, a number of commercially available AT_1R antibodies originally proposed to be specific for AT_1R and used in previous studies have since been found to lack specificity for AT_1R– the authors of these studies strongly recommended the need to test the specificity of all antibodies against AT_1R prior to conducting any future studies (626, 627).

AT_2R is a seven trans-membrane domain G-protein coupled receptor consisting of 363 amino acids with a molecular weight of approximately 40 kDa. AT_2R shares only about 32-34% similar amino acid sequence homology with AT_1R (257). In addition to Ang-II, AT_2R has a high affinity to Ang-III and Ang (1-7) (427, 499). Activation of AT_2R elicits responses that counteract and help to regulate the actions of cRAS. AT_1R and AT_2R have been found to interact to form receptor complexes (heterodimer) both *in vitro* and *in vivo* regardless of Ang-II binding (641). This physiological cross-talk mechanism could be the potential cause of cross-reactivity between antibodies.

In brain tissue, expression of AT_2R has been found in the vascular wall and high densities are localised in brain areas involved in learning and motor function such as the amygdala, caudate putamen and thalamus (247, 499). In addition, AT_2R is expressed in neurons, astrocytes and microglia of the cortex, hippocampus and basal ganglia (246).

AT_1R and AT_2R expression may be inter-dependent: in AT_2R knockout mice for instance, there is increased expression of AT_1R in the brain (642). In addition, previous studies have showed that dysfunction of AT_2R detrimentally modulates brain morphology and is implicated in learning and memory dysfunction (385, 643). Together these studies highlight the regulatory role of AT_2R in the brain and the importance of accurately characterising the expression of this receptor particularly in AD. However, as for AT_1R, a previous study found that three of the commercially available antibodies against AT_2R are also non-specific and cross-react with AT_1R (628). Thus, testing the specificity of antibodies against AT_2R is also very important for studies aimed to characterise AT_2R receptor expression.

9.11.3 Study aims and hypothesis

The aims of the study described in this chapter were:

(i) To investigate the specificity of previously untested commercially available antibodies against AT_1R, AT_1aR and AT_2R.

(ii) To explore the specificity of a commercially available AT_2R sandwich ELISA kit.

We wished to identify AT_1R and AT_2R specific antibodies that will be useful as research tools to allow more accurate characterisation of these receptors in AD.

9.11.4 Methods

9.11.4.1 Study Samples

9.11.4.1.1 Transfected cell lysates

HEK cells that had been stably transfected to overexpress AT_1aR, AT_1bR and AT_2R were kindly provided by Prof. Jeremy Henley's lab (University of Bristol). I tested the specificity of several commercially available AT_1R and AT_2R antibodies to specifically detect AT_1R and AT_2R in HEK cell lines that were transfected with Green fluorescent protein (GFP) tagged or un-tagged AT_1aR, AT_1bR, AT_2R. Cell lysates were produced and total protein level within each cell lysates had been previously measured.

9.11.4.1.2 Exploration of AT_1R antibody specificity

In this study, three commercially available AT_1R antibodies were tested by western blotting: rabbit AGTR1 polyclonal antibody (ThermoFisher, PA5-20812), rabbit anti-AGTR1 (Sigma-Aldrich, SAB3500209), and rabbit anti-AT1 receptor polyclonal antibody (Enzo, BML-SA608). In addition, two AT_1aR antibodies were kindly gifted from Dr Atticus Hainsworth (St George's University of London). These included the rodent versions of AT_1R, a non-selective AT_1a receptor polyclonal antibody and an AT_1a selective receptor polyclonal antibody. Details of the primary and secondary antibodies are described previously in Appendix II: section 9.2.1 (Table 9.13 and Table 9.14 respectively). Further information on the immunogen, specificity and applications of the commercially available AT_1R antibodies is listed in Table 9.40.

Table 9.40 Characteristics of AT_1R and AT_2R antibodies used in this study

Antibody	Immunogen	Specificity	Application
AGTR1 polyclonal antibody (ThermoFisher, PA5-20812)	A 16 amino acid peptide near the centre of human AGTR1.	Human, Mouse, Rat	Immunocytochemistrey (ICC) Immunofluorescence (IF) Immunohistochemistry (IHC) Western Blot (WB)
Anti-AGTR1(Sigma-Aldrich, SAB3500209)	AGTR1 antibody was raised against a 16 amino acid peptide sequence near the centre of human AGTR1.	Human, Mouse, Rat	Immunofluorescence (IF) Immunohistochemistry (IHC) Western Blot (WB) Indirect enzyme-linked immunosorbent assay (ELISA)
AT1 receptor polyclonal antibody (Enzo, BML-SA608)	Synthetic peptide corresponding to amino acids 4-18 of human AT1.	Human, Mouse, Rat	Immunocytochemistrey (ICC) Western Blot (WB) Flow cytometry (FC)
Anti-Angiotensin II Type 2 Receptor antibody (Abcam, ab92445)	Synthetic peptide within human angiotensin II Type 2 Receptor amino acid sequence 300-400 (C terminal).	Human, Mouse, Rat	Western Blot (WB) Immunoprecipitation (IP)

9.11.4.2 Western blotting for AT1R

A standard protocol of the western blot procedure is described in detail in chapter 2 (section 2.4). In summary, for the detection of AT_1R in HEK cell lysate samples, the membrane was blocked in 10% milk/TBST buffer for 1 hour. After it had been washed with 0.05% TBST (3x 15 minutes) at room temperature on a shaker, the membrane was then incubated with either AGTR1 polyclonal antibody (ThermoFisher, PA5-20812) diluted 1:800, Anti-AGTR1 (Sigma-Aldrich, SAB3500209) diluted 1:800 or AT1 receptor polyclonal antibody (Enzo, BML-SA608) diluted 1:500 in 5% milk/TBST antibody buffer overnight at 4°C (in the fridge) on a shaker. Following a wash step with 0.05% TBST (3x 15 minutes) at room temperature on shaker, the membrane was incubated with a secondary antibody (peroxidase conjugated anti-Rabbit) diluted 1:5000 in 5% milk/TBST for 1 hour. After 3 x 15 minutes washing steps with 0.05% TBST, a chemiluminescent HRP substrate (ECL) (Millipore) was added to the membrane in a 1:1 ratio (5 ml of reagent 1 and 5 ml of reagent 2) for 5 minutes. The images then were acquired using ChemiDoc XRS+ and Image Lab software, version 0.5 (Bio-Rad).

9.11.4.3 Western blotting for AT1aR

For detection of AT_1aR in HEK cell lysate samples, the membrane was blocked in 10% milk/TBST buffer for 1 hour. After it had been washed with 0.05% TBST (3x 15 minutes) at room temperature on a shaker, the membrane was then incubated with either AT1a non-selective receptor polyclonal antibody diluted 1:1000 or AT1a selective receptor polyclonal antibody diluted 1:1000 in 5% milk/TBST antibody buffer overnight at 4°C (in the fridge) on a shaker. Following a wash step with 0.05% TBST (3x 15 minutes) at room temperature on a shaker, the membrane was incubated with a secondary antibody (peroxidase conjugated anti-Rabbit) diluted 1:5000 in 5% milk/TBST for 1 hour. After 3x 15 minutes wash steps with 0.05% TBST, a chemiluminescent HRP substrate (ECL) (Millipore) added to the membrane in a 1:1 ratio (5 ml of reagent 1 and 5 ml of reagent 2) for 5 minutes. The images then were acquired using ChemiDoc XRS+ and assessed using Image Lab software, version 0.5 (Bio-Rad).

9.11.4.4 Validation of AT_2R antibody specificity

A commercially available AT_2R antibody (Anti-Angiotensin II Type 2 Receptor antibody (Abcam, ab92445)) was tested by western blot in HEK cell lysates that overexpressed AT_1aR, AT_1bR and AT_2R. Details of the primary and secondary antibodies are described previously in Appendix II: section 9.2.1 (Table 9.13 and Table 9.14 respectively). Further information on immunogen, specificity and applications of the commercially available AT_2R antibody is listed in Table 10-40.

9.11.4.4.1 Western blotting for AT2R

A standard protocol for western blotting is described in detail in the general methods (section 2.4). In summary, for detection of AT_2R in HEK cell lysate samples, the membrane was blocked in 10% milk/TBST buffer for 1 hour. After it had been washed with 0.05% TBST (3x 15 minutes) at room temperature on a shaker, the membrane was then incubated with rabbit anti-angiotensin II type 2 receptor antibody (Abcam, ab92445) diluted 1:800 in 5% milk/TBST antibody buffer overnight at 4°C (in the fridge) on a shaker. Following a wash step with 0.05% TBST (3x 15 minutes) at room temperature on shaker, the membrane was incubated with a secondary antibody (peroxidase conjugated anti-Rabbit) diluted 1:5000 in 5% milk/TBST for 1 hour. After 3x 15 minutes wash steps with 0.05% TBST, a chemiluminescent HRP substrate (ECL) (Millipore) was added to the membrane in a 1:1 ratio (5 ml of reagent 1 and 5 ml of reagent 2) for 5 minutes. The images then were acquired using ChemiDoc XRS+ and assessed using Image Lab software, version 0.5 (Bio-Rad).

9.11.4.4.2 Human Angiotensin II Receptor 2 (AGTR2) ELISA

Recent studies have measured AT_2R level in different tissues (heart and kidney) using a commercially available ELISA kit (644, 645). I tested the specificity of the same ELISA kit used previously in order to validate its specificity for AT_2R in brain tissue. The concentration of AT_2R was measured in HEK cell lysates transfected to overexpress AT_1aR, AT_1bR and AT_2R using a commercially available quantitative sandwich ELISA kit for the detection of AT_2R (Cloud-Clone Corp.) Following the manufacturer's procedure, all reagents were allowed to reach room temperature before use. Recombinant AT_2R (10-0.156 ng/ml) and diluted cell lysates (1:10) in PBS (all 100 µl) were added to a microplate pre-coated with an antibody specific to AT_2R and incubated for 1 hour at 37°C.

Following five wash steps, 100 µl of detection reagent A was added to each well and incubated for 1 hour at 37°C. After another five wash steps, 100 µl of detection reagent B was added to each well and incubated for 30 minutes at 37°C. After a further set of washes, 90 µl of TMB substrate was added to each well and incubated for 10 minutes at 37°C in the dark. The reaction was stop by adding 50 µl of stop solution and the absorbance was measured immediately at 450nm using a FLUOstar OPTIMA plate reader (BMG labtech).

9.11.5 Results

9.11.5.1 Specificity of AT_1R antibodies

The western blots shown in the representative images below (Figure 9.51) show a similar pattern of immunoreactivity between each of the three commercial AT_1R antibodies tested: AGTR1 polyclonal antibody (ThermoFisher, PA5-20812); Anti-AGTR1 (Sigma-Aldrich, SAB3500209); AT1 receptor polyclonal antibody (Enzo, BML-SA608). For each antibody, a predominant band was observed at the anticipated approximate MW 50-60 kDa in HEK cell lysates that overexpressed AT_1aR and AT_1bR. In addition, several additional non-specific bands were identified at MW higher and lower than 50-60 kDa.

A similar pattern of bands was also identified in HEK cells that overexpressed AT_2R for each of the AT_1R targeting antibodies i.e. all three antibodies were unable to discriminate between AT_1R and AT_2R expression. We also used the antibody to probe for AT_1R in human post-mortem brain tissue (1 AD and 1 control). A dominant band was observed between 50-75 kDa as expected. There were additional bands in brain tissue that differed from HEK cells and were also different between AD and controls.

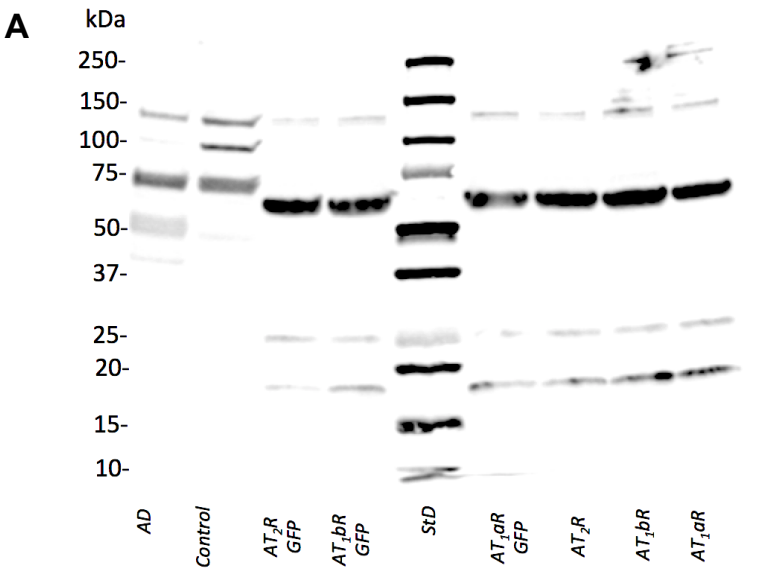

AGTR1 Poly clonal antibody (ThermoFisher, PA5-20812)

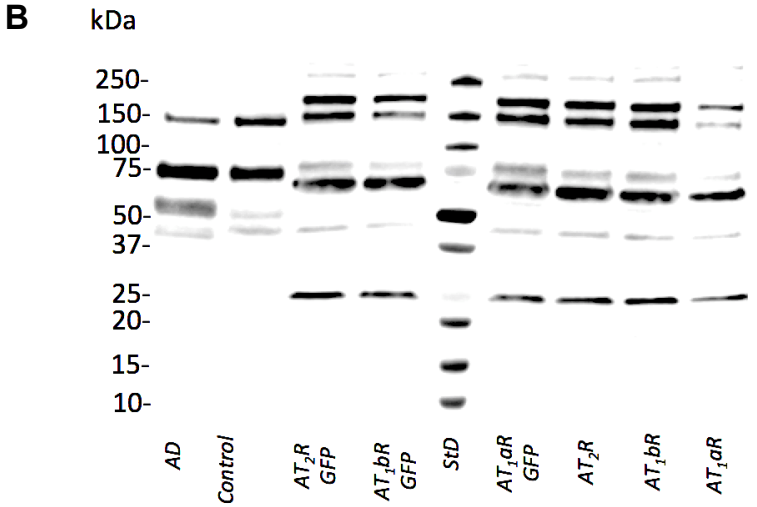

Anti-AGTR1 (Sigma-Aldrich,SAB3500209)

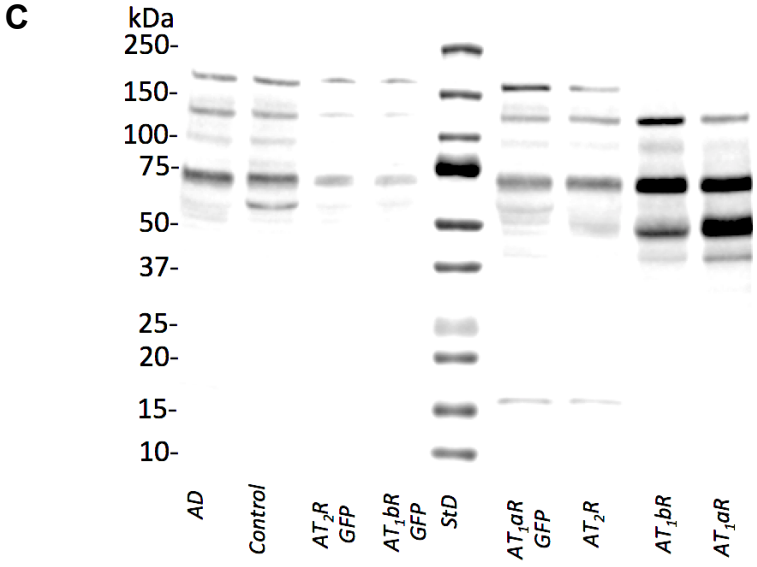

AT1 receptor polyclonal antibody (Enzo, BML-SA608)

Figure 9.51 Western blot of AT1R expression in HEK cell lysates and human post-mortem brain tissue.
AT_1R expression was studied by western blotting in HEK cell lysates transfected with GFP tagged AT_2R, AT_1bR, AT_1aR (lane 3,4 and 6), un-tagged AT_2R, AT_1bR, AT_1aR (lane 7,8,9) and human brain tissue from an AD case and non-disease control (lane 1 and 2). Lane (5) includes a MW marker. Each membrane was exposed to three different anti-AT_1R antibodies respectively: A. (AGTR1 polyclonal antibody (ThermoFisher, PA5-20812), the reported size of AT_1R was between 50-75 kDa and was detected in all samples. B. Anti-AGTR1 (Sigma-Aldrich, SAB3500209), the reported size of AT_1R was between 50-75 kDa and detected in all samples. C. AT1 receptor polyclonal antibody (Enzo, BML-SA608), the reported size of the AT_1R is about 50-75 kDa was detected in all samples. Several bands at different molecular sizes were also observed.

9.11.5.2 Exploring the specificity of AT_1aR antibodies

The specificity of two generously gifted AT_1aR antibodies was tested in HEK cells overexpressing AT_1aR, AT_1bR and AT_2R. We compared an AT_1a non-selective receptor polyclonal antibody and AT_1a selective receptor polyclonal antibody. The western blot images shown below (Figure 9.52) indicate that both antibodies detected a single band at the anticipated MW 50-60 kDa. However, a similar pattern of immunoreactivity was observed in all three HEK cell lysates indicating that both antibodies were unable to discriminate between AT_1aR and AT_1bR, and between AT1aR and AT_2R i.e. they are non-specific.

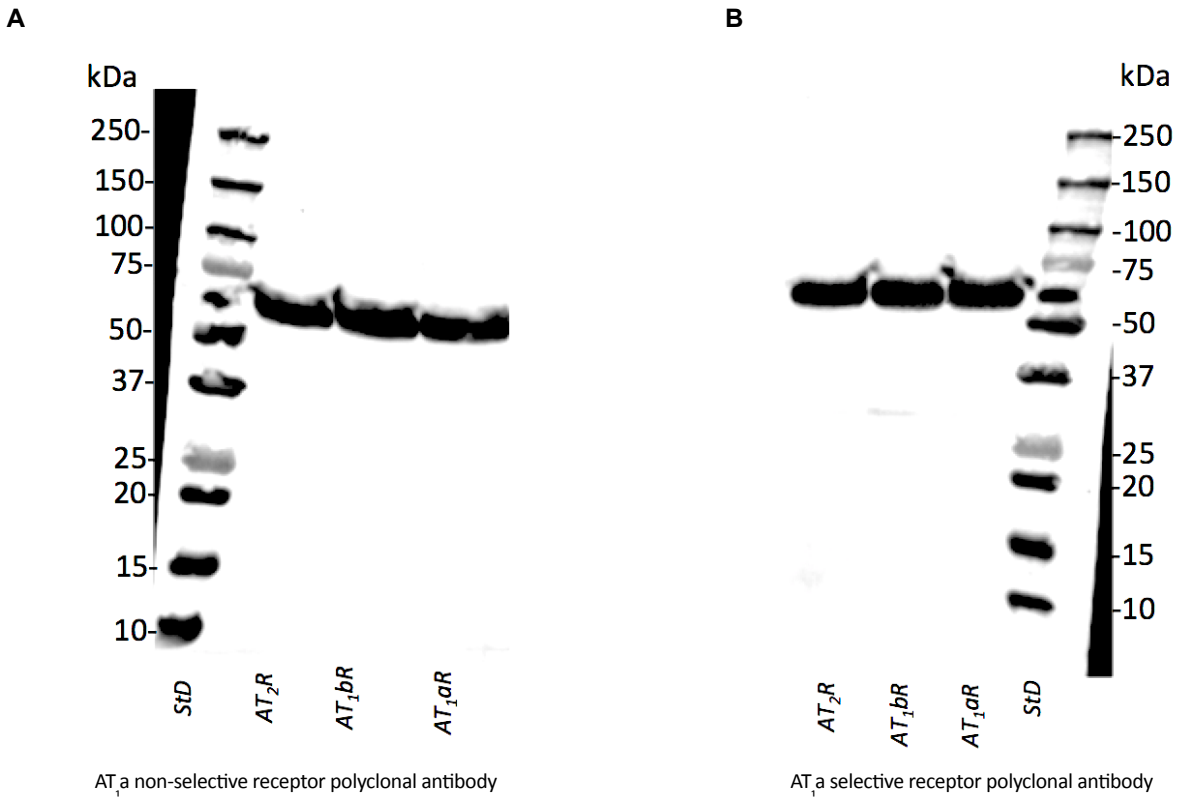

Figure 9.52 Western blot of AT_1aR expression in HEK cell lysates.
AT_1aR expression was tested by western blotting in HEK cell lysates transfected with AT_2R, AT_1bR and AT_1aR. The membranes were labelled with two different antibodies: A. AT_1a non-selective receptor polyclonal antibody, the reported size of AT_1R was between 50-60 kDa and detected in all samples (HEK cell lysates transfected with AT_2R (lane 2), AT_1bR (lane 3) and AT_1aR (lane 4), lane (1) include MW marker. B. AT_1a selective receptor polyclonal antibody, the reported size of AT_1R was between 50-60 kDa and detected in all samples (HEK cell lysates transfected with AT_2R (line 1), AT_1bR (lane 2) and AT_1aR (lane 3), lane (4) include MW marker. The AT_1aR antibodies were kindly gifted from Dr Atticus Hainsworth.

9.11.5.3 Exploration of the specificity of an AT_2R antibody

I also tested the specificity of a previously untested AT_2R antibody (Anti-Angiotensin II Type 2 Receptor antibody (Abcam, ab92445)). The western blot image shown below in (Figure 9.53) shows that the antibody detects a distinct prominent band at approximately the correct predicted molecular weight of ~30 kDa in HEK cells that overexpressed AT_2R-GFP tagged. The detected MW was lower than the expected MW of AT_2R at approximately 40 kDa, however, the expression of this band was noticeably higher in HEK-AT_2R cells compared to HEK-AT_1aR and AT_1bR cells. In addition, this AT_2R antibody detected faint bands at approximately the correct MW of ~30 kDa in human brain

tissue of control and AD case. Surprisingly no bands were observed in untagged HEK-AT_2R, AT_1aR and AT_1bR cells – the reason for this is unclear.

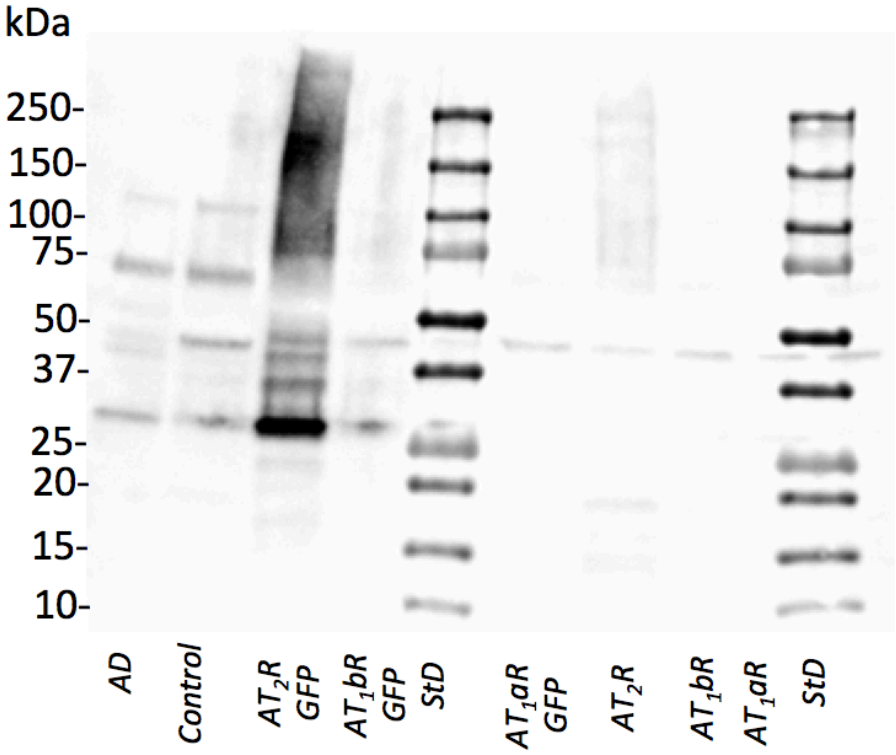

Figure 9.53 Western blot of AT_2R expression in HEK cell lysates.
AT_2R expression was studied by western blotting in HEK cell lysates transfected with GFP tagged AT_2R, AT_1bR, AT_1aR (lane 3,4 and 6), un-tagged AT_2R, AT_1bR, AT_1aR (lane 7, 8, 9) and human brain tissue of AD case and control (lane 1 and 2), lanes (5 and 10) include MW markers. The membrane was exposed to AT2 receptor monoclonal antibody (Abcam, ab92445). The antibody detected AT_2R in cell lysate transfected with AT2R-GFP and reported size of the AT_2R is about 27.9 kDa.

9.11.5.4 Investigating the specificity of Human Angiotensin II Receptor 2 (AGTR2) ELISA

The level of AT_2R was measured in HEK cells that overexpressed AT_1aR, AT_1bR and AT_2R using a commercially avaliable sandwich AT_2R ELISA kit (Cloud-Clone Corp.). We predicted that levels of AT_2R would be higher in HEK cells overexpressing AT_2R compared to the AT_1R (a and b) counterparts. However I detected a similar level of AT_2R in all HEK cell lysates, despite only one line over-expressing AT_2R. I found that the ELISA-measured AT_2R level in HEK cells that overexpressed AT_1aR= 2.473 ng/ml, HEK cell lysate that overexpressed AT_1bR= 3.07 ng/ml and AT_2R level in HEK cell lysate that overexpressed AT_2R= 3.003 ng/ml (Figure 9.54). These data suggest that the

commercially available ELISA is not specific as it was unable to discriminate between AT_1R and AT_2R.

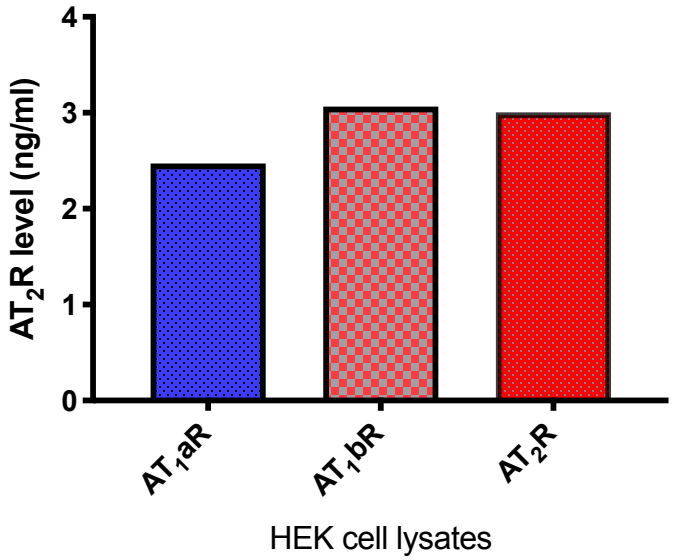

Figure 9.54 ELISA measured AT_2R level in HEK cell lysate overexpressing AT_1aR, AT_1bR and AT_2R.
Bar chart represents the level of AT_2R measured by sandwich ELISA kit (Cloud-Clone Corp. SEA973Hu) in HEK cell lysates transfected with either AT_1aR, AT_1bR or AT_2R. The measurements were performed once.

9.11.6 Discussion

In this chapter, I have investigated the specificity of three AT_1R antibodies, two AT_1aR antibodies (that are rodent sub-types of the human AT_1R), one AT_2R antibody, and a commercial AT_2R ELISA kit, none of which have any reported testing for specificity with a view to being tools for the study of RAS in AD. None of the AT_1R or AT_1aR antibodies were found to be specific and were unable to discriminate between AT_1R and AT_2R, or between AT_1aR and AT_1bR respectively in human tissue and individual HEK cell lines over-expressing AT_1aR, AT_1bR and AT_2R. The AT_2R antibody provided some preliminary and encouraging evidence that it may have selectivity for AT_2R, however, this needs further confirmation. In contrast the commercially available AT_2R sandwich ELISA was non-specific and did not detect a difference in expression of AT_2R compared to either AT_1R sub-types in HEK overexpressing cells. Together these findings indicate, in support of previous research on AT_1R and AT_2R antibodies (626-628) that most of the commercially available AT_1R and AT_2R

reagents are not specific and therefore using them to characterise these two important receptors may generate unreliable results.

These findings have important implications for RAS research in general but particularly at this exciting time in AD research. Given the importance of AT_1R as the main effector receptor of the cRAS and increased expression in several pathophysiological conditions, including AD (528), it has been surprising to find that the characterisation and selectivity of AT_1R antibodies used in most of the studies undertaken have not been validated. AT_1R expression has been reported to be increased in human brain tissue in AD using immunohistochemical staining (91) however, potential changes in the expression and distribution of the receptor has been limited by the lack of specific antibodies. A previous study characterised six commercially available antibodies by western blotting and immunohistochemistry in tissue extracts from AT_1aR knockout and wild-type mice and non-transfected hypothalamic cultured 4B cells with or without AT_1R expression. Their data revealed that none of the tested AT_1R antibodies met the criteria of specificity (627). In this study, I examined the specificity of another three commercially available AT_1R antibodies that have not been tested before.

My findings from western blots of HEK cells transfected with AT_1R, AT_1aR, AT_1bR and AT_2R, showed that all AT_1R antibodies tested recognised a major band at a higher MW between 50-75 kDa consistent with the expected molecular weight of AT_1R. The MW of AT_1R is influenced by the glycosylation level (626). In addition, the AT_1R antibodies detected several additional bands at molecular sizes higher and lower than the major predominant band. Together these data indicate that these antibodies are non-specific and did not follow two of the characterised criteria for specificity of antibodies that state: (i) that antibodies immunoreactivity should correlate with the degree of receptor expression (646, 647), and (ii) that antibodies must detect single bands of appropriate molecular weight. The similar pattern of immunoreactivity of AT_1R antibodies observed could be explained by similar immunogen properties of the antigen, which as seen in (Table 10.40) are all based on the centre area of AT_1R involving the same region of overlapping residues, against which all the three antibodies are raised. My results extend and further support previous studies reporting that commercially available AT_1R antibodies are non-specific and generate unreliable characterisation of this important receptor (626, 627, 648). Both AT_1aR antibodies tested in my study recognized a distinct band at the approximate MW between 50-60 kDa in cells that individually overexpressed AT_1aR, AT_1bR and AT_2R. These results indicate that these AT_1aR antibodies are also non-specific and unfortunately did not discriminate between the two AT_1R subtypes. This could be attributed to the high degree of homology (~95%) between AT_1aR and AT_1bR.

I tested one AT_2R antibody (anti-Angiotensin II Type 2 Receptor antibody (Abcam, ab92445)) that has been used in several studies (649-653). Although, to our knowledge, the specificity of this antibody has not been tested (628), I found that it detected a single band only in cell lysates from HEK cells that overexpressed AT_2R, suggesting that this antibody exhibited specificity against AT_2R. However, the detected band was at a molecular size lower than the expected weight for AT_2R (around 40 kDa) (499). The observed band at an unexpected lower MW could potentially result from cleavage of the GFP tagged protein - a weak fusion linker used in the transfection step (654, 655). In contrast, the commercially available AT_2R sandwich ELISA tested failed to detect a significant difference in the expression of AT_2R and AT_1R in overexpressing HEK cells. This ELISA kit has been used in previous studies that have aimed to measure levels of AT_2R in different tissues (644, 645) - our results indicate that such measurements may have been inaccurate and that there is a need for more rigorous testing and validation of commercially available AT_1R and AT_2R antibodies and kits prior to them being used in research studies.

My results support previous reports suggesting that AT_1R antibodies are non-specific. However, my investigations discussed in this chapter have some limitations which were due to limitations in the time available. This study was limited by characterising the specificity of AT_1R and AT_2R antibodies using just one methodological approach (western blot). Another limitation of this study was that the selected AT_1R antibodies were raised against similar domains of the receptor. Further experimental investigations could be used to further test the specificity of the AT_1R and AT_2R antibodies, or at least of the AT_2R antibody that showed some promising evidence of specificity. Additional and more sensitive methods that could be used are competitive radioligand binding assays and quantitative real-time PCR of the gene within cells to verify whether there is the likelihood or receptor expression. The cross-reactivity between AT_1R and AT_2R is surprising given the low % sequence homology (~35%) but these receptors are now known to form homo- and heterodimers with each other and other RAS receptors (MasR and AT_4R) which adds an additional level of complexity and difficulty to overcome. Perhaps, development of technology such as RNAscope together with immunofluorescence will be able to map the distribution on these receptors with confidence in future studies.

In conclusion, this study highlights that there is ongoing need to identify more specific antibodies or alternative approaches to map the distribution and expression of AT_1R and AT_2R in AD and other diseases in which RAS is involved. These findings, along with previous studies highlight the need for cautious scepticism around the reported specificity of commercially available antibodies and kits to avoid generating unreliable results and the need for undertaking meaningful internal validation.

Are the commercially available AT_1R and AT_2R antibodies specific to detect these receptors?

AT_1R and AT_2R are the main effector receptors of the cRAS axis, however, the expression and distribution of these major angiotensin receptors remains unclear within the brain due in part to a lack of specific antibodies (528, 626). In this thesis, I have undertaken pilot studies to examine the specificity of three new commercially available AT_1R antibodies, two AT_1aR antibodies, one AT_2R antibody and one commercially available AT_2R sandwich ELISA kit. I have used HEK cells that have been transfected to overexpress AT_1aR, AT_1bR and AT_2R as the primary test source to explore the specificity of the receptor antibodies using Western blotting.

My findings indicate that none of the tested AT_1R antibodies tested were able to discriminate between AT_1R, AT_1aR and AT_2R. In contrast, I present preliminary encouraging evidence that the AT_2R antibody tested has potential selectivity for AT_2R, however, this needs further confirmation. The AT_2R ELISA kit was also unable to discriminate between HEK cells overexpressing AT_2R and AT_1R variants. Together my findings further support previous studies reporting that several other commercially available AT_1R and AT_2R antibodies are non-specific and thus potentially lead to unreliable and mis-leading characterisation of these important receptors in human and rodent brain tissue across different models of disease (626-628, 648). Some of problems with specificity could be attributed to the homology that exists between AT_1R and AT_2R or the dimerization between these receptors, and the high degree of homology between AT_1aR and AT_1bR (around 95%). My findings indicate that better tools are required to allow detailed characterisation of AT_1R and AT_2R - an urgent requirement in the field that needs more attention in future work. One potential method that could be used to provide some way of getting additional corroborating evidence would be the use of RNA scope and immunofluorescence labelling of receptors to discriminate between AT_1R and AT_2R expression in brain tissue. The characterisation of AT_1R and AT_2R in brain tissue in AD remains an ongoing issue that needs to be overcome and will likely provide hugely important insights into the role of RAS in AD.

References

1. Mehan S, Arora R, Sehgal V, Sharma D, Sharma G. Dementia – A Complete Literature Review on Various Mechanisms Involves in Pathogenesis and an Intracerebroventricular Streptozotocin Induced Alzheimer's Disease. Inflammatory Diseases – Immunopathology, Clinical and Pharmacological Bases, Dr Mahin Khatami (Ed). 2012.
2. Cunningham ELM, B., Herron B, Passmore AP. Dementia. Ulster Med J 2015;84(2):79-87.
3. Winblad B, Amouyel P, Andrieu S, Ballard C, Brayne C, Brodaty H, et al. Defeating Alzheimer's disease and other dementias: a priority for European science and society. Lancet Neurol. 2016;15(5):455-532.
4. Alzheimer's Association. Alzheimer's disease facts and figures. Alzheimers Dement. 2018;14(3):367-429.
5. Cipriani G, Dolciotti C, Picchi L, Bonuccelli U. Alzheimer and his disease: a brief history. Neurol Sci. 2011;32(2):275-9.
6. Caselli RJ, Beach TG, Knopman DS, Graff-Radford NR. Alzheimer Disease: Scientific Breakthroughs and Translational Challenges. Mayo Clin Proc. 2017;92(6):978-94.
7. Alzheimer's Society UK 2015 [Available from: http://bit.ly/1jf4vBm.
8. Kalaria R. Similarities between Alzheimer's disease and vascular dementia. J Neurol Sci. 2002;203-204:29-34.
9. Smith EE. Clinical presentations and epidemiology of vascular dementia. Clin Sci (Lond). 2017;131(11):1059-68.
10. Pendlebury ST, Rothwell PM. Prevalence, incidence, and factors associated with pre-stroke and post-stroke dementia: a systematic review and meta-analysis. . Lancet Neurol. 2009;8(11):1006-18.
11. Jellinger KA. Pathology and pathogenesis of vascular cognitive impairment-a critical update. Front Aging Neurosci. 2013;5:17.
12. Skrobot OA, O'Brien J, Black S, Chen C, DeCarli C, Erkinjuntti T, et al. The Vascular Impairment of Cognition Classification Consensus Study. Alzheimers Dement. 2017;13(6):624-33.
13. Skrobot OA, Black SE, Chen C, DeCarli C, Erkinjuntti T, Ford GA, et al. Progress toward standardized diagnosis of vascular cognitive impairment: Guidelines from the Vascular Impairment of Cognition Classification Consensus Study. Alzheimers Dement. 2018;14(3):280-92.
14. McKeith IG, Mosimann UP. Dementia with Lewy bodies and Parkinson's disease. Parkinsonism Relat Disord. 2004;10 Suppl 1:S15-8.

15. Emre M. Treatment of dementia associated with Parkinson's disease. Parkinsonism Relat Disord. 2007;13:S457-S61.
16. Love S. Neuropathological investigation of dementia: a guide for neurologists. J Neurol Neurosurg Psychiatry. 2005;76 Suppl 5:v8-14.
17. Langa KM, Foster NL, Larson EB. mixed dementia emerging concepts and therapeutic implications. JAMA. 2004;292(23):2901-8.
18. Schneider JA, Arvanitakis Z, Bang W, Bennett dA. Mixed brain pathologies account for most dementia cases in community-dwelling older persons. Neurology. 2007;69(24):2197-204.
19. Raz L, Knoefel J, Bhaskar K. The neuropathology and cerebrovascular mechanisms of dementia. J Cereb Blood Flow Metab. 2016;36(1):172-86.
20. Pan X, Chen X. Clinic, neuropathology and molecular genetics of frontotemporal dementia: a mini-review. Transl Neurodegener. 2013;2:8.
21. Rabinovici GD, Miller BL. Frontotemporal lobar degeneration: epidemiology, pathophysiology, diagnosis and management. CNS Drugs. 2010;24(5):375-98.
22. Nichols E, Szoeke CEI, Vollset SE, Abbasi N, Abd-Allah F, Abdela J, et al. Global, regional, and national burden of Alzheimer's disease and other dementias, 1990–2016: a systematic analysis for the Global Burden of Disease Study 2016. Lancet Neurol. 2019;18(1):88-106.
23. WHO, Dementia 2019 [Available from: https://www.who.int/news-room/fact-sheets/detail/dementia.
24. Prince M, Wimo A, Guerchet M, Ali MG-C, Wu Y-T, Prina M. World Alzheimer report. The global impact of dementia. ADI. 2015.
25. Ahmadi-Abhari S, Guzman-Castillo M, Bandosz P, Shipley MJ, Muniz-Terrera G, Singh-Manoux A, et al. Temporal trend in dementia incidence since 2002 and projections for prevalence in England and Wales to 2040: modelling study. BMJ. 2017;358:j2856.
26. Matthews FE, Arthur A, Barnes LE, Bond J, Jagger C, Robinson L, et al. A two-decade comparison of prevalence of dementia in individuals aged 65 years and older from three geographical areas of England: results of the Cognitive Function and Ageing Study I and II. Lancet. 2013;382(9902):1405-12.
27. Matthews FE, Stephan BC, Robinson L, Jagger C, Barnes LE, Arthur A, et al. A two decade dementia incidence comparison from the Cognitive Function and Ageing Studies I and II. Nat Commun. 2016;7:11398.
28. Joshi A, Ringman JM, Lee AS, Juarez KO, Mendez MF. Comparison of clinical characteristics between familial and non-familial early onset Alzheimer's disease. J Neurol. 2012;259(10):2182-8.

29. Reitz C, Mayeux R. Alzheimer disease: epidemiology, diagnostic criteria, risk factors and biomarkers. Biochem Pharmacol. 2014;88(4):640-51.
30. Serrano-Pozo A, Frosch MP, Masliah E, Hyman BT. Neuropathological alterations in Alzheimer disease. Cold Spring Harb Perspect Med. 2011;1(1):a006189.
31. Perl DP. Neuropathology of Alzheimer's disease. Mt Sinai J Med. 2010;77(1):32-42.
32. Iwatsubo T, Odaka A, Suzuki N, Mizusawa H, Nukina N, Ihara Y. Visualization of A beta 42(43) and A beta 40 in senile plaques with ends-specific A beta monoclonals: evidence that an initially deposited species is A beta 42(43). Neuron. 1994;13(1):45-53.
33. Wippold FJ, 2nd, Cairns N, Vo K, Holtzman DM, Morris JC. Neuropathology for the neuroradiologist: plaques and tangles. AJNR Am J Neuroradiol. 2008;29(1):18-22.
34. Bayer TA, Wirths O. Intracellular accumulation of amyloid-Beta - a predictor for synaptic dysfunction and neuron loss in Alzheimer's disease. Front Aging Neurosci. 2010;2:8.
35. Barage SH, Sonawane KD. Amyloid cascade hypothesis: Pathogenesis and therapeutic strategies in Alzheimer's disease. Neuropeptides. 2015;52:1-18.
36. Hasegawa M. Molecular Mechanisms in the Pathogenesis of Alzheimer's disease and Tauopathies-Prion-Like Seeded Aggregation and Phosphorylation. Biomolecules. 2016;6(2).
37. Roy S, Zhang B, Lee VM, Trojanowski JQ. Axonal transport defects: a common theme in neurodegenerative diseases. Acta Neuropathol. 2005;109(1):5-13.
38. Tucker RP. The roles of microtubule-associated proteins in brain morphogenesis: a review. Brain Res Rev. 1990;15:101-20.
39. Go ̈tz J, Chen F, van Dorpe J, Nitsch RM. Formation of Neurofibrillary
Tangles in P301L Tau
Transgenic Mice Induced by Aβ42 Fibrils. Science. 2001;293:1491-5.
40. De Felice FG, Wu D, Lambert MP, Fernandez SJ, Velasco PT, Lacor PN, et al. Alzheimer's disease-type neuronal tau hyperphosphorylation induced by A beta oligomers. Neurobiol Aging. 2008;29(9):1334-47.
41. Jin M, Shepardson N, Yang T, Chen G, Walsh D, Selkoe DJ. Soluble amyloid beta-protein dimers isolated from Alzheimer cortex directly induce Tau hyperphosphorylation and neuritic degeneration. Proc Natl Acad Sci U S A. 2011;108(14):5819-24.
42. Love S, Nicoll AJ, Hughes A, Wilcock GK. APOE and cerebral amyloid angiopathy in the elderly. Neuroreport. 2003;14(11):1535-6.
43. Love S, Chalmers K, Ince P, Esiri M, Attems J, Jellinger K, et al. Development, appraisal, validation and implementation of a consensus protocol for the assessment of cerebral amyloid angiopathy in post-mortem brain tissue. Am J Neurodegener Dis. 2014;3(1):19-32.

44. Ghiso J, Tomidokoro Y, Revesz T, Frangione B, Rostagno A. Cerebral Amyloid Angiopathy And ALzheimer's Disease. Hirosaki Igaku 2010;61 (Suppl):S111–S24.

45. Love S, Miners JS. Cerebrovascular disease in ageing and Alzheimer's disease. Acta Neuropathol. 2016;131(5):645-58.

46. Hardy J, Selkoe DJ. The Amyloid Hypothesis of Alzheimer's Disease:
Progress and Problems on the Road to Therapeutics. Science. 2002;297:353-6.

47. Chen JX, Yan SS. Role of mitochondrial amyloid-beta in Alzheimer's disease. J Alzheimers Dis. 2010;20 Suppl 2:S569-78.

48. Selkoe DJ, Hardy J. The amyloid hypothesis of Alzheimer's disease at 25 years. EMBO Mol Med. 2016;8(6):595-608.

49. Bateman RJ, Xiong C, Benzinger TL, Fagan AM, Goate A, Fox NC, et al. Clinical and biomarker changes in dominantly inherited Alzheimer's disease. N Engl J Med. 2012;367(9):795-804.

50. Jack CR, Wiste HJ, Botha H, Weigand SD, Therneau TM, Knopman DS, et al. The bivariate distribution of amyloid-beta and tau: relationship with established neurocognitive clinical syndromes. Brain. 2019;142(10):3230-42.

51. Gralle M, Ferreira ST. Structure and functions of the human amyloid precursor protein: the whole is more than the sum of its parts. Prog Neurobiol. 2007;82(1):11-32.

52. Kang J, Lemaire H-G, Unterbeck A, Salbaum JM, Masters CL, Grzeschikt K-H, et al. The precursor of Alzheimer's disease amyloid A4 protein resembles a cell-surface receptor. Nature. 1987;325:733-6.

53. Vassar R, Bennett BD, Babu-Khan S, Kahn S, Mendiaz EA, Denis P, et al. β-Secretase Cleavage of Alzheimer's Amyloid Precursor Protein by the Transmembrane Aspartic Protease BACE. Science. 1999;286(5440):735-41.

54. Allinson TM, Parkin ET, Turner AJ, Hooper NM. ADAMs Family Members As Amyloid Precursor Protein □-Secretase
. J Neurosci Res. 2003;74:342-52.

55. Kimberly WT, LaVoie MJ, Ostaszewski BL, Ye W, Wolfe MS, Selkoe DJ. Gamma-secretase is a membrane protein complex comprised of presenilin, nicastrin, Aph-1, and Pen-2. Proc Natl Acad Sci U S A. 2003;100(11):6382-7.

56. Kehoe PG, Miners S, Love S. Angiotensins in Alzheimer's disease - friend or foe? Trends Neurosci. 2009;32(12):619-28.

57. Scheuner D, Eckman C, Jensen M, Song X, Citron M, Suzuki N, et al. Secreted amyloid ~-protein similar to that in the senile plaques of Alzheimer1s disease is increased in vivo by the presenilin 1 and 2 and APP mutations linked to familial Alzheimer1s disease. Nat Med. 1996;2(8):864-70.

58. Shen J, Kelleher RJ, III. The presenilin hypothesis of Alzheimer's disease: evidence for a loss-of-function pathogenic mechanism. Proc Natl Acad Sci U S A. 2007;104(2):403-9.

59. Glabe CG. Common mechanisms of amyloid oligomer pathogenesis in degenerative disease. Neurobiol Aging. 2006;27(4):570-5.

60. Glabe CG. Structural classification of toxic amyloid oligomers. J Biol Chem. 2008;283(44):29639-43.

61. Walsh DM, Selkoe DJ. A beta oligomers - a decade of discovery. J Neurochem. 2007;101(5):1172-84.

62. Murphy MP, LeVine H, 3rd. Alzheimer's disease and the amyloid-beta peptide. J Alzheimers Dis. 2010;19(1):311-23.

63. Zou K, Kim D, Kakio A, Byun K, Gong JS, Kim J, et al. Amyloid beta-protein (Abeta)1-40 protects neurons from damage induced by Abeta1-42 in culture and in rat brain. J Neurochem. 2003;87(3):609-19.

64. Haass C, Selkoe DJ. Soluble protein oligomers in neurodegeneration: lessons from the Alzheimer's amyloid beta-peptide. Nat Rev Mol Cell Biol. 2007;8(2):101-12.

65. Palop JJ, Mucke L. Amyloid-beta-induced neuronal dysfunction in Alzheimer's disease: from synapses toward neural networks. Nat Neurosci. 2010;13(7):812-8.

66. Welander H, Franberg J, Graff C, Sundstrom E, Winblad B, Tjernberg LO. Abeta43 is more frequent than Abeta40 in amyloid plaque cores from Alzheimer disease brains. J Neurochem. 2009;110(2):697-706.

67. Saito T, Suemoto T, Brouwers N, Sleegers K, Funamoto S, Mihira N, et al. Potent amyloidogenicity and pathogenicity of Abeta43. Nat Neurosci. 2011;14(8):1023-32.

68. Kim J, Onstead L, Randle S, Price R, Smithson L, Zwizinski C, et al. Abeta40 inhibits amyloid deposition in vivo. J Neurosci. 2007;27(3):627-33.

69. Huang Y, Mucke L. Alzheimer mechanisms and therapeutic strategies. Cell. 2012;148(6):1204-22.

70. Weller RO, Massey A, Kuo Y, Roher AE. Cerebral Amyloid Angiopathy: Accumulation of Aβ in Interstitial Fluid Drainage Pathways in Alzheimer’s Disease. Ann N Y Acad Sci. 2000;903:110-7.

71. Yoon SS, Jo SA. Mechanisms of Amyloid-beta Peptide Clearance: Potential Therapeutic Targets for Alzheimer's Disease. Biomol Ther (Seoul). 2012;20(3):245-55.

72. Wyss-Coray T. Inflammation in Alzheimer disease: driving force, bystander or beneficial response? Nat Med. 2006;12(9):1005-15.

73. Sagare AP, Deane R, Zetterberg H, Wallin A, Blennow K, Zlokovic BV. Impaired lipoprotein receptor-mediated peripheral binding of plasma amyloid-beta is an early biomarker for mild cognitive impairment preceding Alzheimer's disease. J Alzheimers Dis. 2011;24(1):25-34.

74. Sehgal N, Gupta A, Valli RK, Joshi SD, Mills JT, Hamel E, et al. Withania somnifera reverses Alzheimer's disease pathology by enhancing low-density lipoprotein receptor-related protein in liver. Proc Natl Acad Sci U S A. 2012;109(9):3510-5.

75. Miners JM, Barua N, Kehoe PG, Gill S, Love S. Aβ-Degrading Enzymes: Potential for Treatment of Alzheimer Disease. J Neuropathol Exp Neurol. 2011;70(11):944-59.

76. Miners JS, Helmond ZV, Chalmers K, Wilcock G, Love S, Kehoe PG. Decreased Expression and Activity of Neprilysin in Alzheimer Disease Are Associated With Cerebral Amyloid Angiopathy. J Neuropathol Exp Neurol. 2006;65(10):1012-21.

77. Miners JS, Kehoe PG, Love S. Immunocapture-based fluorometric assay for the measurement of insulin-degrading enzyme activity in brain tissue homogenates. J Neurosci Methods. 2008;169(1):177-81.

78. Miners JS, Ashby E, Van Helmond Z, Chalmers KA, Palmer LE, Love S, et al. Angiotensin-converting enzyme (ACE) levels and activity in Alzheimer's disease, and relationship of perivascular ACE-1 to cerebral amyloid angiopathy. Neuropathol Appl Neurobiol. 2008;34(2):181-93.

79. Liu S, Liu J, Miura Y, Tanabe C, Maeda T, Terayama Y, et al. Conversion of Abeta43 to Abeta40 by the successive action of angiotensin-converting enzyme 2 and angiotensin-converting enzyme. J Neurosci Res. 2014;92(9):1178-86.

80. Nalivaeva NN, Beckett C, Belyaev ND, Turner AJ. Are amyloid-degrading enzymes viable therapeutic targets in Alzheimer's disease? J Neurochem. 2012;120 Suppl 1:167-85.

81. Hu J, Igarashi A, Kamata M, Nakagawa H. Angiotensin-converting enzyme degrades Alzheimer amyloid beta-peptide (A beta); retards A beta aggregation, deposition, fibril formation; and inhibits cytotoxicity. J Biol Chem. 2001;276(51):47863-8.

82. Oba R, Igarashi A, Kamata M, Nagata K, Takano S, Nakagawa H. The N-terminal active centre of human angiotensin-converting enzyme degrades Alzheimer amyloid beta-peptide. Eur J Neurosci. 2005;21(3):733-40.

83. Zou K, Yamaguchi H, Akatsu H, Sakamoto T, Ko M, Mizoguchi K, et al. Angiotensin-converting enzyme converts amyloid beta-protein 1-42 (Abeta(1-42)) to Abeta(1-40), and its inhibition enhances brain Abeta deposition. J Neurosci. 2007;27(32):8628-35.

84. Kehoe PG, Russ C, McIlroy S, Williams H, Holmans P, Holmes C, et al. Variation in DCP1, encoding ACE, is associated with susceptibility to Alzheimer disease. Nature America Inc. 1999;21:71-2.

85. Narain Y, Yip A, Murphy T, Brayne C, Easton D, Evans JG, et al. The ACE gene and Alzheimer's disease susceptibility. J Med Genet 2000;37:695-7.

86. Kehoe PG, Katzov H, Feuk L, Bennet AM, Johansson B, Wiman B, et al. Haplotypes extending across ACE are associated with Alzheimer's disease. Hum Mol Genet. 2003;12(8):859-67.

87. Kehoe PG, Katzov H, Andreasen N, Gatz M, Wilcock GK, Cairns NJ, et al. Common variants of ACE contribute to variable age-at-onset of Alzheimer's disease. Hum Genet. 2004;114(5):478-83.

88. Elkins JS, Douglas VC, Johnston SC. Alzheimer disease risk and genetic variation in ACE A meta-analysis. Neurology. 2004;62:363–8.

89. Lehmann DJ, Cortina-Borja M, Warden DR, Smith AD, Sleegers K, Prince JA, et al. Large meta-analysis establishes the ACE insertion-deletion polymorphism as a marker of Alzheimer's disease. Am J Epidemiol. 2005;162(4):305-17.

90. Miners JS, Helmond ZV, Raiker M, Love S, Kehoe PG. ACE variants and association with brain Aβ levels in Alzheimer's disease

. Am J Transl Res 2011;3(1):73-80.

91. Savaskana E, Hockb C, Olivieria G, Bruttela S, Rosenbergc C, Hulette C, et al. Cortical alterations of angiotensin converting enzyme, angiotensin II and AT1 receptor in Alzheimer's dementia. Neurobiol Aging. 2001;22:541-6.

92. He M, Ohrui T, Maruyama M, Tomita N, Nakayama K, Higuchi M, et al. ACE activity in CSF of patients with mild cognitive impairment and Alzhimer disease. Neurology. 2006;67(7):1309-10.

93. Forman MS, Trojanowski JQ, Lee VM-Y. Neurodegenerative diseases: a decade of discoveries paves the way for therapeutic breakthroughs. Nat Med. 2004;10(10):1055-63.

94. Eftekharzadeh B, Daigle JG, Kapinos LE, Coyne A, Schiantarelli J, Carlomagno Y, et al. Tau Protein Disrupts Nucleocytoplasmic Transport in Alzheimer's Disease. Neuron. 2018;99(5):925-40 e7.

95. Du X, Wang X, Geng M. Alzheimer's disease hypothesis and related therapies. Transl Neurodegener. 2018;7:2.

96. Braak H, Braak E. Diagnostic Criteria for Neuropathologic Assessment of Alzheimer's Disease. Neurobiol Aging. 1997;18(S4):S85-S8.

97. Morris M, Maeda S, Vossel K, Mucke L. The many faces of tau. Neuron. 2011;70(3):410-26.

98. Engel T, Hernandez F, Avila J, Lucas JJ. Full reversal of Alzheimer's disease-like phenotype in a mouse model with conditional overexpression of glycogen synthase kinase-3. J Neurosci. 2006;26(19):5083-90.

99. Jembrek M, Babić M, Pivac N, Hof P, Šimić G. Hyperphosphorylation of tau by GSK-3β in Alzheimer's disease: The interaction of Aβ and sphingolipid mediators as a therapeutic target. Transl Neurosci. 2013;4(4).

100. Jin N, Yin X, Yu D, Cao M, Gong CX, Iqbal K, et al. Truncation and activation of GSK-3beta by calpain I: a molecular mechanism links to tau hyperphosphorylation in Alzheimer's disease. Sci Rep. 2015;5:8187.

101. Lee VM, Goedert M, Trojanowski JQ. Neurodegenerative tauopathies. Annu Rev Neurosci. 2001;24:1121-59.

102. Lewis J, Dickson DW, Lin W, Chisholm L, Corral A, Jones G, et al. Enhanced Neurofibrillary Degeneration in Transgenic Mice Expressing Mutant Tau and APP. Science. 2001;293(5534):1487-91.

103. Oddo S, Caccamo A, Kitazawa M, Tseng BP, LaFerla FM. Amyloid deposition precedes tangle formation in a triple transgenic model of Alzheimer's disease. Neurobiol Aging. 2003;24(8):1063-70.

104. Hu X, Li X, Zhao M, Gottesdiener A, Luo W, Paul S. Tau pathogenesis is promoted by Aβ1-42 but not Aβ1-40. Mol Neurodegener. 2014;9(52).

105. Braak H, Thal DR, Ghebremedhin E, Tredici KD. Stages of the Pathologic Process in Alzheimer Disease: Age Categories From 1 to 100 Years. J Neuropathol Exp Neurol. 2011;70(11):960-9.

106. Nunes-Tavares N, Santos LE, Stutz B, Brito-Moreira J, Klein WL, Ferreira ST, et al. Inhibition of choline acetyltransferase as a mechanism for cholinergic dysfunction induced by amyloid-beta peptide oligomers. J Biol Chem. 2012;287(23):19377-85.

107. Bartus RT, Dean III RL, Beer B, Lipp AS. The Cholinergic Hypothesis of GeriatricMemory Dysfunction. Science. 1982;217(4558):408-14.

108. Haam J, Yakel JL. Cholinergic modulation of the hippocampal region and memory function. J Neurochem. 2017;142 Suppl 2:111-21.

109. Lieo A, Greenberg SM, Growdon JH. Current pharmacotherapy for Alzheimer’s disease. Annu Rev Med. 2006;57:513-33.

110. de la Torre JC, Mussivand T. Can disturbed brain microcirculation cause Alzheimer’s disease? Neurol Res. 1993;15(3):146-53.

111. Grammas P, Tripathy D, Sanchez A, Yin X, Luo J. Brain microvasculature and hypoxia-related proteins in Alzheimer’s disease. Int J Clin Exp Pathol 2011;4(6):616-27.

112. Kalaria RN, Akinyemi R, Ihara M. Does vascular pathology contribute to Alzheimer changes? J Neurol Sci. 2012;322(1-2):141-7.

113. Kelleher RJ, Soiza RL. Evidence of endothelial dysfunction in the development of Alzheimer’s disease:

Is Alzheimer’s a vascular disorder? Am J Cardiovasc Dis. 2013;3(4):197-226.

114. Bell RD, Winkler EA, Sagare AP, Singh I, LaRue B, Deane R, et al. Pericytes control key neurovascular functions and neuronal phenotype in the adult brain and during brain aging. Neuron. 2010;68(3):409-27.

115. Qiu L, Ng G, Tan EK, Liao P, Kandiah N, Zeng L. Chronic cerebral hypoperfusion enhances Tau hyperphosphorylation and reduces autophagy in Alzheimer's disease mice. Sci Rep. 2016;6(23964).
116. Kalaria RN. Vascular basis for brain degeneration: faltering controls and risk factors for dementia. Nutr Rev. 2010;68 Suppl 2:S74-87.
117. Zlokovic BV. Neurovascular pathways to neurodegeneration in Alzheimer's disease and other disorders. Nat Rev Neurosci. 2011;12(12):723-38.
118. Iturria-Medina Y, Sotero RC, Toussaint PJ, Mateos-Perez JM, Evans AC, Alzheimer's Disease Neuroimaging I. Early role of vascular dysregulation on late-onset Alzheimer's disease based on multifactorial data-driven analysis. Nat Commun. 2016;7:11934.
119. Tuppo EE, Arias HR. The role of inflammation in Alzheimer's disease. Int J Biochem Cell Biol. 2005;37(2):289-305.
120. Bolos M, Perea JR, Avila J. Alzheimer's disease as an inflammatory disease. Biomol Concepts. 2017;8(1):37-43.
121. Guerreiro R, Bilgic B, Guven G, Bras J, Rohrer J, Lohmann E, et al. Novel compound heterozygous mutation in TREM2 found in a Turkish frontotemporal dementia-like family. Neurobiol Aging. 2013;34(12):2890 e1-5.
122. Colonna M, Wang Y. TREM2 variants: new keys to decipher Alzheimer disease pathogenesis. Nat Rev Neurosci. 2016;17(4):201-7.
123. Song W, Hooli B, Mullin K, Jin SC, Cella M, Ulland TK, et al. Alzheimer's disease-associated TREM2 variants exhibit either decreased or increased ligand-dependent activation. Alzheimers Dement. 2017;13(4):381-7.
124. Salter MW, Stevens B. Microglia emerge as central players in brain disease. Nat Med. 2017;23(9):1018-27.
125. Hong S, Beja-Glasser VF, Nfonoyim BM, Frouin A, Li S, Ramakrishnan S, et al. Complement and microglia mediate early synapse loss in Alzheimer mouse models. Science. 2016;352(6286):712-6.
126. Paolicelli RC, Jawaid A, Henstridge CM, Valeri A, Merlini M, Robinson JL, et al. TDP-43 Depletion in Microglia Promotes Amyloid Clearance but Also Induces Synapse Loss. Neuron. 2017;95(2):297-308 e6.
127. McGeer PL, McGeer EG. Targeting microglia for the treatment of Alzheimer’s disease. Expert Opin Ther Targets. 2015;19(4):497-506.
128. Bronzuoli MR, Iacomino A, Steardo L, Scuderi C. Targeting neuroinflammation in Alzheimer's disease. J Inflamm Res. 2016;9:199-208.
129. Jevtic S, Sengar AS, Salter MW, McLaurin J. The role of the immune system in Alzheimer disease: Etiology and treatment. Ageing Res Rev. 2017;40:84-94.

130. Guerreiro R, Bras J. The age factor in Alzheimer's disease. Genome Med. 2015;7:106.

131. Riedel BC, Thompson PM, Brinton RD. Age, APOE and sex: Triad of risk of Alzheimer's disease. J Steroid Biochem Mol Biol. 2016;160:134-47.

132. Masters CL, Bateman R, Blennow K, Rowe CC, Sperling RA, Cummings JL. Alzheimer's disease. Nat Rev Dis Primers. 2015;1:15056.

133. Lanoiselee HM, Nicolas G, Wallon D, Rovelet-Lecrux A, Lacour M, Rousseau S, et al. APP, PSEN1, and PSEN2 mutations in early-onset Alzheimer disease: A genetic screening study of familial and sporadic cases. PLoS Med. 2017;14(3):e1002270.

134. Patterson C, Feightner JW, Garcia A, Hsiung GY, MacKnight C, Sadovnick AD. Diagnosis and treatment of dementia: 1. Risk assessment and primary prevention of Alzheimer disease. CMAJ. 2008;178(5):548-56.

135. Nizzari M, Thellung S, Corsaro A, Villa V, Pagano A, Porcile C, et al. Neurodegeneration in Alzheimer disease: role of amyloid precursor protein and presenilin 1 intracellular signaling. J Toxicol. 2012;2012:187297.

136. Corder EH, Saunders AM, Strittmatter WJ, Schmechel DE, Gaskell PC, Small GW, et al. Gene dose of apolipoprotein E type 4 allele and the risk of Alzheimer’s disease in late onset families. Science. 1993;261(5123):921-3.

137. Raber J, Huang Y, Ashford JW. ApoE genotype accounts for the vast majority of AD risk and AD pathology. Neurobiol Aging. 2004;25(5):641-50.

138. Genin E, Hannequin D, Wallon D, Sleegers K, Hiltunen M, Combarros O, et al. APOE and Alzheimer disease: a major gene with semi-dominant inheritance. Mol Psychiatry. 2011;16(9):903-7.

139. Leduc V, Jasmin-Belanger S, Poirier J. APOE and cholestrol homeostasis in Alzheimer’s disease. Trends Mol Med. 2010;16(10):469-77.

140. Mahley RW, Weisgraber KH, Huang Y. Apolipoprotein E: structure determines function, from atherosclerosis to Alzheimer's disease to AIDS. J Lipid Res. 2009;50 Suppl:S183-8.

141. Saunders AM, Strittmatter WJ, Schmechel D, George-Hyslop PH, Pericak-Vance MA, Joo SH, et al. Association of apolipoprotein E allele epsilon 4 with late-onset familial and sporadic Alzheimer’s disease. Neurology. 1993;43(8):1467-72.

142. Kuusisto J, Koivisto K, Kervinen K, Mykkanen L, Helkala E-L, Vanhanen M, et al. Association of apolipoproteinE phenotypes with late onset Alzheimer'sdisease:population based study. BMJ. 1994;309:636-368.

143. Reiman EM, Chen K, Liu X, Bandy D, Yu M, Lee W, et al. Fibrillar amyloid-beta burden in cognitively normal people at 3 levels of genetic risk for Alzheimer's disease. Proc Natl Acad Sci U S A. 2009;106(16):6820-5.

144. Villemagne VL, Pike KE, Chetelat G, Ellis KA, Mulligan RS, Bourgeat P, et al. Longitudinal assessment of Abeta and cognition in aging and Alzheimer disease. Ann Neurol. 2011;69(1):181-92.
145. Moffat SD, Szekely CA, Zonderman AB, Kabani NJ, Resnick SM. Longotudinal change in hippocampal volume as a function of apolipoprotein E genotype. Neurology. 2000;55(1):134-6.
146. Lambert JC, Heath S, Even G, Campion D, Sleegers K, Hiltunen M, et al. Genome-wide association study identifies variants at CLU and CR1 associated with Alzheimer's disease. Nat Genet. 2009;41(10):1094-9.
147. Harold D, Abraham R, Hollingworth P, Sims R, Gerrish A, Hamshere ML, et al. Genome-wide association study identifies variants at CLU and PICALM associated with Alzheimer's disease. Nat Genet. 2009;41(10):1088-93.
148. Hollingworth P, Harold D, Sims R, Gerrish A, Lambert JC, Carrasquillo MM, et al. Common variants at ABCA7, MS4A6A/MS4A4E, EPHA1, CD33 and CD2AP are associated with Alzheimer's disease. Nat Genet. 2011;43(5):429-35.
149. Naj AC, Jun G, Beecham GW, Wang LS, Vardarajan BN, Buros J, et al. Common variants at MS4A4/MS4A6E, CD2AP, CD33 and EPHA1 are associated with late-onset Alzheimer's disease. Nat Genet. 2011;43(5):436-41.
150. Lambert JC, Ibrahim-Verbaas CA, Harold D, Naj AC, Sims R, Bellenguez C, et al. Meta-analysis of 74,046 individuals identifies 11 new susceptibility loci for Alzheimer's disease. Nat Genet. 2013;45(12):1452-8.
151. Seshadri S, Fitzpatrick AL, Ikram MA, DeStefano AL, Gudnason V, Boada M, et al. Genome-wide analysis of genetic loci associated with Alzheimer disease. JAMA. 2010;303(18):1832-40.
152. Lee JH, Cheng R, Barral S, Reitz C, Medrano M, Lantigua R, et al. Identification of novel loci for Alzheimer disease and replication of CLU, PICALM, and BIN1 in Caribbean Hispanic individuals. Arch Neurol. 2011;68(3):320-8.
153. Kunkle BW, Grenier-Boley B, Sims R, Bis JC, Naj AC, Boland A, et al. Genetic meta-analysis of diagnosed Alzheimer's disease identifies new risk loci and implicates Aβ, tau, immunity and lipid processing. Nat Genet. 2019;51(3):414-30.
154. Meng Y, Baldwin CT, Bowirrat A, Waraska K, Inzelberg R, Friedland RP, et al. Association of Polymorphisms in the Angiotensin-Converting Enzyme Gene with Alzheimer Disease in an Israeli Arab Community. Am J Hum Genet. 2006;78:871-7.
155. Achouri-Rassas A, Ali NB, Cherif A, Fray S, Siala H, Zakraoui NO, et al. Association between ACE polymorphism, cognitive phenotype and APOE E4 allele in a Tunisian population with Alzheimer’s disease. J Neural Transm (Vienna). 2016;123(3):317-21.

156. Beydoun MA, Beydoun HA, Gamaldo AA, Teel A, Zonderman AB, Wang Y. Epidemiologic studies of modifiable factors associated with cognition and dementia: systematic review and meta-analysis. BMC Public Health. 2014;14:643.

157. Anstey KJ, Cherbuin N, Budge M, Young J. Body mass index in midlife and late-life as a risk factor for dementia: a meta-analysis of prospective studies. Obes Rev. 2011;12(5):e426-37.

158. Vagelatos NT, Eslick GD. Type 2 diabetes as a risk factor for Alzheimer's disease: the confounders, interactions, and neuropathology associated with this relationship. Epidemiol Rev. 2013;35:152-60.

159. Debette S, Seshadri S, Beiser A, Au R, Himali JJ, Palumbo C, et al. Midlife vascular risk factor exposure accelerates structural brain aging and cognitive decline. Neurology. 2011;77:461-8.

160. Solomon A, Kivipelto M, Wolozin B, Zhou J, Whitmer RA. Midlife serum cholesterol and increased risk of Alzheimer's and vascular dementia three decades later. Dement Geriatr Cogn Disord. 2009;28(1):75-80.

161. Sun X, He G, Qing H, Zhou W, Dobie F, Cai F, et al. Hypoxia facilitates Alzheimer's disease pathogenesis by up-regulating BACE1 gene expression. Proc Natl Acad Sci U S A. 2006;103(49):18727-32.

162. Kennelly SP, Lawlor BA, Kenny RA. Blood pressure and dementia - a comprehensive review. Ther Adv Neurol Disord. 2009;2(4):241-60.

163. Goldstein FC, Levey AI, Steenland NK. High blood pressure and cognitive decline in mild cognitive impairment. J Am Geriatr Soc. 2013;61(1):67-73.

164. Lobanova I, Qureshi AI. The association between cardiovascular risk factors and progressive hippocampus volume loss in persons with Alzheimer’s disease. JVIN. 2014;14:52-5.

165. Cifuentes D, Poittevin M, Dere E, Broqueres-You D, Bonnin P, Benessiano J, et al. Hypertension accelerates the progression of Alzheimer-like pathology in a mouse model of the disease. Hypertension. 2015;65(1):218-24.

166. Barnes LL, Bennett DA. Alzheimer's disease in African Americans: risk factors and challenges for the future. Health Aff (Millwood). 2014;33(4):580-6.

167. Gardner RC, Burke JF, Nettiksimmons J, Kaup A, Barnes DE, Yaffe K. Dementia risk after traumatic brain injury vs nonbrain trauma: the role of age and severity. JAMA Neurol. 2014;71(12):1490-7.

168. Ownby RL, Crocco E, Acevedo A, John V, Loewenstein D. Depression and risk for Alzheimer disease: systematic review, meta-analysis, and metaregression analysis. Arch Gen Psychiatry. 2006;63(5):530-8.

169. Diniz BS, Butters MA, Albert SM, Dew MA, Reynolds CF, 3rd. Late-life depression and risk of vascular dementia and Alzheimer's disease: systematic review and meta-analysis of community-based cohort studies. Br J Psychiatry. 2013;202(5):329-35.
170. Chang WP, Liu ME, Chang WC, Yang AC, Ku YC, Pai JT, et al. Sleep apnea and the risk of dementia: a population-based 5-year follow-up study in Taiwan. PLoS One. 2013;8(10):e78655.
171. Chen PL, Lee WJ, Sun WZ, Oyang YJ, Fuh JL. Risk of dementia in patients with insomnia and long-term use of hypnotics: a population-based retrospective cohort study. PLoS One. 2012;7(11):e49113.
172. Rolland Y, Abellan van Kan G, Vellas B. Physical activity and Alzheimer's disease: from prevention to therapeutic perspectives. J Am Med Dir Assoc. 2008;9(6):390-405.
173. Smith PJ, Blumenthal JA. Diet and Neurocognition: Review of Evidence and Methodological Considerations. Curr Aging Sci. *2010*;*3*(1):57-66.
174. Lourida I, Soni M, Thompson-Coon J, Purandare N, Lang IA, Ukoumunne OC, et al. Mediterranean Diet, Cognitive Function, and Dementia A Systematic Review. Epidemiology. 2013;24(4):479-89.
175. Morris MC, Tangney CC, Wang Y, Sacks FM, Bennett DA, Aggarwal NT. MIND diet associated with reduced incidence of Alzheimer's disease. Alzheimers Dement. 2015;11(9):1007-14.
176. Scarmeas N, Levy G, Tang M-X, Manly J, Stern Y. Influence of leisure activity on the incidence of Alzheimer’s Disease
. Neurology. 2001;26(12):2236-42.
177. Valenzuela M, Scachdev P. Can cognitive excercise prevent the onset of dementia? Systematic review of randomized clinical trials with longitudinal follow-up. Am J Geriatr Psychiatry. 2009;17(3):179-87.
178. Karp A, Paillard-Borg S, Wang HX, Silverstein M, Winblad B, Fratiglioni L. Mental. physical and social components in leisure activities equally contribute to decrease dementia risk. Dement Geriatr Cogn Disord. 2006;21(2):65-73.
179. Vertesi A, Lever JA, Molloy DW, Sanderson B, Tuttle I, Pokoradi L, et al. Standardized Mini-Mental State Examination
Use and interpretation. Can Fam Physician. 2001;47:2018-23.
180. Chapman KR, Bing-Canar H, Alosco ML, Steinberg EG, Martin B, Chaisson C, et al. Mini Mental State Examination and Logical Memory scores for entry into Alzheimer's disease trials. Alzheimers Res Ther. 2016;8:9.

181. Trzepacz PT, Hochstetler H, Wang S, Walker B, Saykin AJ, Alzheimer's Disease Neuroimaging I. Relationship between the Montreal Cognitive Assessment and Mini-mental State Examination for assessment of mild cognitive impairment in older adults. BMC Geriatr. 2015;15:107.

182. Karas G, Scheltens P, Rombouts S, van Schijndel R, Klein M, Jones B, et al. Precuneus atrophy in early-onset Alzheimer's disease: a morphometric structural MRI study. Neuroradiology. 2007;49(12):967-76.

183. Klunk WE, Engler H, Nordberg A, Wang Y, Blomqvist G, D.P. H, et al. Imaging Brain Amyloid in Alzheimer's Disease with Pittsburgh Compound-B. Ann Neurol. 2004;55(3):306-19.

184. Camus V, Payoux P, Barre L, Desgranges B, Voisin T, Tauber C, et al. Using PET with 18F-AV-45 (florbetapir) to quantify brain amyloid load in a clinical environment. Eur J Nucl Med Mol Imaging. 2012;39(4):621-31.

185. Colloby SJ, Taylor JP, Firbank MJ, McKeith IG, Williams ED, O'Brien JT. Covariance 99mTc-exametazime SPECT patterns in Alzheimer's disease and dementia with Lewy bodies: utility in differential diagnosis. J Geriatr Psychiatry Neurol. 2010;23(1):54-62.

186. Ewers M, Zhong Z, Burger K, Wallin A, Blennow K, Teipel SJ, et al. Increased CSF-BACE 1 activity is associated with ApoE-epsilon 4 genotype in subjects with mild cognitive impairment and Alzheimer's disease. Brain. 2008;131(Pt 5):1252-8.

187. Olsson B, Lautner R, Andreasson U, Ohrfelt A, Portelius E, Bjerke M, et al. CSF and blood biomarkers for the diagnosis of Alzheimer's disease: a systematic review and meta-analysis. Lancet Neurol. 2016;15(7):673-84.

188. McKhann GM, Knopman DS, Chertkow H, Hyman BT, Jack CR, Jr., Kawas CH, et al. The diagnosis of dementia due to Alzheimer's disease: recommendations from the National Institute on Aging-Alzheimer's Association workgroups on diagnostic guidelines for Alzheimer's disease. Alzheimers Dement. 2011;7(3):263-9.

189. Montine TJ, Phelps CH, Beach TG, Bigio EH, Cairns NJ, Dickson DW, et al. National Institute on Aging-Alzheimer's Association guidelines for the neuropathologic assessment of Alzheimer's disease: a practical approach. Acta Neuropathol. 2012;123(1):1-11.

190. Hyman BT, Phelps CH, Beach TG, Bigio EH, Cairns NJ, Carrillo MC, et al. National Institute on Aging-Alzheimer's Association guidelines for the neuropathologic assessment of Alzheimer's disease. Alzheimers Dement. 2012;8(1):1-13.

191. Rogers SL, Doody RS, Mohs RC, Friedhoff LT. Donepezil improves cognition and global function in alzheimer disease: a 15-week, double-blind, placebo-controlled study. Donepezil Study Group. Arch Intern Med. 1998;158(9):1021-31.

192. Rösler M, Anand R, Cicin-Sain A, Gauthier S, Agid Y, Dal-Bianco P, et al. Efficacy and safety of rivastigmine in patients with Alzheimer's disease: international randomised controlled trial. BMJ. 1999;318:633-40.
193. Raskind MA, Peskind ER, Wessel T, Yuan W. Galantamine in AD: A 6-month randomized, placebo-controlled trial with a 6-month extension. Te Galantamine USA-1 Study Group. Neurology. 2000;54(12):2261-8.
194. Reisberg B, Doody R, Stoffler A, Schmitt F, Ferris S, Mobius HJ, et al. Memantine in moderate-to-severe Alzheimer's disease. N Engl J Med. 2003;348(14):1333-41.
195. Han JY, Besser LM, Xiong C, Kukull WA, Morris JC. Cholinesterase Inhibitors May Not Benefit Mild Cognitive Impairment and Mild Alzheimer Disease Dementia. Alzheimer Dis Assoc Disord. 2019;33(2):87-94.
196. Knapp M, King D, Romeo R, Adams J, Baldwin A, Ballard C, et al. Cost-effectiveness of donepezil and memantine in moderate to severe Alzheimer's disease (the DOMINO-AD trial). Int J Geriatr Psychiatry. 2017;32(12):1205-16.
197. Cummings JL, Morstorf T, Zhong K. Alzheimer's disease drug-development pipeline: few candidates, frequent failures. Alzheimers Res Ther. 2014;6(37).
198. Cummings J, Lee G, Mortsdorf T, Ritter A, Zhong K. Alzheimer's disease drug development pipeline: 2017. Alzheimers Dement (N Y). 2017;3(3):367-84.
199. Groot C, Hooghiemstra AM, Raijmakers PG, van Berckel BN, Scheltens P, Scherder EJ, et al. The effect of physical activity on cognitive function in patients with dementia: A meta-analysis of randomized control trials. Ageing Res Rev. 2016;25:13-23.
200. Farina N, Tabet N, Rusted J. Habitual physical activity (HPA) as a factor in sustained executive function in Alzheimer-type dementia: a cohort study. Arch Gerontol Geriatr. 2014;59(1):91-7.
201. Aguirre E, Woods RT, Spector A, Orrell M. Cognitive stimulation for dementia: a systematic review of the evidence of effectiveness from randomised controlled trials. Ageing Res Rev. 2013;12(1):253-62.
202. Alagiakrishnan K, McCracken P, Feldman H. Treating vascular risk factors and maintaining vascular health: is this the way towards successful cognitive ageing and preventing cognitive decline? Postgrad Med J. 2006;82(964):101-5.
203. McGuinness B, Tood S, Passmore P, Bullock R. Blood pressure lowering in patients without prior cerebrovascular disease for prevention of cognitive impairment and dementia. Cochrane Database syst Rev. 2009;7(4):CD004034.

204. Power MC, Weuve J, Gagne JJ, McQueen MB, Viswanathan A, Blacker D. The association between blood pressure and incident Alzheimer disease: a systematic review and meta-analysis. Epidemiology. 2011;22(5):646-59.

205. Elias MF, Wolf PA, D'Agostino RB, Cobb J, White LR. Untreated Blood Pressure Level Is Inversely Related to Cognitive Functioning: The Framingham Study. AJE. 1993;138(6):353-64.

206. Launer LJ, Ross GW, Petrovitchc H, Masaki K, Foley D, White LR, et al. Midlife blood pressure and dementia: the Honolulu–Asia aging study. Neurobiol Aging. 2000;21:94-55.

207. Elias MF, Elias PK, Sullivan LM, Wolf PA, D'Agostino RB. Lower cognitive function in the presence of obesity and hypertension: the Framingham heart study. Int J Obes Relat Metab Disord. 2003;27(2):260-8.

208. Kuo HK, Jones RN, Milberg WP, Tennstedt S, Talbot L, Morris JN, et al. Effect of blood pressure and diabetes mellitus on cognitive and physical functions in older adults: a longitudinal analysis of the advanced cognitive training for independent and vital elderly cohort. J Am Geriatr Soc. 2005;53(7):1154-61.

209. Tzourio C. Hypertension, cognitive decline, and
dementia: an epidemiological perspective. Dialogues Clin Neurosci. 2007;9:61-70.

210. Waldstein SR, Rice SC, Thayer JF, Najjar SS, Scuteri A, Zonderman AB. Pulse pressure and pulse wave velocity are related to cognitive decline in the Baltimore Longitudinal Study of Aging. Hypertension. 2008;51(1):99-104.

211. Gifford KA, Badaracco M, Liu D, Tripodis Y, Gentile A, Lu Z, et al. Blood pressure and cognition among older adults: a meta-analysis. Arch Clin Neuropsychol. 2013;28(7):649-64.

212. Skoog I, Lernfelt B, Landahl S, Palmertz B, Andreasson LA, Nilsson L, et al. 15-year longitudinal study of blood pressure and dementia. Lancet. 1996;347(9009):1141-5.

213. Qiu C, Winblad B, Viitanen M, Fratiglioni L. Pulse pressure and risk of Alzheimer disease in persons aged 75 years and older: a community-based, longitudinal study. Stroke. 2003;34(3):594-9.

214. Kivipelto M, Helkala E-L, Laakso MP, Hänninen T, Hallikainen M, Alhainen K, et al. Midlife vascular risk factors and Alzheimer's disease in later life: longitudinal, population based study. BMJ. 2001;322:1447-51.

215. Freitag MH, Peila R, Masaki K, Petrovitch H, Ross GW, White LR, et al. Midlife pulse pressure and incidence of dementia: the Honolulu-Asia Aging Study. Stroke. 2006;37(1):33-7.

216. Yamada M, Kasagi F, Sasaki I, Masunari N, Mimori Y, Suzuki G. Association Between Dementia and Midlife Risk Factors:
the Radiation Effects Research Foundation Adult Health Study. JAGS. 2003;51:410-4.

217. Morris MC, Scherr PA, Hebert LE, Glynn RJ, Bennett DA, Evans DA. Association of Incident Alzheimer Disease and Blood Pressure Measured From 13 Years Before to 2 Years After Diagnosis in a Large Community Study. Arch Neurol. 2001;58:1640-6.

218. Walker VM, Kehoe PG, Martin RM, Davies NM. Repurposing antihypertensive drugs for the prevention of Alzheimer's disease: a Mendelian randomization study. Int J Epidemiol. 2019.

219. Corrada MM, Hayden KM, Paganini-Hill A, Bullain SS, DeMoss J, Aguirre C, et al. Age of onset of hypertension and risk of dementia in the oldest-old: The 90+ Study. Alzheimers Dement. 2017;13(2):103-10.

220. De Heus RAA, Olde Rikkert MGM, Tully PJ, Lawlor BA, Claassen J, Group NS. Blood Pressure Variability and Progression of Clinical Alzheimer Disease. Hypertension. 2019;74(5):1172-80.

221. Scott JA, Braskie MN, Tosun D, Thompson PM, Weiner M, DeCarli C, et al. Cerebral Amyloid and Hypertension are Independently Associated with White Matter Lesions in Elderly. Front Aging Neurosci. 2015;7:221.

222. Uiterwijk R, Staals J, Huijts M, de Leeuw PW, Kroon AA, van Oostenbrugge RJ. MRI progression of cerebral small vessel disease and cognitive decline in patients with hypertension. J Hypertens. 2017;35(6):1263-70.

223. Dufouil C, Chalmers J, Coskun O, Besancon V, Bousser MG, Guillon P, et al. Effects of blood pressure lowering on cerebral white matter hyperintensities in patients with stroke: the PROGRESS (Perindopril Protection Against Recurrent Stroke Study) Magnetic Resonance Imaging Substudy. Circulation. 2005;112(11):1644-50.

224. Firbank MJ, Wiseman RM, Burton EJ, Saxby BK, O'Brien JT, Ford GA. Brain atrophy and white matter hyperintensity change in older adults and relationship to blood pressure. Brain atrophy, WMH change and blood pressure. J Neurol. 2007;254(6):713-21.

225. Poels MM, Ikram MA, van der Lugt A, Hofman A, Niessen WJ, Krestin GP, et al. Cerebral microbleeds are associated withworse cognitive function: the Rotterdam Scan Study. Neurology. 2012;78(5):326-33.

226. Faraco G, Iadecola C. Hypertension: a harbinger of stroke and dementia. Hypertension. 2013;62(5):810-7.

227. Verhaaren BF, Vernooij MW, de Boer R, Hofman A, Niessen WJ, van der Lugt A, et al. High blood pressure and cerebral white matter lesion progression in the general population. Hypertension. 2013;61(6):1354-9.

228. Beauchet O, Celle S, Roche F, Bartha R, Montero-Odasso M, Allali G, et al. Blood pressure levels and brain volume reduction: a systematic review and meta-analysis. J Hypertens. 2013;31(8):1502-16.

229. Iadecola C, Gottesman RF. Neurovascular and Cognitive Dysfunction in Hypertension. Circ Res. 2019;124(7):1025-44.

230. Sparks DL, Scheff SW, Liu H, Landers TM, Coyne CM, Hunsaker III JC. Increased incidence of neurofibrillary tangles (NFT) in non-demented individuals with hypertension. J Neurol Sci. 1995;131:162-9.

231. Petrovitch H, Ross GW, Steinhorn SC, Abbott RD, Markesbery W, Davis D, et al. AD lesions and infarcts in demented and non-demented Japanese-American men. Ann Neurol. 2005;57(1):98-103.

232. Beach TG, Wilson JR, Sue LI, Newell A, Poston M, Cisneros R, et al. Circle of Willis atherosclerosis: association with Alzheimer's disease, neuritic plaques and neurofibrillary tangles. Acta Neuropathol. 2007;113(1):13-21.

233. Hoffman LB, Schmeidler J, Lesser GT, Beeri MS, Purohit PD, Grossman HT, et al. Less Alzheimer disease neuropathology in medicated hypertensive than nonhypertensive persons. Neurology. 2009;72:1720-6.

234. Toledo JB, Toledo E, Weiner MW, Jack CR, Jr., Jagust W, Lee VM, et al. Cardiovascular risk factors, cortisol, and amyloid-beta deposition in Alzheimer's Disease Neuroimaging Initiative. Alzheimers Dement. 2012;8(6):483-9.

235. Langbaum JB, Chen K, Launer LJ, Fleisher AS, Lee W, Liu X, et al. Blood pressure is associated with higher brain amyloid burden and lower glucose metabolism in healthy late middle-age persons. Neurobiol Aging. 2012;33(4):827 e11-9.

236. Rodrigue KM, Rieck JR, Kennedy KM, Devous MD, Sr., Diaz-Arrastia R, Park DC. Risk factors for beta-amyloid deposition in healthy aging: vascular and genetic effects. JAMA Neurol. 2013;70(5):600-6.

237. Hughes TM, Kuller LH, Barinas- Mitchell EJ, Mackey RH, McDade EM, Klunk WE, et al. Pulse wave velocity is associated with β-amyloid deposition in the brains of very elderly adults. Neurology. 2013;81:1711–8.

238. Zhu D, Shi J, Zhang Y, Wang B, Liu W, Chen Z, et al. Central angiotensin II stimulation promotes beta amyloid production in Sprague Dawley rats. PLoS One. 2011;6(1):e16037.

239. Faraco G, Park L, Zhou P, Luo W, Paul SM, Anrather J, et al. Hypertension enhances Abeta-induced neurovascular dysfunction, promotes beta-secretase activity, and leads to amyloidogenic processing of APP. J Cereb Blood Flow Metab. 2016;36(1):241-52.

240. Nation DA, Edland SD, Bondi MW, Salmon DP, Delano-Wood L, Peskind ER, et al. Pulse pressure is associated with Alzheimer biomarkers in cognitively normal older adults. Neurology. 2013;81:2014-27.

241. Nation DA, Edmonds EC, Bangen KJ, Delano-Wood L, Scanlon BK, Han SD, et al. Pulse pressure in relation to tau-mediated neurodegeneration, cerebral amyloidosis, and progression to dementia in very old adults. JAMA Neurol. 2015;72(5):546-53.

242. Jacobson EJ, Salehmoghaddam S, Dorman JA, Land S, Back C, Barrio J. The effect of blood control on cognitive function (the focus study). Am J Hypertens. 2001;14:55A-6A.

243. Lithell H, Hansson L, Skoog I, Elmfeldt D, Hofman A, Olofsson B, et al. The Study on COgnition and Prognosis in the Elderly (SCOPE); outcomes in patients not receiving add-on therapy after randomization. J Hypertens. 2004;22(8):1605-12.

244. Fyhrquist F, Saijonmaa O. Renin-angiotensin system revisited. J Intern Med. 2008;264(3):224-36.

245. Carey RM, Siragy HM. Newly recognized components of the renin-angiotensin system: potential roles in cardiovascular and renal regulation. Endocr Rev. 2003;24(3):261-71.

246. Jackson L, Eldahshan W, Fagan SC, Ergul A. Within the Brain: The Renin Angiotensin System. Int J Mol Sci. 2018;19(3).

247. Mogi M, Iwanami J, Horiuchi M. Roles of Brain Angiotensin II in Cognitive Function and Dementia. Int J Hypertens. 2012;2012:169649.

248. Te Riet L, van Esch JH, Roks AJ, van den Meiracker AH, Danser AH. Hypertension: renin-angiotensin-aldosterone system alterations. Circ Res. 2015;116(6):960-75.

249. Donoghue M, Hsieh F, Baronas E, Godbout K, Gosselin M, Stagliano N, et al. A Novel Angiotensin-Converting Enzyme–Related Carboxypeptidase (ACE2) Converts Angiotensin I to Angiotensin 1-9

. Circ Res 2000;87:e1-e9.

250. Tipnis SR, Hooper NM, Hyde R, Karran E, Christie G, Turner AJ. A human homolog of angiotensin-converting enzyme. Cloning and functional expression as a captopril-insensitive carboxypeptidase. J Biol Chem. 2000;275(43):33238-43.

251. Xia H, Lazartigues E. Angiotensin-converting enzyme 2 in the brain: properties and future directions. J Neurochem. 2008;107(6):1482-94.

252. Santos RA, Simoes e Silva AC, Maric C, Silva DM, Machado RP, de Buhr I, et al. Angiotensin-(1-7) is an endogenous ligand for the G protein-coupled receptor Mas. Proc Natl Acad Sci U S A. 2003;100(14):8258-63.

253. Gironacci MM, Cerniello FM, Longo Carbajosa NA, Goldstein J, Cerrato BD. Protective axis of the renin-angiotensin system in the brain. Clin Sci (Lond). 2014;127(5):295-306.

254. Xu P, Sriramula S, Lazartigues E. ACE2/ANG-(1-7)/Mas pathway in the brain: the axis of good. Am J Physiol Regul Integr Comp Physiol. 2011;300(4):R804-17.

255. Gironacci MM, Vicario A, Cerezo G, Silva MG. The depressor axis of the renin-angiotensin system and brain disorders: a translational approach. Clin Sci (Lond). 2018;132(10):1021-38.
256. Yugandhar VG, Clark MA. Angiotensin III: a physiological relevant peptide of the renin angiotensin system. Peptides. 2013;46:26-32.
257. Wright JW, Harding JW. The brain RAS and Alzheimer's disease. Exp Neurol. 2010;223(2):326-33.
258. Puertas Mdel C, Martinez-Martos JM, Cobo M, Lorite P, Sandalio RM, Palomeque T, et al. Plasma renin-angiotensin system-regulating aminopeptidase activities are modified in early stage Alzheimer's disease and show gender differences but are not related to apolipoprotein E genotype. Exp Gerontol. 2013;48(6):557-64.
259. Engeli S, Negrel R, Sharma AM. Physiology and Pathophysiology of the Adipose Tissue Renin-Angiotensin System. Hypertension. 2000;35:1270-7.
260. Navar LG, Harrison-Bernard LM, Nishiyama A, Kobori H. Regulation of Intrarenal Angiotensin II in Hypertension. Hypertension. 2002;39(2 Pt 2):316-22.
261. Dostal DE. The cardiac renin–angiotensin system: novel signaling mechanisms related to cardiac growth and function. Regul Peptides. 2000;91:1-11.
262. Bader M, Ganten D. Update on tissue renin-angiotensin systems. J Mol Med (Berl). 2008;86(6):615-21.
263. Cuadra AE, Shan Z, Sumners C, Raizada MK. A current view of brain renin-angiotensin system: Is the (pro)renin receptor the missing link? Pharmacol Ther. 2010;125(1):27-38.
264. Steckelings UM, Rompe F, Kaschina E, Unger T. The evolving story of the RAAS in hypertension, diabetes and CV disease: moving from macrovascular to microvascular targets. Fundam Clin Pharmacol. 2009;23(6):693-703.
265. Garg M, Royce SG, Tikellis C, Shallue C, Batu D, Velkoska E, et al. Imbalance of the renin-angiotensin system may contribute to inflammation and fibrosis in IBD: a novel therapeutic target? Gut. 2019;DOI: 10.1136/gutjnl-2019-318512.
266. Nehme A, Zouein FA, Zayeri ZD, Zibara K. An Update on the Tissue Renin Angiotensin System and Its Role in Physiology and Pathology. J Cardiovasc Dev Dis. 2019;6(2).
267. Farag E, Maheshwari K, Morgan J, Sakr Esa WA, Doyle DJ. An update of the role of renin angiotensin in cardiovascular homeostasis. Anesth Analg. 2015;120(2):275-92.
268. Passos-Silva DG, Brandan E, Santos RA. Angiotensins as therapeutic targets beyond heart disease. Trends Pharmacol Sci. 2015;36(5):310-20.
269. Nguyen Dinh Cat A, Touyz RM. A new look at the renin-angiotensin system--focusing on the vascular system. Peptides. 2011;32(10):2141-50.

270. von Bohlen und Halbach O, Albrecht D. The CNS renin-angiotensin system. Cell Tissue Res. 2006;326(2):599-616.

271. Phillips MI, Sumners C. Angiotensin II in central nervous system physiology. Regul Pept. 1998;78:1-11.

272. Bertram D, Coote JH. Inhibitory Effects Of Angiotensin II on Barosensitive rostal Ventrolateral Medulla Neurons Of The Rat. Clin Exp Pharmacol Physiol. 2001;28:1112-4.

273. Bunag RD, Eriksson L, Tanabe S. Baroreceptor Reflex Enhancement by Chronic Intracerebroventricular Infusion of Enalapril in Normotensive Rats. Hypertension. 1990;15(3):284-90.

274. LIorens-Cortes C, Mendelsohn FA. Organisation and functional role of the brain angiotensin system. JRAAS. 2002;Suppl 1:S39-48.

275. Bourassa EA, Fang X, Li X, Sved AF, Speth RC. AT(1) angiotensin II receptor and novel non-AT(1), non-AT(2) angiotensin II/III binding site in brainstem cardiovascular regulatory centers of the spontaneously hypertensive rat. Brain Res. 2010;1359:98-106.

276. Heringer-Walther S, Batista EN, Walther T, Khosla MC, Santos RA, Campagnole-Santos MJ. Baroreflex Improvement in SHR After ACE Inhibition Involves Angiotensin-(1-7). Hypertension. 2001;37:1309-14.

277. Guimaraes PS, Santiago NM, Xavier CH, Velloso EP, Fontes MA, Santos RA, et al. Chronic infusion of angiotensin-(1-7) into the lateral ventricle of the brain attenuates hypertension in DOCA-salt rats. Am J Physiol Heart Circ Physiol. 2012;303(3):H393-400.

278. Nautiyal M, Shaltout HA, de Lima DC, do Nascimento K, Chappell MC, Diz DI. Central angiotensin-(1-7) improves vagal function independent of blood pressure in hypertensive (mRen2)27 rats. Hypertension. 2012;60(5):1257-65.

279. Xue B, Zhang Z, Johnson RF, Guo F, Hay M, Johnson AK. Central endogenous angiotensin-(1-7) protects against aldosterone/NaCl-induced hypertension in female rats. Am J Physiol Heart Circ Physiol. 2013;305(5):H699-705.

280. Oscar CG, Muller-Ribeiro FC, de Castro LG, Martins Lima A, Campagnole-Santos MJ, Santos RA, et al. Angiotensin-(1-7) in the basolateral amygdala attenuates the cardiovascular response evoked by acute emotional stress. Brain Res. 2015;1594:183-9.

281. Sriramula S, Xia H, Xu P, Lazartigues E. Brain-targeted angiotensin-converting enzyme 2 overexpression attenuates neurogenic hypertension by inhibiting cyclooxygenase-mediated inflammation. Hypertension. 2015;65(3):577-86.

282. Marchesi C, Paradis P, Schiffrin EL. Role of the renin-angiotensin system in vascular inflammation. Trends Pharmacol Sci. 2008;29(7):367-74.

283. Williams B, Baker AQ, Gallacher B, Lodwick D. Angiotensin II increases vascular permeability factor gene expression by human vascular smooth muscle cells. Hypertension. 1995;25(5):913-7.
284. Alvarez A, Cerda-Nicolas M, Naim Abu Nabah Y, Mata M, Issekutz AC, Panes J, et al. Direct evidence of leukocyte adhesion in arterioles by angiotensin II. Blood. 2004;104(2):402-8.
285. Piqueras L, Kubes P, Alvarez A, O'Connor E, Issekutz AC, Juan V. Esplugues JV, et al. Angiotensin II Induces Leukocyte–Endothelial Cell Interactions In Vivo Via AT1 and AT2 Receptor–Mediated P-Selectin Upregulation. Circulation 2000;102:2118-23.
286. Nobuhiko A, Suganuma E, Babaev VR, Fogo A, Swift LL, Linton MF, et al. Angiotensin II amplifies macrophage-driven atherosclerosis. Arterioscler Thromb Vasc Biol. 2004;24(11):2143-8.
287. Han C, Liu J, Liu X, Li M. Angiotensin II induces C-reactive protein expression through ERK1/2 and JNK signaling in human aortic endothelial cells. Atherosclerosis. 2010;212(1):206-12.
288. Dandona P, Kumar V, Aljada A, Ghanim H, Syed T, Hofmayer D, et al. Angiotensin II receptor blocker valsartan suppresses reactive oxygen species generation in leukocytes, nuclear factor-kappa B, in mononuclear cells of normal subjects: evidence of an antiinflammatory action. J Clin Endocrinol Metab. 2003;88(9):4496-501.
289. Benicky J, Sanchez-Lemus E, Honda M, Pang T, Orecna M, Wang J, et al. Angiotensin II AT1 receptor blockade ameliorates brain inflammation. Neuropsychopharmacology. 2011;36(4):857-70.
290. Saavedra JM. Angiotensin II AT(1) receptor blockers as treatments for inflammatory brain disorders. Clin Sci (Lond). 2012;123(10):567-90.
291. Villapol S, Saavedra JM. Neuroprotective effects of angiotensin receptor blockers. Am J Hypertens. 2015;28(3):289-99.
292. Jiang T, Gao L, Guo J, Lu J, Wang Y, Zhang Y. Suppressing inflammation by inhibiting the NF-kappaB pathway contributes to the neuroprotective effect of angiotensin-(1-7) in rats with permanent cerebral ischaemia. Br J Pharmacol. 2012;167(7):1520-32.
293. Sriramula S, Cardinale JP, Lazartigues E, Francis J. ACE2 overexpression in the paraventricular nucleus attenuates angiotensin II-induced hypertension. Cardiovasc Res. 2011;92(3):401-8.
294. Thomas MC, Pickering RJ, Tsorotes D, Koitka A, Sheehy K, Bernardi S, et al. Genetic Ace2 deficiency accentuates vascular inflammation and atherosclerosis in the ApoE knockout mouse. Circ Res. 2010;107(7):888-97.
295. Kamel AS, Abdelkader NF, Abd El-Rahman SS, Emara M, Zaki HF, Khattab MM. Stimulation of ACE2/ANG(1-7)/Mas Axis by Diminazene Ameliorates Alzheimer's Disease in the D-Galactose-Ovariectomized Rat Model: Role of PI3K/Akt Pathway. Mol Neurobiol. 2018;55(10):8188-202.
296. Farkas E, Luiten PG. Cerebral microvascular pathology in aging and Alzheimer's disease. Prog Neurobiol. 2001;64:575–611.

297. Jeynes B, Provias J. The possible role of capillary cerebral amyloid angiopathy in Alzheimer lesion development: a regional comparison. Acta Neuropathol. 2006;112(4):417-27.
298. Thal DR, Griffin WS, de Vos RA, Ghebremedhin E. Cerebral amyloid angiopathy and its relationship to Alzheimer's disease. Acta Neuropathol. 2008;115(6):599-609.
299. Montagne A, Nation DA, Pa J, Sweeney MD, Toga AW, Zlokovic BV. Brain imaging of neurovascular dysfunction in Alzheimer's disease. Acta Neuropathol. 2016;131(5):687-707.
300. Pluta R, Furmaga-Jablonska W, Maciejewski R, Ulamek-Koziol M, Jablonski M. Brain ischemia activates beta- and gamma-secretase cleavage of amyloid precursor protein: significance in sporadic Alzheimer's disease. Mol Neurobiol. 2013;47(1):425-34.
301. Shiota S, Takekawa H, Matsumoto SE, Takeda K, Nurwidya F, Yoshioka Y, et al. Chronic intermittent hypoxia/reoxygenation facilitate amyloid-beta generation in mice. J Alzheimers Dis. 2013;37(2):325-33.
302. Villarreal AE, Barron R, Rao KS, Britton GB. The effects of impaired cerebral circulation on Alzheimer’s disease pathology: evidence from animal studies. J Alzheimers Dis. 2014;42(3):707-22.
303. Kerridge C, Kozlova DI, Nalivaeva NN, Turner AJ. Hypoxia Affects Neprilysin Expression Through Caspase Activation and an APP Intracellular Domain-dependent Mechanism. Front Neurosci. 2015;9:426.
304. Lall R, Mohammed R, Ojha U. What are the links between hypoxia and Alzheimer's disease? Neuropsychiatr Dis Treat. 2019;15:1343-54.
305. Pluta R, Jablonski M, Ulamek-Koziol M, Kocki J, Brzozowska J, Januszewski S, et al. Sporadic Alzheimer's disease begins as episodes of brain ischemia and ischemically dysregulated Alzheimer's disease genes. Mol Neurobiol. 2013;48(3):500-15.
306. Wierenga CE, Hays CC, Zlatar ZZ. Cerebral blood flow measured by arterial spin labeling MRI as a preclinical marker of Alzheimer's disease. J Alzheimers Dis. 2014;42 Suppl 4:S411-9.
307. Di Marco LY, Farkas E, Martin C, Venneri A, Frangi AF. Is Vasomotion in Cerebral Arteries Impaired in Alzheimer's Disease? J Alzheimers Dis. 2015;46(1):35-53.
308. Kiryk A, Pluta R, Figiel I, Mikosz M, Ulamek M, Niewiadomska G, et al. Transient brain ischemia due to cardiac arrest causes irreversible long-lasting cognitive injury. Behav Brain Res. 2011;219(1):1-7.
309. Li J, Wang YJ, Zhang M, Fang CQ, Zhou HD. Cerebral ischemia aggravates cognitive impairment in a rat model of Alzheimer's disease. Life Sci. 2011;89(3-4):86-92.
310. Cohan CH, Neumann JT, Dave KR, Alekseyenko A, Binkert M, Stransky K, et al. Effect of cardiac arrest on cognitive impairment and hippocampal plasticity in middle-aged rats. PLoS One. 2015;10(5):e0124918.

311. Miners JS, Palmer JC, Tayler H, Palmer LE, Ashby E, Kehoe PG, et al. Abeta degradation or cerebral perfusion? Divergent effects of multifunctional enzymes. Front Aging Neurosci. 2014;6:238.
312. Barker R, Wellington D, Esiri MM, Love S. Assessing white matter ischemic damage in dementia patients by measurement of myelin proteins. J Cereb Blood Flow Metab. 2013;33(7):1050-7.
313. Barker R, Ashby EL, Wellington D, Barrow VM, Palmer JC, Kehoe PG, et al. Pathophysiology of white matter perfusion in Alzheimer's disease and vascular dementia. Brain. 2014;137(Pt 5):1524-32.
314. Thomas T, Miners S, Love S. Post-mortem assessment of hypoperfusion of cerebral cortex in Alzheimer's disease and vascular dementia. Brain. 2015;138(Pt 4):1059-69.
315. Miners JS, Palmer JC, Love S. Pathophysiology of Hypoperfusion of the Precuneus in Early Alzheimer's Disease. Brain Pathol. 2016;26(4):533-41.
316. Kagiyama T, Kagiyama S, Phillips MI. Expression of angiotensin type 1 and 2 receptors in brain after transient middle cerebral artery occlusion in rats. Regul Pept. 2003;110:241-7.
317. Nishimura Y, Ito T, Saavedra JM. Angiotensin II AT1 Blockade Normalizes Cerebrovascular Autoregulation and Reduces Cerebral Ischemia in Spontaneously Hypertensive Rats. Stroke. 2000;31:2478-86.
318. Saavedra JM, Benicky J, Zhou J. Mechanisms of the Anti-Ischemic Effect of Angiotensin II AT(1) Receptor Antagonists in the Brain. Cell Mol Neurobiol. 2006;26(7-8):1099-111.
319. Ito T, Yamakawa H, Bregonzio C, Terron JA, Falcon-Neri A, Saavedra JM. Protection against ischemia and improvement of cerebral blood flow in genetically hypertensive rats by chronic pretreatment with an angiotensin II AT1 antagonist. Stroke. 2002;33(9):2297-303.
320. Grotha W, Blumea A, Gohlkea P, Ungerb T, Culmana J. Chronic pretreatment with candesartan improves recovery from focal cerebral ischaemia in rats. J Hypertens. 2003;21(11):2175-82.
321. Lu Q, Zhu Y-Z, Wong PT-H. Neuroprotective effects of candesartan against cerebral ischemia in spontaneously hypertensive rats. Neuroreport. 2005;16(17):1963-7.
322. Li JM, Mogi M, Iwanami J, Min LJ, Tsukuda K, Sakata A, et al. Temporary pretreatment with the angiotensin II type 1 receptor blocker, valsartan, prevents ischemic brain damage through an increase in capillary density. Stroke. 2008;39(7):2029-36.
323. Mecca AP, O'Connor TE, Katovich MJ, Sumners C. Candesartan pretreatment is cerebroprotective in a rat model of endothelin-1-induced middle cerebral artery occlusion. Exp Physiol. 2009;94(8):937-46.
324. Willis LM, El-Remessy AB, Somanath PR, Deremer DL, Fagan SC. Angiotensin receptors blockers and angiogenesis: clinical and experimental evidence. Clin Sci (Lond). 2011;120(8):307-19.

325. Ferreira AJ, Santos RA, Bradford CN, Mecca AP, Sumners C, Katovich MJ, et al. Therapeutic implications of the vasoprotective axis of the renin-angiotensin system in cardiovascular diseases. Hypertension. 2010;55(2):207-13.

326. Mecca AP, Regenhardt RW, O'Connor TE, Joseph JP, Raizada MK, Katovich MJ, et al. Cerebroprotection by angiotensin-(1-7) in endothelin-1-induced ischaemic stroke. Exp Physiol. 2011;96(10):1084-96.

327. Regenhardt RW, Mecca AP, Desland F, Ritucci-Chinni PF, Ludin JA, Greenstein D, et al. Centrally administered angiotensin-(1-7) increases the survival of stroke-prone spontaneously hypertensive rats. Exp Physiol. 2014;99(2):442-53.

328. Zhang Y, Lu J, Shi J, Lin X, Dong J, Zhang S, et al. Central administration of angiotensin-(1-7) stimulates nitric oxide release and upregulates the endothelial nitric oxide synthase expression following focal cerebral ischemia/reperfusion in rats. Neuropeptides. 2008;42(5-6):593-600.

329. Chen J, Zhao Y, Chen S, Wang J, Xiao X, Ma X, et al. Neuronal over-expression of ACE2 protects brain from ischemia-induced damage. Neuropharmacology. 2014;79:550-8.

330. Zheng JL, Li GZ, Chen SZ, Wang JJ, Olson JE, Xia HJ, et al. Angiotensin converting enzyme 2/Ang-(1-7)/mas axis protects brain from ischemic injury with a tendency of age-dependence. CNS Neurosci Ther. 2014;20(5):452-9.

331. Lu J, Jiang T, Wu L, Gao L, Wang Y, Zhou F, et al. The expression of angiotensin-converting enzyme 2-angiotensin-(1-7)-Mas receptor axis are upregulated after acute cerebral ischemic stroke in rats. Neuropeptides. 2013;47(5):289-95.

332. Harrison C, Acharya KR. ACE for all - a molecular perspective. J Cell Commun Signal. 2014;8(3):195-210.

333. Guang C, Phillips RD, Jiang B, Milani F. Three key proteases--angiotensin-I-converting enzyme (ACE), ACE2 and renin--within and beyond the renin-angiotensin system. Arch Cardiovasc Dis. 2012;105(6-7):373-85.

334. Riordan JF. Angiotensin-I-converting enzyme and its relatives. Genome Biol. 2003;4(8):225.

335. Kaur P, Muthuraman A, Kaur M. The implications of angiotensin-converting enzymes and their modulators in neurodegenerative disorders: current and future perspectives. ACS Chem Neurosci. 2015;6(4):508-21.

336. Hooper NM, Turner AJ. An ACE structure. Nat Struct Biol. 2003;10(3).

337. Danilov SM, Sadovnikova E, Scharenborg N, Balyasnikova IV, Svinareva DA, Semikina EL, et al. Angiotensin-converting enzyme (CD143) is abundantly expressed by dendritic cells and discriminates human monocyte-derived dendritic cells from acute myeloid leukemia-derived dendritic cells. Exp Hematol. 2003;31(12):1301-9.

338. McKinley MJ, Albiston AL, Allen AM, Mathai ML, May CN, McAllen RM, et al. The brain renin–angiotensin system: location and physiological roles. Int J Biochem Cell Biol. 2003;35(6):901-18.
339. Skidgel RA, Erdos EG. Angiotensin converting enzyme (ACE) and neprilysin hydrolyze neuropeptides: a brief history, the beginning and follow-ups to early studies. Peptides. 2004;25(3):521-5.
340. Xiao Z, Cilz NI, Kurada L, Hu B, Yang C, Wada E, et al. Activation of neurotensin receptor 1 facilitates neuronal excitability and spatial learning and memory in the entorhinal cortex: beneficial actions in an Alzheimer's disease model. J Neurosci. 2014;34(20):7027-42.
341. Keiser AA, Matazel KS, Esser MK, Feifel D, Prus AJ. Systemic administration of the neurotensin NTS(1)-receptor agonist PD149163 improves performance on a memory task in naturally deficient male brown Norway rats. Exp Clin Psychopharmacol. 2014;22(6):541-7.
342. Yamada D, Wada E, Amano T, Wada K, Sekiguchi M. Lack of neurotensin type 1 receptor facilitates contextual fear memory depending on the memory strength. Pharmacol Biochem Behav. 2010;96(3):363-9.
343. Zou K, Maeda T, Watanabe A, Liu J, Liu S, Oba R, et al. Abeta42-to-Abeta40- and angiotensin-converting activities in different domains of angiotensin-converting enzyme. J Biol Chem. 2009;284(46):31914-20.
344. Fuchs S, Xiao HD, Hubert C, Michaud A, Campbell DJ, Adams JW, et al. Angiotensin-converting enzyme C-terminal catalytic domain is the main site of angiotensin I cleavage in vivo. Hypertension. 2008;51(2):267-74.
345. Sun X, Becker M, Pankow K, Krause E, Ringling M, Beyermann M, et al. Catabolic attacks of membrane-bound angiotensin-converting enzyme on the N-terminal part of species-specific amyloid-beta peptides. Eur J Pharmacol. 2008;588(1):18-25.
346. Zou K, Liu J, Watanabe A, Hiraga S, Liu S, Tanabe C, et al. Abeta43 is the earliest-depositing Abeta species in APP transgenic mouse brain and is converted to Abeta41 by two active domains of ACE. Am J Pathol. 2013;182(6):2322-31.
347. Hemming ML, Selkoe DJ. Amyloid beta-protein is degraded by cellular angiotensin-converting enzyme (ACE) and elevated by an ACE inhibitor. J Biol Chem. 2005;280(45):37644-50.
348. Eckman EA, Adams SK, Troendle FJ, Stodola BA, Kahn MA, Fauq AH, et al. Regulation of steady-state beta-amyloid levels in the brain by neprilysin and endothelin-converting enzyme but not angiotensin-converting enzyme. J Biol Chem. 2006;281(41):30471-8.
349. Denayer T, Stöhr T, Roy MV. Animal models in translational medicine: Validation and prediction. Eur J Mol Clin Med. 2014;2(1).

350. Pound P, Ritskes-Hoitinga M. Is it possible to overcome issues of external validity in preclinical animal research? Why most animal models are bound to fail. J Transl Med. 2018;16(1):304.
351. Katzov H, Chalmers K, Palmgren J, Andreasen N, Johansson B, Cairns NJ, et al. Genetic variants of ABCA1 modify Alzheimer disease risk and quantitative traits related to beta-amyloid metabolism. Hum Mutat. 2004;23(4):358-67.
352. Rigat B, Hubert C, Alhenc-Gelas F, Cambien F, Corvol P, Soubrier F. An Insertion/Deletion Polymorphism in the Angiotensin I-converting Enzyme Gene Accounting for Half the Variance of Serum Enzyme Levels. J Clin Invest. 1990;86:1343-6.
353. Lazaroni TL, Raslan AC, Fontes WR, de Oliveira ML, Bader M, Alenina N, et al. Angiotensin-(1-7)/Mas axis integrity is required for the expression of object recognition memory. Neurobiol Learn Mem. 2012;97(1):113-23.
354. Miners S, Ashby E, Baig S, Harrison R, Tayler H, Speedy E, et al. Angiotensin-converting enzyme levels and activity in Alzheimer's disease: differences in brain and CSF ACE and association with ACE1 genotypes. Am J Transl Res. 2009;1(2):163-77.
355. Arregui A, Perry EK, Rossor M, Tomlinson BE. Angiotensin converting enzyme in Alzheimer's disease increased activity in caudate nucleus and cortical areas. J Neurochem. 1982;38(5):1490-2.
356. Barnes NM, Cheng CH, Costali B, Naylor RJ, Williams TJ, Wischik CM. Angiotensin converting enzyme density is increased in temporal cortex from patients with Alzheimer's disease. Eur J Pharmacol. 1991;200:289-92.
357. Savaskan E. The role of the brain renin-angiotensin system in neurodegenerative disorders. Curr Alzheimer Res. 2005;2(1):29-35.
358. Wang J, Ho L, Chen L, Zhao Z, Zhao W, Qian X, et al. Valsartan lowers brain beta-amyloid protein levels and improves spatial learning in a mouse model of Alzheimer disease. J Clin Invest. 2007;117(11):3393-402.
359. Takeda S, Sato N, Takeuchi D, Kurinami H, Shinohara M, Niisato K, et al. Angiotensin receptor blocker prevented beta-amyloid-induced cognitive impairment associated with recovery of neurovascular coupling. Hypertension. 2009;54(6):1345-52.
360. Dong YF, Kataoka K, Tokutomi Y, Nako H, Nakamura T, Toyama K, et al. Perindopril, a centrally active angiotensin-converting enzyme inhibitor, prevents cognitive impairment in mouse models of Alzheimer's disease. FASEB J. 2011;25(9):2911-20.
361. AbdAlla S, Langer A, Fu X, Quitterer U. ACE inhibition with captopril retards the development of signs of neurodegeneration in an animal model of Alzheimer's disease. Int J Mol Sci. 2013;14(8):16917-42.

362. Ongali B, Nicolakakis N, Tong XK, Aboulkassim T, Papadopoulos P, Rosa-Neto P, et al. Angiotensin II type 1 receptor blocker losartan prevents and rescues cerebrovascular, neuropathological and cognitive deficits in an Alzheimer's disease model. Neurobiol Dis. 2014;68:126-36.
363. Ferrington L, Miners JS, Palmer LE, Bond SM, Povey JE, Kel-ly PA, et al. Angiotensin II-inhibiting drugs have no effect on intraneu- ronal Aβ or oligomeric Aβ levels in a triple transgenic mouse model of Alzheimer's disease. Am J Transl Res. 2011;3(2):197-208.
364. Soto ME, van Kan GA, Nourhashemi F, Gillette-Guyonnet S, Cesari M, Cantet C, et al. Angiotensin-converting enzyme inhibitors and Alzheimer's disease progression in older adults: results from the Reseau sur la Maladie d'Alzheimer Francais cohort. J Am Geriatr Soc. 2013;61(9):1482-8.
365. O'Caoimh R, Healy L, Gao Y, Svendrovski A, Kerins DM, Eustace J, et al. Effects of centrally acting angiotensin converting enzyme inhibitors on functional decline in patients with Alzheimer's disease. J Alzheimers Dis. 2014;40(3):595-603.
366. Li NC, Lee A, Whitmer RA, Kivipelto M, Lawler E, Kazis LE, et al. Use of angiotensin receptor blockers and risk of dementia in a predominantly male population: prospective cohort analysis. BMJ. 2010;340:b5465.
367. Davies NM, Kehoe PG, Ben-Shlomo Y, Martin RM. Associations of anti-hypertensive treatments with Alzheimer's disease, vascular dementia, and other dementias. . J Alzheimers Dis. 2011;26(4):699-708.
368. Kehoe PG, Davies NM, Martin RM, Ben-Shlomo Y. Associations of angiotensin targeting antihypertensive drugs with mortality and hospitalization in primary care patients with dementia. J Alzheimers Dis. 2013;33(4):999-1008.
369. Barthold D, Joyce G, Wharton W, Kehoe P, Zissimopoulos J. The association of multiple anti-hypertensive medication classes with Alzheimer's disease incidence across sex, race, and ethnicity. PLoS One. 2018;13(11):e0206705.
370. Ding J, Davis-Plourde KL, Sedaghat S, Tully PJ, Wang W, Phillips C, et al. Antihypertensive medications and risk for incident dementia and Alzheimer's disease: a meta-analysis of individual participant data from prospective cohort studies. Lancet Neurol. 2020;19(1):61-70.
371. Lerman LO, Kurtz TW, Touyz RM, Ellison DH, Chade AR, Crowley SD, et al. Animal Models of Hypertension: A Scientific Statement From the American Heart Association. Hypertension. 2019;73(6):e87-e120.
372. Anthony CS, Masuyer G, Sturrock ED, Acharya KR. Structure Based Drug Design of Angiotensin-I Converting Enzyme Inhibitors. Curr Med Chem. 2012;19(6):845-55.

373. Douglas RG, Sharma RK, Masuyer G, Lubbe L, Zamora I, Acharya KR, et al. Fragment-based design for the development of N-domain-selective angiotensin-1-converting enzyme inhibitors. Clin Sci (Lond). 2014;126(4):305-13.
374. Nchinda AT, Chibale K, Redelinghuys P, Sturrock ED. Synthesis and molecular modeling of a lisinopril-tryptophan analogue inhibitor of angiotensin I-converting enzyme. Bioorg Med Chem Lett. 2006;16(17):4616-9.
375. Denti P, Sharp SK, Kroger WL, Schwager SL, Mahajan A, Njoroge M, et al. Pharmacokinetic evaluation of lisinopril-tryptophan, a novel C-domain ACE inhibitor. Eur J Pharm Sci. 2014;56:113-9.
376. Ehlers MR, Abrie JA, Sturrock ED. C domain-selective inhibition of angiotensin-converting enzyme. JRAAS. 2013;14(2):189-92.
377. Kehoe PG, Blair PS, Howden B, Thomas DL, Malone IB, Horwood J, et al. The Rational and Design of the Reducing Pathology in Alzheimer's Disease through Angiotensin TaRgeting (RADAR) trial. J Alzheimers Dis. 2018;61(2):803-14.
378. Wharton W, Goldstein FC, Tansey MG, Brown AL, Tharwani SD, Verble DD, et al. Rationale and Design of the Mechanistic Potential of Antihypertensives in Preclinical Alzheimer's (HEART) Trial. J Alzheimers Dis. 2018;61(2):815-24.
379. Gironacci MM. Angiotensin-(1-7): beyond its central effects on blood pressure. Ther Adv Cardiovasc Dis. 2015;9(4):209-16.
380. Thomas MA, Fleissner G, Stohr M, Hauptfleisch S, Lemmer B. Localization of components of the renin-angiotensin system in the suprachiasmatic nucleus of normotensive Sprague-Dawley rats: part A. angiotensin I/II, a light and electron microscopic study. Brain Res. 2004;1008(2):212-23.
381. Thomas MA, Fleissner G, Stohr M, Hauptfleisch S, Lemmer B. Localization of components of the renin-angiotensin system in the suprachiasmatic nucleus of normotensive Sprague-Dawley rats: part B. angiotensin II (AT1)-receptors, a light and electron microscopic study. Brain Res. 2004;1008(2):224-35.
382. O.V. H, Albrecht D. Angiotensin II Inhibits Long-Term Potentiation within the Lateral Nucleus of the Amygdala through AT1 Receptors. Peptides. 1998;19(6):1031-6.
383. Tchekalarova J, Albrecht D. Angiotensin II suppresses long-term depression in the lateral amygdala of mice via L-type calcium channels. Neurosci Lett. 2007;415(1):68-72.
384. Gard PR. The role of angiotensin II in cognition and behaviour. Eur J Pharmacol. 2002;438:1-14.
385. Maul B, von Bohlen und Halbach O, Becker A, Sterner-Kock A, Voigt JP, Siems WE, et al. Impaired spatial memory and altered dendritic spine morphology in angiotensin II type 2 receptor-deficient mice. J Mol Med (Berl). 2008;86(5):563-71.

386. Dai HL, Hu WY, Jiang LH, Li L, Gaung XF, Xiao ZC. p38 MAPK Inhibition Improves Synaptic Plasticity and Memory in Angiotensin II-dependent Hypertensive Mice. Sci Rep. 2016;6:27600.
387. Foulquier S, Namsolleck P, Van Hagen BT, Milanova I, Post MJ, Blankesteijn WM, et al. Hypertension-induced cognitive impairment: insights from prolonged angiotensin II infusion in mice. Hypertens Res. 2018;41(10):817-27.
388. Wiesmann M, Roelofs M, van der Lugt R, Heerschap A, Kiliaan AJ, Claassen JA. Angiotensin II, hypertension and angiotensin II receptor antagonism: Roles in the behavioural and brain pathology of a mouse model of Alzheimer's disease. J Cereb Blood Flow Metab. 2017;37(7):2396-413.
389. Liu J, Liu S, Matsumoto Y, Murakami S, Sugakawa Y, Kami A, et al. Angiotensin type 1a receptor deficiency decreases amyloid beta-protein generation and ameliorates brain amyloid pathology. Sci Rep. 2015;5:12059.
390. Tian M, Zhu D, Xie W, Shi J. Central angiotensin II-induced Alzheimer-like tau phosphorylation in normal rat brains. FEBS Lett. 2012;586(20):3737-45.
391. Li Z, Mo N, Li L, Cao Y, Wang W, Liang Y, et al. Surgery-Induced Hippocampal Angiotensin II Elevation Causes Blood-Brain Barrier Disruption via MMP/TIMP in Aged Rats. Front Cell Neurosci. 2016;10:105.
392. Takane K, Hasegawa Y, Lin B, Koibuchi N, Cao C, Yokoo T, et al. Detrimental Effects of Centrally Administered Angiotensin II are Enhanced in a Mouse Model of Alzheimer Disease Independently of Blood Pressure. J Am Heart Assoc. 2017;6(4).
393. Kehoe PG, Hibbs E, Palmer LE, Miners JS. Angiotensin-III is increased in Alzheimer's disease in association with Amyloid-β and Tau pathology. J Alzheimers Dis. 2017;58(1):203-14.
394. Zimmerman MC, Lazartigues E, Sharma RV, Davisson RL. Hypertension caused by angiotensin II infusion involves increased superoxide production in the central nervous system. Circ Res. 2004;95(2):210-6.
395. Levi-Marpillat N, Macquin-Mavier I, Tropeano AI, Parati G, Maison P. Antihypertensive drug classes have different effects on short-term blood pressure variability in essential hypertension. Hypertens Res. 2014;37(6):585-90.
396. de Gasparo M, Catt KJ, Inagami T, Wright JW, Unger T. International union of pharmacology. XXIII. The angiotensin II receptors. Pharmacol Rev. 2000;52(3):415-72.
397. Labandeira-Garcia JL, Rodriguez-Perez AI, Garrido-Gil P, Rodriguez-Pallares J, Lanciego JL, Guerra MJ. Brain Renin-Angiotensin System and Microglial Polarization: Implications for Aging and Neurodegeneration. Front Aging Neurosci. 2017;9:129.

398. Zhang TL, Fu JL, Geng Z, Yang JJ, Sun XJ. The neuroprotective effect of losartan through inhibiting AT1/ASK1/MKK4/JNK3 pathway following cerebral I/R in rat hippocampal CA1 region. CNS Neurosci Ther. 2012;18(12):981-7.

399. Haraguchi T, Iwasaki K, Takasaki K, Uchida K, Naito T, Nogami A, et al. Telmisartan, a partial agonist of peroxisome proliferator-activated receptor gamma, improves impairment of spatial memory and hippocampal apoptosis in rats treated with repeated cerebral ischemia. Brain Res. 2010;1353:125-32.

400. Braszko JJ, Wincewicz D, Jakubow P. Candesartan prevents impairment of recall caused by repeated stress in rats. Psychopharmacology (Berl). 2013;225(2):421-8.

401. Wincewicz D, Braszko JJ. Angiotensin II AT1 receptor blockade by telmisartan reduces impairment of spatial maze performance induced by both acute and chronic stress. JRAAS. 2015;16(3):495-505.

402. Anil Kumar KV, Nagwar S, Thyloor R, Satyanarayana S. Anti-stress and nootropic activity of drugs affecting the renin-angiotensin system in rats based on indirect biochemical evidence. JRAAS. 2015;16(4):801-12.

403. Hamel E, Royea J, Ongali B, Tong XK. Neurovascular and Cognitive failure in Alzheimer's Disease: Benefits of Cardiovascular Therapy. Cell Mol Neurobiol. 2016;36(2):219-32.

404. Fogari R, Mugellini A, Zoppi A, Derosa G, Pasotti C, Fogari E, et al. Influence of losartan and atenolol on memory function in very elderly hypertensive patients. J Hum Hypertens. 2003;17(11):781-5.

405. Fogari R, Mugellini A, Zoppi A, Marasi G, Pasotti C, Poletti L, et al. Effects of valsartan compared with enalapril on blood pressure and cognitive function in elderly patients with essential hypertension. Eur J Clin Pharmacol. 2004;59(12):863-8.

406. Wolozin B, Lee A, Lee A, Whitmer R, Kazis L. Use of angiotensin receptor blockers is associated with a lower incidence and progression of Alzheimer's disease. Alzheimers Dement. 2008;4:T118-T.

407. Kalra J, Prakash A, Kumar P, Majeed AB. Cerebroprotective effects of RAS inhibitors: Beyond their cardio-renal actions. JRAAS. 2015;16(3):459-68.

408. Guimond MO, Gallo-Payet N. The Angiotensin II Type 2 Receptor in Brain Functions: An Update. Int J Hypertens. 2012;2012:351758.

409. Mateos L, Perez-Alvarez MJ, Wandosell F. Angiotensin II type-2 receptor stimulation induces neuronal VEGF synthesis after cerebral ischemia. Biochim Biophys Acta. 2016;1862(7):1297-308.

410. Jing F, Mogi M, Sakata A, Iwanami J, Tsukuda K, Ohshima K, et al. Direct stimulation of angiotensin II type 2 receptor enhances spatial memory. J Cereb Blood Flow Metab. 2012;32(2):248-55.

411. Min LJ, Mogi M, Tsukuda K, Jing F, Ohshima K, Nakaoka H, et al. Direct stimulation of angiotensin II type 2 receptor initiated after stroke ameliorates ischemic brain damage. Am J Hypertens. 2014;27(8):1036-44.
412. Wan Y, Wallinder C, Plouffe B, Beaudry H, Mahalingam AK, Wu X, et al. Design, Synthesis, and Biological Evaluation of the First Selective Nonpeptide
AT2 Receptor Agonist. J Med Chem. 2004;47(24):5995-6008.
413. Sakata A, Mogi M, Iwanami J, Tsukuda K, Min LJ, Fujita T, et al. Sex-different effect of angiotensin II type 2 receptor on ischemic brain injury and cognitive function. Brain Res. 2009;1300:14-23.
414. Kawajiri M, Mogi M, Higaki N, Matsuoka T, Ohyagi Y, K Tsukuda K, et al. Angiotensin-converting enzyme (ACE) and ACE2 levels in the cerebrospinal fluid of patients with multiple sclerosis. Mult Scler. 2009;15:262-5.
415. Rocha NP, Scalzo PL, Barbosa IG, de Campos-Carli SM, Tavares LD, de Souza MS, et al. Peripheral levels of angiotensins are associated with depressive symptoms in Parkinson's disease. J Neurol Sci. 2016;368:235-9.
416. Jiang T, Zhang YD, Zhou JS, Zhu XC, Tian YY, Zhao HD, et al. Angiotensin-(1-7) is Reduced and Inversely Correlates with Tau Hyperphosphorylation in Animal Models of Alzheimer's Disease. Mol Neurobiol. 2016;53(4):2489-97.
417. Kehoe PG, Wong S, Al Mulhim N, Palmer LE, Miners JS. Angiotensin-converting enzyme 2 is reduced in Alzheimer's disease in association with increasing amyloid-beta and tau pathology. Alzheimers Res Ther. 2016;8(1):50.
418. Doobay MF, Talman LS, Obr TD, Tian X, Davisson RL, Lazartigues E. Differential Expression of Neuronal ACE2 in Transgenic Mice with Overexpression of the Brain Renin-angiotensin System. Am J Physiol Regul Integr Comp Physiol. 2007;292(1):R373–R81.
419. Wang XL, Iwanami J, Min LJ, Tsukuda K, Nakaoka H, Bai HY, et al. Deficiency of angiotensin-converting enzyme 2 causes deterioration of cognitive function. NPJ Aging Mech Dis. 2016;2:16024.
420. Gallagher PE, Chappell MC, Ferrario CM, Tallant EA. Distinct roles for ANG II and ANG-(1-7) in the regulation of angiotensin-converting enzyme 2 in rat astrocytes. Am J Physiol Cell Physiol. 2006;290(2):C420-6.
421. Evans CE, Miners JS, Piva G, Willis CL, Heard DM, Kidd EJ, et al. ACE2 activation protects against cognitive decline and reduces amyloid pathology in the Tg2576 mouse model of Alzheimer's disease. Acta Neuropathol. 2020.
422. Block CH, Santos RA, Brosnihan KB, Ferrario CM. Immunocytochemical Localization of Angiotensin-(1-7) in the Rat Forebrain. Peptides. 1989;9:1395-401.

423. Chappell MC, Brosnihan KB, Diz DI, Ferrario CM. Identification of Angiotensin-(1-7) in Rat Brain. J Biol Chem. 1989;264(28):16518-23.
424. Li H, Liu X, Ren Z, Gu J, Lu Y, Wang X, et al. Effects of Diabetic Hyperglycemia on Central Ang-(1-7)-Mas-R-nNOS Pathways in Spontaneously Hypertensive Rats. Cell Physiol Biochem. 2016;40(5):1186-97.
425. Costa-Besada MA, Valenzuela R, Garrido-Gil P, Villar-Cheda B, Parga JA, Lanciego JL, et al. Paracrine and Intracrine Angiotensin 1-7/Mas Receptor Axis in the Substantia Nigra of Rodents, Monkeys, and Humans. Mol Neurobiol. 2018;55(7):5847-67.
426. Fraga-Silva RA, Ferreira AJ, Dos Santos RA. Opportunities for targeting the angiotensin-converting enzyme 2/angiotensin-(1-7)/mas receptor pathway in hypertension. Curr Hypertens Rep. 2013;15(1):31-8.
427. Santos RA, Ferreira AJ, Verano-Braga T, Bader M. Angiotensin-converting enzyme 2, angiotensin-(1-7) and Mas: new players of the renin-angiotensin system. J Endocrinol. 2013;216(2):R1-R17.
428. Karnik SS, Singh KD, Tirupula K, Unal H. Significance of angiotensin 1-7 coupling with MAS1 receptor and other GPCRs to the renin-angiotensin system: IUPHAR Review 22. Br J Pharmacol. 2017;174(9):737-53.
429. Xie W, Zhu D, Ji L, Tian M, Xu C, Shi J. Angiotensin-(1-7) improves cognitive function in rats with chronic cerebral hypoperfusion. Brain Res. 2014;1573:44-53.
430. Jiang T, Yu JT, Zhu XC, Zhang QQ, Tan MS, Cao L, et al. Angiotensin-(1-7) induces cerebral ischaemic tolerance by promoting brain angiogenesis in a Mas/eNOS-dependent pathway. Br J Pharmacol. 2014;171(18):4222-32.
431. Lu J, Zhang Y, Shi J. Effects of intracerebroventricular infusion of angiotensin-(1-7) on bradykinin formation and the kinin receptor expression after focal cerebral ischemia-reperfusion in rats. Brain Res. 2008;1219:127-35.
432. Hellner K, Walther T, Schubert M, Albrecht D. Angiotensin-(1-7) enhances LTP in the hippocampus through the G-protein-coupled receptor Mas. Mol Cell Neurosci. 2005;29(3):427-35.
433. Albrecht D. Angiotensin-(1-7)-induced plasticity changes in the lateral amygdala are mediated by COX-2 and NO. Learn Mem. 2007;14(3):177-84.
434. Uekawa K, Hasegawa Y, Senju S, Nakagata N, Ma M, Nakagawa T, et al. Intracerebroventricular Infusion of Angiotensin-(1-7) Ameliorates Cognitive Impairment and Memory Dysfunction in a Mouse Model of Alzheimer's Disease. J Alzheimers Dis. 2016;53(1):127-33.
435. Jiang T, Tan L, Gao Q, Lu H, Zhu XC, Zhou JS, et al. Plasma angiotensin-(1-7) is a potential Biomarker for Alzheimer’s disease. Curr Neurovasc Res. 2016;13(2):96-9.

436. Young D, Waitches G, Birchmeier C, Fasano O, Wigler M. Isolation and characterization of a new cellular oncogene encoding a protein with multiple potential transmembrane domains. Cell. 1986;45(5):711-9.

437. Alenina N, Bohme I, Bader M, Walther T. Multiple non-coding exons and alternative splicing in the mouse Mas protooncogene. Gene. 2015;568(2):155-64.

438. Becker LK, Etelvino GM, Walther T, Santos RA, Campagnole-Santos MJ. Immunofluorescence localization of the receptor Mas in cardiovascular-related areas of the rat brain. Am J Physiol Heart Circ Physiol. 2007;293(3):H1416-24.

439. Brett A, Kaar a, Rae MG. The Mas receptor does not modulate group I metabotropic receptor-mediated calcium signals in control or transgenic Alzheimer's disease (3xTg-AD) mouse hippocampal neurons. JNRBM. *In Press*.

440. Chen JL, Zhang DL, Sun Y, Zhao YX, Zhao KX, Pu D, et al. Angiotensin-(1-7) administration attenuates Alzheimer's disease-like neuropathology in rats with streptozotocin-induced diabetes via Mas receptor activation. Neuroscience. 2017;346:267-77.

441. Bennion DM, Haltigan E, Regenhardt RW, Steckelings UM, Sumners C. Neuroprotective mechanisms of the ACE2-angiotensin-(1-7)-Mas axis in stroke. Curr Hypertens Rep. 2015;17(2):3.

442. Castro CH, Santos RA, Ferreira AJ, Bader M, Alenina N, Almeida AP. Evidence for a functional interaction of the angiotensin-(1-7) receptor Mas with AT1 and AT2 receptors in the mouse heart. Hypertension. 2005;46(4):937-42.

443. Tetzner A, Gebolys K, Meinert C, Klein S, Uhlich A, Trebicka J, et al. G-Protein-Coupled Receptor MrgD Is a Receptor for Angiotensin-(1-7) Involving Adenylyl Cyclase, cAMP, and Phosphokinase A. Hypertension. 2016;68(1):185-94.

444. Gembardt F, Grajewski S, Vahl M, Schultheiss HP, Walther T. Angiotensin metabolites can stimulate receptors of the Mas-related genes family. Mol Cell Biochem. 2008;319(1-2):115-23.

445. Tirupula KC, Desnoyer R, Speth RC, Karnik SS. Atypical signaling and functional desensitization response of MAS receptor to peptide ligands. PLoS One. 2014;9(7):e103520.

446. Lautner RQ, Villela DC, Fraga-Silva RA, Silva N, Verano-Braga T, Costa-Fraga F, et al. Discovery and characterization of alamandine: a novel component of the renin-angiotensin system. Circ Res. 2013;112(8):1104-11.

447. Villela DC, Passos-Silva DG, Santos RA. Alamandine: a new member of the angiotensin family. Curr Opin Nephrol Hypertens. 2014;23(2):130-4.

448. Qaradakhi T, Apostolopoulos V, Zulli A. Angiotensin (1-7) and Alamandine: Similarities and differences. Pharmacol Res. 2016;111:820-6.

449. Soares ER, Barbosa CM, Campagnole-Santos MJ, Santos RAS, Alzamora AC. Hypotensive effect induced by microinjection of Alamandine, a derivative of angiotensin-(1-7), into caudal ventrolateral medulla of 2K1C hypertensive rats. Peptides. 2017;96:67-75.
450. Li P, Chen XR, Xu F, Liu C, Li C, Liu H, et al. Alamandine attenuates sepsis-associated cardiac dysfunction via inhibiting MAPKs signaling pathways. Life Sci. 2018;206:106-16.
451. Liu C, Yang CX, Chen XR, Liu BX, Li Y, Wang XZ, et al. Alamandine attenuates hypertension and cardiac hypertrophy in hypertensive rats. Amino Acids. 2018;50(8):1071-81.
452. Jesus ICG, Scalzo S, Alves F, Marques K, Rocha-Resende C, Bader M, et al. Alamandine acts via MrgD to induce AMPK/NO activation against ANG II hypertrophy in cardiomyocytes. Am J Physiol Cell Physiol. 2018;314(6):C702-C11.
453. Zylka MJ, Dong X, Southwell AL, Anderson DJ. Atypical expansion in mice of the sensory neuron-specific Mrg G protein-coupled receptor family. Proc Natl Acad Sci U S A. 2003;100(17):10043-8.
454. Dong X, Han S-K, Zylka MJ, Simon MI, Anderson DJ. A Diverse Family of GPCRs Expressed in Specific Subsets of Nociceptive Sensory Neurons. Cell. 2001;106:619–32.
455. Santos RAS, Sampaio WO, Alzamora AC, Motta-Santos D, Alenina N, Bader M, et al. The ACE2/Angiotensin-(1-7)/MAS Axis of the Renin-Angiotensin System: Focus on Angiotensin-(1-7). Physiol Rev. 2018;98(1):505-53.
456. Schleifenbaum J. Alamandine and Its Receptor MrgD Pair Up to Join the Protective Arm of the Renin-Angiotensin System. Front Med (Lausanne). 2019;6:107.
457. Albrecht D. Physiological and pathophysiological functions of different angiotensins in the brain. Br J Pharmacol. 2010;159(7):1392-401.
458. Wright JW, Kawas LH, Harding JW. The development of small molecule angiotensin IV analogs to treat Alzheimer's and Parkinson's diseases. Prog Neurobiol. 2015;125:26-46.
459. Wright JW, Harding JW. The brain renin-angiotensin system: a diversity of functions and implications for CNS diseases. Pflugers Arch. 2013;465(1):133-51.
460. Marc Y, Llorens-Cortes C. The role of the brain renin-angiotensin system in hypertension: implications for new treatment. Prog Neurobiol. 2011;95(2):89-103.
461. Padia SH, Kemp BA, Howell NL, Gildea JJ, Keller SR, Carey RM. Intrarenal angiotensin III infusion induces natriuresis and angiotensin type 2 receptor translocation in Wistar-Kyoto but not in spontaneously hypertensive rats. Hypertension. 2009;53(2):338-43.
462. Wang HX, Zhang QF, Zeng XJ, Wang W, Tang CS, Zhang LK. Effects of angiotensin III on protein, DNA, and collagen synthesis of neonatal cardiomyocytes and cardiac fibroblasts in vitro. J Cardiovasc Pharmacol Ther. 2010;15(4):393-402.

463. Speth RC, Karamyan VT. The significance of brain aminopeptidases in the regulation of the actions of angiotensin peptides in the brain. Heart Fail Rev. 2008;13(3):299-309.
464. Gard PR, Fidalgo S, Lotter I, Richardson C, Farina N, Rusted J, et al. Changes of renin-angiotensin system-related aminopeptidases in early stage Alzheimer's disease. Exp Gerontol. 2017;89:1-7.
465. De Mota N, Iturrioz X, Claperon C, Bodineau L, Fassot C, Roques BP, et al. Human brain aminopeptidase A: biochemical properties and distribution in brain nuclei. J Neurochem. 2008;106(1):416-28.
466. Zini S, Masdehors P, Lenkei Z, Fournie-Zaluski MC, Roques BP, Corvol P, et al. Aminopeptidase A: Distribution In Rat Brain Nuclei And Increased Activity In Spontaneously Hypertensive Rats. Neuroscience. 1997;78(4):1187-93.
467. Wright JW, Mizutani S, Harding JW. Focus on Brain Angiotensin III and Aminopeptidase A in the Control of Hypertension. Int J Hypertens. 2012;2012:124758.
468. Fournie-Zaluski MC, Fassot C, Valentin B, Djordjijevic D, Reaux-Le Goazigo A, Corvol P, et al. Brain renin-angiotensin system blockade by systemically active aminopeptidase A inhibitors: a potential treatment of salt-dependent hypertension. Proc Natl Acad Sci U S A. 2004;101(20):7775-80.
469. Brannstrom K, Ohman A, Nilsson L, Pihl M, Sandblad L, Olofsson A. The N-terminal region of amyloid beta controls the aggregation rate and fibril stability at low pH through a gain of function mechanism. J Am Chem Soc. 2014;136(31):10956-64.
470. Noble F, Banisadr G, Jardinaud F, Popovici T, Lai-Kuen R, Chen H, et al. First Discrete Autoradiographic Distribution Of Aminopeptidase N In Various Structure Of Rat Brain And Spinal Cord Using The Selective Iodinated Inhibitor [125I]RB 129. Neuroscience. 2001;105(2):479-88.
471. Banegas I, Prieto I, Vives f, Alba F, de Gasparo M, Segarra AB, et al. Brain Aminopeptidases and Hypertension. JRAAS. 2006;7(3):129-34.
472. Chai SY, Bastias MA, Clune EF, Matsacos DJ, Mustafa T, Lee JH, et al. Distribution of angiotensin IV binding sites (AT4 receptor) in the human forebrain, midbrain and pons as visualised by in vitro receptor autoradiography. J Chem Neuroanat. 2000;20:339–48.
473. Wright JW, Yamamoto BJ, Harding JW. Angiotensin receptor subtype mediated physiologies and behaviors: New discoveries and clinical targets. Prog Neurobiol 2008;84(2):157-81.
474. Albiston AL, McDowall SG, Matsacos D, Sim P, Clune E, Mustafa T, et al. Evidence that the angiotensin IV (AT(4)) receptor is the enzyme insulin-regulated aminopeptidase. J Biol Chem. 2001;276(52):48623-6.
475. Farag E, Sessler DI, Ebrahim Z, Kurz A, Morgan J, Ahuja S, et al. The renin angiotensin system and the brain: New developments. J Clin Neurosci. 2017;46:1-8.

476. Krama´r EA, Armstrong DL, Ikeda S, Waynerd MJ, Harding JW, Wright JW. The effects of angiotensin IV analogs on long-term potentiation within the CA1 region of the hippocampus in vitro. Brain Res. 2001;897:114-21.

477. Wayner MJ, Armstrong DL, Phelix CF, Wright JW, Harding JW. Angiotensin IV enhances LTP in rat dentate gyrus in vivo. Peptides. 2001;22:1403-14.

478. Davis CJ, Kramar EA, De A, Meighan PC, Simasko SM, Wright JW, et al. AT4 receptor activation increases intracellular calcium influx and induces a non-N-methyl-D-aspartate dependent form of long-term potentiation. Neuroscience. 2006;137(4):1369-79.

479. De Bundel D, Smolders I, Vanderheyden P, Michotte Y. Ang II and Ang IV: unraveling the mechanism of action on synaptic plasticity, memory, and epilepsy. CNS Neurosci Ther. 2008;14(4):315-39.

480. Wright JW, Stubley L, Pederson ES, Krama´r EA, Hanesworth JM, Harding JW. Contributions of the Brain Angiotensin IV–AT4 Receptor Subtype System to Spatial Learning. J Neurosci. 1999;19(10):3952–61

481. Lee J, Albiston AL, Allen AM, Mendelsohn FA, Ping SE, Barrett GL, et al. Effect of I.C.V. injection of AT4 receptor ligands, NLE1-angiotensin IV and LVV-hemorphin 7, on spatial learning in rats. Neuroscience. 2004;124(2):341-9.

482. Braszko JJ, Walesiuk A, Wielgat P. Cognitive Effects Attributed to Angiotensin II may Result from its Conversion to Angiotensin IV. JRAAS. 2006;7(3):168-74.

483. Golding BJ, Overall AD, Brown G, Gard PR. Strain differences in the effects of angiotensin IV on mouse cognition. Eur J Pharmacol. 2010;641(2-3):154-9.

484. Paris JJ, Eans SO, Mizrachi E, Reilley KJ, Ganno ML, McLaughlin JP. Central administration of angiotensin IV rapidly enhances novel object recognition among mice. Neuropharmacology. 2013;70:247-53.

485. Holownia A. Effect of angiotensin IV on the acquisition of the water maze task and ryanodine channel function. Pharmacol Biochem Behav. 2003;76(1):85-91.

486. Gard PR, Daw P, Mashhour ZS, Tran P. Interactions of angiotensin IV and oxytocin on behaviour in mice. JRAAS. 2007;8(3):133-8.

487. Wright JW, Clemens JA, Jill A. Panetta JA, Smalstig EB, Weatherly LS, Krama´r EA, et al. Effects of LY231617 and angiotensin IV on ischemia-induced deficits in circular water maze and passive avoidance performance in rats. Brain Res. 1996;717:1-11.

488. Pederson ES, Krishnan R, Harding JW, Wright JW. A role for the angiotensin AT4 receptor subtype in overcoming scopolamine-induced spatial memory deficits. Regul Peptides. 2001;102:147–56.

489. Albiston AL, Pederson ES, Burns P, Purcell B, Wright JW, Harding JW, et al. Attenuation of scopolamine-induced learning deficits by LVV-hemorphin-7 in rats in the passive avoidance and water maze paradigms. Behav Brain Res. 2004;154(1):239-43.

490. Olson ML, Cero IJ. Intrahippocampal Norleucine(1)-Angiotensin IV mitigates scopolamine-induced spatial working memory deficits. Peptides. 2010;31(12):2209-15.

491. Benoist CC, Wright JW, Zhu M, Appleyard SM, Wayman GA, Harding JW. Facilitation of hippocampal synaptogenesis and spatial memory by C-terminal truncated Nle1-angiotensin IV analogs. J Pharmacol Exp Ther. 2011;339(1):35-44.

492. McCoy AT, Benoist CC, Wright JW, Kawas LH, Bule-Ghogare JM, Zhu M, et al. Evaluation of metabolically stabilized angiotensin IV analogs as procognitive/antidementia agents. J Pharmacol Exp Ther. 2013;344(1):141-54.

493. Royea J, Zhang L, Tong XK, Hamel E. Angiotensin IV Receptors Mediate the Cognitive and Cerebrovascular Benefits of Losartan in a Mouse Model of Alzheimer's Disease. J Neurosci. 2017;37(22):5562-73.

494. Krama´r EA, Harding JW, Wright JW. Angiotensin II- and IV-induced changes in cerebral blood flow Roles of AT1 AT2, and AT4 receptor subtypes. Regul Pept. 1997;68:131-8.

495. Braszko JJ. Indispensable role of the voltage-gated calcium channels in the procognitive effects of angiotensin IV. Brain Res Bull. 2017;130:118-24.

496. Fernando RN, Larm J, Albiston AL, Chai SY. Distribution and cellular localization of insulin-regulated aminopeptidase in the rat central nervous system. J Comp Neurol. 2005;487(4):372-90.

497. Fernando RN, Albiston AL, Chai SY. The insulin-regulated aminopeptidase IRAP is colocalised with GLUT4 in the mouse hippocampus--potential role in modulation of glucose uptake in neurones? Eur J Neurosci. 2008;28(3):588-98.

498. Albiston AL, Diwakarla S, Fernando RN, Mountford SJ, Yeatman HR, Morgan B, et al. Identification and development of specific inhibitors for insulin-regulated aminopeptidase as a new class of cognitive enhancers. Br J Pharmacol. 2011;164(1):37-47.

499. Wright JW, Harding JW. Brain renin-angiotensin--a new look at an old system. Prog Neurobiol. 2011;95(1):49-67.

500. Lew RA, Mustafa T, Ye S, McDowall SG, Chai SY, Albiston AL. Angiotensin AT4 ligands are potent, competitive inhibitors of insulin regulated aminopeptidase (IRAP). J Neurochem. 2003;86(2):344-50.

501. Albiston AL, Morton CJ, Ng HL, Pham V, Yeatman HR, Ye S, et al. Identification and characterization of a new cognitive enhancer based on ihibition of insulin-regulated aminopeptidase. FASEB J. 2008;22(12):4209-17.

502. Mountford SJ, Albiston AL, Charman WN, Ng L, Holien JK, Parker MW, et al. Synthesis, structure-activity relationships and brain uptake of a novel series of benzopyran inhibitors of insulin-regulated aminopeptidase. J Med Chem. 2014;57(4):1368-77.
503. Chai SY, Fernando R, Peck G, Ye SY, Mendelsohn FA, Jenkins TA, et al. The angiotensin IV/AT4 receptor. Cell Mol Life Sci. 2004;61(21):2728-37.
504. Yeatman HR, Albiston AL, Burns P, Chai SY. Forebrain neurone-specific deletion of insulin-regulated aminopeptidase causes age related deficits in memory. Neurobiol Learn Mem. 2016;136:174-82.
505. Nakamura T, Mizuno S. The discovery of hepatocyte growth factor (HGF) and its significance for cell biology, life sciences and clinical medicine. Proc Jpn Acad Ser B Phys Biol Sci. 2010;86(6):588-610.
506. Tyndall SJ, Walikonis RS. The receptor tyrosine kinase Met and its ligand hepatocyte growth factor are clustered at excitatory synapses and can enhance clustering of synaptic proteins. Cell Cycle. 2006;5(14):1560-8.
507. Kawas LH, Benoist CC, Harding JW, Wayman GA, Abu-Lail NI. Nanoscale mapping of the Met receptor on hippocampal neurons by AFM and confocal microscopy. Nanomedicine. 2013;9(3):428-38.
508. Sharma S. Hepatocyte growth factor in synaptic plasticity and Alzheimer's disease. Sci World J. 2010;10:457-61.
509. Tsuboi Y, Kakimoto K, Nakajima M, Akatsu H, Yamamoto T, Ogawa K, et al. Increased hepatocyte growth factor level in cerebrospinal fluid in Alzheimer’s disease. Acta Neurol Scand. 2003;107:81-6.
510. Tyndall SJ, Patel SJ, Walikonis RS. Hepatocyte growth factor-induced enhancement of dendritic branching is blocked by inhibitors of N-methyl-D-aspartate receptors and calcium/calmodulin-dependent kinases. J Neurosci Res. 2007;85(11):2343-51.
511. Lee J, Chai S, Mendelsohn FA, Morris MJ, Allen AM. Potentiation of cholinergic transmission in the rat hippocampus by angiotensin IV and LVV-hemorphin-7. Neuropharmacology. 2001;40:618-23.
512. Lim CS, Walikonis RS. Hepatocyte growth factor and c-Met promote dendritic maturation during hippocampal neuron differentiation via the Akt pathway. Cell Signal. 2008;20(5):825-35.
513. Chen SD, Wu CL, Lin TK, Chuang YC, Yang DI. Renin inhibitor aliskiren exerts neuroprotection against amyloid beta-peptide toxicity in rat cortical neurons. Neurochem Int. 2012;61(3):369-77.
514. Dong YF, Kataoka K, Toyama K, Sueta D, Koibuchi N, Yamamoto E, et al. Attenuation of brain damage and cognitive impairment by direct renin inhibition in mice with chronic cerebral hypoperfusion. Hypertension. 2011;58(4):635-42.

515. Hou DR, Wang Y, Zhou L, Chen K, Tian Y, Song Z, et al. Altered angiotensin-convering enzyme and its effects on the brain in a rat model of Alzheimer disease. Chin Med J (Engl). 2008;121(22):2320-3.

516. Ali MR, Abo-Youssef AM, Messiha BA, Khattab MM. Tempol and perindopril protect against lipopolysaccharide-induced cognition impairment and amyloidogenesis by modulating brain-derived neurotropic factor, neuroinflammation and oxido-nitrosative stress. Naunyn Schmiedebergs Arch Pharmacol. 2016;389(6):637-56.

517. Goel R, Bhat SA, Hanif K, Nath C, Shukla R. Perindopril Attenuates Lipopolysaccharide-Induced Amyloidogenesis and Memory Impairment by Suppression of Oxidative Stress and RAGE Activation. ACS Chem Neurosci. 2016;7(2):206-17.

518. Hemming ML, Selkoe DJ, Farris W. Effects of Prolonged Angiotensin-converting Enzyme Inhibitor Treatment on Amyloid β-Protein Metabolism in Mouse Models of Alzheimer Disease. Neurobiol Dis. 2007;26(1):273-81.

519. Bernstein KE, Koronyo Y, Salumbides BC, Sheyn J, Pelissier L, Lopes DH, et al. Angiotensin-converting enzyme overexpression in myelomonocytes prevents Alzheimer's-like cognitive decline. J Clin Invest. 2014;124(3):1000-12.

520. Hajjar IM, Keown M, Lewis P, Almor A. Angiotensin converting enzyme inhibitors and cognitive and functional decline in patients with Alzheimer's disease: an observational study. Am J Alzheimers Dis Other Demen. 2008;23(1):77-83.

521. Wharton W, Zhao L, Steenland K, Goldstein FC, Schneider JA, Barnes LL, et al. Neurofibrillary tangles and conversion to mild cognitive impairment with certain antihypertensives. J Alzheimers Dis. 2019;70(1):153-61.

522. Danielyan L, Klein R, Hanson LR, Buadze M, Schwab M, Gleiter CH, et al. Protective effects of intranasal losartan in the APP/PS1 transgenic mouse model of Alzheimer disease. Rejuvenation Res. 2010;12(2-3):195-201.

523. Mogi M, Tsukuda K, Li JM, Iwanami J, Min LJ, Sakata A, et al. Inhibition of cognitive decline in mice fed a high-salt and cholesterol diet by the angiotensin receptor blocker, olmesartan. Neuropharmacology. 2007;53(8):899-905.

524. Mogi M, Li JM, Tsukuda K, Iwanami J, Min LJ, Sakata A, et al. Telmisartan prevented cognitive decline partly due to PPAR-gamma activation. Biochem Biophys Res Commun. 2008;375(3):446-9.

525. Tsukuda K, Mogi M, Iwanami J, Min LJ, Sakata A, Jing F, et al. Cognitive deficit in amyloid-beta-injected mice was improved by pretreatment with a low dose of telmisartan partly because of peroxisome proliferator-activated receptor-gamma activation. Hypertension. 2009;54(4):782-7.

526. Tota S, Kamat PK, Awasthi H, Singh N, Raghubir R, Nath C, et al. Candesartan improves memory decline in mice: involvement of AT1 receptors in memory deficit induced by intracerebral streptozotocin. Behav Brain Res. 2009;199(2):235-40.
527. Ellul J, Archer N, Foy CM, Poppe M, Boothby H, Nicholas H, et al. The effects of commonly prescribed drugs in patients with Alzheimer's disease on the rate of deterioration. J Neurol Neurosurg Psychiatry. 2007;78(3):233-9.
528. Wright JW, Harding JW. Contributions by the Brain Renin-Angiotensin System to Memory, Cognition, and Alzheimer's Disease. J Alzheimers Dis. 2019;67(2):469-80.
529. Kulemina LV, Ostrov DA. Prediction of off-target effects on angiotensin-converting enzyme 2. J Biomol Screen. 2011;16(8):878-85.
530. Mascolo A, Sessa M, Scavone C, De Angelis A, Vitale C, Berrino L, et al. New and old roles of the peripheral and brain renin-angiotensin-aldosterone system (RAAS): Focus on cardiovascular and neurological diseases. Int J Cardiol. 2017;227:734-42.
531. Zhong J, Basu R, Guo D, Chow FL, Byrns S, Schuster M, et al. Angiotensin-converting enzyme 2 suppresses pathological hypertrophy, myocardial fibrosis, and cardiac dysfunction. Circulation. 2010;122(7):717-28, 18 p following 28.
532. Singh Y, Singh K, Sharma PL. Effect of combination of renin inhibitor and Mas-receptor agonist in DOCA-salt-induced hypertension in rats. Mol Cell Biochem. 2013;373(1-2):189-94.
533. Bodineau L, Frugiere A, Marc Y, Inguimbert N, Fassot C, Balavoine F, et al. Orally active aminopeptidase A inhibitors reduce blood pressure: a new strategy for treating hypertension. Hypertension. 2008;51(5):1318-25.
534. Gao J, Marc Y, Iturrioz X, Leroux V, Balavoine F, LIorens-Cortes C. A new strategy for treating hypertension by blocking the activity of the brain renin-angiotensin system with aminopeptidase A inhibitors. Clin Sci (Lond). 2014;127(3):135-48.
535. Balavoine F, Azizi M, Bergerot D, De Mota N, Patouret R, Roques BP, et al. Randomised, double-blind, placebo-controlled, dose-escalating phase I study of QGC001, a centrally acting aminopeptidase a inhibitor prodrug. Clin Pharmacokinet. 2014;53(4):385-95.
536. Carmona AK, Schwager SL, Juliano MA, Juliano L, Sturrock ED. A continuous fluorescence resonance energy transfer angiotensin I-converting enzyme assay. Nat Protoc. 2006;1(4):1971-6.
537. Kehoe PG. The renin-angiotensin-aldosterone system and Alzheimer’s disease? JRAAS. 2003;4(2):80-93.
538. Kehoe PG. The Coming of Age of the Angiotensin Hypothesis in Alzheimer's Disease: Progress Toward Disease Prevention and Treatment? J Alzheimers Dis. 2018;62(3):1443-66.

539. Bertram L, McQueen MB, Mullin K, Blacker D, Tanzi RE. Systematic meta-analyses of Alzheimer disease genetic association studies: the AlzGene database. Nat Genet. 2007;39(1):17-23.
540. Marioni RE, Harris SE, Zhang Q, McRae AF, Hagenaars SP, Hill WD, et al. GWAS on family history of Alzheimer's disease. Transl Psychiatry. 2018;8(1):99.
541. Ohrui T, Matsui T, Yamaya M, Arai H, Ebihara S, Maruyama M, et al. Angiotensin-Converting Enzyme Inhibitors And Incidence Of Alzheimer's Disease In Japan. JAGS. 2004;52(4):649-50.
542. Wharton W, Goldstein FC, Zhao L, Steenland K, Levey AI, Hajjar I. Modulation of Renin-Angiotensin System May Slow Conversion from Mild Cognitive Impairment to Alzheimer's Disease. J Am Geriatr Soc. 2015;63(9):1749-56.
543. Rouch L, Cestac P, Hanon O, Cool C, Helmer C, Bouhanick B, et al. Antihypertensive drugs, prevention of cognitive decline and dementia: a systematic review of observational studies, randomized controlled trials and meta-analyses, with discussion of potential mechanisms. CNS Drugs. 2015;29(2):113-30.
544. Khachaturian AS, Zandi PP, Lyketsos CG, Hayden KM, Skoog I, Norton MC, et al. Antihypertensive medication use and incident Alzheimer disease: the Cache County Study. Arch Neurol. 2006;63(5):686-92.
545. van Helmond Z, Miners JS, Kehoe PG, Love S. Higher soluble amyloid beta concentration in frontal cortex of young adults than in normal elderly or Alzheimer's disease. Brain Pathol. 2010;20(4):787-93.
546. Ferrer I, Santpere G, Arzberger T, Bell J, Blanco R, Boluda S, et al. Brain Protein Preservation Largely Depends on the Postmortem Storage Temperature: Implications for Study of Proteins in Human Neurologic Diseases and Management of Brain Banks: A BrainNet Europe Study. J Neuropathol Exp Neurol. 2007;66(1):35-46.
547. Burger D, Reudelhuber TL, Mahajan A, Chibale K, Sturrock ED, Touyz RM. Effects of a domain-selective ACE inhibitor in a mouse model of chronic angiotension II-dependent hypertension. Clin Sci (Lond). 2014;127(1):57-63.
548. Liu S, Ando F, Fujita Y, Liu J, Maeda T, Shen X, et al. A clinical dose of angiotensin-converting enzyme (ACE) inhibitor and heterozygous ACE deletion exacerbate Alzheimer's disease pathology in mice. J Biol Chem. 2019;294(25):9760-70.
549. Toropygin IY, Kugaevskaya EV, Mirgorodskaya OA, Elisseeva YE, Kozmin YP, Popov IA, et al. The N-domain of angiotensin-converting enzyme specifically hydrolyzes the Arg-5-His-6 bond of Alzheimer's Abeta-(1-16) peptide and its isoAsp-7 analogue with different efficiency as evidenced by quantitative matrix-assisted laser desorption/ionization time-of-light mass spectrometry. Rapid Commun Mass Spectrom. 2008;22(2):231-9.

550. Kugaevskaya EV, Veselovsky AV, Indeykina MI, Solovyeva NI, Zharkova MS, Popov IA, et al. N-domain of angiotensin-converting enzyme hydrolyzes human and rat amyloid-beta(1-16) peptides as arginine specific endopeptidase potentially enhancing risk of Alzheimer's disease. Sci Rep. 2018;8(1):298.

551. Fang L, Geng M, Liu C, Wang J, Min W, Liu J. Structural and molecular basis of angiotensin-converting enzyme by computational modeling: Insights into the mechanisms of different inhibitors. PLoS One. 2019;14(4):e0215609.

552. Anthony CS, Corradi HR, Schwager SL, Redelinghuys P, Georgiadis D, Dive V, et al. The N domain of human angiotensin-I-converting enzyme: the role of N-glycosylation and the crystal structure in complex with an N domain-specific phosphinic inhibitor, RXP407. J Biol Chem. 2010;285(46):35685-93.

553. Hay M, Polt R, Heien ML, Vanderah TW, Largent-Milnes TM, Rodgers K, et al. A Novel Angiotensin-(1-7) Glycosylated Mas Receptor Agonist for Treating Vascular Cognitive Impairment and Inflammation-Related Memory Dysfunction. J Pharmacol Exp Ther. 2019;369(1):9-25.

554. Crozier RA, Ajit SK, Kaftan EJ, Pausch MH. MrgD activation inhibits KCNQ/M-currents and contributes to enhanced neuronal excitability. J Neurosci. 2007;27(16):4492-6.

555. Milasta S, Pediani J, Appelbe S, Trim S, Wyatt M, Cox P, et al. Interactions between the Mas-related receptors MrgD and MrgE alter signalling and trafficking of MrgD. Mol Pharmacol. 2006;69(2):479-91.

556. Morley JE, Armbrecht HJ, Farr SA, Kumar VB. The senescence accelerated mouse (SAMP8) as a model for oxidative stress and Alzheimer's disease. Biochim Biophys Acta. 2012;1822(5):650-6.

557. Lopez Verrilli MA, Rodriguez Fermepin M, Longo Carbajosa N, Landa S, Cerrato BD, Garcia S, et al. Angiotensin-(1-7) through Mas receptor up-regulates neuronal norepinephrine transporter via Akt and Erk1/2-dependent pathways. J Neurochem. 2012;120(1):46-55.

558. Freund M, Walther T, von Bohlen Und Halbach O. Effects of the angiotensin-(1-7) receptor Mas on cell proliferation and on the population of doublecortin positive cells within the dentate gyrus and the piriform cortex. Eur Neuropsychopharmacol. 2014;24(2):302-8.

559. Arroja MM, Reid E, McCabe C. Therapeutic potential of the renin angiotensin system in ischaemic stroke. Exp Transl Stroke Med. 2016;8:8.

560. Chang AY, Li FC, Huang CW, Wu JC, Dai KY, Chen CH, et al. Interplay between brain stem angiotensins and monocyte chemoattractant protein-1 as a novel mechanism for pressor response after ischemic stroke. Neurobiol Dis. 2014;71:292-304.

561. Wallis MG, Lankford MF, Keller SR. Vasopressin is a physiological substrate for the insulin-regulated aminopeptidase IRAP. Am J Physiol Endocrinol Metab. 2007;293(4):E1092-102.

562. Diwakarla S, Nylander E, Gronbladh A, Vanga SR, Khan YS, Gutierrez-de-Teran H, et al. Aryl Sulfonamide Inhibitors of Insulin-Regulated Aminopeptidase Enhance Spine Density in Primary Hippocampal Neuron Cultures. ACS Chem Neurosci. 2016;7(10):1383-92.

563. Diwakarla S, Nylander E, Gronbladh A, Vanga SR, Khan YS, Gutierrez-de-Teran H, et al. Binding to and Inhibition of Insulin-Regulated Aminopeptidase by Macrocyclic Disulfides Enhances Spine Density. Mol Pharmacol. 2016;89(4):413-24.

564. Vanga SR, Savmarker J, Ng L, Larhed M, Hallberg M, Aqvist J, et al. Structural Basis of Inhibition of Human Insulin-Regulated Aminopeptidase (IRAP) by Aryl Sulfonamides. ACS Omega. 2018;3(4):4509-21.

565. Seyer B, Diwakarla S, Burns P, Hallberg A, Grnbladh A, Hallberg M, et al. Insulin-regulated aminopeptidase inhibitor-mediated increases in dendritic spine density are facilitated by glucose uptake. J Neurochem. 2019.

566. Holownia A, Braszko JJ. The effect of angiotensin II and IV on ERK1/2 and CREB signalling in cultured rat astroglial cells. Naunyn Schmiedebergs Arch Pharmacol. 2007;376(3):157-63.

567. McNay EC, Pearson-Leary J. GluT4: A central player in hippocampal memory and brain insulin resistance. Exp Neurol. 2020;323:113076.

568. Pearson-Leary J, McNay EC. Intrahippocampal administration of amyloid-beta(1-42) oligomers acutely impairs spatial working memory, insulin signaling, and hippocampal metabolism. J Alzheimers Dis. 2012;30(2):413-22.

569. Palmer JC, Barker R, Kehoe PG, Love S. Endotheline-1 is elevated in Alzheimer's disease and upregulated by amyloid-β . J Alzheimers Dis. 2012;29(4):853-61.

570. Braszko JJ, Kulakowska A, Wisniewski K. Angiotensin II and Its 3-7 Fragment Improve Recognition But Not Spatial Memory in Rats. Brain Res Bull. 1995;37(6):627-31.

571. Handa RK. Metabolism Alters the Selectivity of Angiotensin-(1-7) Receptor Ligands for Angiotensin Receptors. J Am Soc Nephrol. 2000;11:1377-86.

572. Werno MW, Chamberlain LH. S-acylation of the Insulin-Responsive Aminopeptidase (IRAP): Quantitative analysis and Identification of Modified Cysteines. Sci Rep. 2015;5:12413.

573. Jiang T, Gao L, Shi J, Lu J, Wang Y, Zhang Y. Angiotensin-(1-7) modulates renin-angiotensin system associated with reducing oxidative stress and attenuating neuronal apoptosis in the brain of hypertensive rats. Pharmacol Res. 2013;67(1):84-93.

574. Lee S, Evans MA, Chu HX, Kim HA, Widdop RE, Drummond GR, et al. Effect of a Selective Mas Receptor Agonist in Cerebral Ischemia In Vitro and In Vivo. PLoS One. 2015;10(11):e0142087.

575. Oliveira-Lima OC, Pinto MC, Duchene J, Qadri F, Souza LL, Alenina N, et al. Mas receptor deficiency exacerbates lipopolysaccharide-induced cerebral and systemic inflammation in mice. Immunobiology. 2015;220(12):1311-21.
576. Liu M, Shi P, Sumners C. Direct anti-inflammatory effects of angiotensin-(1-7) on microglia. J Neurochem. 2016;136(1):163-71.
577. Jiang T, Xue L, Yang Y, Wang Q, Xue X, Ou Z, et al. AVE0991, a nonpeptide analogue of Ang-(1-7), attenuates aging- related neuroinflammation. Aging. 2018;10(4):645-57.
578. Saavedra JM. Beneficial effects of Angiotensin II receptor blockers in brain disorders. Pharmacol Res. 2017;125(Pt A):91-103.
579. Sumners C, Horiuchi M, Widdop RE, McCarthy C, Unger T, Steckelings UM. Protective arms of the renin-angiotensin-system in neurological disease. Clin Exp Pharmacol Physiol. 2013;40(8):580-8.
580. Mogi M, Kawajiri M, Tsukuda K, Matsumoto S, Yamada T, Horiuchi M. Serum levels of renin-angiotensin system components in acute stroke patients. Geriatr Gerontol Int. 2014;14(4):793-8.
581. Tao MX, Xue X, Gao L, Lu JL, Zhou JS, Jiang T, et al. Involvement of angiotensin-(1-7) in the neuroprotection of captopril against focal cerebral ischemia. Neurosci Lett. 2018;687:16-21.
582. Royea J, Martinot P, Hamel E. Memory and cerebrovascular deficits recovered following angiotensin IV intervention in a mouse model of Alzheimer's disease. Neurobiol Dis. 2020;134:104644.
583. Naveri L, Stromberg C, Saavedra JM. Angiotensin IV Reverses the Acute Cerebral Blood Flow Reduction After Experimental Subarachnoid Hemorrhage in the Rat
. J Cerebr Blood F Met. 1994;14:1096-9.
584. Dalmay F, Mazouz H, Allard J, Pesteil F, Achard JM, Fournier A. Non-AT1-receptor-mediated protective effect of angiotensin against acute ischaemic stroke in the gerbil. JRAAS. 2001;2(2):103-06.
585. Faure S, Chapot R, Tallet D, Javellaud J, Achard JM, Oudart N. Cerebroprotective Effect Of Angiotensin IV
In Experimental Ischemic Stroke In The Rat Mdiated By AT4 Receptors. J Physiol Pharmacol. 2006;57(3):329-42.
586. Pham V, Albiston AL, Downes CE, Wong CH, Diwakarla S, Ng L, et al. Insulin-regulated aminopeptidase deficiency provides protection against ischemic stroke in mice. J Neurotrauma. 2012;29(6):1243-8.
587. Karamyan VT, Stockmeier CA, Speth RC. Human brain contains a novel non-AT1, non-AT2 binding site for active angiotensin peptides. Life Sci. 2008;83(11-12):421-5.
588. Karamyan VT, Arsenault J, Escher E, Speth RC. Preliminary biochemical characterization of the novel, non-AT1, non-AT2 angiotensin binding site from the rat brain. Endocrine. 2010;37(3):442-8.

589. Ray K, Hines CS, Coll-Rodriguez J, Rodgers DW. Crystal structure of human thimet oligopeptidase provides insight into substrate recognition, regulation, and localization. J Biol Chem. 2004;279(19):20480-9.

590. Wangler NJ, Santos KL, Schadock I, Hagen FK, Escher E, Bader M, et al. Identification of membrane-bound variant of metalloendopeptidase neurolysin (EC 3.4.24.16) as the non-angiotensin type 1 (non-AT1), non-AT2 angiotensin binding site. J Biol Chem. 2012;287(1):114-22.

591. Brown CK, Madauss K, Lian W, Beck MR, Tolbert WD, Rodgers DW. Structure of neurolysin reveals a deep channel that limits substrate access. Proc Natl Acad Sci U S A. 2001;98(6):3127-32.

592. Rioli V, Gozzo FC, Heimann AS, Linardi A, Krieger JE, Shida CS, et al. Novel natural peptide substrates for endopeptidase 24.15, neurolysin, and angiotensin-converting enzyme. J Biol Chem. 2003;278(10):8547-55.

593. Rashid M, Wangler NJ, Yang L, Shah K, Arumugam TV, Abbruscato TJ, et al. Functional up-regulation of endopeptidase neurolysin during post-acute and early recovery phases of experimental stroke in mouse brain. J Neurochem. 2014;129(1):179-89.

594. Rabey FM, Karamyan VT, Speth RC. Distribution of a novel binding site for angiotensins II and III in mouse tissues. Regul Pept. 2010;162(1-3):5-11.

595. Vincent B, Beaudet A, Dauch P, Vincent J, Checler F. Distinct Properties of Neuronal and Astrocytic Endopeptidase 3.4.24.16: A Study on Differentiation, Subcellular Distribution, and Secretion Processes. J Neurosci 1996;16(16):5049-59.

596. Fontenele-Neto JD, Massarelli EE, Garrido PA, Beaudet A, Ferro ES. Comparative Fine Structural Distribution of Endopeptidase 24.15 (EC3.4.24.15) and 24.16 (EC3.4.24.16) in Rat Brain. J Comp Neurol. 2001;438:399-410.

597. Woulfe J, Checler F, Beaudet A. Light and electron microscopic localization of the neutral metalloendopeptidase EC 3.4.24.16 in the mesencephalon of the rat. Eur J Neurosci. 1992;4(12):1309-19.

598. Jones ES, Vinh A, McCarthy CA, Gaspari TA, Widdop RE. AT2 receptors: functional relevance in cardiovascular disease. Pharmacol Ther. 2008;120(3):292-316.

599. Wangler NJ, Jayaraman S, Zhu R, Mechref Y, Abbruscato TJ, Bickel U, et al. Preparation and preliminary characterization of recombinant neurolysin for in vivo studies. J Biotechnol. 2016;234:105-15.

600. Checler F, Ferro ES. Neurolysin: From Initial Detection to Latest Advances. Neurochem Res. 2018;43(11):2017-24.

601. Rashid M, Arumugam TV, Karamyan VT. Association of the novel non-AT1, non-AT2 angiotensin binding site with neuronal cell death. J Pharmacol Exp Ther. 2010;335(3):754-61.

602. Teixeira PF, Masuyer G, Pinho CM, Branca RMM, Kmiec B, Wallin C, et al. Mechanism of Peptide Binding and Cleavage by the Human Mitochondrial Peptidase Neurolysin. J Mol Biol. 2018;430(3):348-62.

603. Yamauchi R, Wada E, Kamichi S, Yamada D, Maeno H, Delawary M, et al. Neurotensin type 2 receptor is involved in fear memory in mice. J Neurochem. 2007;102(5):1669-76.

604. Laszlo K, Toth K, Kertes E, Peczely L, Ollmann T, Lenard L. Effects of neurotensin in amygdaloid spatial learning mechanisms. Behav Brain Res. 2010;210(2):280-3.

605. Manberg PJ, Youngblood WW, Nemeroff CB, Rossor MN, Iversen LL, Prange AJ, et al. Regional distribution of neurotensin in human brain. J Neurochem. 1982;38(6):1777-80.

606. Benzing WC, Mufson EJ, Jennes L, Armstrong DM. Reduction of neurotensin immunoreactivity in the amygdala in Alzheimer's disease. Brain Res. 1990;537:298-302.

607. Satoh K, Matsumura H. Distribution of Neurotensin-Containing Fibers In The Frontal Cortex Of The Macaque Monkey
. J Comp Neurol. 1990;298:215-23.

608. Hamid EH, Hyde TM, Egan MF, Wolf SS, Herman MH, Nemeroff CB. Neurotensin Receptor Binding Abnormalities in the Entorhinal Cortex in Schizophrenia and Affective Disorders. Biol Psychiatry. 2002;51:795-800.

609. Nykjaer A, Willnow TE. Sortilin: a receptor to regulate neuronal viability and function. Trends Neurosci. 2012;35(4):261-70.

610. Fassio A, Evans G, Grisshammer R, Bolam JP, Mimmack M, Emson PC. Distribution of the neurotensin receptor NTS1 in the rat CNS studied using an amino-terminal directed antibody. Neuropharmacology. 2000;39:1430-42.

611. Woodworth HL, Perez-Bonilla PA, Beekly BG, Lewis TJ, Leinninger GM. Identification of Neurotensin Receptor Expressing Cells in the Ventral Tegmental Area across the Lifespan. eNeuro. 2018;5(1).

612. Jansen KL, Faull RL, Dragunow M, Synek BL. Alzheimer’s disease: Changes in Hippocampal N-Methyl-D-Aspartate, Quisqualate, Neurotensin, Adenosine, Benzodiazepine, Serotenin and Opioid Receptors-an Autoradiographic study. Neuroscience. 1990;39(3):613-27.

613. Rowe WB, Kar S, Meaney MJ, Quirion R. Neurotensin receptor levels as a function of brain aging and cognitive performance in the Morris water maze task in the rat. Peptides. 2006;27(10):2415-23.

614. Gahete MD, Rubio A, Córdoba-Chacón J, Gracia-Navarro FK, R.D., Avila J, al. e. Expression of the ghrelin and neurotensin systems is altered in the temporal lobe of Alzheimer's disease patients. J Alzheimers Dis. 2010;22(3):819-28.

615. Hu K, Harper DG, Shea SA, Stopa EG, Scheer FA. Noninvasive fractal biomarker of clock neurotransmitter disturbance in humans with dementia. Sci Rep. 2013;3:2229.
616. Al-Shawi R, Hafner A, Olsen J, Chun S, Raza S, Thrasivoulou C, et al. Neurotoxic and neurotrophic roles of proNGF and the receptor sortilin in the adult and ageing nervous system. Eur J Neurosci. 2008;27(8):2103-14.
617. Checler F. Experimental stroke: neurolysin back on stage. J Neurochem. 2014;129(1):1-3.
618. Ferrier IN, Cross AJ, Johnson JA, Roberts GW, Crow TJ, Corsellis JA, et al. Neuropeptides In Alzheimer Types Dementia. J Neurol Sci. 1983;62:159-70.
619. Yamada K, Uchida S, Takahashi S, Takayama M, Nagata Y, Suzuki N, et al. Effect of a centrally active angiotensin-converting enzyme inhibitor, perindopril, on cognitive performance in a mouse model of Alzheimer's disease. Brain Res. 2010;1352:176-86.
620. Sleegers K, den Heijer T, van Dijk EJ, Hofman A, Bertoli-Avella AM, Koudstaal PJ, et al. ACE gene is associated with Alzheimer's disease and atrophy of hippocampus and amygdala. Neurobiol Aging. 2005;26(8):1153-9.
621. Kauwe JS, Wang J, Mayo K, Morris JC, Fagan AM, Holtzman DM, et al. Alzheimer's disease risk variants show association with cerebrospinal fluid amyloid beta. Neurogenetics. 2009;10(1):13-7.
622. Mesquita Pasqualoto KF. Exploring the C-domain inhibition of angiotensin converting enzyme through novel bradykinin potentiating peptides. Pharm Pharmacol Int J. 2018;6(6).
623. Crecelius A, Gotz A, Arzberger T, Frohlich T, Arnold GJ, Ferrer I, et al. Assessing quantitative post-mortem changes in the gray matter of the human frontal cortex proteome by 2-D DIGE. Proteomics. 2008;8(6):1276-91.
624. Leonhardt J, Villela DC, Teichmann A, Munter LM, Mayer MC, Mardahl M, et al. Evidence for Heterodimerization and Functional Interaction of the Angiotensin Type 2 Receptor and the Receptor MAS. Hypertension. 2017;69(6):1128-35.
625. Patel S, Hussain T. Dimerization of AT2 and Mas Receptors in Control of Blood Pressure. Curr Hypertens Rep. 2018;20(5):41.
626. Herrera M, Sparks MA, Alfonso-Pecchio AR, Harrison-Bernard LM, Coffman TM. Lack of specificity of commercial antibodies leads to misidentification of angiotensin type 1 receptor protein. Hypertension. 2013;61(1):253-8.
627. Benicky J, Hafko R, Sanchez-Lemus E, Aguilera G, Saavedra JM. Six commercially available angiotensin II AT1 receptor antibodies are non-specific. Cell Mol Neurobiol. 2012;32(8):1353-65.
628. Hafko R, Villapol S, Nostramo R, Symes A, Sabban EL, Inagami T, et al. Commercially available angiotensin II At(2) receptor antibodies are nonspecific. PLoS One. 2013;8(7):e69234.

629. Mehta PK, Griendling KK. Angiotensin II cell signaling: physiological and pathological effects in the cardiovascular system. Am J Physiol Cell Physiol. 2007;292(1):C82-97.
630. Savoia C, Schiffrin EL. Vascular inflammation in hypertension and diabetes: molecular mechanisms and therapeutic interventions. Clin Sci (Lond). 2007;112(7):375-84.
631. Padia SH, Carey RM. AT2 receptors: beneficial counter-regulatory role in cardiovascular and renal function. Pflugers Arch. 2013;465(1):99-110.
632. Rompe F, Artuc M, Hallberg A, Alterman M, Stroder K, Thone-Reineke C, et al. Direct angiotensin II type 2 receptor stimulation acts anti-inflammatory through epoxyeicosatrienoic acid and inhibition of nuclear factor kappaB. Hypertension. 2010;55(4):924-31.
633. McCarthy CA, Vinh A, Callaway JK, Widdop RE. Angiotensin AT2 receptor stimulation causes neuroprotection in a conscious rat model of stroke. Stroke. 2009;40(4):1482-9.
634. Phillips MI, de Oliveira EM. Brain renin angiotensin in disease. J Mol Med (Berl). 2008;86(6):715-22.
635. Thomas WG, Mendelsohn FA. Angiotensin receptors: form and function and distribution. Int J Biochem Cell Biol. 2003;35(6):774-9.
636. Bali A, Jaggi AS. Angiotensin as stress mediator: role of its receptor and interrelationships among other stress mediators and receptors. Pharmacol Res. 2013;76:49-57.
637. Hajjar I, Brown L, Mack WJ, Chui H. Impact of Angiotensin receptor blockers on Alzheimer disease neuropathology in a large brain autopsy series. Arch Neurol. 2012;69(12):1632-8.
638. Chiu WC, Ho WC, Lin MH, Lee HH, Yeh YC, Wang JD, et al. Angiotension receptor blockers reduce the risk of dementia. J Hypertens. 2014;32(4):938-47.
639. Arganaraz GA, Konno AC, Perosa SR, Santiago JF, Boim MA, Vidotti DB, et al. The renin-angiotensin system is upregulated in the cortex and hippocampus of patients with temporal lobe epilepsy related to mesial temporal sclerosis. Epilepsia. 2008;49(8):1348-57.
640. Gouveia TL, Frangiotti MI, de Brito JM, de Castro Neto EF, Sakata MM, Febba AC, et al. The levels of renin-angiotensin related components are modified in the hippocampus of rats submitted to pilocarpine model of epilepsy. Neurochem Int. 2012;61(1):54-62.
641. Inuzuka T, Fujioka Y, Tsuda M, Fujioka M, Satoh AO, Horiuchi K, et al. Attenuation of ligand-induced activation of angiotensin II type 1 receptor signaling by the type 2 receptor via protein kinase C. Sci Rep. 2016;6:21613.
642. Armando I, Terron JA, Falcon-Neri A, Takeshi I, Hauser W, Inagami T, et al. Increased angiotensinII AT(1) receptor expression in paraventricular nucleus and hypothalamic-pituitary-adrenal axis stimulation in AT (2) receptor gene disrupted mice. Neuroendocrinology. 2002;76(3):137-47.

643. AbdAlla S, Lother H, el Missiry A, Langer A, Sergeev P, el Faramawy Y, et al. Angiotensin II AT2 receptor oligomers mediate G-protein dysfunction in an animal model of Alzheimer disease. J Biol Chem. 2009;284(10):6554-65.
644. Clancy P, Koblar S, Golledge J. Involvement of Angiotensin II Type 1 and 2 Receptors in Gelatinase Regulation in Human Carotid Atheroma in vitro. J Atheroscler Thromb. 2016;23(7):773-91.
645. Zheng J, Wang J, Pan H, Wu H, Ren D, Lu J. Effects of IQP, VEP and Spirulina platensis hydrolysates on the local kidney renin angiotensin system in spontaneously hypertensive rats. Mol Med Rep. 2017;16(6):8485-92.
646. Saper CB. An open letter to our readers on the use of antibodies. J Comp Neurol. 2005;493(4):477-8.
647. Saper CB. A guide to the perplexed on the specificity of antibodies. J Histochem Cytochem. 2009;57(1):1-5.
648. Elliott KJ, Kimura K, Eguchi S. Lack of specificity of commercial antibodies leads to misidentification of angiotensin type-1 receptor protein. Hypertension. 2013;61(4):e31.
649. Khan N, Muralidharan A, Smith MT. Attenuation of the Infiltration of Angiotensin II Expressing CD3(+) T-Cells and the Modulation of Nerve Growth Factor in Lumbar Dorsal Root Ganglia - A Possible Mechanism Underpinning Analgesia Produced by EMA300, An Angiotensin II Type 2 (AT2) Receptor Antagonist. Front Mol Neurosci. 2017;10:389.
650. Rong R, Hu G, Wang W, Muroya Y, Miura T, Ogawa Y, et al. Angiotensin II upregulates CYP4A isoform expression in the rat kidney through angiotensin II type 1 receptor. Prostaglandins Other Lipid Mediat. 2018;139:80-6.
651. Wang Q, Zhang Y, Le F, Wang N, Zhang F, Luo Y, et al. Alteration in the expression of the renin-angiotensin system in the myocardium of mice conceived by in vitro fertilization. Biol Reprod. 2018;99(6):1276-88.
652. Papali'i-Curtin JC, Brasch HD, van Schaijik B, de Jongh J, Marsh RW, Tan ST, et al. Expression of Components of the Renin-Angiotensin System in Pyogenic Granuloma. Front Surg. 2019;6:13.
653. Shi W, Yuan R, Chen X, Xin Q, Wang Y, Shang X, et al. Puerarin Reduces Blood Pressure in Spontaneously Hypertensive Rats by Targeting eNOS. Am J Chin Med. 2019;47(1):19-38.
654. Chen X, Zaro JL, Shen WC. Fusion protein linkers: property, design and functionality. Adv Drug Deliv Rev. 2013;65(10):1357-69.
655. Mahmood T, Yang PC. Western blot: technique, theory, and trouble shooting. N Am J Med Sci. 2012;4(9):429-34.